

FITHYDRO : Fishfriendly Innovative Technologies for Hydropower. Delivrable 2.2 Working basis of solutions, models, tools and devices and identification of their application range on a regional and overall level to attain self-sustained fish populations

Laurent David, Manon Dewitte

▶ **To cite this version:**

Laurent David, Manon Dewitte. FITHYDRO : Fishfriendly Innovative Technologies for Hydropower. Delivrable 2.2 Working basis of solutions, models, tools and devices and identification of their application range on a regional and overall level to attain self-sustained fish populations. Institut Pprime. 2019, pp.423. ⟨hal-05146760⟩

HAL Id: hal-05146760

https://hal.science/hal-05146760v1

Submitted on 11 Jul 2025

HAL is a multi-disciplinary open access archive for the deposit and dissemination of scientific research documents, whether they are published or not. The documents may come from teaching and research institutions in France or abroad, or from public or private research centers.

L'archive ouverte pluridisciplinaire **HAL**, est destinée au dépôt et à la diffusion de documents scientifiques de niveau recherche, publiés ou non, émanant des établissements d'enseignement et de recherche français ou étrangers, des laboratoires publics ou privés.



HAL Authorization

FIThydro

Fishfriendly Innovative Technologies for Hydropower



Funded by the Horizon 2020 Framework Programme of the European Union

D2.2 Working basis of solutions, models, tools and devices and identification of their application range on a regional and overall level to attain self-sustained fish populations

Project Acronym	FIThydro
Project ID	727830
Work package	2
Project Coordinator	Peter Rutschmann (TUM)
Deliverable Lead	Laurent David (CNRS)
Authors	Manon Dewitte, Laurent David
Contributors	Please refer to the first page of each section
Reviewers	Please refer to the first page of each section
Dissemination Level	Public
Estimated Delivery Date	30.04.2019
Actual Delivery Date	30.04.2019
Version	1

Acknowledgement

This project has received funding from the European Union's Horizon 2020 research and innovation programme under grant agreement No 727830.

Executive Summary

Deliverable 2.2 aims to report on the solutions, methods, tools and devices (SMTDs) used in the FIThydro project. The report is based on the analysis and the experience of the presently available SMTDs tested and applied in 14 FIThydroTest Cases and in lab investigations. The outcome with respect to SMTDs considers both a regional and a more overall focus. The deliverable consist of three parts: First a description of the SMTDs, second, a presentation of the work done and the results reached so far at the test cases, and third, a summary and a discussion including the identified knowledge gaps.

The Test Cases and the objectives investigated at each site were presented in deliverable 2.1, (submitted in October 2018). The activites at the Test Cases could be classified into 5 topics: Upstream and downstream migration, hydropeaking, turbine mortality and hydromorphology and habitat suitability. The progress of the activities at the various Test Cases differs from site to site and therefore the results available in spring 2019 are presented in this deliverable.

Finally, the deliverable closes with a summary and a discussion on the investigated 5 topics, namely: upstream migration, downstream migration, mortality through turbines, hydropeaking, habitat and hydromorphology. The surveys in D2.1 and the findings of D2.2 allowed to extract the appropriateness, constraints and limitation of the mitigation measures at Test Cases and in the laboratories; to deduct the range of application, accuracy and limitation of existing on-site monitoring tools and methods; and finally to identify the knowledge gaps and needs.

Table of Contents

1. Introduction 8
2. Tools and methods – general description 9
2.1 Visible Implant Elastomer 14
2.2 Acoustic Telemetry 15
2.3 Radio Telemetry 19
2.4 Radio Frequency Identification (RFID) with Passive Integrated Transponder – PIT tag 22
2.5 3D Fish Tracking System 26
2.6 3D Sensorless, ultrasound fish tracking 31
2.7 Cassiopée, 1993-2011 33
2.8 BASEMENT 40
2.9 River 2D 42
2.10 CASiMiR 46
2.11 HEC-RAS 50
2.12 OpenFOAM 56
2.13 FLOW-3D 59
2.14 TELEMAC 62
2.15 Bedload monitoring system 64
2.16. Shelter Measurements 67
2.17. GNSS – Global Navigation Satellite Sytem 70
2.18. iRon Differential pressure sensor base artificial lateral line probe 72
2.19. Barotrauma Detection System 75
2.20. Dilution Gauging 78
2.21. Acoustic Doppler Current Profiler - ADCP 80
2.22. Acoustic Doppler Velocimetry (ADV) 83
2.23. Particle Image Velocimetry - PIV 90
2.24. Lidar 94
2.25. Structure from Motion - SfM 98
2.26. Current meter 102
2.27. Hydropeaking indicator 105
2.28. Hydropeaking tool 108
2.29. COSH-TOOL 110
2.30. Sediment Simulation in intakes with Multiblock option 114
2.31. General discussion on the tools – Workshop 25th January 2019, Lisbon, Portugal 116

2.31.1. Laboratory and field measurement techniques 116
2.31.2. Hydraulic and habitat modelling tools....120
2.32. Conclusion....122
3. Results at the Test Cases 123
3.1 Altheim....135
3.2. Anundsjö....136
3.2.1. Passability and attraction at the fishway entrance 137
3.2.2. Bypassed reach and fishway: Flow 140
3.2.3. Reservoir....141
3.2.4. References....143
3.3. Bannwil 144
3.3.1. Downstream fish migration measures (ETHZ, FCO, BKW)....144
3.3.2. Turbine passage: Barotrauma Detection System measurements (TUT, SJE, BKW) 167
3.3.3. Turbine passage: BioPA modelling (VOITH, BKW) 169
3.3.4. References....187
3.4 Bragado 188
3.4.1 Fish community of the Tâmega River basin....188
3.4.2. Fish and habitat analysis....194
3.4.3. Hydropeaking....200
3.4.4. References....214
3.5 Freudenau....217
3.5.1. Fish species 217
3.5.2. Direct impacts on fish....220
3.5.3. Measures for habitat improvement 221
3.5.4. Use of bypass channel....224
3.5.5. Feasibility study for the investigation of fish migration paths with acoustic telemetry 226
3.5.6. Hydraulic modelling with coupled diffusion models for temperature and chemicals 229
3.5.7. Investigation and interpretation of fish swimming paths....229
3.5.8. References....230
3.6 Gotein 232
3.6.1. Efficiency of downstream migration devices....232
3.6.2. Characterization of the flow repartition between the 2 bypass entrances....238
3.6.3. Hydraulic modelling of the fishfriendly water intake 239

3.6.4. References....240
3.7 Guma and Vadocondes....241
3.7.1 Population and habitat analysis....241
3.7.2 Analysis of the conceptual solutions and facilities for fish migration....244
3.7.3 Assessment and improvement of fish mortality in the turbines....245
3.7.4 Spawning areas and hydro-morphology to attain self-sustainable populations 246
3.7.5 Migration facilities and attraction flow....250
3.7.6 Hydraulic modelling of the fishway and its attractiveness....259
3.7.7 References....264
3.8 Günz....266
3.8.1. Improvement of spawning habitats within the fish bypass....266
3.8.2. Population analysis....270
3.9 Ham....277
3.9.1. Study of survival through Archimede screws....277
3.9.2. Fish tracking by acoustic telemetry....280
3.9.3. References....280
3.10 Iller - Legau to Maria Steinbach....281
3.10.1. Population and habitat analysis (BEW)....281
3.10.2. Hydrodynamic modelling (SJE)....283
3.10.3. Telemetry system (INBO)....286
3.10.4. Fish tracks and evaluation – preliminary results (INBO)....297
3.10.5. Migration model (SJE)....302
3.10.6. References....304
3.11 Las Rives....305
3.11.1. Efficiency of downstream migration devices....305
3.11.2. Hydraulic modelling....309
3.11.3. Assessment of global survival rate at Las Rives....324
3.11.4. References....324
3.11.5. Annex 1: Gauging of the discharge in the downstream migration duct and assessment of the total discharge....325
3.12 Schiffmuhle....330
3.12.1 Monitoring of bedload transport through a vortex tube....330
3.12.2 Downstream impact of sediment management at HPPs (NTNU, ETHZ)....339
3.12.3 Efficiency of downstream and upstream migration devices (ETHZ, FCO, LKW, AF-CONSULT)....342

2.12.4. Habitat modelling (SJE, TUT) 342
3.12.4 References....367
3.13 Trois-Villes 370
3.13.1. Efficiency of downstream migration devices....370
3.13.2. Hydraulic modelling 375
3.13.3. References 380
3.14. Conclusion....380
4. Upstream migration 381
4.1. Specific tools for upstream migration....382
4.1.1. Fish Monitoring....382
4.1.2. Field measurements....385
4.1.3. Hydraulic modelling tools 385
4.2. Application Ranges 387
4.2.1. In France....387
4.2.2. In Spain....393
4.2.3. In Belgium 396
4.2.4. In Portugal....399
4.2.5. In Germany 399
4.2.6. In Switzerland....400
4.2. Knowledge gaps....400
4.3. References....402
5. Downstream migration....403
5.1. Specific tools and devices for downstream migration 404
5.1.1. Fish monitoring....404
5.1.2. Field hydraulic measurements....405
5.1.3. Hydraulic numerical modelling....407
5.2. Design criteria and application ranges....407
5.2.1. In France....407
5.2.2. In Switzerland....408
5.2.3. In Belgium 409
5.3. Results and knowledge gaps....409
5.3.1. France....410
5.3.2. Switzerland 410
5.3.3. Belgium 411
5.4. Conclusions....412

5.5. References 413
6. Passage through turbine 414
6.1. Background to fish mortality in hydraulic machines 415
6.2. Injury and mortality of fish due to turbine passage 416
6.2.1. Strike and gaps 416
6.2.2. Pressure and cavitation 416
6.2.3. Shear and turbulence 416
6.2.4. Indirect mortality 417
6.3. Discussion on tools and methods 417
6.3.1. Hydraulic machines 417
6.3.2. Machine modification, management and further mitigation measures 423
6.3.3. Fish mortality assessment 425
6.3.4. Application range 428
6.4. Knowledge gaps 432
6.4.1. Required SMTDs for fish mortality in turbines 432
6.4.2. Work on SMTDs for fish mortality in turbines 435
6.4.3. Conclusion 443
6.5. References 444
7. Hydropeaking 450
7.1. Introduction 451
7.2. Knowledge gaps and needs 451
7.2.1. Hydropeaking impacts 451
7.2.2. Mitigation measures 453
7.3. Tools for hydropeaking assessment and related knowledge gaps 453
7.4. Appropriateness, constraints and limitation of the mitigation measures 454
7.5. Range of application, accuracy and limitation of existing on-site monitoring tools and methods 456
7.6. References 456
8. Hydromorphology 459
8.1. Specific tools for hydromorphology 459
8.1.1. Sediment Management for habitat improvement 459
8.1.2. Vortex Tube / Bedload monitoring 461
8.1.3. Bathymetry measurements with ADCP 462
8.1.4. Habitat modelling with Casimir 462
8.1.5. Double averaging method 463
8.2. Knowledge Gaps and application ranges 464

8.2.1. Sediment Management 464
8.2.2. Swimming paths and Casimir 465
8.2.3. Double Averaging Method 465
8.3. Lessons learned / recommendations 466
8.4. References 467
9. Conclusion 471
10 Acknowledgement 471
11. Appendix 472
11.1. A-1 Programs of the workshops the 25th January 2019 in Lisbon, Portugal 472

1. Introduction

FIThydro is focussing on 5 main areas of hydropower impact: migration, mortality, habitats, sediments and monitoring. After the state of the art review conducted in D2.1 about the solutions, methods, tools and devices (SMTDs) and the identification of the knowledge gaps, the current deliverable aims to report on the analysis of the presently available SMTDs tested at the Test Cases and in the lab and the potential SMTDs on both a regional and an overall European level. We will study the SMTDs applied at the Test Cases and provide the limitation of the mitigation measures identified. The application range of the SMTDs are defined and their uses are discussed.

After the general description of the SMTDs used at each Test Case and the results of all the Test Cases, we will discuss and compare the tools, present the application ranges of the mitigation measures and identify the knowledge gaps according to five main topics: upstream migration, downstream migration, passage through turbine, hydropeaking and hydromorphology.

Deliverable 2.2 Main Index

- Detailed Table of contents
- Tools and methods – general description
- Results at the Test Cases
- Upstream migration
- Downstream migration
- Passage through turbine
- Hydropeaking
- Hydromorphology

2. Tools and methods – general description

To conduct the activites at the Test Cases, many SMTDs were used. These techniques can be classified into 7 categories: fish tracking, hydraulic modelling, hydraulic measurements, sediment tracking, hydromorphology tools, hydropeaking tools, barotroma sensors.

This part aims to describe the tools and methods used in research study conducted at the Test Cases and to present their application ranges and cross-comparisons. This part of the deliverable is highly linked to workpackage 4. All findings will be part of a wiki system developed in WP4.

Two workshops were organised to present and discuss these tools and methods, during a FIThydro meeting at Lisbon the 25th January 2019. The first one was about field measurements and the second about hydraulic and habitat numerical modelling. The reports on the discussion held during these two meeting are included in this deliverable.

List of tables

Figure 1: Injection of visible implant elastomer. 14
Figure 2: Example of VIE at different spots on fishes 15
Figure 3: Left: VPS array in the river Iller (Germany) covering a fish pass outflow downstream of a hydropower plant (Vemco 180 kHz system). Blue marks are hydrophones containing synchronisation tags and yellow marks are reference tags. Right: example of a silver eel track at the Albert Canal (Belgium) using VPS at 69 kHz. 16
Figure 4: Left: Belgian hydrophone network (2018) consisting of 164 hydrophones. Right: European ETN hydrophone network with 136 different programs, 2948 tagged fish and 55 million detections (source: http://www.lifewatch.be/etn/). 17
Figure 5: Left: two radio transmitters of different size; right: radio telemetry receiver. 20
Figure 6: Brown trout (Salmo trutta) with a radio transmitter in the body cavity and the external antenna. 20
Figure 7: Passive Integrated Transponder source: https://www.oregonrfid.com/new-to-rfid/. 22
Figure 8: Schema of the RFID system (source: Tomanova et al. 2017). 23
Figure 9: Example of a tuning capacitor (source; AFB). 24
Figure 10: Example of a RFID reader (source: AFB). 24
Figure 11: Example of antennas in a downstream migration channel in France (source: Tetard et al., 2017). 25
Figure 12: 3D fish tracking system installed in the etho-hydraulic flume at VAW of ETH Zurich (source: VAW) 27
Figure 13. (a) Camera (acA2000-50gmNIR, Basler) with lens (FE185C086HA-1, Fujifilm), (b) waterproof housing for the camera and lens (Autovimation), (c) high performance computer for camera recording and network switch for camera connection (source: VAW). 28
Figure 14: (a) Stereo view of a camera pair, (b) three detected fish and noise, (c) 2D tracks of three fish (source: VAW). 29
Figure 15: Top view of 3D tracks of three fish from an etho-hydraulic test of fish guidance structure with horizontal bars (source: VAW). 29
Figure 16: Experimental setup for testing and development of the 3D sensorless ultrasound fish tracking. 32
Figure 17: Example of designing a pool-type fishway. 35
Figure 18: Example of computing water levels. 36
- Figure 19: Example of the tool to design a pre-barrage. 37
Figure 20: Tool to design a baffle fishway in Cassiopée. 38
Figure 21: Example of use of Cassiopée in FIThydro at Las Rives, France. 39
Figure 22: Combination of 1D and 2D models in BASEMENT (source: VAW) 40
Figure 23: Graphical user interface of BASEMENT (credits: VAW). 41
Figure 24: Visualization of BASEMENT results with QGIS plugin Crayfish (credits: VAW). ..41
Figure 25: River 2D layout images: (a) R2D_Bed; (b) R2D_Mesh; and (c) River2D. 43
Figure 26: Water depth (m) output from River 2D. Ocreza River, Portugal. 44
Figure 27: Water velocity (m/s) output from River 2D. Ocreza River, Portugal. 44
Figure 28: WUA (m2) for the European Eel. Ocreza River, Portugal. 45
Figure 29: WUA (m2) and discharge in the Ocreza River for Iberian barbel (adult and juvenile), European eel (adult and juvenile) and Gudgeon. 45
Figure 30: CASiMiR model of river stretch and results for adult barbel. 47
Figure 31: Example of an operational mitigation measure: reduced downramping rate. 48
Figure 32: Predicted migration paths based on rheoreactive behaviour of grayling. 48

Back to D2.2 Main index

Figure 33: view of the interface. 49
Figure 34: HEC-RAS graphical user interface (GUI) https://www.hec.usace.army.mil/software/hec-ras/. 51
Figure 35: HEC-RAS outputs (https://www.hec.usace.army.mil/software/hec-ras/): (a) cross-section; (b) profile; (c) rating curve; (d) hydrograph; (e) inundation mapping; and (f) tabular output. 55
Figure 36: Example of turbine inlet (flow in x-direction) modelled using an unstructured computational grid for OpenFOAM simulations (source: VAW). 57
Figure 37: Case directory structure in OpenFOAM (source: CFD Direct ® OpenFOAM) 57
Figure 38: Overview of OpenFOAM structure (source: CFD Direct ® OpenFOAM). 58
Figure 39: Exemplary ParaView visualization of OpenFOAM simulation results showing horizontal flow velocities in a rectangular channel with a curved bar rack (CBR) for horizontal plane at 0.2 m (**a**). Deviation (in percent) of the ratio between tangential vt and normal velocities vn for the MCR compared to the situation without screen 5 cm (**b**) and 40 cm (**c**) upstream of the screen axis. The black arrows represent the flow direction (source: VAW). 58
Figure 40: Location of variables in FLOW-3D computational mesh (source: FLOW-3D) 60
Figure 41: Example of a river power plant geometry set up for FLOW-3D (source: VAW) 61
Figure 42: Exemplary visualization of FLOW-3D simulation results for the case study HPP Banwil showing flow velocities and streamlines at a potential location for fish guidance structures (left) and during spillway operation (right) (source: VAW). 61
Figure 43: Overview of the TELEMAC modeling system (Source: www.opentelemac.org) ... 63
Figure 44. (a) Geophone and accelerometer installed in a watertight housing mounted on an impact plate and exemplary (b) geophone and (c) accelerometer signal of the identical single grain impact. SumIMP denotes the total number of peaks above the threshold amplitude A_{min} for the event shown. A_{maxmax} is the maximum amplitude registered during this event. Only positive amplitude values are considered. 65
Figure 45. (a) Conceptual sketch of the vortex tube functionality and (b) vortex tube outlet at HPP Schiffmühle (source: VAW). 65
Figure 46. (a) Vortex tube outlet with mounted sensors and (b) vortex tube running during the field calibration (source: VAW). 66
Figure 47: Juvenile salmon in the upper layers of river bed sediment (Forseth et al., 2014). 68
Figure 48: Exemplarily shown hiding depth of 2cm (first marker covered) on a tube. 68
Figure 49: Different systems called as GPS. 70
Figure 50: Differential GPS mounted on a remote-controlled boat for bathymetry and discharge measurements. 71
Figure 51: RTK-GPS for single point measurements at very high accuracy (< 1 cm). 71
Figure 52. iRon, the lateral line probe (LLP). NACA0025 body shape.showing the locations of the differential pressure sensors (1-6), and the absolute pressure sensor (7) [3]. 73
Figure 53.Velocity estimation with an artificial lateral line. a) Distribution of pressure over the body of the lateral line. b) Estimation of velocity considering different pressure differences around the body and different shapes [4] 73
Figure 54. Distribution of mean pressure asymmetry for different refuge layouts (R0: control, R1: close triangles, and R2: open triangles) and hydrodynamic scenarios [3] 74
Figure 55: Schematic and dimensions of the BDS, showing the locations of the three pressure transducers and the Inertial Measurement Unit (IMU). Left: side-view of sensor. Right: top-view facing the cap showing the left (L), middle (M) and right (R) pressure ports. 76

Figure 56: Time series plot and overlay of a vertical Kaplan turbine, showing the pressure change as measured by the BDS as it passes through a hydropower plant (turbine illustration courtesy of cfdsupport.com). 77
Figure 57: Dilution gauging in a fishway. Left: making the dilution of the tracer (Rhodamine Wt). Right. Mariotte device for the continuous injection into the fishway. 79
Figure 58. Exemplary ADCPs: (a) Teledyne RiverPro with 5 beams (credit: http://www.teledynemarine.com) and (b) Sontek M9 with 9 beams and S5 with 5 beams (credit: https://www.sontek.com). 80
Figure 59. (a) Teledyne Marine Q-boat of VAW equipped with Riverpro ADCP and DGPS and (b) water surface elevation along the power canal of HPP Schiffmühle (black line: DGPS data and red line: total station data). 81
Figure 60: Workflow used for post-processing of ADCP data 82
Figure 61: Depth averaged flow velocities upstream of the HPP Bannwil measured with the ADCP boat at a discharge of 402 m3/s (background image: © 2018 swisstopo (JD 100041)). 82
Figure 62: ADV device: (a) photograph showing its main components; (b) SonTek 10MHz down-looking ADV and SonTek FlowTracker with side-looking probe; (c) Nortek Vector with down-looking probes and Nortek Vectrino with down-looking and side-looking probes; (d) down. 85
Figure 63: Set-up of a standard 2D PIV system (Raffel et al 2007). 91
Figure 64: LSPIV measurement sequence: (a) imaging the area to be measured (white patterns indicate the natural or added tracers used for visualization of the free surface), (b) the distorted raw image, and (c) the undistorted image with the estimated velocity velocity vectors overlaid on the image (Muste et al. 2008) 92
Figure 65: Swiss grid georeferenced surface velocity field and streamlines measured by AIV, including areas of noisy velocity data. (Note that according to Le Coz et al. (2010), depth averaged velocities can be estimated by multiplying the surface velocity by factors 0.79-0.89, with a central value close to 0.85); (Detert et al. 2019) 93
Figure 66: Basic set up of a Lidar measurement (Mallet 2010). 95
Figure 67: Comparison red vs green laser (Mallet 2010). 95
Figure 68: Discrete Echo and waveform signal comparison for Airborne Laser Scanning (https://commons.wikimedia.org/wiki/File:Airborne_Laser_Scanning_Discrete_Echo_and_Full_Waveform_signal_comparison.svg). 96
Figure 69: Drone picture taken in a height of 50 m over ground showing the residual flow area in Anundsjø HPP, ice cover and the author. 99
Figure 70: First run of a structure from motion evaluation in the lab of NTNU. The blue field indicates the camera position. 99
Figure 71: Screenshot of the Argisoft Photoscan Workflow. 100
Figure 72: Mesh generated from SfM from a section of the residual flow reach of Anundsjø. 101
Figure 73: Current meter: a) mechanic, b) electro-magnetic, c) acoustic. Sources: SEBA hydrométrie, OTT, Sontek. 103
Figure 74: Cutting of a section during the measurement by a flow meter, in red the verticals, the black dots correspond to the measurement points. 104
Figure 75: Operator in the downstream migration channel for measurements with a current meter. 104
Figure 76: Example of flow analysis. 106

Back to D2.2 Main index

Figure 77: Evolution of the Hydropeaking indicator on the Maronne river at Basteyroux station for the whole year and during the spring (mid-march to mid-june); effect of the progressive implementation of mitigation measures since 2001. 107
Figure 78 Principle of the hydropeaking tool for categorization of regulated rivers according to the potential impacts of hydropeaking on fish population. 109
Figure 79. Combinations of hydropeaking effects and vulnerability for total impact assessment 110
Figure 80.The river Lundesokna in Norway downstream of a peaking hydropower plant. COSH-Tool can be used to asses many aspects of peaking operations. 111
Figure 81. Distribution of peak events though the day. 112
Figure 82. Number of peak events per day for each year of the time series. 113
Figure 83. Distribution of peak events (increasing events) per month according to light conditions 113
Figure 84: flow chart of the executable SSIIM. 114
Figure 85: List of all available parameters. 115
Figure 86: Examples of simulations with SSIIM. 116

List of Tables

Table 1: shelter availability depending on the number of shelter available 69
Table 2: Technical specifications of the commercial ATS Sensor Fish Model ARC800 and the BDS developed in the FITHydro project. 77
Table 3: Levels of hydrologic perturbation due to hydropeaking events. 107
Table 4. List of parameters computed by COSH-Tool. 111

2.1 Visible Implant Elastomer

Type: device

Suitable for monitoring aquatic fauna in all phases of mitigation measures (planning, implementation, maintenance)

Introduction:

Visible Implant Elastomer (VIE) Tags are coloured tags (https://www.nmt.us/visible-implant-elastomer/). They are implanted in translucent tissue of several animals, mainly used in fish, but also in crustaceans, cephalopods, reptiles, amphibians, small mammals, etc. (Figure 1). VIE consists of two liquid components (colour component and curing agent) which are mixed just before the tagging, changing into a solid state in a short time (1-2 hours). VIE are injected subcutaneously with syringes or specialist injection systems, in clear tissue areas and there are several colours available, with and without fluorescence.



Figure 1: Injection of visible implant elastomer.

Application:

The main goal of tagging with VIE is the visual recognition of individuals. This can be achieved with a unique code, depending on the number of animals, colours and tagging places available. Obtaining results is based on mark and recapture techniques, and usually as a complement of another tracking system. The main application is focused on temporary habitat use studies. In the case of fishways, tagging fish downstream, upstream and inside the fishway, and recapturing some of them, can provide information about their movements.

In contrast to other tag devices smaller individuals (even less than five centimetres) can be tagged with VIE and the cost per tag is quite low (€ cents per tag per millilitre of product and

day of tagging). However, about costs, it is necessary to also take into account the need for fish samples, or video recording devices that are required for the recaptures.



Figure 2: Example of VIE at different spots on fishes

Other information:

More information about range size and species with links to research papers can be found here: https://www.nmt.us/versatile-vie/

There are other types of tags with similar characteristics and/or applications. For example: VI Alpha tags (https://www.nmt.us/vi-alpha/), Anchor tags (https://www.hallprint.com/), piercing tags (https://nationalband.com/fish-tags/).

Contact information:

https://www.nmt.us

Authors	Javier Sanz Ronda (ITAGRA)
Reviewers	Robert Boes (ETHZ)

2.2 Acoustic Telemetry

Type: method

Introduction:

Together with radio and PIT telemetry, acoustic telemetry is a biotelemetry technique that has been used on fish for over 60 years. The principle of acoustic telemetry consists of the communication between an emitting tag (fish) and a receiving device (hydrophone) by means of an acoustic signal to determine the location of the tag (fish). This location can provide useful information about migration, individual behaviour, habitat use, passage efficiency, predation, etc. Acoustic telemetry uses lower radio frequency signals (69-500 kHz) compared to radio telemetry (30-300 MHz), which both have advantages and disadvantages. A major drawback of acoustic compared to radio telemetry used to be the poor reading range in turbulent water

systems. Recent developments countered this drawback by using higher frequency signals. Nowadays, also more challenging environments like noisy, shallow and reflective water systems are suitable for acoustic telemetry. This evolution also allows positioning many tagged animals with sub-meter accuracy at the same time. Another unique advantage of acoustic telemetry is its capability to be used in salt and deep water. These features make this technique suitable to conduct fish behaviour studies that are able to address multiple research questions, even for diadromous fish species. Besides a single registration of a fish (1D or presence/ absence), more and more research is done to gather fish tracks in 2D or even 3D at specific sites like migration obstacles, fish passes and hydropower stations (Figure 3). The principle of this precise positioning of fish is based on the difference in detection time of a tag that is positioned in between at least 3 receiving hydrophones. Depending on the producer of the tags and hydrophones, the acoustics work at different kHz ranges. When the producer is VEMCO, then the 2D/3D positioning system is called VPS and this works at either 69 kHz or 180 kHz. Initially, this VPS (Vemco Positioning System) was mainly used in big lakes using 69 kHz tags, but recently small-scale accurate fish tracking is possible using a higher 180 kHz frequency. The choice for one or the other frequency depends on the system studied and the study objectives. Typically, the VPS array is equipped with reference and synchronisation tags to monitor system performance and to correct for clock drift between different submerged hydrophones. Figure 3 shows a VPS array conducted at the Fithydro case study of the river Iller (Altusried, Germany, left) and another one in the Albert Canal (Ham, Belgium, right).

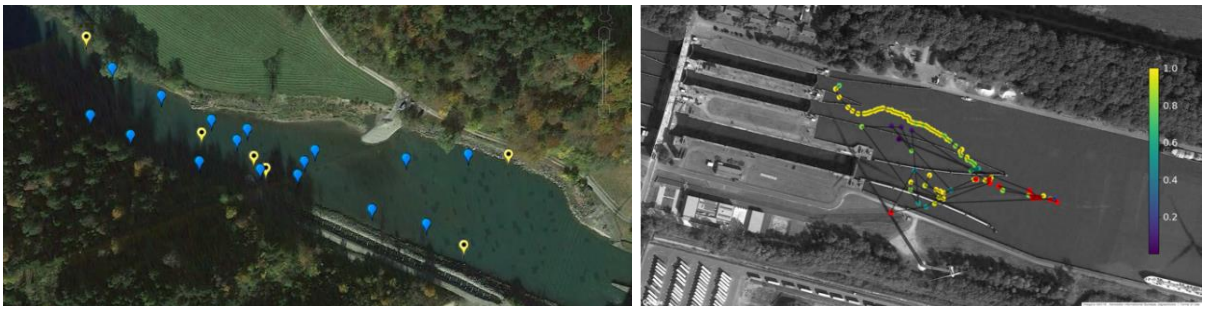


Figure 3: Left: VPS array in the river Iller (Germany) covering a fish pass outflow downstream of a hydropower plant (Vemco 180 kHz system). Blue marks are hydrophones containing synchronisation tags and yellow marks are reference tags. Right: example of a silver eel track at the Albert Canal (Belgium) using VPS at 69 kHz.

Application:

The most comprehensive use of acoustic fish telemetry has been done on the **large scale 1D** migration research. In this setup hydrophones are spread along a lake, a river or a canal and fish are detected when passing these hydrophones. Numerous examples of fish migration studies in large rivers and lakes around the world have been published so far. The advantages of this research technique are found in its good performance in deep and salt water and its large detection range in such situations. Many of these migration studies were conducted on diadromous fish species like eel and salmonids. The typical study design consists of 69 kHz hydrophones and tags with a diameter between 7 and 13 mm. The hydrophones can be moored close to the river banks if the detection range of the tags covers the whole width of the river. In lake or estuary systems, hydrophones can be attached to buoys. This range depends on the tag output power (136-162 dB) and the environmental conditions (noise). Tags are custom-made and programmed to fit the research demands. The determining factors for the setup of a 1D acoustic system are the fish species of interest, its environment and the specific research questions. When studying smaller species or juvenile fish, tag size will limit the battery

life. Big rivers with strong currents will require more hydrophones and/or tags with a higher output (so a shorter battery life). When spatial and temporal changes of a certain migration are expected, tags could be programmed in different steps in which the duration, the power output and the signal delay can be changed. During or after the study period, hydrophones have to be lifted for data download by means of Bluetooth connection to a PC. Hydrophones at 69 kHz can operate for more than one year before the battery has to be changed. A single hydrophone can store 1.6 million detections. These unique detections are the result of a so called 'PPM' signal (Pulse Position Modulation), which is a ping train of 8 consecutive pings. The separation between each of these individual pings results in a unique ID. The recently developed tags and hydrophones that work on 180 kHz can emit and detect HR (High Residency) coded signals beside PPM coded signals. An HR coded signal is emitted as one ping and does not exist of consecutive ping trains. Hence, the emission time of the code is reduced much and one signal is emitted in less than one second. Consequently, the chance of collision of codes of multiple tagged fish that are within the same detection zone of a hydrophone is reduced. Next, the delay between two consecutive code emissions can be reduced as well, down to one second, allowing more frequent fish positioning (more fish positions per time unit). High frequency tags are smaller compared to the 69 kHz tags (smallest tag diameter is 4 mm). A network of receivers can be used to conduct research on several species at a large scale (Figure 4).



Figure 4: Left: Belgian hydrophone network (2018) consisting of 164 hydrophones. Right: European ETN hydrophone network with 136 different programs, 2948 tagged fish and 55 million detections (source: http://www.lifewatch.be/etn/).

The Belgian hydrophone network has been used to study both upstream and downstream fish migration of 10 different fish species in the freshwater part and 5 more in the North Sea and the estuary of river Schelde (Reubens et al., 2018; Verhelst et al., 2018). The network is funded by INBO (Research Institute for Nature and Forest; www.inbo.be), VLIZ (Flanders Marine Institute; www.vliz.be) and Lifewatch (EU; http://www.lifewatch.be/en/fish-acoustic-receiver-network).

In recent years acoustic telemetry is used to generate fish tracks at certain sites of interest. The same gear that is used for 1D tracking can be used for **2D and 3D tracking**, so fish tags can be programmed to be deployed in both designs. To retrieve 3D data, the tags have to include a pressure sensor. The post processing of calculated positions to gather accurate fish tracks is still challenging. Tracks can suffer either by insufficient or excessive filtering.

Within the Fithydro project, a high frequency VPS array was installed in the river Iller (Altusried, Germany, Figure 3, left). Processing raw data of 25 graylings (*Thymallus thymallus*) and 22 barbels (*Barbus barbus*) resulted in more than 15 million unfiltered fish positions.

Other information:

Acoustic fish telemetry suppliers worldwide:

- ATS, 470 First Avenue NW, Isanti, MN 55040, USA
- *HTI, 715 NE Northlake Way, Seattle, WA 98105*: **recent partnership with Vemco**
- Lotek Wireless Inc., 115 Pony Drive, Newmarket, Ontario, Canada L3Y 7B5
- Thelma Biotel, Sluppenveien 10, 7037 Trondheim, Norway, EU
- Sonotronics, 3169 S Chrysler Ave, Tucson, AZ 85713, USA
- Vemco, 20 Angus Morton Drive, Bedford, Nova Scotia, Canada B4B 0L9

Hydrophones can differ regarding the frequency used, the ability to measure other variables (tilt, temperature, …), whether it is cabled or not, etc. The price for one submersible hydrophone ranges from 1.000 to over 3.000 € (without VAT). Tags are available in an endless number of different settings and sizes. The price range of acoustic tags is between 180 and 500 €. A lot of other gear like portable hydrophones, automatic acoustic release systems, remote communication, etc. are available these days.

References:

Some examples of 1D acoustic studies using different suppliers of acoustic gear:

Bass, A. L., T. O. Haugen, & L. A. Vøllestad, 2014. Distribution and movement of European grayling in a subarctic lake revealed by acoustic telemetry. Ecology of Freshwater Fish 23: 149–160.

Behrmann-Godel, J., & Eckmann, R., 2003. A preliminary telemetry study of the migration of silver European eel (Anguilla anguilla L.) in the River Mosel, Germany. Ecology of Freshwater Fish 12: 196–202.

Besson, M., T. Trancart, A. Acou, F. Charrier, V. Mazel, A. Legault, & E. Feunteun, 2016. Disrupted downstream migration behaviour of European silver eels (Anguilla anguilla, L.) in an obstructed river. Environmental Biology of Fishes .

Breine, J., I. S. Pauwels, P. Verhelst, L. Vandamme, R. Baeyens, J. Reubens, & J. Coeck, 2017. Successful external acoustic tagging of twaite shad Alosa fallax (Lacépède 1803). Fisheries Research 191: 36–40.

Bultel, E., Lasne, E., Acou, A., Guillaudeau, J., Bertier, C., & Feunteun, E. (2014). Migration behaviour of silver eels (Anguilla anguilla) in a large estuary of Western Europe inferred from acoustic telemetry. Estuarine, Coastal and Shelf Science, 137(0), 23-31. doi:http://dx.doi.org/10.1016/j.ecss.2013.11.023

Hayden TA, Holbrook CM, Fielder DG, Vandergoot CS, Bergstedt RA, Dettmers JM, et al. (2014) Acoustic Telemetry Reveals Large-Scale Migration Patterns of Walleye in Lake Huron. PLoS ONE 9(12): e114833. https://doi.org/10.1371/journal.pone.0114833

More than 1000 research papers on Vemco acoustic telemetry research can be consulted via https://vemco.com/publications-database/

A couple of 100 papers that used Lotek gear can be found here: http://www.lotek.com/search

Examples of 2D and 3D research outputs:

Andrews, K. S., N. Tolimieri, G. D. Williams, J. F. Samhouri, C. J. Harvey, & P. S. Levin, 2011. Comparison of fine-scale acoustic monitoring systems using home range size of a demersal fish. Marine Biology 158: 2377–2387.

Espinoza, M., T. Farrugia, D. Webber, F. Smith, & C. Lowe, 2011. Testing a new acoustic technique to quantify fine-scale, long-term fish movements. Fisheries Research 108: 364-371.

Fowler, A. J., C. Huveneers, & M. T. Lloyd, 2017. Insights into movement behaviour of snapper (Chrysophrys auratus, Sparidae) from a large acoustic array. Marine and Freshwater Research 68: 1438–1453.

Roy, R., L. Westrelin, E. Tissot, E. De Oliveira, & C. Argillier, 2014. Activity patterns of three piscivorous species in a reservoir studied with the Vemco Positioning System. 144ème réunion annuelle de l'American Fisheries Society 18 p.

Vergeynst, J., R. Baeyens, I. Pauwels, T. De Mulder, I. Nopens, & A. Mouton, 2016. The behaviour of downstream migrating European eel at sluices and turbines. , http://lib.ugent.be/catalog/pug01:8075115.

Williams-Grove, L. J., & S. T. Szedlmayer, 2017. Depth preferences and three-dimensional movements of red snapper, Lutjanus campechanus, on an artificial reef in the northern Gulf of Mexico. Fisheries Research 190: 61–70.

Contact information:

Authors	Johan Coeck (INBO), Ine Pauwels (INBO), Raf Baeyens (INBO)
Reviewers	Robert Boes (ETHZ)

2.3 Radio Telemetry

Type: Telemetry techniques

Suitable for fish migration studies, mitigation, monitoring (see list) in planning and success evaluation phases

Introduction:

Radio telemetry is mainly used in freshwater (shallow streams and rivers) with a conductivity of < 500-1000 µSiemens/cm. A radio transmitter emits electromagnetic energy in the radio frequency range (between 30-300 MHz) and provides a possibility for remotely locating a fish. Digitally coded transmitters emit a unique code. A system can operate up to 1000 coded transmitters on one single frequency.

It is a gear intensive technique with the following components:

- Transmitter (emitting the signal, attached to the fish, with battery and an antenna, Figure 5, left)
- Mobile or fixed receiving antenna, capturing the radio signal, different types available; often loop or Yagi antenna are used.
- Receiver, converting the radio signal into an electronic/audible form in order to identify the tagged fish (Figure 5, right)
- Data logger, operates the receiver when the operator is absent
- Cables/connectors connect the antenna to the receiver

The transmitters should be adjusted to the size of fish and the study goal. The transmitter weight should not exceed 2 % of the fish weight. Different sensors can record temperature, depth, and pressure. Miniaturization made transmitters with 0.2 g possible. Therefore small fishes (12-15 cm total length) can be equipped with these tiny transmitters.



Figure 5: Left: two radio transmitters of different size; right: radio telemetry receiver.

The transmitters are implanted into the body cavity of the fish (Figure 6). Gastric (oesophagus) insertion or external attachment may be possible. The conductivity of the water and the depth of the transmitter in the river are the most critical parameters in detecting the radio signals.



Figure 6: Brown trout (Salmo trutta) with a radio transmitter in the body cavity and the external antenna.

Application:

Radio telemetry is a standard tool for the study of spatial ecology and migration of fishes. It can be applied for a variety of fish migration studies. The passage corridor at a hydropower plant can be evaluated and information is gathered how the fish is approaching the site. The

searching phase in front of a hydropower plant can be documented for downstream and upstream migrations.

Stationary and mobile tracking are often used. Stationary tracking continuously tracks a signal, but its application is limited to specific sites. Fish presence or absence at a site, and passage and movement rates between sites can be detected (Eiler, 2012). Mobile tracking allows the survey of an extended area.

The application for radio telemetry at hydropower plants is mainly detecting passage routes and linear migrations in a river system. However, acoustic telemetry (section 2.2) became very popular and is more suitable for studies with the goal of documenting the detailed behaviour patterns of fishes in front of a hydropower plant (forebay). There are certain advantages and disadvantages for acoustic and radio telemetry. Both methods are adequate depending on the study objectives.

Radio telemetry is applied worldwide. Beeman et al (2012) published a comprehensive study on the effects of hydroelectric dams on fish populations on the Columbia River and on the Snake River. The downstream migration of Chinook salmon and anadromous rainbow trout at different sites were extensively documented.

Radio telemetry studies will be applied within the FIThydro project in the Aare River (HP Bannwil) to study the migration corridor and the timing of the migration. Mainly cyprinid fish species will be tracked. The main question is if fish are using the spillway corridor or if they migrate with the main flow through the turbine intakes. On the whole, the downstream migration of cyprinid fish species at hydropower plants has been incompletely studied so far and the Bannwil Test Case should contribute to a better understanding of cyprinid fish migration.

Other information:

Radio telemetry is gear-intensive with high initial costs for the equipment, but also for transmitters, the preparation and station installation. Radio telemetry experiments have to be considered as animal experiments and special permissions from the local authorities are needed.

References:

Beeman, J. W., E. E. Hockersmith & J. R. Stevenson. 2012. Design and performance of radio telemetry systems for assessing juvenile fish passage at three hydroelectric dams. Pages 281-302 in N. S. Adams, J. W. Beeman & J. H. Eiler. Editors. Telemetry techniques: a user guide for fisheries research. American Fisheries Society, Bethesda, Maryland.

Eiler, J. H. 2012. Tracking aquatic animals with radio telemetry. Pages 163-204 in N. S. Adams, J. W. Beeman & J. H. Eiler. Editors. Telemetry techniques: a user guide for fisheries research. American Fisheries Society, Bethesda, Maryland.

Contact information:

Author of the document: Armin Peter

Authors	Armin Peter (FCO)
Reviewers	Robert Boes (ETHZ)

2.4 Radio Frequency Identification (RFID) with Passive Integrated Transponder – PIT tag

Date: 1973

Type: Tool (fish tracking)

Suitable for animal tracking (movements), useful for upstream and downstream mitigation measures during implementation and maintenance of the mitigation measure

Introduction:

RFID (Radio Frequency Identification) system uses PIT (Passive Integrated Transponder) tags to detect and follow individuals. The PIT tags (Figure 7), each with a unique alphanumeric code, are of small size and benefit of indefinite operational life (no battery is required). When entering in the detection area of a RFID antenna (Figure 8), the reader is responsible of powering and communicating with the tag. The tag antenna captures energy from a tag and transfers the tag's ID.

Low Frequency RFID uses magnetic fields that can go through water in contrast to high frequency RFID. Owing to the shorter detection range (less than 2 m perpendicular to the antenna plane) RFID technology is mainly suitable for smaller systems. Two different technologies can be used (source: https://www.oregonrfid.com/resources/hdx-fdx/):

- Half duplex RFID (HDX): A half duplex RFID reader generates short magnetic pulses that wirelessly charge a capacitor (Figure 9) inside an HDX tag. When the charge field turns off, the tag uses the stored power to send the tag number back to the reader (Figure 10) without interference from the reader.
- Full duplex RFID (FDX): Full duplex RFID generates a continuous magnetic field which powers the tag to respond immediately. Tags repeat their message, while powered by the field, up to 30 times per second.



Figure 7: Passive Integrated Transponder source: https://www.oregonrfid.com/new-to-rfid/.

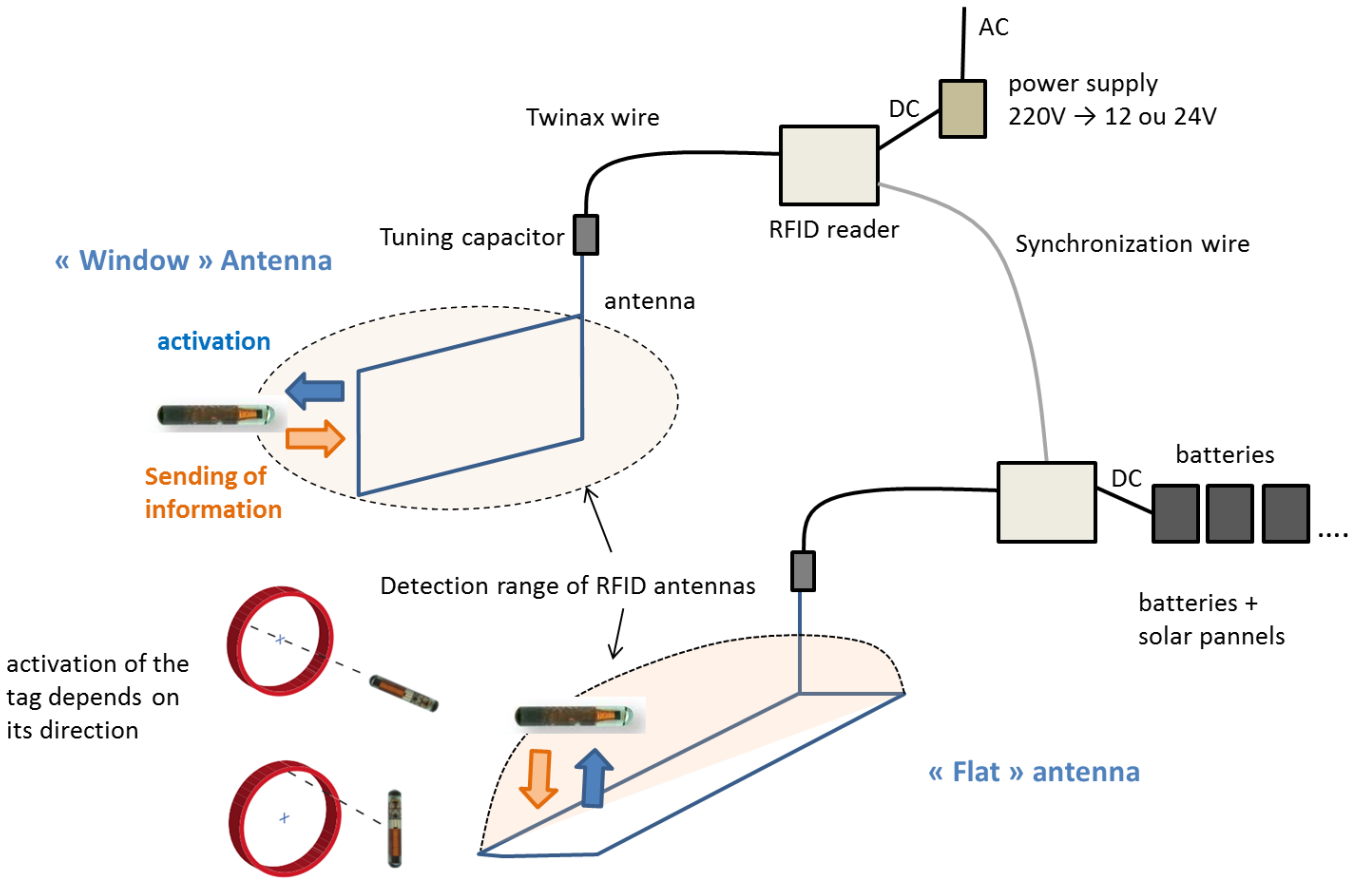


Figure 8: Schema of the RFID system (source: Tomanova et al. 2017).

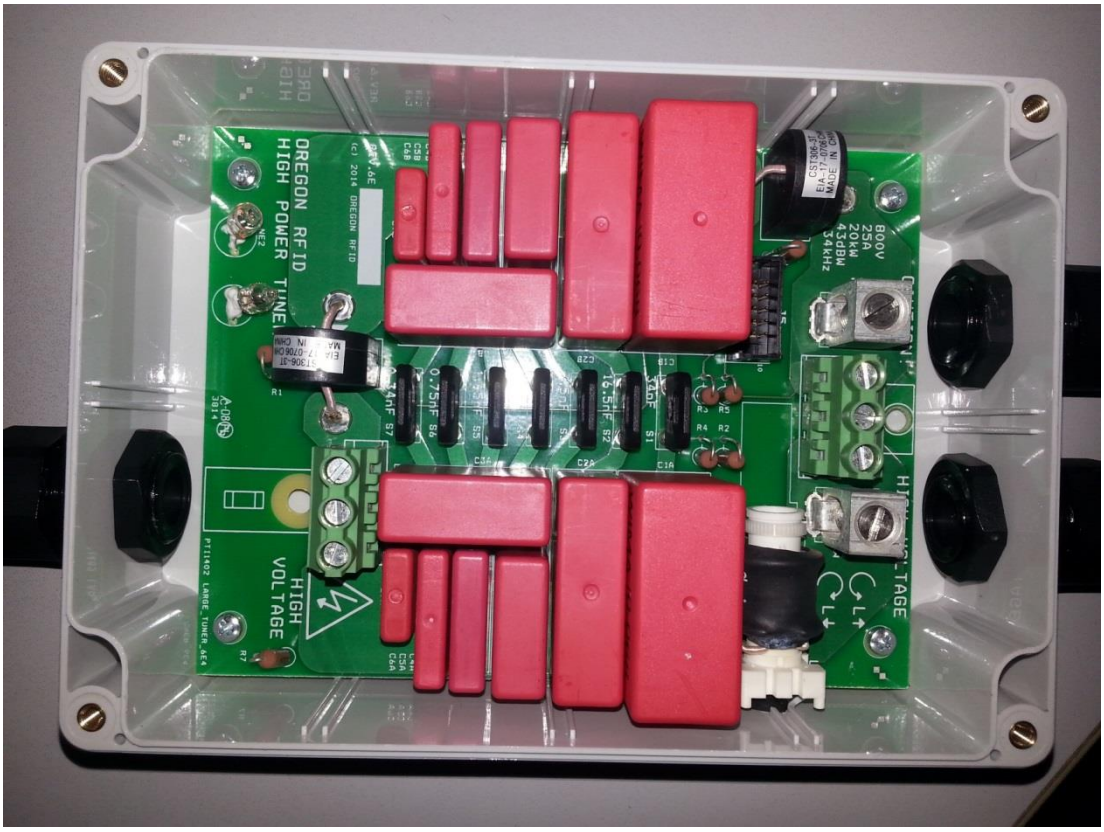


Figure 9: Example of a tuning capacitor (source; AFB).

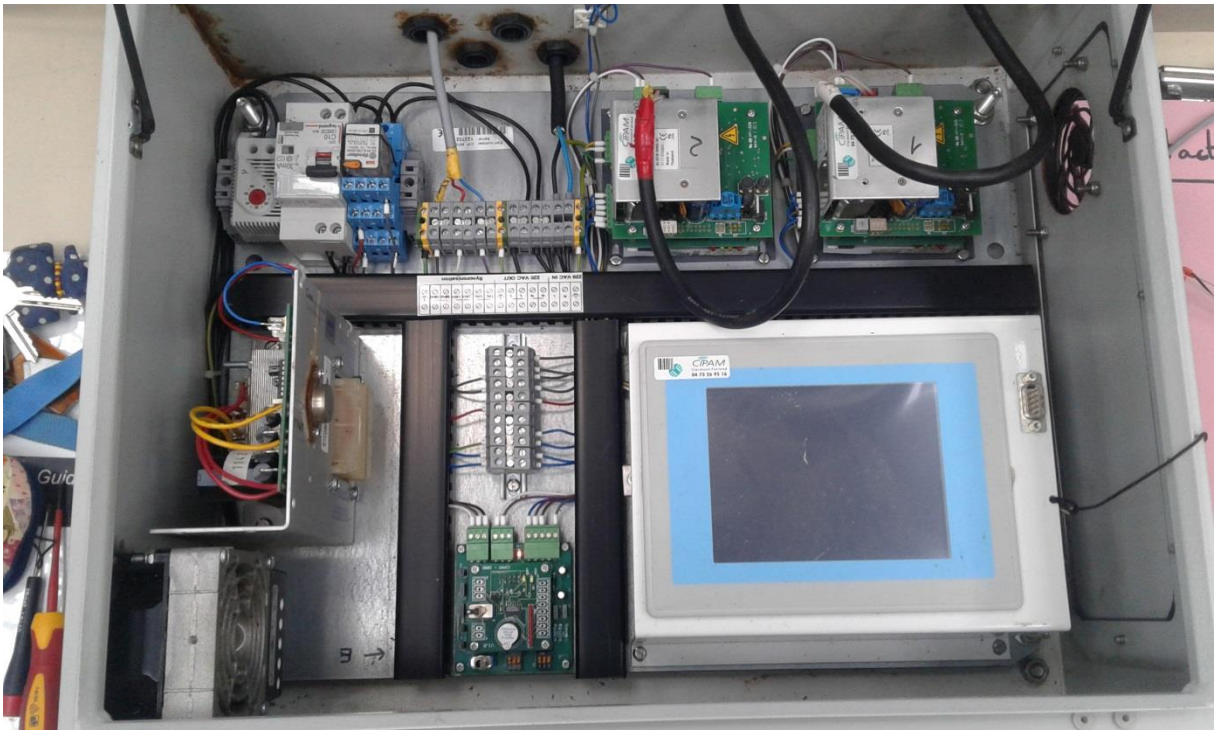


Figure 10: Example of a RFID reader (source: AFB).

The whole system has to be supplied by DC power, powered by different ways:

- Battery;
- Solar;
- Thermoelectric generator;
- Micro hydro (to charge the batteries);
- A power supply can transform the AC power to DC power.

Application:

The RFID technique is used in FIThydro Test Cases in order to follow fishes to study their migration paths, their behaviour and to assess the efficiency of upstream and downstream migration devices and other mitigation measures on habitat.

The PIT tag has to be inserted in the fish by surgical act. For this, the fishes are anaesthetized. The tag is inserted either using a syringe or through a small incision in the abdominal cavity or muscle. Most researchers (Jepsen et al., 2005) adhere to the principle that the weight of the tag should not exceed 2 % of the total weight of the fish.

As for all experiments with living beings, the regulatory obligation must be respected: the personnel must be qualified, the company/organism must be certified and obtain the agreement of an ethics committee. The 3R rule (replace, reduce, refine) must be applied.

This technology allows tagging of very small fishes due to the small size of the tag. It allows following fishes over several years since the tag has no battery and a quasi-endless lifetime. The drawbacks are the size of the antennas and the detection range. Due to the large number of code existing, a large number of fishes can be tagged. It is not sensible to turbidity, or thermal stratification.

One threshold is the effect of metal on the detection ranges of the antennas. Indeed metal is disrupting the signal. For example, it will not be possible to install an antenna in a metal baffle fish pass.

In FIThydro this technology has been used to assess the efficiency of downstream migration devices (Figure 11), fish passes and fish behaviour systems.



Figure 11: Example of antennas in a downstream migration channel in France (source: Tetard et al., 2017).

Other information:

The costs of the technology are acceptable: around 2 € per tag. A reader costs from 2000 to 5000 €.

References:

https://www.oregonrfid.com/

Tomanova, S.; Guillemin, A.; Destouches J.P.; Allou, A., 2017, ***Journée d'échange technique AFB – Utilisation de la RFID***, 13-15 novembre 2017

European committee for standardization, 2018, ***Water quality – Guidance for assessing the efficiency and related metrics of fish passage solutions using telemetry***

Tétard, S.; Tomanova, S.; Courret, D.; Sagnes, P. ; Alric, A. ; De Oliveira, E. ; Lagarrigue, T. ; Frey, A. (2017), ***The efficiency of inclined and oriented racks to prevent Atlantic salmon smolts from entering the turbines, International conference on engineering and ecohydrology for fish passage***

Jepsen N, Schreck C, Clements S, Thorstad E: ***A Brief Discussion on the 2% tag/Bodymass Rule of Thumb.*** *In Aquatic Telemetry: Advances and Applications – Proceedings of the Fifth Conference on Fish Telemetry: 9–13 June 2005; Ustica, Italy. Edited by: Spedicato MT, Lembo G, Marmulla G. Rome: FAO; 2005:255–259.*

Contact information:

Authors	Manon Dewitte (CNRS); Sylvie Tomanova (AFB)
Reviewers	Robert Boes (ETHZ)

2.5 3D Fish Tracking System

Developed by: VAW, ETH Zurich,

Type: Device, Methods

Suitable for 3D fish tracking in etho-hydraulic tests in the laboratory conditions in all phases (planning, implementation)

Introduction:

Laboratory investigations with live-fish, i.e. so-called etho-hydraulic tests, serve to understand interactions between the hydraulics of fish protection technologies and fish behaviour and hence to improve the current design of fish passages or develop new technologies. For laboratory application, VAW of ETH Zurich developed a three dimensional (3D) fish tracking system consisting of synchronous vertically submerged cameras and a MATLAB-based 3D tracking software to determine fish locations in the flow from the recorded videos (Figure 12).

Typically, the behaviour of aquatic fauna is documented by manual protocol written down by biologists and (optional) supplementary video recording. The main drawbacks of both techniques are (i) time consuming, (ii) low time resolution, (iii) low spatial resolution, and (iv) providing only qualitative information. The present 3D fish tracking system overcomes such

drawbacks by automatically and accurately providing 3D swimming tracks on a larger metric space at a milliseconds time resolution.

The software tracks several fish in 3D. Swimming path-time diagrams give a distinct 'big picture' of the fish movement, which helps to identify fish preferred and disliked regions. Furthermore, detailed 3D path analyses of fish interactions and fish velocities are provided as well. The details of the system are documented below. Although the 3D fish tracking system is developed for laboratory use, it may be applied in an adapted version in the field to monitor fish movements or counting, as long as the visual observation is not compromised by turbidity.



Figure 12: 3D fish tracking system installed in the etho-hydraulic flume at VAW of ETH Zurich (source: VAW)

Application:

Within the scope of FIThydro, VAW investigates two types of fish guidance structures (FGS), namely with horizontal (Figure 12) and vertical curved bars. These FGSs are tested with four different fish species under various hydraulic conditions to evaluate their fish guidance efficiencies and to understand fish behaviour. To this end, the 3D fish tracking system is further developed and tested in these etho-hdyraulic (live-fish) investigations. The present system is similar to that currently used by the German Federal Institute for Hydraulic Engineering (BAW) in Karlsruhe together with the German Federal Institute of Hydrology (BfG, 2018; Detert *et al.*, 2018).

The present system consists of up to five cameras arranged in a streamwise series facing vertically upwards through the water surface, each with a distance of 1.5 m (Figure 13). Model acA2000-50gmNIR cameras from *Basler* are used and equipped with a 185° fisheye lens of FE185C086HA-1 (Fujifilm) (Figure 13a). The camera resolution is 3 MPx. Each camera and lens are waterproofed using a housing from *Autovimation* (Figure 13b). A GigE Vision 2.0 network with a Precision Time Protocol (PTP) IEEE1588 provided synchronous measurements with frame rates kept constant at 20 fps (Figure 13c). For larger control volume and longer areas, the actual system including the network switch and the high performance PC can theoretically be equipped with up to 48 cameras. However, the frame rate will be lower then.

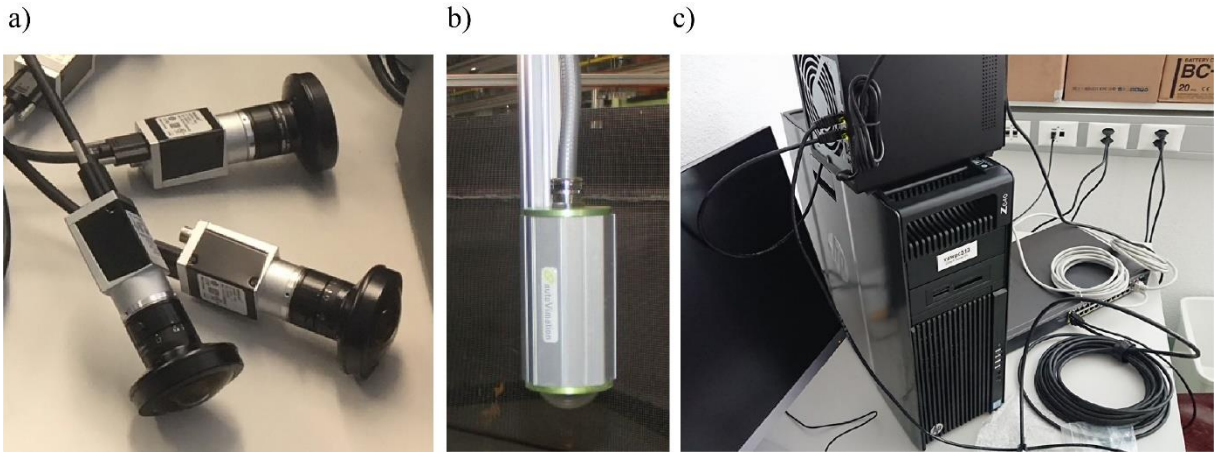


Figure 13. (a) Camera (acA2000-50gmNIR, Basler) with lens (FE185C086HA-1, Fujifilm), (b) waterproof housing for the camera and lens (Autovimation), (c) high performance computer for camera recording and network switch for camera connection (source: VAW).

An adapted software by Fujifilm Switzerland is used to set-up cameras and record videos. The etho-hydraulic flume is illuminated with 7x1000 W halogen lamps (Figure 12, right). Calibration of the system is essential and made in three steps: finding intrinsic and extrinsic parameters for each of the five cameras using a checkboard, calibrating five stereo cameras according to the overlapping views of camera pairs, and finally performing a rigid transformation of all stereo camera pairs to a global flume coordinate system (Figure 14a, Detert et al., 2018).

3D fish tracking is based on the detection of moving fish in each frame and associating the detections corresponding to the same fish over time. These are done by using a background subtraction algorithm and a Karman filter in MATLAB (Detert et al., 2018). The primary results of motion-based tracking are tracks in a distorted and uncalibrated 2D image frame coordinate system for each camera. Figure 14a and c show the three detected fish and noises caused by reflections from the glass window and their 2D tracks over time. After undistorting such frames and stereo calibrating the cameras, the 2D fish tracks are transferred to a 3D metric-space according to their epipolar geometry based on the camera parameters derived from the calibration (Figure 15).

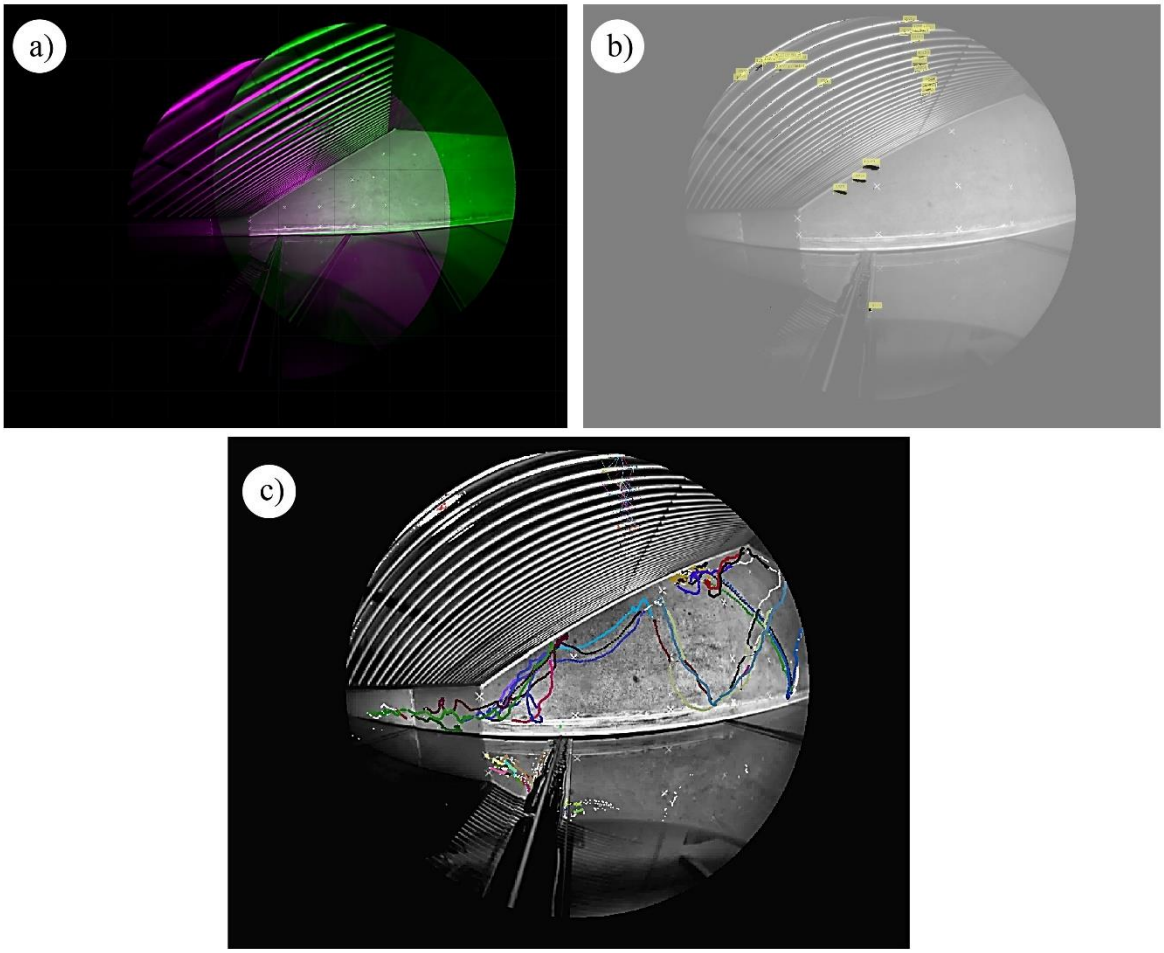


Figure 14: (a) Stereo view of a camera pair, (b) three detected fish and noise, (c) 2D tracks of three fish (source: VAW).

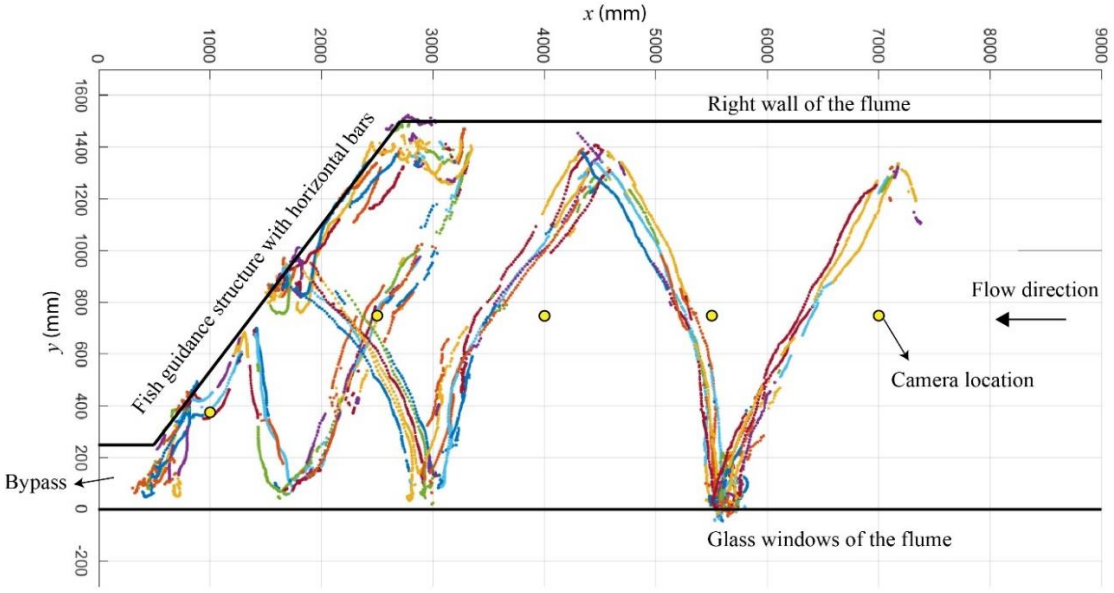


Figure 15: Top view of 3D tracks of three fish from an etho-hydraulic test of fish guidance structure with horizontal bars (source: VAW).

Back to D2.2 Main index

The etho-hydraulic tests were done for a flow depth of 90 cm, flume width of 150 cm, distance of 150 cm between the cameras and average flow velocities up to 0.7 m/s. Under such conditions, the 3D fish tracking system provided fish positions in 3D with an accuracy of about ±5 cm and 20 fps. The challenges for a successful implementation of the system are: assignment of individual fish to the tracks, constant illumination of the flow, camera distortion, air bubbles and suspended sediment and humid conditions for the cameras.

Overall, despite some shortcomings such as noise due to reflections from the glass windows, the 3D fish tracking system works well, provides important information on fish behaviour affected by fish guidance structures and has the potential for further etho-hydraulic studies.

Other information:

The total costs of the present system is approx. 40'000 USD=35'000 € including camera set-up and recoding software. For current costs of the equipment, we recommend to ask the corresponding supplier listed below. Note that a cheaper camera and lens set-up can significantly reduce the total cost of the system. The MATLAB-based 3D tracking code developed by VAW will be freely available.

References:

BfG (German Federal Institute of Hydrology), 2018. The behaviour of fish in fishways – BfG and BAW's ethohydraulic tests. Annual report of 2016/2017, pp.43. https://doi.org/10.5675/bfg-jahresbericht_2016/2017.

Detert, M., Schütz, C., Czerny, R. (2018). Development and test of a 3D fish-tracking videometry system for an experimenal flume. *In Proc. River Flow 2018 - Ninth International Conference on Fluvial Hydraulics*, E3S Web of Conferences 40: 03018. https://doi.org/10.1051/e3sconf/20184003018

Links to the suppliers of equipment:

Basler Camera:

https://www.baslerweb.com/en/products/cameras/area-scan-cameras/ace/aca2000-50gmnir/

Fujifilm lens:

http://www.fujifilm.com/products/optical_devices/pdf/cctv/fa/fisheye/fe185c086ha-1.pdf

Camera waterproof enclosure:

https://www.autovimation.com/index.php/en/selection-guide-enclosures

Software for 3D fish tracking:

It will be available on request.

Contact information:

Authors	Ismail Albayrak (VAW, ETHZ), Martin Detert (ETHZ)
Reviewers	Robert Boes (ETHZ)

2.6 3D Sensorless, ultrasound fish tracking

Developed by: Chair of Hydraulic and Water Resources Engineering, Chair of Non-Destructive Testing, TU Munich

Type: Device

Suitable for sensorless 3D tracking and adaptive fish migration management

Introduction:

The device (Figure 16) works without tagging fish and is similar to 3D tomographic imaging. It detects fish in rivers with high spatial and temporal resolution over a distance of a couple of hundred meters. Ultra-sonic transducers (receivers and emitters) are positioned in the water. When one transducer emits the others receive the signal. Emitting and receiving cycles around the devices with high frequency. As the resolution is in the range of only a few centimetres it is expected to measure the length of fish and even the species by the shape of the fish bladder.

Application:

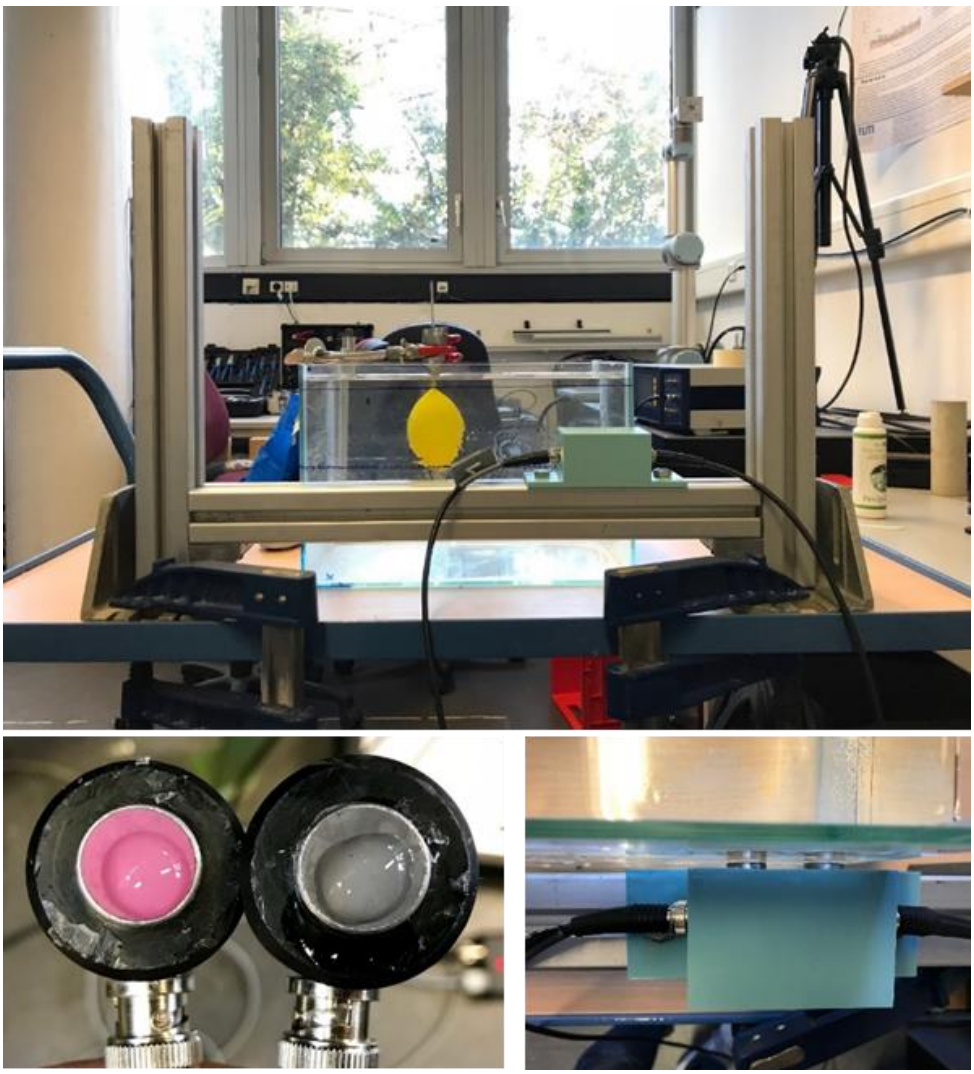


Figure 16: Experimental setup for testing and development of the 3D sensorless ultrasound fish tracking.

The device can be used to detect sensorless fish in 3D. This cannot only be used to track fish in 3D but also to adapt operation of a hydropower plant to the needs of migrating fish. During the FIThydro project the TRL level needs to be raised from TRL4 to TRL5. So far, only first results are available and they show good potential. However, there is still a long way to go for a first prototype application in real rivers.

Other information:

European patent applied (application 15 188 223.0-1020)

Contact information:

Authors	Peter Rutschmann (TUM)
Reviewers	Robert Boes (ETHZ)

2.7 Cassiopée, 1993-2011

French agency for biodiversity (AFB)

Type: Tool (model)

Calculation tool to help sizing upstream migration fish passes (during planning)

Introduction:

Cassiopée is a computing software for fish pass designers. It allows studying pool-type fishways, baffle fishways and pre-barrage (for futher information on the different type of fishways please see first deliverable of WP2 D2.1).

It has been developed by Myriad Software Ltd in 1993, under the scientific direction of Michel Larinier and Jean-Pierre Porcher. It runs on Windows systems and two updates were held in 1996 and 2011.

It only addresses users familiar with designing fish passes. In the process of designing a fish pass, the function of Cassiopée is to compute variables characterizing its operating and to present clear and explicit results.

Application:

Cassiopée allows to determine flow and water level for sizing or verifying correct operation for:

- pool-type fishways (with plunging or streaming flow notches, submerged orifices, single or double vertical slots);
- baffle fishways (with Denil type, Fatou type, super-active type or chevron type baffles);
- pre-barrages (with rectangular weir, triangular weir or semi-triangular weir).

For pool-type fishways, three computing tools allow to determine the geometry of the basins, given the target flow and drop between pools, water levels in the pools and volumetric dissipated power criteria set by the designer. A fourth tool allows to compute the size (width and depth) and to altitudinally set the first wall and first basin, given the upstream water level and flow, drop between pools, water levels in the pools and volumetric dissipated power criteria (altimeter setting of other walls and basins is obtained by substraction from the first wall and basin the drop between pools).

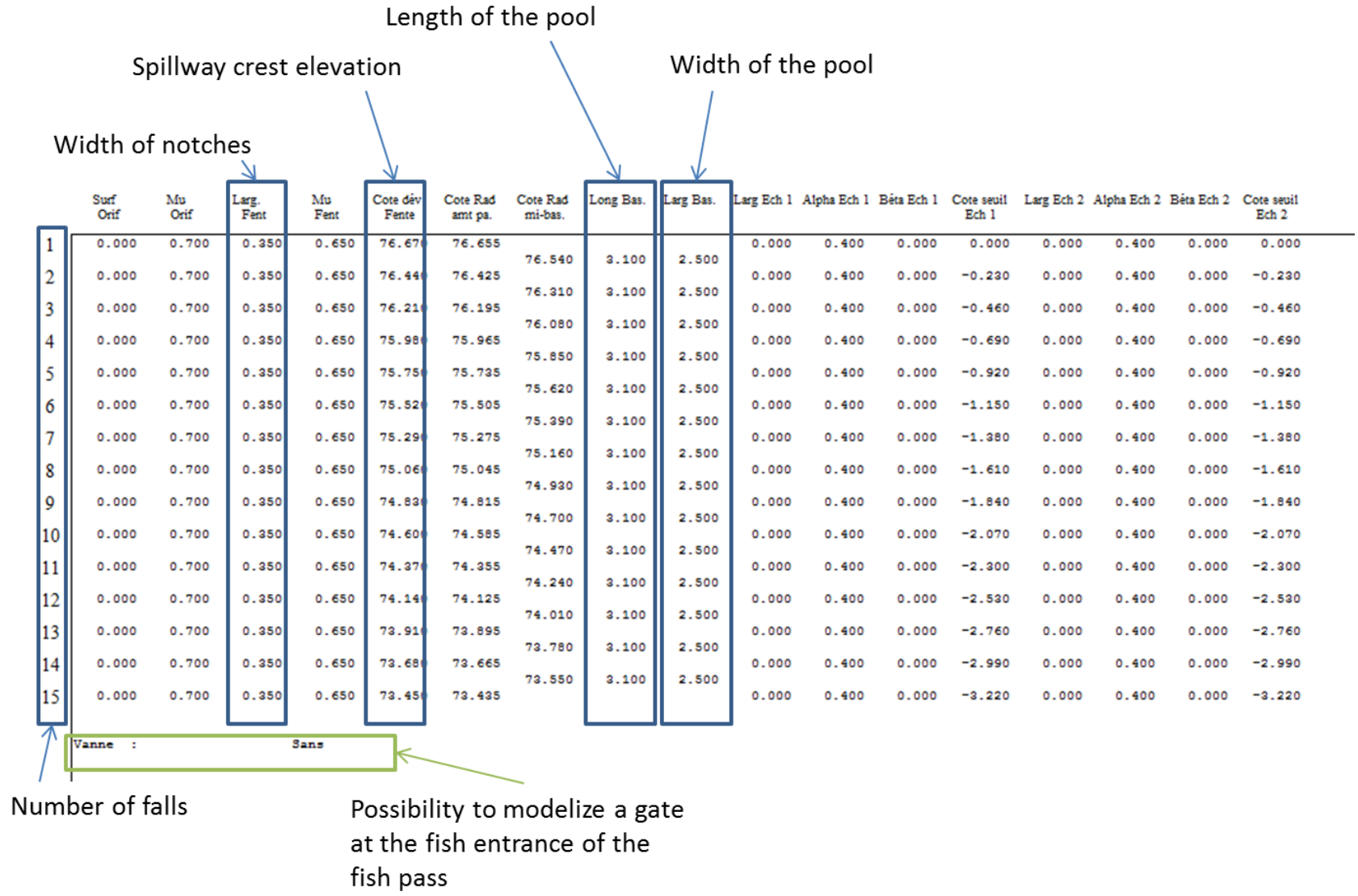
For pre-barrage, it is possible to associate different types of weir (for example, two rectangular weirs with two levels of crest and a semi-triangular weir). The geometry of pre-barrages can be complex and it is possible to provide flows between basins from upstream to downstream but also between the upstream and any basin.

For baffle fishways, after setting the geometry, the software allows to determine level-discharge and flow velocity-discharge relationships. It also allows to compute the number of baffles and the elevations of the first and last baffle and corresponding bottom, from upstream and downstream water levels.

Cassiopée also has 3 computing tools:

- KIVI: tool to simulate the working conditions of a thin weir (Kindsvater and Cater formula) for submerged flow or not (Villemonte coefficient);

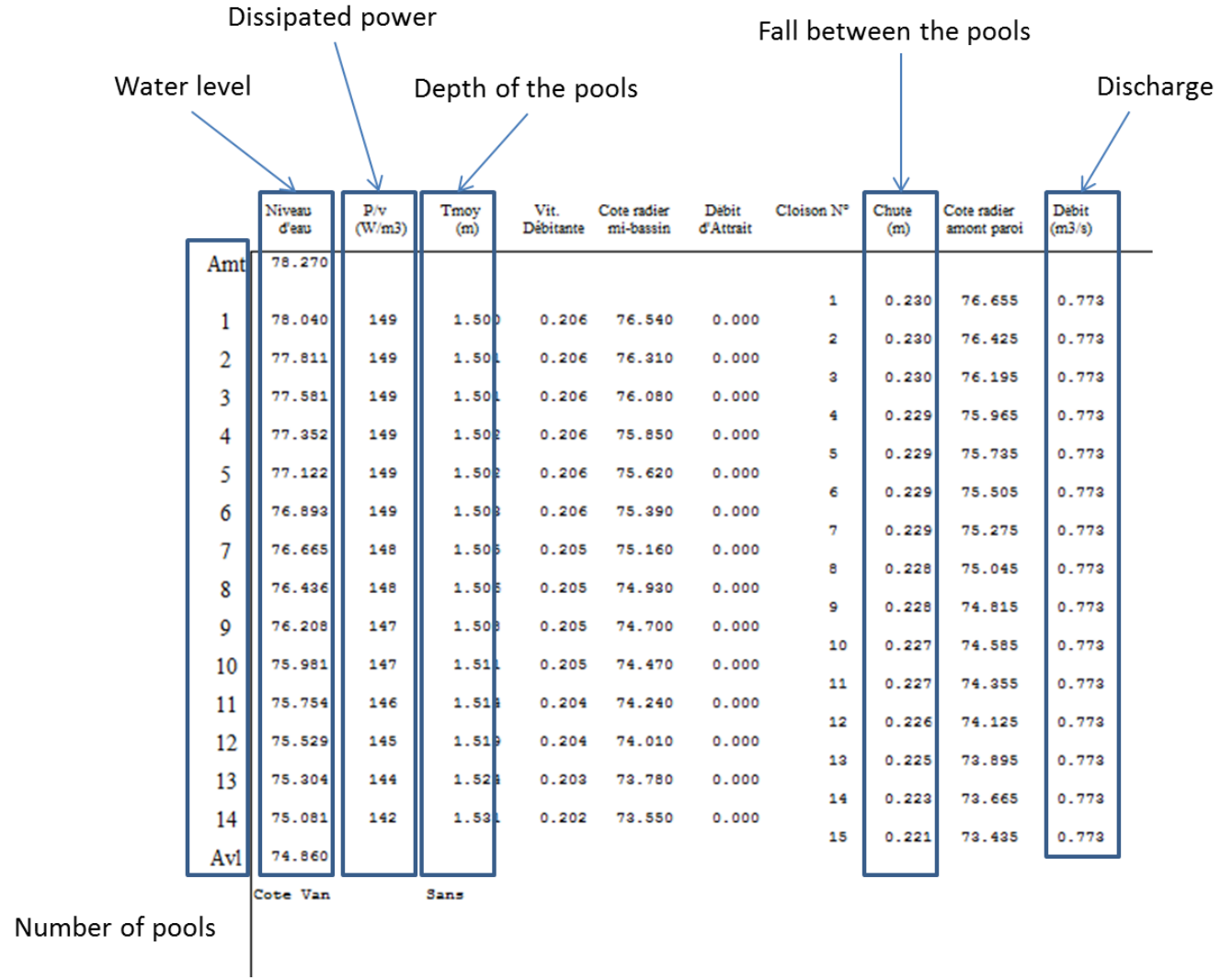
- MOODY: tool to compute the discharge or the head loss of a flow in full pipes;
- DEVER: a tool to compute the relationship between upstream water level and discharge transiting at a weir (simple or composed of different spillways with different characteristics).
- Examples of the software application are given in Figure 17 to Figure 20.



	Surf Orif	Mu Orif	Larg. Fent	Mu Fent	Cote dév Fente	Cote Rad amt pa.	Cote Rad mi-bas.	Long Bas.	Larg Bas.	Larg Ech 1	Alpha Ech 1	Béta Ech 1	Cote seuil Ech 1	Larg Ech 2	Alpha Ech 2	Béta Ech 2	Cote seuil Ech 2
1	0.000	0.700	0.350	0.650	76.670	76.655				0.000	0.400	0.000	0.000	0.000	0.400	0.000	0.000
							76.540	3.100	2.500								
2	0.000	0.700	0.350	0.650	76.440	76.425				0.000	0.400	0.000	-0.230	0.000	0.400	0.000	-0.230
							76.310	3.100	2.500								
3	0.000	0.700	0.350	0.650	76.210	76.195				0.000	0.400	0.000	-0.460	0.000	0.400	0.000	-0.460
							76.080	3.100	2.500								
4	0.000	0.700	0.350	0.650	75.980	75.965				0.000	0.400	0.000	-0.690	0.000	0.400	0.000	-0.690
							75.850	3.100	2.500								
5	0.000	0.700	0.350	0.650	75.750	75.735				0.000	0.400	0.000	-0.920	0.000	0.400	0.000	-0.920
							75.620	3.100	2.500								
6	0.000	0.700	0.350	0.650	75.520	75.505				0.000	0.400	0.000	-1.150	0.000	0.400	0.000	-1.150
							75.390	3.100	2.500								
7	0.000	0.700	0.350	0.650	75.290	75.275				0.000	0.400	0.000	-1.380	0.000	0.400	0.000	-1.380
							75.160	3.100	2.500								
8	0.000	0.700	0.350	0.650	75.060	75.045				0.000	0.400	0.000	-1.610	0.000	0.400	0.000	-1.610
							74.930	3.100	2.500								
9	0.000	0.700	0.350	0.650	74.830	74.815				0.000	0.400	0.000	-1.840	0.000	0.400	0.000	-1.840
							74.700	3.100	2.500								
10	0.000	0.700	0.350	0.650	74.600	74.585				0.000	0.400	0.000	-2.070	0.000	0.400	0.000	-2.070
							74.470	3.100	2.500								
11	0.000	0.700	0.350	0.650	74.370	74.355				0.000	0.400	0.000	-2.300	0.000	0.400	0.000	-2.300
							74.240	3.100	2.500								
12	0.000	0.700	0.350	0.650	74.140	74.125				0.000	0.400	0.000	-2.530	0.000	0.400	0.000	-2.530
							74.010	3.100	2.500								
13	0.000	0.700	0.350	0.650	73.910	73.895				0.000	0.400	0.000	-2.760	0.000	0.400	0.000	-2.760
							73.780	3.100	2.500								
14	0.000	0.700	0.350	0.650	73.680	73.665				0.000	0.400	0.000	-2.990	0.000	0.400	0.000	-2.990
							73.550	3.100	2.500								
15	0.000	0.700	0.350	0.650	73.450	73.435				0.000	0.400	0.000	-3.220	0.000	0.400	0.000	-3.220

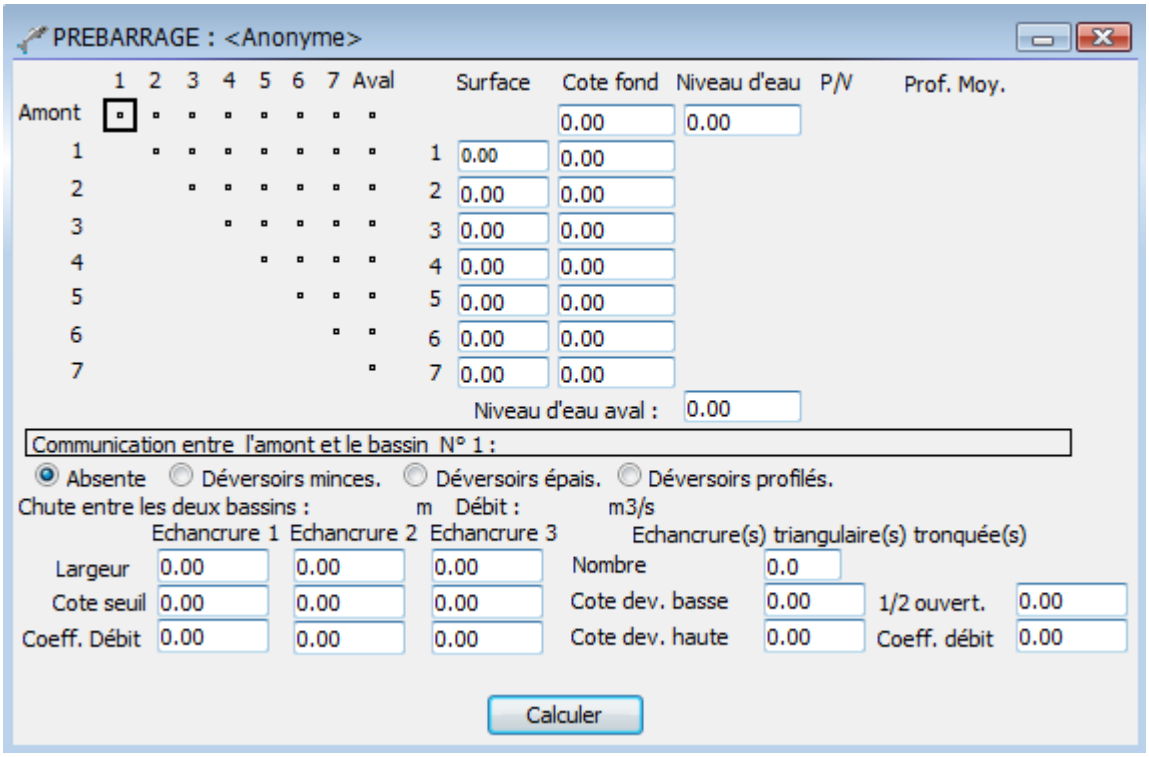
Vanne : Sans

Figure 17: Example of designing a pool-type fishway.



	Niveau d'eau	P/v (W/m3)	Tmoy (m)	Vit. Débitante	Cote radier mi-bassin	Débit d'Attrait	Cloison N°	Chute (m)	Cote radier amont paroi	Débit (m3/s)
Amt	78.270									
							1	0.230	76.655	0.773
1	78.040	149	1.500	0.206	76.540	0.000				
							2	0.230	76.425	0.773
2	77.811	149	1.501	0.206	76.310	0.000				
							3	0.230	76.195	0.773
3	77.581	149	1.501	0.206	76.080	0.000				
							4	0.229	75.965	0.773
4	77.352	149	1.502	0.206	75.850	0.000				
							5	0.229	75.735	0.773
5	77.122	149	1.502	0.206	75.620	0.000				
							6	0.229	75.505	0.773
6	76.893	149	1.503	0.206	75.390	0.000				
							7	0.229	75.275	0.773
7	76.665	148	1.505	0.205	75.160	0.000				
							8	0.228	75.045	0.773
8	76.436	148	1.505	0.205	74.930	0.000				
							9	0.228	74.815	0.773
9	76.208	147	1.508	0.205	74.700	0.000				
							10	0.227	74.585	0.773
10	75.981	147	1.511	0.205	74.470	0.000				
							11	0.227	74.355	0.773
11	75.754	146	1.514	0.204	74.240	0.000				
							12	0.226	74.125	0.773
12	75.529	145	1.519	0.204	74.010	0.000				
							13	0.225	73.895	0.773
13	75.304	144	1.523	0.203	73.780	0.000				
							14	0.223	73.665	0.773
14	75.081	142	1.531	0.202	73.550	0.000				
							15	0.221	73.435	0.773
Avl	74.860									

Figure 18: Example of computing water levels.



- *Figure 19: Example of the tool to design a pre-barrage.*

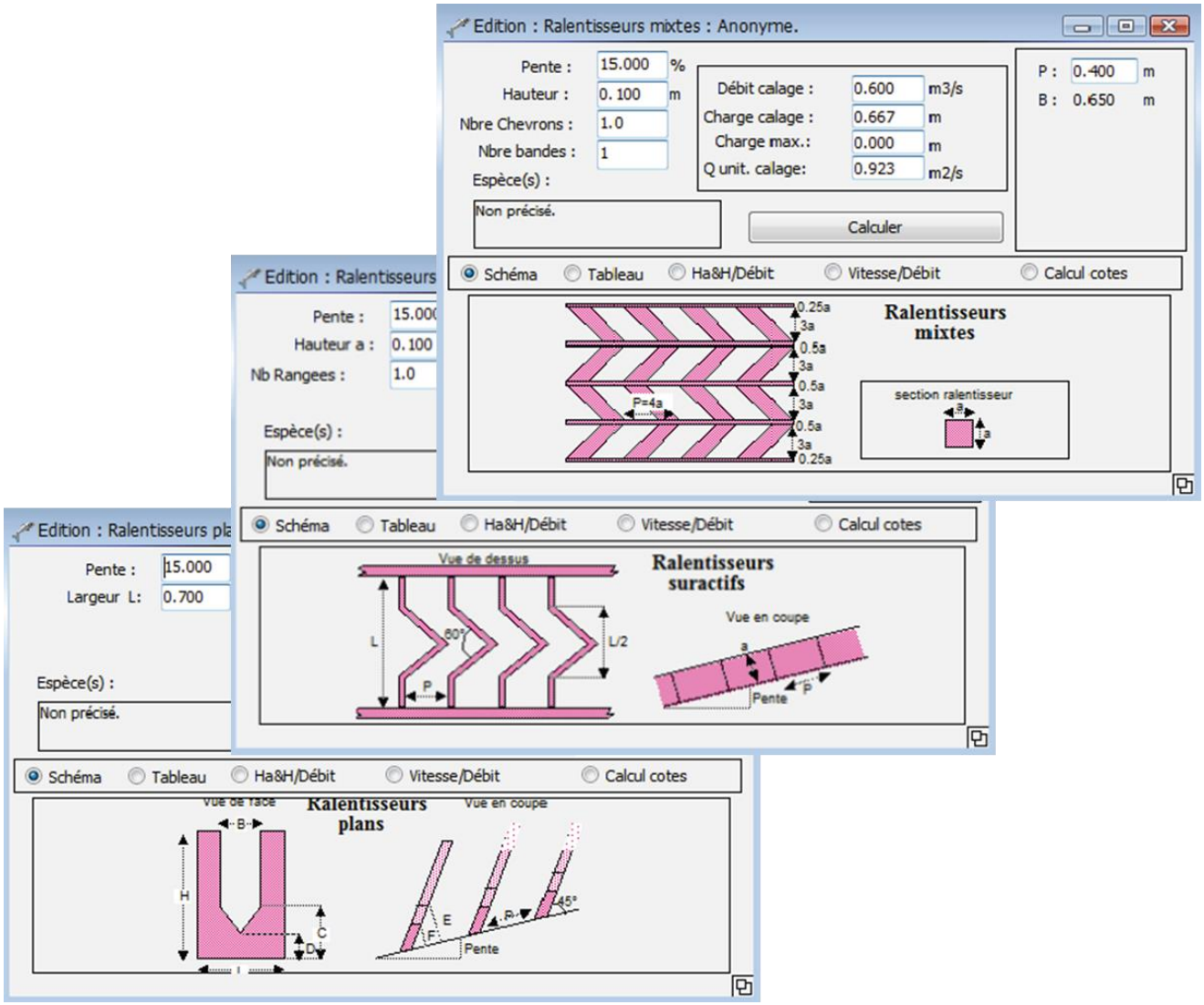


Figure 20: Tool to design a baffle fishway in Cassiopée.

In FIThydro, we used Cassiopée to assess the downstream migration discharges in the downstream migration channels at several French Test Cases (Figure 21).

Based on a topographical survey at the Test Case, the topographic data are entered in the DEVER tool in order to assess the global discharge since it is controlled by a weir. It also allows to refine the discharge coefficient of the control weir and to correct the discharge taking into account the approach velocities of the flow upstream of the weir.

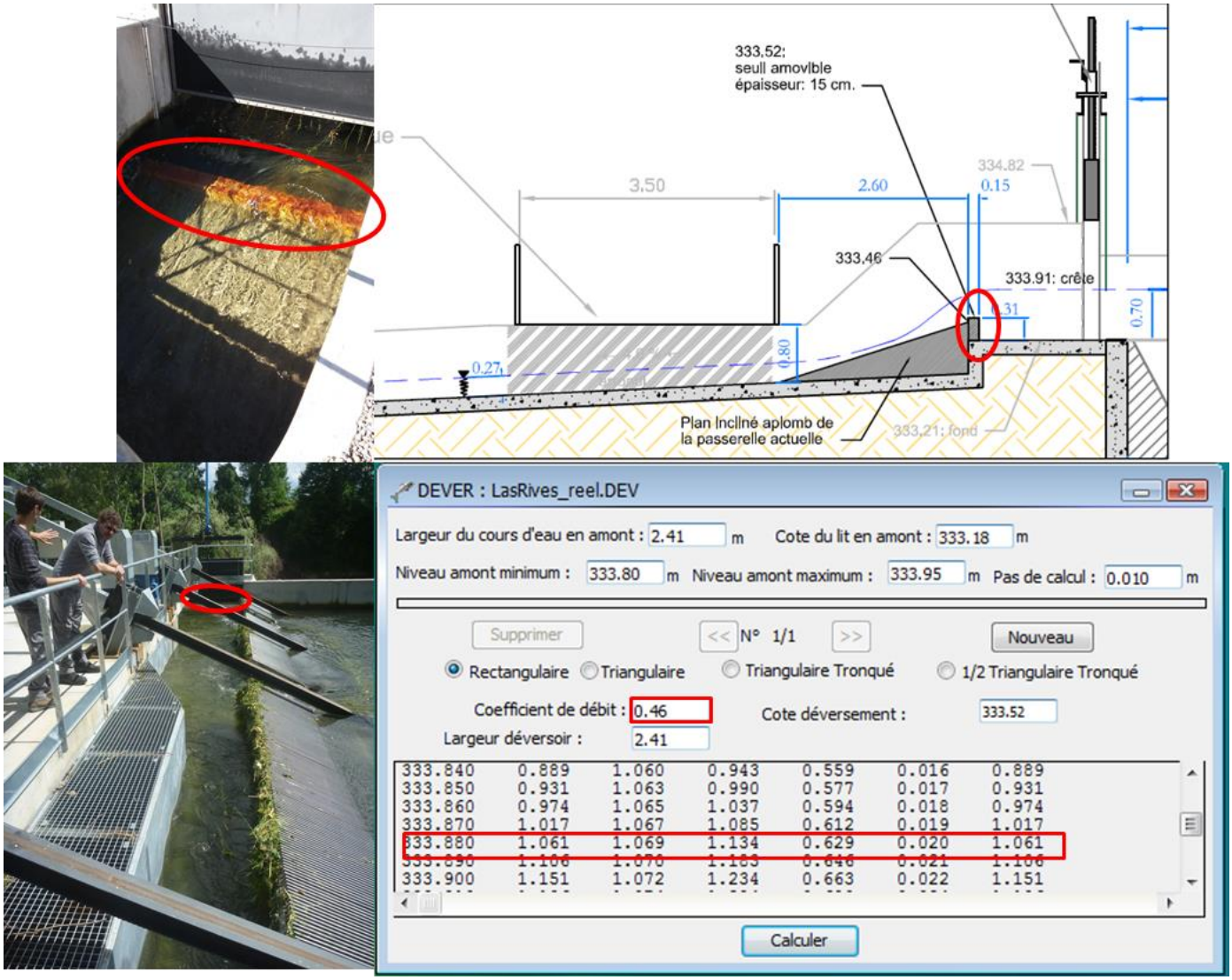


Figure 21: Example of use of Cassiopée in FIThydro at Las Rives, France.

Other information:

This software is free but not openly accessible. It is distributed after training on fishway design provided by AFB.

References:

Michel Larinier et Jean-Pierre Porcher, 1996, Cassiopée – Logiciel d'aide au calcul pour le concepteur de passes à poissons – Notice d'utilisation, Conseil Supérieur de la Pêche 1993

Sylvain Richard, 2018, Cassiopée – Logiciel d'aide au calcul pour le concepteur de passe à poisson, Formation continue AFB, Dispositifs de franchissement piscicole, Toulouse 11-15 juin 2018

Contact information :

Authors	Manon Dewitte (CNRS), Sylvain Richard (AFB)
Reviewers	Robert Boes (ETHZ)

2.8 BASEMENT

Developed by: Laboratory of hydraulics, hydrology and glaciology (VAW) of ETH Zurich

Date: May 2018 (Version 2.8)

Type: tool, freeware

Suitable for river hydro- and morphodynamics in all phases (planning, implementation, maintenance)

Introduction:

BASEMENT (BAsic Simulation EnvironMENT) is a numerical software for the simulation of hydro- and morphodynamics in rivers. The main motivation for the development of the software is to provide a powerful user-friendly tool that facilitates basic applications for practitioners as well as advanced model configurations for research. The underlying one- and two-dimensional models are based on the Saint-Venant equations for the hydrodynamics, the Exner-Hirano equations for bed load transport and an advection-diffusion approach with source terms for suspended sediment transport. Mentionable special features of the software are arbitrary combinations of 1D and 2D model domains (Figure 22), a PID controller for various monitoring values and the use of an unstructured dual-mesh to improve topographic accuracy.

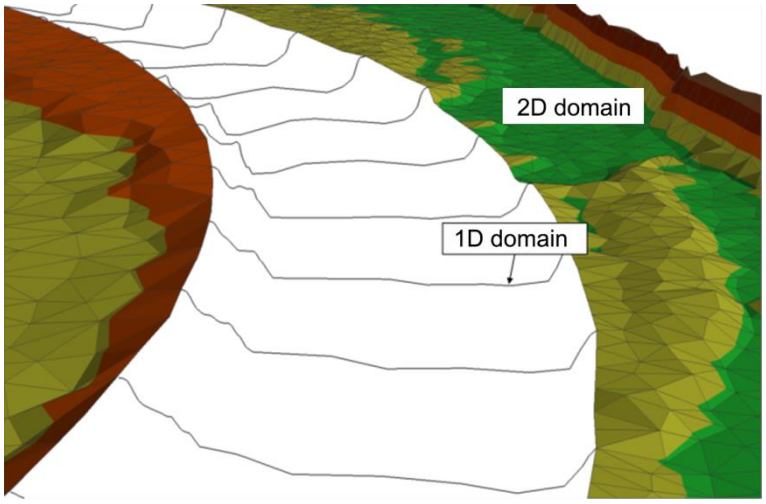


Figure 22: Combination of 1D and 2D models in BASEMENT (source: VAW)

Application:

The 1D model of BASEMENT is based on river cross sections and its main application are river reaches where the level of detail is less important. The 2D model uses a triangular computational grid to reproduce the topography and can be applied to more detailed and complex problems than the 1D model, e.g. the inundation or river bar formation. BASEMENT supports Windows as well as Linux platforms and includes a graphical user interface (GUI) which supports the user during the model setup and simulation process (Figure 23). For grid generation, the QGIS plugin BASEmesh is provided by the developers and for visualization of the results, among others, the QGIS plugin Crayfish (QGIS 2.8) from Lutra Consulting (https://www.lutraconsulting.co.uk) can be used (Figure 24).

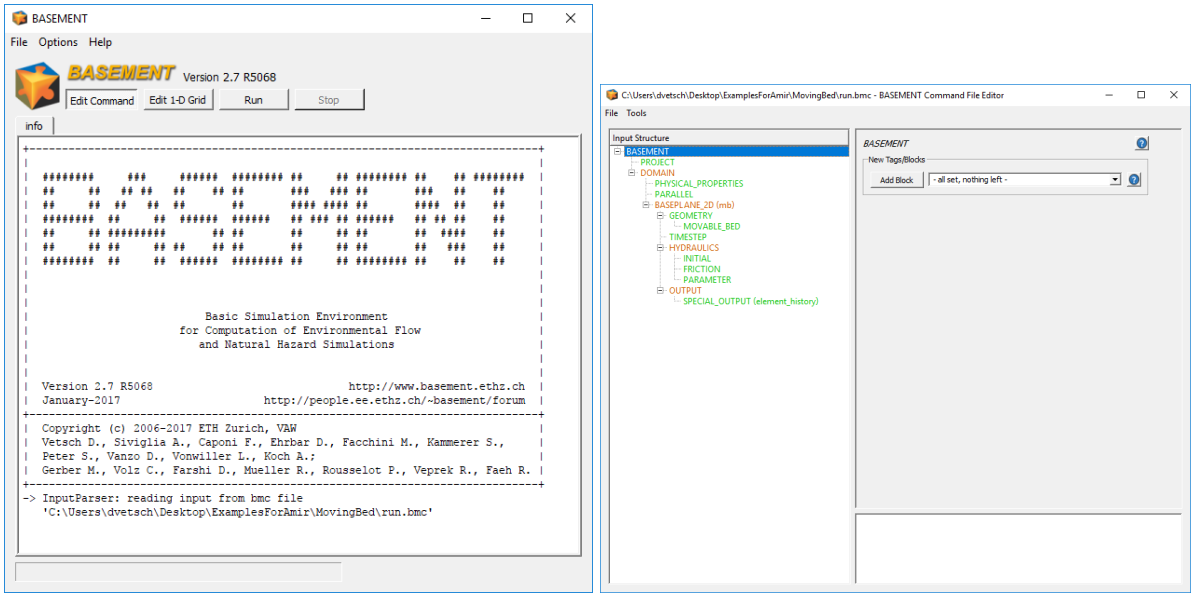


Figure 23: Graphical user interface of BASEMENT (credits: VAW).

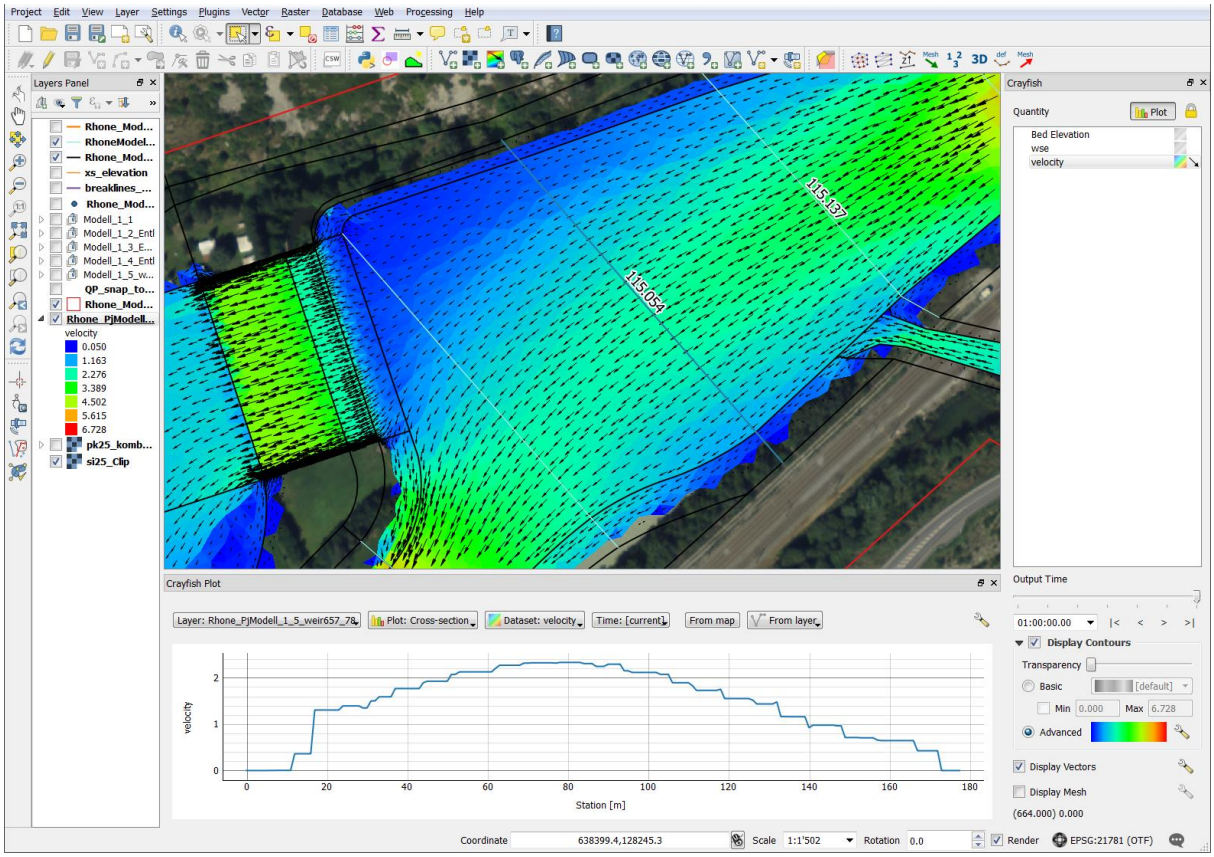


Figure 24: Visualization of BASEMENT results with QGIS plugin Crayfish (credits: VAW).

Other information:

In addition to the use on regular Windows and Linux workstations, the upcoming version 3.0 of BASEMENT (March 2019) is designed to run on graphical processing units (GPUs) and distributed memory computer clusters allowing engineers to tackle problems with very large computational domains or long simulation time.

References:

Vetsch D., Siviglia A., Caponi F., Ehrbar D., Gerke E., Kammerer S., Koch A., Peter S., Vanzo D., Vonwiller L., Facchini M., Gerber M., Volz C., Farshi D., Mueller R., Rousselot P., Veprek R., Faeh R. 2018. System Manuals of BASEMENT, Version 2.8. Laboratory of Hydraulics, Glaciology and Hydrology (VAW). ETH Zurich. Available from http://www.basement.ethz.ch.

Contact information:

Website (download, tutorials, etc.): www.basement.ethz.ch

Email: basement@ethz.ch

Authors	David Vetsch
Reviewers	Robert Boes (ETHZ)

2.9 River 2D

Developed by: collaboratively between the Freshwater Institute in Winnipeg, the Civil and Environmental Department of the University of Alberta in Edmonton, the Midcontinent Ecological Science Center of the U.S. Geological Survey in Ft. Collins, and the Fisheries Division of the Alberta Government in Cochrane.

Date: 2002

Type: Computer model

Suitable for Environmental flow (hydropeaking) mitigation measure in all phases (planning, implementation, maintenance)

Introduction:

The River 2D is a two dimensional depth-averaged finite element hydrodynamic model that has been customized for fish habitat evaluation studies (Steffler, 2000). The River2D model simulates hydraulic conditions in natural rivers from topographic data input, and uses the habitat suitability curves containing known biological preference data, to calculate the potential habitat for specific species life-history stages by obtaining the Weighted Usable Area (WUA).

The model suite consists of four programs: R2D_Bed, R2D_Ice, R2D_Mesh and River2D (Figure 25). R2D_Bed was designed for editing bed topography data while R2D_Ice is intended for developing ice topographies to be used in the modelling of ice-covered domains. The R2D_Mesh program is used for the development of computational meshes that will ultimately be input for River2D. The latter is then used to solve for the water depths and velocities using the 2D shallow water equations throughout the discretized domain. The habitat model to calculate the WUA is incorporated in the River2D program.

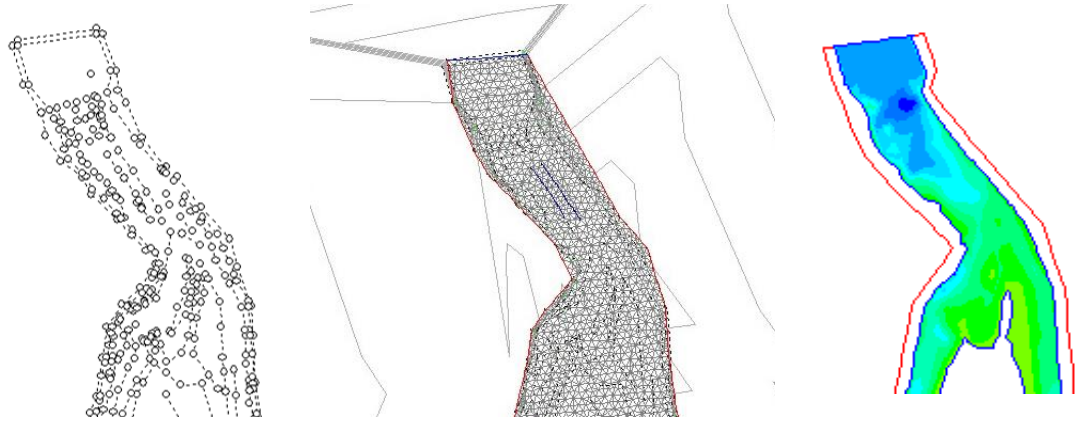


Figure 25: River 2D layout images: (a) R2D_Bed; (b) R2D_Mesh; and (c) River2D.

Application:

The River2D can be used to calculate the water depths and velocities for any point in the river reach. The final goal is to calculate the WUA for a given fish species and life-stages by using Habitat Suitability Curves.

As input data, the model requires channel bed topography, roughness and transverse eddy viscosity distributions, boundary conditions, and initial flow conditions. Boundary conditions usually take the form of a specified total discharge at inflow sections and fixed water surface elevations at outflow sections. Locating flow boundaries some distance away from areas of interest is important to reduce the effect of boundary conditions uncertainties. The 2D finite element model works with a triangular irregular mesh.

Topography forms the template of the modelling mesh which is draped over the boundary surface and which forms the basis for the numerical solution to the governing flow equations. The challenge of building a mesh is to distribute the nodes in such a way that the most accurate solution is obtained for a particular purpose. Closely spaced nodes in areas of high interest, gradual changes in node spacing, and regularity of elements are important considerations.

Outputs from the model are two (horizontal) velocity components and a depth at each point or node (Figure 26 and Figure 27). Velocity distributions in the vertical are assumed to be uniform and pressure distributions are assumed to be hydrostatic.

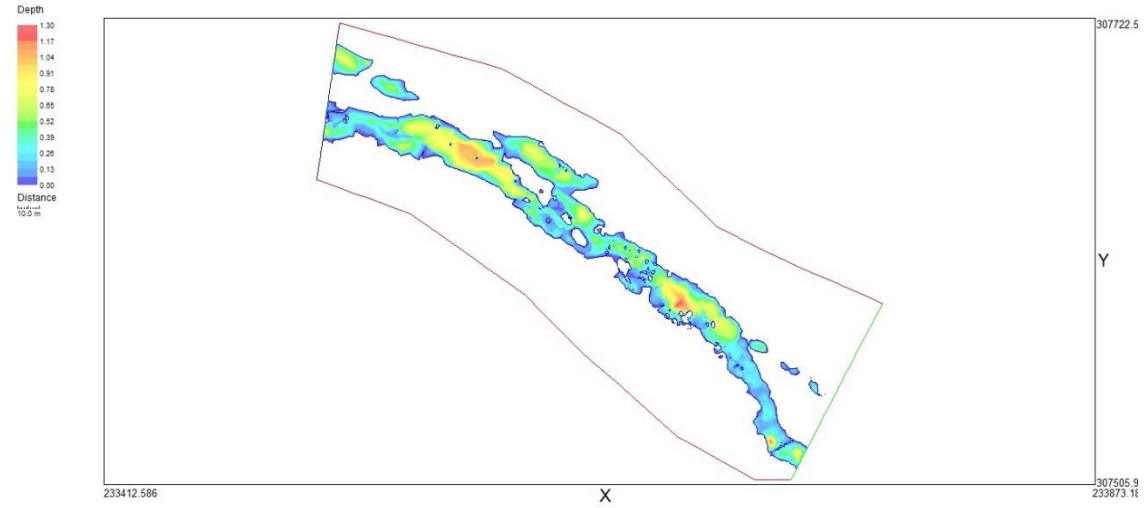


Figure 26: Water depth (m) output from River 2D. Ocreza River, Portugal.

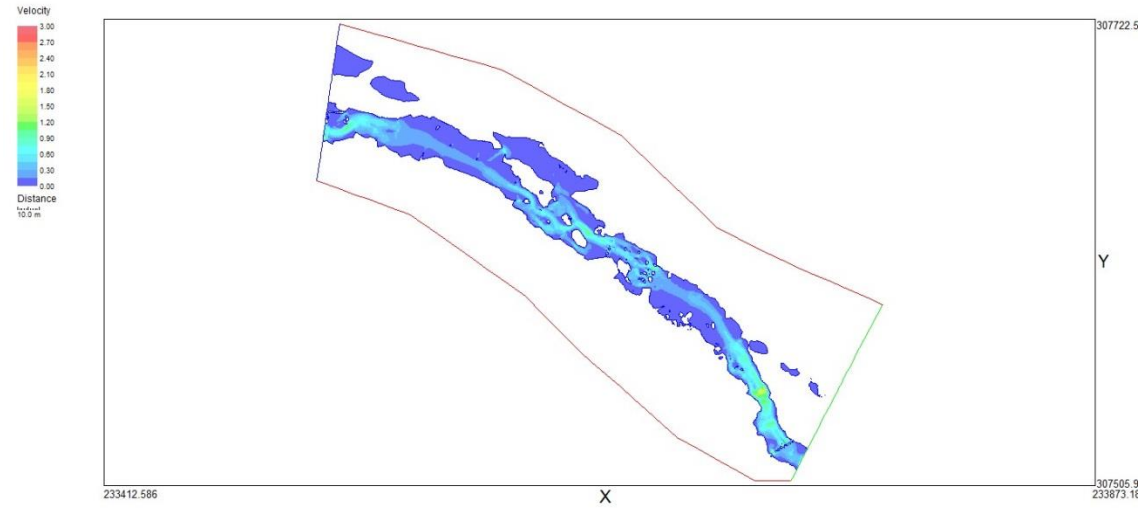


Figure 27: Water velocity (m/s) output from River 2D. Ocreza River, Portugal.

The fish habitat component of River2D is based on the Weighted Usable Area (WUA) (Bovee et al., 1998) concept used in the PHABSIM family of fish habitat models. The WUA is calculated as an aggregate of the product of a Composite Suitability Index (CSI, range 0.0 - 1.0) evaluated at every node in the domain and the "tributary area" associated with that node in the finite element mesh. The Suitability Index (SI) for each parameter is evaluated by linear interpolation from an appropriate Habitat Suitability Curves (HSC) to be supplied separately. Velocities and depths are taken directly from the hydrodynamic component of the model. The channel index values may depend on channel substrate or cover for different fish species and life stages. These values are interpolated from a separate channel index file to the computational nodes. The interpolation may be linear (continuous) or nearest neighbour (discrete). At the last stage, the River 2D computes the WUA (Figure 28) as the product, harmonic mean, or minimum value.

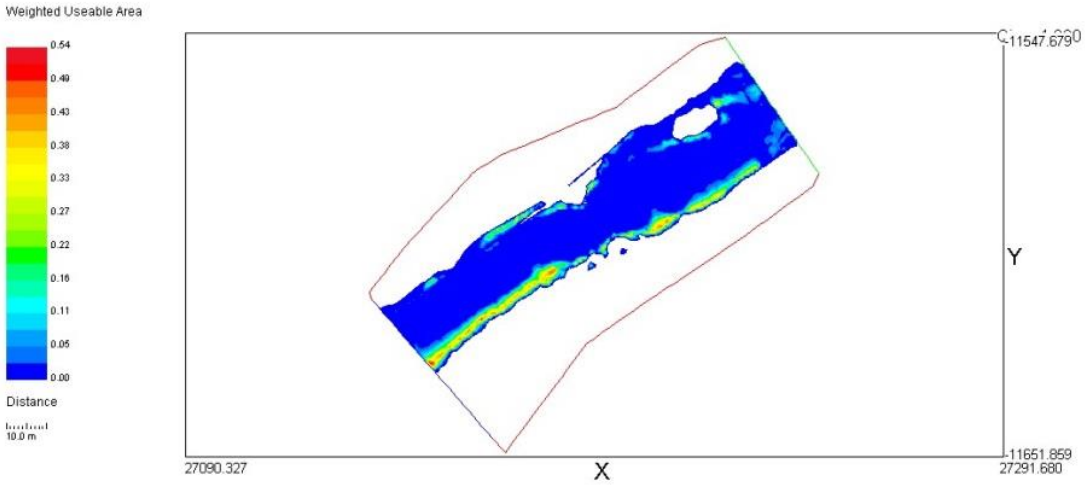


Figure 28: WUA (m2) for the European Eel. Ocreza River, Portugal.

For habitat studies, the assumption is that the habitat is optimal when it reaches a maximum value of WUA (Figure 29).

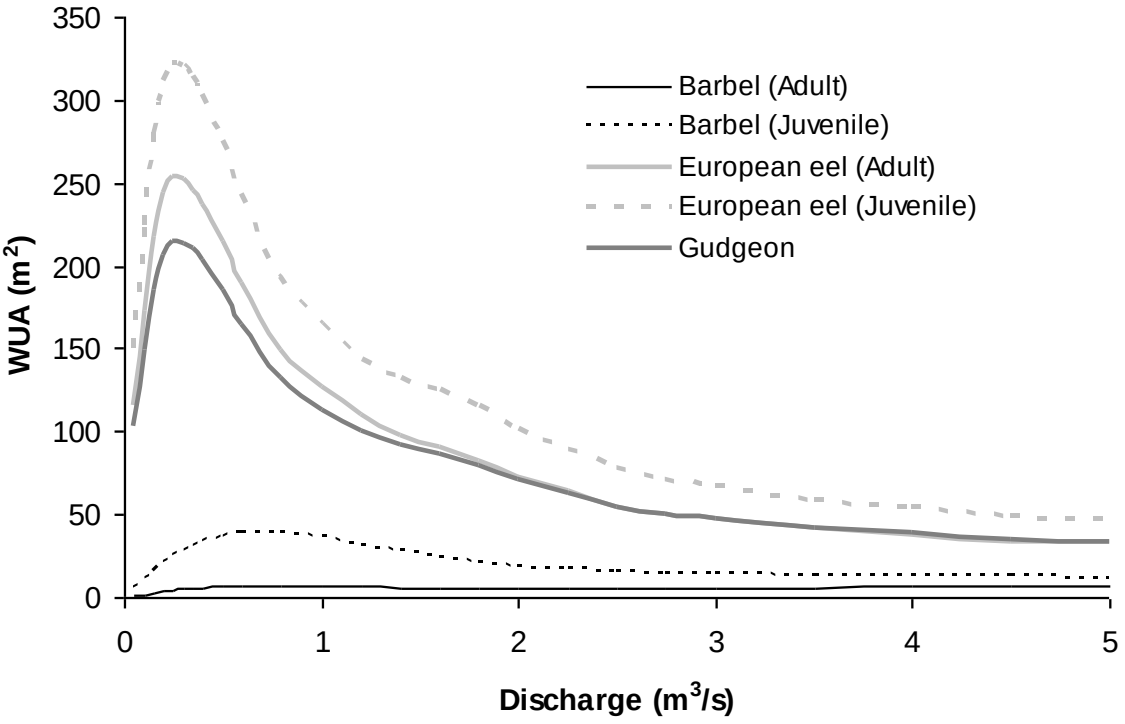


Figure 29: WUA (m2) and discharge in the Ocreza River for Iberian barbel (adult and juvenile), European eel (adult and juvenile) and Gudgeon.

The River 2D has been widely used to access the environmental flows (Rivaes et al., 2017), to study fish movements due to hydropeaking (Boavida et al., 2017; Yarnell et al., 2012), to calculate the suitability of spawning grounds (Gard, 2009), and for river restoration studies (Boavida et al., 2010; García de Jalón and Gortázar, 2007; Lacey and Millar, 2004).

Other information:

The River 2D is a freeware available on the internet: http://www.river2d.ualberta.ca/

References:

Boavida, I., Harby, A., Clarke, K.D., Heggenes, J., 2017. Move or stay: habitat use and movements by Atlantic salmon parr (Salmo salar) during induced rapid flow variations. Hydrobiologia 785, 261–275. https://doi.org/10.1007/s10750-016-2931-3

Boavida, I., Santos, J.M., Cortes, R., Pinheiro, A.N., Ferreira, M.T., 2010. Assessment of instream structures for habitat improvement for two critically endangered fish species. Aquat. Ecol. 45, 113–124. https://doi.org/10.1007/s10452-010-9340-x

Bovee, K.D., Lamb, B.L., Bartholow, J.M., Stalnaker, C.B., Taylor, J., Henriksen, J., Tatlor, J., Henriksen, J., 1998. Stream Habitat Analysis using the Instream Flow Incremental Methodology. U.S. Goelogical Surv. Biol. Resour. Div. Inf. Technol. Rep.

García de Jalón, D., Gortázar, J., 2007. Evaluation of instream habitat enhancement options using fish habitat simulations: case-studies in the river Pas (Spain). Aquat. Ecol. 41, 461–474. https://doi.org/10.1007/s10452-006-9030-x

Gard, M., 2009. Comparison of spawning habitat predictions of PHABSIM and River2D models. Int. J. River Basin Manag. 7, 55–71. https://doi.org/10.1080/15715124.2009.9635370

Lacey, R.W.J., Millar, R.G., 2004. Reach scale hydraulic assessment of instream salmonid habitat restoration. J. Am. Water Resour. Assoc. 4, 1631–1644. https://doi.org/10.1111/j.1752-1688.2004.tb01611.x

Rivaes, R., Boavida, I., Santos, J.M., Pinheiro, A.N., Ferreira, T., 2017. Importance of considering riparian vegetation requirements for the long-term efficiency of environmental flows in aquatic microhabitats. Hydrol. Earth Syst. Sci. 21. https://doi.org/10.5194/hess-21-5763-2017

Steffler, P., 2000. Software River2D. Two Dimensional Depth Averaged Finite Element Hydrodynamic Model. University of Alberta, Canada.

Yarnell, S.M., Lind, A.J., Mount, J.F., 2012. DYNAMIC FLOW MODELLING OF RIVERINE AMPHIBIAN HABITAT WITH APPLICATION TO REGULATED FLOW MANAGEMENT. River Res. Appl. 177–191. https://doi.org/10.1002/rra

Contact information:

http://www.river2d.ualberta.ca/

Authors	Isabel Boavida (IST)
Reviewers	Robert Boes (ETHZ)

2.10 CASiMiR

CASiMiR-Fish, CASiMiR-Hydropeaking, CASiMiR-Migration

Developed by: SJE Ecohydraulic Engineering GmbH, Matthias Schneider, Ianina Kopecki

Type: Tool (Computer model)

Suitable for

CASiMiR-Fish → environmental flow, morphological mitigation, impact of river engineering in planning and maintenance phases

CASiMiR-Hydropeaking → environmental flow, morphological mitigation, operational mitigation to reduce hydropeaking impacts on fish in planning and maintenance phases

CASiMiR-Migration → assessment and optimization of attraction flow for upstream migration gation measures (see list) in planning, implementation, and maintenance phases

Introduction:

CASiMiR is a software package with different modules aiming at the assessment of impacts of human measures on river ecology.

CASiMiR-Fish is a habitat suitability model that imports results of 2D hydrodynamic modelling and relates them to the requirements of aquatic species, such as different life stage of fish species, macroinvertebrates or macrophytes. The model delivers quantitative information on the quality and availability of hydro-morphological habitats and their changes, caused by changes in hydrology (temporal flow features), hydraulics (spatial flow feature) and morphology (Figure 30). In contrast to other habitat suitability models, it is based on a multivariate approach that is able to integrate rules for the description of habitat requirements. These rules are generated based on data evaluation and/or ecological expertise.

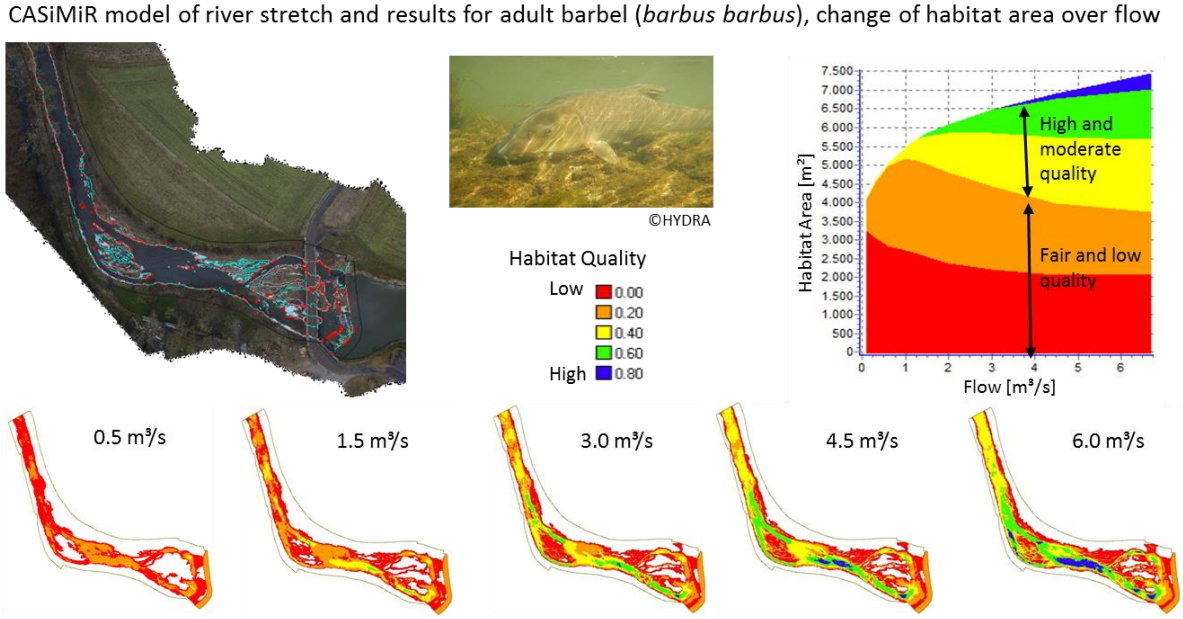


Figure 30: CASiMiR model of river stretch and results for adult barbel.

CASiMiR-Hydropeaking is a model able to process unsteady flow data for habitat risk assessment. Dynamic parameters as ramping rates (water level changes over time) are used to assess the stranding risk or drift risk for young fish during rapidly changing flows that occur in rivers under hydropeaking impact (Figure 31). Additionally, the “habitat persistence” as an indicator for the sustainability of habitats for organisms with restricted mobility (larvae, macroinvertebrates) can be quantified and assessed for different scenarios of turbine operation and morphological mitigation.

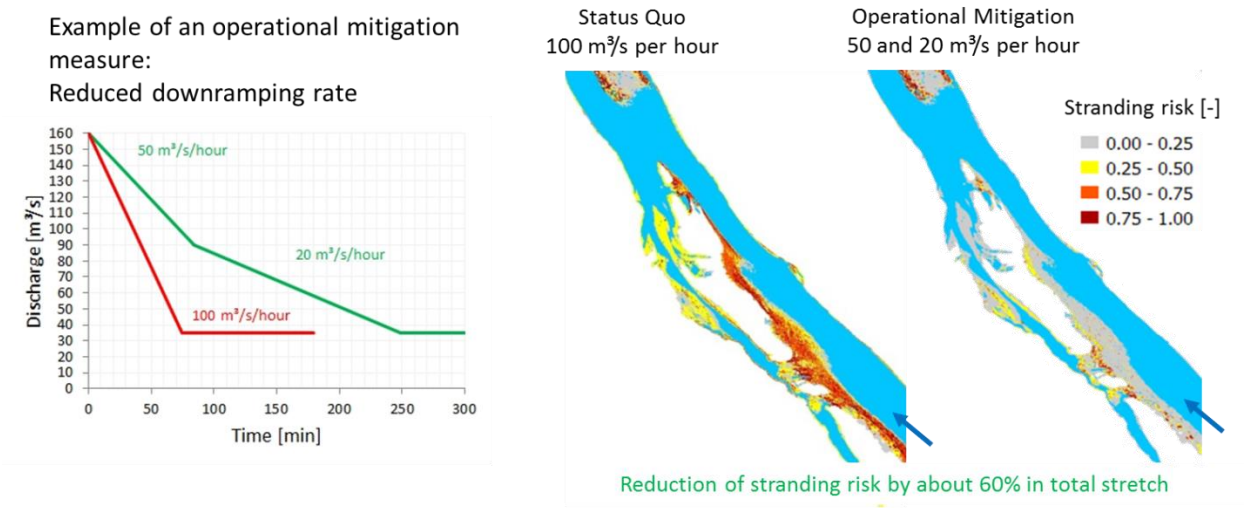


Figure 31: Example of an operational mitigation measure: reduced downramping rate.

CASiMiR-Migration is an agent-based model developed within FITHYDRO. It is used to assess the effectiveness of the attraction flow downstream of fish passes. It is based on the evaluation of hydraulic features such as flow velocity-magnitude, -direction and -gradient as well as morphological features such as river bottom gradients, vicinity of flow obstacles to predict favorable and unfavorable swimming paths for migratory fish (Figure 32).

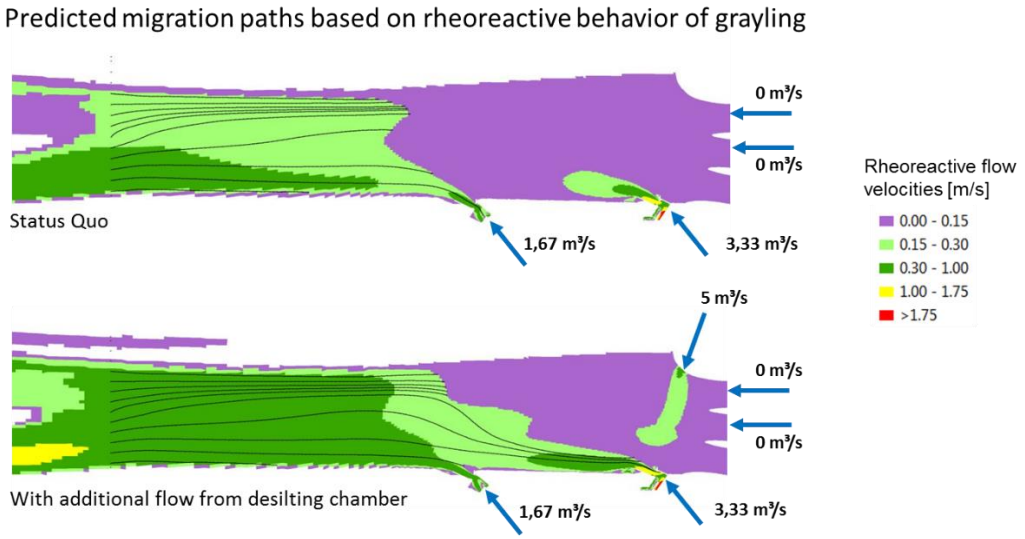


Figure 32: Predicted migration paths based on rheoreactive behaviour of grayling.

Application:

CASiMiR integrates interfaces for several 2D hydrodynamic models such as Hydro-AS_2D, SRH, BASEMENT, FLUMEN, River2D. The model has been applied in rivers of most different dimensions, types and stretches with lengths between several 10 meters to sections of several dozens of kilometres length (Figure 33).

CASiMiR is unique in that it makes use of physical and biological parameters through the application of expert knowledge using fuzzy logic-based rule systems, but can also use the standard preference function method as well. The main advantages of using habitat simulation models are:

- The ecological condition of an aquatic ecosystem is directly coupled with the living conditions of the typical resident species.

- The use of habitat models allows for the effects of changing flow rates and structural characteristics to be account for and can be used to predict their impacts.
- Changes to the flow rate and morphology result primarily in impacting the water depth, flow velocity, and substrate conditions, all of which are major factors in determining the habitat suitability and can be directly evaluated with numerical models.
- Due to the direct relationship between habitat conditions and flow rate, a quantitative basis can be established whereby an overall ecological assessment of the habitat requirements can be performed.

Other information:

Base versions of CASiMiR are free for download under www.casimir-software.de. Advanced versions can be purchased via mailbox@sjeweb.de. Scientific and commercial licenses are available.

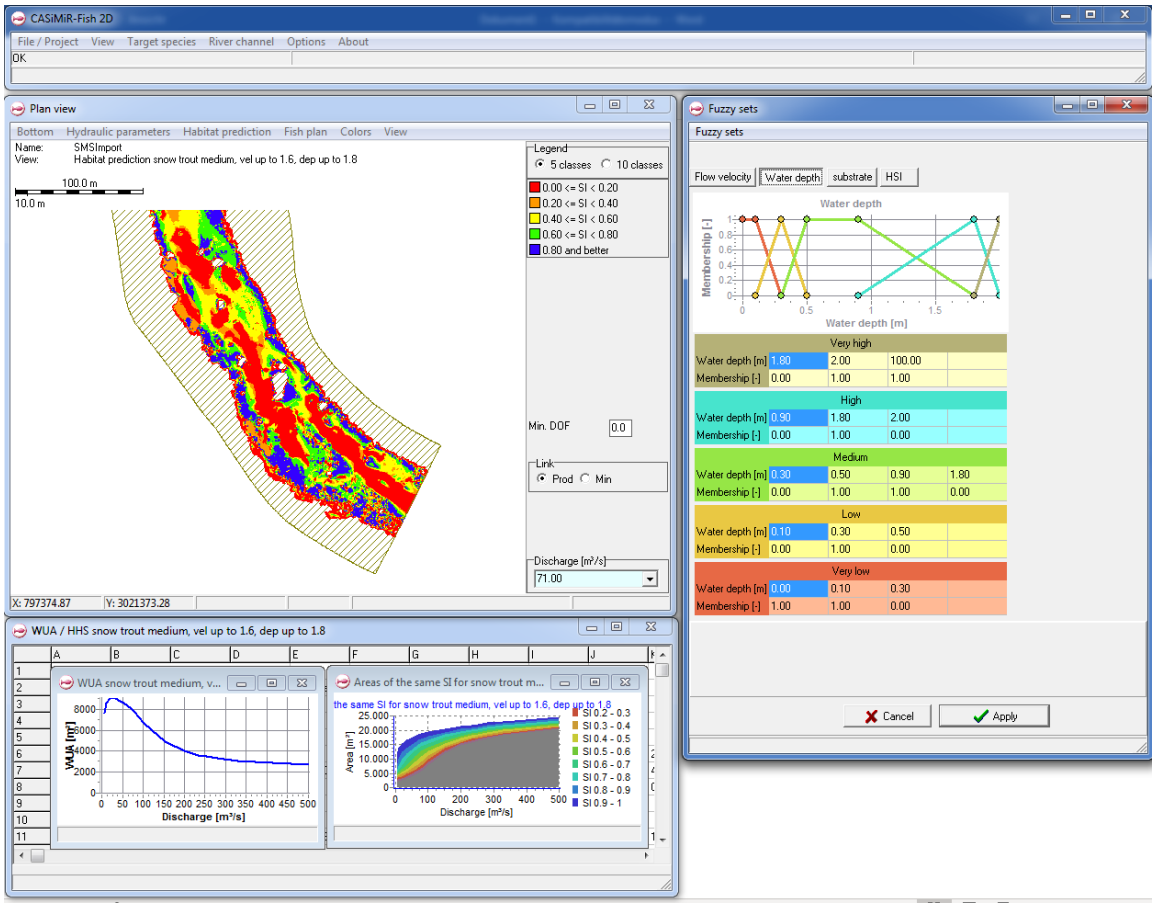


Figure 33: view of the interface.

References:

Noack, M., Schneider, M. and Wieprecht, S. (2013): The Habitat Modelling System CASiMiR: A Multivariate Fuzzy Approach and its Applications; in Ecohydraulics: An Integrated Approach, Chapter 6 (75-93); Editors I. Maddock, A. Harby, P. Kemp, P. Wood, John Wiley & Sons Ltd

Schneider, M., Kopecki, I., Tuhtan, J., Sauterleute, J., Zinke, P., Bakken, T., Zakowski, T., Merigoux, S. (2016): A Fuzzy Rule-based Model for the Assessment of Macrobenthic Habitats under Hydropeaking Impact. River Research and Applications, 1467-1535

Kopecki, I., Tuhtan, J., Schneider, M., Ortlepp, J., Thonhauser, S., Schletterer, M. (2014): Assessing Fishway Attraction Flows Using an Ethohyraulic Approach. 3rd IAHR Europe Congress, Porto, April 14-16.

Contact information:

www.casimir-software.de

Authors	Matthias Schneider (SJE)
Reviewers	Robert Boes (ETHZ)

2.11 HEC-RAS

Developed by: CEIWR-HEC, the Hydrologic Engineering Center an organization of the United States Corps of Engineers (USACE) Institute for Water Resources

Type: Tool (computer model)

Suitable for open channel flow analysis, including sediment and water quality modelling, thus suitable for use in all mitigation measures (habitat, environmental flow, sediments, downstream fish migration, and upstream fish migration) and phases (planning, implementation, maintenance).

Introduction:

HEC-RAS (Hydrologic Engineering Center-River Analysis System) is a freely available and widely used software tool for open channel flow analysis. The first version of the software, originally developed as a one-dimensional (1D) open channel flow analysis tool, was released in July 1995. In 2016 the ability to perform two-dimensional (2D) modelling was added. The current version allows users to perform 1D steady flow and 1D/2D unsteady flow modelling, sediment transport/mobile bed computations, and water temperature/water quality modelling for a full network of natural and constructed channels, or a single river reach, under the same graphical user interface (GUI) (Figure 34).

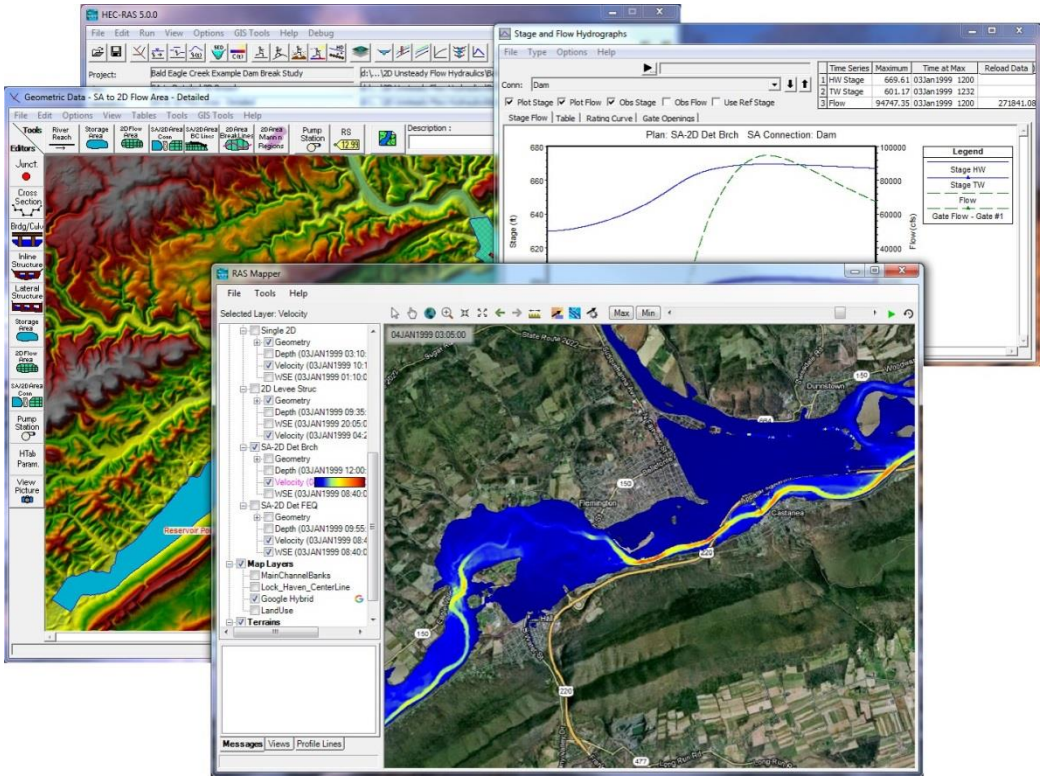


Figure 34: HEC-RAS graphical user interface (GUI) https://www.hec.usace.army.mil/software/hec-ras/.

The basic computational procedure of HEC-RAS for steady flow is based on the solution of the 1D energy equation, the energy losses are evaluated by friction (Manning's equation) and contraction/expansion (coefficient multiplied by the change in velocity head). The momentum equation may be used in situations where the water surface is rapidly varied (e.g. hydraulic jumps, bridges, river confluences). For the 1D unsteady flow computation, HEC-RAS solves the full, dynamic, 1D Saint Venant Equation using an implicit finite difference method. For the 2D modelling the software solves either the 2D Saint Venant equations, often referred to as the shallow water equations (with optional momentum additions for turbulence and Coriolis effects) or the 2D Diffusion Wave equations. This is user-selectable, giving modellers more flexibility. The shallow water equations solver disregards vertical velocities and assumes hydrostatic pressure, whereas the diffusive wave approximation solver additionally omits unsteady, advection and turbulent viscous terms, which narrows the range of applicability but has many computational advantages. Thus, in general, selection of the 2D Diffusion Wave equations allows the software to run faster, and has greater stability properties, whereas the 2D Saint-Venant equations are applicable to a wider range of problems.

The 2D unsteady flow equations solver uses an Implicit Finite Volume algorithm. The implicit solution algorithm allows for larger computational time steps than explicit methods. The Finite Volume method guarantees improved stability and robustness over traditional finite difference and finite element techniques with the wetting and drying of 2D cells being very robust.

The 1D and 2D solution algorithms are tightly coupled on a time step basis with an option to iterate between 1D and 2D flow transfers within a time step. This allows for direct feedback at each time step between the 1D and 2D flow elements.

The 2D modelling has a flexible mesh generation allowing the user to generate a computation grid that is a mixture of structured and unstructured mesh types with the possibility of containing a mixture of cell shapes (the model is limited to elements with up to eight sides) and sizes. A user can customize a mesh to suit the terrain, containing predominantly large

orthogonal grid cells (which simplifies the numerical discretization, making it more efficient), and where needed smaller cells, orientated appropriately along controlling terrain such as road crests, or along important river channels.

Within HEC-RAS each computational cell and cell face is based on the details of the underlying terrain, which is referred to as “high resolution subgrid model”. This allows larger cell sizes without compromising the resolution of the results, since it still accurately represents the underlying terrain, with gains in the modelling time.

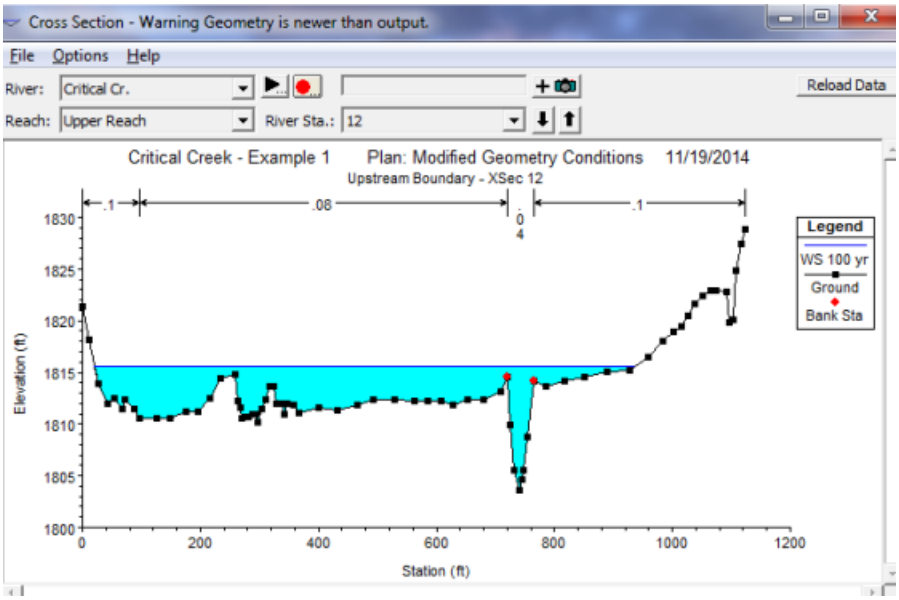
Application:

HEC-RAS has a wide range of applications; it can be applied to river/open channel flow analysis, river rehabilitation/restoration studies, floodplain determination studies, hydraulic structures design and analysis (e.g. bridges, weirs, culverts), sediment transport studies, scour/deposition analysis, dam break analysis (e.g. timing of flood, flood inundation), and water quality analysis.

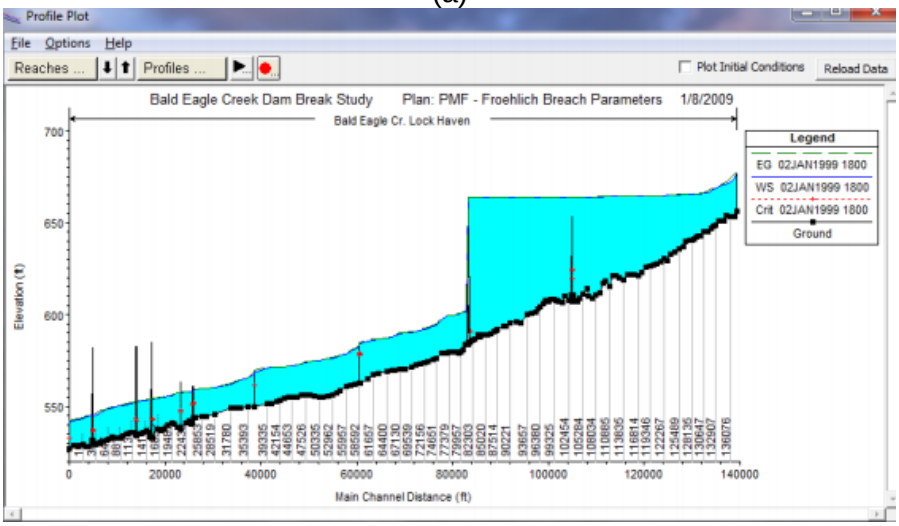
As input data, it requires geometry data, like topography (e.g. surveyed cross sections, digital elevation model), energy losses (e.g. roughness, expansions and contractions), and hydraulic structures (e.g. bridges, culverts, weirs). Hydrology data (e.g. gauging stations data, measured/observed flow and water depth data), is also needed, for calibration/validation and/or boundary conditions. If sediment transport or water quality studies are intended, sediment data (e.g. representative material, appropriate transport equations, appropriate sorting and fall velocity methods) and water quality data (e.g. meteorological data, nutrients data) are required, respectively.

HEC-RAS has an internal GIS tool (RAS Mapper) which provides flexible viewing and manipulation of integrated 1D and 2D results, greatly enhancing the pre- and post-processing capabilities of data within the software.

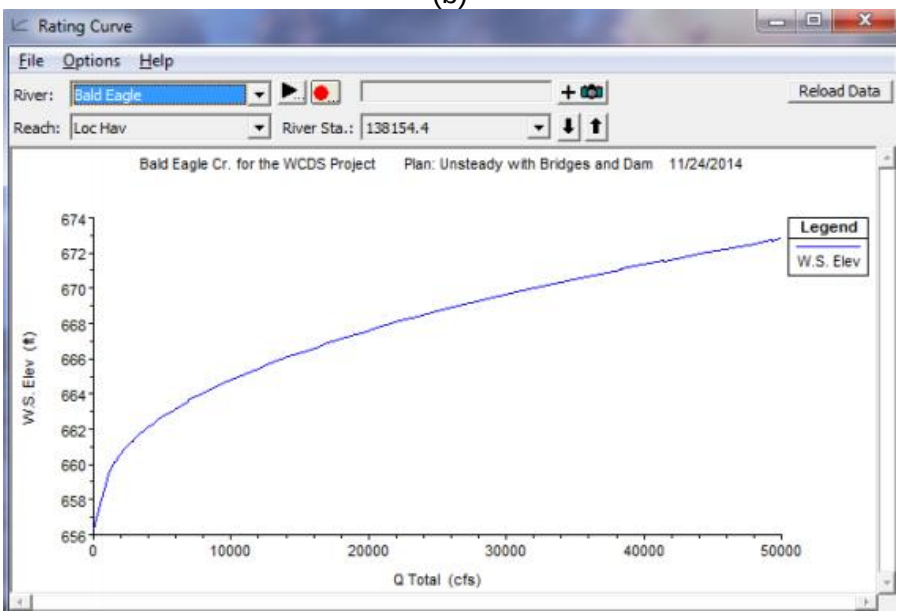
Outputs of HEC-RAS include graphics, like X-Y plots of the river system schematic, cross-sections (Figure 35a), profiles (Figure 35b), rating curves (Figure 35c), hydrographs (Figure 35d), and inundation mapping (Figure 35e). Inundation maps can contain multiple background layers, like terrain and aerial photography, and additional geospatial data can be generated for the analysis of velocity, shear stress, stream power, ice thickness and floodway encroachment data. Tabular output (Figure 35f) is available with the possibility of selecting pre-defined tables or developing customized tables. The graphical and tabular output can be exported to other software, such as a word-processor or a spreadsheet.



(a)

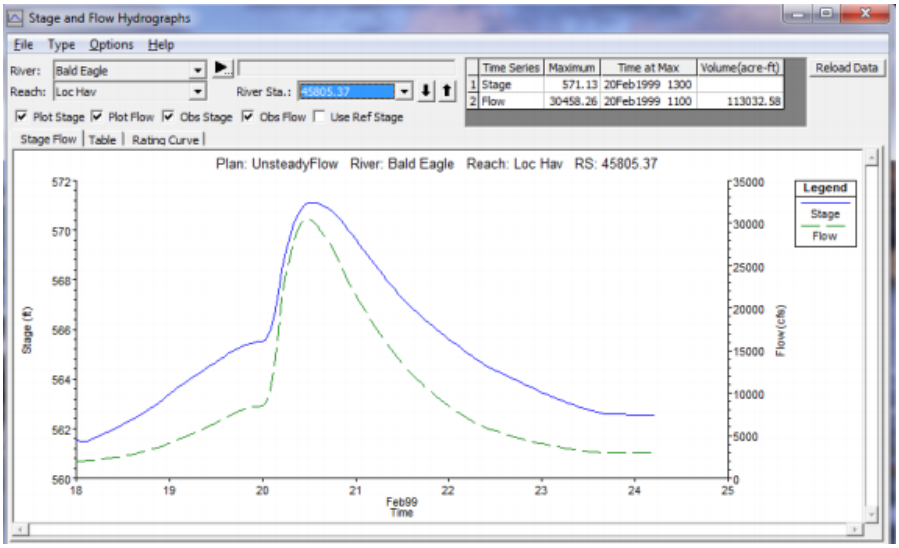


(b)

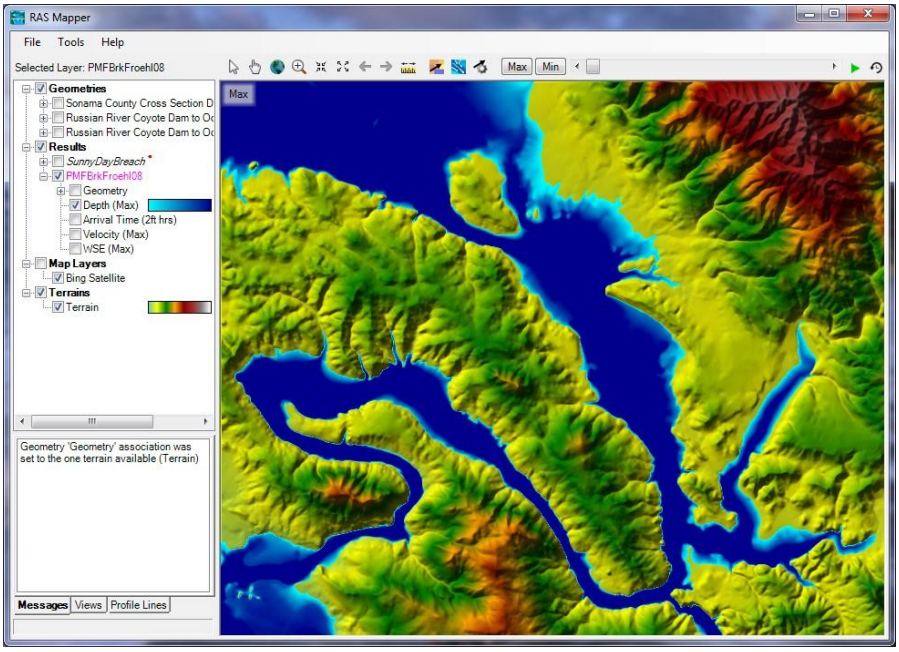


(c)

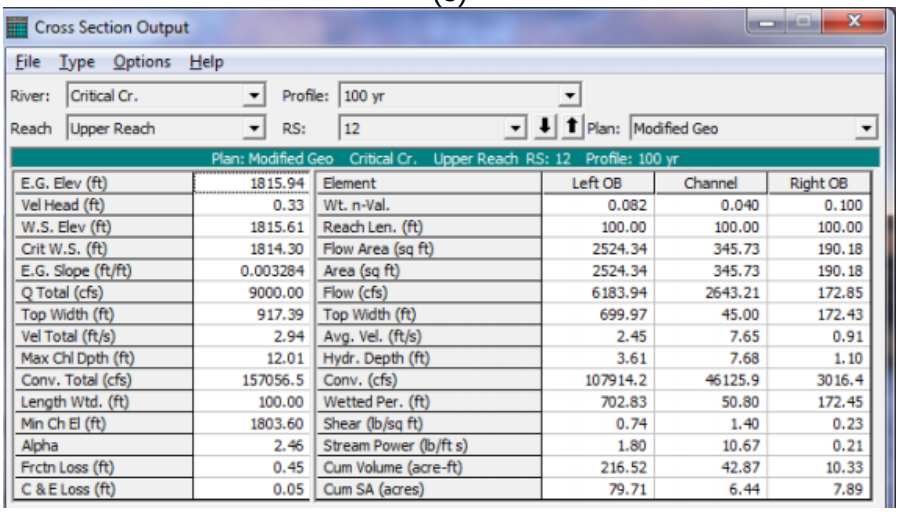
Back to D2.2 Main index



(d)



(e)



Cross Section Output

File Type Options Help

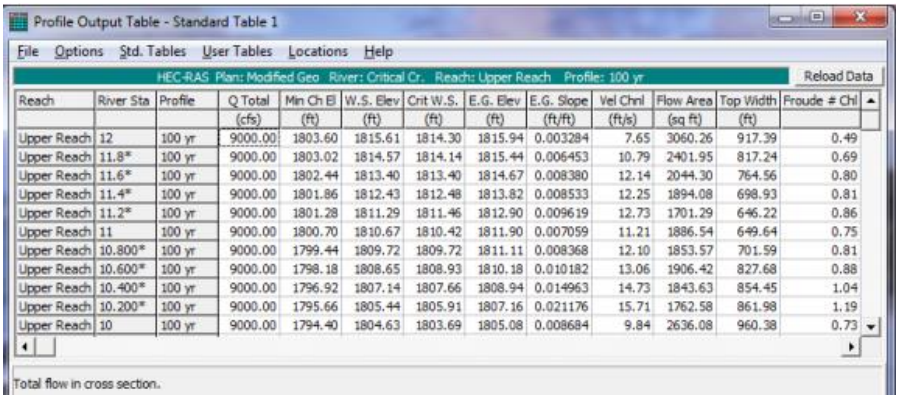
River: Critical Cr. Profile: 100 yr

Reach Upper Reach RS: 12 Plan: Modified Geo

Plan: Modified Geo Critical Cr. Upper Reach RS: 12 Profile: 100 yr

		Element	Left OB	Channel	Right OB
E.G. Elev (ft)	1815.94				
Vel Head (ft)	0.33	Wt. n-Val.	0.082	0.040	0.100
W.S. Elev (ft)	1815.61	Reach Len. (ft)	100.00	100.00	100.00
Crit W.S. (ft)	1814.30	Flow Area (sq ft)	2524.34	345.73	190.18
E.G. Slope (ft/ft)	0.003284	Area (sq ft)	2524.34	345.73	190.18
Q Total (cfs)	9000.00	Flow (cfs)	6183.94	2643.21	172.85
Top Width (ft)	917.39	Top Width (ft)	699.97	45.00	172.43
Vel Total (ft/s)	2.94	Avg. Vel. (ft/s)	2.45	7.65	0.91
Max Chl Dpth (ft)	12.01	Hydr. Depth (ft)	3.61	7.68	1.10
Conv. Total (cfs)	157056.5	Conv. (cfs)	107914.2	46125.9	3016.4
Length Wtd. (ft)	100.00	Wetted Per. (ft)	702.83	50.80	172.45
Min Ch El (ft)	1803.60	Shear (lb/sq ft)	0.74	1.40	0.23
Alpha	2.46	Stream Power (lb/ft s)	1.80	10.67	0.21
Frctn Loss (ft)	0.45	Cum Volume (acre-ft)	216.52	42.87	10.33
C & E Loss (ft)	0.05	Cum SA (acres)	79.71	6.44	7.89

Back to D2.2 Main index



Reach	River Sta	Profile	Q Total	Min Ch El	W.S. Elev	Crit W.S.	E.G. Elev	E.G. Slope	Vel Chnl	Flow Area	Top Width	Froude # Chl
			(cfs)	(ft)	(ft)	(ft)	(ft)	(ft/ft)	(ft/s)	(sq ft)	(ft)	
Upper Reach	12	100 yr	9000.00	1803.60	1815.61	1814.30	1815.94	0.003284	7.65	3060.26	917.39	0.49
Upper Reach	11.8*	100 yr	9000.00	1803.02	1814.57	1814.14	1815.44	0.006453	10.79	2401.95	817.24	0.69
Upper Reach	11.6*	100 yr	9000.00	1802.44	1813.40	1813.40	1814.67	0.008380	12.14	2044.30	764.56	0.80
Upper Reach	11.4*	100 yr	9000.00	1801.86	1812.43	1812.48	1813.82	0.008533	12.25	1894.08	698.93	0.81
Upper Reach	11.2*	100 yr	9000.00	1801.28	1811.29	1811.46	1812.90	0.009619	12.73	1701.29	646.22	0.86
Upper Reach	11	100 yr	9000.00	1800.70	1810.67	1810.42	1811.90	0.007059	11.21	1886.54	649.64	0.75
Upper Reach	10.800*	100 yr	9000.00	1799.44	1809.72	1809.72	1811.11	0.008368	12.10	1853.57	701.59	0.81
Upper Reach	10.600*	100 yr	9000.00	1798.18	1808.65	1808.93	1810.18	0.010182	13.06	1906.42	827.68	0.88
Upper Reach	10.400*	100 yr	9000.00	1796.92	1807.14	1807.66	1808.94	0.014963	14.73	1843.63	854.45	1.04
Upper Reach	10.200*	100 yr	9000.00	1795.66	1805.44	1805.91	1807.16	0.021176	15.71	1762.58	861.98	1.19
Upper Reach	10	100 yr	9000.00	1794.40	1804.63	1803.69	1805.08	0.008684	9.84	2636.08	960.38	0.73

(f)

Figure 35: HEC-RAS outputs (https://www.hec.usace.army.mil/software/hec-ras/): (a) cross-section; (b) profile; (c) rating curve; (d) hydrograph; (e) inundation mapping; and (f) tabular output.

The current version (5.0.6) cannot perform sediment transport and water quality modelling in 2D flow areas, nor use HEC-RAS bridge modelling capabilities inside of a 2D flow area, nor connect pump stations to 2D flow area cells.

Other information:

HEC-RAS is freely available in the public domain in: https://www.hec.usace.army.mil/software/hec-ras/

Since the software is continuously under development, users are encouraged to submit suggestions, requests for enhancement, or report any bugs, or possible errors, so current limitations and new additions are worked on to have solutions and improvements in future versions.

The 2D modelling is done with a multi-processor based solution algorithm (parallel computing) to take advantage of multiple processors on a computer, allowing it to run much faster than on a single processor.

HEC-RAS is compatible with several GIS software. HEC-GEO-RAS is an extension for ArcGIS which allows for the pre-processing of geometric data to import to HEC-RAS and the post-processing of the results. It was developed by CEIWR-HEC together with ESRI (Environmental System Research Institute). RiverGIS is a QGIS plugin for creating HEC-RAS flow model geometry from spatial data, it is free software released under the GNU General Public License.

References:

Hydrologic Engineering Center, 2018. Benchmarking of the HEC-RAS Two-Dimensional Hydraulic Modeling Capabilities, April 2018, U.S. Army Corps of Engineers, Davis, California.

Hydrologic Engineering Center, 2016. HEC-RAS River Analysis System, Applications Guide, Version 5.0, February 2016, U.S. Army Corps of Engineers, Davis, California.

Hydrologic Engineering Center, 2016. HEC-RAS River Analysis System, Hydraulic Reference Manual, Version 5.0, February 2016, U.S. Army Corps of Engineers, Davis, California.

Hydrologic Engineering Center, 2016. HEC-RAS River Analysis System, User´s Manual, Version 5.0, February 2016, U.S. Army Corps of Engineers, Davis, California.

Hydrologic Engineering Center, 2016. HEC-RAS River Analysis System, 2D Modeling User´s Manual, Version 5.0, February 2016, U.S. Army Corps of Engineers, Davis, California.

Hydrologic Engineering Center, 2018. HEC-RAS River Analysis System, Supplemental User´s Manual, Version 5.0, April 2018, U.S. Army Corps of Engineers, Davis, California.

Hydrologic Engineering Center, 2018. HEC-RAS Verification and Validation Tests, Version 5.0, April 2018, U.S. Army Corps of Engineers, Davis, California.

https://www.hec.usace.army.mil/software/hec-ras/

https://www.hec.usace.army.mil/software/hec-ras/documentation.aspx

Contact information:

hec.ras@usace.army.mil

Authors	Ana Quaresma (IST)
Reviewers	Robert Boes (ETHZ)

2.12 OpenFOAM

Developed by: OpenCFD Ltd / OpenFOAM Foundation

Date: 12.12.2018 (OpenFOAM release v1812)

Type: Tool, open source CFD software, GNU Public License (GPL)

Suitable for assessment of hydrodynamics in all phases (planning, implementation, maintenance)

Introduction:

OpenFOAM is a C++ toolbox for simulation of general continuum mechanics problems including the Navier-Stokes equations that mathematically describe the 3D motion of fluids. For simulations of free-surface gravity flows, the prebuilt Eulerian' solver *interFOAM* is most suitable. The *interFOAM* solver identifies the interface between water and air based on the Volume Of Fluid (VOF) method and uses the PIMPLE algorithm for pressure-velocity coupling. The governing flow equations can be solved in combination with different approaches for turbulence modelling. In *OpenFOAM*, Reynolds-averaged Navier-Stokes (*RANS*) models using one or two equation turbulence models (e.g. *k-ε* model) as well as more computationally expensive large eddy simulation (LES) methods are available. An advantage of *OpenFOAM*, besides its free availability, is the use of body-fitted or unstructured computational grids. The additional use of polyhedral cells (in addition to hexahedral cells) allows even complex geometries to be accurately mapped (Figure 36).

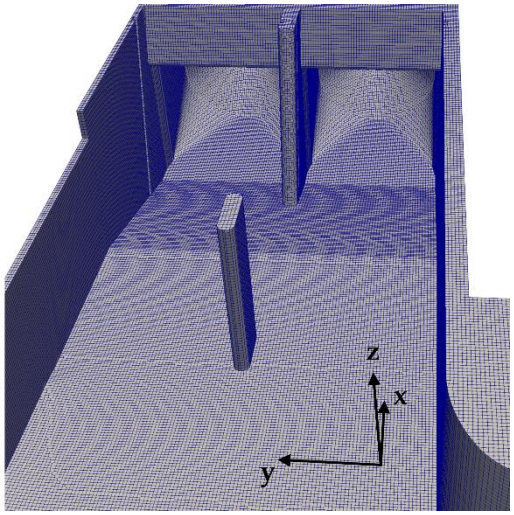


Figure 36: Example of turbine inlet (flow in x-direction) modelled using an unstructured computational grid for OpenFOAM simulations (source: VAW).

Application:

The operating system for *OpenFOAM* is Linux and there is no official Graphical User Interface (GUI). The basic directory structure for an *OpenFOAM* case containing the minimum set of files required to run an application is shown in Figure 37. All the files can be accessed with a text editor. In the *system* directory, the parameters associated with the solution procedure itself are defined (e.g. start/end time, solution schemes). The *constant* directory contains the description of the mesh and files specifying the physical properties. The *time* directories contain data files that can be either initial values, boundary conditions or results written to file.

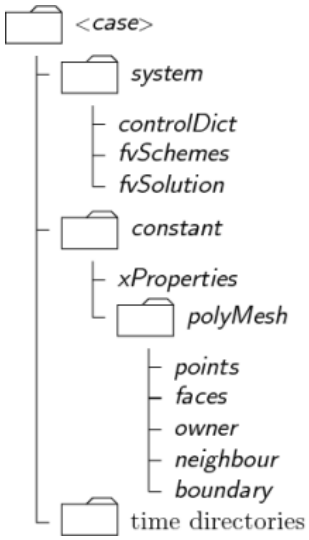


Figure 37: Case directory structure in OpenFOAM (source: CFD Direct ® OpenFOAM)

OpenFOAM is supplied with a pre- and post-processing environment. The interface to the pre- and post-processing are *OpenFOAM* utilities, thereby ensuring consistent data handling across all environments. The overall structure of *OpenFOAM* is shown in Figure 38.

In the pre-processing, simple meshes containing blocks of hexahedral cells can be generated by the *blockMesh* utility. For more complex geometries, the *snappyHexMesh* utility automatically generates meshes containing split-hexahedral cells by iteratively refining the

starting mesh and morphing the resulting split-hex mesh to the triangulated surface of solid geometrical structures like power plant facilities (see Figure 37). Solid structures are represented in the form of stereolithographic files (*STL*).

The main post-processing tool provided with *OpenFOAM* is the reader module *paraFoam* that uses *ParaView*, an open-source visualization software to display geometry, computational mesh and simulation results (Figure 38).

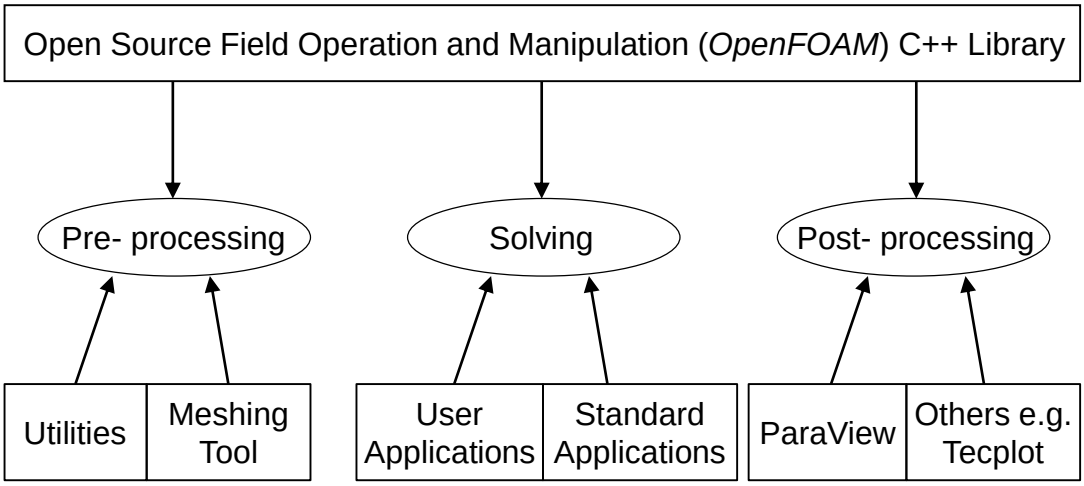


Figure 38: Overview of OpenFOAM structure (source: CFD Direct ® OpenFOAM).

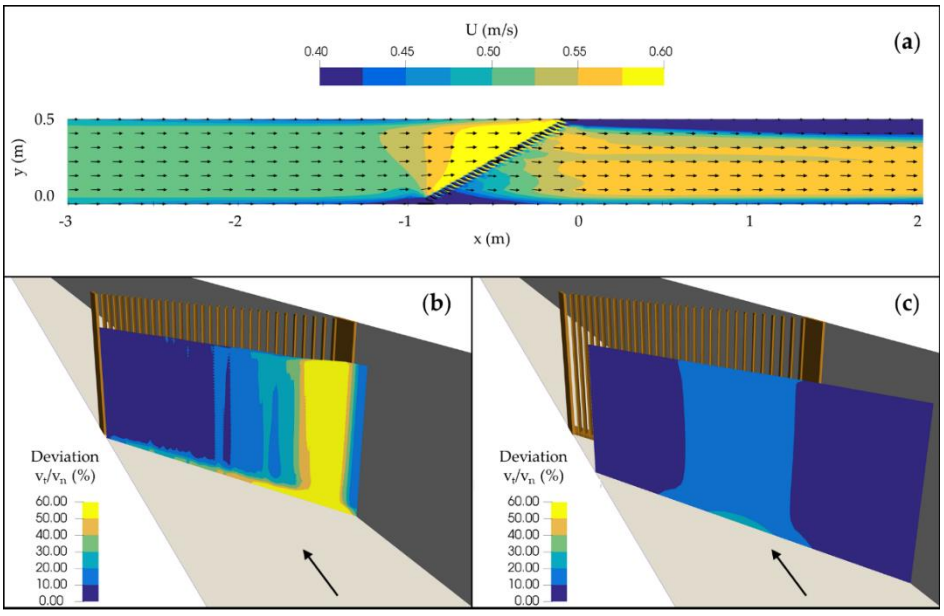


*Figure 39: Exemplary ParaView visualization of OpenFOAM simulation results showing horizontal flow velocities in a rectangular channel with a curved bar rack (CBR) for horizontal plane at 0.2 m (**a**). Deviation (in percent) of the ratio between tangential v_t and normal velocities v_n for the MCR compared to the situation without screen 5 cm (**b**) and 40 cm (**c**) upstream of the screen axis. The black arrows represent the flow direction (source: VAW).*

Other information:

General advantages & disadvantages of the tool (no claim for completeness)

+ Open source software	− Complex model setup (no GUI)
+ Accurate representation of complex geometries due to unstructured or body-fitted computational grids	− Definition of boundary and initial condition requires in depth knowledge of underlying concepts
+ Growing user community (forum)	− No standardized documentation

References:

Feigenwinter, L., Vetsch, D., Kammerer, S., Kriewitz, R.C., Boes, R.M. (2018) Conceptual Approach for Positioning of Fish Guidance Screens Using CFD and expert knowledge. *Sustainability*, under review.Fuentes-Perez, J.F., Silva, A.T., Tuhtan, J.A., Garcia-Vega, A., Carbonell-Baeza, R., Musall, M., Kruusmaa, M. (2018). 3D modelling of non-uniform and turbulent flow in vertical slot fishways. *Environmental Modelling and Software*, *99*, 156-169, doi:10.1016/j.envsoft.2017.09.011.

Gisen, D.C., Weichert, R.B,; Nestler, J.M. (2017) Optimizing attraction flow for upstream fish passage at a hydropower dam employing 3D Detached-Eddy Simulation. *Ecological Engineering*, *100*, 344-353, doi:10.1016/j.ecoleng.2016.10.065.

Raynal, S., Chatellier, L., David, L., Courret, D., Larinier, M. (2013). Numerical Simulations of Fish-Friendly Angled Trashracks at Model and Real Scale. *Proceedings of the 35th Iahr World Congress, Vols I and II*, 2557-2566.

Contact information:

OpenFOAM download: https://www.openfoam.com / https://openfoam.org

User guide and tutorials: https://www.openfoam.com/documentation

Paraview: https://www.paraview.org

Authors	Stephan Kammerer (VAW, ETHZ), David Vetsch (VAW, ETHZ)
Reviewers	Robert Boes (ETHZ)

2.13 FLOW-3D

Developed by: Flow Science, Inc (Santa Fe, New Mexico, USA)

Date: 11.2016 (FLOW-3D release v11.2)

Type: Tool (Commercial CFD software)

Suitable for assessment of hydrodynamics in all phases (planning, implementation, maintenance)

Introduction:

FLOW-3D is a commercial CFD simulation software that focusses on free-surface flows in a wide range of industrial applications and physical processes. The software solves the Navier-Stokes equations that mathematically describe the 3D motion of fluids. The domain is subdivided into several mesh blocks containing rectangular grid cells (structured mesh). Fluid velocities and pressures are located at staggered mesh locations as shown for a typical grid cell in Figure 40.

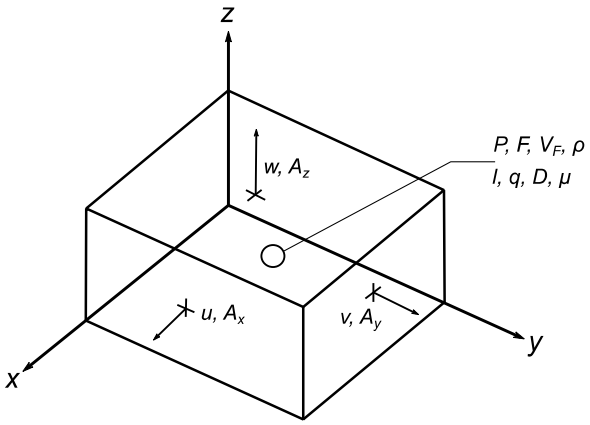


Figure 40: Location of variables in FLOW-3D computational mesh (source: FLOW-3D)

The numerical model involves the following variables: velocities (*u,v,w*) and fractional areas (*A*) at the centers of cell-faces, pressures (*P*), fluid fractions (*F*), fractional volumes (V_F), densities (ρ), internal energy (*I*), turbulence quantities for energy (*q*), dissipation (*D*) and viscosity (μ) are located at cell centres.

In *FLOW-3D*, one or two equation turbulence models (e.g. *k-ε* model), as well as more computationally expensive large eddy simulation (LES) methods, are available for turbulence modelling.

Wall boundaries and other solid geometrical structures like power plant facilities are embedded in the orthogonal mesh by the so called *FAVOR*^{TM} method. This algorithm defines the fractional face areas and fractional volumes of the cells that are open to fluid flow. Thus, the mesh does not have to be fit around complex geometry during the pre-processing. In order to properly capture the free-surface dynamics, the *Volume of Fluid* (*VOF*) method is applied in *FLOW-3D.*

Application:

FLOW-3D supports Windows as well as Linux platforms and includes a powerful graphical user interface (GUI) which supports the user during the model setup and simulation process.

3D solid structures are imported into the GUI in the form of stereolithographic files (*STL*). Figure 41 shows the exemplary geometry set-up of the FIThydro case study hydropower plant (HPP) Bannwil in Canton Bern, Switzerland for *FLOW-3D*. Definition of mesh blocks and mesh resolution, as well as boundary and initial conditions, can is done in the GUI. The use of multiple mesh blocks allows for local refinement at areas of interest. Small obstacles, complex geometries and thin channels that are small compared to the overall domain size can be accurately resolved using so called conforming mesh blocks. In *FLOW-3D* “conforming mesh” means, that the transition between solid and void or solid and fluid is resolved with a nested finer mesh within a defined overlap length compared to the surrounding block.

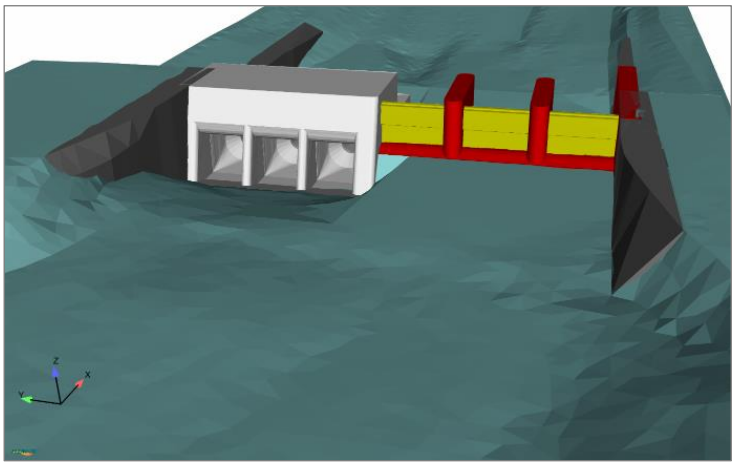


Figure 41: Example of a river power plant geometry set up for FLOW-3D (source: VAW)

The software license includes the post-processing tool *FlowSight*, designed to deliver sophisticated visualizations of *FLOW-3D* results. Arbitrary 2D clips along spline pathways, 3D clips and transparencies, volume rendering, advanced data time series plotting and calculators, streamline and vector plots are available in *FlowSight* (Figure 42). Alternatively, the result files can be visualized using other free (e.g. *ParaView*) or commercial (e.g. *Tecplot*) CFD visualization software.

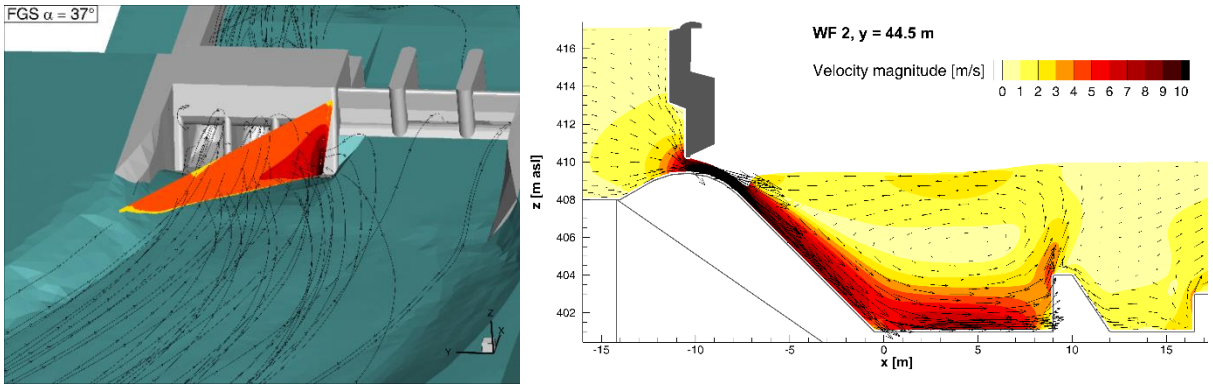


Figure 42: Exemplary visualization of FLOW-3D simulation results for the case study HPP Banwil showing flow velocities and streamlines at a potential location for fish guidance structures (left) and during spillway operation (right) (source: VAW).

Other information:

In addition to the use on regular Windows and Linux workstations, the High Performance Computing (HPC) version of *FLOW-3D* is designed to run on distributed memory computer clusters allowing engineers to tackle problems with very large computational domains or long simulation time. For users with limited access to hardware resources, the HPC version is also available on the *FLOW-3D CLOUD* computing service.

General advantages & disadvantages of the tool (no claim for completeness)

+ Relatively easy to use due to GUI and integrated pre and post-processing
+ Detailed documentation available
+ Access to HPC services via Cloud

− Commercial software (licenses costs)
− Source code not available
− Cartesian gird

References:

Kammerer, S., Lutz, N., Vetsch, D., Kriewitz, K. R., Früh, H. (2018). Beurteilung der Unterhaltspflicht eines Regulierwehrs mit Kraftwerk mittels 3D Simulationen, *19.*

Wasserbausymposium Graz 2018, Graz, Austria, pp.237-244, Graz: Verlag der Technischen Universität Graz, September 18-20.

Duguay, J., Lacey, R.W.J., Gaucher, J. (2017). A case study of a pool and weir fishway modeled with OpenFOAM and FLOW-3D. *Ecological Engineering*. 103. 31-42. doi: 10.1016/j.ecoleng.2017.01.042.

Duguay, J., Lacey, R.W.J. (2014), Use of Numerical Hydraulic Modeling to Improve Fish Passage at Perched Culverts. *Canadian Journal of Civil Engineering*, 2016, 43(2): 173-181. dx.doi.org/10.1139/cjce-2014-043

Contact information:

FLOW-3D webpage: https://www.flow3d.com/

Water & Environmental applications: https://www.flow3d.com/industries/water-environmental/

Authors	Stephan Kammerer (VAW, ETHZ), David Vetsch (VAW, ETHZ)
Reviewers	Robert Boes (ETHZ)

2.14 TELEMAC

Developed by: Laboratoire National d'Hydraulique et Environnement (LNHE), part of the R&D group of Électricité de France.

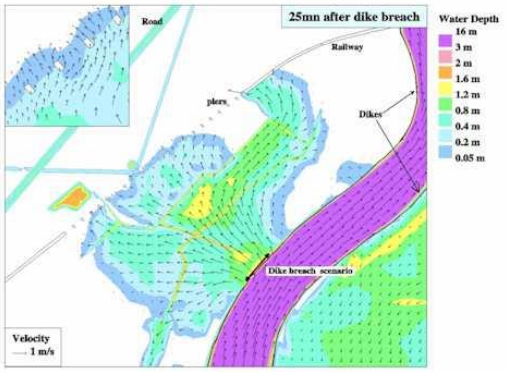
Date: 1991 and later

Type: Computer model

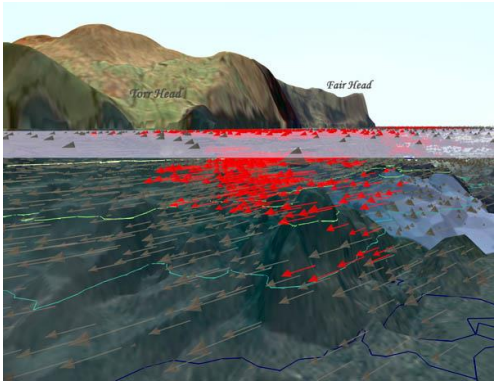
Suitable for 2D and 3D hydro-morphological computations in rivers

Introduction:

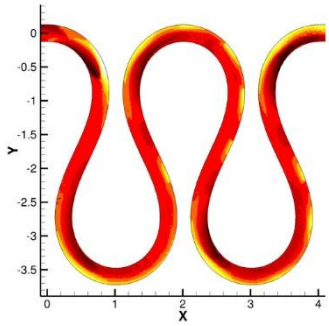
An international consortium of research institutes, agencies and companies manages the open source software TELEMAC (www.opentelemac.org). Originally developed in France, the software is now freely available and the FORTRAN-based source code is open for developers and users. The software is structured in modules, which can be coupled depending on the purpose. The most common module is Telemac-2D, which is a 2D depth averaged, shallow water based hydrodynamic solver for free surface flows. The more complex model,Telemac-3D, provides RANS averaged three dimensional information on the flow. Both modules can be coupled to Sisyphe, the morphological module, representing sediment transport. Figure 43 provides an overview of some selected modules. For completeness, the others are Artemis and Tomawac (for wave and coastal areas), Nestor (extension for Sisyphe), and the one-dimensional solver Mascaret.



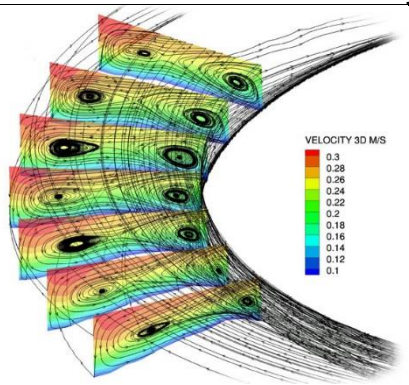
Telemac2D: Modeling of an embankment failure



Telemac-3D: Threedimensional velocity field



Telemac2d+Sisyphe: Morphodynamic evolution in meandering bars



Telemac-3d+Sisyphe:Threedimensional flow pattern and bed deformation

Figure 43: Overview of the TELEMAC modeling system (Source: www.opentelemac.org)

Application:

TELEMAC is well suited to model flow and hydro-morphological processes in rivers, by using either a classical, two-dimensional shallow-water approach or a fully 3D RANS based Navier-Stokes solver. The program has a large number of empirical bed-load and suspended load transport formulae implemented. Additionally customized developments and extensions can be implemented as described below.

Other information:

The availability of the source code makes TELEMAC suitable for developments, extensions and research purposes, beyond the existing framework. On the TELEMAC homepage information on user-specific developments can be found in a source code repository or in the proceedings of the user community events. For example, at TUM the following user-specific extensions have been developed or are currently under development:

- Development for sediment transport to improve the process description and the stability of the code.
- Integration of innovative, data-driven methods instead of classical, morphological simulation approaches.
- Further code optimization for one of the fastest High-Performance-Computer worldwide.
- Concept to provide the computational grid, to estimate relevant parameters and to perform an automated, iterative model calibration.

Summary:

TELEMAC is a powerful program with a large user community. The open-source strategy and support of the consortium makes the application user-friendly and suitable for researchers, engineering offices and consultants.

References:

"TELEMAC: A New Numerical Model for Solving Shallow Water Equations", J.C. Galland; N. Goutal; J.M. Hervouet, (1991), , Advances in Water Resources AWREDI, 14 (3): 138-148, Bibcode:1991AdWR...14..138G, doi:10.1016/0309-1708(91)90006-A

"A Finite Volume Solver for 1D Shallow-Water Equations Applied to an Actual River", N. Goutal and F. Maurel, Int. J. Numer. Meth. Fluids 2002; 38:1-19

"MASCARET: a 1-D Open-Source Software for Flow Hydrodynamic and Water Quality in Open Channel Networks", N. Goutal, J.-M. Lacombe, F. Zaoui and K. El-Kadi-Abderrezzak, River Flow 2012 – Murillo (Ed.), pp. 1169-1174

Contact information:

Authors	Peter Rutschmann (TUM), Markus Reisenbüchler (TUM)
Reviewers	Hany Abo el Wafa (TUM)

2.15 Bedload monitoring system

Developed by: VAW, ETH Zurich, Switzerland; Test Case partner: Limmatkraftwerke AG, Baden, Switzerland

Date: 15-02-2019

Type: Device

Suitable for bedload transport monitoring in rivers, torrents and hydraulic structures in all phases (planning, implementation, maintenance)

Introduction:

An indirect Bedload Monitoring System (BMS) is developed for bedload transport monitoring in the vortex tube system installed in the headwater channel of the FIThydro case study hydropower plant (HPP) Schiffmühle. The BMS allows the quantitative assessment of bedload transport in rivers, torrents and hydraulic sediment diversion structures. The measurements support the evaluation of bedload continuity across hydropower plants or other hydraulic structures.

The BMS consists of two passive acoustic sensors, i.e. a geophone (GS-20DX manufactured by Geospace Technologies, Houston TX, USA) and an accelerometer (ICP352C03 manufactured by PCB Piezoelectronics, Depew NY, USA), mounted to an impact plate in a watertight housing (Figure 44a). These sensors do not directly measure bedload transport but register the vibration signals of the impact plate, i.e. oscillations induced by the impingement of passing bedload particles. In the case study HPP, the impact plate is the steel wall of the vortex tube (Figure 44a). The vibration signal output of both sensors is a voltage that is sampled at a frequency of f_s = 51.2 kHz. The raw signals are then transmitted and further processed (Figure 44b, c).

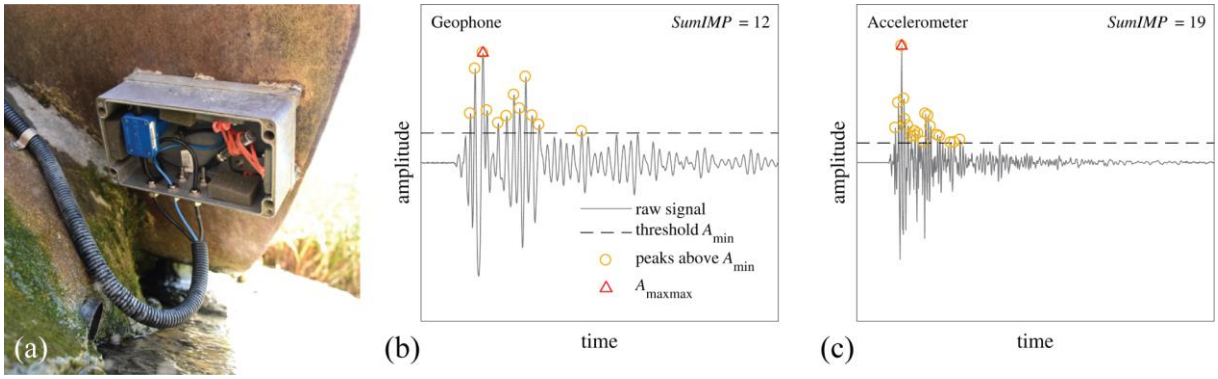


Figure 44. (a) Geophone and accelerometer installed in a watertight housing mounted on an impact plate and exemplary (b) geophone and (c) accelerometer signal of the identical single grain impact. SumIMP denotes the total number of peaks above the threshold amplitude A_{min} for the event shown. A_{maxmax} is the maximum amplitude registered during this event. Only positive amplitude values are considered.

The BMS presented here is similar to the Swiss Plate Geophone System (SPGS) (Rickenmann *et al.* 2012) but includes an additional accelerometer sensor to expand the range of frequencies and hence the potentially detectable particle sizes compared to the SPGS.

The maximum amplitude recorded during a bedload transport event can be related to the maximum grain diameter. Additionally, the sum of impulse counts above a certain amplitude threshold can be related to the transported bedload volume. Both relations are BMS setup- and site-dependent and therefore, a calibration is required to correlate the recorded impact signals to known bedload transport rates, often obtained from traditional bedload sampling (Rickenmann *et al.* 2012). If possible, a calibration in a laboratory flume as well as in the field setting is recommended (Gray *et al.* 2010, Rickenmann *et al.* 2014, Wyss *et al.* 2016a, Wyss *et al.* 2016b, Albayrak *et al.* 2017).

Application:

Within the scope of FIThydro, a BMS consisting of a geophone and accelerometer was installed on the vortex tube at HPP Schiffmühle, which diverts bedload from the headwater channel to the residual flow reach. The vortex tube consists of a steel tube embedded in the side weir, connecting the two parallel channels (Figure 45). A gate valve is positioned in the side weir, which opens automatically when a predefined discharge is exceeded. The opening of the valve automatically triggers the BMS measurements.

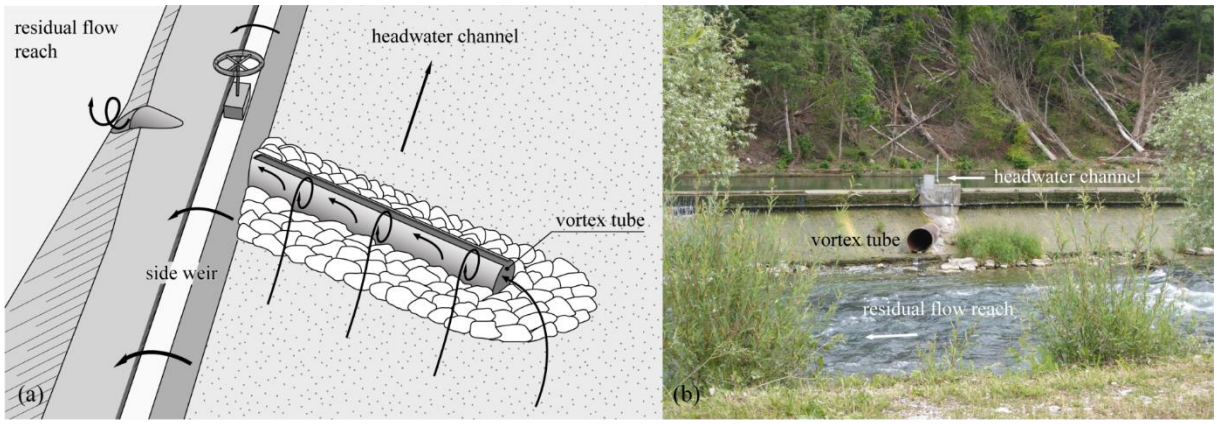


Figure 45. (a) Conceptual sketch of the vortex tube functionality and (b) vortex tube outlet at HPP Schiffmühle (source: VAW).

In contrast to the SPGS, the steel tube is used as an impact plate for the BMS and the sensors are mounted directly onto the outside of the steel tube (Figure 46). Therefore, laboratory calibration was not easily possible. Instead, the system was calibrated in the field by repeatedly dumping sediment samples of known grain size distribution and volume upstream of the vortex tube and subsequently flushing them to the residual flow reach. In addition, drop tests with single grains were performed when the vortex tube was not in operation. The single grain signals help to analyze the influence of grain size, grain form, drop height, and drop location on the amplitude and frequency signals.

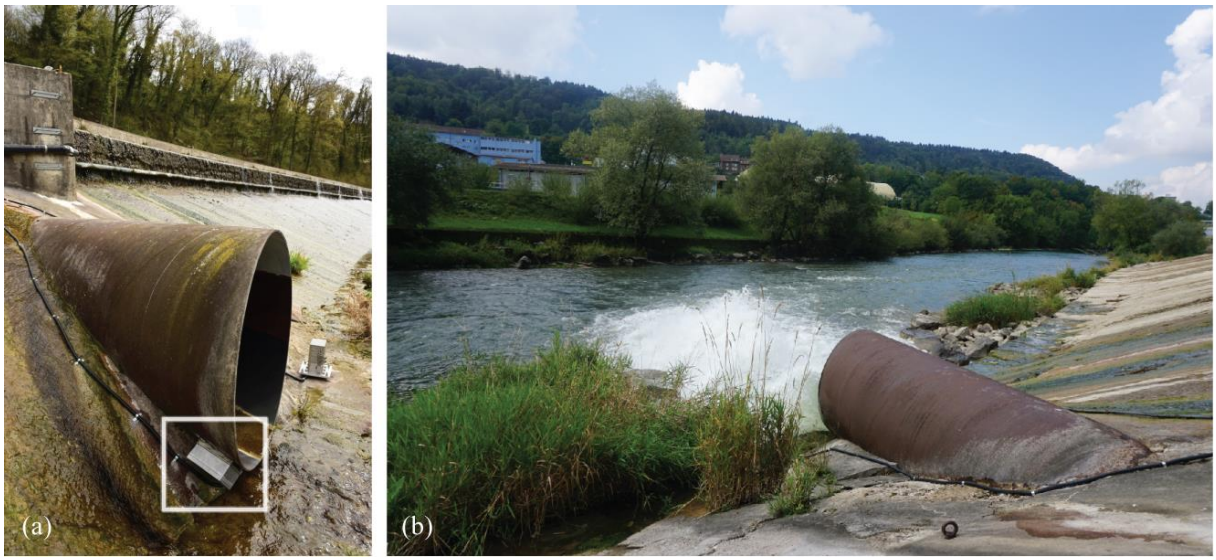


Figure 46. (a) Vortex tube outlet with mounted sensors and (b) vortex tube running during the field calibration (source: VAW).

The first results of the presented BMS are promising, but the data analysis will be further refined and extended. Furthermore, a larger number of recorded flood events is necessary to check the plausibility of the results obtained so far. Overall, it is demonstrated that the measurement principle of the state-of-the-art SPGS can be extended to non-standardized impact plates like steel vortex tubes, and the use of an additional accelerometer sensor, given that appropriate calibration measures are taken.

Other information:

The total costs for the geophone and accelerometer sensors amount to approx. 885-1'330 €. The costs for the field computer, the analog-digital-converter, and the 3G modem are approx. 5'300-6'200 €. Additional costs for the installation, data transmission, and the calibration depending on the site conditions and set-up.

References:

Albayrak, I., Müller-Hagmann, M., Boes, R.M. (2017). Calibration of Swiss Plate Geophone System for bedload monitoring in a sediment bypass tunnel. In *Proc. 2nd Intl. Workshop on Sediment Bypass Tunnels* (Sumi, T., ed.), paper FP16, Kyoto University, Kyoto, Japan

Gray, J.R., Laronne, J.B., Marr, J.D.G. (2010). Bedload-surrogate Monitoring Technologies, *US Geological Survey Scientific Investigations Report 2010-5091*. US Geological Survey: Reston VA.

Rickenmann, D., Turowski, J.M., Fritschi, B., Klaiber, A., Ludwig, A. (2012). Bedload transport measurements at the Erlenbach stream with geophones and automated basket samplers. *Earth Surface Processes and Landforms*, 37, 1000-1011.

Rickenmann, D., Turowski, J.M., Fritschi, B., Wyss, C., Laronne, J., Barzilai, R., Reid, I., Kreisler, A., Aigner, J., Seitz, H., Habersack, H. (2014). Bedload transport measurements with impact plate geophones: comparison of sensor calibration in different gravel-bed streams. *Earth Surface Processes and Landforms*, 39, 928-942.

Wyss, C.R., Rickenmann, D., Fritschi, B., Turowski, J.M, Weitbrecht, V., Boes, R.M. (2016a). Laboratory flume experiments with the Swiss plate geophone bed load monitoring system: 1. Impulse counts and particle size identification. *Water Resources Research*, 52, 7744-7759.

Wyss, C.R., Rickenmann, D., Fritschi, B., Turowski, J.M, Weitbrecht, V., Boes, R.M. (2016b). Laboratory flume experiments with the Swiss plate geophone bed load monitoring system: 2. Application to field sites with direct bed load samples. *Water Resources Research*, 52, 7760-7778.

Contact information:

Authors	Cristina Rachelly (VAW, ETHZ), Ismail Albayrak (VAW, ETHZ)
Reviewers	Robert Boes (ETHZ)

2.16. Shelter Measurements

Developed by: A. G. FINSTAD

Type: tool

Introduction:

The technique was developed by Finstad to estimate the shelter availability for juvenile salmon (Finstad et al. 2007a). In this stage of their life cycle, the salmon seeks shelter in the free spaces of the upper layers of the river bed sediment (Figure 47). The existence and size of such openings to be used as shelter is measured with the described technique. It is relatively easy to be carried out in the field. The method is based on the idea to mimic the small fish by using a plastic tube which has the approximate diameter of such a fish.

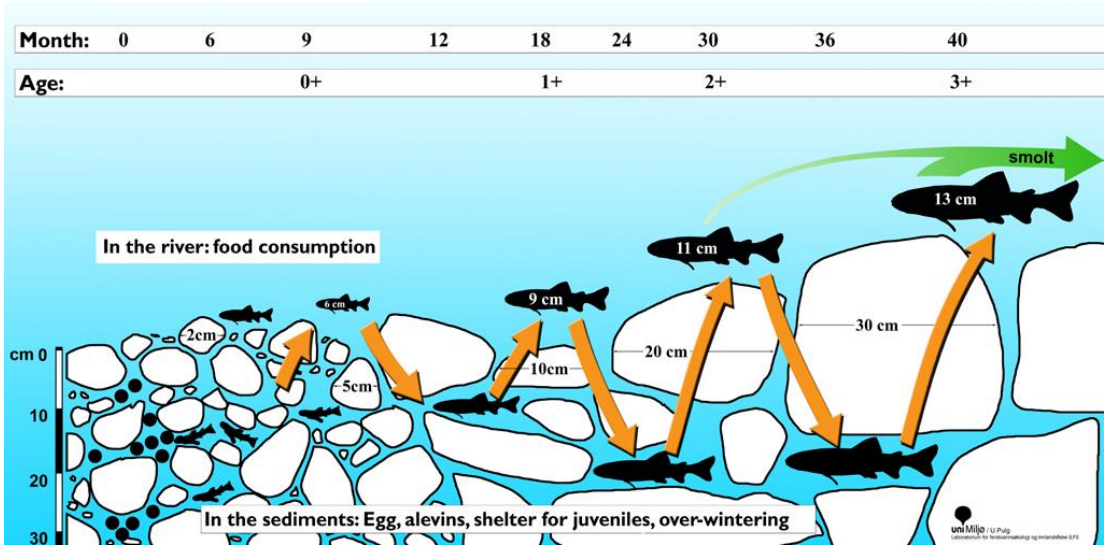


Figure 47: Juvenile salmon in the upper layers of river bed sediment (Forseth et al., 2014).

For salmon Finstad used tubes with five different diameters (5, 10, 13, 16, 22 mm). As a result of their experiments Forseth et al. (2014) suggest the use of a 13mm tube to conduct the tests in an area of about 0.25m^2. The tube is marked according to the three different shelter categories at lengths of 2, 5 and 10 cm to be able to detect certain possible hiding depths. Within the fixed framed area one is aiming to find every hole or opening where one can stick the tube into. The length of the tube (defined by the three rings) which is not visible any more, defines the potential hiding depth (Figure 48).

The post-processing of the data is quite simple and described in the following section.



Figure 48: Exemplarily shown hiding depth of 2cm (first marker covered) on a tube.

In FIThydro this technique shall be applied also to other fish species than the salmon. Therefore we use in addition tubes with diameters of 5 mm and 8 mm.

These results can then be linked to the D5 and D10 grain diameter of the sediment (Szabo-Meszaros et al 2016).

The method was developed in and for Norwegian rivers with large grain sizes. It is currently (also in FIThydro) under investigation if, when using it in rivers with a smaller D50, i.e. smaller grain sizes, this relation still applies or another relation becomes relevant.

Application:

For the measurement the following material is needed:

- one tube with a diameter of 13 mm and marks (rings) at 2, 5 and 10 cm
- one frame (metal or wood) to define the size of the area to be counted on
- something to take notes

The hiding depth thresholds are defined as 2, 5 and 10 cm and often named as class S1 (2 cm – 5 cm), class S2 (5 cm – 10 cm) and class S3 (> 10 cm).

It is recommended that the same person is carrying out the counting, to minimize the human based systematic error as much as possible.

When all values are collected in the field, the counted numbers for the different classes / hiding depth per spot are weighted using the following empirical formula described in Forseth et al (2014):

S1 + S2 x 2 + S3 x 3

Based on the following matrix the shelter availability can be defined:

Table 1: shelter availability depending on the number of shelter available

Shelter Class	Low	Moderate	High
Values for weighted shelter	< 5	5 – 10	> 10

References:

Finstad, A.G., Einum, S., Forseth, T., Ugedal, O., 2007a. Shelter availability affects behaviour, size-dependent and mean growth of juvenile Atlantic salmon. Freshwater Biology 52, 1710–1718. https://doi.org/10.1111/j.1365-2427.2007.01799.x

Finstad, A.G., Forseth, T., Ugedal, O., N?Sje, T.F., 2007b. Metabolic rate, behaviour and winter performance in juvenile Atlantic salmon. Functional Ecology 21, 905–912. https://doi.org/10.1111/j.1365-2435.2007.01291.x

Forseth, T., Harby, A., Ugedal, O., Pulg, U., Fjeldstad, H.-P., Robertsen, G., Barlaup, B.T., Alfredsen, K., Sundt, H., Salveit, S.J., Skoglund, H., Kvingedal, E., Sundt-Hansen, L.E.B., Finstad, A., Einum, S., Arnekleiv, J.V., 2014. Handbook for environmental design in regulated salmon rivers (NINA temahefte No. 53). Norsk institutt for naturforskning, Trondheim, Norway.

Szabo-Meszaros, Marcel, Rüther, N., Alfredsen, K., 2016. Correlation between the shelter of juvenile salmonids and bed substrate, in: Wieprecht, S., Haun, S., Weber, K., Noack, M., Terheiden, K. (Eds.), River Sedimentation: Proceedings of the 13th International Symposium on River Sedimentation (Stuttgart, Germany, 19-22 September, 2016).

Valdimarsson, S.K., Metcalfe, N.B., 1998. Shelter selection in juvenile Atlantic salmon, or why do salmon seek shelter in winter? Journal of Fish Biology 52, 42–49. https://doi.org/10.1111/j.1095-8649.1998.tb01551.x

Contact information:

Authors	Kordula Schwarzwälder (NTNU)
Reviewers	Robert Boes (ETHZ)

2.17. GNSS – Global Navigation Satellite Sytem

Developed by: USA, EU, China, Russia

Type: method

Introduction:

GPS is often used as a synonym for all of the different systems

System	BeiDou	Galileo	GLONASS	GPS
Owner	China	European Union	Russia	United States
Coverage	Regional, global by 2020	Global by 2020	Global	Global
Status	basic service by 2018 to be completed by H1 2020	operating since 2016 2020 completion	Operational	Operational
Precision	10m (Public) 0.1m (Encrypted)	1m (Public) 0.01m (Encrypted)	4.5m – 7.4m	15m (no DGPS or WAAS)

Figure 49: Different systems called as GPS.

Application:

GNSS systems are used to georeferenced measurements. It is usually used in connection with other systems, such as ADCP, Drones, devices for monitoring fish migration, and other devices where the exact location is important.

It is important to be aware of the accuracy of the GNSS data and if it fits the measurement. For bathymetry measurements it is recommended to have accuracy within a few cm, while discharge measurements can be done with accuracy at the submeter level.

There are mainly three different types of GNSS accuracy:

1) Standard, such as in cell phones and car navigation. The accuracy lies within 3-5 m horizontally and 5-20 m vertically. These systems don't receive any correction signal.
2) Advanced receivers, usually referred to as "differential GPS". These are used in most scientific instruments. The accuracy lies below 1 m horizontally and 2 m vertically.
3) RTK-GPS need an internet connection to receive a correction signal. This usually is a real time signal (RTK = Real Time Kinematic), but it is also possible to get the correction for post processing.



Figure 50: Differential GPS mounted on a remote-controlled boat for bathymetry and discharge measurements.



Figure 51: RTK-GPS for single point measurements at very high accuracy (< 1 cm).

Other information:

General accuracy is depending on

- Number of satellites / selective availability
- Angle between the satellites = Dilution of Precision (DOP)
- Reflection from buildings/obstacles = multipath error
- Atmospheric conditions

Only the last point, the atmospheric conditions, can be corrected with the differential and RTK GPS.

References:

https://eos-gnss.com/elevation-for-beginners

https://www.e-education.psu.edu/geog862/node/1828

https://gisgeography.com/gps-accuracy-hdop-pdop-gdop-multipath/

Contact information:

Authors	Markus Peter Först (SWECO), Wolf Dietrich Marchand (SWECO)
Reviewers	Robert Boes (ETHZ)

2.18. iRon Differential pressure sensor base artificial lateral line probe

Developed by: Centre for Biorobotics

Date: 01/11/2016

Type: Tool (device)

Suitable for mitigation related to fishway attraction flows, fish habitats and hydropeaking for the planning, implementation, maintenance phases.

Introduction:

“iRon” is a device that mimics the lateral line sensory system used by fish in nature (artificial lateral line) and that allows the characterization of flow fields from a fish perspective. First artificial lateral lines were developed to provide sensing capabilities to small underwater robots (EU project FILOSE, 2009-2012 [1]) and they were further developed for environmental monitoring in BONUS FishView project (2013-2016) [2].

In contrast to conventional flow measuring devices (such as ADVs, propellers, etc.), they are streamlined bodies which record the spatial distribution of fluid-body interactions at a sampling rate close to that of the sensory organs (up to 400 Hz in the latest designs). From these records, point-based hydrodynamic parameters such as velocity or turbulence metrics can be estimated, but also body-oriented metrics (“flow asymmetry”).

iRon belongs to a new generation of artificial lateral lines where an increase of sensitivity is achieved by the use of differential pressure sensors. It consists of a 0.22 m long NACA025 streamlined body, which measures the pressure gradients simultaneously using six differential pressure sensors (±2000 Pa MPXV7002). In addition, the water depth is measured by the probe using an absolute pressure sensor (0 to 10000 Pa – MPX5010GP) (Figure 52).

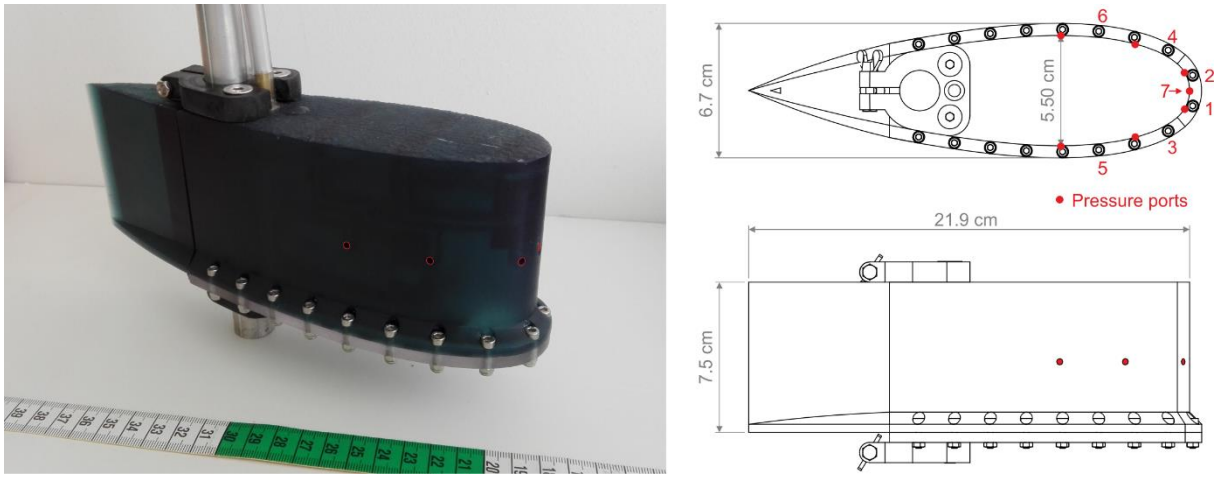


Figure 52. iRon, the lateral line probe (LLP). NACA0025 body shape.showing the locations of the differential pressure sensors (1-6), and the absolute pressure sensor (7) [3].

Application:

Artificial lateral lines have been successfully applied to estimate flow variables such as velocity [4]–[7] turbulence [4], [5] and also for hydrodynamic classification [8], [9] (Figure 53).

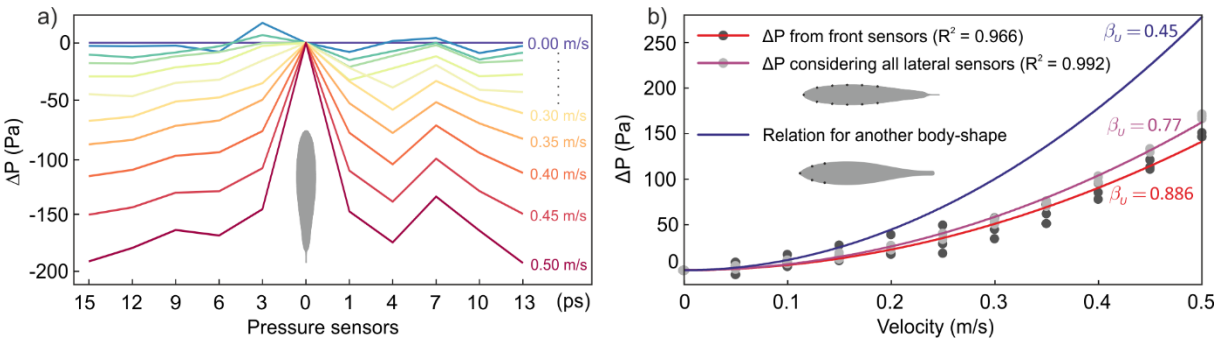


Figure 53.Velocity estimation with an artificial lateral line. a) Distribution of pressure over the body of the lateral line. b) Estimation of velocity considering different pressure differences around the body and different shapes [4].

iRon was specially developed for FIThydro project and was designed to conduct biological assessments. The device has been successfully applied to study fish habitats and their spatial preferences [10] as well as to analyze fish's behavioural responses [3]. To achieve this, the raw data of iRon is translated into body-oriented metrics, mean pressures sensed by the body, pressure fluctuations around the body or asymmetries around the body [10].

In fishways, iRon has shown the potential of characterizing the spatial preferences of fish under variable hydrodynamic scenarios (Video 2) better than standard technologies such as ADV [10]. Among other, this seems to be induced by the higher dimensionality of the iRon that may aid in improving the characterization of fish's hydraulic preferences.

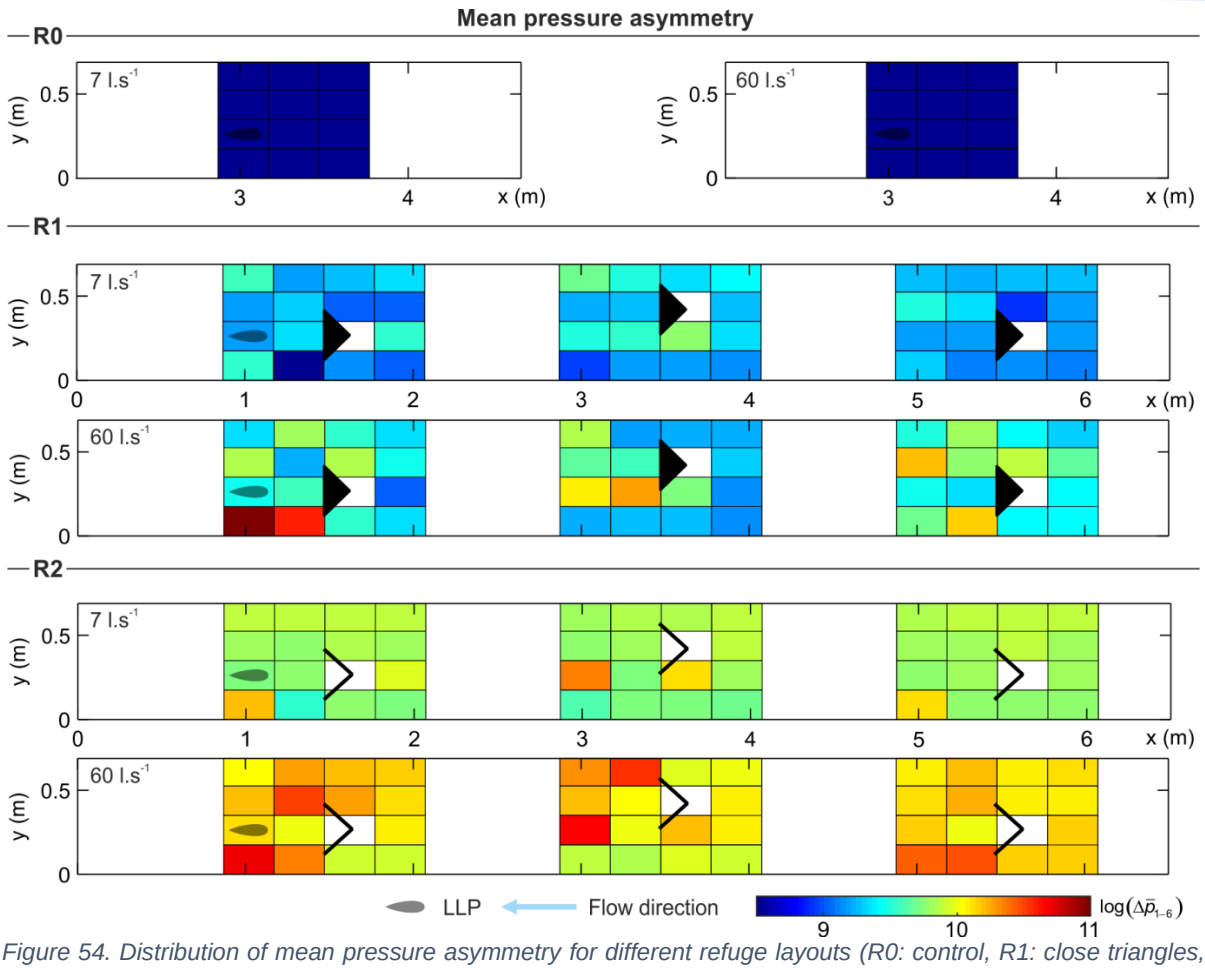


Figure 54. Distribution of mean pressure asymmetry for different refuge layouts (R0: control, R1: close triangles, and R2: open triangles) and hydrodynamic scenarios [3].

Another application of iRon has been the characterization of hydrodynamic signatures generated by different refuge structures under hydropeaking scenarios to after analyse fish behavioural responses [3] (Figure 54). This study, among other results, demonstrated the importance of asymmetric flows in the refugee selection by fish, which generates a unique signature in iRon for each scenario and configuration.

All the characterizations so far have been elaborated considering mean differential pressure recorded by the flow, mean fluctuations of differential pressure and mean asymmetries between both sizes of the body [3], [10]. However, the available data can be further exploited, for instance considering the frequency domains of the recorded signals.

Other information:

iRon is available for use by interested researchers at no cost. Please contact staff at the Centre for Biorobotics for additional information.

References:

[1] "https://cordis.europa.eu/project/rcn/89451/factsheet/en." .

[2] "https://www.bonusportal.org/projects/innovation_2014-2017/fishview."

[3] M. J. Costa, J. F. Fuentes-Pérez, I. Boavida, J. A. Tuhtan, and A. N. Pinheiro, "Fish under pressure: examining behavioural responses of Iberian barbel under simulated hydropeaking with instream structures," *PLoS One*, vol. 14, no. 1, 2019.

[4] J. F. Fuentes-Pérez, J. A. Tuhtan, R. Carbonell-Baeza, M. Musall, G. Toming, N.

Muhammad, and M. Kruusmaa, “Current velocity estimation using a lateral line probe,” *Ecol. Eng.*, vol. 85, pp. 296–300, 2015.

[5] K. Chen, J. A. Tuhtan, J. F. Fuentes-Pérez, G. Toming, M. Musall, N. Strokina, J.-K. Kämäräinen, and M. Kruusmaa, “Estimation of flow turbulence metrics with a lateral line probe and regression,” *IEEE Trans. Instrum. Meas.*, vol. 66, no. 4, pp. 651–660, 2017.

[6] N. Strokina, J.-K. Kamarainen, J. A. Tuhtan, J. F. Fuentes-Perez, and M. Kruusmaa, “Joint Estimation of Bulk Flow Velocity and Angle Using a Lateral Line Probe,” *Instrum. Meas. IEEE Trans.*, vol. 65, no. 3, 2016.

[7] J. F. Fuentes-Pérez, K. Kalev, J. A. Tuhtan, and M. Kruusmaa, “Underwater vehicle speedometry using differential pressure sensors: Preliminary results,” in *IEEE/OES AUV*, 2016, p. 6.

[8] J. A. Tuhtan, N. Strokina, G. Toming, N. Muhammed, M. Kruusmaa, and J.-K. Kämäräinen, “Hydrodynamic classification of natural flows using an artifical lateral line and frequency domain features.,” in *E-proceedings of the 36th IAHR World Congress*, 2015.

[9] J. A. Tuhtan, J. F. Fuentes-Pérez, G. Toming, M. Schneider, R. Schwarzenberger, M. Schletterer, and M. Kruusmaa, “Man-made flows from a fish’s perspective: autonomous classification of turbulent fishway flows with field data collected using an artificial lateral line,” *Bioinspir. Biomim.*, 2018.

[10] J. F. Fuentes-Pérez, M. Eckert, J. A. Tuhtan, M. T. Ferreira, M. Kruusmaa, and P. Branco, “Spatial preferences of Iberian barbel in a vertical slot fishway under variable hydrodynamic scenarios,” *Ecol. Eng.*, vol. 125, pp. 131–142, Dec. 2018.

Contact information:

Authors	Jeffrey Tuhtan (TUT), Juan Fuentes (TUT)
Reviewers	Robert Boes (ETHZ)

2.19. Barotrauma Detection System

Developed by: Centre for Biorobotics, Tallinn University of Technology

Date: 2019.02.15

Type: Tool (device)

Suitable for fish downstream migration, planning, implementation:

Introduction:

The BDS sensor housing consists of two POM plastic end caps and a 4 cm outer diameter polycarbonate plastic tube, with a total length of 14 cm, and mass of 150 g (Figure 55). Neutral buoyancy of the BDS is achieved by estimating the water temperature during deployment (±5 °C) and manually adjusting the length of the sensor by screwing the flat end cap inwards or outwards to modify the total sensor volume. Each hemispherical end cap contains three digital total pressure transducers (MS5837-2BA, TE Connectivity, Switzerland) have a sensitivity of 0.0021 kPa (0.21 mm water column) and are linearly rated for 25 m of water depth, and can be used up to 45 m of water depth using a non-linear correction based on laboratory calibration. Each pressure transducer is equipped with its own on-chip temperature sensor, allowing for all pressure readings to include real-time temperature correction using a 2nd order algorithm. All sensors were tested against a HOBO reference pressure sensor under static and dynamic conditions in a laboratory barochamber. The BDS employs a high-speed digital sampling architecture with a 400 kHz clock rate.

All BDS units are equipped with an atmospheric auto-calibration algorithm. All three transducers are set to a default value of 100 kPa (1000 mbar) at local atmosphere. All sensors are therefore auto-calibrated to local changes in atmospheric pressure which occur during the day, directly before each field deployment. This feature removes the necessity of manually correcting pressure sensor readings.

The BDS units use three pressure sensors for two reasons. The first is to ensure repeatable field measurements with increased fault tolerance. The BDS uses Triple Modular Redundancy (TMR) by including a pressure sensor array in lieu of a single pressure sensor, whose error and failure cannot be controlled during deployment [1]. The second is that multiple sensors allow for the detection of pressure gradients during passage, which may correspond to regions of high shear.

In addition to the three pressure transducers, the BDS sensor also contains a digital 9 degree of freedom inertial measurement unit (IMU) model BNO055 (Bosch Sensortec, Germany) integrating linear accelerometer, gyroscope and magnetometer sensors. In contrast to existing barotrauma sensors, which require extensive post-processing to providing real-time absolute orientation at 100 Hz. The device uses proprietary (Bosch Sensortec, Germany) sensor fusion algorithms to combine the linear accelerometer, gyroscope and magnetometer readings into the body-oriented Euler angles.

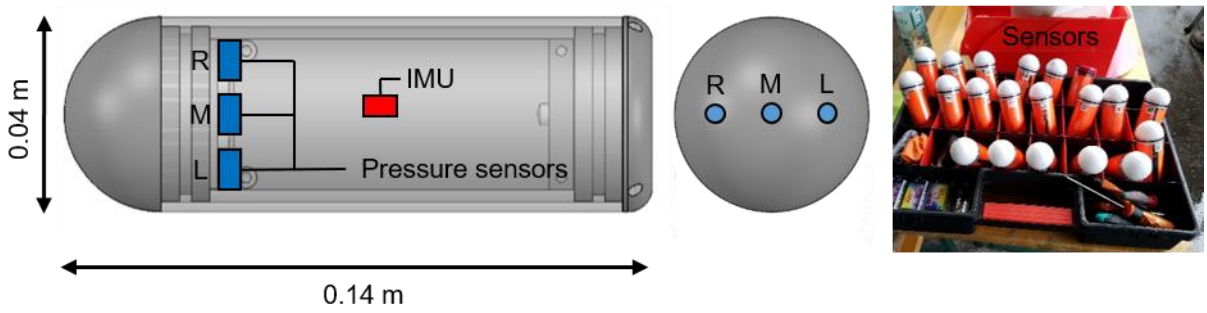


Figure 55: Schematic and dimensions of the BDS, showing the locations of the three pressure transducers and the Inertial Measurement Unit (IMU). Left: side-view of sensor. Right: top-view facing the cap showing the left (L), middle (M) and right (R) pressure ports.

Application:

The sensors are turned on by activating the magnetic switch. Afterwards, they are deployed into the water where they travel through the hydropower plant (Figure 56). Balloon tags inflate, bringing the sensors to the surface, where they are recovered by boat. The data are saved as text files and can be imported into Excel, R, MATLAB and other commonly used software for processing and visualization.

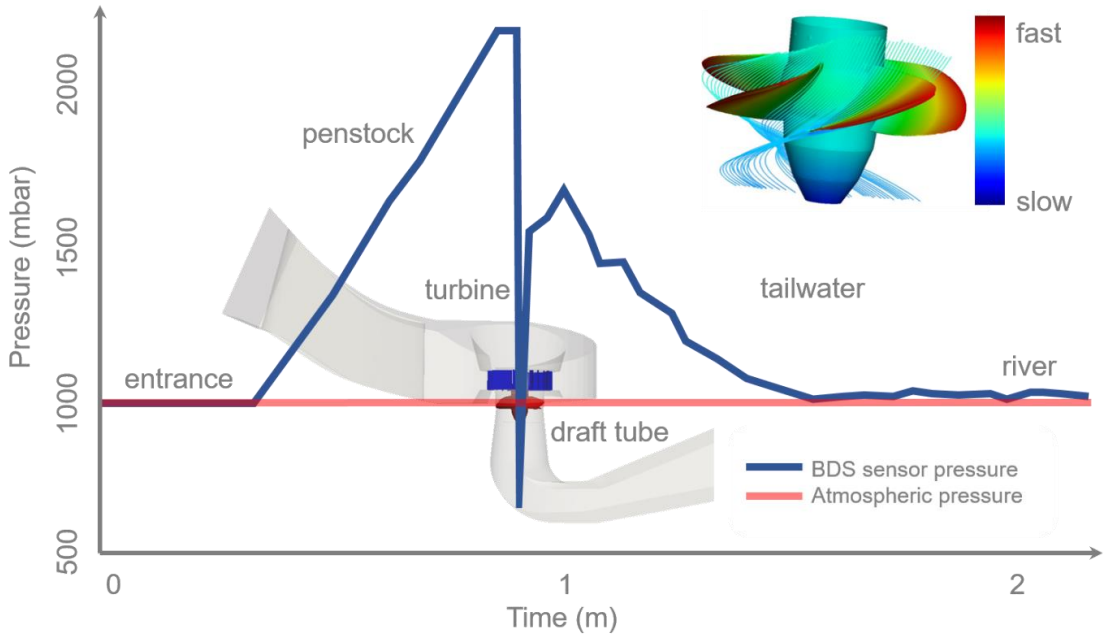


Figure 56: Time series plot and overlay of a vertical Kaplan turbine, showing the pressure change as measured by the BDS as it passes through a hydropower plant (turbine illustration courtesy of cfdsupport.com).

Other information:

The cost of each sensor is 500 EUR. Tests at 5 case study sites have shown that an average of 120 data sets per day can be recovered for each hydropower plant operational scenario (e.g. full load, ½ load).

Table 2: Technical specifications of the commercial ATS Sensor Fish Model ARC800 and the BDS developed in the FITHydro project.

Physical and sensor specifications	**ATS Sensor Fish Model ARC800**	**FITHydro Barotrauma Detection System**
Physical dimensions	89.9 x 24.5 mm (fixed)	143 + 1.25 x 40 mm (adjustable)
Density	1 mg / mm³ (fixed)	1.0 mg / mm³ (adjustable)
Excess mass (wet weight)	0.5 g	+/- 1.15 g
Sensor sampling rate	2048 Hz (analog)	400 kHz (digital), saved at 100 or 250 Hz
Maximum sampling time	4 min	240 min
3D acceleration	0 – 200 g	+/- 16 g
3D rotational velocity	0 – 2000 °/s	+/- 2067 °/s
Pressure	0 - 1399.64 kPa (1 sensor) accuracy: +/- 1.4 kPa	0 - 2941 kPa (3 sensors) accuracy: 0.1 kPa
Temperature sensor	-40 - 125 °C (separate sensor for temperature correction)	-20 - 85 °C (temperature correction on each pressure sensor)

References:

[1] Reddy PV, Nayak M, Rajanna K. 2007 MEMS based pressure sensor with triple modular redundancy. In *Sensors, 2007 IEEE*, pp. 919–921. IEEE

Contact information:

Authors	Jeffrey Tuhtan (TUT)
Reviewers	Robert Boes (ETHZ)

2.20. Dilution Gauging

Type: Method

Suitable for pool type fishway during maintenance

Introduction:

This method requires the release of a known tracer concentration in a section of the river or fishway and the subsequent determination of the tracer concentration in a downstream section. It is based on the dilution relationships between the injection of the tracer and the discharge we want to know. There are two main different methods for the injection of the tracers into the flow: (a) instantaneous or integration method and (b) continuous method.

The discharge for (a) is calculated as:

$$Q = \frac{c_0}{c} \cdot \frac{V}{T}$$

Being c_0 the tracer concentration which is introduced in the watercourse with discharge Q. c is the concentration of the sample in volume V and T is equal to the time needed for the tracer to be transported downstream.

The formulae discharge for (b):

$$Q = q.\frac{c_1}{c_2}$$

Being c_1 the tracer concentration in the injection, q the constant injection flow for the tracer (e.g. using a Mariotte device) and c_2 the tracer concentration at the downstream point.

The choice of the tracer depends on several factors: the chemical characteristics of the water, the suspended sediment, the distance between the injection and measuring section, the type of flow to be measured, the sensitivity of the tracer measurement devices and the possible environmental impact of the tracer. Common tracers used: chemical (NaCl, NaI, NH4Cl) and fluorescent (fluorescein and Rhodamine WT).

It is important to verify some conditions: the tracer cannot be absorbed in the medium and the solution must be well mixed. Emphasizing the last one, it is necessary to assure the good mixing length, which is the distance between the injection and measure sections ensuring a stable concentration of the diluted tracer.

Application:

Experiences of ITAGRA-GEA measuring discharge through dilution gauging

This method has been used for ITAGRA-GEA to measure discharge into the fishways (Bravo-Córdoba y Sanz-Ronda, 2011; Fuentes-Pérez et al., 2016 and 2017; Sanz-Ronda et al., 2016; Bravo-Córdoba et al., 2018). One of the main aims was to improve the accuracy of the discharge coefficients related to technical fishways into the field. It was done through the continuous method, using Rodamine WT as a tracer and a portable fluorometer to measure the fluorescence of the samples (Figure 57).



Figure 57: Dilution gauging in a fishway. Left: making the dilution of the tracer (Rhodamine Wt). Right. Mariotte device for the continuous injection into the fishway.

References:

ISO 9555:1994. Measurement of liquid flow in open channels — Tracer dilution methods for the measurement of steady flow

Tazioli, A. (2011). Experimental methods for river discharge measurements: Comparison among tracers and current meter. Hydrological Sciences Journal – Journal des Sciences Hydrologiques. 56. 1314-1324.

Bravo-Córdoba FJ, Sanz-Ronda FJ. 2011. Evaluación de la eficiencia biológica de una escala de hendiduras verticales para la trucha autóctona (*Salmo trutta* L.) en la Cuenca del Duero. Master's thesis. University of Valladolid, Spain.

Bravo-Córdoba FJ, Sanz-Ronda FJ, Ruiz-Legazpi J, Celestino LF, Makrakis S. 2018. Fishway with two entrance branches: Understanding its performance for potamodromous Mediterranean barbels. Fisheries Management and Ecology 25(1): 12–21.

Fuentes-Pérez JF, Sanz-Ronda FJ, Martínez de Azagra-Paredes A, García-Vega A, Martínez de Azagra A, García-Vega A. 2016. Nonuniform hydraulic behavior of pool-weir fishways: a tool to optimize its design and performance. Ecol Eng 86: 5–12.

Fuentes-Pérez JF, García-Vega A, Sanz-Ronda FJ, Martínez de Azagra Paredes A. 2017. Villemonte's approach: a general method for modelling uniform and non-uniform performance in stepped fishways. Knowl. Manag. Aquat. Ecosyst., 418, 23.

Sanz-Ronda FJ, Bravo-Córdoba FJ, Fuentes-Pérez JF, Castro-Santos T. 2016. Ascent ability of brown trout, Salmo trutta, and two Iberian cyprinids− Iberian barbel, Luciobarbus bocagei, and northern straight-mouth nase, Pseudochondrostoma duriense− in a vertical slot fishway. Knowledge and Management of Aquatic Ecosystems (417): 10.

Contact information:

Authors	Francisco Javier Bravo (ITAGRA)
Reviewers	Robert Boes (ETHZ)

2.21. Acoustic Doppler Current Profiler - ADCP

Developed by: Various Companies

Type: Device

Suitable for flow velocity, turbulent characteristics, discharge, bathymetry and sediment transport measurements in rivers, lakes, reservoirs and oceans in all phases (planning, implementation, maintenance).

Introduction:

Acoustic Doppler Current Profiler (ADCP) allows quick, easy and accurate measurements of 3D velocity time series and bathymetry, and computation of discharges in rivers, estuaries, lakes and reservoirs as well as oceans. ADCP data can be used for calibration of numerical models, hydraulic studies (for example, flow field around hydraulic structures), habitat quality assessment and modelling, hydro-morphologic surveys and sediment studies.

The ADCP is equipped with multi-beams (three up to nine beams, Figure 58), which emit acoustic energy at a known frequency and record the frequency of the acoustic energy backscattered by the particles in the water column. The velocity of the water flow along each beam is computed based on the change in the frequency of the emitted and backscattered acoustic energy, i.e. the Doppler shift. Detailed information on the ADCP working principle and its limitations are described by Simpson (2002). The ADCP beams are positioned to 20 or 30 degree away from the vertical axis. By using a simple trigonometry, 3D velocity components are computed from the Doppler shifts measured with three or four sonar beams. In the latter, a redundant, fourth beam is used to compute error velocity, which is the difference between a velocity measured by one set of three beams and a velocity measured by another set of three beams at the same time (Simpson, 2002). The error velocity is used to evaluate the assumption of horizontal homogeneity. The frequency of the ultrasonic sound transmitted by commercially available ADCPs ranges from 30 kHz to 3000 KHz (Simpson, 2002). ADCP can be used at a fixed position, i.e. stationary, or mounted to a tethered boat, manned boat or a remote-controlled boat (Mueller et al., 2013). Non-stationary i.e. moving boat ADCP measurements yield the flow velocity and direction relative to the boat and hence the velocity of the boat should be accounted for by using either bottom tracking or global positioning system (GPS) to determine true flow velocity.

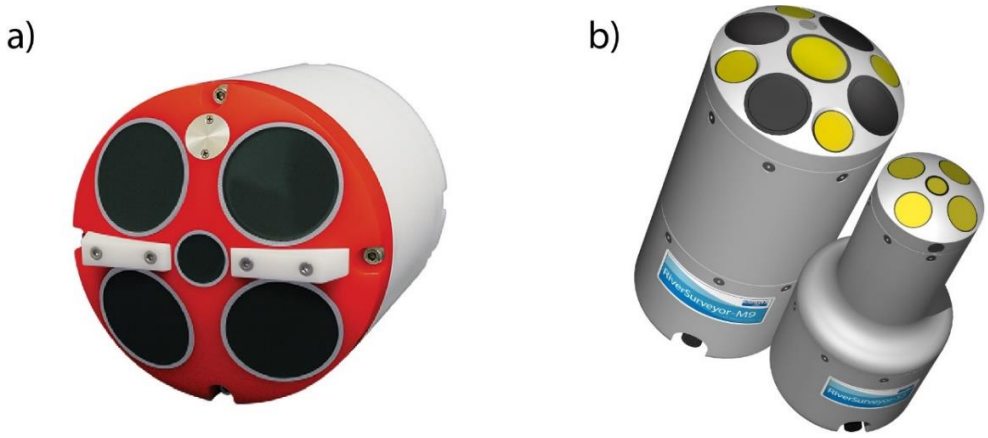


Figure 58. Exemplary ADCPs: (a) Teledyne RiverPro with 5 beams (credit: http://www.teledynemarine.com) and (b) Sontek M9 with 9 beams and S5 with 5 beams (credit: https://www.sontek.com).

Application:

Within the scope of FIThydro, high resolution 3D velocity, as well as bathymetry measurements, have been conducted using an ADCP mounted on a high speed remote-controlled boat at two hydropower plants (HPP) in Switzerland since the beginning of 2018. The models of the ADCP and the boat are River Pro 1200 kHz including piston style four-beam transducer with a 5th, independent 600 kHz vertical beam and Q-Boat purchased from Teledyne Marine, USA, respectively (Figure 59a). An external Differential GPS (DGPS) system from A326 AtlasLink (Hemisphere) was used to accurately measure the positions of the ADCP. One set of the battery for the Q-boat allowed us to make measurements for 4 hours up to 10 hours depending on the flow velocity and field conditions i.e. temperature.

Compass calibration and moving bed tests are conducted before each ADCP measurement at the case study HPPs. The Test Case study HPP Schiffmühle is located on the 35 km long river Limmat between in Untersiggenthal and Turgi near Baden in Switzerland (see the Test Case presentation file for HPP Schiffmühle). Two transects of ADCP at each densely spaced cross-section along the river were enough but high accuracy of altitude data was required for the bathymetry measurements at the HPP and in general. The present DGPS system resulted in ±1m of errors in altitude measurements (Figure 59b, black line). Therefore, use of a total station, which is time consuming, or real-time kinematic (RTK) GPS is recommended to accurately determine water surface and hence bathymetry (Figure 59, red line from total station measurements).

Furthermore, the test results from the HPP Bannwil located on River Aare in canton Bern indicated that averaging of at least 8 transects or even more at each cross-section is needed to obtain robust and smooth velocity field and accurate discharge data at highly turbulent and 3D flows occurring in rivers, turbine inlet and outlets or other hydraulic structures (see the Test Case presentation file for HPP Bannwil).

The ADCP data from both HPPs Schiffmühle and Bannwil are post-processed according to the workflow sketched in Figure 60 using the software WinRiver II (Teledyne software) and velocity mapping toolbox (VMT, Matlab based software for processing and visualizing ADCP data provided by U.S. Geological Survey). Figure 61 shows the depth-averaged velocities at the HPP Bannwil plotted with VMT. VMT can be used with the output files from Sontek ADCPs. For further data analysis and presentation on the maps like river bed changes, Q-GIS (free software) or ARC-GIS (Commercial software) are also recommended.

The present system based on the remote-controlled boat platform has advantages over the tethered boat ADCP application. These are less man-power needed, faster and more measurements in a shorter time, no flow disturbance and interference with beams and smoother movement of the boat.

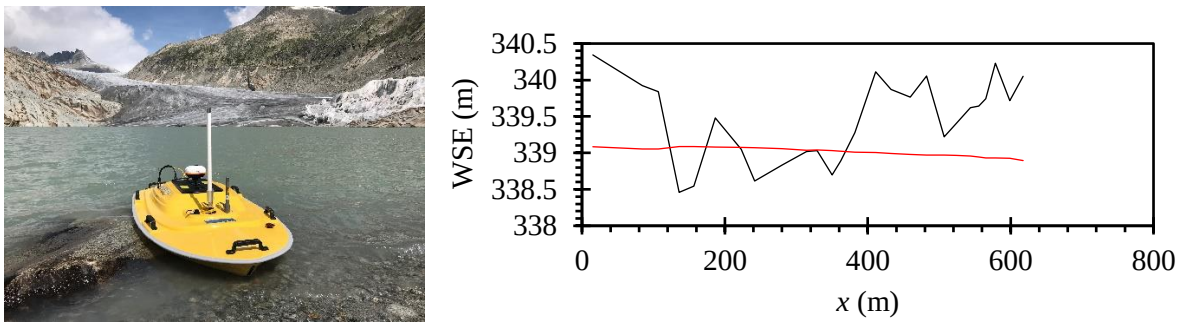


Figure 59. (a) Teledyne Marine Q-boat of VAW equipped with Riverpro ADCP and DGPS and (b) water surface elevation along the power canal of HPP Schiffmühle (black line: DGPS data and red line: total station data).

Back to D2.2 Main index

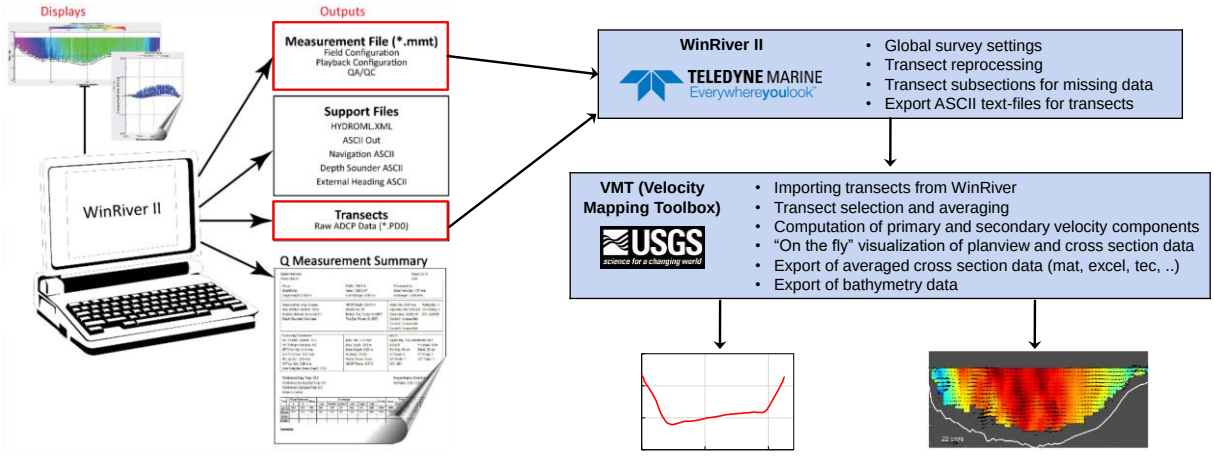


Figure 60: Workflow used for post-processing of ADCP data

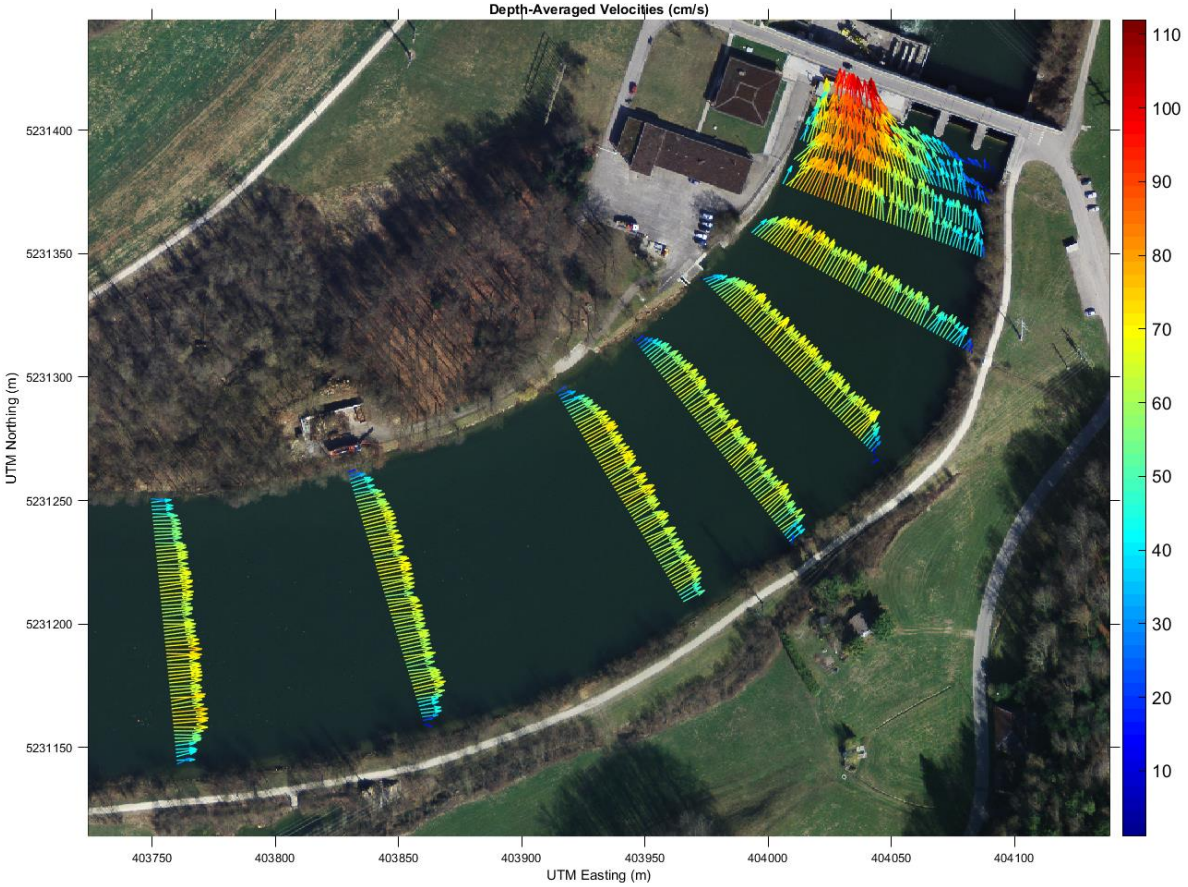


Figure 61: Depth averaged flow velocities upstream of the HPP Bannwil measured with the ADCP boat at a discharge of 402 m3/s (background image: © 2018 swisstopo (JD 100041)).

Other information:

The total costs for the Teledyne RiverPro 1200 kHz, Teledyne Q-boat and DGPS from Hemisphere Atlas link amount to approx. 22'000 €, 21'200 € and 3'340 € respectively. The costs of shipping, VAT, some mounting apparatus and long-range radio modem are excluded. For current costs of the equipment, we recommend to ask the corresponding supplier. Note

that Q-boat can also house Sontek RiverSurveyor M9. Furthermore, a rugged laptop for field use is recommended.

References:

Mueller, D.S., Wagner, C.R., Rehmel, M.S., Oberg, K.A., Rainville, F. (2013). Measuring discharge with acoustic Doppler current profilers from a moving boat (ver. 2.0, December 2013), U.S. Geological Survey Techniques and Methods, book 3, chap. *http://dx.doi.org/10.3133/tm3A22*.

Simpson, M.R. (2002). Discharge measurements using a broadband acoustic Doppler current profiler. Open-file Report 2001-1, https://doi.org/10.3133/ofr011.

Links to the suppliers of equipment:

Teledyne Marine, ADCP RiverPro:

http://www.teledynemarine.com/riverpro-adcp?ProductLineID=13

Teledyne Marine, Q-Boat:

http://www.teledynemarine.com/Lists/Downloads/Q-Boat_1800_Datasheet.pdf

Hemisphere Atlas DPS:

https://hemispheregnss.com/Atlas/atlaslinke284a2-gnss-smart-antenna-1226

Sontek ADCP M9,

https://www.sontek.com/riversurveyor-s5-m9

Software for ADCP data analysis:

Velocity Mapping Toolbox:

https://hydroacoustics.usgs.gov/movingboat/VMT/VMT.shtml

Q-GIS:

https://qgis.org/en/site/

ARC-GIS:

https://www.esri.com/en-us/arcgis/about-arcgis/overview

Contact information:

Authors	Ismail Albayrak (VAW, ETHZ)
Reviewers	Robert Boes (ETHZ)

2.22. Acoustic Doppler Velocimetry (ADV)

Developed by: Nortek, SonTek

Type: Device

Used for velocity measurement, thus suitable for use in all mitigation measures (habitat, environmental flow, sediments, downstream fish migration, and upstream fish migration) and phases (planning, implementation, maintenance).

Introduction:

Acoustic Doppler velocimetry (ADV) is a velocity measurement technique that allows for the measurement of 3D flow velocities by using the Doppler shift principle. ADV operates by emitting short acoustic pulses along a transmitter beam, the central transducer. As the sound bursts propagate through the water, a fraction of the acoustic energy is scattered back by ambient scatterers such as suspended sediments and microbubbles (Kraus et al. 1994, Lohrmann et al. 1995, McLelland & Nicholas 2000).

The ADV comprises a probe connected to the main housing, which contains the electronics, by either a rigid stem or a cable (Figure 62a, b and c). The main housing is connected to a computer by a cable. The sampling volume is located away from the probe (Figure 62d), which reduces the interference of the probe with the flow and measurement point. The reduced probe size also minimizes the flow interference. The probe consists of a transmitter and three or four receivers (Figure 62b and c), which are equally angled and symmetrically arranged around the transmitter (Khorsandi et al. 2012). The fourth receiver provides redundancy improving turbulence measurements. The transmitter emits ultrasound (short acoustic pulse) at a known frequency and the receivers get back the echo of ultrasound (sound-scattering particles) reflected in the water particles with a different frequency. The difference between the frequency emitted and reflected is proportional to water velocity.

The signal-to-noise ratio (SNR) is a measure of the scattering strength, representing the strength of the echo relative to the electronic noise level, and it is a central parameter in ADV operation (Kraus et al. 1994). The acoustic echoes originated at the sampling volume, defined by the intersection of the transmitter and receivers beams (Figure 62d), are detected by the receivers' transducers. The frequency of the echo is Doppler shifted according to the relative motion of the scatterers, assumed to be travelling with the velocity of the fluid flow. The Doppler shift observed at each receiver is proportional to the component of the flow velocity along the bisector of the receiver and transmitter beams. The radial or beam velocities are computed sequentially for each receiver and are then converted to a local Cartesian coordinate system (ux, uy, uz) by using a transformation matrix. This transformation matrix is determined empirically by the manufacturer by calibrating the system at one speed and will remain constant if the physical dimensions or geometry of the probe remain unchanged (Kraus et al. 1994, Lohrmann et al. 1995, McLelland & Nicholas 2000).

The ADV uses a dual pulse-pair scheme with different pulse repetition rates separated by a dwell time (McLelland & Nicholas 2000, García et al. 2005). The longer pair of pulses is used for higher precision velocity estimates while the shorter pulse is used for ambiguity resolution, assuming that the real velocity is beyond the limit resolvable by the longer time lag (García et al. 2005). The pulse repetition rates can be adjusted by choosing the instrument velocity range.

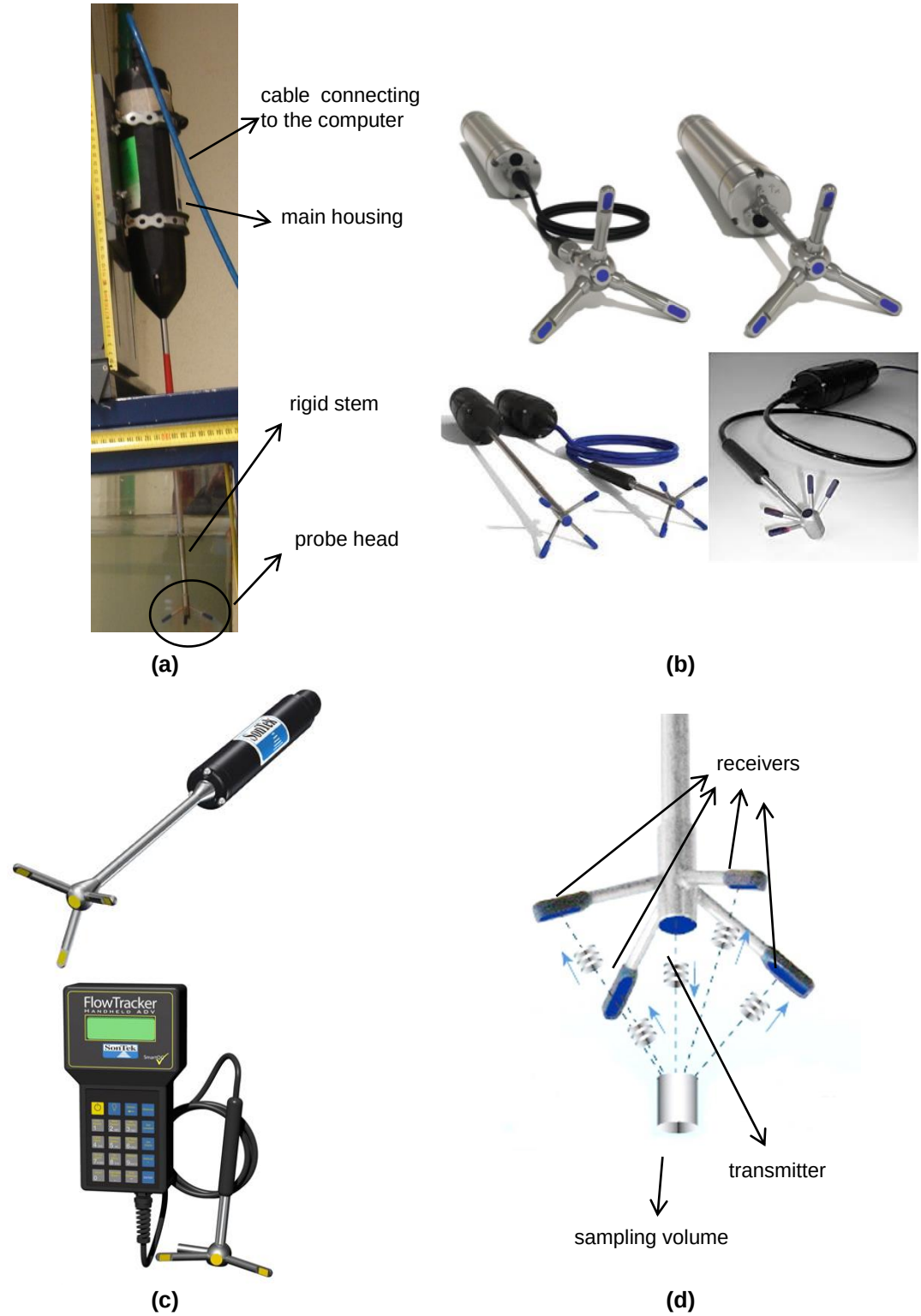


Figure 62: ADV device: (a) photograph showing its main components; (b) SonTek 10MHz down-looking ADV and SonTek FlowTracker with side-looking probe; (c) Nortek Vector with down-looking probes and Nortek Vectrino with down-looking and side-looking probes; (d) down.

It is a widely used technique due to its capability to measure the three components of instantaneous velocities, its robustness and portability, the fact that it does not require calibration and its relatively low cost (Khorsandi et al., 2012, Quaresma et al., 2017). It is also suitable for laboratory and field applications.

ADVs capability of accurately measuring time-averaged velocities has been referred by Lemmin & Rolland (1997), Voulgaris & Trowbridge (1998), Quaresma et al. (2017). On the other hand, the quality of turbulence quantities computed from ADV data has been questioned, and the need for post-processing emphasized (Hurther & Lemmin 2001, Goring & Nikora 2002, Blanckaert & Lemmin 2006, Cea et al. 2007, Parsheh et al. 2010, Khorsandi et al. 2012, Montero et al. 2014, Quaresma et al. 2017). Moreover, it is a point-wise measurement technique, therefore, obtaining maps of time-averaged turbulent flow variables involves placing one single probe in several successive positions, which is time-consuming, or deploying multiple probes (which may be too expensive and impractical) (Quaresma et al. 2017).

It is known that the precision of ADV measurements in turbulent flows is affected by random spikes, including sampling errors linked with analogue/digital conversion, and the Doppler ambiguity process, characterized by the amplitude modulation of the backscattered signal related to the transit time of the acoustical targets through the sampling volume (this error is independent of the flow and depends on the pulse length, set by the velocity range), Doppler noise (which is intrinsic to the measurement principle and is associated with the random motion of targets in the sampling volume), and errors due to the mean velocity gradients in the sampling volume and associated to spatial averaging of the instantaneous flow field within the sampling volume and unresolved turbulent scales that are of the same order of magnitude or smaller than the sampling volume's transverse size (Garbini et al. 1982, Voulgaris & Trowbridge 1998, McLelland & Nicholas 2000, Hurter & Lemmin 2001, Goring & Nikora 2002, Khorsandi et al. 2012). The spatial averaging of fluctuating motion contributes to reducing the variance of the signal; all the other sources of error contribute to increasing it (Hurter & Lemmin 2001).

In recent years several papers have been focusing on the theoretical and experimental identification and characterization of noise sources affecting the turbulence measurements performed with ADV (Garbini et al. 1982, Lohrmann et al. 1994, Voulgaris & Trowbridge 1998, McLelland & Nicholas 2000, Hurther & Lemmin 2001, García et al. 2005). Even when all the manufacturers' precautions are taken into consideration, the signal will have a noise level that affects the values of turbulence parameters (García et al. 2005).

Several post-processing filters have been proposed to reduce the effect of noise resulting from random spikes, namely the phase-space thresholding despiking method of Goring & Nikora (2002), the velocity correlation filter of Cea et al. (2007), and the modified phase-space thresholding despiking method of Parsheh et al. (2010).

On the other hand, the Doppler noise is "white" noise with a Gaussian probability distribution and a flat power spectrum (McLelland & Nicholas 2000, Hurther & Lemmin 2001, García et al. 2005). White noise does not affect the mean velocity values because it has zero mean. Lohrmann et al. (1994), Voulgaris & Trowbridge (1998) and McLelland & Nicholas (2000) showed that the ADV can accurately predict mean velocity and Reynolds shear stresses.

Hurther & Lemmin (2001) proposed a correction method for subtracting the contribution of noise from the mean turbulent parameters. This method takes advantage of the bistatic four-receiver configuration of some ADV instruments, and consequent redundancy in the measurements of the velocity along the axis of the ADV. The variance of the noise and the noise spectrum can thus be determined. The geometrically weighted noise spectrum is then subtracted from the spectra of the longitudinal components. Turbulence intensities are obtained by integration of the latter.

Application:

ADV has been extensively used in flow field characterization in fish migration and fishways studies. Odeh et al. (2002) used ADV to characterize flow turbulence to evaluate its effects on the behaviour of downstream migratory juvenile fish. Puertas et al. (2004) and Liu et al. (2006) conducted ADV measurements to characterize flow patterns and turbulence structures of flow in vertical slot fishways laboratory scale models. To assess the effects of water velocity and turbulence on the behaviour of Iberian barbel in an indoor full scale experimental pool-type fishway with orifices, Silva et al. (2011) used ADV measurements. Also in an indoor full scale experimental pool-type fishway with orifices, Santos et al. (2012) assessed the effect of two flow regimes, created by boulder placement in the flume bottom, in the upstream movements of Iberian barbel by performing ADV measurements to characterize the flow field. Branco et al. (2013) used ADV to characterize the water velocity and turbulence to evaluate the behaviour of two different morpho-ecological cyprinid species facing plunging and streaming flows in an indoor full scale experimental pool-type fishway with orifices and notches. To characterize a vertical slot fishway turning pool flow and validate a CFD model Marriner et al. (2014) performed ADV measurements on the Vianney-Legendre vertical slot fishway in Quebec, Canada. Bombač et al. (2015) performed extensive field measurements of the flow in a VSF, at the Arto – Blanca hydropower plant, and used these measurements to calibrate and verify a CFD model. To assess the effects of hydrodynamics on fish behaviour, and evaluate the upstream passage performance of a potamodromous cyprinid, over an experimental broad-crested weir, Amaral et al. (2016) characterized the flow pattern downstream of the weir with ADV. An et al. (2016) validated a three-dimensional CFD model of a VSF by carrying out velocity measurements in a physical model with ADV. Romão et al. (2017) used ADV measurements to characterize the flow hydrodynamics in an indoor full-scale pool-type fishway for two different vertical slot configurations. Quaresma et al. (2018) used these data to calibrate and validate a three-dimensional CFD model subsequently used to compare the hydrodynamics of two widely used vertical slot fishways (VSF) configurations and three multi slot fishway (MSF) configurations.

Other information:

WinADV, a free Windows-based viewing and post-processing utility for ADV files (Wahl, 2000) is widely used to post-process ADV data.

The Multi-instrument turbulence toolbox (MITT) Open-source MATLAB algorithms for the analysis of high-frequency flow velocity time series datasets from MacVicar et al. (2014), is also available for the post-processing of ADV data.

References:

Amaral SD, Branco P, Silva AT, Katopodis C, Viseu T, Ferreira MT, Pinheiro AN & Santos JM. 2016. Upstream passage of potamodromous cyprinids over small weirs: the influence of key-hydraulic parameters. Journal of Ecohydraulics 1:79-89. doi:10.1080/24705357.2016.1237265

An R, Li J, Liang R & Tuo Y. 2016. Three-dimensional simulation and experimental study for optimizing a vertical slot fishway. Journal of Hydro-environment Research 12:119-129. http://dx.doi.org/10.1016/j.jher.2016.05.005

Blanckaert K & Lemmin U. 2006. Means of noise reduction in acoustic turbulence measurements. Journal of Hydraulic Research 44(1):3–17. doi:10.1080/00221686.2006.9521657

Bombač M, Novak G, Mlacnik J & Četina M. 2015. Extensive field measurements of flow in vertical slot fishway as data for validation of numerical simulations. Ecological Engineering 84:476-484. doi:10.1016/j.ecoleng.2015.09.030

Branco P, Santos JM, Katopodis C, Pinheiro A & Ferreira MT. 2013. Pool-Type Fishways: Two Different Morpho-Ecological Cyprinid Species Facing Plunging and Streaming Flows. PLoS ONE 8(5):e65089. doi:10.1371/journal.pone.0065089

Cea L, Puertas J & Pena L. 2007. Velocity measurements on highly turbulent free surface flow using ADV. Experiments in Fluids 42(3):333–348. doi: 10.1007/s00348-006-0237-3

Doroudian B, Bagherimiyab F & Lemmin U. 2010. Improving the accuracy of four-receiver acoustic Doppler velocimeter (ADV) measurements in turbulent boundary layer flows. Limnology and Oceanography: Methods 8(11):575–591. doi:10.4319/lom.2010.8.0575

Garbini JL, Forster FK & Jorgensen JE. 1982. Measurement of Fluid Turbulence Based on Pulsed Ultrasound Techniques. Part 1. Analysis. Journal of Fluid Mechanics 118:445–470. doi:10.1017/S0022112082001153

García CM, Cantero MI, Niño Y & García MH. 2005. Turbulence Measurements with Acoustic Doppler Velocimeters. Journal of Hydraulic Engineering 131(12):1062-1073. doi:10.1061/(ASCE)0733-9429(2005)131:12(1062)

Goring DG & Nikora VI. 2002. Despiking acoustic Doppler velocimeter data. Journal of Hydraulic Engineering 128(1):117–126. doi: 10.1061/(ASCE)0733-9429(2002)128:1(117)

Hurther D & Lemmin U. 2001. A Correction Method for Turbulence Measurements with a 3D Acoustic Doppler Velocity Profiler. Journal of Atmospheric and Oceanic Technology 18(3):446–458. doi: http://dx.doi.org/10.1175/1520-426(2001)018<0446:ACMFTM>2.0.CO;2

Khorsandi B, Mydlarski L & Gaskin S. 2012. Noise in Turbulence Measurements Using Acoustic Doppler Velocimetry. Journal of Hydraulic Engineering 138(10):829–838. doi:10.1061/(ASCE)HY.1943-7900.0000589

Kraus NC, Lohrmann A & Cabrera R. 1994. New Acoustic Meter for Measuring 3D Laboratory Flows. Journal of Hydraulic Engineering 120(3):406–412. doi:10.1061/(ASCE)0733-9429(1994)120:3(406)

Lemmin U & Rolland T. 1997. Acoustic Velocity Profiler for Laboratory and Field Studies. Journal of Hydraulic Engineering 123(12):1089–1098. doi:10.1061/(ASCE)0733-9429(1997)123:12(1089)

Liu M, Rajaratnam N & Zhu DZ. 2006. Mean flow and turbulence structure in vertical slot fishways. Journal of Hydraulic Engineering 132(8):765–777. doi:10.1061/(ASCE)0733-9429(2006)132:8(765)

Lohrmann A, Cabrera R, Gelfenbaum G & Haines J. 1995. Direct Measurements of Reynolds Stress with an Acoustic Doppler Velocimeter. Proceedings of the IEEE Fifth Working Conference on Current Measurement, IEEE Catalog Number 95CH35724, 205-210. doi:10.1109/CCM.1995.516175

MacVicar B, Dilling S, Lacey J. 2014. Multi-instrument turbulence toolbox (MITT): Open-source MATLAB algorithms for the analysis of high-frequency flow velocity time series datasets. Computers & Geosciences 73:88-98.

Marriner BA, Baki ABM, Zhu DZ, Thiem JD, Cooke SJ & Katopodis C. 2014. Field and numerical assessment of turning pool hydraulics in a vertical slot fishway. Ecological Engineering 63:88-101. doi:10.1016/j.ecoleng.2013.12.010

McLelland SJ & Nicholas AP. 2000. A new method for evaluating errors in high-frequency ADV measurements. Hydrological Processes 14(2):351-366. doi:10.1002/(SICI)1099-1085(20000215)14:2<351::AID-HYP963>3.0.CO;2-K

Montero VGG, Romagnoli M, García CM, Cantero MI, Scacchi G. 2014. Optimization of ADV sampling strategies using DNS of turbulent flow. Journal of Hydraulic Research. 52(6), 862–869.

Nortek. 2004. Nortek Vectrino Velocimeter. User Guide. Rev. C. Nortek AS, Norway.

Odeh M, Noreika JF, Haro A, Maynard A & Castro-Santos T. 2002. Evaluation of the Effects of Turbulence on the Behavior of Migratory Fish. Final Report to the Bonneville Power Administration, Portland, Oregon. Contract 00000022, Project 200005700.

Parsheh M, Sotiropoulos F &Porté-Agel, F. 2010. Estimation of power spectra of acoustic-Doppler velocimetry data contaminated with intermittent spikes. Journal of Hydraulic Engineering 136(6):368–378. doi: 10.1061/(ASCE)HY.1943-7900.0000202

Puertas J, Pena L & Teijeiro T. 2004. Experimental approach to the hydraulics of vertical slot fishways. Journal of Hydraulic Engineering 130(1):10–23. doi:10.1061/(ASCE)0733-9429(2004)130:1(10)

Quaresma AL, Ferreira RML & Pinheiro AN. 2017. Comparative analysis of particle image velocimetry and acoustic Doppler velocimetry in relation to a pool-type fishway flow. Journal of Hydraulic Research. 55(4):582-591. doi: 10.1080/00221686.2016.1275051

Quaresma AL, Romão F, Branco P, Ferreira MT, Pinheiro AN. 2018. Multi slot versus single slot pool-type fishways: a modelling approach to compare hydrodynamics. Ecological Engineering 122:197-206. https://doi.org/10.1016/j.ecoleng.2018.08.006

Romão F, Quaresma AL, Branco P, Santos JM, Amaral S, Ferreira MT, Katopodis C & Pinheiro AN. 2017. Passage performance of two Cyprinids with Different Ecological Traits in a Fishway with Distinct Vertical Slot Configurations. Ecological Engineering. 105:180-188. doi: http://dx.doi.org/10.1016/j.ecoleng.2017.04.031

Santos JM, Branco PJ, Silva AT, Katopodis C, Pinheiro AN, Viseu T & Ferreira MT. 2012. Effect of two flow regimes on the upstream movements of the Iberian barbel (Luciobarbus bocagei) in an experimental pool-type fishway. Journal of Applied Ichthyology 29(2):425-430. doi: 10.1111/jai.12043

Silva AT, Santos JM, Ferreira MT, Pinheiro AN & Katopodis C. 2011. Effects of water velocity and turbulence on the behaviour of Iberian barbel (Luciobarbus bocagei, Steindachner, 1864) in an experimental pool-type fishway. River Research and Applications 27(3):360–373. doi:10.1002/rra.1363

Voulgaris G & Trowbridge JH. 1998. Evaluation of the acoustic Doppler velocimeter (ADV) for turbulence measurements. Journal of Atmospheric and Oceanic Technology 15(1):272–289. doi: http://dx.doi.org/10.1175/1520-0426(1998)015<0272:EOTADV>2.0.CO;2

Wahl T. 2000. Analyzing ADV Data Using WinADV. Joint Conference on Water Resource Engineering and Water Resources Planning and Management. ASCE, Minneapolis, pp.1–10. https://doi.org/10.1061/40517(2000)300

Contact information:

Nortek

https://www.nortekgroup.com/

e-mail: inquiry@nortekgroup.com

SonteK

https://www.sontek.com

e-mail: inquiry@sontek.com

Authors	Ana Quaresma (IST)
Reviewers	Robert Boes (ETHZ)

2.23. Particle Image Velocimetry - PIV

used by: [ETHZ / NTNU]

Type: method and device

It can be used in all phases, as it is a measurement method / device]

Introduction:

Particle Image Velocimetry (PIV)
The particle image velocimetry (PIV), also described in FIThydro deliverable 2.1, is an optical technique to measure the velocity of a fluid by measuring the velocity of the movement of particles transported in this fluid assuming that the particles are transported with the fluid without losses or disturbances.

The main devices used for this technique are:

- A source of light (for PIV usually a laser, however strong LED lights become more popular)
- At least one camera (in case of a 3D or volume measurement up to at least 4 cameras)
- Synchronizer to be able to automatically synchronize the camera (times when the pictures are taken) with the laser, otherwise, the pictures would not be properly illuminated
- Software for evaluation of the results
- Mostly also tracer particles as seeding

PIV is an instantaneous method to measure the flow. The main set-up includes usually a laser as a source of light (see Figure 63). With this laser, a so called laser sheet, a plain area within the fluid which is enlightened with the laser is created. All particles transported with the fluid are supposed to reflect the light and become visible like that. This effect can be supported by the use of special tracer particles (which are quite costly, so this is only recommended for lab use).

A camera takes pictures of the moving particles in predefined very short time intervals Δt. Based on the known Δt the flow velocity can be calculated using special algorithms to evaluate the movement of the seeding points visible in the picture. The evaluation of the pictures uses an Eulerian' approach. To be able to evaluate the distances on the pictures the system needs to be calibrated. As both, the time between the two pictures as well as the distance one particle has moved comparing these pictures the particle and hence the fluid velocity can be calculated.

To be able to achieve good results it is necessary to mind certain rules such as that one particle on the resulting picture should have the size of approx.. 2-3 pixel etc. It is highly recommended to get a detailed view into the literature (i.a. Raffel et al 2007) before starting with a measurement.

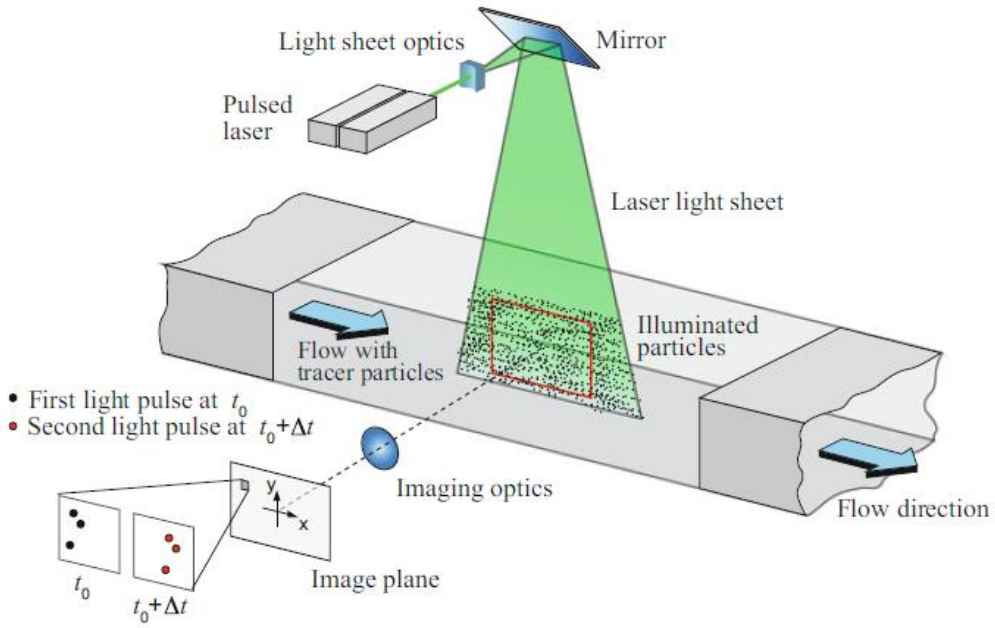


Figure 63: Set-up of a standard 2D PIV system (Raffel et al 2007).

The PIV can be bought as a complete system, usually including the software. Different companies such as ILA Laser applications, Dantec or LaVision offer this possibility including support. Some research institutions and universities also develop their own codes for post-processing depending on their needs or build the laser or camera system on their own.

Large Scale PIV (LS-PIV) or Airborne Image Velocimetry (AIV)

Based on the idea of PIV the so called Large Scale PIV (LS-PIV) or Airborne Image Velocimetry (AIV) was developed. As “Large Scale” with the increasing technical possibilities became a quite wide meaning the term AIV is more correct nowadays and used hereinafter.

The measurement and evaluation technique is basically the same set-up and underlying theory as PIV and adapts this for use on large scale mainly in the field. As mentioned above the term large scale is not defined, generally, it means more than lab size with about max. 1.5m x 1.5m for very good conditions. Such as a PIV the AIV is an optical system used to measure flow velocities, other than the PIV mainly surface velocities in 2D.

Instead of Laser as a source of light, the AIV uses the sun. This might become a problem for the evaluation of the pictures when direct sun is present, as reflections will affect the quality of the results.

The camera is often mounted on a UAV to ensure a sufficient size of the pictures taken as a result of greater distance and angle (Figure 64). Seeding is recommended for a sufficient quality of results. As the seeding, other than for the use with PIV, is used in a natural environment and most likely it will not be possible to collect it back behind the area of interest it is necessary to use seeding which is biodegradable such as wood chips or maize flips

(packing material). Any other material which is biodegradable and available can be used as well as long as it is following the flow and is visible on the pictures taken.

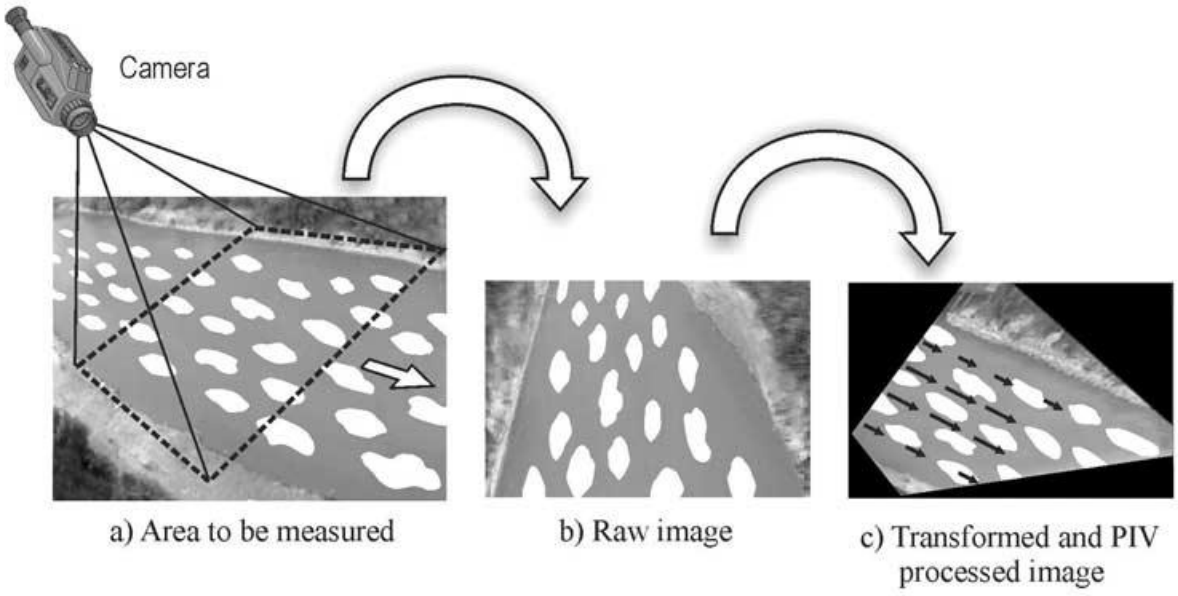


Figure 64: LSPIV measurement sequence: (a) imaging the area to be measured (white patterns indicate the natural or added tracers used for visualization of the free surface), (b) the distorted raw image, and (c) the undistorted image with the estimated velocity velocity vectors overlaid on the image (Muste et al. 2008)

Application:

For the application, the study area needs to be well known and targets need to be distributed in the area to ensure a defined distance for calibration on the pictures. As due to the huge amount of seeding needed for one run, not too many tests can be run and it is highly recommended to prepare the experiment properly.

- Set up of targets (either own targets such as wooden crosses or coded targets can be used). The coded targets are especially of interest in case the measurement shall be combined with a Structure from Motion measurement
- preparation of the drone, best case would be an automated flight route, however, also manual flights are possible without any problem
- preparation of any other measurement devices to be used at the same time, when the seeding starts floating everything needs to run smoothly
- preparation of the team which is responsible for spreading the seeding: based on a detailed planning it needs to be ensured, that the seeding is present in a sufficient amount under the drone, hence visible in the picture taken.
- In general, it depends on the camera of the resolution and frequency for pictures or movies is better
- A second run of the experiment would be recommended

After the data collection in the field, the more time consuming part is the data evaluation. Therefore different software can be used. Usually all variations of commercial products such as the PIV software of DanTec, ILA or LaVision. Further free software such as PIVlab can be used.

Depending on the software different levels of own effort are necessary when it comes to rectification of the pictures (Detert et al. 2015; Patalano et al 2017). The software is, when using PIVlab, MATLAB based and the basic idea is the same as for a standard PIV.

The results generated are surface velocities in the measured areas (Figure 65).

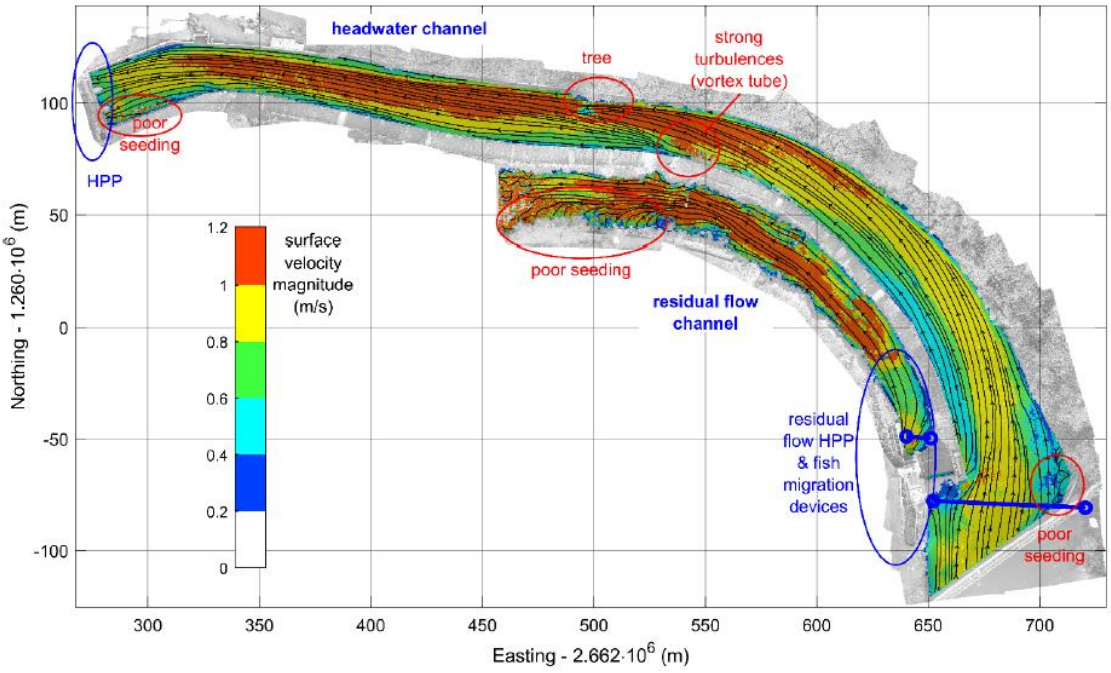


Figure 65: Swiss grid georeferenced surface velocity field and streamlines measured by AIV, including areas of noisy velocity data. (Note that according to Le Coz et al. (2010), depth averaged velocities can be estimated by multiplying the surface velocity by factors 0.79-0.89, with a central value close to 0.85); (Detert et al. 2019)

Other information:

Costs depend mainly on the staff needed for conducting the experiment and in case a commercial software is used for evaluation on the license costs.

Authors	Kordula Schwarzwälder (NTNU)
Reviewers	Robert Boes (ETHZ)

References:

Detert, M., & Weitbrecht, V. (2014). Helicopter-based surface PIV experiments at Thur River. Proceedings of the Seventh International Conference on River Flow, Lausanne, Switzerland, 2003–2008.

Detert, M., & Weitbrecht, V. (2015). Estimation of flow discharge by an airborne velocimetry system. First International SHF-Conference on Drones et hydraulique, Paris-Cachan, France.

Detert, M., Weitbrecht, V., (2015). A low-cost airborne velocimetry system: proof of concept. Journal of Hydraulic Research 53, 532–539. https://doi.org/10.1080/00221686.2015.1054322

Detert, M., Cao, L. & Albayrak, I. (2019). Airborne image velocimetry measurements at the hydropower plant Schiffmühle on Limmat river, Switzerland. HydroSenSoft, International Symposium and Exhibition on Hydro-Environment Sensors and Software, Madrid, Spain, ISBN: 978-90-824846-4-9

Dramais, G., Le Coz, J., Camenen, B., & Hauet, A. (2011). Advantages of a mobile LSPIV method for measuring flood discharges and improving stage-discharge curves. Journal of Hydroenviromental Research, 5, 301–312.

Fujita, I., & Hino, T. (2003). Unseeded and seeded PIV measurementsof river flows video from a helicopter. Journal of Visualization, 6, 245–252.

Fujita, I., & Kunita, Y. (2011). Application of aerial LSPIV to the 2002 flood of the Yodo River using a helicopter mounted high density video camera. Journal of Hydroenvironmental Research, 5, 323–331.

Gunawan, B., Sun, X., Sterling, M., Shiono, K., Tsubaki, R., Rameshwaran, P., Knight, D.W., Chandler, J.H., Tang, X., Fujita, I., 2012. The application of LS-PIV to a small irregular river for inbank and overbank flows. Flow Measurement and Instrumentation 24, 1–12. https://doi.org/10.1016/j.flowmeasinst.2012.02.001

Le Coz, J., Hauet, A., Pierrefeu, G., Dramais, G., Camenen, B., 2010. Performance of image-based velocimetry (LSPIV) applied to flash-flood discharge measurements in Mediterranean rivers. Journal of Hydrology 394, 42–52. https://doi.org/10.1016/j.jhydrol.2010.05.049

Muste, M., Fujita, I., & Hauet, A. (2008). Large-scale particle image velocimetry for measurements in riverine environments. Special Issue on Hydrologic Measurements, Water Resources Research, 44, doi:10.1029/2008WR006950.

Muste, M., Hauet, A., Fujita, I., Legout, C., Ho, H.-C., 2014. Capabilities of Large-scale Particle Image Velocimetry to characterize shallow free-surface flows. Advances in Water Resources 70, 160–171. https://doi.org/10.1016/j.advwatres.2014.04.004

Pagano, C., Tauro, F., Porfiri, M., & Grimaldi, S. (2014). Development and testing of an unmanned aerial vehicle for large scale particle image velocimetry. Proceedings of ASEM 2014 Dynamic Systems and Control Conference, San Antonio,USA, DSCC2014-5838.

Thielicke, W., & Stamhuis, E. J. (2014). PIVlab: Time-resolved digital Particle Image Velocimetry tool for MATLAB (version: 1.35). http://dx.doi.org/10.6084/m9.figshare.1092508.

Weitbrecht, V., Kühn, G., & Jirka, G. H. (2002). Large-scale PIV-measurements at the surface of shallow water flows. Flow Measurement and Instrumentation, 13, 237–245.

2.24. Lidar

Type: tool

Introduction:

Lidar is a measurement technique that measures the distance from a georeferenced laser sensor to a ground target by illuminating the target with the pulsed light (Figure 66). The sensor detects the reflected pulses. The time shifts in laser return and wavelengths can then be used to make digital 3-D representations of the target areas, e.g. a river section. The laser pulses can have different wavelengths, most commonly red and green.

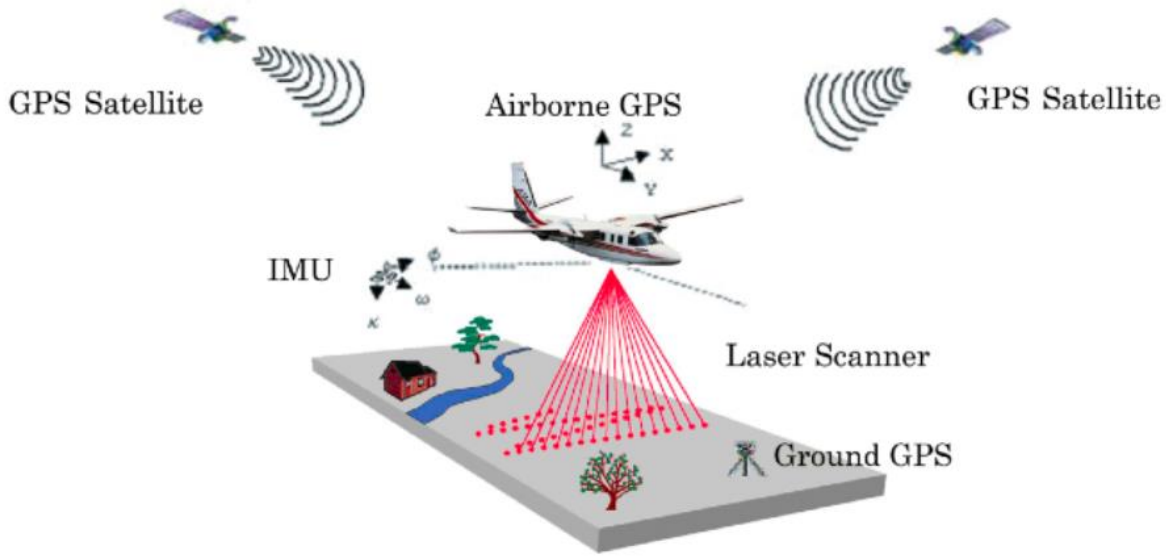


Figure 66: Basic set up of a Lidar measurement (Mallet 2010).

The red laser is more common and therefore cheaper. However, other than the NeoDyn Yag laser it can not penetrate the water surface. Therefore the green laser (wavelength 532nm) is most preferred in scientific and especially river related measurements (Figure 67). However, a certain distance from the source of the light to the eye of any person passing accidentally the measurement must be guaranteed due to safety reasons. This is usually not a problem, as this application is used for large scale approached, mainly with so called Airborne Laser Scanning (ALS) where the laser is mounted to a small plane, a helicopter or even a large (more than 15 kg load) drone.

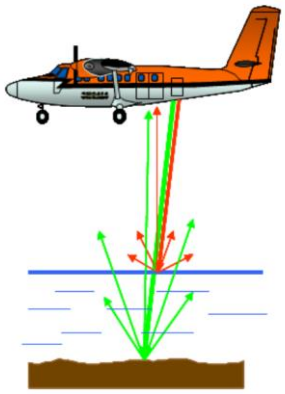


Figure 67: Comparison red vs green laser (Mallet 2010).

Application:

As the laser and also the plane or helicopter are a quite expensive set of devices, the measurements are usually taken by private contractors. Most of the time the client is a municipality, the government or a hydropower operator interested in the geometry of floodplains and the bathymetry of rivers.

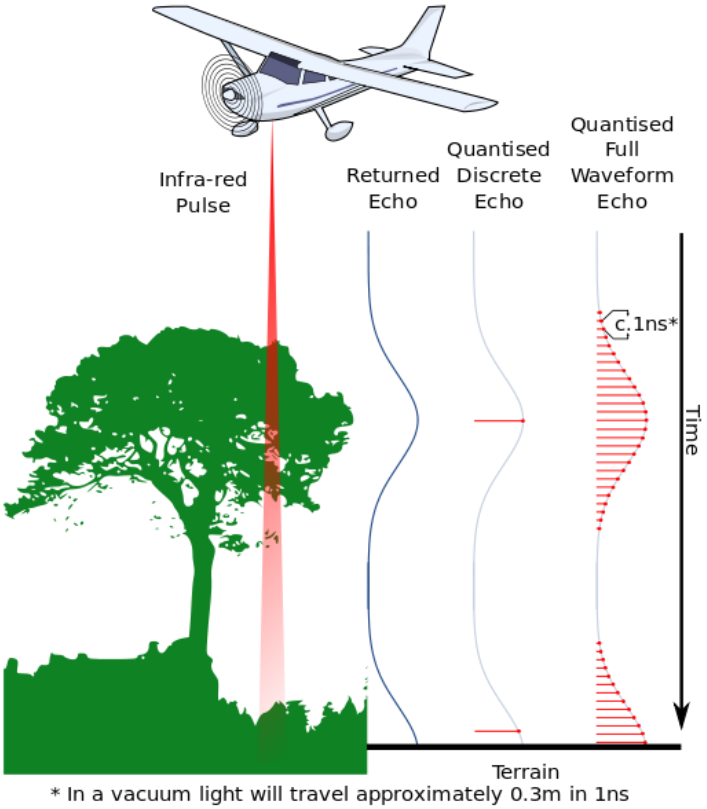


Figure 68: Discrete Echo and waveform signal comparison for Airborne Laser Scanning (https://commons.wikimedia.org/wiki/File:Airborne_Laser_Scanning_Discrete_Echo_and_Full_Waveform_signal_comparison.svg).

In Norway, most of the rivers are currently measured with a red laser (hence no underwater registrations). These are relatively easily available for research institutions through public website hoydedata.no. Also available at the website are green laser derived bathymetry of a selection of river reaches.

The penetration depth of the green laser through water depends highly on turbidity, flow velocity, reflections on the surface / waves and water depth. It also depends most probably on the type of suspended load. Thus, green laser measurements are in many cases supplied with echosounding data.

Problems can also be caused by any other overlap of objects such as trees above ground or submerged vegetation above river bottoms (Figure 68). This can lead to blurred areas and various z-data (height marker) for the same x/y coordinates.

The measurements generate a point cloud. Post-processing is usually done in a specific software (also freeware) as is the case many other applications (such as SfM). However, as it is a usual output format, it is not a specific part of the Lidar system.

References:

Bizzi, S., Demarchi, L., Grabowski, R.C., Weissteiner, C.J., Van de Bund, W., 2016. The use of remote sensing to characterise hydromorphological properties of European rivers. Aquatic Sciences 78, 57–70. https://doi.org/10.1007/s00027-015-0430-7

Brock, J.C., Purkis, S.J., 2009. The Emerging Role of Lidar Remote Sensing in Coastal Research and Resource Management. Journal of Coastal Research 10053, 1–5. https://doi.org/10.2112/SI53-001.1

Brock und Purkis - 2009 - The Emerging Role of Lidar Remote Sensing in Coast.pdf, n.d.

Costa, B.M., Battista, T.A., Pittman, S.J., 2009. Comparative evaluation of airborne LiDAR and ship-based multibeam SoNAR bathymetry and intensity for mapping coral reef ecosystems. Remote Sensing of Environment 113, 1082–1100. https://doi.org/10.1016/j.rse.2009.01.015

Costa et al. - 2009 - Comparative evaluation of airborne LiDAR and ship-.pdf, n.d.

Gao, J., 2009. Bathymetric mapping by means of remote sensing: methods, accuracy and limitations. Progress in Physical Geography 33, 103–116. https://doi.org/10.1177/0309133309105657

Hilldale, R.C., Raff, D., 2008. Assessing the ability of airborne LiDAR to map river bathymetry. Earth Surface Processes and Landforms 33, 773–783. https://doi.org/10.1002/esp.1575

Hilldale und Raff - 2008 - Assessing the ability of airborne LiDAR to map riv.pdf, n.d.

Irish, J.L., White, T.E., 1998. Coastal engineering applications of high-resolution lidar bathymetry. Coastal Engineering 35, 47–71. https://doi.org/10.1016/S0378-3839(98)00022-2

Kinzel, P.J., Legleiter, C.J., Nelson, J.M., 2013. Mapping River Bathymetry With a Small Footprint Green LiDAR: Applications and Challenges : Mapping River Bathymetry with a Small Footprint Green LiDAR: Applications and Challenges. JAWRA Journal of the American Water Resources Association 49, 183–204. https://doi.org/10.1111/jawr.12008

Langhammer, J., Janský, B., Kocum, J., Minařík, R., 2018a. 3-D reconstruction of an abandoned montane reservoir using UAV photogrammetry, aerial LiDAR and field survey. Applied Geography 98, 9–21. https://doi.org/10.1016/j.apgeog.2018.07.001

Langhammer, J., Janský, B., Kocum, J., Minařík, R., 2018b. 3-D reconstruction of an abandoned montane reservoir using UAV photogrammetry, aerial LiDAR and field survey. Applied Geography 98, 9–21. https://doi.org/10.1016/j.apgeog.2018.07.001

Lejot, J., Delacourt, C., Piégay, H., Fournier, T., Trémélo, M.-L., Allemand, P., 2007. Very high spatial resolution imagery for channel bathymetry and topography from an unmanned mapping controlled platform. Earth Surface Processes and Landforms 32, 1705–1725. https://doi.org/10.1002/esp.1595

Lükő, G., Rüther, D.N., n.d. UAV BASED HYDROMORPHOLOGICAL MAPPING OF A RIVER REACH TO IMPROVE HYDRODYNAMIC NUMERICAL MODELS 1.

Lükő, G., Rüther, D.N., n.d. UAV Based Hydromorphological Mapping of a River Reach to Improve Hydrodynamic Numerical Models.

Marcus, W.A., Fonstad, M.A., 2008. Optical remote mapping of rivers at sub-meter resolutions and watershed extents. Earth Surface Processes and Landforms 33, 4–24. https://doi.org/10.1002/esp.1637

Mallet C., 2010; LIDAR aéroportéstopographiques & bathymétriques ; https://www.umr-cnrm.fr/ecole_lidar/IMG/pdf/Mallet-Topo_Bathy_Veget.pdf

Saylam, K., Brown, R.A., Hupp, J.R., 2017. Assessment of depth and turbidity with airborne Lidar bathymetry and multiband satellite imagery in shallow water bodies of the Alaskan North Slope. International Journal of Applied Earth Observation and Geoinformation 58, 191–200. https://doi.org/10.1016/j.jag.2017.02.012

Wang, C.-K., Philpot, W.D., 2007. Using airborne bathymetric lidar to detect bottom type variation in shallow waters. Remote Sensing of Environment 106, 123–135. https://doi.org/10.1016/j.rse.2006.08.003

Wang und Philpot - 2007 - Using airborne bathymetric lidar to detect bottom .pdf, n.d.

Zhang, K., Yang, F., Zhang, H., Su, D., Li, Q., 2017. Morphological characterization of coral reefs by combining lidar and MBES data: A case study from Yuanzhi Island, South China Sea: MORPHOLOGICAL STUDY OF CORAL REEF. Journal of Geophysical Research: Oceans 122, 4779–4790. https://doi.org/10.1002/2016JC012507

Zhang, K., Frey, H.C., 2006. Road Grade Estimation for On-Road Vehicle Emissions Modeling Using Light Detection and Ranging Data. Journal of the Air & Waste Management Association 56, 777–788. https://doi.org/10.1080/10473289.2006.10464500

Contact information:

Authors	Kordula Schwarzwälder (NTNU)
Reviewers	Robert Boes (ETHZ)

2.25. Structure from Motion - SfM

Type: tool and device

Introduction:

The technique of structure from motion was developed for the gaming industry to allow fast and easy 3D detection and evaluation of bodies. With this technique, it is possible, based on pictures of an object taken with a camera to combine these pictures and based on a software evaluation There are several approaches to generate a 3D model from SfM. In incremental SFM (Schönberger & Frahm 2016), camera poses are solved and added one by one. In global SFM (Govindu 2001), the poses of all cameras are solved for at the same time.

The best result can be achieved when taking pictures from every angle around the object. However, this is not possible for rivers, depending on the river bank vegetation only a flight directly above but with no relevant angle to the sides is possible (Figure 69).

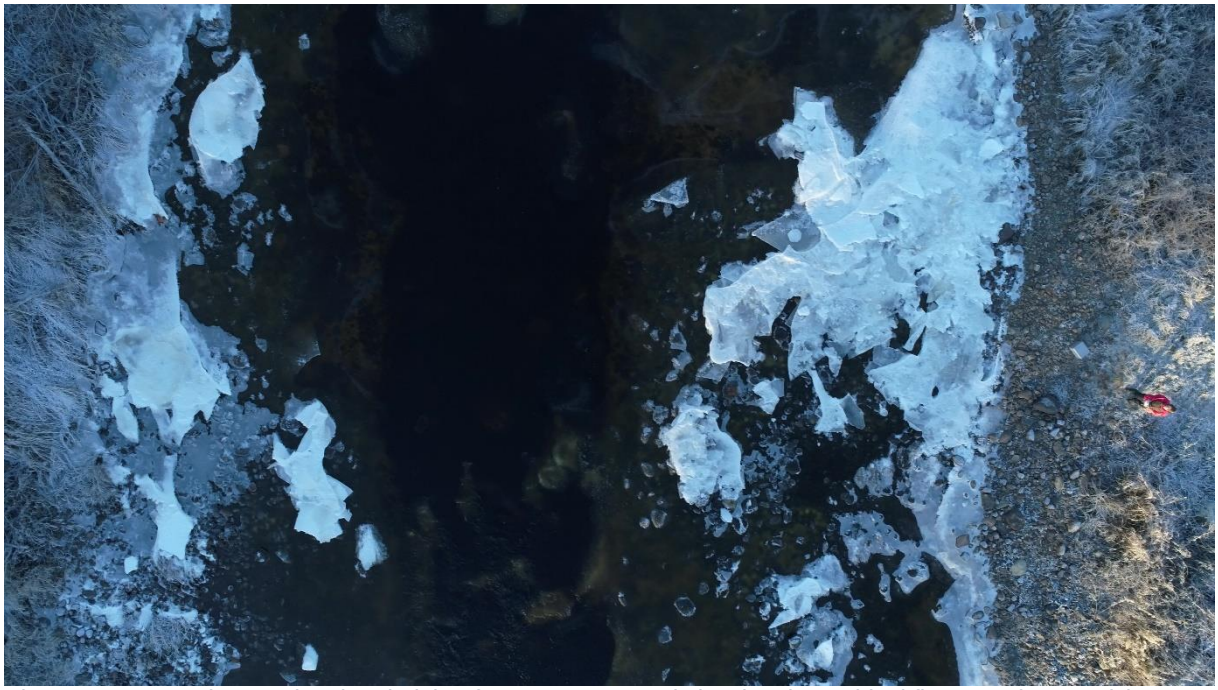


Figure 69: Drone picture taken in a height of 50 m over ground showing the residual flow area in Anundsjø HPP, ice cover and the author.

The same problem might appear when using the technique in the lab (Figure 70).

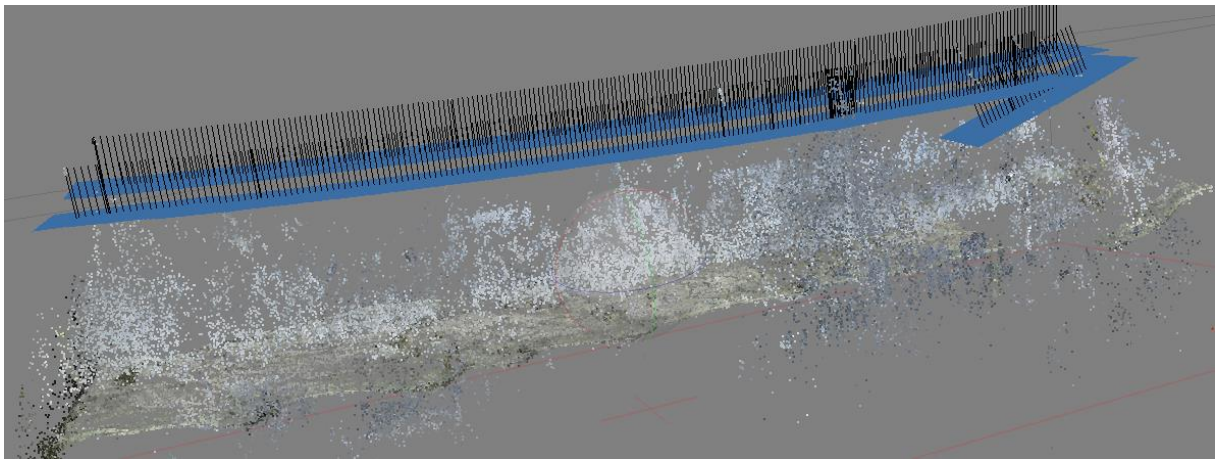


Figure 70: First run of a structure from motion evaluation in the lab of NTNU. The blue field indicates the camera position.

For a sufficient accuracy of the results, at least a camera with a high quality GPS sensor needs to be used. The use of targets or even coded targets would be more favourable, however. Without a clear positioning of the pictures in the space, the result would not be correct as the cameras could not be located correctly in dependency to each other. Targets on the ground, especially for field measurements, are highly recommended. The position of the targets can be measured with a GPS and the targets can be redetected later in the pictures.

Depending on the software used this process of “re-finding” can be done automatically or needs to be done manually.

Again, there are different types of software available, commercial and non-commercial ones. As there is a very fast development and most non-commercial tools need a lot of experience with picture modifications etc. it is recommended, despite the costs, to use a commercial one such as Agisoft Photoscan for instance.

In this software, the user can follow relatively easy the workflow provided by the program (Figure 71) to produce a DEM.

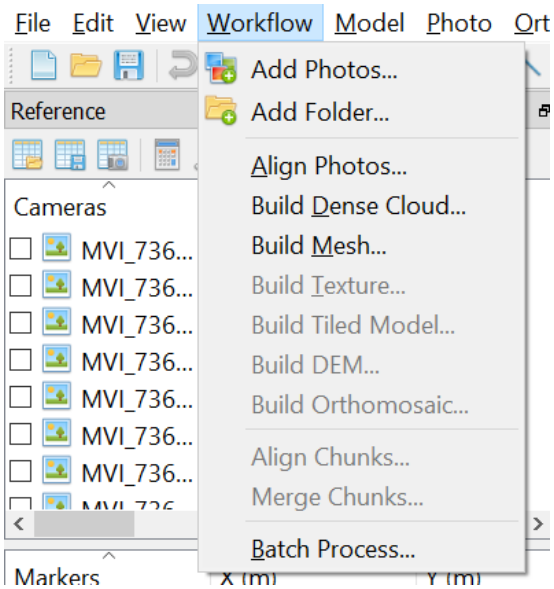


Figure 71: Screenshot of the Argisoft Photoscan Workflow.

Application:

As for other picture-based evaluation methods, the data processing is the most demanding part of the measurement. When starting with the measurements in the field, it is highly recommended to use targets. The rough workflow is as follows:

- Putting targets on the ground with sufficient visibility. The quality of the results increases in case there are two to three targets visible in every picture. Hence the distribution of the targets depend on the flight height of the camera.
- The camera is usually mounted on a drone, however other constructions as a crane etc. are possible.
- Speed and height over ground depend on the area to be evaluated.
- In case large areas need to be covered an automated flight route programmed for the drone would be useful.
- Starting and landing the drone can be a crucial point, especially in the case this is done automatically and the connection is nut sufficient.
- Further problems can be caused by wind (for the flying performance) and by reflections (for the resulting pictures).

Once the measurements are done the evaluation is the most crucial point. Depending on the number of pictures evaluated the result quality de- or increases and in a reverse way the computer performance and power needed in- or decreases (Figure 72).

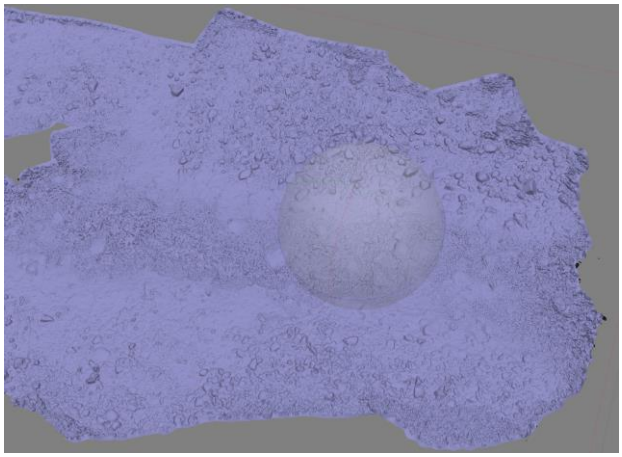


Figure 72: Mesh generated from SfM from a section of the residual flow reach of Anundsjø.

Other information:

The highest cost is the software license in case a commercial product is used.

References:

Alfredsen, K., Haas, C., Tuthan, J., Zinke, P., 2018. Brief Communication: Mapping river ice using drones and structure from motion.

Bouhoubeiny, E., Germain, G., Druault, P., 2011. Time-Resolved PIV investigations of the flow field around cod-end net structures. Fisheries Research 108, 344–355. https://doi.org/10.1016/j.fishres.2011.01.010

Buscombe, D., 2016a. Spatially explicit spectral analysis of point clouds and geospatial data. Computers & Geosciences 86, 92–108. https://doi.org/10.1016/j.cageo.2015.10.004

Buscombe, D., 2016b. Spatially explicit spectral analysis of point clouds and geospatial data. Computers & Geosciences 86, 92–108. https://doi.org/10.1016/j.cageo.2015.10.004

Cunliffe, A.M., Brazier, R.E., Anderson, K., 2016. Ultra-fine grain landscape-scale quantification of dryland vegetation structure with drone-acquired structure-from-motion photogrammetry. Remote Sensing of Environment 183, 129–143. https://doi.org/10.1016/j.rse.2016.05.019

Flammang, B.E., Lauder, G.V., Troolin, D.R., Strand, T.E., 2011. Volumetric imaging of fish locomotion. Biol. Lett. 7, 695–698. https://doi.org/10.1098/rsbl.2011.0282

Govindu, V.M. (2001). "Combining two-view constraints for motion estimation". IEEE Computer Society Conference on Computer Vision and Pattern Recognition

Koci, J., Jarihani, B., Leon, J.X., Sidle, R., Wilkinson, S., Bartley, R., 2017. Assessment of UAV and Ground-Based Structure from Motion with Multi-View Stereo Photogrammetry in a Gullied Savanna Catchment. ISPRS International Journal of Geo-Information 6, 328. https://doi.org/10.3390/ijgi6110328

Kothnur, P.S., Tsurikov, M.S., Clemens, N.T., Donbar, J.M., Carter, C.D., 2002. Planar imaging of CH, OH, and velocity in turbulent non-premixed jet flames. Proceedings of the Combustion Institute 29, 1921–1927. https://doi.org/10.1016/S1540-7489(02)80233-4

Langhammer, J., Lendzioch, T., Miřijovský, J., Hartvich, F., 2017. UAV-Based Optical Granulometry as Tool for Detecting Changes in Structure of Flood Depositions. Remote Sensing 9, 240. https://doi.org/10.3390/rs9030240

LI, S., CHENG, W., WANG, M., CHEN, C., 2011. The flow patterns of bubble plume in an MBBR. Journal of Hydrodynamics, Ser. B 23, 510–515. https://doi.org/10.1016/S1001-6058(10)60143-6

Lükő, G., Rüther, D.N., n.d. UAV BASED HYDROMORPHOLOGICAL MAPPING OF A RIVER REACH TO IMPROVE HYDRODYNAMIC NUMERICAL MODELS 1.

Lükő, G., Rüther, D.N., n.d. UAV Based Hydromorphological Mapping of a River Reach to Improve Hydrodynamic Numerical Models.

Morgan et al. - 2017 - Application of Structure-from-Motion photogrammetr.pdf, n.d.

Morgan, J.A., Brogan, D.J., Nelson, P.A., 2017. Application of Structure-from-Motion photogrammetry in laboratory flumes. Geomorphology 276, 125–143. https://doi.org/10.1016/j.geomorph.2016.10.021

Paterson, D.M., Black, K.S., 1999. Water Flow, Sediment Dynamics and Benthic Biology, in: D.B. Nedwell and D.G. Raffaelli (Ed.), Advances in Ecological Research. Academic Press, pp. 155–193.

Schönberger, J.L & Frahm, J.M. (2016). "Structure-from-Motion Revisited" (PDF). IEEE Computer Society Conference on Computer Vision and Pattern Recognition.

Tytell, E.D., 2011. BUOYANCY, LOCOMOTION, AND MOVEMENT IN FISHES | Experimental Hydrodynamics, in: Anthony P. Farrell (Ed.), Encyclopedia of Fish Physiology. Academic Press, San Diego, pp. 535–546.

Vázquez-Tarrío, D., Borgniet, L., Liébault, F., Recking, A., 2017. Using UAS optical imagery and SfM photogrammetry to characterize the surface grain size of gravel bars in a braided river (Vénéon River, French Alps). Geomorphology 285, 94–105. https://doi.org/10.1016/j.geomorph.2017.01.039

Westoby et al. - 2012 - ‘Structure-from-Motion’ photogrammetry A low-cost.pdf, n.d.

Westoby, M.J., Brasington, J., Glasser, N.F., Hambrey, M.J., Reynolds, J.M., 2012. ‘Structure-from-Motion’ photogrammetry: A low-cost, effective tool for geoscience applications. Geomorphology 179, 300–314. https://doi.org/10.1016/j.geomorph.2012.08.021

Contact information:

Authors	Kordula Schwarzwälder (NTNU)
Reviewers	Robert Boes (ETHZ)

All pictures taken by the author (and some by her drone Phantom 4).

2.26. Current meter

Developed by: Reinhardt Woltman, 1786

Type: Tool

Field measurements at all phases

Introduction:

The first devices to measure flow velocities appeared during the 1780s with the first mechanical current meter which counts the rotations of a propeller and links it to the flow velocity (by proportionality principle).

Today there are 3 different techniques to assess the flow velocity: mechanically, electromagnetically, and acoustically (Figure 73). The acoustic current meters using the Doppler Effect are not presented here, as these tools (ADCP, ADV, etc.) are presented separately.

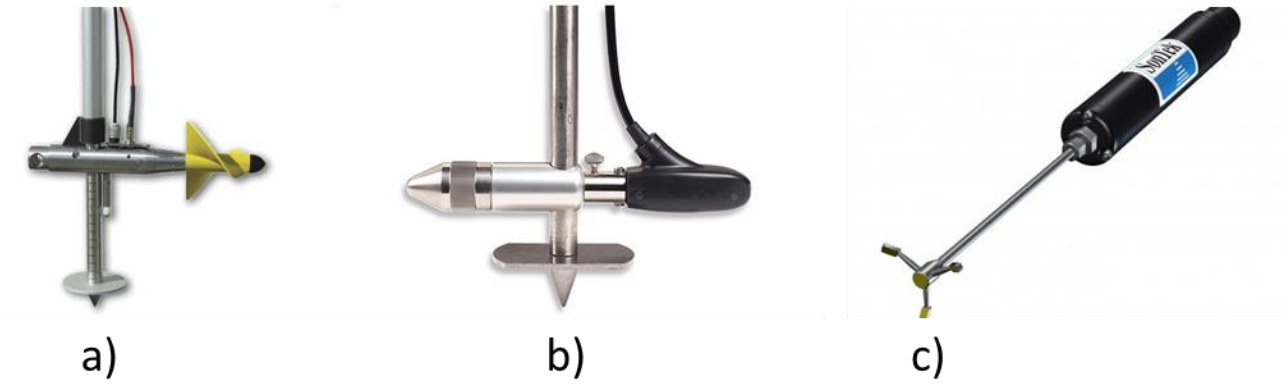


Figure 73: Current meter: a) mechanic, b) electro-magnetic, c) acoustic. Sources: SEBA hydrométrie, OTT, Sontek.

Application:

For a mechanical flow meter, the rotation of the propeller produces an electrical impulse detected and recorded by a counter connected to the current meter.

The electromagnetic flow meter uses the Faraday law. The sensor creates a magnetic field between two electrodes located at the end of the probe. The flow velocity is deduced from the measurement of the electromagnetic force generated by the passage of water through the magnetic field.

The measurement conditions of discharge through flow velocity fields are regulated by the European standard NF EN ISO 748.

The velocities are measured along a cross section at verticals. The number of verticals (n) depends on the width of the channel:

- Width of channel $<$ 0,5 m, $n = 5$ or 6
- Width of channel $>$ 0,5 m and $<$ 1 m, $n = 6$ or 7
- Width of channel $>$ 1 m and $<$ 3 m, $n = 7$ or 12
- Width of channel $>$ 3 m and $<$ 5 m, $n = 13$ to 16
- Width of channel $>$ 5 m, $n \geq 22$

One method among others to measure the mean velocity on each vertical is to measure the velocity in one or several measurement points at different water levels on the vertical. The number of measurements points for each vertical depends on the water level. For example, only one point is needed for water level <20 cm at 60% of the water level. If there are only 2 measurement points, they should be at 20 and 80% of the water level, and the mean velocity corresponds to the average of the two measured velocities. In the following example, 6

measurements were selected (Figure 74). The example is linked to the velocity profile inside a downstream migration channel, which is not logarithmic.

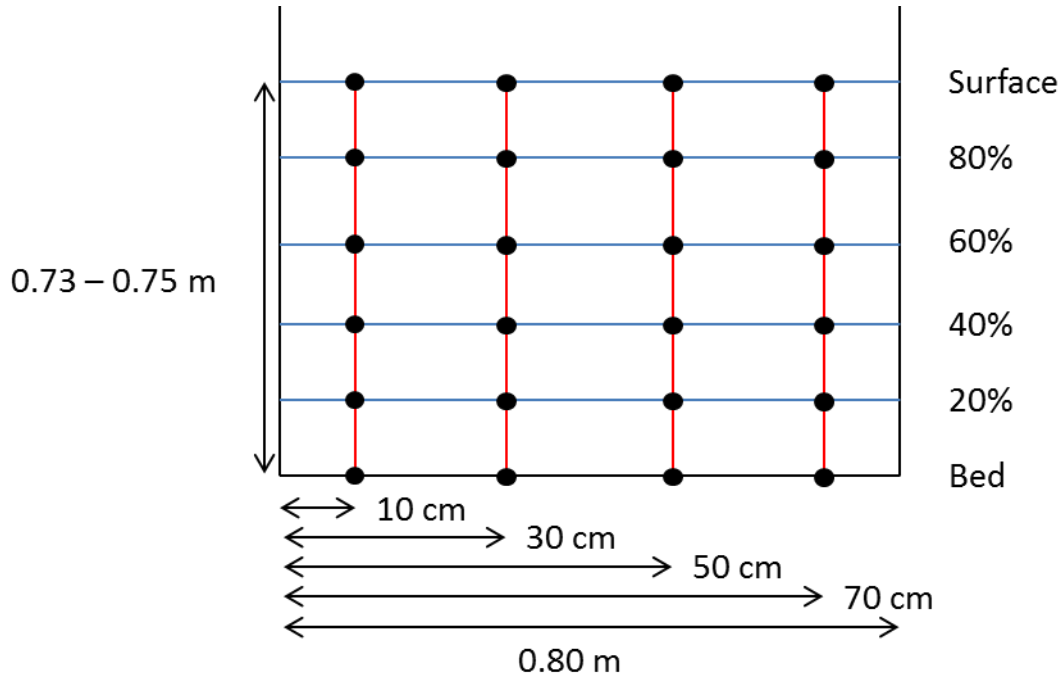


Figure 74: Cutting of a section during the measurement by a flow meter, in red the verticals, the black dots correspond to the measurement points.

To do the measurements, the operator needs to be equipped with waders and to be in the stream (Figure 75).



Figure 75: Operator in the downstream migration channel for measurements with a current meter.

By the method of mean section, the mean velocity between the banks and the closer verticals can be calculated. The mean velocity on each vertical is calculated that way, in the case of 6 measurement points:

$$V_{mean\ section} = 0.1(V_s + 2V_{0.8} + 2V_{0.6} + 2V_{0.4} + 2V_{0.2} + V_{pf})$$

Then a mean velocity is calculated for each flow section between the verticals and the closer bank; by making an average for the sections without including the banks, and by applying the following formula:

$$V_{mean\ section} = \frac{m}{m+1} * V_{mean\ closer\ vertical}$$

where *m* is a parameter depicting the characteristics of the river bed or of the wall. *m* is generally comprised between 5 and 7 but can be equal to 10 if the walls are really smooth. If *m*=4 the river bed and the walls are rough.

The discharge per section can be calculated according to standard EN ISO 748:2007:

$$Q_{section} = V_{mean\ section} * H_{water\ mean} * L_{flow}$$

Where $H_{water\ mean}$ is the mean water level and L_{flow} is the width of the channel.

In order to have the total discharge, all discharges per section have to be added.

The most recent devices have the possibility to directly treat the data and give the discharge on the cross section.

https://www.ott.com/en-uk/products/water-flow-3/ott-mf-pro-water-flow-meter-968/

Other information:

Several companies commercialise these technologies.

At the French Test Cases an electromagnetic flow meter Marsh McBirney, FLO-MATE 2000 is used.

References:

Aurélien Despax, 2016, Incertitude des mesures de débit des cours d'eau au courantomètre, Amélioration desméthodes analytiques et apports des essais interlaboratoires, Ingénierie de l'environnement, UniversitéGrenoble Alpes, 2016

Manon Dewitte, Dominique Courret, Fatma Lemkecher, Laurent David, 2019, Presentation of Las Rives Test Case, FIThydro

https://www.ott.com/en-uk/products/water-flow-3/ott-mf-pro-water-flow-meter-968/

Authors	Manon Dewitte (CNRS), Dominique Courret (AFB)
Reviewers	Robert Boes (ETHZ)

2.27. Hydropeaking indicator

Developed by: French Agency For Biodiversity, Ecohydraulic Team AFB-IMFT, Courret D, Larinier M and Baran P.

Date: 2014

Type: Tool (computer model)

Suitable for environmental flow (hydropeaking) mitigation measure in all phases (planning, implementation, maintenance)

Introduction:

Hydropeaking at hydroelectric facilities (more than 150 in France) generates sudden changes in flow in the river and can affect the composition, the abundance and the structure of fish and invertebrates populations over long distances. The objectives of the “Hydropeaking indicator” tool are (1) to characterize hydropeaks within hydrograph and (2) to produce a synthetic indicator of hydrological disturbance, related to the impacts on fish populations.

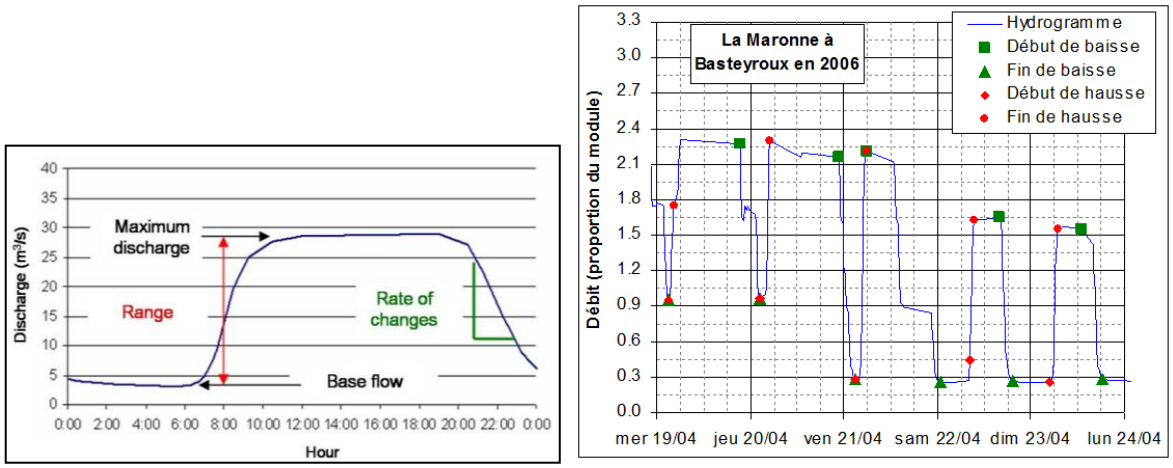


Figure 76: Example of flow analysis.

From the analysis of 97 stations and 1575 years of flow data, rates of change of natural flow variations have been first characterized (Figure 76) within 8 ranges between 5% and 4 times the mean inter-annual discharge. Formulas representing the "fastest variations possible naturally" and taking into account the type of change (increase or decrease), the size of the stream (via the mean inter-annual discharge) and the flow range over which the variation takes place have been constructed and then used to discriminate hydropeaks and natural events.

From the analysis of 80 stations and 491 years of flow data affected by hydropeaking, a method was developed to identify, within the hydrograph, hydropeaks whose characteristics are beyond what can occur in natural hydrology, using 3 criteria: a minimum range (≥ 10% of the mean inter-annual discharge and ≥ 20% of the hydropeak base flow), a minimal rate of change (> to the maximum natural rate of change) and an upper limit on the maximum flow rate (to remove flood events).

A synthetic indicator differentiating 5 levels of hydrological disturbance induced by hydropeaking regimes was constructed (Figure 77). The level of disturbance of each of the 491 years of flow data was evaluated by 3 expert operators according to the knowledge of the biological impacts of hydropeaking. The linear discriminant analysis allows reproducing this classification using 5 characteristic parameters of hydropeaking regimes (87% of correct reclassification).

Table 3: Levels of hydrologic perturbation due to hydropeaking events.

Level	Colour	Levels of hydrologic perturbation due to hydropeaking events
0		Hydrology natural or hardly disturbed.
1	Blue	Noticeable hydrologic perturbation.
2	Green	Hydrologic perturbation marked.
3	Yellow	Hydrologic perturbation very marked.
4	Orange	High hydrologic perturbation.
5	Red	Very high hydrologic perturbation.

Application:

The hydropeaking Indicator needs discharge time series as input file, with a fixed or variable time step. This time step should be short to precisely describe the hydropeaks (< 0.5-1 h). The indicator can be produced per year or per period corresponding to biological phases / seasons. Its automated calculation requires knowing only the mean inter-annual flow of the river and the maximum turbine discharge of the hydropower plant upstream.

The hydropeaking Indicator produces (1) a set of parameters that characterizes each hydropeak (base flow, maximum flow, rate of change…) and their statistics, and (2) the score provided by the discriminant analysis and the level of perturbation.

Examples show that the indicator is sensitive to changes in hydropower plant management and allows appreciating the spatial and temporal changes in hydropeaking regimes, including the damping in the downstream direction (Figure 77). This indicator is a tool for managers of "pre-diagnosis" of biological impacts and for monitoring spatial and temporal changes in hydropeaking.

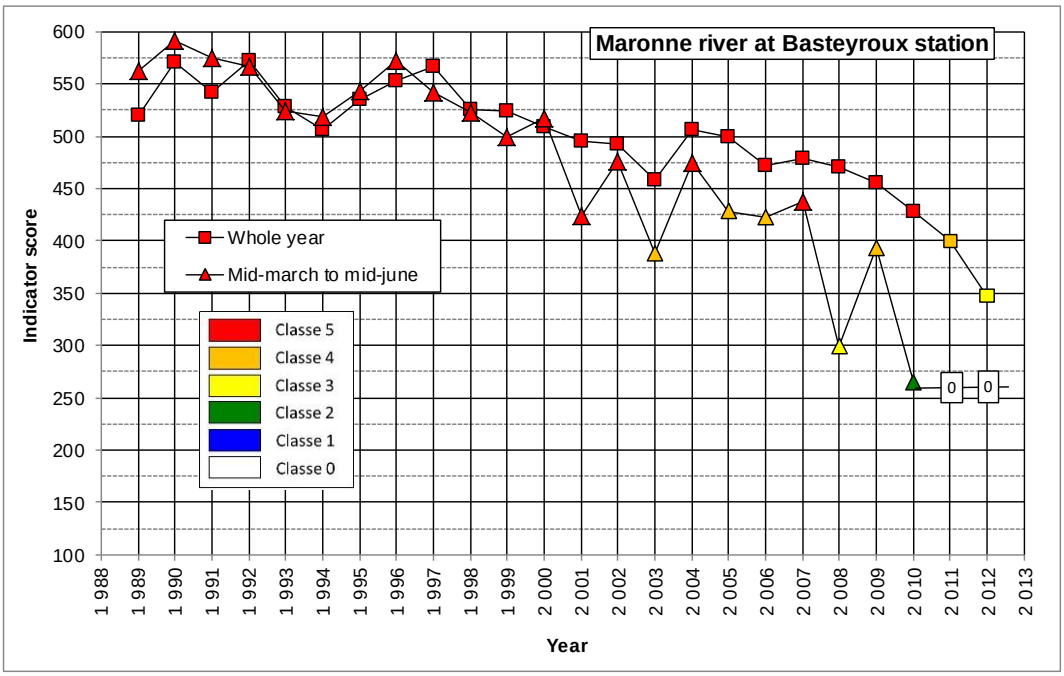


Figure 77: Evolution of the Hydropeaking indicator on the Maronne river at Basteyroux station for the whole year and during the spring (mid-march to mid-june); effect of the progressive implementation of mitigation measures since 2001.

Other information:

The Hydropeaking Indicator is implemented in an Excel sheet, using a macro coded in Visual Basic. The tool can be transmitted for free by the Ecohydraulic Team AFB-IMFT after agreement.

References:

Courret D, 2010. Etude des gradients des variations de débit naturelles en vue de la fixation des critères pour le repérage des éclusées hydroélectriques. Rapport GHAAPPE RA.09.04.

http://oai.eau-adour-garonne.fr/oai-documents/59478/GED_00000000.pdf

Courret D, Larinier M, Baran P, 2014. Développement d'une méthodologie de caractérisation des éclusées hydroélectriques et Définition d'un indicateur du niveau de la perturbation hydrologique induite (seconde version). Rapport GHAAPPE RA.14.02.

Courret D., 2014. Caractérisation de la perturbation hydrologique induite par les régimes d'éclusées hydroélectriques et définition d'un indicateur - Réflexion sur les mesures de mitigation des impacts des éclusées sur les populations de poissons. Thèse de l'INP Toulouse.

http://ethesis.inp-toulouse.fr/archive/00002880/

Contact information:

Authors	Dominique Courret (AFB)
Reviewers	Robert Boes (ETHZ)

2.28. Hydropeaking tool

Developed by: SINTEF Energy Research

Date: Under development

Type: Tool (Excel file)

Suitable for environmental flow (hydropeaking) mitigation measure in all phases (planning, implementation, maintenance)]

Introduction:

The Hydropeaking Tool is a tool for assessing the impacts of hydropeaking on fish populations in regulated rivers. It is available as an Excel file.

The hydropeaking tool is based on a method for assessing impacts from hydropeaking developed for salmonids at SINTEF Energy as a part of the CEDREN EnviPeak project (Norwegian Research Council, Grant number 193818).

The Hydropeaking Tool is currently under development in FitHydro for the Iberian barbel and the grayling, in addition to salmonids. Factors that determine the assessment will be modified or adding for these species. Criteria and thresholds will be adjusted too.

Application:

In the Hydropeaking tool, the impacts from hydropeaking are divided into two axis: direct effects from hydropeaking and vulnerability of the fish population to hydropeaking. The *effect* axis characterises the possible ecological impacts of peaking from how physical conditions such as flow, water level and water covered area changes, given the hydropower system and

river morphology. The *vulnerability* axis characterises how vulnerable the system is to further influence from peaking. Both axis may be evaluated separately, but we also provide a system to combine them and obtain an overall assessment of hydropeaking (Figure 78). The starting point for the evaluation of the current situation is a regulated river without peaking operations.

The current version of the Hydropeaking Tool is available in Excel®. The user has to enter the input values for effects and vulnerability parameters for the studied rivers in the corresponding tables. These input values can be obtained from numerical modelling, analysis of water level/discharge time series, and fieldwork.

The outputs from the Hydropeaking Tool are the score of effects factors, the score of vulnerability factors, and the score for the combined assessment (Figure 79).

The Hydropeaking Tool aims at being used to assess existing or planned hydropeaking. It also gives the user a possibility to see which parameters have a low score, helping to identify where mitigation should be concentrated.

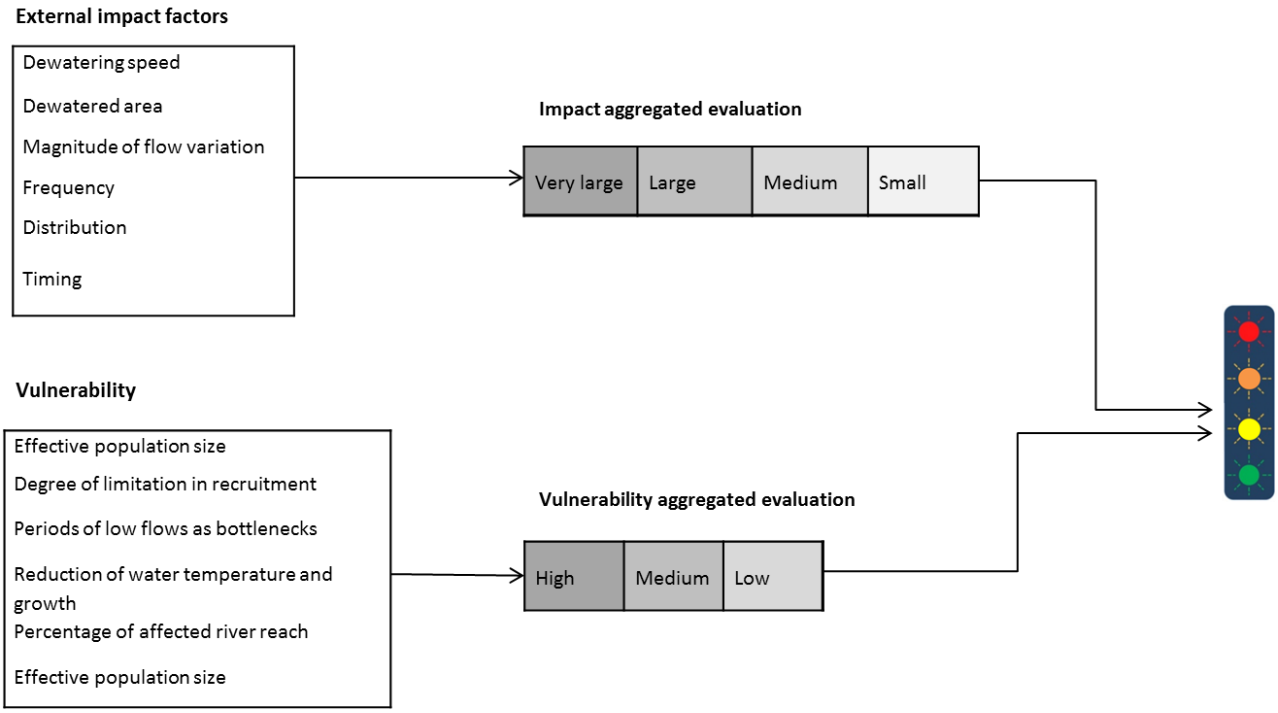
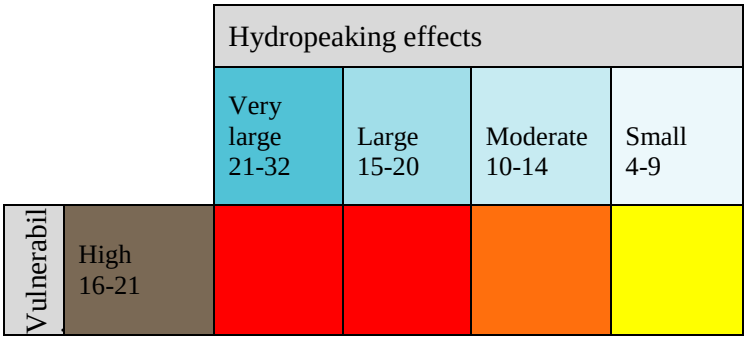


Figure 78 Principle of the hydropeaking tool for categorization of regulated rivers according to the potential impacts of hydropeaking on fish population.



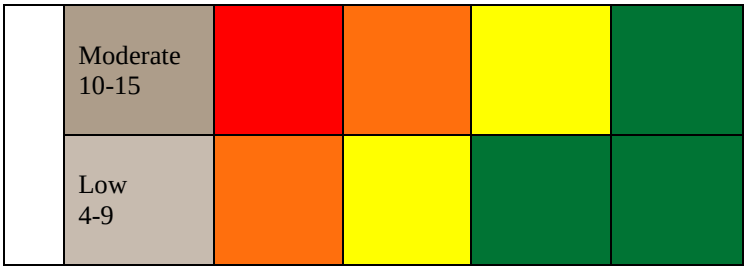


Figure 79. Combinations of hydropeaking effects and vulnerability for total impact assessment

Other information:

The Hydropeaking tool will be a deliverable of the FitHydro project.

References:

Harby et al., J. 2016. A method to assess impacts from Hydropeaking. *Proceedings of 11th International Symposium on Ecohydraulics, Melbourne, Australia.*

Bakken, T.H., Forseth, T and Harby (2016), Miljøvirkninger av effektkjøring: kunnskapsstatus og råd til forvaltning og industri. NINA Special Report 62, Trondheim, Norway.

Forseth, T and Harby (2014), A. Handbook for environmental design in regulated salmon rivers. NINA Special Report 53, Trondheim, Norway.

CEDREN www.cedren.no

Contact information:

Authors	Julie Charmasson (SINTEF)
Reviewers	Robert Boes (ETHZ)

2.29. COSH-TOOL

Developed by: SINTEF Energy Research

Date: 27-11-2018

Type: Tool (computer model)

Suitable for environmental flow (hydropeaking) mitigation measure in all phases (planning, implementation, maintenance)

Introduction:

The COSH-Tool is a software written in Python used for quantifying fluctuations in water level and discharge which may occur in rivers subjected to hydropeaking. The COSH-Tool was developed at SINTEF Energy as a part of the CEDREN EnviPeak project (Norwegian Research Council, Grant number 193818) with the aim of providing characteristics of hydropeaking events in regulated rivers in order to classify the hydropeaking regimes of rivers.

The tool enables the analysis of long time series of water level or discharge by applying an automated processing to the time series. It provides a set of indicators that characterize fluctuations of water level and discharge in rivers and lakes/reservoirs.



Figure 80.The river Lundesokna in Norway downstream of a peaking hydropower plant. COSH-Tool can be used to asses many aspects of peaking operations.

Application:

The COSH-Tool can be applied to any water level or discharge time series provided by measurements (field work, Figure 80) or simulation (numerical modelling). The analysis of the time series using the COSH-Tool does not require any coding from the user and is executed through an interface.

Input files:

The input file is a water level or discharge time series. The COSH-Tool handles time series with typical time steps ranging from a minute to an hour.

Output files:

The COSH-Tool computes a set of parameters that characterise water level and discharge fluctuations. The parameters can be classified into three categories: 1) magnitude of the variations; 2) timing and speed; and 3) frequency. The parameters are listed in Table 4.

Table 4. List of parameters computed by COSH-Tool.

	Parameter	**Unit**
Magnitude	Flow	m^3/s
	Stage	m
	Flow maximum/minimum of a flow increase	m^3/s
	Flow maximum/minimum of a flow decrease	m^3/s
	Stage maximum/minimum of a flow increase	m
	Stage maximum/minimum of a flow decrease	m
	Flow ratio of a flow increase/decrease	-
Scale of time	Mean rate of flow increase/decrease	$m^3/(s*h)$

	Mean rate of stage increase/decrease	cm/h
	Maximal rate of flow increase/decrease	$m^3/(s*h)$
	Maximal rate of stage increase/decrease	cm/h
	Time of the start/end of a flow increase	hh:mm
	Time of the start/end of a flow decrease	hh:mm
	Duration between a flow increase and a flow decrease	min
	Duration between a flow decrease and a flow increase	min
Frequency	Count of flow increases/decreases per year	-
	Portion of days with *n* flow increases/decreases per day	-
	Portion of flow increases/decreases during daylight, twilight, darkness	-

The output of the COSH-Tool consists in a table with statistics of the magnitude and timing parameters (category 1 and 2) and a set of corresponding graphs. Statistics are min, max, mean, median, standard deviation and percentiles. They can be computed for the entire time series, as well as on a monthly, seasonal and yearly basis. Statistics are also displayed in the form of box plots.

The COSH-Tool provides also values and graphs for all frequency parameters (category 3), namely distribution of peaks through the day (Figure 81), number of peaks per day for each year of the time series (Figure 82), and the total number of peak events per year.

Additionally, the light conditions (day, twilight, darkness) at the time of the occurrence of the peaks can be computed. A graph provides the proportion of peaks occurring at the different types of light conditions per month (Figure 83).

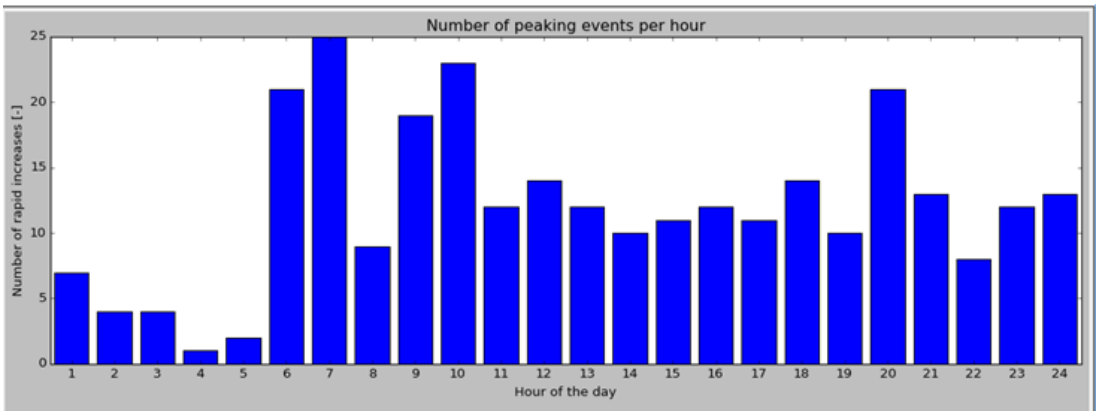


Figure 81. Distribution of peak events though the day.

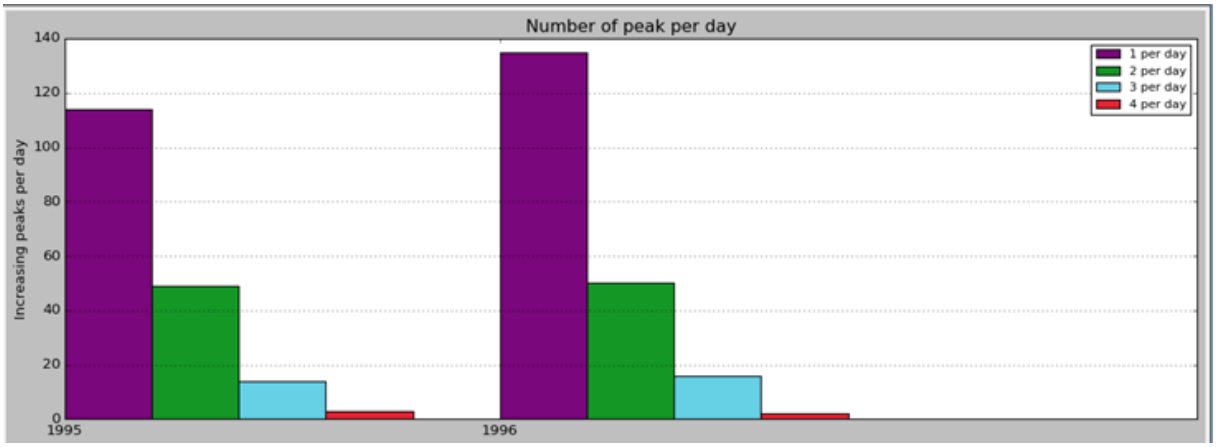


Figure 82. Number of peak events per day for each year of the time series.

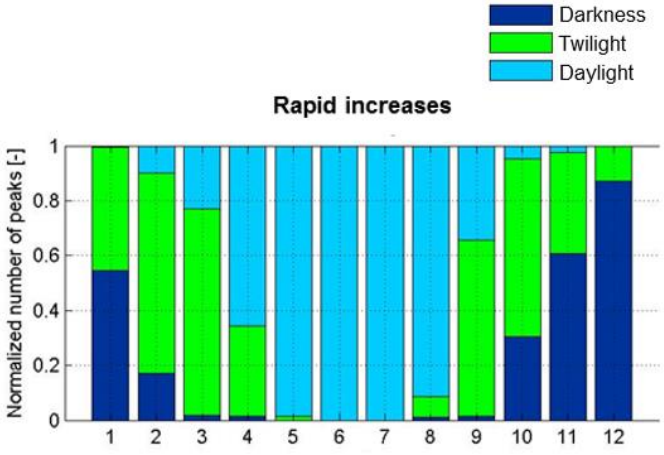


Figure 83. Distribution of peak events (increasing events) per month according to light conditions

Other information:

The COSH-Tool is free of use after agreement with SINTEF Energy Research.

References:

Sauterleute J. and Charmasson J. (2014). A computational tool for the characterisation of rapid fluctuations in flow and stage in rivers caused by hydropeaking. *Environmental Modelling & Software* **55**:266-278.

Charmasson, J. (2016). COSH-Tool, a computational tool for the characterization of rapid fluctuations in flow and stage in rivers caused by hydropeaking. *Proceedings of 11th International Symposium on Ecohydraulics, Melbourne, Australia.*

Caetano, L., Pinheiro, A. and Boavida, I. 2018. Analysis of the effects of a hydropower plant in the downstream fish habitat. COSH-tool application. *Proceedings of 12th International Symposium on Ecohydraulics, Tokyo, Japan.*

Contact information:

Authors	Julie Charmasson (SINTEF)
Reviewers	Robert Boes (ETHZ)

2.30. Sediment Simulation in intakes with Multiblock option

Developed by: NTNU

Type: Tool, numerical simulation

Suitable for habitat related to hydraulics and sediment (substarte) mitigations measures in all phases (planning, implementation, maintenance)

Introduction:

SSIIM is a numerical model to simulate the hydraulics and sediment transport including bed changes as well as various other parameters related to water quality in fluvial environment. It solves the Reynolds-averaged Navier-Stokes equations in all three directions and calculates the turbulent kinetic energy and dissipation through the standard k-ε model. The calculated bed changes are directly coupled to the time steps in the hydraulic computations. SSIIM can use both, an unstructured and a structured grid to discretize the domain of interest.

Application:

After downloading the SSIIM executable from the webpage mentioned below, the text files control and koordina have to be established. The control file lists all the control parameter which SSIIM is supposed to execute. There are various parameters depending on the results the user wants to achieve. The koordina file is used to describe the geometry of interest.

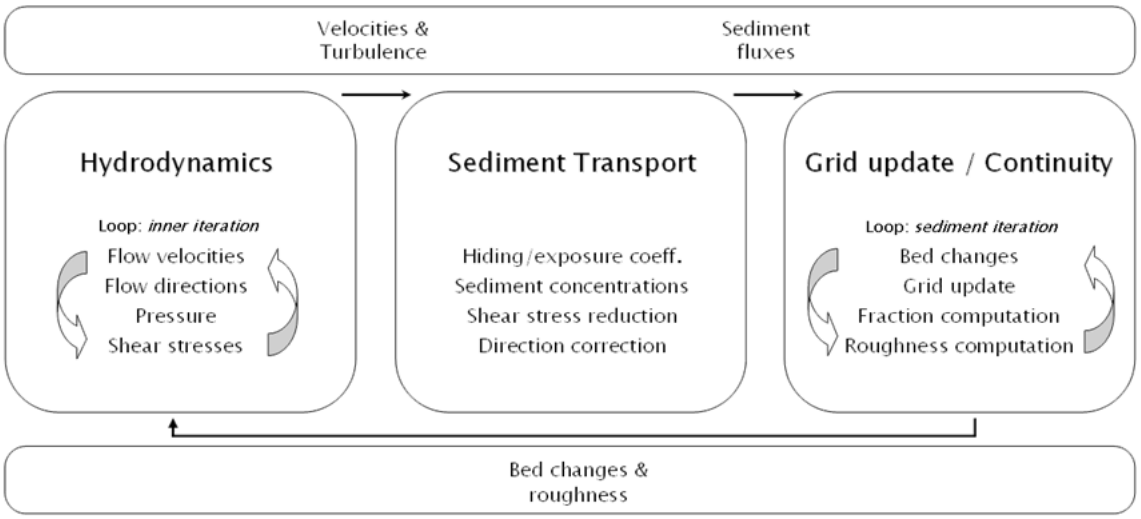


Figure 84: flow chart of the executable SSIIM.

Figure 84 shows the flow chart in which way SSIIM is working.

The application of the user does not require any coding, however, the user has to specify certain parameters and the geometry as text in the above mentioned files. These files are generated with any text editor and linked to the main executable. A detailed description can be taken from the manual (Olsen, 2018). The application varies from the most basic simulation of a steady state hydraulic computation to the most complex one, when combining unsteady flow with multiple sediment sizes and wetting and drying of parts of the geometry.

INPUT:

To start a most basic version of a time dependent sediment transport model of a river reach you have to have the geometry in terms of a point cloud file, the discharge $Q_{in=out}$, the

waterlevel height at the downstream end of the reach and the prevailing sediment grain size distribution at the river bed.

OUTPUT:

All the available output parameters can be displayed in the graphical user interface and copied into the clipboard (Figure 85). In addition, it is possible to use a separate post processing toll, like freeware Paraview (https://en.wikipedia.org/wiki/ParaView) or commercialized Tecplot (https://en.wikipedia.org/wiki/Tecplot).

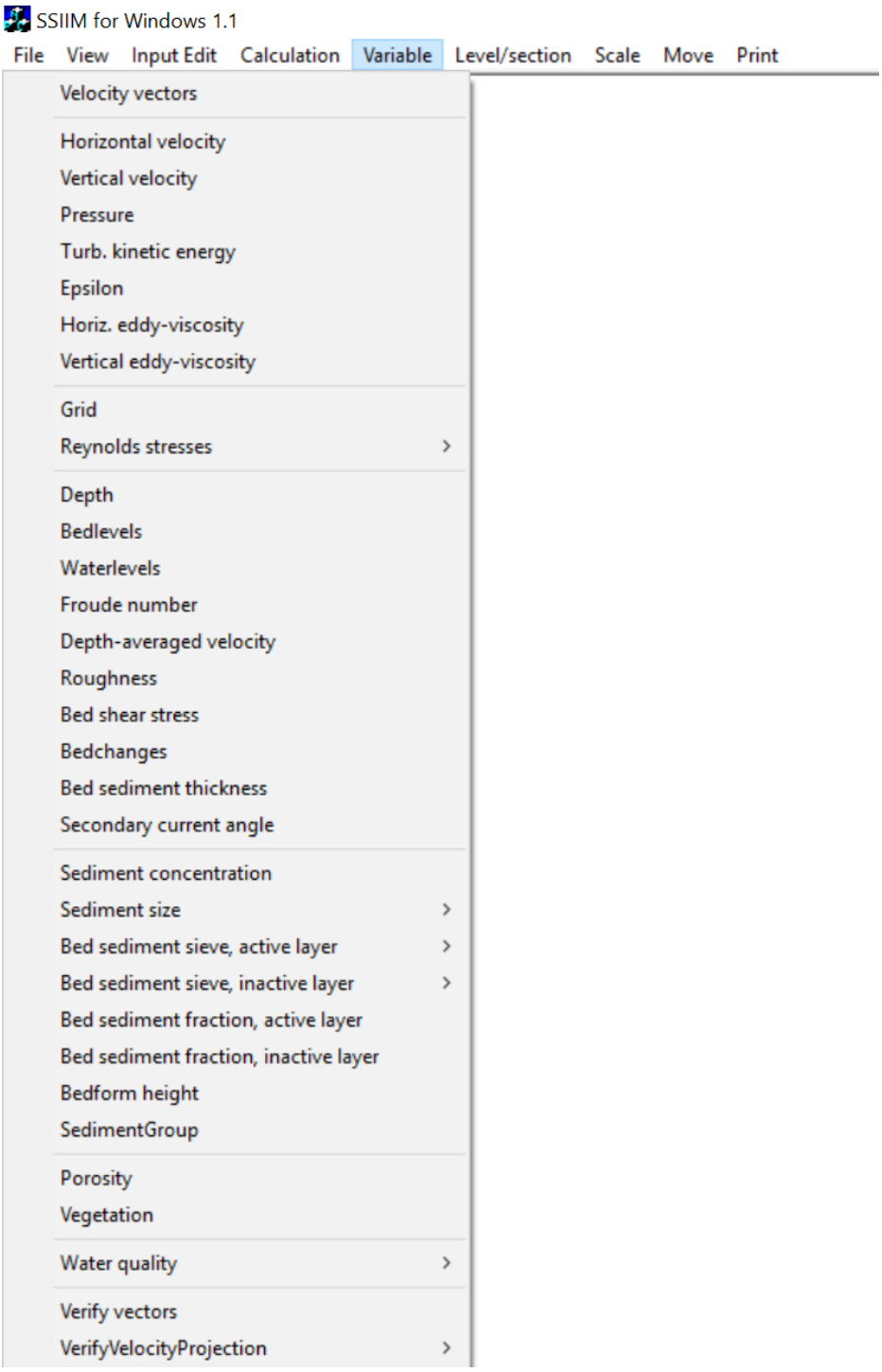


Figure 85: List of all available parameters.

EXAMPLES:

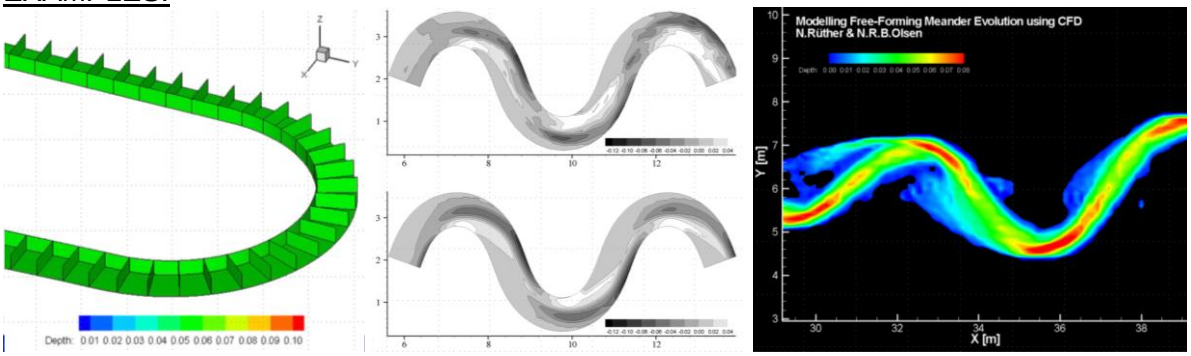


Figure 86: Examples of simulations with SSIIM.

Other information:

The numerical model can be download free of charge at the webpage listed below. There is a large user group and information is available at many places.

References:

Olsen, N.R.B. (2018), SSIIM user manual (http://folk.ntnu.no/nilsol/ssiim/manual5.pdf)

Contact information:

http://folk.ntnu.no/nilsol/ssiim/

Authors	Nils Rüther (NTNU)
Reviewers	Robert Boes (ETHZ)

2.31. General discussion on the tools – Workshop 25th January 2019, Lisbon, Portugal

Workshops on Laboratory and field measurement techniques and hydraulic and habitat measurements within FIThydro were held in Lisbon on the 25th January 2019. The workshops aimed to present the laboratory and field measurement techniques and the hydraulic and habitat modelling tools. The presentations had to address the following questions:

1) How and why is this technique used in FIThydro? How are the results prepared? Is there anything special to mention as e.g. special knowledge or high effort for post-processing of data or special preparations before you can start the experiment/measurement? Which questions can be answered using this technique and which cannot (application range and restrictions)? What are the challenges/limitations of using the technique (practical problems/advice)?

2) How can we make results comparable? How many cross sections do we need? What is the min/max level of detailedness we can achieve? Which file format is needed/ does the outcome feature?

Each presentation was followed by a short discussion. The results of these discussions are presented below.

The programs of the two workshops are available in the appendix.

2.31.1. Laboratory and field measurement techniques

- Measuring velocity fields using ADV and LLP by Ana Quaresma (IST-ID) (see 2.22)

The quantitative difference in terms of costs of the ADV when compared to PIV depends on the case and the seeding needed. The commercial PIV equipment itself is much more expensive than the ADV and also seeding in PIV can have a high cost (depending on the type and quantity needed). The post-processing needed for the PIV data is more demanding in time and computational effort. However, the sampling point of an ADV is larger so for higher gradient the error is larger, too. The limitations of assembling several ADV devices to measure are mainly the acquisition of the devices, the space needed to their assembly and also the synchronization needed for the measurements to obtain 2D maps of velocity fields.

- Large-scale PIV systems by Kordula Schwarzwälder (NTNU) (see section 2.23)

In general, the field application of large-scale PIV systems can result in high cost. Whereas the equipment itself is getting cheaper as the technology (e.g. for cameras and drones) develops very fast, high costs might occur due to field conditions and the high number of field workers required for the seeding purpose but also for calibration and post-processing. This technique needs several people to be executed (for the proper distribution of the seeding) and it might not be possible to be applied in wider rivers. The seeding should follow the flow and be biodegradable (one of the seeding used in this experiment consisted of a type of corn). Wind is an issue with the Large-scale PIV as it can hinder the seeding to follow the flow, but also reflection and shadows can influence the result. This technique is generally restricted to surface velocity measurements. Calibration and post-processing is needed as in any PIV system.

- Field experiences with an ADCP mounted on a remotely-operated boat by Ismail Albayrak (ETHZ) (see 2.21)

This equipment allows obtaining relatively quickly high resolution 3D velocity fields and bathymetry information as a side product. Both velocity and bathymetry data can be used for 3D numerical model construction, calibration and validation. One of the challenges/limitations for the bathymetric measurements is to measure the water surface level (altimetry) accurately, which depends on the GPS. Although the current and widely used DGPS devices provide longitude and latitude coordinate in an accuracy of -±6 cm, their accuracy drops to approx. ±40 cm for altitude measurements depending on the model of the DGPS device. To overcome this problem, a novel and low-cost technology ublox RTK-GPS (https://www.u-blox.com/en/product/c94-m8p), in comparison with traditional DGPS calibrations is already integrated into the ADCP system and will be tested in the field by ETHZ. With the new ublox RTK-GPS, ±2 cm of accuracy in altitude measurements is expected. The ADCP and Q boat system allows measurements in wide and deep rivers more easily than other methods (because of the remotely operated boat). This equipment provides moving bed data, which can be used to measure bedload transport, but calibration is needed.

This equipment is quite costly but also offers technical specifications which can provide measurements with high accuracy. One advantage of this ADCP is that its 5th beam working at 600 Hz provides a direct measurement of vertical velocity and flow depth up to 120 m. Water temperature and suspended solid concentration may limit the velocity and water depth measurements obtained from its 4 beams working at 1200 Hz. Other limitations include the number of transects that must be performed to represent adequately the flow field and unmeasured discharge in near-shore areas and close to the bottom. Increasing the number of transects increases the accuracy of velocity data, in particular in highly turbulent flows. The ADCP can also be used to measure suspended sediment concentrations, but the signal to noise ratio becomes a problem here and calibration with concentration data obtained with other techniques such as water sampling is needed for this approach. Further, it has to be

mentioned that an autonomous tour of the boat depends highly on the accuracy of the map material and needs to be tested very carefully.

- Global Navigation Satellite Systems in Hydraulic Measurements by Markus Först (SWECO) (see 2.17)

The accuracy depends on several factors: the number of satellites and availability; the angle between satellites; reflections from buildings or other obstacles and atmospheric conditions. Bathymetry measurements are generally more affected by the accuracy than discharge measurements. For instance, for bathymetric measurements, steeper slopes need higher precision and hence a very narrow mesh compared to gentle slopes. This technique needs a stationary station.

- Ecological Intelligence: merging models, maps, sensors and drone imagery with machine learning and big data by Jeffrey Tuhtan (TalTech)

We should focus on big data, which are already available from several different origins. It is important to link the data and the Solutions, Methods, Tools and Devices (SMTD) we are studying and applying in FIThydro. Furthermore, the data from the Test Cases in FIThydro should be applied on a bigger scale. We should learn from Precision Agriculture that already uses the same methods such as Machine Learning to link and interoperate the different methods and technologies. However, there is still the need to get more biological information as basic input and the existing techniques should be linked and used for that so also some funding (thinking about further research) should come from the biological science side. It is also crucial not only to collect huge amounts of data but to clarify in advance how can we organize and share the data.

- General discussion on the topic

The question on how to combine all results has been raised. Very often the approach is not the good one: measures in the field and then reflection on what to do with the data. The right approach is to do field measurements with a precise goal (for example bathymetry measurements in order to build a hydraulic model).

Before doing field measurements, an exercise should be done: hypothesis on what kind of data we want, we need and what we want to obtain from these data. It leads to the way to obtain these. And the big data needs to be linked to real data, too, so the learning part, especially for machine learning and ANN, is quite crucial.

- Acoustic telemetry: fish tracking in 1, 2 and 3-D by Johan Coeck (INBO) (see 2.2)

The technology of both, the telemetry transmitters and receivers has been evolving. For instance, even predation can be studied by an ID change that happens when stomach acids digest a polymer of the transmitter (predation tag). High frequency telemetry (HR signal transmission) offers a better solution for studies conducted near the turbines because the signal pinging and transmission is much faster and thus more reliable (less interference). It can be used in fresh and salt water, thus it offers more possibilities to monitor different life cycle stages of diadromous fish species. Combining 2-D and 3-D acoustic telemetry offers advantages to monitor fish behaviour because it provides information about depth preferences used by the fish.

Questions arose on the sampling size (number of fish) needed to obtain statistically significant results, however, in telemetry studies, one of the major concerns about the sample size is directly related to monetary costs of the equipment, i.e. the number of transmitters.

- Radio telemetry systems in the Aare River by Armin Peter (Peter FishConsulting) (see 2.3)

Radio telemetry is mainly restricted to freshwater because water conductivity must be less than 1000°µS/cm, which is why it can only be performed in shallow streams and rivers. The transmitters' insertion in fish was referred. The weight of the transmitter should not exceed 2% of the total weight of the fish. This rule of thumb was emphasized and the body cavity was referred to be the preferable fish area to insert the transmitter. There are already very small transmitters, for instance, a fish of 12 cm (e.g. bullhead) may be marked with a very small transmitter. The size of the transmitter must be selected according to the size of the fish and the objective of the study because smaller transmitters also have less battery. There is also the possibility to attach tags externally; however, these are not working well and clearly might influence the behaviour of the fish. The number of receivers increases the range of the detected signals but it also increases the cost of the study. The prices have not changed much with the years; it is still an expensive system. It has limited depth information although fish can be detected over long river distances. The question on the sampling size needed to obtain statistically significant results was mentioned again.

- Fishtracking: PIT-Tag Technique by Manon Dewitte (CNRS-Pprime) (see 2.4)

The low cost and small size of the tags are big advantages. The absence of a battery is the greatest advantage of the PIT tag since it allows the production of much smaller tags that can be used on smaller organisms, which will last all the lifetime of the fish. However, the location of antennas is important and noise sources need to be evaluated (for example metal materials near the PIT-Tag antennas receivers can cause problems). Comparing the full-duplex (FDX) and half-duplex (HDX) systems, the later does not have the same interference issues as the FDX systems and, therefore, may be recommended to avoid noise interference.

- 3D Ultrasonic Fish Tracking – current state of the experiment by Peter Rutschmann (TUM) (see 2.6)

This technique is used for other objectives, for example, in concrete, but it should work in water, too. It is still in a very preliminary stage. The pilot studies suggest that this technology will be able to identify fish species based on the fish bladder's shape.

- 3D fish tracking system for etho-hydraulic investigations by Ismail Albayrak (ETHZ) (see 2.5)

A 3D fish tracking system is developed for etho-hydraulic laboratory tests at VAW, ETH Zurich (live-fish tests). The system consists of IP cameras with fish eye lenses, lamps, network switches, high performance computer for video recording and data analysis and fish tracking software developed by VAW. A simple calibration of the cameras is needed. The lighting conditions are very important. Tracking of individual fish in a group of fish is challenging because of fish overlapping in the view of cameras. Aerated flows and turbidity can also affect fish detection. Visual noise such as light reflection from the glass walls cause problems of fish detection but can be eliminated during the post processing of the data or by covering the glass windows with a dark foil. Overall, the system has relatively high costs because of professional cameras, lenses and waterproof housing. However, using GoPro or cheaper cameras can reduce the overall cost of the system.

- How to link shelter availability and sediment by Kordula Schwarzwälder (NTNU) (see 2.16)

The method is based on the use of a plastic pipe mimicking a small fish seeking shelter. As nothing else is needed than a frame, a pipe and notes it is a very cheap and fast method to collect information about the shelter availability. Recommendations about the data processing were suggested: the data should be processed in a software like MATLAB or R. If so, the post-processing is fast and simple. A restriction is the fact, that the information is only collected for the area above the interstitial, hence the results cover only a certain type of shelter. To reduce the error, the sampling should be performed by the same person.

2.31.2. Hydraulic and habitat modelling tools

- Hydropeaking indicator by Dominique Courret (AFB) (see 2.27)

The thresholds of the categories are different from the ones in Norway, indeed the tool has been developed in France. The tool is built on French study cases; it has not yet been tested elsewhere nor adapted to other regions.

The approach is based on hydrological statistics, how can we link it to ecology? Some biological data linked to hydrological data already exist like recruitment. But we need years of data for each parameter and there is not enough hindsight for now. The relationship between the indicators is not always well acknowledged.

There is no paper released for now, only Dominique's thesis manuscript.

- Cosh tool by Julie Charmasson (SINTEF) (see 2.29)

The best time step for the hydrological data is around 10 minutes. Less will be too long to process. More will increase the risk of missing an event, definitely 1 hour is much too long.

How is it possible to make a difference between natural events and artificial peaks? The user gives the mean rate of change of peaks, it is different for natural events and hydropeaks. So the tool can detect the difference.

- Hydropeaking assessment tool by Julie Charmasson (SINTEF) (see 2.28)

2 types of factors: effect factor and vulnerability factor. For the last one, the scoring goes from 4 to 32 and not from 7 to 32 - why? The vulnerability score has been reduced because of the possibility of "improvement". For example, during low flow periods, there is more water in the river stretch because the HPP induces a "regulation", so the vulnerability score is reduced.

It is important to note that the tool has been developed for salmonids. The tool is now being adapted in FIThydro to make the tool usable for other species. It will be tested in the GKI Inn (Austria) and Bragado (Portugal) Test Cases for the grayling and the Iberian barbel and the Grayling.

- General discussion on presented hydropeaking tools

In the tools developed in Norway, the comparison is made between hydropeaking and regulated rivers, does it make sense also in other countries? The effect of hydropeaking is assessed by comparison on a river with a HPP with and without hydropeaking.

In France, hydropeaking is compared with the natural state of the river. The global effect of the HPP is assessed and not only the effect of hydropeaking.

The tools are not yet accessible, but a publication about the hydropeaking assessment tool exists. Tests are being performed in order to assess the applicability of the Cosh tool.

- River 2D by Isabel Boavida (IST) (see 0)

Shallow waters are a limitation of the software because it induces numerical instabilities.

Another limitation is that some factors of the model are not changing during simulation, for example, shadow due to trees during the day influences the habitat, but this factor cannot change during the simulation according to the time of the day.

It also does not consider the arithmetic mean to calculate the Weighted Usable Area (WUA) contrarily

The last released version is from 2010, which is also a limitation when compared to other software.

- Casimir by Matthias Schneider (SJE)

It is possible to map the substrate but precise data are needed.

For now, the work has been done with graylings because we know their behaviour. When the flow is low, they usually do not move. When there is enough flow graylings are swimming against it. The habitat preferences are also known for graylings.

It is possible to use this software on a large scale, not only on a local scale. It is possible to run the model dynamically, it has already been done, but it takes longer and it is possible only for short stretches (not for 40 km).

- 1D/2D (HEC-RAS) by Ana Quaresma (IST)

The sediment module of HEC-RAS is challenging because you need to have sediment data to calibrate and validate it, and this data is most of the time not available. Since there are six different transport functions available, and these are all empirical there is a big variability in the results obtained by their application so, to choose the appropriate transport formula among those proposed by the software, sediment data to calibrate the model and also to validate the results are needed.

One of its strengths is to combine 1D and 2D easily which enables its use with large river systems. Flexible mesh generation with combined structured and unstructured mesh types is another advantage of the software. The mesh can be adapted according to the terrain controlling features (finer mesh around the dam and key features of the terrain that will control water movement). HEC-RAS uses high resolution sub-grid modelling which allows the use of larger cell sizes with gains in the computational time without compromising the resolution of the results since the underlying terrain resolution is still kept and accurately represented.

- Basement by David Vetsch (ETHZ)

The last version of the software can be 40 times faster thanks to the use of several graphic cards at the same time (but only Nvidia cards).

- 3d (Openfoam + Flow 3D) by David Vetsh (ETHZ)

Multiphase flow can be accurately modelled using Openfoam which solves an equation for each phase.

In FIThydro, 3D modelling is used to assess the influence/role of a guiding screen on the flow.

To look at close details, Openfoam should be preferred. For more engineering considerations/practical use, Flow 3D should be used, indeed it is often used for design approaches.

Star CCM+ is another 3D tool.

- Sediment modelling by Nils Rüther (NTNU)

The bedload transport is studied at the HPP Schiffmühle Test Case: the substrate grain diameter distribution is being studied according to the hydrology to correlate it with the substrate shelter availability and predict shelter availability.

To perform this numerical modelling sediment inflow is needed for the boundary conditions and also to validate numerical model results. According to Nils and Ismail this data is available or will be estimated.

2.32. Conclusion

All the SMTDs presented are used at the Test Cases to conduct different activites addressing upstream migration, downstream migration, passage through turbine, hydropeaking and hydromorphology-habitat. Their application ranges will be discussed in sections 4 to 8.

These presentations will later be available and updated online in a wiki system (WP4).

The 5 following sections are discussions on FIThydro main topics: upstream migration, downstream migration, passage through turbines, hydropeaking and hydromorphology. They aim to extract the appropriateness, constraints and limitations of the mitigation measures at Test Cases and in the laboratories; to deduct the range of application, accuracy and limitation of existing on-site monitoring tools and methods; and finally to identify the knowledge gaps and needs.

As all the results of the Test Cases are not yet available, some lessons will be learnt later in the project and will be part and completed in a wiki system (WP4) as a living product.

3. Results at the Test Cases

In this deliverable, the work done at 14 FIThydro Test Cases spread over 4 regions: France and Belgium, the Alpine region, the Iberian Peninsula and Scandinavia is presented.

Several activities are conducted at each Test Case. Each site has been presented in deliverable D2.1. While in this deliverable, only the activities at the Test Cases will be presented. For more precise detail about the configuration of the site or the objective of the activites at each Test Case, please refer to D2.1 delivered to the EU in October 2018.

The activities conducted at the Test Case address 5 topics: upstream migration, downstream migration, passage through turbine, hydropeaking and hydromorphologie/habitat. As all results are not yet avalailable, some information is still missing. At the end of the project – November 2020 – a document for each Test Case will be avalaible in order to gather the presentation of the site, the objectives and the results of the activities.

However, some of the activites at the Test Cases will be conducted in the context of WP3. For further information, please refer to the deliverables of WP3 and WP4.

Test Case	Authors	Reviewers
Altheim	Cornelia Felber (UNIPER)	Peter Rutschmann (TUM)
Altusried	Tobias Epple (BEW), Ine Pauwels (INBO), Matthias Schneider (SJE)	Peter Rutschmann (TUM)
Anundsjoe	Kordula Schwarzwälder (NTNU), Angela Odelberg (Statkraft), Claudia Strobl (TUM)	Alte Harby (SINTEF)
Bannwil	Ismail Albayrak (VAW, ETH Zürich), Stephan Kammerer(VAW, ETH Zürich), David Vetsch (VAW, ETH Zürich), Robert Boes (VAW, ETH Zürich), Armin Peter (FCO), Jeffrey Tuhtan (TUT), Ulli Stoltz (VOITH) and Carl Robert Kriewitz-Byun (BKW)	Ismail Albayrak (ETHZ)
Bragado	Isabel Boavida (IST)	Antonio Pinheiro (IST)
Freudenau	Walter Reckendorfer (Verbund)	Peter Rutschmann (TUM)
Gotein	Manon Dewitte (CNRS), Laurent David (CNRS), Dominique Courret (AFB)	Laurent David (CNRS)
Günz	Thomas Lechner (IBF UMWELT)	Peter Rutschmann (TUM)
Guma and Vadocondes	Javier Sanz-Ronda (SAVASA), Francisco Godinho (HYDROERG)	Antonio Pinheiro (IST)
Ham	Ine Pauwels (INBO)	Laurent David (CNRS)
Las Rives	Manon Dewitte (CNRS), Laurent David (CNRS), Dominique Courret (AFB)	Laurent David (CNRS)
Schiffmuhle	Ismail Albayrak (VAW, ETH Zürich), Muhammadreza Maddahi (VAW, ETH Zürich), Cristina Rachelly (VAW, ETH Zürich), Martin Detert (VAW, ETH Zürich), Robert Boes (VAW, ETH Zürich), Armin Peter (FCO), Christian Milzow (AF-Consult), Jeffry Tuhtan (TUT), Kordula Schwarzwälder (NTNU), Nils Ruther (NTNU), Andreas Doessegger (LKW)	Ismail Albayrak (ETHZ)
Trois Villes	Manon Dewitte (CNRS), Laurent David (CNRS), Dominique Courret (AFB)	Laurent David (CNRS)

List of figures

Figure 69: Drone picture taken in a height of 50 m over ground showing the residual flow area in Anundsjø HPP, ice cover and the author. 99
Figure 70: First run of a structure from motion evaluation in the lab of NTNU. The blue field indicates the camera position. 99
Figure 71: Screenshot of the Argisoft Photoscan Workflow. 100
Figure 72: Mesh generated from SfM from a section of the residual flow reach of Anundsjø. 101
Figure 73: Current meter: a) mechanic, b) electro-magnetic, c) acoustic. Sources: SEBA hydrométrie, OTT, Sontek. 103
Figure 74: Cutting of a section during the measurement by a flow meter, in red the verticals, the black dots correspond to the measurement points. 104
Figure 75: Operator in the downstream migration channel for measurements with a current meter. 104
Figure 76: Example of flow analysis. 106
Figure 77: Evolution of the Hydropeaking indicator on the Maronne river at Basteyroux station for the whole year and during the spring (mid-march to mid-june); effect of the progressive implementation of mitigation measures since 2001. 107
Figure 78 Principle of the hydropeaking tool for categorization of regulated rivers according to the potential impacts of hydropeaking on fish population. 109
Figure 79. Combinations of hydropeaking effects and vulnerability for total impact assessment 110
Figure 80.The river Lundesokna in Norway downstream of a peaking hydropower plant. COSH-Tool can be used to asses many aspects of peaking operations..... 111
Figure 81. Distribution of peak events though the day. 112
Figure 82. Number of peak events per day for each year of the time series. 113
Figure 83. Distribution of peak events (increasing events) per month according to light conditions..... 113
Figure 84: flow chart of the executable SSIIM. 114
Figure 85: List of all available parameters. 115
Figure 86: Examples of simulations with SSIIM. 116
Figure 87 : Map (tilted, North is left) of Anundsjø showing the different areas according to tab. 1 137
Figure 88 : The Sontek M9, one mounted on a kayak (left) and an autonomous boat (right) 138
Figure 89 : ADV measurements in the bypassed reach..... 140
Figure 90: First results from the SfM measurements in the residual flow reach 141
Figure 91: Barrier guiding towards the fishway entrance approx. in the middle of the lake (red line)..... 142
Figure 92 : Flow velocity in front of the turbine with very shallow areas in most parts (less than 1 m) and the deep areas of the intake..... 142
Figure 93: Teledyne Marine Q-boat of VAW equipped with ADCP probe and GPS antenna. 145
Figure 94: Workflow used for post-processing of ADCP data (modified from [2]). 145
Figure 95: Location of variables in FLOW-3D computational mesh [1]. 146
Figure 96: Model domain (within model boundary) and topographic data used to set up the numerical 3D model (background image: © 2018 swisstopo (JD 100041))..... 147
Figure 97: Riverbed bathymetry in coordinate system of the 3D model. 147

Back to D2.2 Main index

Figure 98: Power plant components represented in the 3D model, view from upstream (left) and downstream (right) 148
Figure 99: Grid resolution of the 3D model with full domain (on top) and exemplary grid refinement for restart simulations of a particular subdomain (at bottom)..... 149
Figure 100: Hydro-acoustic imaging setup with DIDSON and ARIS sonar systems in front of the trash rack. 6 different positions were covering the area in front of the trash rack. View in flow direction. 151
Figure 101: ARIS sonar system at HPP Bannwil. Left: ARIS explorer sonar mounted on an arm of the Palfinger trash rack cleaner. Right: lowered arm with ARIS system in data recording status. 151
Figure 102: Depth-averaged flow velocities [cm/s] upstream of HPP Bannwil measured with boat-mounted ADCP at a discharge of 402 m^3/s (background image: © 2018 swisstopo (JD 100041)). 152
Figure 103: Contour plot of streamwise flow velocities about 6 m upstream of turbine inlets for Q_T = 402 m^3/s (view in flow direction). 153
Figure 104: Effect of transect averaging about 50 m downstream of the turbine outlets for Q_T = 143 m^3/s (view in flow direction). 154
Figure 105: Comparison of the simulation results (top) with the ADCP measurements (bottom, average of two transects) for a discharge of 402 m^3/s about 20 m upstream of the turbine inlets (view in flow direction). 155
Figure 106: Comparison of the simulation results (top) with the ADCP measurements (bottom, average of 6 transects) for a discharge of 143 m^3/s about 40 m downstream of the turbine outlets (view in flow direction). 156
Figure 107: Potential positions of fish guidance structures upstream of the HPP Bannwil (background image: © 2018 swisstopo (JD 100041)). 157
Figure 108: Normal (left) and tangential (right) flow velocities at potential FGS positions upstream of the turbine inlets for scenario 1a for FGS angled at 45° (top) and 37° (bottom). 158
Figure 109: Normal (left) and tangential (right) flow velocities at potential FGS positions upstream of the turbine inlets for scenario 1b for FGS angled at 45° (top) and 37° (bottom). 159
Figure 110: General turbine admission flow direction for turbine discharge only (left, scenario 1) and combined turbine and weir discharge (right, scenario 2). 159
Figure 111: Normal (left) and tangential (right) flow velocities at potential FGF positions upstream of the turbine inlets for scenario 2a for FGS angled at 45° (top) and 37° (bottom). 160
Figure 112: Velocity magnitudes at weir discharge for scenario 2a: Gate flow occurs at field 2 and 3, field 1 is closed. The depicted cross section is extracted at position y = 44.5 m in the middle of WF 2. 162
Figure 113: Velocity magnitudes at weir discharge for scenario 2b: Overflow occurs at WF 1, 2 and 3 plus gate flow at WF1. The depicted cross section is extracted at position y = 44.5 m in the middle of WF 2. 163
Figure 114: Number of detected fishes and time of registration for all 6 positions at HPP Bannwil intake trash rack. The red lines indicate data gaps. 164
Figure 115: Total body length [cm[vs. frequency distribution of detected fishes at HPP Bannwil intake trash rack. Blue bars: pooled data for the 5 runs, red bar: continuous data, only position VI 165
Figure 116: Swimming depth of all fishes registered during the continuous data analysis at position VI at HPP Bannwil intake trash rack (N=49). The colors serve only for a better identification of the individuals. 165

Figure 117: Barotrauma Detection System (BDS) and illustration of the multiple regions in which pressure changes occur that fish experience during turbine passage (vertical Kaplan). 168
Figure 118: Annual discharge of Bannwil in 2017 according to the three machine units.... 170
Figure 119: Annual Load Duration Curve (simultaneous). 170
Figure 120: Normalized Hill Chart of Bannwil HPP. 171
Figure 121: BioPA probability distribution and dose- response of pressure Nadir [1]..... 173
Figure 122: CAD Model of the Bulb Turbine in Bannwil. 174
Figure 123: Intensity Distribution. 176
Figure 124: Strike Probability Distribution. 176
Figure 125: Blade Strike Survival Curve for salmon [5]. 177
Figure 126: Comparing different Fish Length's. 179
Figure 127: Fish Passage Hill Chart of Pressure. 181
Figure 128: Fish Passage Hill Chart of TKE. 182
Figure 129: Fish Passage Hill Chart of Shear Stress 183
Figure 130:Fish Passage Hill Chart of Strike. 184
Figure 131: Combined Fish Passage Hill Chart for 10 m Acclimation Depth. 185
Figure 132 - Places with fish assemblage data in the Tâmega River basin (presence-absence, depicted by a blue circle). 189
Figure 133 - Distribution of Pseudochondrostoma duriense in the Tâmega River basin. Sampling site with species presence is denoted by a green circle, whereas sampling sites with absence are denoted by a blue circle. The species occur in the Avelames River. 190
Figure 134 - Distribution of Squalius carolitertii in the Tâmega River basin. Sampling site with species presence is denoted by a green circle, whereas sampling sites with absence are denoted by a blue circle. The species occur in the Avelames River. 191
Figure 135 - Distribution of Luciobarbus bocagei in the Tâmega River basin. Sampling site with species presence is denoted by a green circle, whereas sampling sites with absence are denoted by a blue circle. 191
Figure 136 - Distribution of Salmo trutta fario in the Tâmega River basin. Sampling site with species presence is denoted by a green circle, whereas sampling sites with absence are denoted by a blue circle. 192
Figure 137 - Distribution of Lepomis gibbosus in the Tâmega River basin. Sampling site with species presence is denoted by a green circle, whereas sampling sites with absence are denoted by a blue circle. 192
Figure 138 - Factor 1 and 2 of the PCA performed on the matrix of presence-absence of fish species in 55 electrofishing surveys made throughout the Tâmega River basin. Eigenvalues were 3.52 and 1.77, respectively, for the first and second factor. 193
Figure 139 – Bragado HPP scheme. Localization of the weir, HPP and key-section. 195
Figure 140 - Mean monthly real and simulated turbined flows during 20010/11 until 2015/16. 196
Figure 141 – Mean monthly flows at Bragado HPP scheme. 197
Figure 142 – Fish survey at Bragado ; a) upstream Bragado weir ; b) downstream Bragado HPP 197
Figure 143 – Topography survey in the river reach downstream Bragado HPP 198
Figure 144 – River bed topography at the upstream river reach. 199
Figure 145 - River bed topography at the downstream river reach. 200
Figure 146 – Flow series from October 1st 2010 to September 30th 2016 at the key-section downstream Bragado HPP. 202
Figure 147 – Number of rapid increases (N_{inc}) and decreases (N_{dec}) per year for the Avelames River downstream Bragado HPP 203
Figure 148 – T_{high} and T_{low} along the 6 years flow series. 204

Figure 149 – Cumulative distribution of time span after a rapid increase and after a rapid decrease. 205
Figure 150 – Number of rapid increases and rapid decreases per day. 206
Figure 151 – Number of rapid increases and rapid decreases during the day. 206
Figure 152 - Percentage of rapid increases and decreases according to daylight conditions (daylight, twilight and darkness). 207
Figure 153 – Monthly distribution of rapid increases and rapid decreases according to light conditions, i.e. daylight, twilight and darkness. 207
Figure 154 – a) Electrofishing at the upstream river reach ; b) Fish measurements: weight and length. 208
Figure 155 – Operator carrying the portable antenna looking for marked fish on the a) upstream river reach, and b) downstream river reach. 209
Figure 156 – Number of fish individuals detected and not detected by species during the seasons late Spring and late Summer. 211
Figure 157 – Macroinvertebrates sampling. 212
Figure 158: Relative abundance 219
Figure 159: Relative biomass 219
Figure 160: Constructed shallow water areas (r-km 1936) out of gravel have a high ecological value especially for rheophilic fish species. 221
Figure 161: Side arm (r-km 1923). 222
Figure 162: Artificial back-water (r-km 1928.5). 223
Figure 163: Fish by-pass system Freudenau. Triangles indicate fish larvae sampling points, circles indicate electrofishing points; length of the sections (m) and slope (%) are given beneath each section name (from Meulenbroek et al. 2018b, adapted after Eberstaller et al. 2001). 224
Figure 164: Relative abundances of flow guilds and number of species for the given sections. Bars indicate relative abundance of flow guilds for juvenile and adult of all caught fish; numbers within each category show the number of species per guild; numbers in parentheses indicate the total number of species per section (from Meulenbroek et al. 2018b). 225
Figure 165: Test array using six hydrophones close to the influx building Langentzersdorf. Yellow dots indicate the positive positioning of a test tag. The dots describe the path of the test tag. Hydrophones are indicated by blue squares. 227
Figure 166: Test array power station Freudenau. Eight hydrophones are tested in the proximity of the power station to test the positioning success with test tags. 228
Figure 167: Mounting construction for open water hydrophones. 228
Figure 168: Mounting construction for the deployment at the power station 228
Figure 169: Digital elevation model of the Danube below the HPP Freudenau and the fishway 229
Figure 170: Tagging of fishes a) mark of 23 mm used b) and c) surgical insertion of the mark in the fish (source: (Tomanova, et al., 2018)). 232
Figure 171: Schematic representation of the HPP and the antennas 233
Figure 172: Pictures of the HPP and location of the antennas (source: (Tomanova, et al., 2018)). 234
Figure 173: Distribution of released fishes' size, non-detected fishes' size and detected in the downstream migration channel fishes' size (source: (Tomanova, et al., 2018)). 236
Figure 174: Upstream view of the water intake and the two bypasses 238
Figure 175: Electrofishing sample downstream of Guma fishway 241
Figure 176: Left: Barotrauma sensors and fake probes with floating devices after the recovery used in the pre-test in Vadocondes HPP. Right: an example of output data of pressure (Y axis) along the time (X axis) registered by the sensors. 246
Figure 177: Potential area for spawning and cone net for trapping fish larvae. 247

Figure 178: Potential spawning areas in the study reach. The downstream limit is Vadocondes HPP (section 1) and the upstream limit is the dam in Guma Village (section 2). Potential spawning areas are numerated from downstream to upstream (see table 10). 248
Figure 179: Fish larvae light trap. Right: bottom view of the trap without the net and the light. (modified from Pérez et al 2009) 250
Figure 180: Marking procedure with Visible Implant Elastomer. Left: yellow elastomer in the dorsal fin (fish from Guma fishway). Right: red elastomer near the anal fin (fish from downstream of Vadocondes fishway). 251
Figure 181: Passive Integrated Transponder Tagging. 251
Figure 182: PIT tag antennas system (Oregon RFID® reader). Left: multiplexer reader with batteries and charge controller. Laptop is connected through an inverter. Right: hand-made RFID antenna with four loops of coil (2.5 mm2) enclosed in PVC pipe. 252
Figure 183: Left: table with field surgery equipment for radio tagging. Right: Detail of Luciobarbus bocagei anaesthetized and sutured, with the gills submerged into the water with supply oxygen and the body of the fish secured (position and humidity) with the foam. 253
Figure 184: Proportion of barbels that located the fishway as a function of release date (month/day/year). 255
Figure 185: Fishway location and ascent success of Guma fishway, related to flow discharge and water temperature. Turbine discharge was affected by operational problems until 29th June. Water head refers to the difference between water level upstream and downstream. 256
Figure 186: Scheme of movement for barbels with radiotag: map of the section under study where radiotracking was done once a week since July to October 2018. 258
Figure 187: Scheme of movement for barbels with radiotag: graph of fish movements along the time (X axis) as a function of the distance from Guma HPP 259
Figure 188: Left: Guma HPP fishway. Right: Guma HPP modelled fishway geometry..... 260
Figure 189: Hydraulic data acquisition on Guma HPP. Left: Doppler bathymetry in the turbine tailrace. Right: topographic survey of bathymetry sections. 261
Figure 190: Example of bathymetry results of one section in Guma downstream reach. Up: current velocity; Middle: flow discharge; Down: water depth..... 261
Figure 191: Photos from drone flight over Guma HPP..... 262
Figure 192: Downstream river stretch under study. Left: terrain elevation. Right: HEC-RAS 2D model area. 262
Figure 193: 3D fishway model preliminary results. Top: 3D flow and water surface configuration. Middle: 3D flow coloured by velocity magnitude. Bottom: Velocity magnitude and streamlines in two regular pools at y = 0.15 m (right located notch axis) 264
Figure 194: Placing gravel into Wattenweiler fishway. 266
Figure 195: Location of gravel input at Wattenweiler fishway. 267
Figure 196 Location of gravel input at Ellzee fishway. 267
Figure 197 Location of gravel input at Waldstetten fishway. 268
Figure 198 spawn of nase on fresh gravel..... 269
Figure 199 Spawn of nase at fishway Ellzee. 269
Figure 200 Electric fishing at Höselhurst fishway. 270
Figure 201 Aerial photo Walddstetten fishway..... 271
Figure 202 Aerial photo Ellzee fishway..... 272
Figure 203 Aerial photo fishladder Wattenweiler 273
Figure 204 Aerial photo Höselhurst fishway. 274
Figure 205: Aerial photo Deisenhausen, fishway..... 275
Figure 206: BDS deployment at Ham from 20-22.06.2018. A) Sensors outfitted with balloon tags ready for deployment. B) Sensor destroyed by crush event. C) Deployment of BDS into the Archimedes screw. D) Recovery downstream via balloon tags in a hand net. 278

Figure 207: Drone used for the aerial survey (left), Ground control point (GCP, right)..... 283
Figure 208: river bathymetry, derived by cross section interpolation (top), higher resolution derived by underwater SfM evaluation 284
Figure 209 : Flow registered at gage Kempten, approx. 8 km upstream of the Test Case site (from : https://www.hnd.bayern.de/pegel/iller_lech/kempten) 285
Figure 210 : Model results for 10 m³/s (top) and 60 m³/s (bottom), water depth (left), flow velocity (right) 286
Figure 211: Schematic view of the detection range (outside the grey area within the dashed circle) of one autonomous hydrophone fixed at the bottom of a river. Tagged fish that are within the detection range (green encircled tags) are logged (ID code) as being present at each time stamp that their emitted signal is heard by the hydrophone. ID codes of tagged fish outside of the detection range of the hydrophone are not logged at those time stamps because they are not heard by the hydrophone and are thus assumed absent from the detection range of the hydrophone. One hydrophone can only define presence/absence and not the exact position of the tag within its detection range (1 dimensional acoustic telemetry). 287
Figure 212: Schematic view of 2 dimensional acoustic telemetry. The relative position of a tagged fish towards the hydrophones (black bottles) is calculated based on the theory of the propagation speed of sound through water and info on the timing of emission of the tag signal and its detection on minimally three hydrophones. Subsequent positions give an idea (red line) of the track that the fish has swum (blue line)..... 288
Figure 213: Pictures of the mooring of the reference tags (a) and the hydrophones with steel pyramid constructions (c) attached to a steel chain that is anchored at both sides of the river and runs over the river bottom (b). In total 16 pyramid constructions where attached to 7 chains spread over the study area. The hydrophone is held vertically by attachment to the top of the pyramid in picture c. 291
Figure 214: (a) Locations of the 16 hydrophones (blue marks) and 6 refefence tags (yellow marks) as positioned with a Trimble GPS at installation and recovery. (b) Location of all 19 hydrophones in the study, and 6 reference tags of the VPS network. (c) Zoom on the locations of the two hydrophones in the fish pass. 293
Figure 215: Indication of the number of grayling (top and right fish pictures) and barbel (left fish pictures) and their catch and release location in the study area. Yellow dots indicate locations where fish were caught electrically, whereas the green dot indicates the location of the counting pool, which was also used to catch studied fish. Further biometric info and info on the catch method is listed in Table 51. 297
Figure 216: Discharge (in m³/s) of the river Iller in Kempten during the studied period (see also Figure 209). 298
Figure 217: Results of first test runs with current version of migration model for 10 (A), 20 (B) and 60 m³/s (C), yellow pins indicate the start position of virtual fish, black lines the predicted track..... 303
Figure 218: Radio telemetry material used: a) mark F1720 for Atlantic salmon smolts, b) aerial loop antenna, c) immersed strand antenna, d) receiving station RC4500 from ATS..... 307
Figure 219: Set of detection antennas installed at Las Rives 307
Figure 220: Pictures of the ADCP StreamPro assembled on its trimaran and the probe with a closer view of the 4 sensors..... 309
Figure 221 : Support and movement carts system allowing the deployment of the ADCP. 310
Figure 222: Positioning of the ADCP measurements transects at Las Rives. 312
Figure 223: Diagram of the components of analysed velocity; longitudinal view (top) and plan view (down)..... 313
Figure 224: Positioning of the gaugings in the downstream migration duct at Las Rives. .. 314
Figure 225: Example of an electro-magnetic flow meter..... 315

Figure 226: Cutting of a section during the measure by a flow meter, in red the verticals, the black dots correspond to the measurement points. 315
Figure 227: Variation of water level and total discharge of the Ariège during the measures at Las Rives. 317
Figure 228: Out of water bar rack at Las Rives, in the red rectangle, the grid is clogged in order to better guide fishes to the bypasses 319
Figure 229: cartographies of the dimensionless velocities V_x/V_0 (up) and V_z/V_0 (down) measured at Las Rives. 321
Figure 230: Cartographies of Vt/V0 measured at Las Rives 322
Figure 231: Cartographies of V_n/V_0 measured at Las Rives. 323
Figure 232: Cartography of ratio V_t/V_n measured at Las Rives. 323
Figure 233: Cartography of V_y/V_0 of transect located 2 m upstream the top of the bar rack (about 0.15 m upstream the entrance of the outlets). Positive direction is oriented from the right bank to the left bank. The location of the outlets is indicated by the vertical dotted lines. 324
Figure 234: Expression of the discharge coefficient for a thick weir with a plane crest and sharp edges (source: (Le Coz, et al., 2011)). 328
Figure 235: Expression of discharge coefficient for a weir with thin wall and rectangular section (Le Coz, et al., 2011)..... 329
Figure 236: Abacus for the determination of Cr for a weir with thin wall and rectangular section (Le Coz, et al., 2011)..... 329
Figure 237: calculated discharge by Devers tool (C=0.46). 329
Figure 238: (a) Conceptual sketch of the vortex tube functionality and (b) the vortex tube at HPP Schiffmühle. 330
Figure 239: Overview of the data set collected between April 13, 2018 and December 23, 2018. The discharge data (FOEN hydrometric station ID 2243) for October, November, and December 2018 is not yet available. The vortex tube is automatically opened for $Q > Q_{open}$ and closed for $Q < Q_{close}$. Flood events are labeled with their start date. The bottom panel informs about the installation dates of the sensors and restrictions on the data availability due to operational problems of either the HPP or the data recording system. The test events are not displayed individually. 331
Figure 240: The bedload monitoring setup with (a) the housing and the geophone and (b) the housing mounted to the vortex tube and all sensors installed. 332
Figure 241: Exemplary (a) geophone and (b) accelerometer signal of the same grain impact. SumIMP denotes the total number of peaks above the threshold amplitude A_{min} for the event shown. A_{maxmax} is the maximum amplitude registered during this event. Only positive amplitude values are considered. 333
Figure 242: The setup for water level measurements with (a) the housing, (b) the sensor, and (c) the installation next to the vortex tube outlet. 333
Figure 243: Grain size distribution of the four gravel mixtures used in the field calibration. The legend indicates whether the grain size sample was processed by square-hole sieving (sieve) or by BASEGRAIN analysis (BG). 334
Figure 244: Field calibration on September 4, 2018 with (a) an excavator set up on a float and (b) the outlet of the vortex tube during a calibration run. 336
Figure 245: The maximum amplitude A_{maxmax} as a power law function of the maximum transported grain size D_{max} for each field calibration runs. 336
Figure 246: Linear relation between the total transported bedload volume V_b and the sum of impulses SumIMP during the field calibration runs for (a) geophone data and (b) accelerometer data. 337
Figure 247: The linear regression between the total transported bedload volume V_b and the sum of impulses SumIMP fitted to the calibration runs and the resulting bedload volumes for

the flood events and weekly flushings for (a) geophone data and (b) accelerometer data. Note that the flood events were only recorded by the geophone, as the accelerometer was not yet installed..... 338
Figure 248: Locations of the sediment sampling in March 2018 340
Figure 249: Results of sieving (red dashed), pebble count (green dotted) and BASEGRAIN (blue line) at spot number 5..... 341
Figure 250: Shelter needs and availabilities depending on the different body sizes of salmons for different ages (Forseth et al., 2014). 342
Figure 251: ADCP and Q-boat. 343
Figure 252: ADCP data analysis workflow..... 344
Figure 253: Velocity and bathymetry measurement locations at HPP Schiffmühle in March 2018..... 344
Figure 254: Velocity and bathymetry measurement locations at HPP Schiffmühle in October 2018..... 345
Figure 255: Water surface elevation measurements using a total station and a target on the boat..... 345
Figure 256: 3D snapshot view to the dry topography area observed by Regionalwerke Baden AG. 346
Figure 257: DJI Phantom 4 Pro and Ecofoam as seeding particles. 348
Figure 258: PIT-Tag antennas (left picture in the nature-like fish pass, right picture in the vertical-slot pass. 348
Figure 259: left: bleak with 12 mm PIT-tag, right: barbel, one of the most abundant species in the Limmat River..... 349
Figure 260: 3D geometry of the residual HPP with upstream (left) and downstream (right) parts. 350
Figure 261: Available bathymetric cross sections, green (this project) and orange (FOEN, 2013). 351
Figure 262: Flow duration curves established based on 1997-2018 Limmat flow data for the four sub-periods of fish migration. 352
Figure 263: Bathymetry of upstream and downstream flow reaches of the residual flow HPP Schiffmühle in March (a) and October (b) 2018..... 354
Figure 264: Photos of residual flow reach in March (a) and October (b) 2018. 355
Figure 265: Depth-averaged velocity profiles from ADCP measurements at HPP Schiffmühle in (a) March and (b) October 2018. Note that the left and right colorbars are for the residual flow reach and headrace channel, respectively. 356
Figure 266: Depth-averaged velocity profiles (a) and streamlines (b) from ADCP measurements at HPP Schiffmühle in October 2018..... 357
Figure 267: Velocity distribution along the HBR-BS in October 2018. 358
Figure 268: Velocity measurement points inside the bypass and velocity data (a) and average velocity in front of the bypass (b)..... 358
Figure 269: Geo-referenced surface velocity field measured using AIV on 2018/03/13 between 11:00-11:45 at a flow discharge of 71–72 m^3/s, with exemplary areas of misleading (noisy) velocity data highlighted by black ellipses. 360
Figure 270: Geo-referenced surface velocity streamlines computed from AIV results. 361
Figure 271: Total length of tagged fishes (N=2'331) belonging to 17 fish species. Only 5 individuals were larger than 300 mm..... 362
Figure 272: A) Lateral line probe can be used easily, and requires a short field training. B) The LLP measurements can be made directly in the attraction flow jet. C) Close-up view of the LLP near the top of the water column, illustrating the water flow around the probe body. D) A measuring tape extended in the field along the jet core facilitates reproducible measurement locations for future studies using ADV or LLP. 365

Figure 273: Top images show LLP and ADV measurement locations at the Schiffmühle case study site which correspond to the near, mid- and far-field regions of the jet core. Lower image depicts the vertical measurement locations for the LLP and ADV in order to capture the hydrodynamic conditions of the jet core at the bottom, middle and top of the water column. 366
Figure 274: Tagging of fishes a) mark of 23 mm used b) and c) surgical insertion of the mark in the fish (source: (Tomanova, et al., 2018)). 370
Figure 275: Schematic representation of the HPP and the antennas 371
Figure 276: Pictures of the HPP and location of the antennas (source: (Tomanova, et al., 2018)). 372
Figure 277: Distribution of released fishes' size, non-detected fishes' size and detected in the downstream migration channel fishes' size (source: (Tomanova, et al., 2018)). 374

List of tables

Table 5 :Measurements conducted by NTNU and SWECO during the first and second field campaign in 2018 (see Figure 7 for location of sites that are described by a-e in the table) 136
Table 6: Scenarios simulated with the numerical 3D model..... 150
Table 7: Overview of the BDS text file data format. Each of the 27 columns corresponds to a different variable saved during turbine passage at 100 Hz (magnetometer 20 Hz), units given in parentheses. 167
Table 8: investigated operating points..... 172
Table 9: Fish Length Scores. 179
Table 10: Performance Score of Load cases at Acclimation Depth of 5 m. 179
Table 11 - Basin area for the Tâmega and Avelames River basins. Including the Spanish part of the basin. 188
Table 12 - Fish taxa occurring in the Tâmega River basin..... 189
Table 13 – Fish survey at river reach upstream Bragado weir and downstream Bragado HPP 198
Table 14 – Threshold values for analysis of the water level time series for Avelames River. 203
Table 15 – Values of Hydropeaking Impact (HP) and Threshold (TR) values for Avelames River downstream Bragado HPP considering the Carolli et al. (2015) methodology..... 208
Table 16 – Fish PITtagged in the upstream and downstream river reach. 208
Table 17 – Number of fish records for each species in late spring and late summer. 211
Table 18 - Proportion of each species in the specimens marked and detected in the downstream reach. 211
Table 19 – Macroinvertebrate present in the "kick" samples..... 212
Table 20 – Macroinvertebrates present in the drift samples. 213
Table 21: Fish ecological "Leitbild" (Leitbild according to BAW / IGF 2017); key species (l) in red, typical companion species (b) in orange, rare companion species (s) in yellow 217
Table 22: Number of fishes and their size for each batch, date and time of release on Gotein's site (source : (Tomanova, et al., 2018))..... 232
Table 23: Detection efficiency (%) of the antennas in the downstream migration channel (source: (Tomanova, et al., 2018)). 233
Table 24: number and distribution of detected or non-detected fishes in the different ways at Gotein (in blue: batches released in the evening) (source: (Tomanova, et al., 2018)). 235

Back to D2.2 Main index

Table 25: Timing of passage of smolts for the different batches, in grey the batches released in the evening (source: (Tomanova, et al., 2018)). 237
Table 26: Summary of the distribution of fishes among the different ways, passage rate through turbines (this study) and their mortality rates (according (Voegtlé, 2010)), and global passage efficiency taking into account passage over the spillway, the downstream migration device and survival after passage through turbines (Tomanova, et al., 2018). 237
Table 27: Calculation of the discharge over the weir 238
Table 28: Distribution of discharge in the different outlets 239
Table 29: Fish species of the study area (based on literature and previous studies review as well as during the fish samples). 242
Table 30: Preliminary results of the number of individuals captured during the samples from May to September 2018, by species and sampling point. 242
Table 31: Preliminary results of the length distribution of fish by species and sampling point: median (first and third quartiles) in mm 243
Table 32: Potential spawning areas between Vadocondes HPP and Guma village dam (see figure 9) 248
Table 33: Spawning areas (figure 9) and confirmation of fish larvae presence by species (X) for benthic spawners 249
Table 34: Number of marked fish with Visible Implant Elastomer from May to September 2018, by species and sampling point. 253
Table 35: Number of recaptured fish with Visible Implant Elastomer from May to September 2018, by species and sampling point. (In brackets: first number indicates the number of fish marked in the same sampling point in which it has been recaptured / second number indicates fish marked in different sampling points). 254
Table 36: Characteristics of fish sample (Luciobarbus bocagei) tagged with PIT tag for the analysis of upstream migration. There are three different sources of fish (all of them upstream the release place). [median (first quartile – third quartile)] 254
Table 37: Summary of the ascent time of Luciobarbus bocagei in Guma fishway, as a function of the source of the fish, in hours. Time is obtained between antenna 1 and antenna 4, corresponding to a total water head of 8 m (31 pools with mean water drops of 0.25 m. 257
Table 38: Barbels (Luciobarbus bocagei) that were radiotagged (see figure 13 for details of their movements) 257
Table 39 Fishstock inventory: Waldstetten fishway, 17.08.2018. 271
Table 40 Fishstock inventory: Ellzee fishway, 17.08.2018. 272
Table 41 Fishstock inventory: Wattenweiler fishway, 29.08.2018. 273
Table 42 Fishstock inventory: Höselhurst fishway, 7.9.2018. 274
Table 43 Fishstock inventory: Deisenhausen fishway, 23.8.2018. 276
Table 44: Ensemble statistics of BDS deployment at Ham (n = 30), Q = 3 m³/s. 279
Table 45: Ensemble statistics of BDS deployment at Ham (n = 28), Q = 4 m³/s. 279
Table 46: Ensemble statistics of BDS deployment at Ham (n = 33), Q = 5 m³/s. 279
Table 47: Results of the electrical fishing session at 12.04.2017 in the downstream area of HPP Altusried 282
Table 48: Results of the electrical fishing session at 10.07.2018 in the downstream area of HPP Altusried 282
Table 49: flows covered with model and hydrological characteristic 285
Table 50: Overview of the type of devices (hydrophones and tags) used in this study and their specifications. The sensors in the hydrophones log temperature, tilt of the hydrophone and background noise. 293
Table 51: Info on the 47 individual wild fish of two species (barbel and grayling) that were tagged and tracked in this study. 295

Table 52: Indication of the number of days that a tagged fish was detected in the VPS network and if the fish swum up the fish ladder or not, till where and only once or multiple times, and the date that a fish was caught in the counting pool if any catch occurred..... 300
Table 53: Size of tagged fishes 308
Table 54: Efficiency of the batches for released smolts at Las Rives in spring 2017 308
Table 55: Mean discharge and velocity allowing the results to be dimensionless. 317
Table 56: Total discharge transiting through the downstream migration duct, and distribution of the discharges between the outlets at Las Rives..... 318
Table 57: Variation of water levels during the measures 325
Table 58: Exploitation of measured velocities at Las Rives at the first point of gauging..... 325
Table 59: Exploitation of measured velocities at Las Rives at the second point of gauging326
Table 60: Measured data for the calculation of the total discharge thanks to the discharge formula..... 327
Table 61: Determination table of A1 coefficient (source (Le Coz, et al., 2011)) 328
Table 62 : Recorded flood events between April 13, 2018 and December 23, 2018..... 331
Table 63: Characteristic grain sizes and the geometric standard deviation $\sigma_g = (d_{84}/d_{16})^{1/2}$ of the sediment mixtures used in the field calibration and in the turbine inlet (BG = BASEGRAIN, sieve = square-hole sieve). 334
Table 64: Field calibration runs of September 4, 2018. The duration includes the opening and closing time of the vortex tube. The material was dumped in between the calibration runs, when the vortex tube was closed. 335
Table 65: List of the different methods applied at the testing spots 341
Table 66: Limmat flow conditions and prescribed residual flows during fish migration periods in spring and fall..... 352
Table 67: Calibration of roughness values 352
Table 68: Fish monitoring results 363
Table 69 : Pressure-based variables from LLP measurements. 366
Table 70: Number of fishes and their size for each batch, date and time of release on Trois-Villes' site (source : (Tomanova, et al., 2018))..... 370
Table 71: Detection efficiency (%) of the antennas in the downstream migration channel (source: (Tomanova, et al., 2018)). 371
Table 72: number and distribution of detected fishes or not in the different ways at Trois-Villes (in blue: batches released in the evening) a) with b) without fishes detected in the dump channel (source: (Tomanova, et al., 2018))..... 373
Table 73: Timing of passage of smolts for the different batches, in grey the batches released in the evening (source: (Tomanova, et al., 2018)). 375
Table 74: Summary of the distribution of fishes among the different ways, passage rate through turbines (this study) and their mortality rates (according (Voegtlé, 2010)), and global passage efficiency taking into account passage over the spillway, the downstream migration device and survival after passage through turbines (Tomanova, et al., 2018). 375
Table 75 : Calculation of the discharge over the weir 379

3.1 Altheim

The waterbody 1_F429 suffers from a substantial lack of dynamic habitat development. Especially in heavily modified water bodies nature like fish ways offer the possibility to improve the ecological potential essentially. Creating connectivity can be combined with spawning grounds and habitats for juvenile fish. Often the availability of habitats is even more important for the development of the population than the mere connectivity. On the other hand, nature-like fish passes often require a significant amount of maintenance due to their length, the difficult balance between what is “nature” and what is functionality and also the maintenance of hydromorphological structures with an all year steady flow.

Along river Isar, the existing drainage stitches have been used for long nature-like fish passes. The assessment within FIThydro is designed to evaluate the benefit of artificial habitat structures within nature-like fish passes for fish and macroinvertebrates.

Mapping of the available structures in the 3.5 km long fish pass

Currently, the quality of the structures in the fish pass is not defined. During the original design, some structures had been implemented to enable the development of habitats, but the availability of these structures is not given anymore. Therefore, the full length of the fish pass needs to be mapped to track all currently available structures in the fish pass. All structures need to be mapped including water depths, flow velocities and substrate conditions. Moreover, the existing structures need to be evaluated regarding their benefit for fish. Therefore, certain structures are to be observed via video monitoring to assess the usage frequency by fish. Moreover, the usability of spawning shall be evaluated.

Development of an improved structural concept in two steps

Based on the eco-mapping and the knowledge about the benefit of the existing structures, a concept is to be developed containing 5-6 standard structures and a geographical plan in which areas to implement them (concept to be available by end of 2018). The assignment will differentiate between the minimum amount of structures needed and the maximum number of structures (2-step approach) that can be implemented to find the optimum allowing the spawning grounds and juvenile habitats in the fish pass needed. Especially for operators the amount of structures is essential, as they require significant effort for maintenance to ensure their usability in the future. The structures shall be installed in the winter months January / February 2019 and evaluated during the spawning time in 2019.

Evaluation of the effort for the maintenance of the fish pass

The nature-like fish pass did long suffer from driftwood getting stuck at it’s upstream end. To solve this, a floating wooden bar had been installed to drift off branches and boughs. In the course of FIThydro, implemented measures shall be evaluated according to their effectiveness to support the development of self-sustaining fish populations, but also regarding the costs and effort for construction and maintenance. Accordingly, at Test Case Altheim the effort for the maintenance of the fish pass will be described, differentiating between regular maintenance measures and ad-hoc measures. Moreover, the description will point out, which measures are related to the length of the fish pass and which are general measures regardless of length. This evaluation will feed back into the cost effectiveness analysis within FIThydro.

3.2. Anundsjö

At this test case the FIThydro partners NTNU, SWECO, CNRS and TUM work together on the tasks mentioned in section 2. In general, NTNU is responsible for the sediment and habitat evaluations including adaption of the Double Averaging Method (DAM) to field use. NTNU supports SWECO in ADCP measurements to collect information about velocity and bathymetry (see also Table 5). These datasets on hydraulics and geometry are the input data for CNRS and TUM, both conducting numerical simulations. CNRS is evaluating the flow structure in the reservoir and its effects on smolt migration., TUM will run numerical simulations where the outlet of the turbines meet the bypassed reach of the river to assess passability and the attractionof fish.

During the first year of field studies, various measurements were conducted by NTNU and SWECO to prepare the relevant data sets to work on the objectives as described above.

Table 5 :Measurements conducted by NTNU and SWECO during the first and second field campaign in 2018 (see Figure 7 for location of sites that are described by a-e in the table)

#	Type of measurement	Location	Type of data	Further use of data	Reference in section 2
1	ADCP	Reservoir (a)	Bathymetry / velocimetry	Numerical simulation of the flow structure in the lake	2.22
2	SfM	Fishway (b)	Geometry	Potential use for further development of the DAM	2.25
3	Salt	Fishway (b)	Discharge	See 2	
4	GPS	Fishway (b)	Geometry	See 2	2.17
5	ADCP	Junction tunnel outlet / residual flow (c)	Bathymetry / velocimetry	Numerical simulation of the flow structure and the possible attraction of fish into the residual flow in this area	2.22
6	GPS	Junction tunnel outlet / residual flow (c)	Geometry	See 5	2.17
7	ADV	Residual Flow Reach (d)	Velocity	Potential use for further development of the DAM	2.22
8	SfM	Residual Flow Reach (d)	Geometry	Potential use for further development of the DAM	2.25
9	GPS	Residual Flow Reach (d)	Geometry	See 8	2.17

10	ADCP	Junction downstream area (e)	Bathymetry / velocimetry	See 5	2.22
11	GPS	Junction downstream area (e)	Geometry	See 5	2.17



Figure 87 : Map (tilted, North is left) of Anundsjø showing the different areas according to tab. 1

3.2.1. Passability and attraction at the fishway entrance

3.2.1.1. Data

The passability and attraction at the fishway entrance and at the downstream end of the bypassed reach will be evaluated by running numerical simulations by TUM. As basis for the model simulations, NTNU and SWECO collected flow and bathymetry data in the respective area.

The data sets were collected upstream and downstream of the junction of the bypassed reach and tunnel outlet (Figure 87**Error! Reference source not found.**, c), towards the tunnel outlet and more downstream towards the lake-like river widenings (Figure 87, e).

3.2.1.2. Methodology

The **hydraulic measurements** were mainly conducted with two Acoustic Doppler Current Profilers (ADCP) from Sontek M9 (Figure 88).



Figure 88 : The Sontek M9, one mounted on a kayak (left) and an autonomous boat (right)

Cross sections in the relevant areas were measured using these two devices. The measurements were conducted in June 2018. These cross sections were complemented by additional loops in between which do not contribute to the velocity information. As the two devices were mounted on different types of boats (a kayak and a boat operated by remote control) it was possible to conduct very efficient and detailed measurements (~48000 data points) even in shallow areas. The water level was measured also with a GPS to ensure a sufficient calibration and accuracy.

As the turbine was shut during this time the measured discharge of 2,2 – 2,5 m3/s resulted only from the water spilled over the weir plus the discharge of the fishway (measured: 0,8 m3/s). For the measurements two transects directly downstream the junction of turbine outlet and residual flow reach were chosen and measured several times with the ADCP.

The area around the confluence of the bypassed reach and the outlet of the power plant will be modeled and simulated. In order to perform hydrodynamic simulation, and flow field (specifically velocity field) calculations in this domain, two different scenarios are defined. Since the power plant must shut down and release the discharge through the gates during the specific hours, in the first scenario, the hydrodynamic simulation will be performed without operating the hydropower plant. In the second scenario, the presence of the operating hydropower plant will be considered in simulations. To achieve this aim, the TELEMAC-MASCARET system has been proposed for the hydrodynamic modeling. All modules of the system are based on unstructured grids and finite-element or finite volume algorithms. The model system includes 2D and 3D hydrodynamic modules (TELEMAC-2D and TELEMAC-3D), and a spectral wave propagation model (TOMAWA). TELEMAC-2D module solves the shallow water equations with several options for the horizontal dispersion terms (e.g. depth-averaged k–ε model, Elder model, and constant eddy viscosity models) and source terms (e.g. atmospheric pressure gradients, Coriolis force, etc.). The numerical discretization includes a choice of classical methods for the advection terms. The use of implicit schemes enables relaxation of the limitation on time steps (typically, values of a CFL-numbers up to 10 or 50 are acceptable). Recently, ideas stemming from finite volume techniques have been coupled with these implicit schemes to ensure monotonicity of depth and sediment concentrations, as well as mass conservation at machine accuracy. TELEMAC-3D solves the Reynolds-Averaged Navier-Stokes (RANS) equations in unstructured meshes obtained by a super-imposition of 2D meshes of triangles. The 3D model can be applied to capture the effect of vertical recirculation cells as well as stratification effects, assuming a hydrostatic or non-hydrostatic pressure distribution. As this study is focusing mainly on the hydrodynamic simulation in the fish path, it is recommended to apply TELEMAC-3D which provides information in vertical direction.

3.2.1.3. Results

The turbines were shut-off during the field campaign and hence the flow situation were not representative for normal operation. Therefore, the ADCP measurements showed very low water velocities. Tthis cannot be seen as representative and therefore needs to be used only for calibration and validation of the model.

The bathymetry data showed relatively shallow areas in the bypassed reach and deep areas just at the tunnel outlet. In addition, a lot of driftwood was present in the downstream areas.

3.2.2. Bypassed reach and fishway: Flow

3.2.2.1. Data

The residual flow reach will be used to develop the Double Averaging Method (DAM) (Nikora et al 2007 a, b; Navaratnam et al 2018) further. Currently this method is developed and only tested under lab conditions. At the test site in Anundsjø, we will adapt this method to field conditions. Further measurements, mainly of the geometry were taken in the fishway. However, the tests showed that the residual flow corresponds better to the requirements for comparing the DAM field results with the lab results due to its broader variety of currents.

3.2.2.2. Methodology

For this method first Acoustic Doppler Velocimeter (ADV) tests were run in the bypassed reach. Therefore, a cross section was chosen with a mix of shallow and deep water zones. Three ADV vectrino probes from Nortek were used to collect point measurements at three different spots at the same time (Figure 89) following a predefined raster.



Figure 89 : ADV measurements in the bypassed reach

Based on ongoing investigations and tests in the lab these measurements will be evaluated, repeated, and used to develop the DAM for field use.

Geometry data were mapped using the "Structure from motion" technique (SfM) with an UVA Phantom 4. These measurements are used to predefine certain spots in the residual flow reach

where tests on the habitat availability will be conducted in 2019. The method is described in more detail in 3.2.3. This will be done by the use of the Finstad method for shelter mapping (Finstad et al 2007), as also conducted in the test site in Schiffmühle in Switzerland. The data sets are tested for further use to collect information about the sediment distribution. This depends highly on the quality of the results which can be achieved with SfM and is still in the evaluation process. In addition, four cross sections were measured in the field with the UVA, to be able to evaluate the drone data with a sufficient accuracy of detected coordinates. These data are linked to the SfM results via the use of targets.

3.2.2.3. Results

First results are available as a very basic geometry for a certain area of the residual flow reach (Figure 90).The work will continue in 2019.

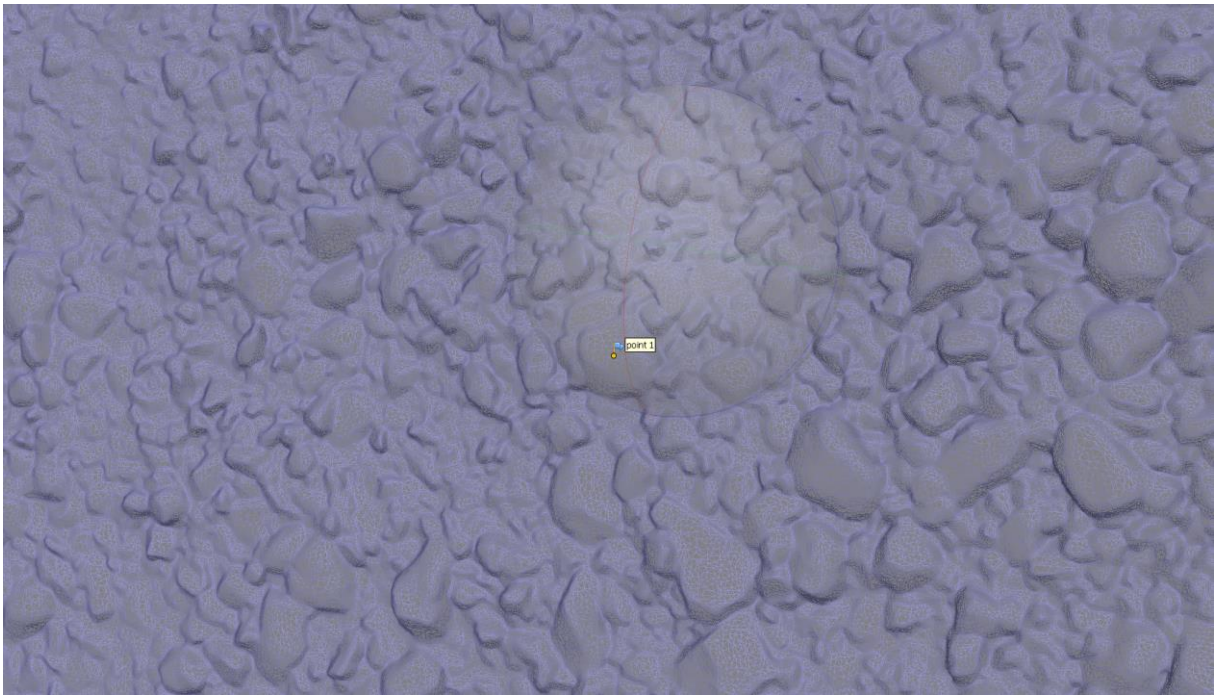


Figure 90: First results from the SfM measurements in the residual flow reach

3.2.3. Reservoir

3.2.3.1. Data

In the reservoir, the behaviour and swimming paths of smolts are of high interest. As the smolts hardly can be detected in the VAKI fish counter at the entrance to the fishway, no information are available. To allow a first rough idea about possible paths based on the flows and currents in the reservoir, a numerical simulation of this area at the turbine inlet will be conducted by CNRS with OPENFOAM. First, the model of the reservoir with the entrance of the turbine will be calibrated with the same inlet conditions recorded in the second field campaign. Then, guiding walls will be tested at a different location to provide an optimal solution for guiding the fish to the fishway. SWECO and NTNU collected velocity and bathymetry data in the reservoir. For information about the devices please see chapter 2.

3.2.3.2. Methodology

The ADCP measurements were conducted in lines and loops in a pattern which ensured a detailed description of the bathymetry in the reservoir, comparable to chapter 3.1. As the reservoir is divided by a temporal floating guidance structure (Figure 91) that affects the water velocity, this was considered for the measurements. The bathymetry data are measured with ~50000 data points for the reservoir area.



Figure 91: Barrier guiding towards the fishway entrance approx. in the middle of the lake (red line)

On the shoreline at the southern and south-eastern part of the reservoir, a lot of water plants and shallow depths hindered the measurements (Figure 92). As mentioned in 3.1, the turbine was shut off (turbine discharge 0 m3/s), therefore also these velocity results can only be used for calibration and validation.

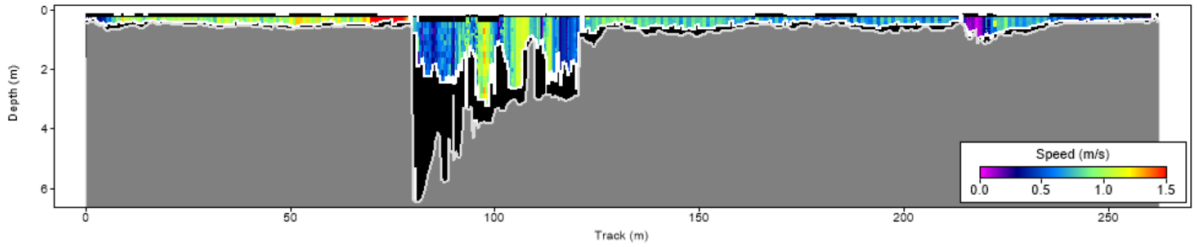


Figure 92 : Flow velocity in front of the turbine with very shallow areas in most parts (less than 1 m) and the deep areas of the intake

Back to D2.2 Main index

3.2.3.3. Results
Upcoming

3.2.4. References

Finstad, A.G., Einum, S., Forseth, T., Ugedal, O., 2007. Shelter availability affects behaviour, size-dependent and mean growth of juvenile Atlantic salmon. Freshwater Biology 52, 1710–1718. https://doi.org/10.1111/j.1365-2427.2007.01799.x

Navaratnam, C.U., Aberle, J., Qin, J., Henry, P.-Y., 2018. An experimental investigation on the flow resistance over a porous gravel-bed surface and its non-porous counterpart. E3S Web of Conferences 40, 05073. https://doi.org/10.1051/e3sconf/20184005073

Nikora, V., McEwan, I., McLean, S., Coleman, S., Pokrajac, D., Walters, R., 2007a. Double-Averaging Concept for Rough-Bed Open-Channel and Overland Flows: Theoretical Background. Journal of Hydraulic Engineering 133, 873–883. https://doi.org/10.1061/(ASCE)0733-9429(2007)133:8(873)

Nikora, V., McLean, S., Coleman, S., Pokrajac, D., McEwan, I., Campbell, L., Aberle, J., Clunie, D., Koll, K., 2007b. Double-averaging concept for rough-bed open-channel and overland flows: Applications. JOURNAL OF HYDRAULIC ENGINEERING-ASCE 133, 884–895. https://doi.org/10.1061/(ASCE)0733-9429(2007)133:8(884)

3.3. Bannwil

3.3.1. Downstream fish migration measures (ETHZ, FCO, BKW)

The current situation is documented through field monitoring and 3D numerical modelling in the area near the powerhouse and the weir of HPP Bannwil. The monitoring comprises the characterization of the flow field with velocity measurements using Acoustic Doppler Current Profiler (ADCP) and a survey of the fish movements. The latter is made with Aris Sonar and radio telemetry techniques.

Spill flow or water release may be the simplest means of transporting fish past HPP obstacles, which can be also cost-effective when the downstream migration period of the target species is short or migration occurs during high river flows. This option and the effect of the HPP operation on the flow field and fish migration for different load cases, e.g. with and without spillway flow, are investigated by measuring flow velocities as well as monitoring fish movements. The obtained hydraulic data is used to calibrate and validate the numerical model.

Applying this model to different structural and/or operational scenarios allows to come up with solutions to improve fish migration at reduced energy losses. For the former, the innovative fish guidance structures (FGS) further developed in WP3, Task 3.5 (by etho-hydraulic modelling in the VAW laboratory) is used as a basis. The hydraulic conditions at potential locations of FGS including bypass are studied with the numerical model.

3.3.1.1. Data

Data are collected from the field campaigns, the HPP operator and literature.

3.3.1.2. Methodology

- Velocity and bathymetry measurements near the HPP using ADCP
- Survey of the fish movements using ARIS Sonar and radio telemetry techniques
- 3D numerical modelling using the software *FLOW-3D*

3.3.1.2.1. ADCP measurements

High-resolution 3D velocity and bathymetry measurements, were conducted using an ADCP mounted on a remote-controlled Q-Boat from *Teledyne Marine*. The River Pro 1200 kHz ADCP including piston style four-beam transducer with a 5th, independent 600 kHz vertical beam was used (Figure 93). In addition to the ADCP probe, the boat is also equipped with a differential GPS system (Hemisphere AtlasLink) with a position accuracy of about 0.1 m. The application range for the ADCP device range from 0 to 5 m/s as well as flow depths between 0.5 and 25 m.



Back to D2.2 Main index

Figure 93: Teledyne Marine Q-boat of VAW equipped with ADCP probe and GPS antenna.

In the scope of this project, two field campaigns were conducted at HHP Bannwil. The first campaign took place at a river discharge of 402 m^3/s on 23 April 2018. The main goal was to acquire additional cross sections of the riverbed to complete the 3D bathymetry for the numerical model. Furthermore, cross sectional flow velocities were measured for model validation. Generally, at one location (cross section) several ADCP transects are acquired, whereby one transect corresponds to one crossing of the river approximately perpendicular to the main flow direction. Depending on the width of the river (at HPP Bannwil about 120 m in the upstream and 90 m in the downstream reaches) it may take up to 10 min to record a single transect. For comparison with the steady state flow field resulting from the numerical model, an average of several ADCP transects is needed. The main goal of the second campaign on 19 September 2018 (discharge 143 m^3/s) was to conduct repeated transect measurements for an in-depth analysis of transect averaging. The post processing was done according to the workflow sketched in Figure 94 using the software WinRiver II[1] and VMT[2].

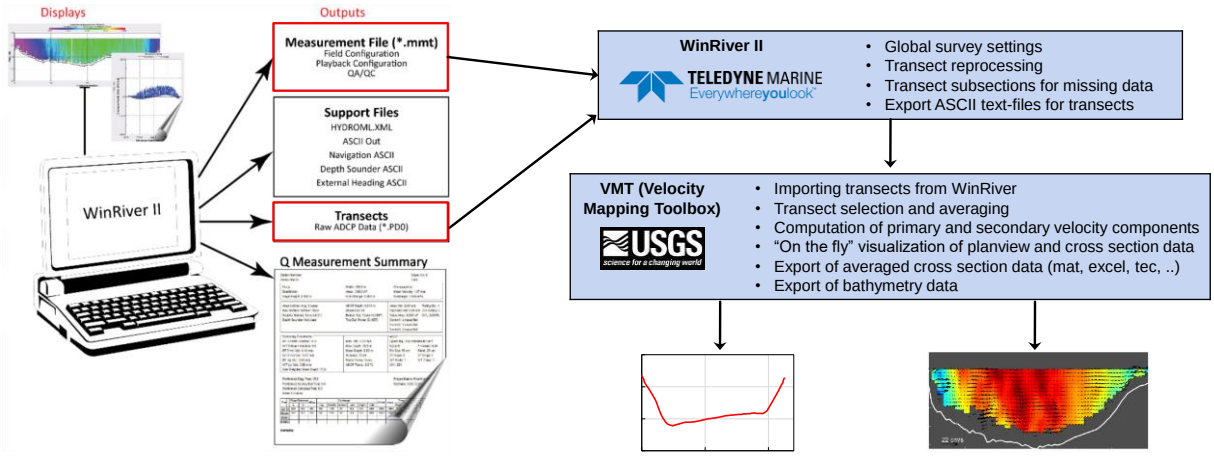


Figure 94: Workflow used for post-processing of ADCP data (modified from [2]).

3.3.1.2.2. Numerical modelling

General model theory

The 3-dimensional motion of fluid can be mathematically described by the *Navier-Stokes* equations considering conservation of mass and momentum. The software *FLOW-3D* is used, numerically solving the *Reynolds*-averaged *Navier-Stokes* (RANS) equations within the computational domain. The domain is subdivided into several mesh blocks containing rectangular grid cells (structured mesh). Fluid velocities and pressures are located at staggered mesh locations as shown for a typical grid cell in Figure 95.

[1] Data collection and post processing software provided by U.S. Geological Survey
[2] Matlab based software for processing and visualizing ADCP data provided by U.S. Geological Survey

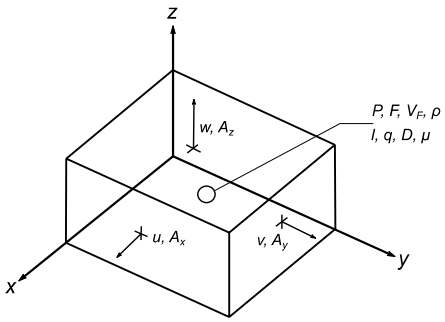


Figure 95: Location of variables in FLOW-3D computational mesh [1].

The numerical model involves the following variables: u velocities and fractional areas A_x at the centers of cell-faces normal to the x-direction, v velocities and fractional areas A_y at the centers of cell-faces normal to the y-direction and w velocities and fractional areas A_z at the centers of cell-faces normal to the z-direction, pressures (P), fluid fractions (F), fractional volumes (V_F), densities (ρ), internal energy (I), turbulence quantities for energy (q), dissipation (D) and viscosity (μ) are located at cell centres [1].

Wall boundaries and other solid geometrical structures like the weir body and the powerhouse are embedded in the mesh by the so called FAVOR^{TM} method defining the fractional face areas and fractional volumes of the cells that are open to fluid flow. In order to properly capture the free-surface dynamics, the *Volume of Fluid* (*VOF*) method is applied in *FLOW-3D* [1]. Because of computer memory and processing time limitations, the full spectrum of turbulent fluctuations cannot be resolved by the equations of mass and momentum conservation. Hence turbulence models are required to close the RANS equations. For this study, the Renormalized-Group k-ε (RNG) turbulence model is used.

Model setup

The topographic data used to set up the Aare river bathymetry are shown in Figure 96. The modelled Aare river reach covers about 500 m upstream and 250 m downstream of the weir in order to minimize the effects of boundary conditions. This is of particular importance with regard to flow deviation by the river bend upstream of the HPP. In addition to the GEWISS profiles[3] that have a rather coarse resolution in streamwise direction (cross sectional data every 100 to 300 m), intermediate cross sections were acquired by means of the ADCP measurements. In order to capture the river curvature accurately, further cross sections were interpolated. Together with break-lines defined at the toe of the bank and other significant slope transitions, the riverbed topography was triangulated using GIS and AutoCAD software. The weir is used as a reference for the local coordinate system of the 3D model (Figure 96 and Figure 97).

[3] River cross sections from official survey of the Swiss Federal Office for the Environment (FOEN)

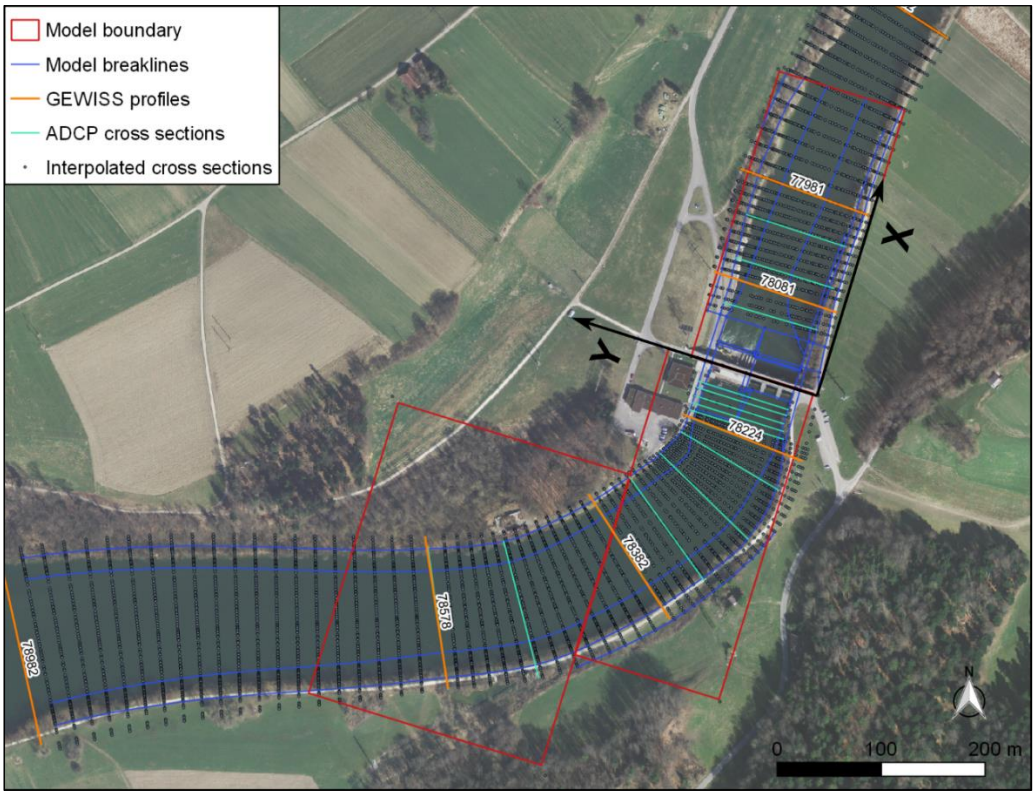


Figure 96: Model domain (within model boundary) and topographic data used to set up the numerical 3D model (background image: © 2018 swisstopo (JD 100041)).

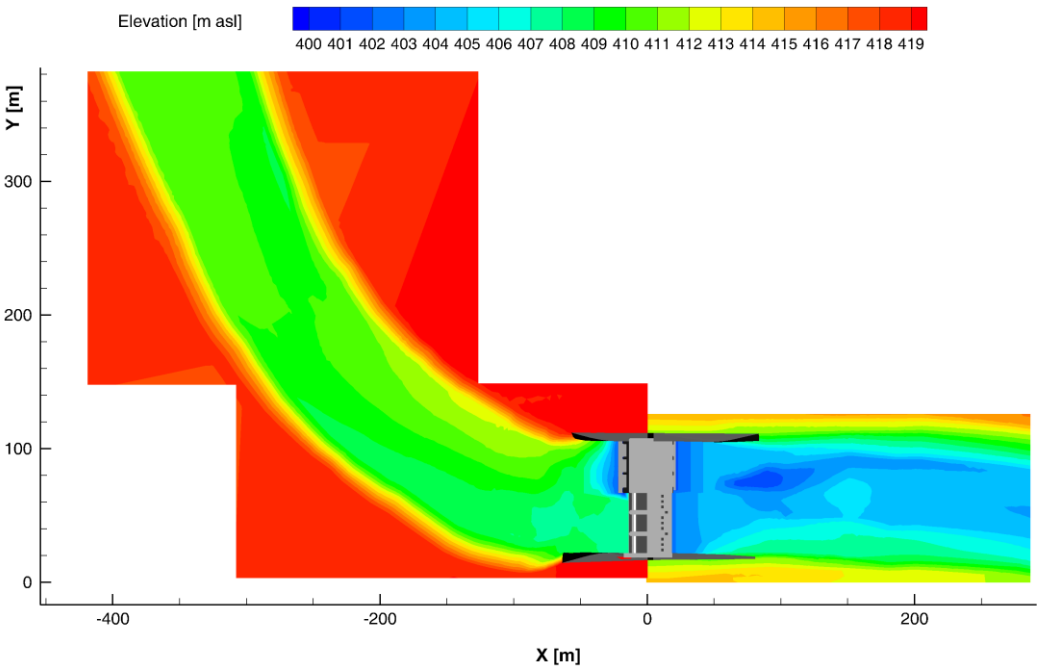


Figure 97: Riverbed bathymetry in coordinate system of the 3D model.

Construction plans provided by the operator were used to model the 3D hydraulic structures like the powerhouse, the weir body and the gates. Such solid structures were designed using

CAD software tools and imported into *FLOW-3D* in the form of stereolithographic files (STL). For the purpose of simplification, the three radial gates with flaps were replaced by simple sluice gates (see Figure 98). Furthermore, turbine runners, flow distributors and trash racks are not geometrically resolved in the model. So-called baffles were used to account for flow resistance of these structural elements. In *FLOW-3D* baffles represent surfaces and therefore do not affect the volume fraction. The baffle geometry snaps to the cell faces of the mesh (see Figure 95), leading to a stair-stepped shape of an originally curved baffle geometry [1]. The user can define different properties such as porosity and linear or quadratic loss coefficients for each baffle. For the current model, the baffles loss coefficients were calibrated in order to match water surface elevations and the discharge distributions between turbines and weir with the measurement data.

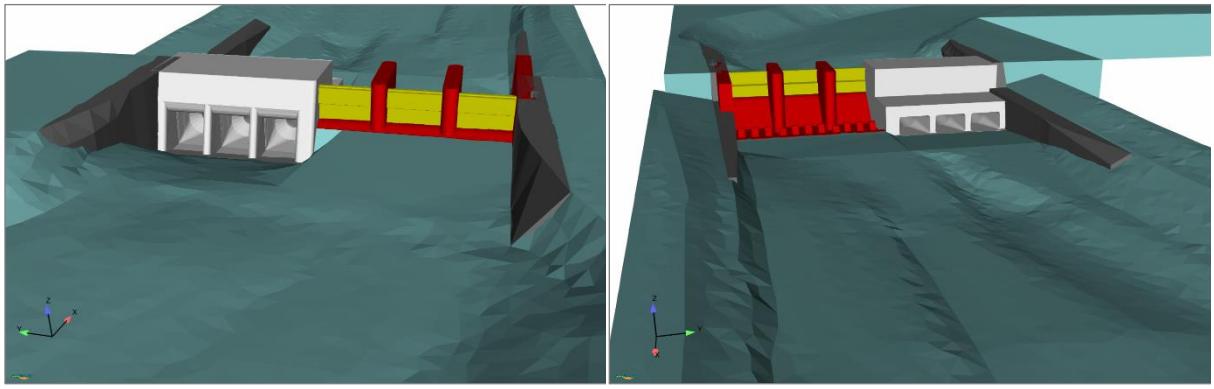
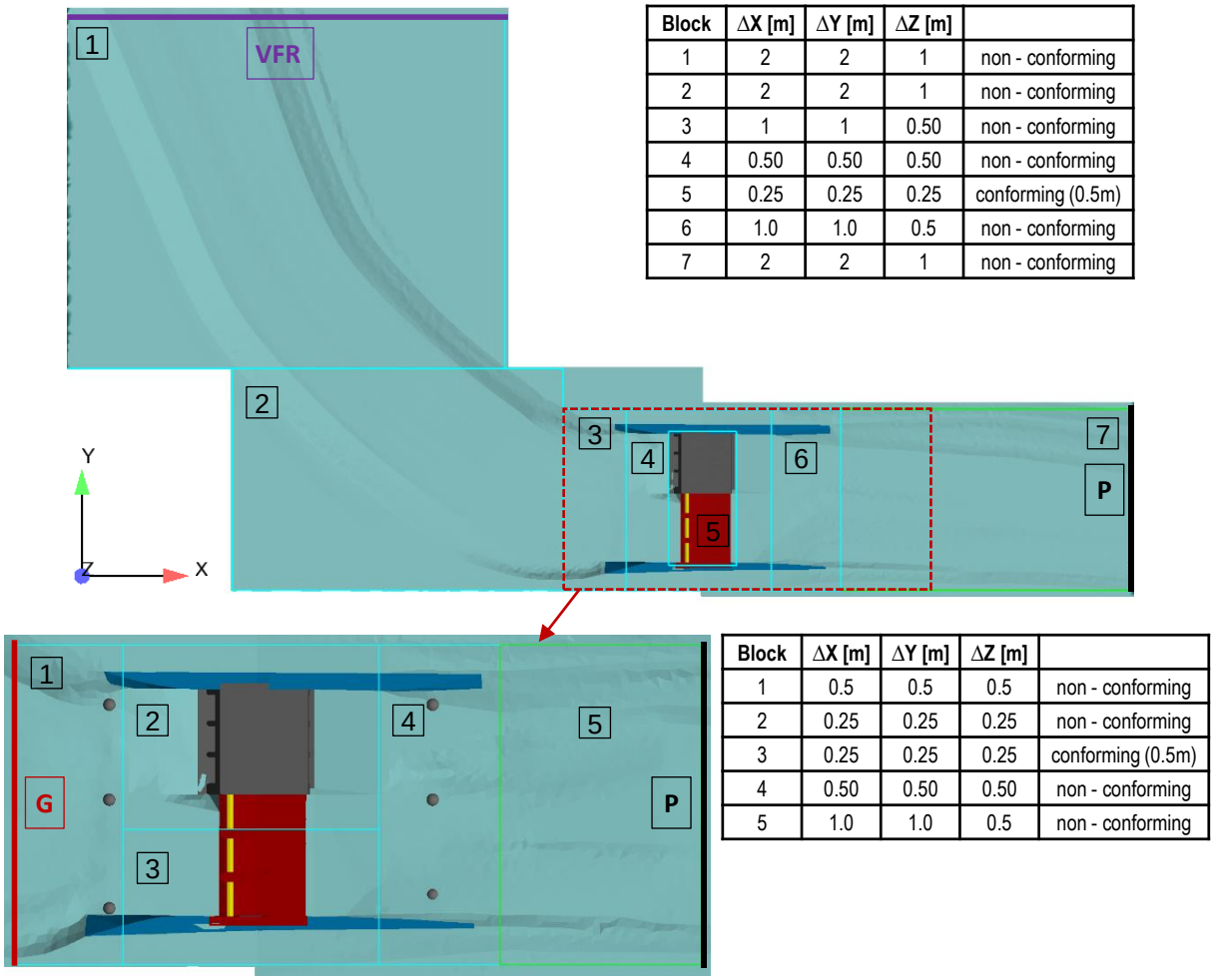


Figure 98: Power plant components represented in the 3D model, view from upstream (left) and downstream (right)

The structured computational mesh of *FLOW-3D* may consist of an arbitrary number of single mesh blocks to cover the model domain. The spatial grid resolution in Cartesian coordinate directions may differ for each mesh block. At first, simulations for the entire model domain were performed. An upstream boundary condition of type volume flow rate (VFR) was used at mesh block 1 (see Figure 99). By specifying the water surface elevation hydrostatic pressure (P) was defined as downstream boundary condition for mesh block 7. The closer to the area of interest, the higher the spatial mesh resolution is. To resolve the power plant structure accurately, a conforming mesh with a resolution of 0.25 m (*x*, *y* and *z*) was specified for mesh block 5. In *FLOW-3D* “conforming mesh” means that the transition between solid and void or solid and fluid is resolved with a nested finer mesh within a defined overlap length compared to the surrounding block. After a steady state solution is reached for the full domain, this solution can be used as restart information for a smaller subdomain model with a finer mesh resolution (bottom of Figure 99). As upstream boundary condition for the restart simulation, a so-called “grid overlay” (G) can be applied. Thus, restart data from the original simulation are used to set flow parameters upstream of mesh block 1. The concept of restart simulations for smaller domains allows for more detailed modelling of particular regions of interest, for example, close to the turbine inlets or the stilling basin downstream of the weir. The computational grids consist of roughly 4 to 6 Mio active fluid cells depending on the scenario.



Block	ΔX [m]	ΔY [m]	ΔZ [m]	
1	2	2	1	non - conforming
2	2	2	1	non - conforming
3	1	1	0.50	non - conforming
4	0.50	0.50	0.50	non - conforming
5	0.25	0.25	0.25	conforming (0.5m)
6	1.0	1.0	0.5	non - conforming
7	2	2	1	non - conforming

Block	ΔX [m]	ΔY [m]	ΔZ [m]	
1	0.5	0.5	0.5	non - conforming
2	0.25	0.25	0.25	non - conforming
3	0.25	0.25	0.25	conforming (0.5m)
4	0.50	0.50	0.50	non - conforming
5	1.0	1.0	0.5	non - conforming

Figure 99: Grid resolution of the 3D model with full domain (on top) and exemplary grid refinement for restart simulations of a particular subdomain (at bottom).

Simulation scenarios

In the scope of the numerical investigations, four different flow conditions were simulated (Table 6). The discharges simulated for scenario 1a and 1b correspond to the hydraulic conditions observed during the ADCP measurement campaigns and were used for model validation. The total and turbine discharges are termed Q_{tot} and Q_T, respectively. For scenario 2a, 231 m^3/s are diverted over the weir as gate flow (Q_{LG}), while the turbine flow is at full load (Q_T =454 m^3/s). During scenario 2b, both gate flow (Q_{LG}) and overflow (Q_{UG}) occur and the total weir discharge (Q_W=Q_{UG}+Q_{LG}) amounts to 106 m^3/s), while the turbine flow is again at quasi full load. For all scenarios, discharge and water surface elevation measurements were provided by the HPP operator.

Back to D2.2 Main index

Table 6: Scenarios simulated with the numerical 3D model.

	Scenario	Q_T [m³/s]	Q_W [m³/s]	Q_{UG} [m³/s]	Q_{LG} [m³/s]	Q_{tot} [m³/s]	Exceedance duration of total flow [d/a]
1. Turbine discharge	1a	402	0	0	0	402	57
	1b	143	0	0	0	143	338
2. Combined discharge	2a	454	231	0	231	685	4
	2b	448	106	75	31	553	20

3.3.1.2.3. Fish monitoring

Hydro-acoustic analysis

From June 19 -21, 2018 a hydro-acoustic investigation of fish behaviour was carried out at HPP Bannwil. The aim of the study was to detect fish in front of the trash rack and to evaluate their position and behaviour in order to gain basic knowledge of their horizontal and vertical distribution and to support the development of measures for fish protection. To this end, a downward-directed imaging sonar recorded video-like data at six different positions along the trash rack (Fig. 14). Overall, five runs were conducted within 3 days: for the first four runs data were recorded for 15 min at each position, whereas during the last run the sampling interval was set to 1 hour. Figure 15 gives an overview of the experimental setup in front of the trash rack. As it became apparent during the field campaign that very low numbers of fish were present, the sonar was left to record data at position VI in between the runs (continuous data). Data processing was carried out with the post-processing software package sonar5 professional and ARISFish.

The data were analysed by measuring the body length of each individual and localizing its first and last appearance in the beam. The spatial distributions, as well as swimming directions, were derived from these data. Independently, the paths of six individuals were tracked in order to evaluate the smoothness of motion and behaviour in detail. Figure 15 shows the set-up of the ARIS explorer sonar mounted on an arm of the Palfinger trash rack cleaning system at HPP in Bannwil.

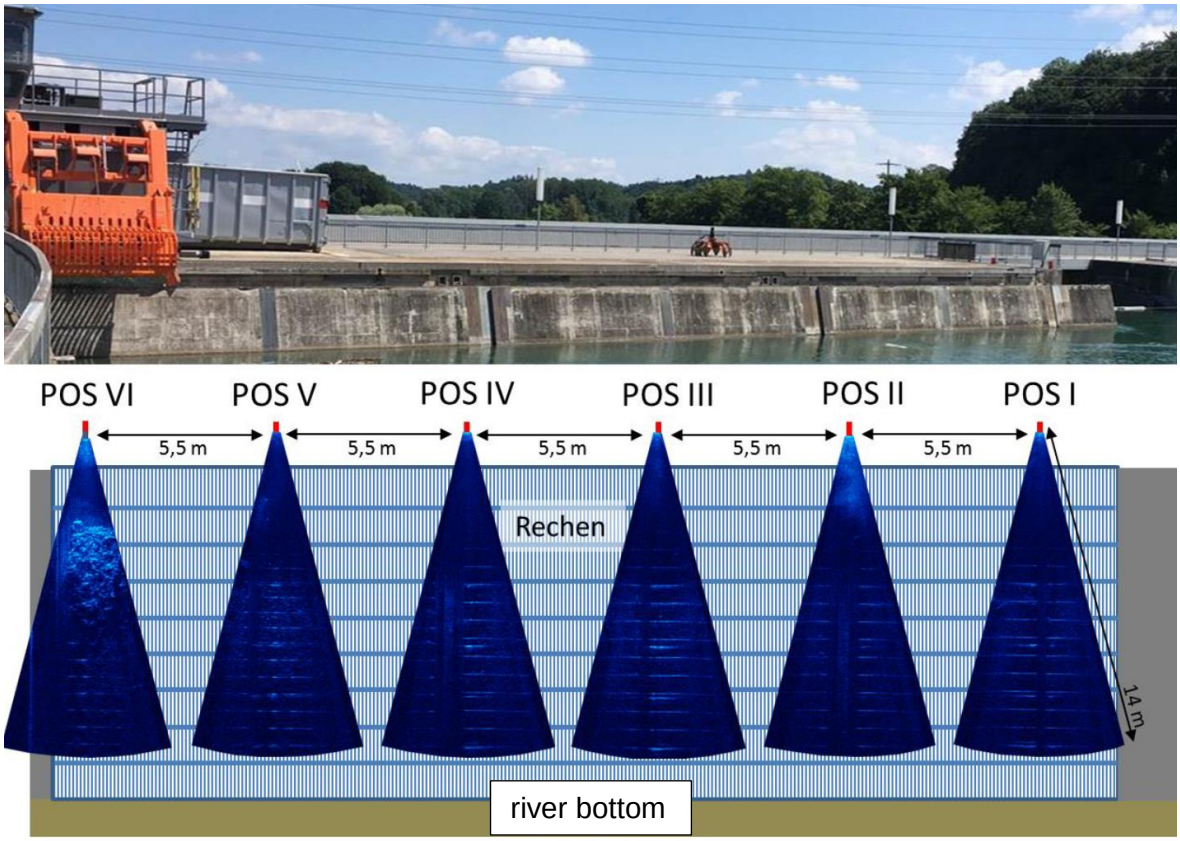


Figure 100: Hydro-acoustic imaging setup with DIDSON and ARIS sonar systems in front of the trash rack. 6 different positions were covering the area in front of the trash rack. View in flow direction.

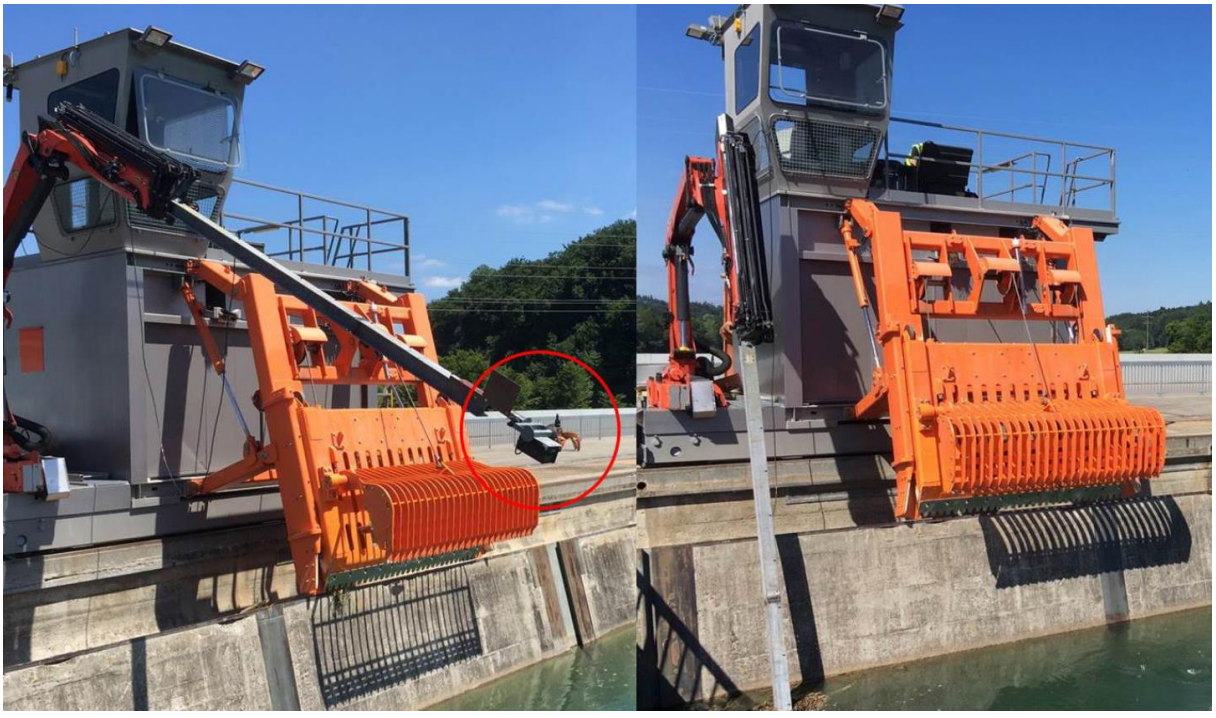


Figure 101: ARIS sonar system at HPP Bannwil. Left: ARIS explorer sonar mounted on an arm of the Palfinger trash rack cleaner. Right: lowered arm with ARIS system in data recording status.

Radio Telemetry:

A radio telemetry system was selected and purchased. The installation and first analysis will be carried out in 2019.

3.3.1.3. Results

To be completed

3.3.1.3.1. ADCP measurements

Field campaign 1: Q = 402 m^3/s

Selected results of the first ADCP campaign are shown in Figures 16 and 17. For the given discharge of 402 m^3/s, the depth-averaged velocities upstream of the HPP are in a range from about 0.7 m/s to 1.1 m/s, depending on the distance from the turbine inlets. The effect of the turbines is clearly visible as the current is concentrated in the left half of the river and towards the inlets. Close to the weir, the flow is almost parallel to the weir axis and a return flow occurs at the right bank.

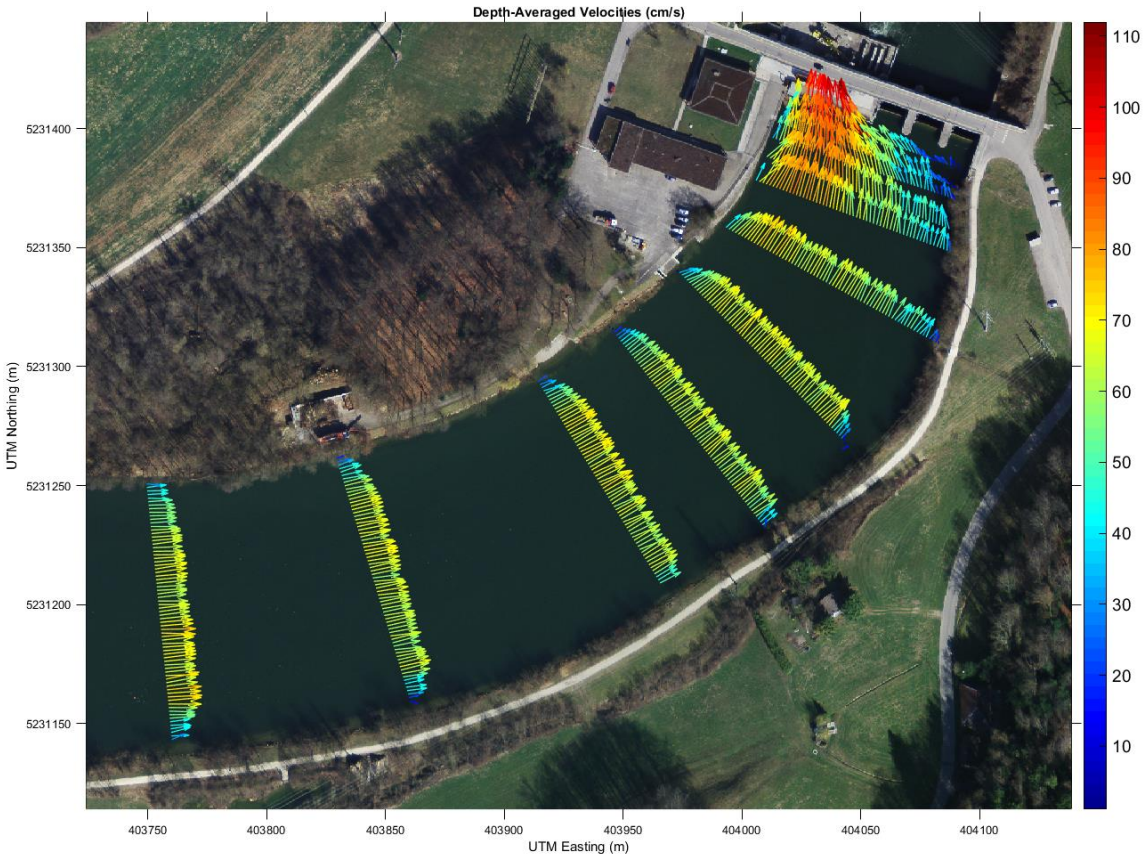


Figure 102: Depth-averaged flow velocities [cm/s] upstream of HPP Bannwil measured with boat-mounted ADCP at a discharge of 402 m^3/s (background image: © 2018 swisstopo (JD 100041)).

The cross section closest to the turbines was recorded about 6 m upstream of the trash rack (see Figure 103). The maximum approach flow velocities in streamwise direction reach up to 1.4 m/s and are located about 3 m above the bottom in front of the inlet of turbine 1 (left turbine). Even slight backwards flow can be observed about 43 m from the left bank in front of the pillar

between the powerhouse and the weir. Transversal flow velocities point towards the turbine inlets and reach about 0.5 to 1 m/s. As can be observed in Figure 103, the lowermost 2 m of the cross section cannot be captured with the ADCP probe due to so-called side lobe interference. This interference of the acoustic beams is caused by reflections from the bottom and may lead to a loss of vertical profiling range of up to 15 % of the total flow depth [3].

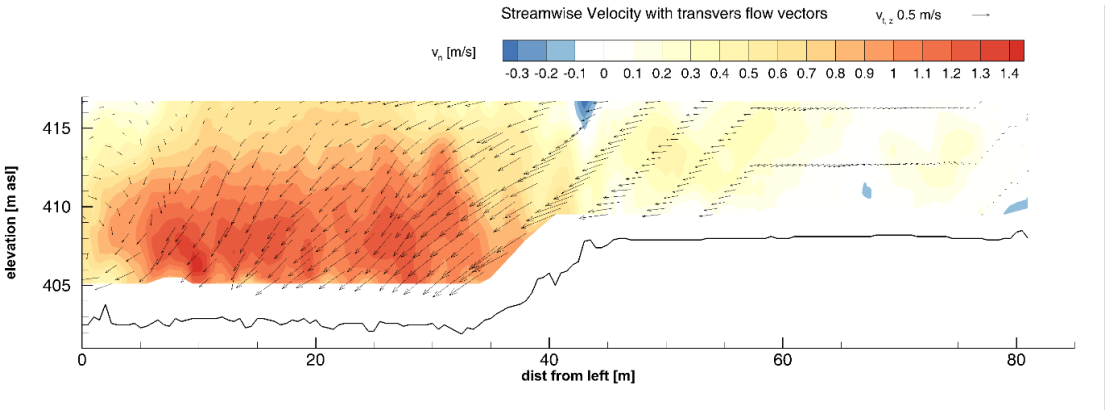


Figure 103: Contour plot of streamwise flow velocities about 6 m upstream of turbine inlets for Q_T = 402 m³/s (view in flow direction).

Campaign 2: Q = 143 m³/s

Due to the very dry weather conditions in summer 2018, the discharge of the Aare River decreased significantly to only 143 m³/s on the day of the second campaign in September 2018. Only turbines 1 and 2 (left and central) were in operation then. Transects were repeatedly recorded downstream of the HPP as shown in Figure 104.

The highest velocities of about 1.4 m/s are observed close to the left riverbank. Due to the turbine outflow similar to a jet flow, a clockwise backward circulation occurs downstream of the HPP which leads to negative streamwise velocities of up to 0.5 m/s towards the right riverbank. When analysing one single ADCP transect, one can observe quite high velocities gradients and generally high fluctuations (Fig. 18a). The more transects are being averaged, the more homogeneous the flow velocities become. Averaging the values of up to 8 transects at one cross section leads to robust and smooth results, i.e. no major changes of the flow quantities result for more than 8 transects. Therefore, it is recommended to acquire a minimum of 8 transects at each cross-section. Such averaged flow field over 8 transects can be used for comparison with the results of the numerical model.

Back to D2.2 Main index

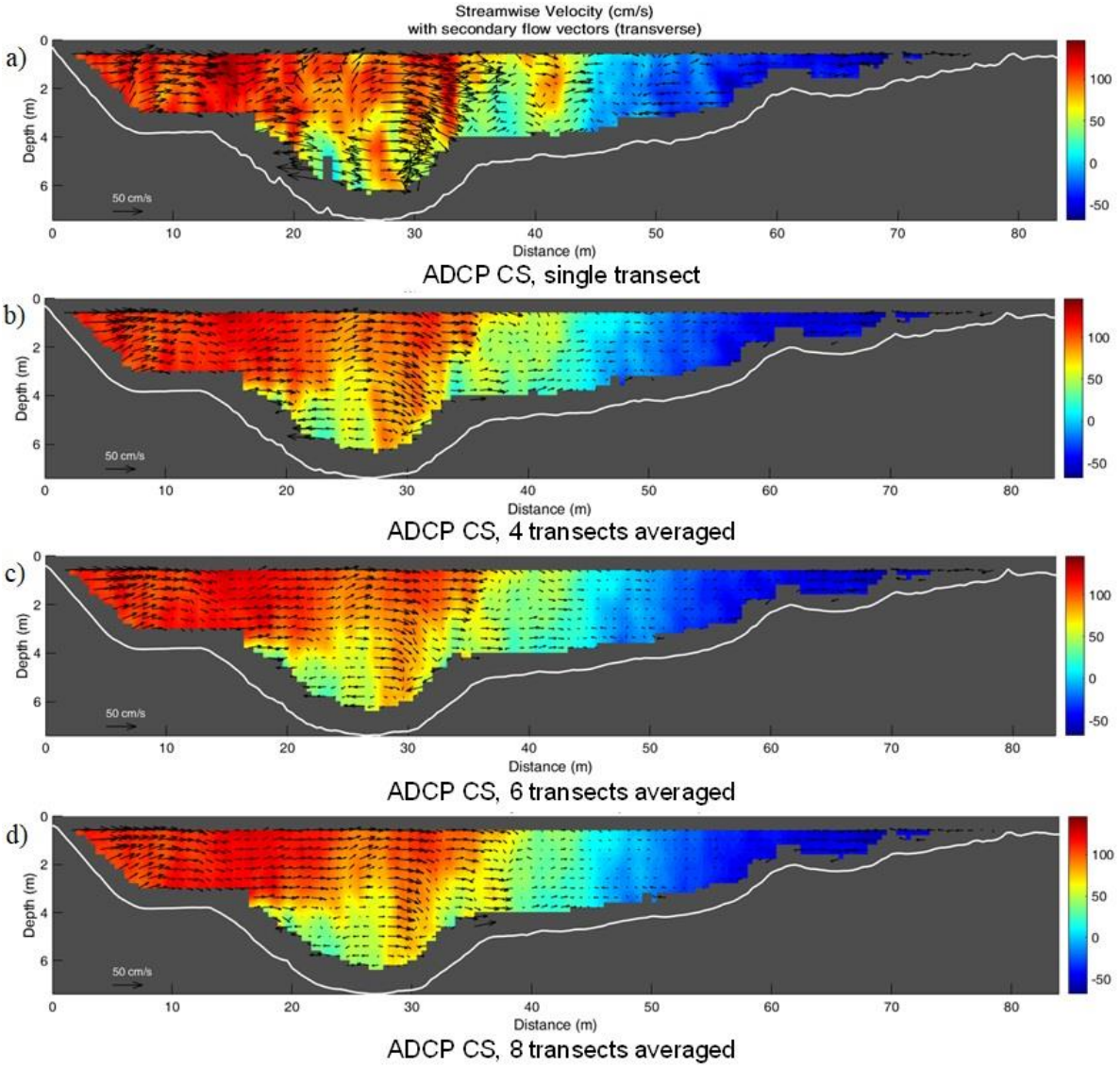


Figure 104: Effect of transect averaging about 50 m downstream of the turbine outlets for Q_T = 143 m^3/s (view in flow direction).

3.3.1.3.2. Numerical modelling

Model validation (Scenarios 1a and 1b)

For all scenarios, the simulated water surface elevations upstream and downstream of the HPP as well as the discharge distribution between the weir and turbines match with the measured surface elevations and turbine discharges, respectively, provided by the operator. For further validation, the simulated flow velocities at certain cross sections are compared with the results of the ADCP measurements for the same hydraulic conditions. Streamwise velocities, as well as transversal flow vectors for a discharge of 402 m3/s (scenario 1a), are compared in Figure 105. The exemplary cross section is located about 20 m upstream of the turbine inlets. In general, the simulated and measured flow fields match. It should be noted that for scenario 1a only two ADCP transects were measured and averaged during the post-processing. Hence, the agreement between measured and simulated velocities is only fair.

Back to D2.2 Main index

The maximum simulated velocities reach about 0.8 m/s and are slightly lower than the measured velocities. The area of high velocities in front of the turbine inlets from 2 to about 40 m from the left riverbank agree very well with the observations. Consistently, both profiles show significant transverse velocity components pointing towards the turbine inlets with a magnitude of approximately 0.8 m/s.

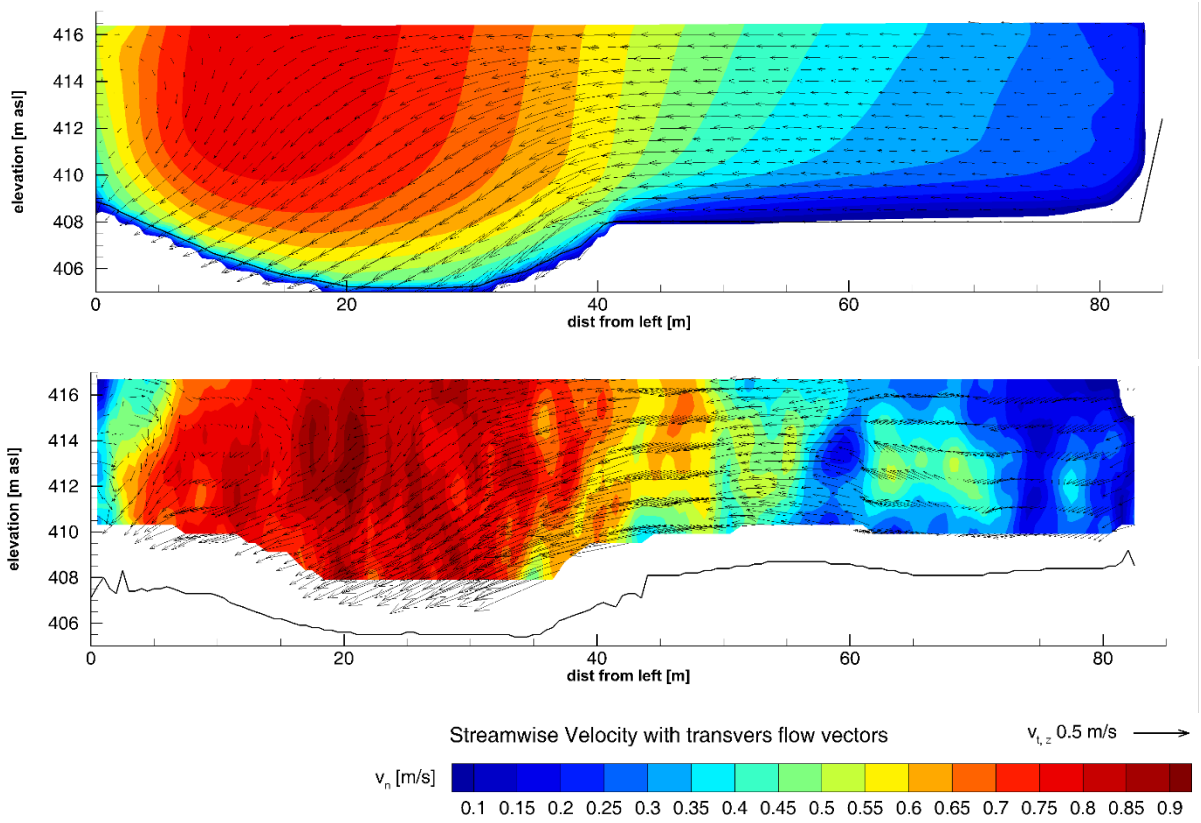


Figure 105: Comparison of the simulation results (top) with the ADCP measurements (bottom, average of two transects) for a discharge of 402 m³/s about 20 m upstream of the turbine inlets (view in flow direction).

Flow velocities for a discharge of 143 m³/s (scenario 1b) downstream of the turbine outlets are compared in Figure 106. For scenario 1b, 6 ADCP transects were averaged. Therefore, the flow velocities are more homogeneous and match well with the results of the simulations. In both cases, the maximum positive flow velocities in the left half of the cross section reach about 1.55 m/s. Due to the fact that the turbine runners are not included in the numerical model, it is not possible to fully capture the vorticity indicated by the significant vertical velocity components in the ADCP data (especially between 0 and about 35 m from the left riverbank). The regions showing negative streamwise velocities are almost identical in both plots with the maximum values of 0.55 m/s.

On the basis of comparison for scenarios 1a and 1b, it is concluded that the numerical 3D model is capable to simulate the major flow pattern upstream and downstream of the HPP (velocity magnitudes, flow directions, water surface elevations). So far, this is verified for conditions with turbine discharge only. Therefore, further ADCP measurements will be conducted for conditions with weir operation to also validate model scenarios with an Aare discharge of more than 450 m³/s.

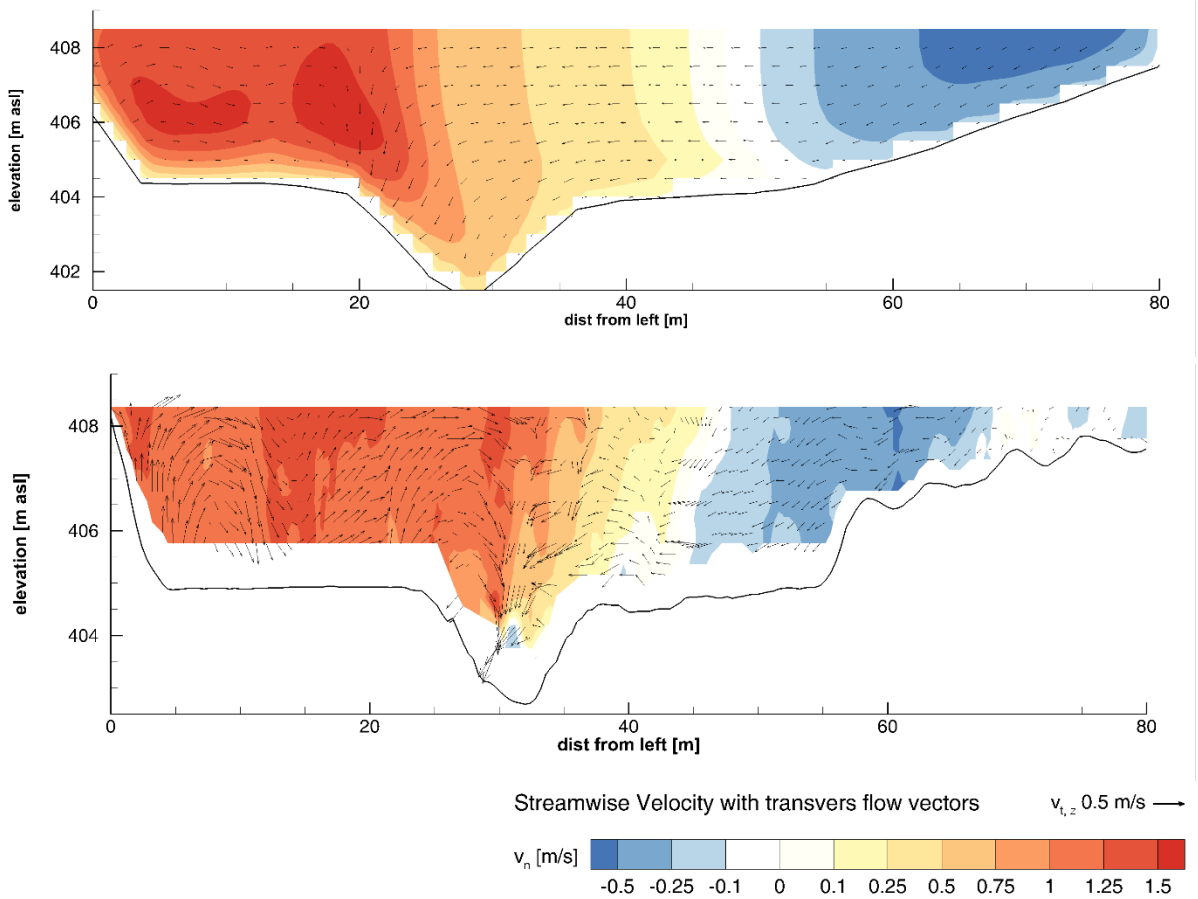


Figure 106: Comparison of the simulation results (top) with the ADCP measurements (bottom, average of 6 transects) for a discharge of 143 m³/s about 40 m downstream of the turbine outlets (view in flow direction).

Positioning of FGS

FGSs in the form of racks with either horizontally or vertically oriented bars are supposed to prevent migrating fish from swimming through the turbines and guide them along the screen axis to an alternative bypass and into the downstream reach. The FGSs are positioned with a certain horizontal angle $\alpha \leq 45°$ towards the approach flow in order to provide a ratio between the tangential v_t and normal v_n flow velocity components larger than one. This ratio is considered a suitable criterion to assess the potential guiding efficiency of a FGS. Furthermore, the normal flow velocities at the FGS should not exceed the maximum sustained swimming speed of the target fish species in order to prevent fish from being pressed against the FGS.

The numerical 3D model is a powerful tool in order to simulate normal and tangential flow velocities at any desired cross section of the computational domain for various discharges and operational conditions. A conceptual approach for the positioning of FGS using numerical 3D simulations was developed at VAW [4]. The advantage of the proposed procedure is that hydraulic conditions at potential FGS can be assessed without resolving the actual geometrical structure of the bars in detail. Such a detailed implementation would lead to an enormous number of very small computational cells (more than 50 Mio), which would make a practical model application at large-scale river power plants such as HPP Bannwil unfeasible.

For the purpose of planning future FGS at HPP Bannwil, the hydraulic conditions of two potential positions upstream of the turbine inlets have been investigated by means of 3D model

Back to D2.2 Main index

simulations. Locations of a FGS with an angle of α = 45 ° and a length of about 58 m as wells as another one with an angle of α = 37° and a length of about 80 m are shown in Figure 21. The latter promises a better ratio of tangential and normal velocities especially for the on-site conditions with the powerhouse being located at the inside of a river bend.

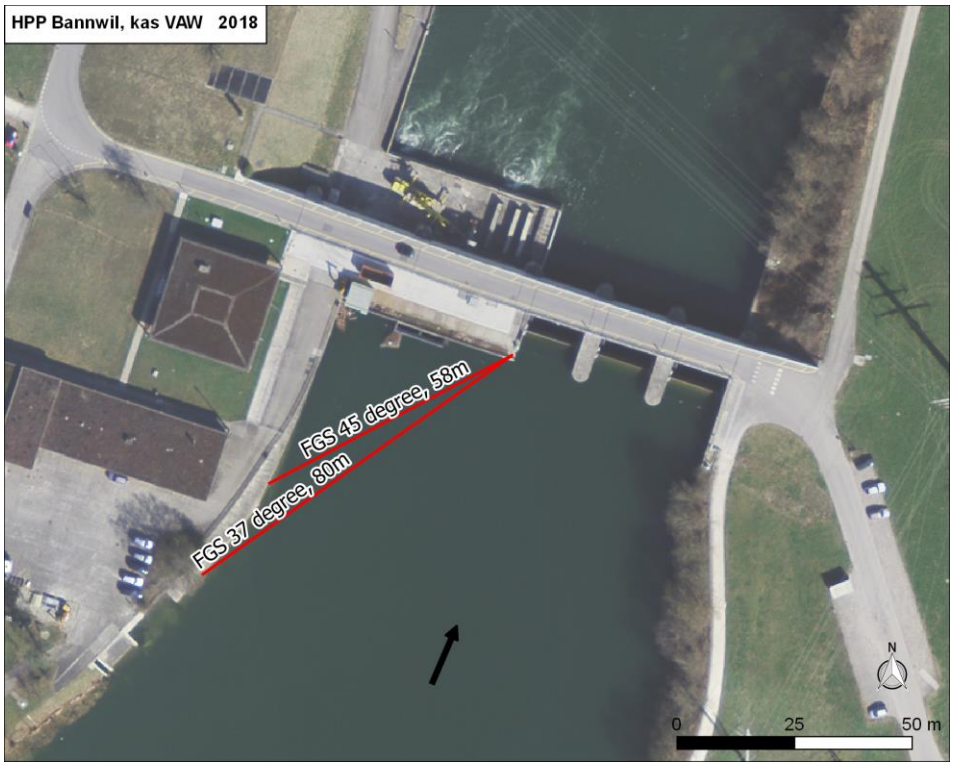


Figure 107: Potential positions of fish guidance structures upstream of the HPP Bannwil (background image: © 2018 swisstopo (JD 100041)).

As seen from Figure 108, the site-specific conditions at HPP Bannwil lead to quite high normal velocity components at the potential FGS positions. Apart from a small area close to the left riverbank near the water surface, v_n exceeds v_t at the considered locations. This holds for an angle of 45° as well as 37°. With respect to fish guidance efficiency, unfavourable conditions arise in front of the pillar between the powerhouse and weir field 1, where negative tangential velocities up to -0.8 m/s occur.

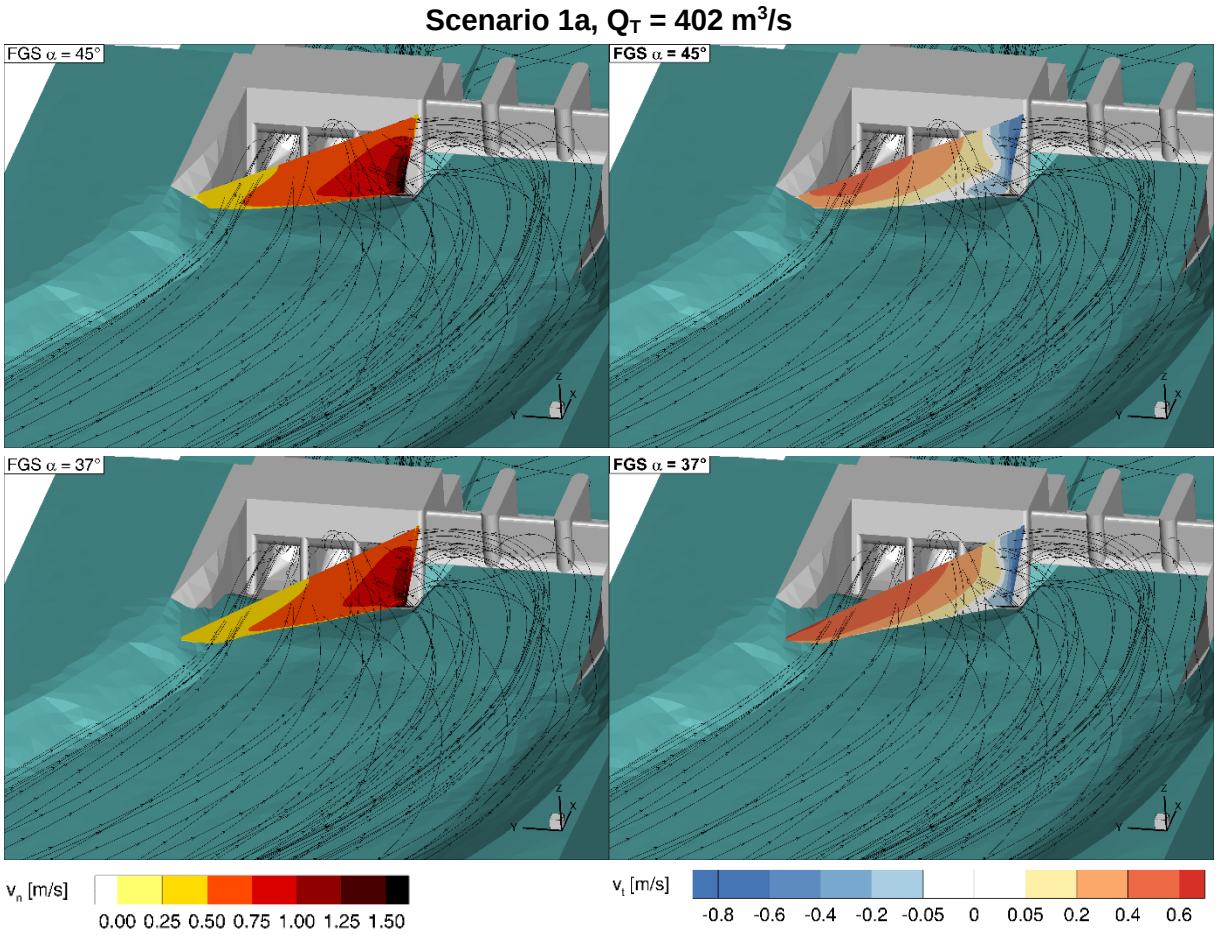


Figure 108: Normal (left) and tangential (right) flow velocities at potential FGS positions upstream of the turbine inlets for scenario 1a for FGS angled at 45° (top) and 37° (bottom).

For scenario 1b maximum v_n values of about 0.35 m/s are reached at an angle of 45 ° (Figure 109). Although normal velocities are generally lower compared to scenario 1a because of lower turbine discharge, the ratio v_t and v_n is smaller than unity for this case. Also, negative tangential velocities increase because only turbine 1 and 2 are in operation.

For both scenarios with turbine discharge only, the hydraulic conditions at the potential FGS position are rather unfavourable. The main reason is the location of the powerhouse on the inside of the river bend, which leads to a curved turbine admission flow at which the streamlines are almost perpendicular to the FGS over a wide range of the screen, both for turbine flow only (Figure 110, left) and combined turbine and weir flow (Figure 110, right). The detailed knowledge about the hydraulic conditions can also be used for positioning of a bypass. Since fish shall be guided along the screen, this would result in a bypass close to the pillar towards the weir. Again, the negative tangential velocities in this area might prevent such a bypass position. An improvement of the hydraulic conditions might be achieved by modification of the shape and/or upstream extent of the pillar. Another option would be the use of multiple guidance screens at different angles α to avoid perpendicular or even opposite admission flow close to the pillar. The 3D model can also be used for such an optimization process of the FGS positioning since modified structural components can be added to the model quite easily.

Back to D2.2 Main index

Furthermore, also economical and structural aspects of such large FGS have to be considered. However, this is not subject of this investigation.

Scenario 1b, Q_T = 143 m³/s

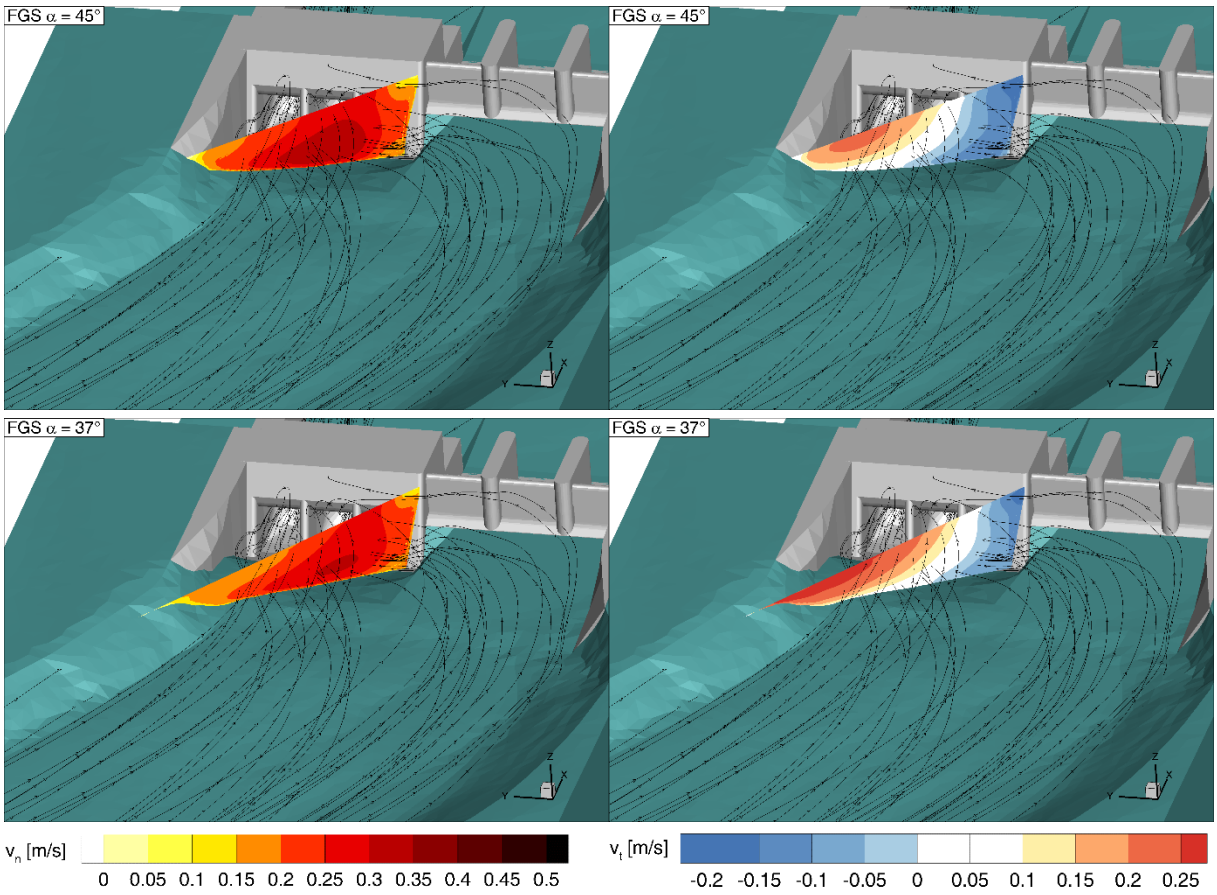


Figure 109: Normal (left) and tangential (right) flow velocities at potential FGS positions upstream of the turbine inlets for scenario 1b for FGS angled at 45° (top) and 37° (bottom).

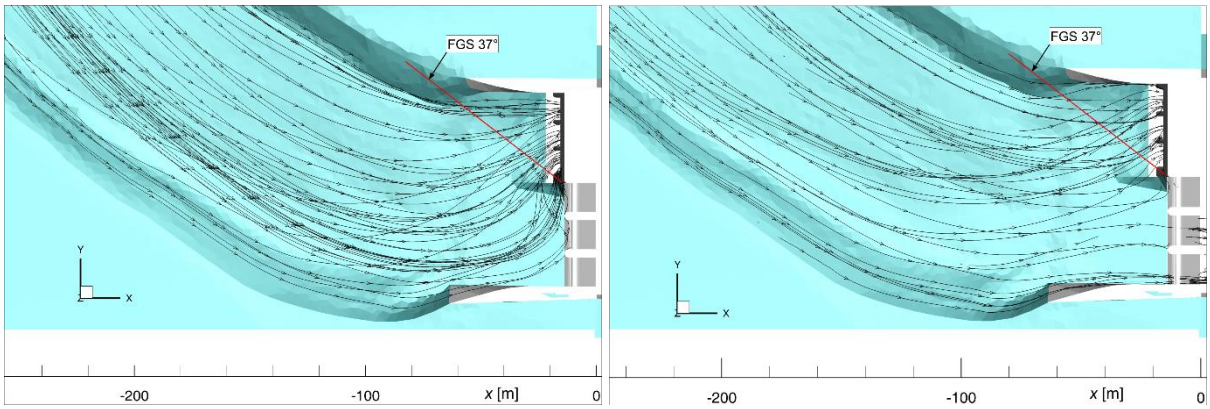


Figure 110: General turbine admission flow direction for turbine discharge only (left, scenario 1) and combined turbine and weir discharge (right, scenario 2).

Back to D2.2 Main index

In case of weir discharge, the hydraulic conditions along the screen are slightly improved due to more head-on approach flow, but the flow attack angle is still not favourable from a fish guidance perspective (Figure 110, right). The backwards tangential flow close to the pillar is reduced compared to scenario 1 (Figure 111). Nevertheless, normal velocities are even higher for scenario 2a because of an increased turbine discharge of 450 m^3/s (design discharge). Especially for an angle of $\alpha = 45°$, v_n still exceeds v_t over a wide range of the FSG and v_n might be too high in view of the sustained swimming speed of the target fish species. In principle, weir operation could be a measure to provide better hydraulic conditions at the FGS. However, weir discharge only occurs on about 42 days per year at HPP Bannwil (see D2.1, informations about hydrology). Furthermore, the large drop over the weir of up to 9 m as well as the hydraulic forces occurring in the stilling basin should be considered. The hydraulic conditions at the weir will be analysed subsequently.

Scenario 2a, Q_T = 450 m^3/s, Q_W = 231 m^3/s

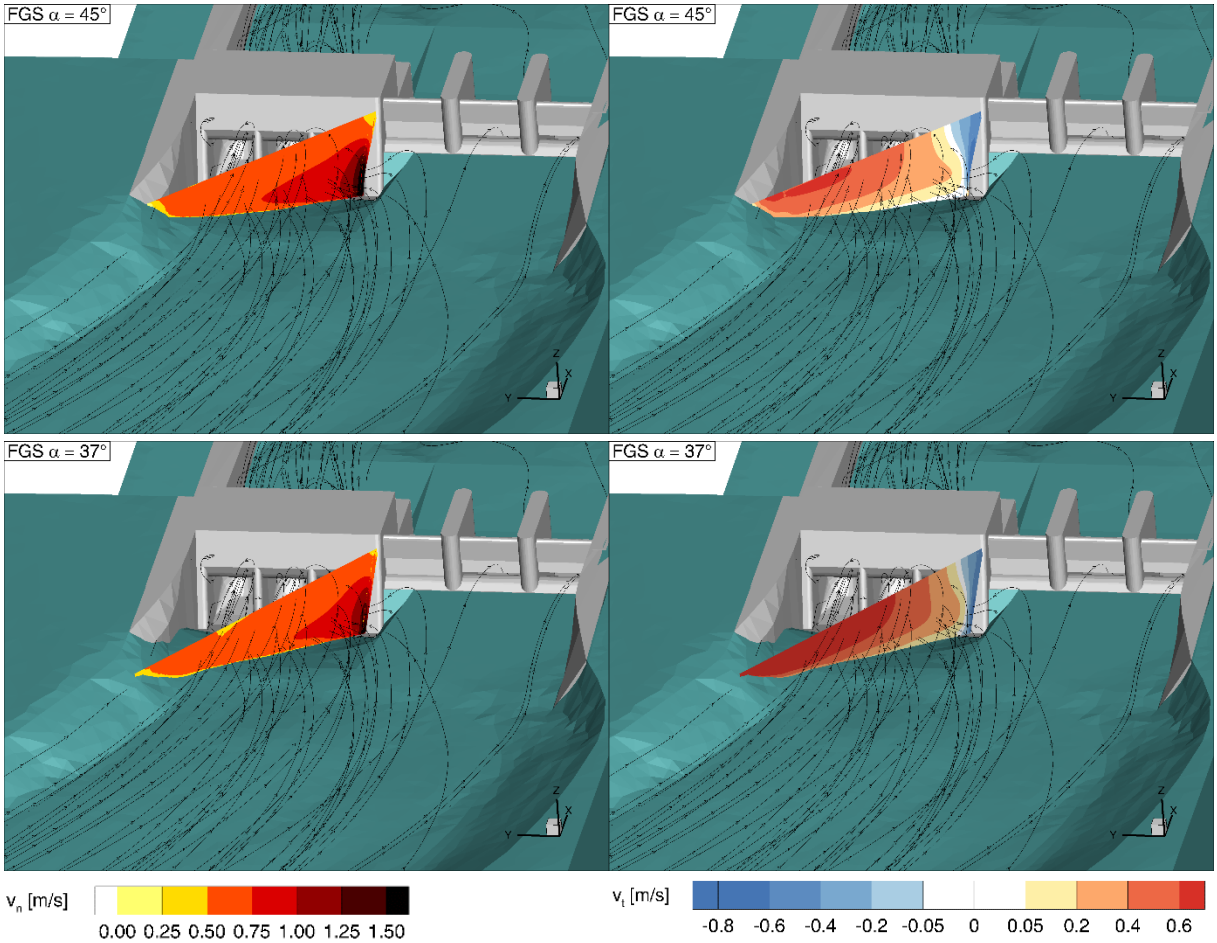


Figure 111: Normal (left) and tangential (right) flow velocities at potential FGF positions upstream of the turbine inlets for scenario 2a for FGS angled at 45° (top) and 37° (bottom).

Weir passage

During scenario 2a the gates of the weir fields (WF) 2 and 3 are open and 231 m^3/s are released via the weir. This leads to flow velocities of up to 10 m/s at the weir crest (Figure 112). At the bottom of the stilling basin, velocities reach up to 7 m/s. The impact velocity at the baffle

Back to D2.2 Main index

blocks at *x* = 9 m is about 5 m/s, which is a potential threat for fish migrating downstream via the weir. The vectors in the sectional plot of Figure 112 clearly show the roller in the basin with backwards circulation at a magnitude of up to 3 m/s close to the water surface.

During scenario 2b, overflow at all weir fields plus gate flow at WF 3 occur and 106 m^3/s are released via the weir. The overflow jet reaches velocities of up to 10 m/s (Figure 27). At the bottom of the stilling basin, velocities reach up to 5 m/s. The impact velocity at the baffle blocks at x = 9 m is about 2 to 3 m/s. which might be a potential threat for fish migrating downstream via the weir. Similar to scenario 2a, the roller inside the basin occurs with a backward circulation at a magnitude of up to 2 m/s for this scenario.

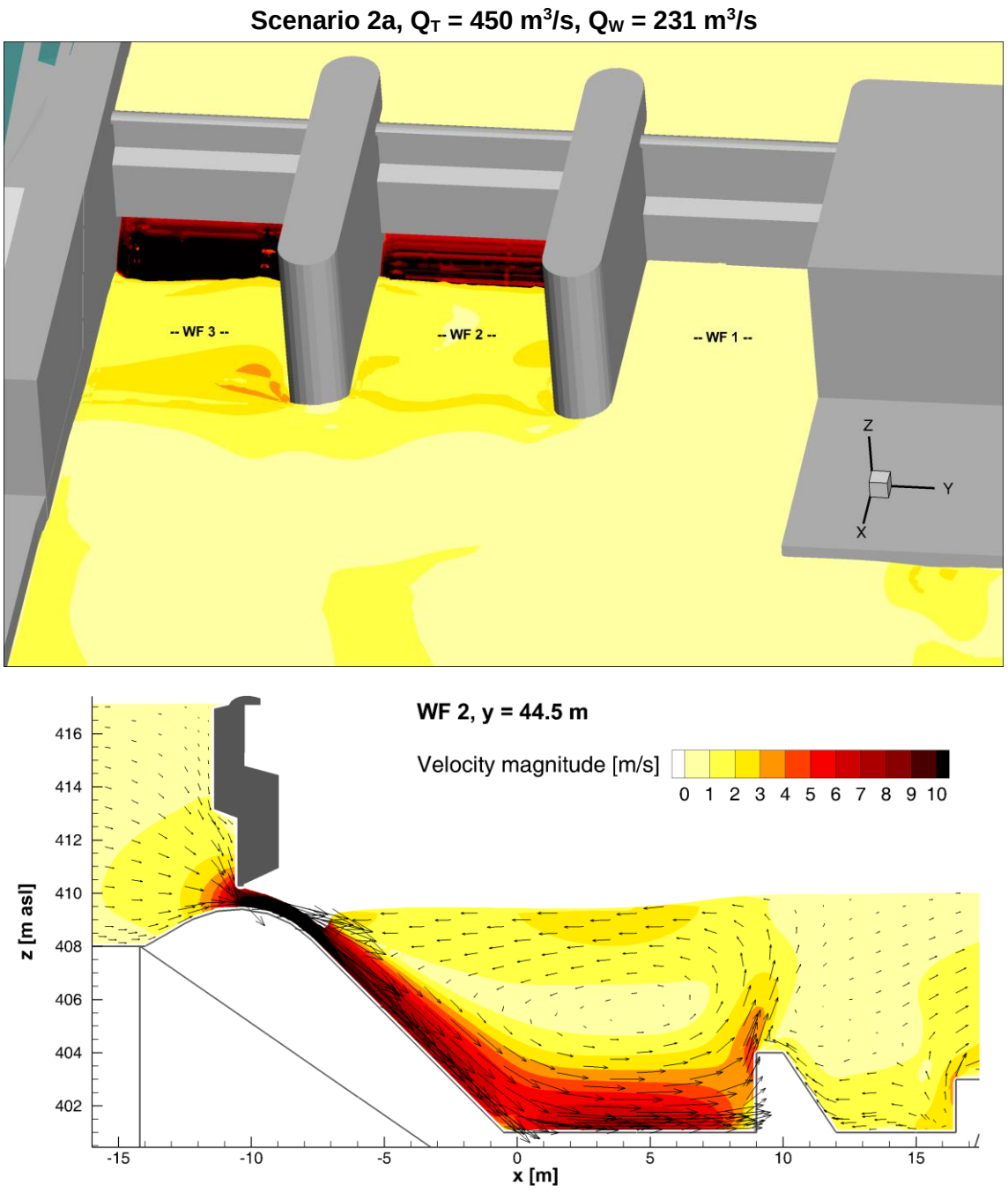


Figure 112: Velocity magnitudes at weir discharge for scenario 2a: Gate flow occurs at field 2 and 3, field 1 is closed. The depicted cross section is extracted at position y = 44.5 m in the middle of WF 2.

Back to D2.2 Main index

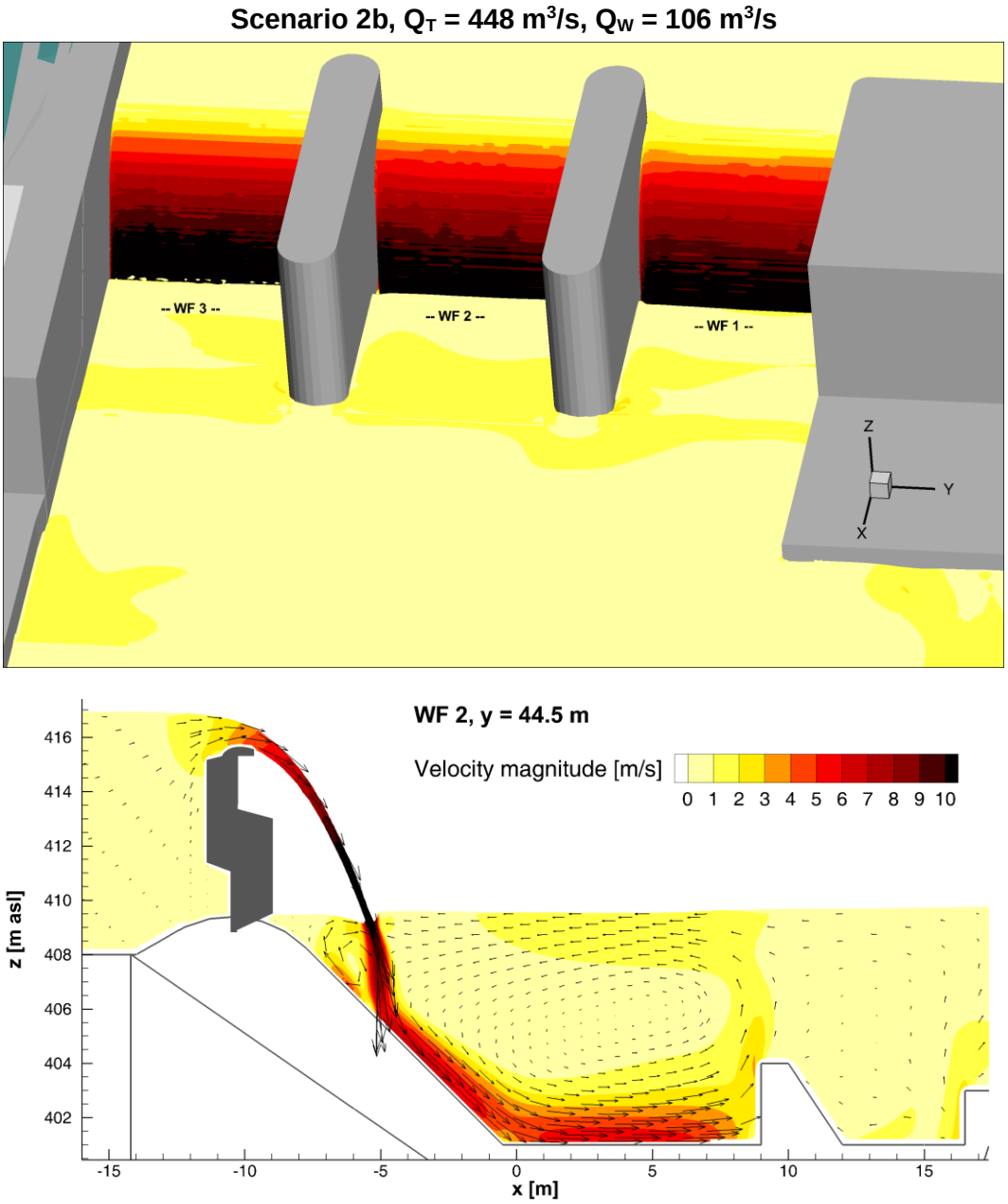


Figure 113: Velocity magnitudes at weir discharge for scenario 2b: Overflow occurs at WF 1, 2 and 3 plus gate flow at WF1. The depicted cross section is extracted at position y = 44.5 m in the middle of WF 2.

Discussion of the results for fish passage over the weir

[7] and [8] published considerable material dealing with Atlantic Salmon mortality at spillway passage. Passage through spillway may cause direct physical injury, increased exposure to predation, temperature change, atmospheric gas supersaturation, sub-lethal effects and/or stranding below the spillway. Neither large nor small fish can sustain impact velocity larger than 16 m/s when they fall in free-fall conditions. Above this critical flow velocity, significant damage occurs such as injuries to the gills, eyes and internal organs. The terminal velocities are approx. 16 m/s for fish in a 10 cm -13 cm size range and 58 m/s for fish in 60 cm. The smaller fish reach their terminal velocity at approx. 30.5 m fall height. At HPP Bannwil, the

Back to D2.2 Main index

overflow velocities of up to 10 m/s (scenario 2b) are below the terminal velocities of small fish and hence no fish injuries is expected due to fall velocities. However, due to back-roll and possible atmospheric gas supersaturation (>100%) in the stilling basin in both scenarios 2a and b, fish are exposed to predation and strike to baffle blocks and gas-bubble disease, respectively. The latter, i.e. the phenomenon of total dissolved gas supersaturation (TDGS), has become of scientific interest mainly due to observations at the Columbia River (US), mainly at deep stilling basins of some 20 m depth where gas becomes dissolved. Exposure to TDGS can be fatal to fish and other aquatic organisms causing a so-called Gas Bubble Trauma (GBT) [6]. At Bannwil, TDGS is unlikely, however, as the hydrostatic pressure in the stilling basin is below critical values according to observation. It is also possible to model the phenomenon of air entrainment with the numerical 3D model, which could provide an estimate of the risk for GBT associated to downstream fish migration via weir discharge.

3.3.1.3.3. Fish monitoring

The results of the data analysis show only little fish passage through the trash rack. 25 fishes were counted during the 5 runs. The highest number of fishes was recorded at position VI with 7 fishes. In addition during the continuous recording at position VI 49 fishes were detected. Figure 28 shows the number of detected fish and the registration time for all positions, while Figure 29 shows the length / frequency distribution of the detected fishes.

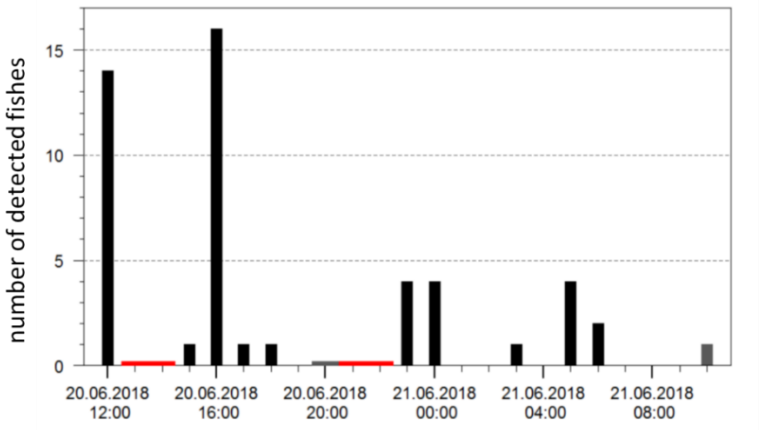


Figure 114: Number of detected fishes and time of registration for all 6 positions at HPP Bannwil intake trash rack. The red lines indicate data gaps.

Back to D2.2 Main index

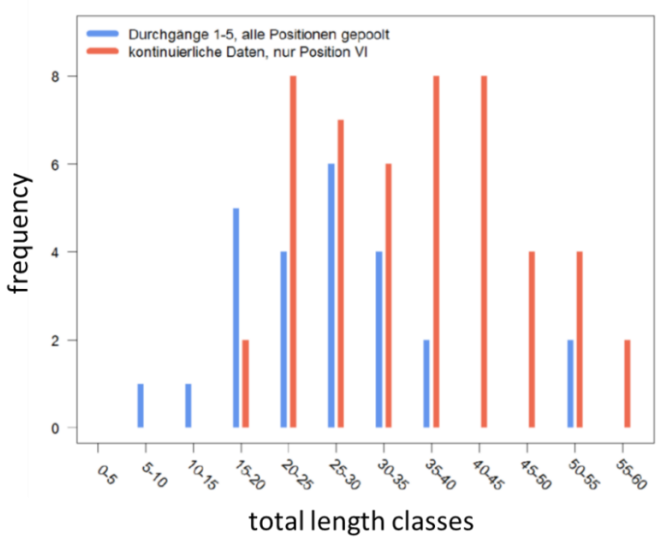


Figure 115: Total body length [cm[vs. frequency distribution of detected fishes at HPP Bannwil intake trash rack. Blue bars: pooled data for the 5 runs, red bar: continuous data, only position VI .

The behaviour of fishes in front of the trash rack in terms of swimming depth is documented in Fig. 30. The range of the observed fish swimming depth at position VI is between 2.3 and 14.5 m below the water surface. Individuals concentrate at depths between 4 and 8 m. However, during the 5 runs, only few fishes were detected at this depth range.

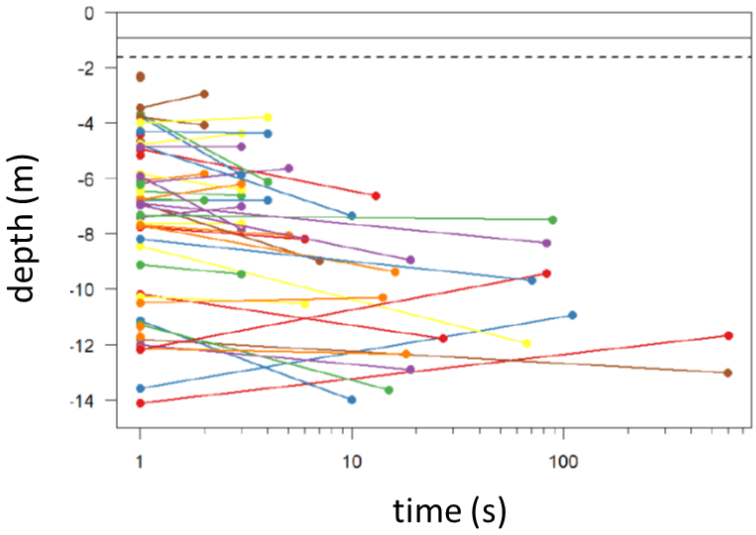


Figure 116: Swimming depth of all fishes registered during the continuous data analysis at position VI at HPP Bannwil intake trash rack (N=49). The colors serve only for a better identification of the individuals.

In summary, fish lengths ranged from 5 to 60 cm and individuals were detected at depths from 2.3 to 14.5 m below the water surface. The swimming motion was directed downwards in 70% and towards the concrete wall on the left riverbank in 55 % of the cases. The tracking of 6 individuals revealed two different kinds of behaviour: 3 passed through the sonar beam in a straight motion at comparatively high speeds, whereas the remaining 3 stayed in the beam

much longer, slowly moving up- and downwards in front of the left concrete wall. The distribution of fish locations is neither vertically nor horizontally homogeneous.

Additional hydroacoustic observations would be interesting at another time of the year (e.g. in late autumn).

3.3.1.4. Conclusions & Outlook

We documented the current situation and investigated the efficiency of spill flow or water release as an operational measure at HPP Bannwil by means of field monitoring and 3-D numerical modelling in the area near the powerhouse and weir. The monitoring comprises:

- characterization of the flow field using ADCP
- 3D numerical simulation
- survey of the fish movements using ARIS Sonar and radio telemetry techniques

Two field campaigns were conducted to measure river bathymetry and flow velocities around the HPP with discharges Q = 402 and 143 m^3/s using an ADCP. The ADCP data were used to construct the 3D numerical model of the HPP and calibrate and validate the model. The 3D numerical model was capable to simulate the major flow patterns upstream and downstream of the HPP (velocity magnitudes, flow directions, water surface elevations), and the simulated flow fields matched well with the measured data.

For the purpose of planning future FGS at HPP Bannwil, the hydraulic conditions of two potential positions upstream of the turbine inlets were investigated by means of the 3D model simulations. Locations of a FGS with an angle of α = 45 ° and a length of about 58 m as wells as another one with an angle of α = 37° and a length of about 80 m were studied. For both scenarios with turbine discharge only, the hydraulic conditions at the potential FGS position are rather unfavourable. It is recommended to use the 3D model for an optimization process since such FGS can be added to the model quite easily.

Spillway or weir passage as an operational measure was numerically studied for the different scenarios. The results indicate that the spillway velocities are lower than the critical impact velocities of small and large fish and hence no injury is expected. However, due to back-roll and potentially atmospheric gas supersaturation (>100%) in the stilling basin in both studied scenarios, fish can be exposed to predation and strike to baffle blocks and gas-bubble disease, respectively.

The fish monitoring study with hydro-acoustic technique provided fish behaviour data in front of the turbine intakes. However, the results do not allow to draw a general conclusion on fish behaviour in front of the turbine intake due to the low number of detected fish during the field campaign. Therefore, a further study is recommended at another time of the year, e.g. in late autumn.

We plan to conduct ADCP measurements in 2019 when the discharge is higher than the design discharge of the HPP and hence weirs are in operation. These data will be used to further validate the numerical model for the scenarios of weir operations. Moreover, fish monitoring will be continued using a radio telemetry technique in 2019. Finally, the collected fish monitoring and hydraulic data will be used to develop measures to improve down fish migration.

3.3.2. Turbine passage: Barotrauma Detection System measurements (TUT, SJE, BKW)

Dynamic pressure fluctuations experienced by fish during the turbine and spillway passages will be studied at HPP Bannwil using a Barotrauma Detection System (BDS) developed at TUT. The data will be analysed and the results will be provided to Voith (WP2) for BioPA model by TUT. VOITH will build a CFD model of turbines at HPP Bannwil, run the model and compare model results with the BDS results. The results will be used for WP 3.3. Furthermore, VOITH will use the same CFD-models and focus on different operating modes to evaluate the possibility of adapting the operation for certain time periods. Finally, the results from TUT and VOITH will be provided to TUM for fish turbine mortality assessment. SJE might help TUT for the field measurements and the analysis of BDS data.

3.3.2.1. Data

Data will be collected from the field campaign and literature. A complete list of the time series data collected by the sensors can be found in Table 3.

3.3.2.1.1. Methodology

In order to analyse the survival possibilities of fishes in hydroelectric turbines through swimming, we built in cooperation with the TUT Biorobotics Center “fish surrogates” that contain a plurality of underwater sensors. The device housing is made of a strong and durable polycarbonate, and the mechanical design of the entire device allows it to withstand and record turbine blade strike events. The electronics are equipped with three precision avionics-grade pressure sensors, which also measure the sensors temperature and an inertial measurement unit that stores the absolute orientation, linear acceleration, rotation rate and magnetic field. The devices automatically calibrate themselves after each use.

At a minimum, 30 data sets for each flow scenario should be recovered. This will take a minimum of one full 8-hour work day for each flow scenario. Based on previous BDS site investigations, it is recommended that one day be allocated for testing the injection system and training the on-site staff for deployment, recovery and quality control during the field work. **Therefore, a minimum of 3 full workdays will be required at Bannwil to conduct the FITHydro BDS field work.**

Table 7: Overview of the BDS text file data format. Each of the 27 columns corresponds to a different variable saved during turbine passage at 100 Hz (magnetometer 20 Hz), units given in parentheses.

Col 1	**Col 2**	**Col 3**	**Col 4**	**Col 5**	**Col 6**	**Col 7**	**Col 8**	**Col 9**
Timestamp (ms)	Pressure left (hPa)	Left temp (°C)	Pressure center (hPa)	Center temp (°C)	Pressure right (hPa)	Right temp (°C)	Euler angle X (deg.)	Euler angle Y (deg.)
Col 10	**Col 11**	**Col 12**	**Col 13**	**Col 14**	**Col 15**	**Col 16**	**Col 17**	**Col 18**
Euler angle Z (deg.)	Quat. X (-)	Quat. Y (-)	Quat. Z (-)	Quat. W (-)	Magnet. X (µT)	Magnet. Y (µT)	Magnet. Z (µT)	Dynamic linear accel. X (m/s²)
Col 19	**Col 20**	**Col 21**	**Col 22**	**Col 23**	**Col 24**	**Col 25**	**Col 26**	**Col 27**
Dynamic linear accel. Y (m/s²)	Dynamic linear accel. Z (m/s²)	Rate gyro X (rad/s)	Rate gyro Y (rad/s)	Rate gyro Z (rad/s)	Calibration status magnet. (0-3)	Calibration status accel. (0-3)	Calibration status gyro. (0-3)	Sum calibration status (0-9)

Back to D2.2 Main index

Fish undergo extreme conditions:

- Pressure rate of change of 100m water column in less than 1 sec
- Blade strike > 10 g acceleration
- Flow velocities of 10-20 m/s near turbine blade

Barotrauma Detection System (BDS) are capable of recording these extreme conditions:

- Span: +/- 5 bar (~50m of water level)
- Recording rate: configurable 100Hz / 250Hz (4096/1024 samples/recorded value)
- Absolute orientation of sensors to compare position during passage
- Inertial measurement unit: 3D linear acceleration, 3D body rotation rate, 3D magnetic field
- Temperature compensation of each individual pressure sensor
- Only barotrauma sensors with triple modular redundance (3x identical, independent pressure sensors)
- First barotrauma sensor with auto-levelling to reference atmospheric pressure (100 kPa)
- First barotrauma sensor capable of directly measuring pressure gradients (shear) as well as pressure magnitudes
- Length/diameter: 14.5cm/4cm
- Housing materials: Polycarbonate (tube body) / Polyoxymethylene (end caps)
- Impact tested up to 3000 g

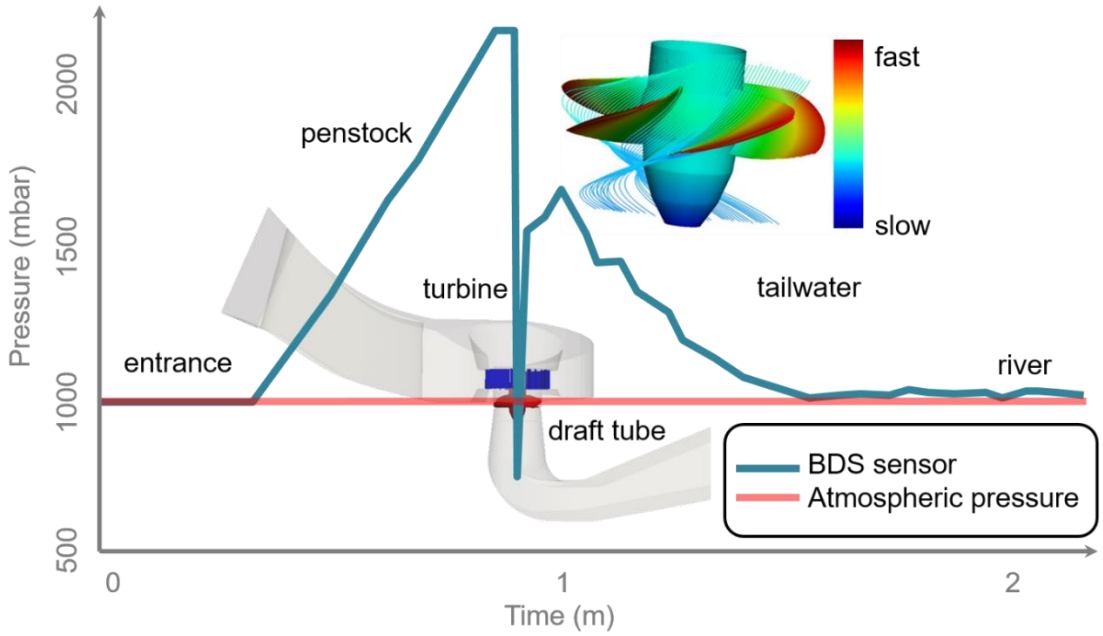


Figure 117: Barotrauma Detection System (BDS) and illustration of the multiple regions in which pressure changes occur that fish experience during turbine passage (vertical Kaplan).

3.3.2.2. Results

The results of the BDS are a statistical analysis of the time series data for each of the sensor modes (e.g. pressure, acceleration, etc.). The following parameters are calculated for each

individual measurement: min, max, mean, median, standard deviation, Q1, Q3 and the number of blade strikes. These statistical parameters are then aggregated according to the flow scenario (full or half-load) and injection location (low, mid, high) into ensembles representing the distributions of each parameters. In this way, each hydropower plant can be compared using a set of reproducible, statistically-derived parameters. For example, if the number of blade strikes differs between flow scenarios but only significantly between two different injection heights, it is possible to “drill down” into the data by comparing the ensemble statistics to gain insight into the physical environment during passage and suggest corrective measures such as installing fish avoidance targeted at a particular location.

3.3.2.3. Conclusions

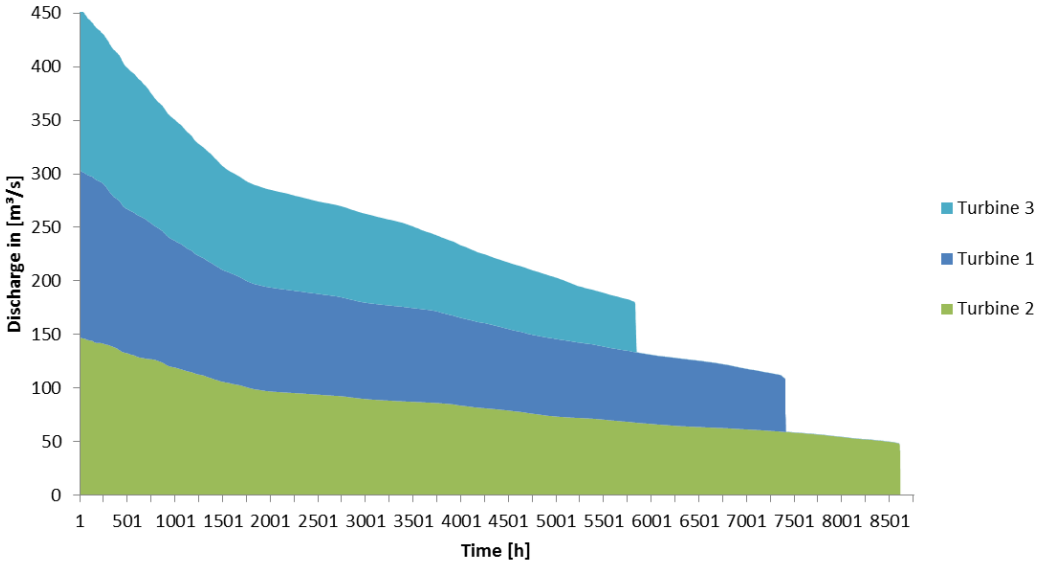
Upcoming

3.3.3. Turbine passage: BioPA modelling (VOITH, BKW)

To analyse the fish passage through a turbine, Voith Hydro set up a CFD model of the turbine passage at HPP Bannwil. Different operating conditions were simulated to evaluate the possibility of adapting the operation for a certain period. In a second step, the results will also be compared with BDS measurement results, see chapter 3.3.2. The results will be used for WP 3.3. Furthermore, all results from TUT and VOITH will be provided to TUM for fish turbine mortality assessment.

3.3.3.1. Data

With the help of the operating characteristics of the last 6 years, it was possible to determine in which operating points the turbines of Bannwil HPP were frequently operated and thus more relevant for the analyses of the impact on the fish population [12]. The operating data consists of 15-minute measured values of the flow, generator power and the corresponding opening angle of the wicket gate. Figure 118 shows the flow duration curve in 2017. Comparing between the years reveals that the machines alternate to have a similar number of operating hours in a multi-year perspective. In 2017, the turbine of unit 2 had the highest operating time with 8760h.



Back to D2.2 Main index

Figure 118: Annual discharge of Bannwil in 2017 according to the three machine units.

The power plant operation of the simultaneously operated turbines results in the annual load duration curve shown in Figure 119. It is visible that either all 3 turbines or 2 turbines are running simultaneously over the year. Each unit has about the same discharge, which is important to determine the tailwater level and estimate the fish passage of the entire system.

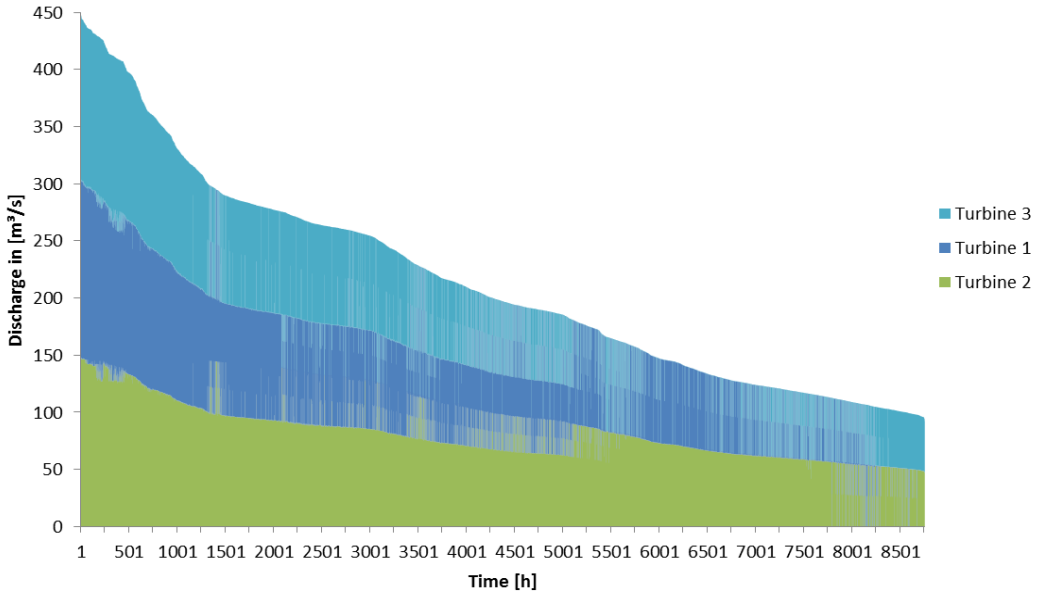


Figure 119: Annual Load Duration Curve (simultaneous).

The hill-chart of the turbines is shown in Figure 120, runner opening angle, wicket gate opening angle and efficiency are normalized to 100%.

Back to D2.2 Main index

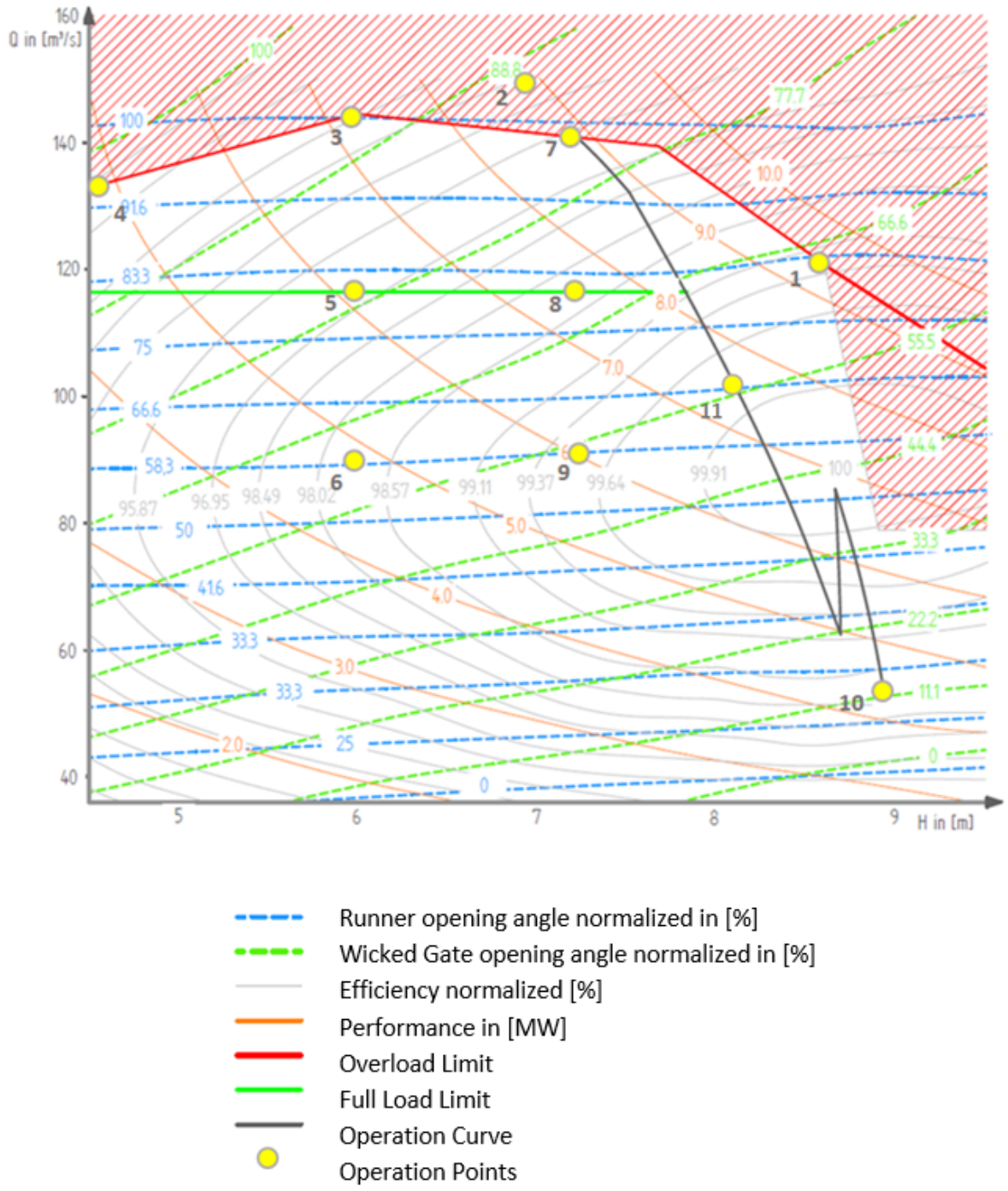


Figure 120: Normalized Hill Chart of Bannwil HPP.

The operation curve is shown in grey. The full load limit is marked in green, as well as the overload limit in red. The illustrated operating points t01 to t09 are the operating conditions for which a CFD simulation has been performed. An important operating point is t07, as it is directly on the line of application of the turbine and is often operated according to the evaluated operating data.

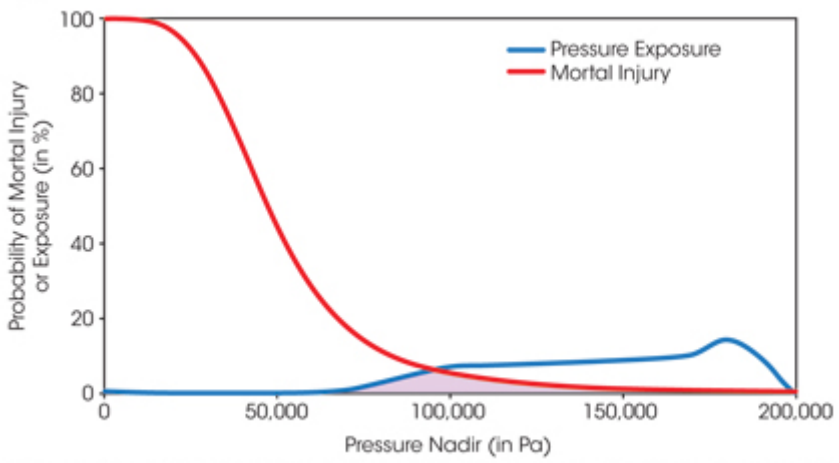
The investigated operating points are listed below:

Table 8: investigated operating points

Load case	Head [m]	Discharge [m³/s]	Wicket Gate Angle [%]	Runner Angle [%]
1	8.65	122	65	82
2	6.95	150	87	100
3	6	144	91	31
4	4	133	98	95
5	6	116.5	78	79
6	6	90	60	58
7	7.2	142	78	97
8	7.2	116.5	67	79
9	7.2	90	54	58
10	9.8	68	11	28
11	8.2	100	56	66

3.3.3.2. Methodology

To evaluate the influence of the turbine passage on the fish a biological performance assessment (BioPA) developed by Pacific Northwest National Laboratory (PNNL) is used. The analysis is based on a CFD simulation of the turbine assuming that a fish pathway follows a streamline through the turbine. The information of stressor exposure, including pressure, strike, shear and turbulence can be extracted from the streamlines and leads to an exposure probability based on the total amount of streamlines applied. To obtain a measure of injury risk, the estimated exposure to the stressors during turbine passage is related to the fish response to them. The so-called dose response value is multiplied with the exposure probability at that stress level, obtained from the exposure estimate. Integrating these risks overall values of the stressor variable yields to the BioPA score (Figure 121). The BioPA score is high when the risk of passage injury is low. Richmond et al. describe in detail how the baseline BioPA score for the existing turbine unit at Priest Rapids was calculated [9]. It is understood that the score does not, at this time, represent a passage-survival estimate. The score should only be used to estimate the relative risk of one design compared to another. A scenario (a specific design and operating point) receiving a higher score than another scenario can be considered to have a lower injury risk to passing fish. The absolute risk cannot be reliably quantified at the present time.



$$P_{Mortality} = \int (P_e \cdot P_m)\, dx$$

P_e=exposure probability of stressor

P_m=exposure mortality of fish

Figure 121: BioPA probability distribution and dose- response of pressure Nadir [1].

As the BioPA considers both fish response to a given stress level and exposure probability, the results provide additional insight into evaluating the size of the affected region within the turbine. For example, a geometry that produces a lower pressure within a small region of the water passage may have a negligible influence on the calculated risk of injuries through pressure. Developing an alternate turbine geometry that addresses the low-pressure region may result in higher component costs and lower turbine performance, without impacting the expected fish survival rate. The BioPA provides a systematic way to evaluate trade-offs associated with various hydraulic solutions.

3.3.3.2.1. Application on Test Case Bannwil

As a basis for the modelling of the HPP Bannwil, the 3D-CAD in Figure 122 was created based on the drawings of the power plant, which were kindly made available by BKW. Unfortunately, the geometry of the runner renewed in 1996 by Escher Wyss could not be made available in the original. For the studies, a runner geometry from Voith Hydro, which was designed for a similar operating range and an equivalent specific speed, was used. Significant for the later simulation are in particular the wicket gate section, the runner and the draft tube. The inlet area of the power plant was also modelled to investigate its effect on the fish passage.

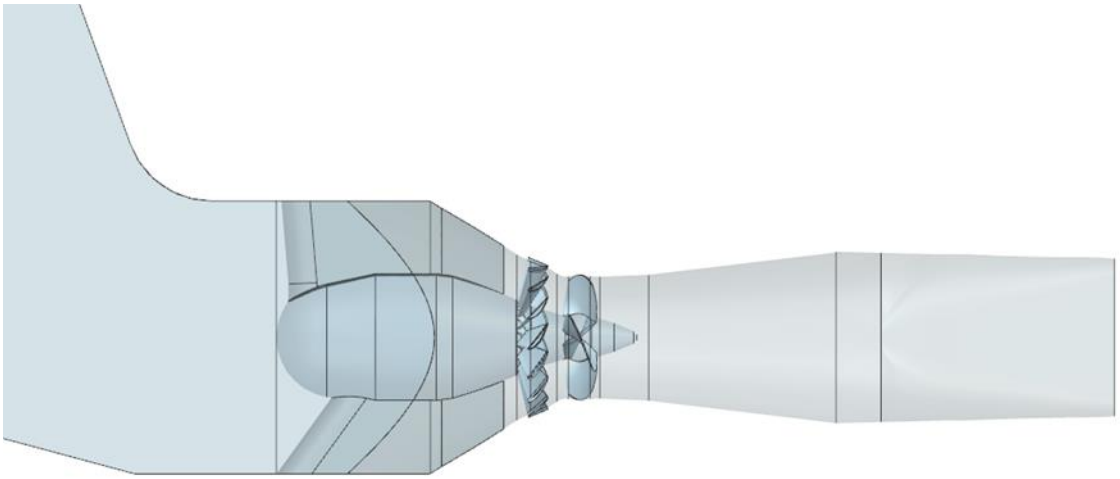


Figure 122: CAD Model of the Bulb Turbine in Bannwil.

The CFD calculations for this study are stationary and calculated with the k-ω SST turbulence model. The whole 360°-machine was modelled, and simulations were performed at prototype size. The inflow condition was set to be mass flow and flow direction. The pressure level at the outlet is set to a constant pressure. The mesh generation of wicket gate, runner and draft tube was done with a Voith in-house tool, the inlet region was meshed with ANSYS ICEM. The results of the CFD were then analysed by extracting the required stressor variables from the streamlines and further post-processed by using the available dose response data of salmon available in BioPA. For the analysis of the streamlines, an ANSYS CFX macro was created to simplify the process compared to the Tecplot post-processing routine used in BioPA. Comparisons of results showed no significant difference in the results [11]. In the following, the post-processing routine is described in more detail.

3.3.3.2.2. Creating the streamlines

Starting the evaluation process, the first step is to create streamlines within the flow field, which assumes that the fish floats through the turbine as a buoyant body. The number of streamlines can be determined variably by the user. However, the streamlines should be densly distributed to roughly correspond to the size of the fish to be examined. This covers all areas where the fish possibly could swim through. A sensitivity study showed that a streamline number of 5000 is sufficient for this case.

The streamlines are a standard post-processing object from CFX which describes the path that a particle with no mass takes through the fluid domain. „The path is calculated using a Runge-Kutta method of vector variable integration with variable time step control.” [10, Chap. 10.4]

BioPA uses the program Tecplot for this step. Again, streamlines are created throughout all domains. The variable of the turbulent kinetic energy is directly taken over from the CFD simulation results. The pressure and the shear strain rate are calculated within Tecplot. To achieve the same results as in BioPA, the formulas are identical. The key benefit of the new routine is that the variables can be automatically created internally in CFX regardless of turbine type and orientation.

To make the data of the streamlines usable for the program, each streamline is represented as a sequence of points with X, Y, Z.-coordinates. The extreme values of the variables presented below, as well as the velocities in each direction, are written in a large matrix and exported into a file. This contains all the basic information needed in the further process.

3.3.3.2.3. Pressure

As the pressure at the outlet of the turbine domain is set to 0 as a default for stationary CFD, the atmospheric pressure p_{atm} and the hydrostatic pressure p_{stat} must be included. The static pressure at each point of the turbine results from the density, the gravitational constant and the height difference of the respective point to the tailwater surface.

The following applies for the pressure:

$$P_{abs} = P_{CFD} + P_{atm} + P_{stat}$$

$$P_{stat} = \rho \cdot g \cdot (Z_{maxOutlet} - Z)$$

3.3.3.2.4. Turbulent Kinetic Energy

The turbulent kinetic energy is automatically part of the result file of Ansys CFX. The turbulent kinetic energy is defined from Ansys CFX. Ansys calculates the turbulent kinetic energy with the turbulent intensity I_{def} set to 5%. U_s, limits the speed to 0.01 m/s by the result of 0 for the turbulent kinetic energy, if there is an initial zero velocity . U_{IG} is the estimated velocity at the beginning. U_ω, is the product of the simulation average length scale and the rotation rate. “This term is designed to produce a suitable velocity scale for rotating domains.” [10, Chapter 3.2.10.1]

The turbulent kinetic energy yields [10]:

$$TKE = \frac{3}{2}\,(I_{def}\,\max(U_s|U_{IG}|U_w))^2$$

3.3.3.2.5. Shear Strain Rate

The shear strain rate is the change in deformation over time. With the strain rate tensor in each direction:

$$SSR = \sqrt{2 \cdot \left(\left(\frac{\partial U_x}{\partial_x}\right)^2 + \left(\frac{\partial U_y}{\partial_y}\right)^2 + \left(\frac{\partial U_z}{\partial_z}\right)^2\right) + \left(\frac{\partial U_x}{\partial_y} + \frac{\partial U_y}{\partial_{yx}}\right)^2 + \left(\frac{\partial U_x}{\partial_z} + \frac{\partial U_z}{\partial_x}\right)^2 + \left(\frac{\partial U_y}{\partial_z} + \frac{\partial U_z}{\partial_y}\right)^2}$$

3.3.3.2.6. Strike

To approximate the thickness of the blade leading edge a geometrical approach is chosen. It is defined by the diameter of the smallest possible circle within the leading edge at several cylindrically arranged cuts through the runner blade. In BioPA the cuts are made parrallel throughout the blade. The runner must then be placed in a defined position. The advantage of circular cuts is the independency of the coordinate system.

The created data files of the streamlines and blade thicknesses are now combined. The location of each streamline just above the leading edge of the blade is determined and the velocity information is extracted there. The points can be seen in Figure 123. The colouring describes the speed. In this case approximately from 5 m/s (blue) up to 25 m/s (red). The velocity increases with radius, i.e. with distance from the turbine axis.

The blade thickness is based on the radial streamline position at the blade leading edge and calculated by interpolation.

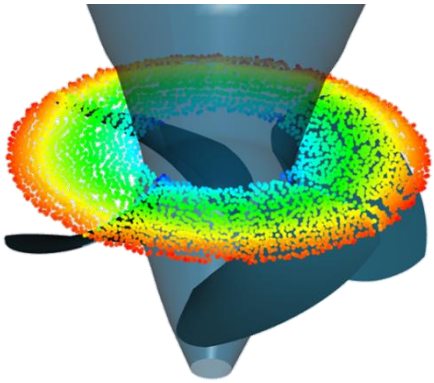


Figure 123: Intensity Distribution.

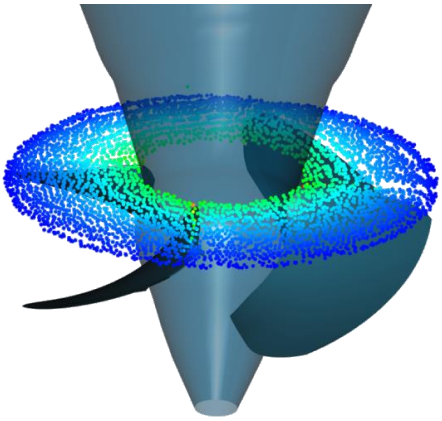


Figure 124: Strike Probability Distribution.

The probability of hitting the blade is calculated. The basis for this is the strike equation below, which is extended by a term which also includes the blade thickness. With the sum of the ratios of fish length *l*, speed *V* and the entrance edge thickness T_b, in relation to the velocity in axial direction, the number of revolutions *n* and the number of blades *N*, the probability of an impact is:

$$P_{Strike} = n \cdot \frac{N}{60} \cdot \left(\frac{l}{V} + \frac{T_b}{V_{axial}}\right)$$

The probability of strike is shown in Figure 124. It ranges from about 2% (blue) at the shroud to 15% (green) at the hub.

The ratio of leading edge thickness to the fish length and the impact velocity of the fish on the blade are important parameters for the strike evaluation. The difference of the tangential speed of the fish and the peripheral velocity of the blade gives the intensity of the impact. The velocity of the rotating blade in (tangential direction) at each diameter is calculated using:

$$v_{tangBlade} = 2 \cdot \pi \cdot r_x \cdot \frac{n}{360}$$

The tangential velocity of the flow is the scalar product of the unit vector in tangential blade direction and the flow velocity in the XY plane.

$$v_{Intensity} = abs(v_{tangBlade} - v_{tangFlow})$$

To calculate the survival probability of the strike itself, additionally to the blade thickness and the intensity, the biological data is needed. The biological data gives the mortality rate of the fish as a function of the ratio of fish length to blade thickness, which becomes valid at the critical speed shown in Figure 125.

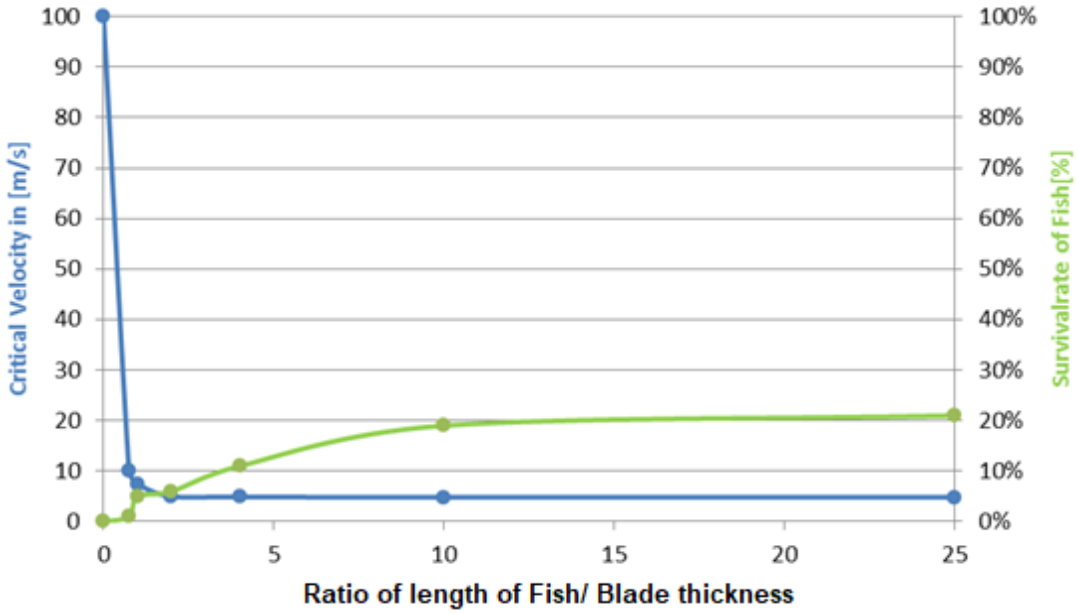


Figure 125: Blade Strike Survival Curve for salmon [5].

The blade thicknesses and the calculated intensity, as well as the ratio of fish length to blade thickness, are used to derive the survival rate.

The following cases are distinguished:

1. If the speed at the blade (intensity of impact) is below the associated critical speed v_{crit}, the fish will survive:

$$P_{Survival} = 1 \quad \text{for} \quad v_{Intensity} \leq v_{crit}$$

2. If the speed on the blade (intensity of the impact) is above the associated critical speed v_{crit}, the survival rate is calculated with:

$$P_{Survival} = 1 + m_r * \left(v_{Intensity} - v_{crit}\right) \quad \text{for} \quad v_{Intensity} \geq v_{crit}$$

The combination of the fish strike probability, P_{strike} and the fish survival probability, $P_{survival}$ after the strike, results in the overall strike mortality probability, $P_{StrikeMortality}$. The calculated survival probability $P_{Survival}$ thus reduces the mortality rate.

$$P_{StrikeMortality} = P_{Strike} \cdot (1 - P_{Survival})$$

3.3.3.3. Results

In the following results of the analysis of the Bannwil Test Case are presented first. They will be further refined in the upcoming months. More detailed information on the work can be found in [11]. All presented results are based on the dose-response data for salmon, which is available from literature. All stressors are rated equally for now. The influence of entering location, fish size, acclimation depth and the impact of different operating points are investigated

Back to D2.2 Main index

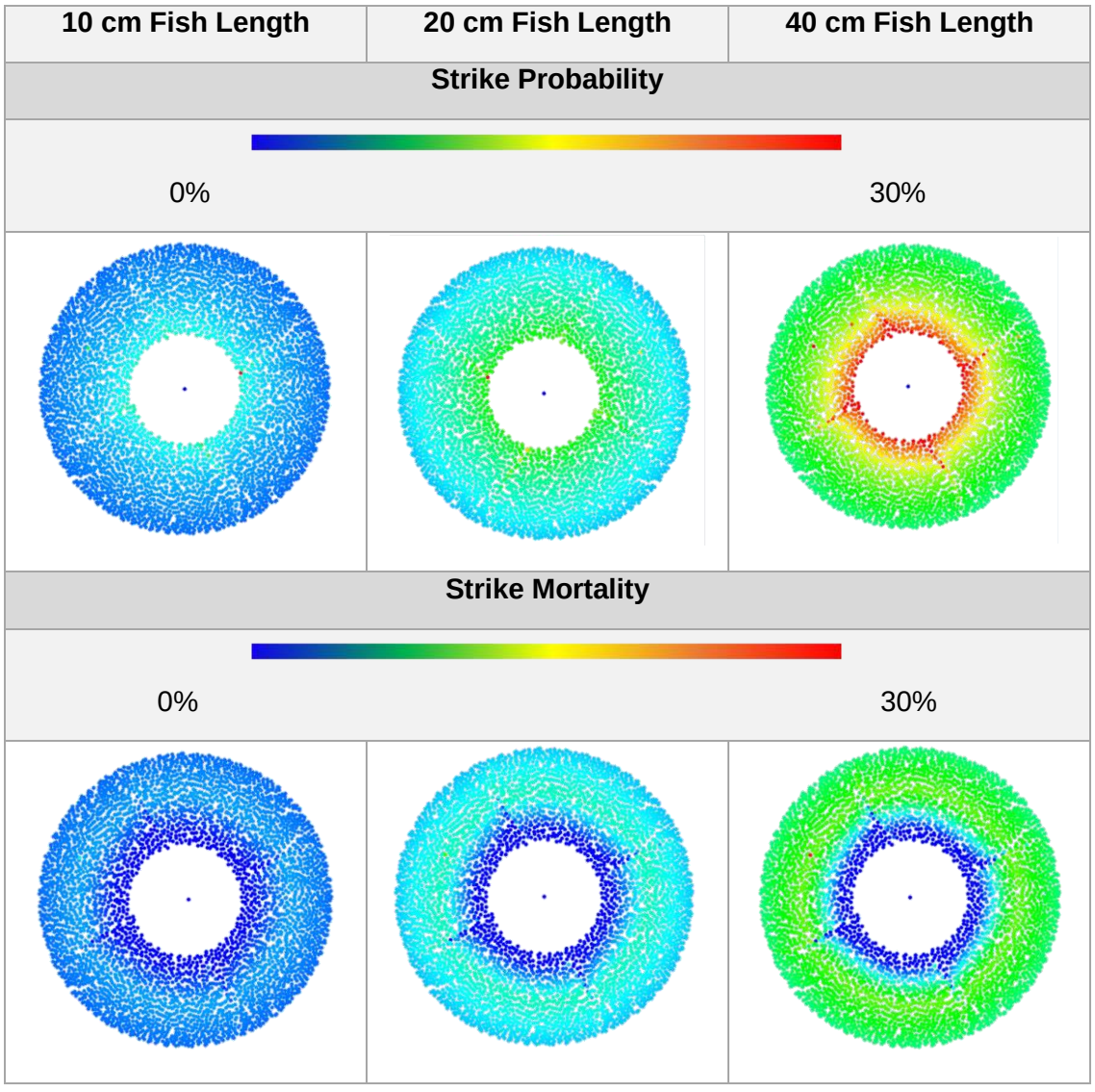
3.3.3.3.1. Influence of entering location

Some preliminary investigations were performed, which showed an influence on the survival probability of the fish based on the entering location to the turbine. Before presenting the outcome of these investigations further studies are required to confirm the first results.

3.3.3.3.2. Fish length

For the evaluation of the strike, the fish length is set to a standard value of 10 cm. This corresponds to a young migrating salmon. The consideration of the survival probability for larger fish at the example of load case 7 is shown here.

The formula for calculating the probability of a fish hitting the runner depends on the length of the fish and on the relation of fish size to the blade thickness. An increase in mortality rate is expected with increasing fish length. Figure 126 shows the strike probability and the strike mortality increasing with the size of the fish. In a second step it would be useful to have biological data available for the species of interest at Bannwil HPP.



Back to D2.2 Main index

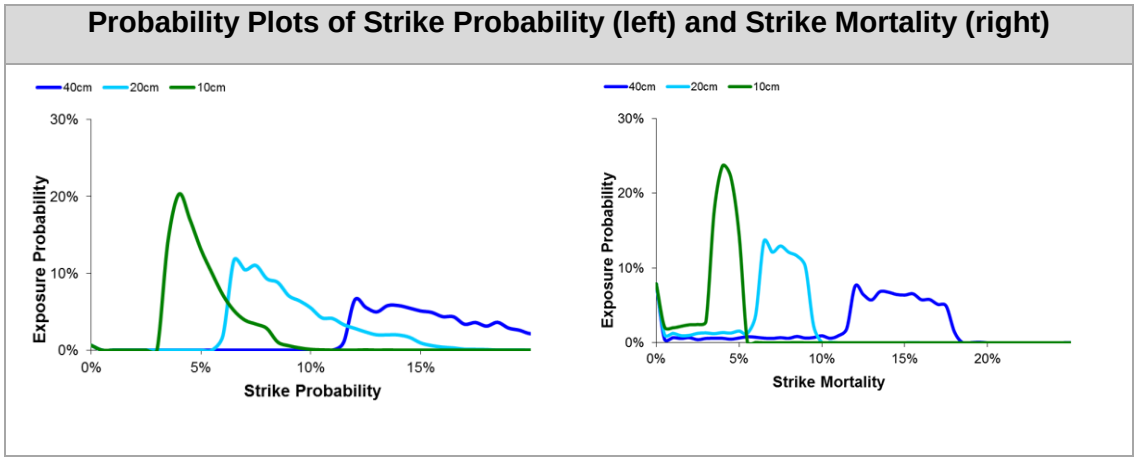


Figure 126: Comparing different Fish Length's.

The performance scores are listed in Table 9: Fish Length ScoresTable 9:

Table 9: Fish Length Scores.

	Strike
10cm	96.45
20cm	93.55
40cm	87.77

3.3.3.3.3. Influence of Operating Points

The evaluation of individual load cases regarding advanced fish passage helps to identify individual damage mechanisms and to evaluate them. To rate a whole power plant, however, this consideration is not sufficient. It requires the evaluation of a complete set of operating points to create a better understanding of which parameters affect the fish passage through the turbine of an entire power plant. Therefore, 11 operating points were selected and each simulated with a 360°-CFD model. All evaluations are made using the CFX post-processing tool. The final fish mortality performance score is calculated using the BioPA Excel Sheet. The performance score is then converted into a "traffic light" scoring system from 1 to 10. Where 10 is the best score and corresponds to the BioPA score of 100. The scoring of 1 corresponds to 70 in BioPA (Table 5).

Table 10: Performance Score of Load cases at Acclimation Depth of 5 m.

Loadcase	Head [m]	Discharge [m³/s]	Pressure Score	TKE Score	Strain Score	Strike Score	Average Score
1	8.65	122	7.98	8.57	9.99	8.26	8.70
2	6.95	150	6.08	8.61	9.99	8.11	8.20
3	6	144	5.95	8.61	9.99	8.11	8.16
4	4	133	6.75	8.43	9.98	7.97	8.28

5	6	116.5	8.63	8.81	10.00	8.02	8.86
6	6	90	9.28	8.87	10.00	7.91	9.02
7	7.2	142	6.27	8.70	9.99	8.22	8.30
8	7.2	116.5	8.57	8.84	9.98	8.12	8.88
9	7.2	90	9.18	8.87	10.00	7.99	9.01
10	9.8	68	5.57	6.53	9.90	8.32	7.58
11	8.2	100	8.93	8.87	10.00	8.00	8.95

This standardization is intended to prevent the performance scores from being confused with absolute survival rates and to give a better overview.

The results are interpolated 3-dimensionally over the head and the discharge flow to get iso-curves for a characteristic evaluation diagram. The hill chart shows isolines indicating the fish passage score. Below results for the stressors pressure, turbulent kinetic energy, strain and strike are presented. The characteristic diagram reads like a typical hill-chart. The load case 10 is disregarded since this is very unlikely to occur during turbine operation.

3.3.3.3.4. Pressure

In Figure 127 the fish passage environment for the different acclimation depths are plotted. It turns out that the probability of survival decreases in all cases towards higher discharges. For the head, an optimum head of 6.4m can be identified. It is clear that flow conditions around the runner have a major impact on the pressure rating. Also, the acclimation depth of the fish has a significant influence. One can argue if the applicable head has a direct influence on the acclimation head, but it seems only reasonable if the river has a larger depth for a significant amount of time. For the tail water level assumptions have been made, which need to be compared to the plant data.

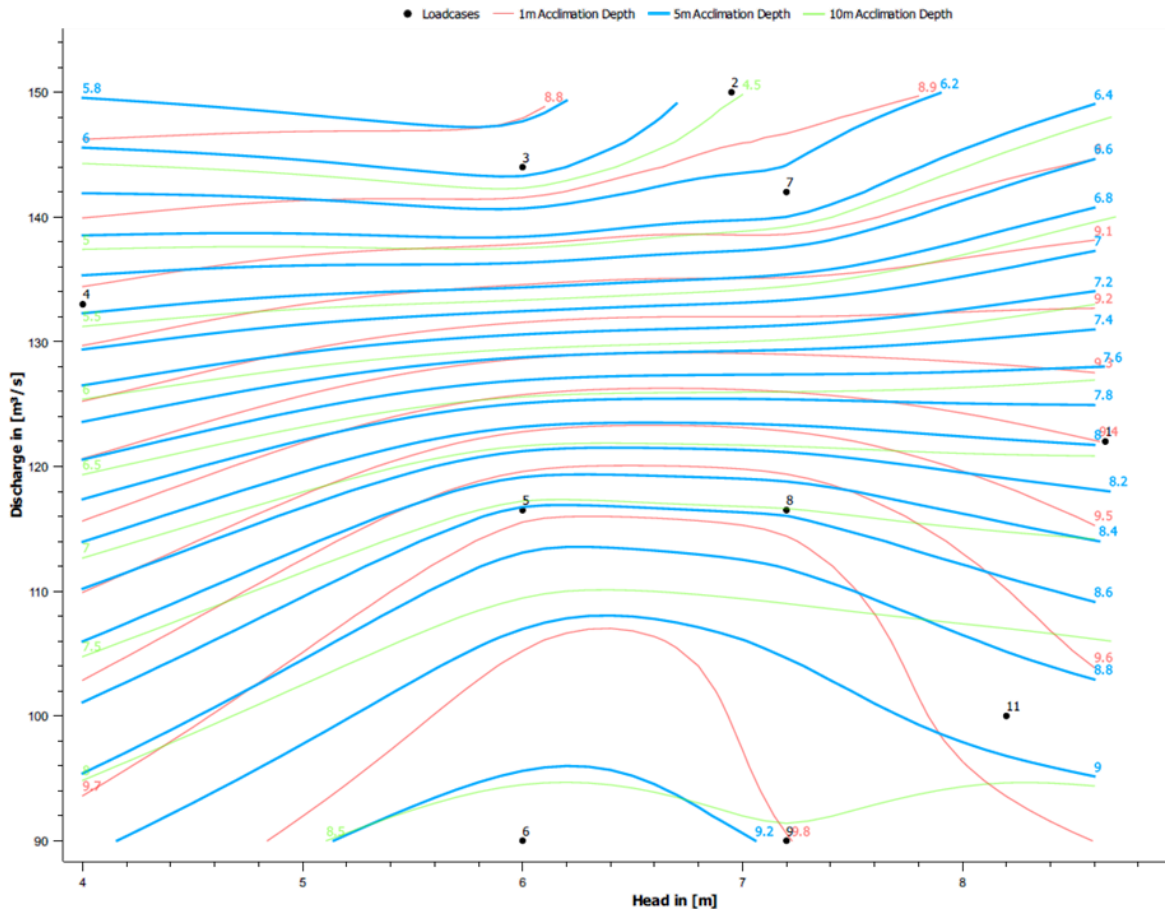


Figure 127: Fish Passage Hill Chart of Pressure.

3.3.3.3.5. Turbulent Kinetic Energy

In Figure 128 the fish passage score of the stressor turbulent kinetic energy is presented. In addition to the scores on the isolines, they are coloured by the score value. One can clearly see that the best score is in the optimum range of the turbine. The smaller the turbulence, the lower the absolute losses and the better the efficiency of the turbine. Both for fish and for the turbine, a flow without vortex and flow separation is most favourable.

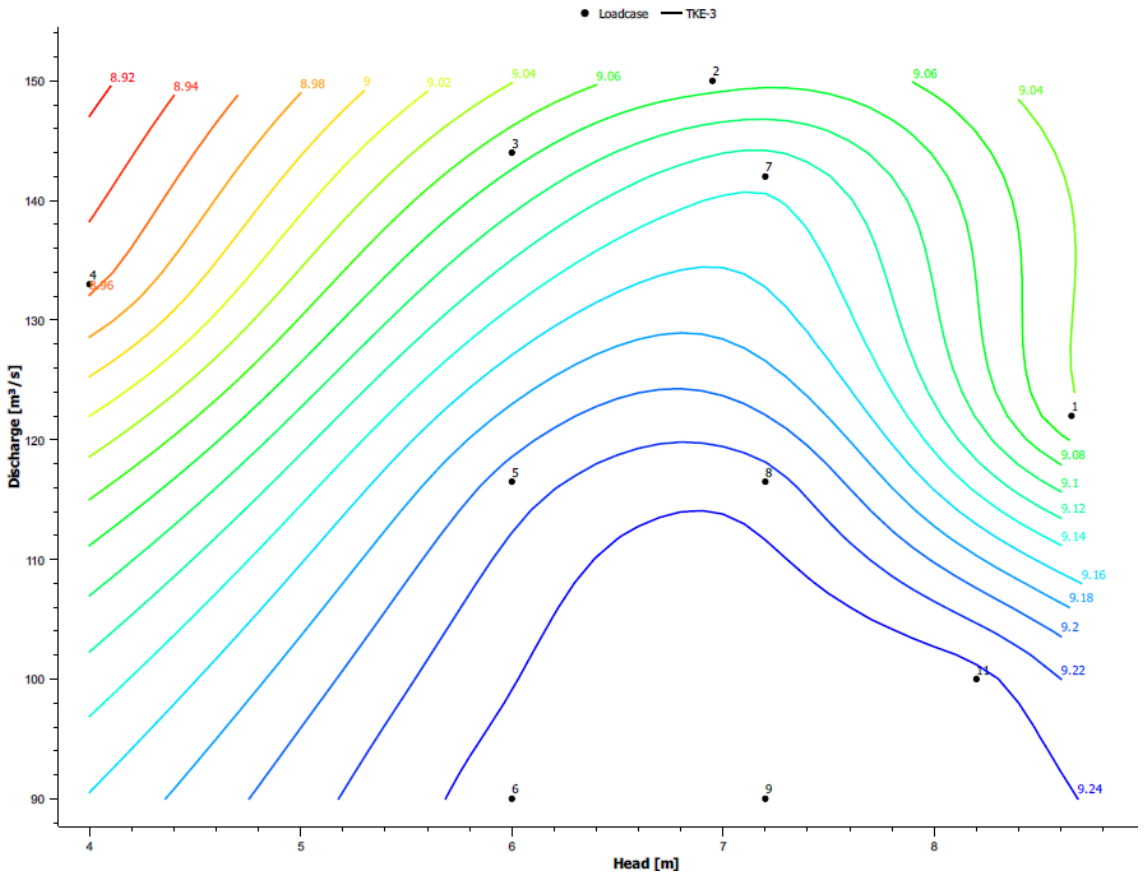


Figure 128: Fish Passage Hill Chart of TKE.

3.3.3.3.6. Shear Stress

The shear stress score is shown in Figure 129. Overall, the score is very high and the impact on fish therefore low. The critical points for shear are at the leading edges of the blades. The differences appear for example because of different blade openings. Anyhow, almost all maximum values of the shear strain are below the harmful limit of 400 1/s².

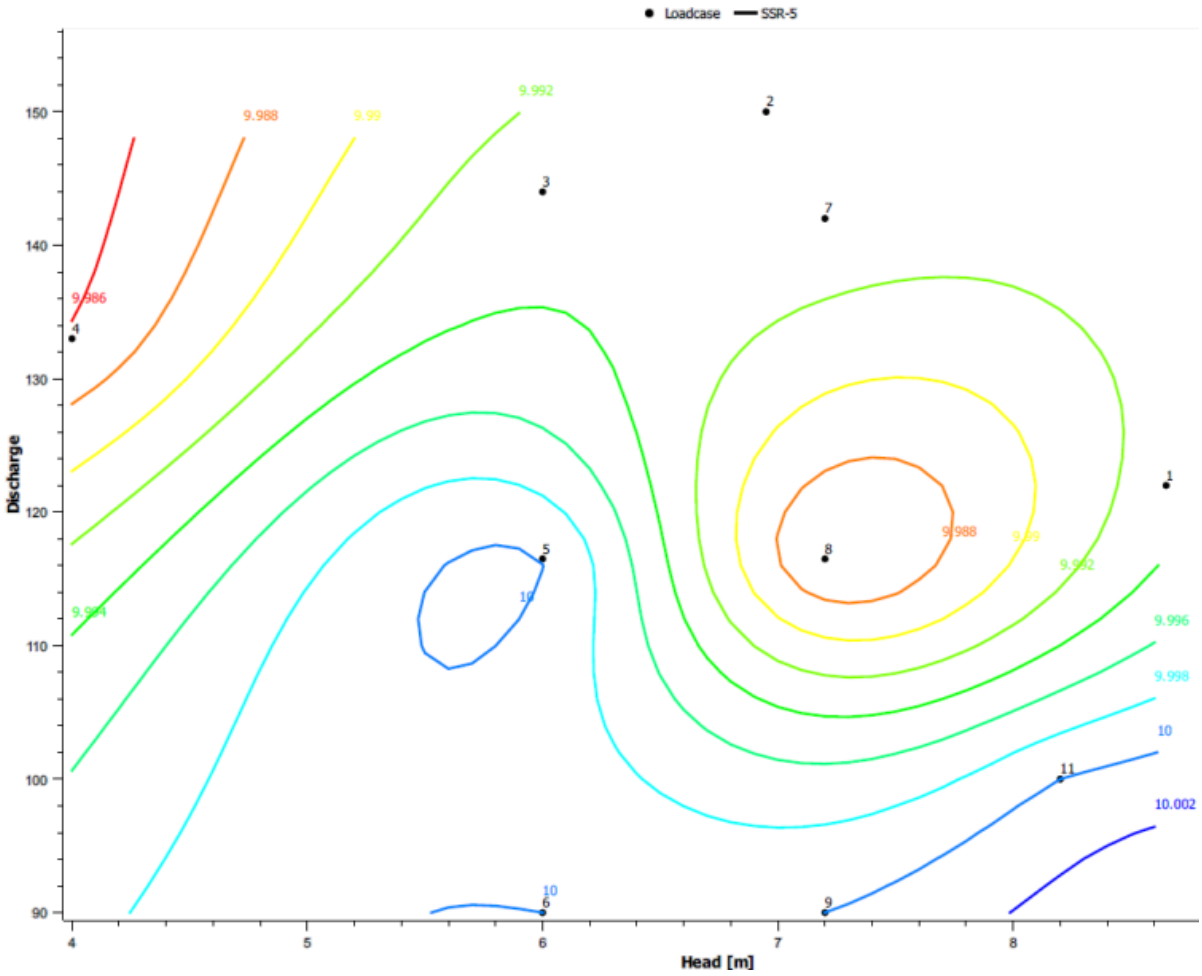


Figure 129: Fish Passage Hill Chart of Shear Stress.

3.3.3.3.7. Strike

The strike score is peaking at high heads and large volume flows. However, the fish passage score has a rather small range of variation. For smaller heads, the lower flow velocity leads to a higher risk of a hit. Anyhow the intensity of the hit is slightly smaller. For smaller blade openings the same effect is valid. Hits with the blade leading edge are recognized in this model but no secondary hits on the blade.

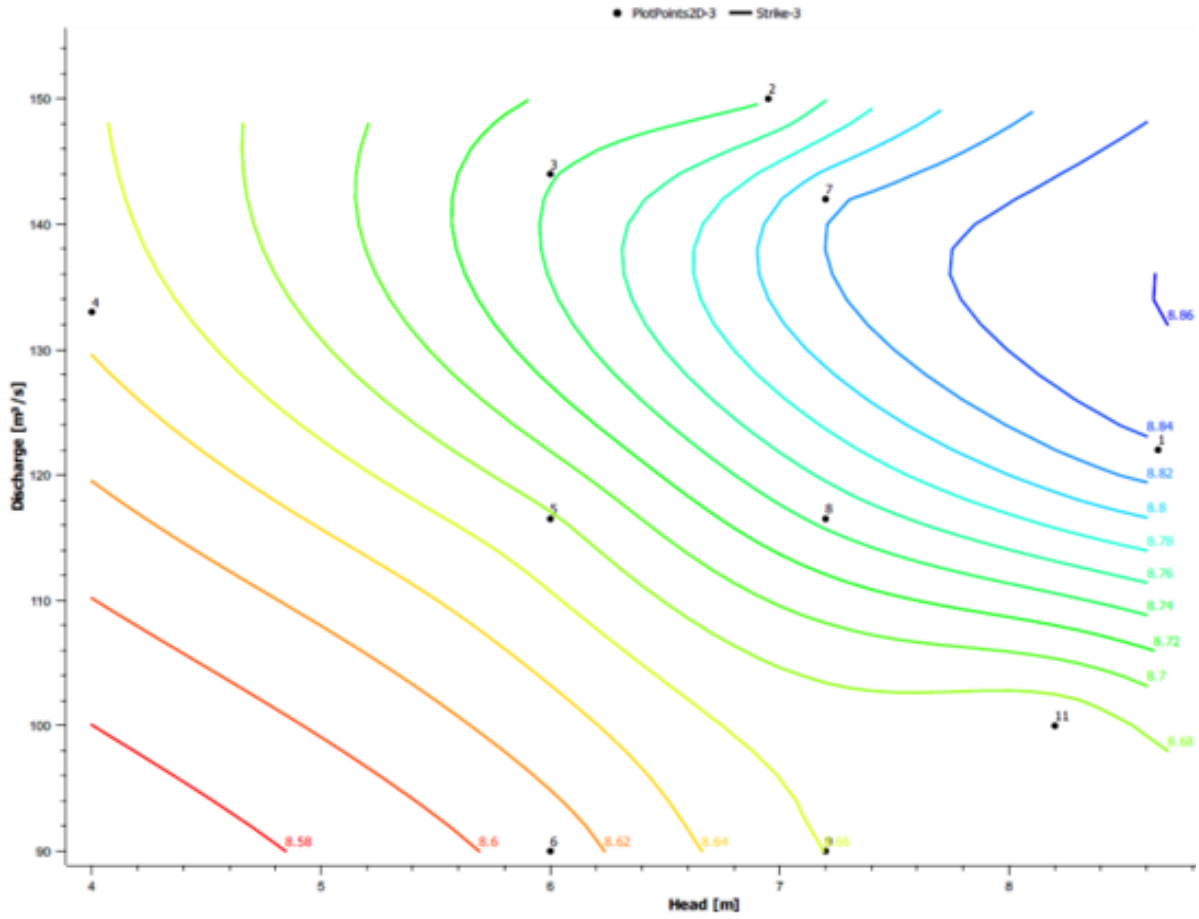


Figure 130:Fish Passage Hill Chart of Strike.

3.3.3.3.8. Combined Results

The Hill charts show that individual stressors behave differently. It can also be stated that in some cases additional operating points are required to obtain a more complete picture. In a first analysis, the results are averaged equally and therefore the stressor with the highest impact dominates. Depending on turbine size, revolutions of the runner and above all on the type of fish, a different weighting of the stressors seems to be necessary. For example, if pressure sensitivity plays only a minor role for a fish species, the stressor should get a smaller weighting factor.

With the operating data of the power plant and the representative operating points an “average fish passage friendliness" can be estimated. In this case, all stressors are weighted equally.

For this consideration, the operating data of the power plant of the year 2017 are linked with the average fish passage score. In addition, the fish passage rating was calculated for 2 running machines. If one looks at the annual flow duration curve (Figure 118) it is visible that below a flow rate of approx. 150 m³/s only 2 machines run at the same time. The average fish friendliness score for the power plant Bannwil is about 9.1 considering an acclimation depth of 5 m, while for 10 m the scoring is around 8.5. The combined hill-chart for the fish passage score can be seen for the 10 m acclimation depth in Figure 131. Regarding the depth of the

river, an acclimation depth of 5 m seems more realistic for HPP Banwill. For an absolute rating of fish survival, this factor apparently plays an important role.

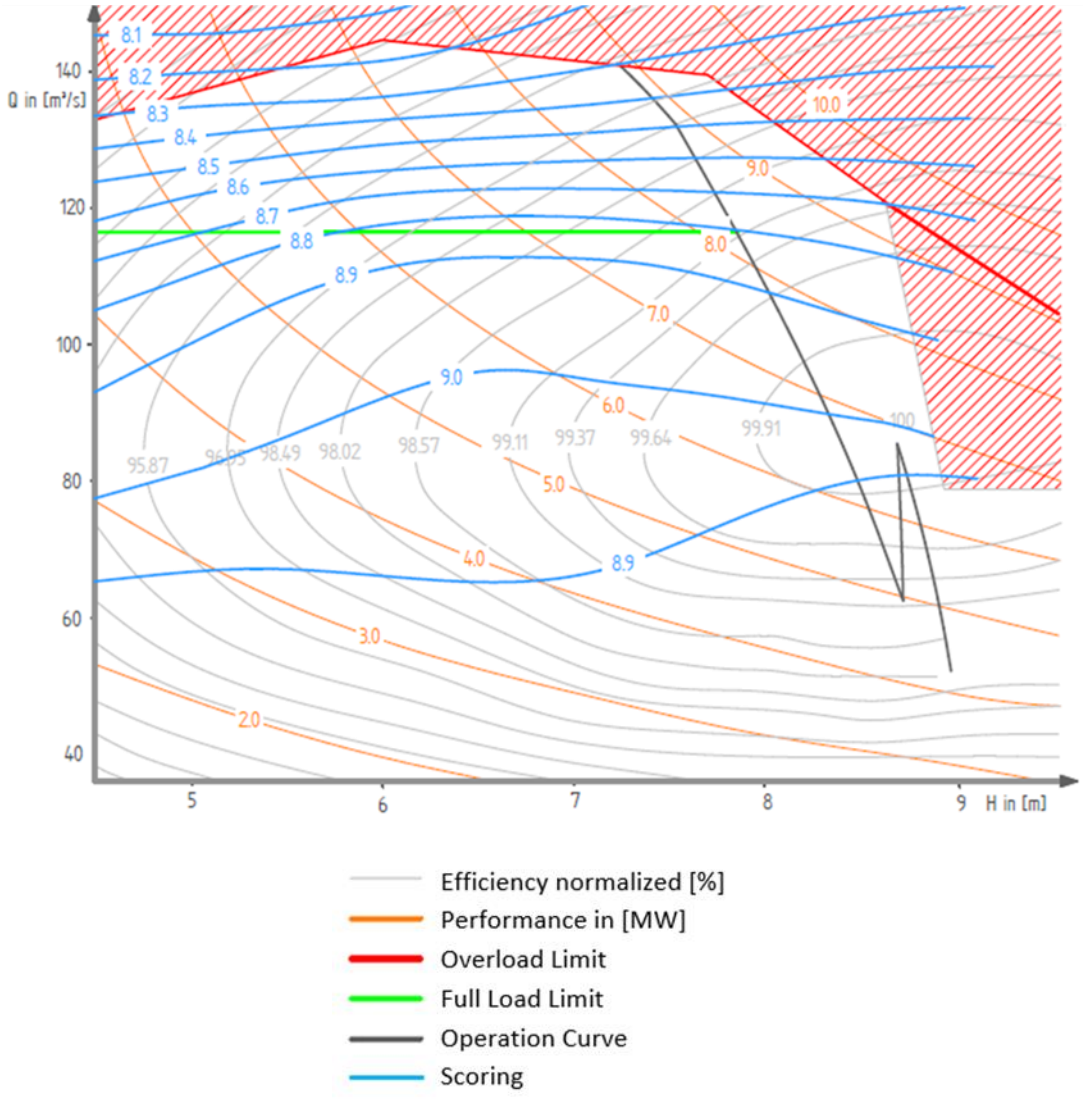


Figure 131: Combined Fish Passage Hill Chart for 10 m Acclimation Depth.

3.3.3.4. Conclusions

These first results indicate the potential of the CFD based turbine passage assessment It is possible to include the turbine operation in the assessment and to generate improved operating schemes. The fish passage hill charts show how the operating condition (head and discharge) have different effects for the relevant stressors. Also, the influence of fish size and entering location can be detected. For the pressure stressor, the acclimation depth of the fish is an important variable. The investigations are on-going and will be further refined in the next months.

The CFD results are reliable for main operating conditions, while for extreme operating conditions transient calculations might become necessary. The evaluation of the results so far assumes that the fish follows a streamline. Additionally, the evaluation is still restricted to the biological response data available in literature. To rate all species relevant in the Aare river, the dose response data needs to be generated with laboratory tests or adapted by expert assessment. The post-processing on streamlines is a statistical approach, which seems most promising to obtain a representative result. Potential movement of fish during turbine passage is still an open topic and difficult to assess. The BioPA assessment is a relative approach and does not deliver absolute survival rates for now. Further investigations will focus on the weighting of the different stressors based on the one hand on machine boundaries and on the other hand on biological data depending on the fish species.

3.3.4. References

[1] Flow Science, Inc., 2016, FLOW-3D User Manual, Release 11.2.3, USA 2016.

[2] WinRiver II, Software User's Guide. Teledyne RD Instruments 2018.

[3] U.S. Geological Survey, Streamgaging, Fact Sheet 2005-3131 (2007) available from: https://hydroacoustics.usgs.gov/

[4] Feigenwinter, L.; Vetsch, D.F.; Kammerer, S.; Kriewitz, C.R.; Boes, R.M. (2019). Conceptual approach for positioning of fish guidance structures using CFD and expert knowledge. Sustainability, 11(6), 1646; https://doi.org/10.3390/su11061646

[5] Crew, A.V,. Keatley, B.E., and Phelps A.M. 2017. Literature review: Fish mortality risks and international regulations associated with downstream passage through hydroelectric facilities. Can. Tech. Rep. Fish. Aquat. Sci. 3207: iv + 47 p

[6] Fidler, L.E. (1988) Gas Bubble Trauma in Fish. University of British Columbia. doi: 10.14288/1.0097966

[7] Ruggles C.P. (1980). A review of the downstream migration of Atlantic salmon. Canadian technical report of fisheries and aquatic sciences No. 952.

[8] Ruggles, C.P., Murray, D.G. (1983). A review of fish response to spillways. Canadian technical report of fisheries and aquatic sciences No. 1172.

[9] Richmond, C. (2014). Computational Tools to Assess Turbine Biological Performance, Hydro Review Volume 6

[10] ANSYS CFX Help, CFX-Solver Theory Guide, 2009

[11] Jäger, S. (2018): Investigation of the fish passage through Bulb Turbines by means of flow simulation.

[12] BKW Energie AG: Power plant drawings and operational data

3.4 Bragado

3.4.1 Fish community of the Tâmega River basin

3.4.1.1 Introduction

The Iberian fish fauna has a high level of endemism, occupying a unique position in the European ichthyofauna (Doadrio 2001; Reyjol *et al.* 2007). The specificity of the Iberian ichthyofauna is highlighted in a number of studies, namely in the typologies developed within the European FAME project (FAME Project - Development, Evaluation and Implementation of a Standardized Fish-based Assessment Method for the Ecological Status of European Rivers: http://fame.boku.ac.at), where the river basins of the Iberian Peninsula clearly stood out from the other European river basins.

To frame the research conducted in the Bragado HPP, a short review of the available information on the fish assemblages of the Tâmega River basin was conducted. The review aims to establish the fish fauna of the river basin and the major factors likely responsible for shaping the composition of fish assemblages in this Douro River sub-basin (Table 11).

Table 11 - Basin area for the Tâmega and Avelames River basins. Including the Spanish part of the basin.

River basin	Area (km^2)
Douro/Duero	98370
Tâmega	3231
Avelames	93

3.4.1.2 Methodology

The fish assemblages of the Tâmega River basin were studied during the last 20 years (including research studies, environmental impact assessments and monitoring studies) (e.g. Cortes *et al.* 1990; Rodriguez-Ruiz & Granado-Lorencio 1992; Ferreira *et al.* 2000; INAG 2001; Madeira 2002; Filipe 2004; Oliveira *et al.* 2007; Godinho unpublished results). From those studies, data on fish species presence-absence in electrofishing surveys were gathered for 55 fluvial reaches (Figure 132) and used to prepare a matrix (sampling reaches x species occurrence). The fish occurrence data were examined to assess global taxa distribution throughout the basin and were subjected to Principal Component Analysis (PCA) to highlight major assemblage patterns. Species occurring in less than 10% of the fish surveys were not considered to prevent analysis distortion (Godinho *et al.* 2014). PCA was run using STATISTICA (StatSoft 2000).

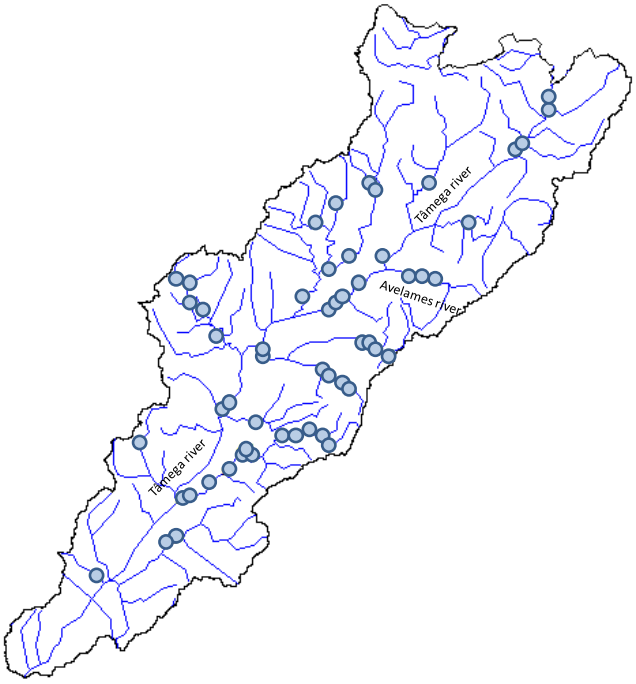


Figure 132 - Places with fish assemblage data in the Tâmega River basin (presence-absence, depicted by a blue circle).

3.4.1.3 Results

In the Tâmega River basin, 18 fish species have been collected in electrofishing surveys, including 55.6% introduced taxa and six Iberian endemism (Table 12). Nevertheless, most introduced species are still restricted to the Tâmega River itself or to the terminal part of some tributaries. The number of species varied from 1 to a maximum of 9 per sampling reach (average richness ± SD = 3.24 ± 2.00). Species richness was higher in the Tâmega River (5.73 ± 1.95) than in its tributaries (2.61 ± 1.47).

The Tâmega River basin includes some of the endangered biological units in Europe, presenting three species listed in Annex II of the Community Directive 97/62/EC (animal and plant species of Community interest whose conservation is designated as special areas of conservation). According to the Portuguese Red Book (Cabral *et al.* 2005), two of the species present in the basin have a threat status.

Most common species in the basin (occurring at least in 20% of the sampling reaches) included the following: Iberian barbel (*Luciobarbus bocagei*), Iberian nase (*Pseudochondrostoma duriense*), Iberian chub (*Squalius carolitertii*), brown trout (*Salmo trutta fario*) and pumpkinseed sunfish (*Lepomis gibbosus*) (Figure 133, Figure 134, Figure 135,Figure 136, andFigure 137).

Table 12 - Fish taxa occurring in the Tâmega River basin.

Taxa	**Common name**	**Conservation status**		
		Portuguese Red List of threatened species	Directive 97/62/CE	IUCN Red List of threatened species
Anguillidae				
Anguilla anguilla	European eel	Endangered	Not evaluated	Critically endangered
Cyprinidae				

Back to D2.2 Main index

Achondrostoma oligolepis	Iberian curved mouth nase	Least concern	Anexo II	Not evaluated
Alburnus alburnus	ablete	introduced		
Carassius auratus	crucian carp			
Cyprinus carpio	common carp			
Gobio lozanoi	Iberian gudgeon			
Luciobarbus bocagei	Iberian barbel	Least concern	Anexo V	Least concern
Pseudochondrostoma duriense	Duero nase	Least concern	Anexo II	Vulnerable
Squalius alburnoides	Calandino	Vulnerable	Anexo II	Vulnerable
Squalius carolitertii	Iberian chub	Least concern	Not evaluated	Least concern
Cobitidae				
Cobitis paludica	Iberian loach	translocated		
Salmonidae				
Oncorhynchus mykiss	rainbow trout	introduced		
Salmo trutta	brown trout	Least concern	Not evaluated	Least concern
Atherinidae				
Atherina boyeri	sand smelt	Data deficient	Not evaluated	Least concern
Poeciliidae				
Gambusia holbrooki	mosquitofish	introduced		
Centrarchidae				
Lepomis gibbosus	pumpkinseed sunfish	introduced		
Micropterus salmoides	largemouth bass			
Percidae				
Sander lucioperca	pikeperch	introduced		

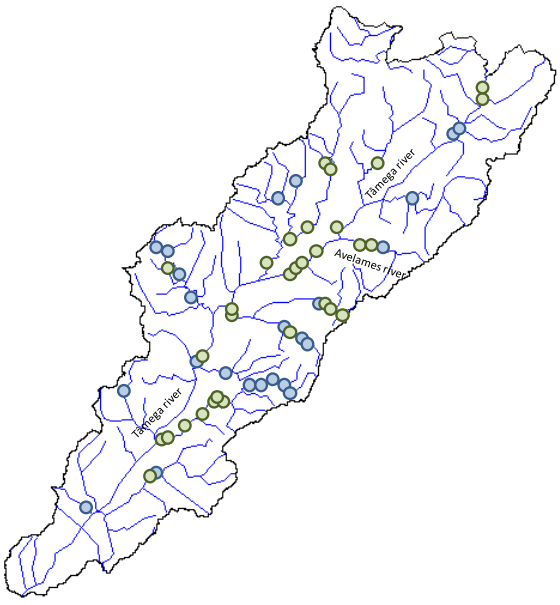


Figure 133 - Distribution of Pseudochondrostoma duriense in the Tâmega River basin. Sampling site with species presence is denoted by a green circle, whereas sampling sites with absence are denoted by a blue circle. The species occur in the Avelames River.

Back to D2.2 Main index

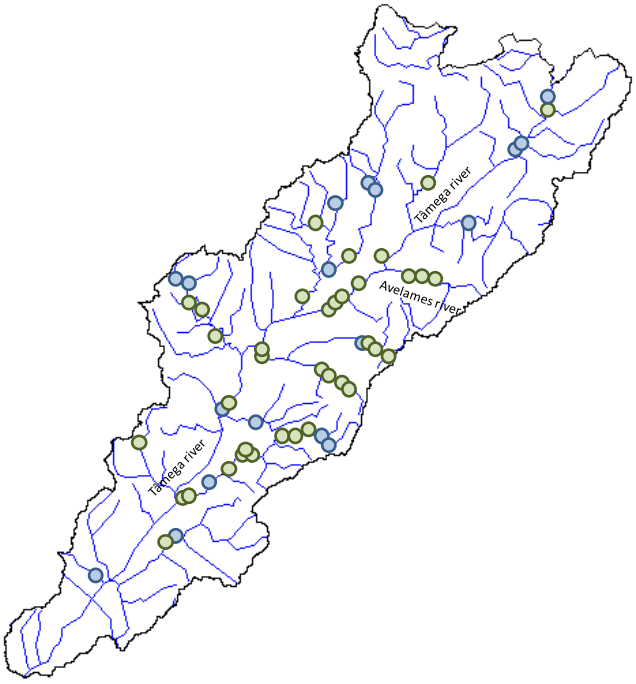


Figure 134 - Distribution of Squalius carolitertii in the Tâmega River basin. Sampling site with species presence is denoted by a green circle, whereas sampling sites with absence are denoted by a blue circle. The species occur in the Avelames River.

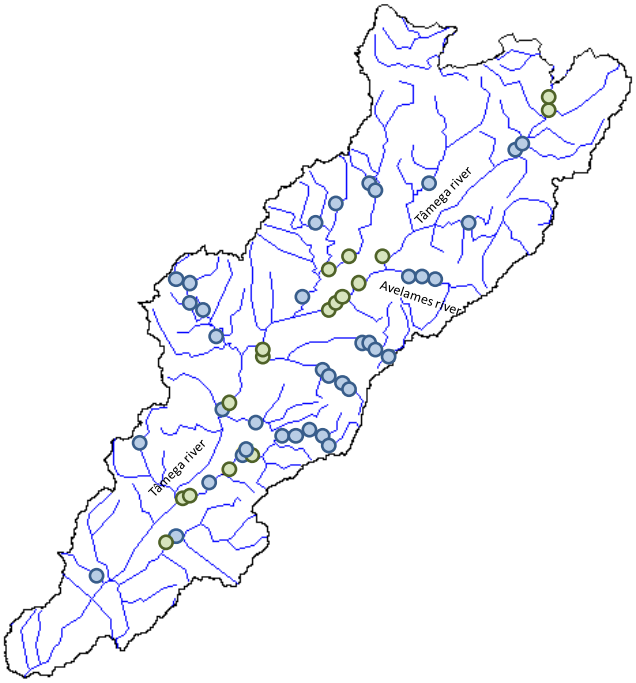


Figure 135 - Distribution of Luciobarbus bocagei in the Tâmega River basin. Sampling site with species presence is denoted by a green circle, whereas sampling sites with absence are denoted by a blue circle.

Back to D2.2 Main index

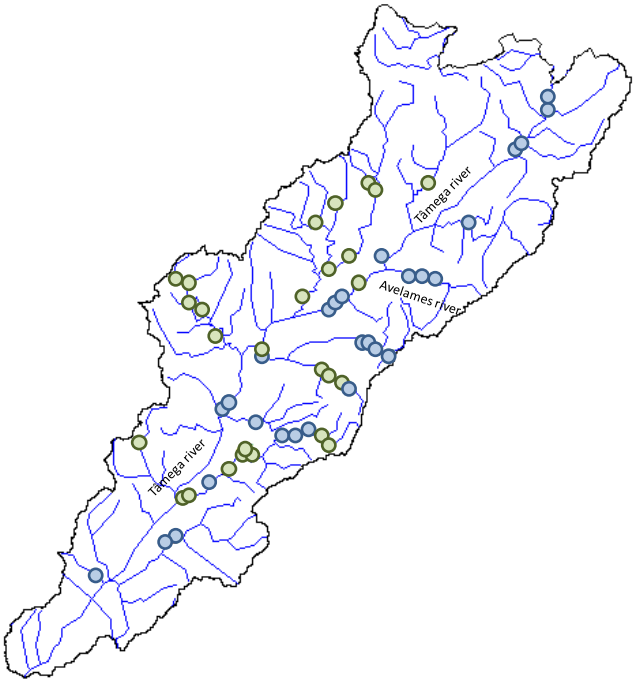


Figure 136 - Distribution of Salmo trutta fario in the Tâmega River basin. Sampling site with species presence is denoted by a green circle, whereas sampling sites with absence are denoted by a blue circle.

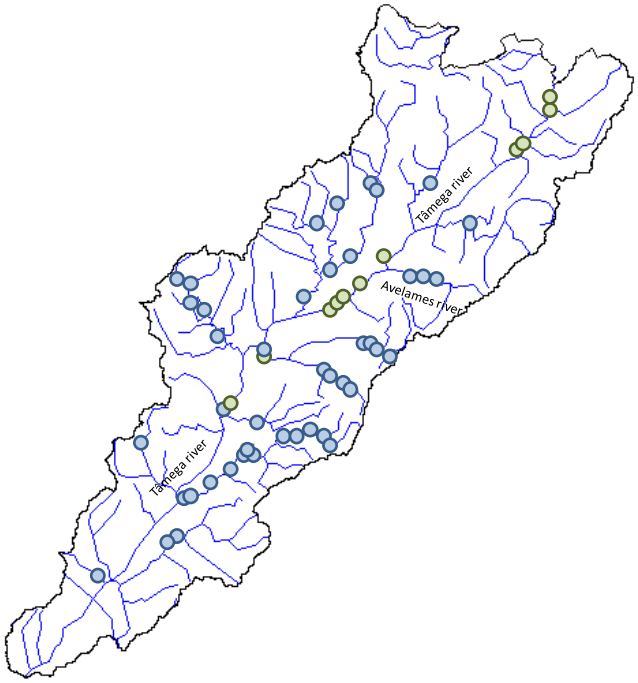


Figure 137 - Distribution of Lepomis gibbosus in the Tâmega River basin. Sampling site with species presence is denoted by a green circle, whereas sampling sites with absence are denoted by a blue circle.

Back to D2.2 Main index

Iberian chub was the most common species in the electrofishing surveys, occurring in 67% of the reaches, followed by the Iberian nase (present in 56% of the surveys) and brown trout (present in 49% of the surveys).

The first two factors of the PCA performed accounted for 58.8% of the variation in fish assemblage composition (Figure 138). Overall, a general gradient in fish species occurrence was depicted from the Tâmega River to its tributaries. Brown trout, being present mostly in tributaries, was separated from the remaining species, particularly the eel and pumpkinseed sunfish that occurred only in the Tâmega River. The Gudgeon (*Gobio lozanoi*) and the barbel occurred mostly in the main river and at larger tributaries, whereas the other native cyprinids (chub, nase, calandino and *A. oligolepis*) occurred both in the main river and tributaries, being frequently associated to the same sampling reach.

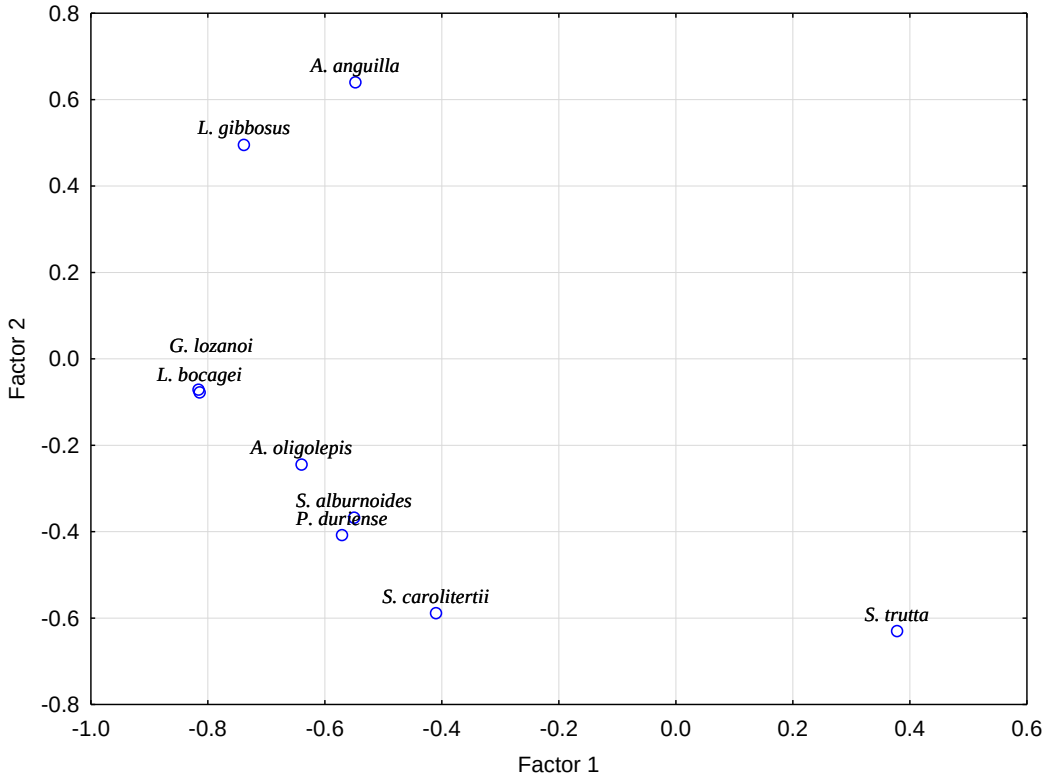


Figure 138 - Factor 1 and 2 of the PCA performed on the matrix of presence-absence of fish species in 55 electrofishing surveys made throughout the Tâmega River basin. Eigenvalues were 3.52 and 1.77, respectively, for the first and second factor.

3.4.1.4 Discussion

The Tâmega River basin presents a native fish community characterized by brown trout and several endemic cyprinids. The species richness increase from tributaries to the main river, although some of this increase was related to the presence of introduced species.

The fish community presents a pattern of variation along the basin that is somewhat similar to that observed in other Northern Portuguese basins, with the increase in the presence of trout and the decrease in the presence of cyprinids as we progress towards headwaters (e.g. Godinho *et al.* 1998; Ferreira *et al.* 2000; Santos *et al.* 2004). Elsewhere, this fish zonation is related to environmental variables such as water temperature and dissolved oxygen, with

warmer temperatures in the lowland main rivers preventing the presence of trout. In addition to this global variation, other patterns are also evident from the data, such as the predominance of the larger sized barbel in the main river, whereas the other, smaller cyprinids, can also occur in small streams.

The fish community of the Avelames River sampled in 1996 before the construction of the Bragado HPP showed assemblages composed exclusively of native cyprinids. In accordance with the Avelames River characteristics, the fish assemblages do not include either trout or the larger sized barbel, being dominated by chub and nase.

3.4.2. Fish and habitat analysis

3.4.2.1. Methodology

To analyse the habitat and the fish population at Bragado HPP two river reaches were initially selected in the Avelames River, one upstream the Bragado weir (hereafter upstream) (41º34'34.95''N, 7º38'51.37''W, *c.* 502 m a.s.l.), and another downstream the tailrace of Bragado powerhouse (hereafter downstream) (41º34'53.27''N, 7º40'50.95''W, *c.* 337 m a.s.l.). Both river reaches length is *c.* 150 m. The two reaches were considered to allow a broader analysis of the aquatic habitat modifications due to the presence of the HPP.

The upstream river reach would act as the reference because it is not affected by hydropeaking. However, due to the existence of a quarry that was releasing polluted water into the river; we did not consider the upstream river reach with respect to direct comparisons with the downstream river reach. Also, the results concerning the fish community were not promising with a low number of individuals and species found at different sampling campaigns.

The river bed topography was surveyed at both reaches to allow the modelling for different discharges. The river reach downstream Bragado powerhouse will be modelled with a 2D and a 3D model to assess the fish mesohabitats.

Because Avelames River is an ungauged watershed, to obtain a reliable forecast of the discharges under natural conditions along the river reach were Bragado HPP is installed a regionalization model for mainland Portugal (Portela 2014) was applied, based on the following equation:

$$Q_2 = Q_1 \times Qmod_2 \div Qmod_1 \qquad \text{Equation 1}$$

where *Q* refers to a daily/subdaily discharge (m^3/s) and *Qmod* is the long term mean annual discharge (m^3/s). Index 1 relates to a gauged watershed with discharge records and index 2 to an ungauged watershed. In the applications accomplished, different ungauged watersheds were considered along Avelames River. Furthermore, a computational simulation algorithm approach was applied to simulate the Bragado HPP operation scheme and to assess the flows downstream the tailrace of the powerhouse at a daily and subdaily scales.

To characterize the local fish assemblages, a survey by means of electrofishing was done at both river reaches. Fishes were captured in the upstream and downstream river reaches of Avelames River by electrofishing over the entire reach, using an electrofishing gear (Hans Grassl IG- 200), according to European norms - CEN EN 14011:2003, Water quality - Sampling of fish with electricity (European Committee for Standardization–CEN [CEN 2003]) and national guidelines (INAG 2008). After electrofishing fish were sorted by species, measured for total length (TL), weighted for total weight (TW) and released at the local of collection.

3.4.2.2. Results

3.4.2.2.1. Hydrology

The mean daily discharges used to establish the natural regime for the Avelames River were obtained at Santa Marta do Alvão gauging station (watershed area of 48.8 km^2), located at Louredo River, also belonging to Tâmega River watershed. Because Louredo and Avelames River present similar morphological characteristics and mean annual flow depths we could apply the regionalization/transposition procedure from the gauging station to the HPP.

Based on the regionalization procedure, two discharge series under natural conditions were obtained: one at the section of the weir of the Bragado HPP and another for the intermediate watershed between the weir and the powerhouse sections (watershed areas of 78.8 and 6.2 km^2, respectively). Because the discharge series refer to daily discharges, in order to have subdaily discharges, a constant value was considered along each day.

The simulation model for the daily operation of the HPP considered the mass balance equation (Equation 2) provided that the volume of water stored in the reservoir does not exceed its capacity (Equation 3), according to:

$$Va - Ve - L = \Delta S \qquad \text{Equation 2}$$

$$S \leq C \qquad \text{Equation 3}$$

where *Va* is the inflow volume at the section of the weir , *Ve* is the outflow volume (i.e. the turbined flow, the Eflow, and the water spilled over the weir), *L* are the infiltration/evaporation losses volume, Δ*S* is the change of the volume stored in the reservoir and *C* is the reservoir capacity.

According to the Bragado HPP operation, once the Eflow is released, discharges over the weir occur whenever the inflow exceeds the scheme design discharge and the available storage capacity is not enough the store the excess inflow volume.

To analyse the hydropeaking, the study adopted as key section a cross section located downstream the powerhouse tailrace, as represented in Figure 139. The discharge (and therefore the respective flow volume) at that section is given by the sum of the following parcels: Eflow, hypothetical discharges over the weir, turbined discharge, and contribution of the intermediate watershed (6.2 km^2), between the weir and the tailrace of the HPP.

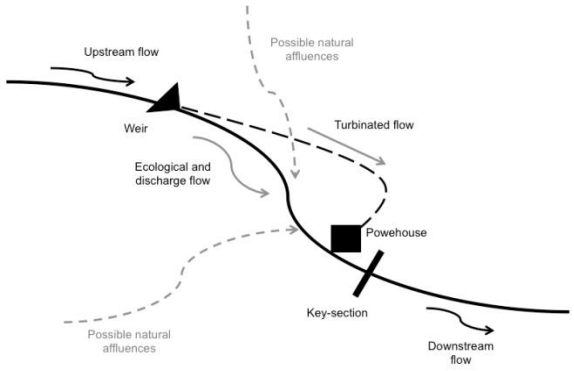


Figure 139 – Bragado HPP scheme. Localization of the weir, HPP and key-section.

Back to D2.2 Main index

The algorithm to simulate the daily operation of Bragado HPP was validated by comparing the computed turbined flows and the energy production with the corresponding real values. The energy produced was calculated based on the estimates of the turbined volumes, according to Equation 4.

$$E = V_{turb} \times H_d / (\frac{3600}{9.8\eta}) \quad \text{Equation 4}$$

where, for a given time interval, E is the energy (GWh); V_{turb} is the turbined volume (hm^3); H_d is the design net head (m) and η is a global efficiency of the HPP.

The comparison between the mean monthly values of the simulated and measured turbined discharges is shown at Figure 140.

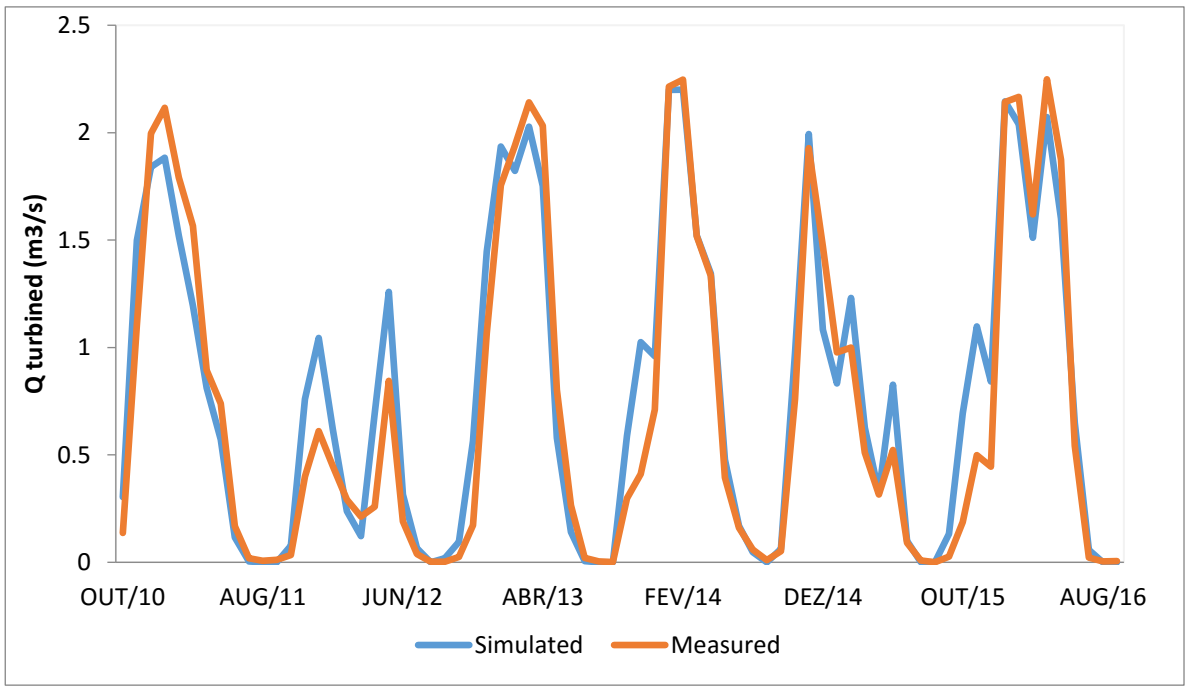


Figure 140 - Mean monthly real and simulated turbined flows during 20010/11 until 2015/16.

The previous figure shows that the computed and registered mean monthly discharges agree quite well. It should be noted that, for simplicity, the simulation algorithm did not consider the concentration of energy production out of the empty hours.

Considering the simulation model, the contributions to the downstream river reach are showed in Figure 141.

Back to D2.2 Main index

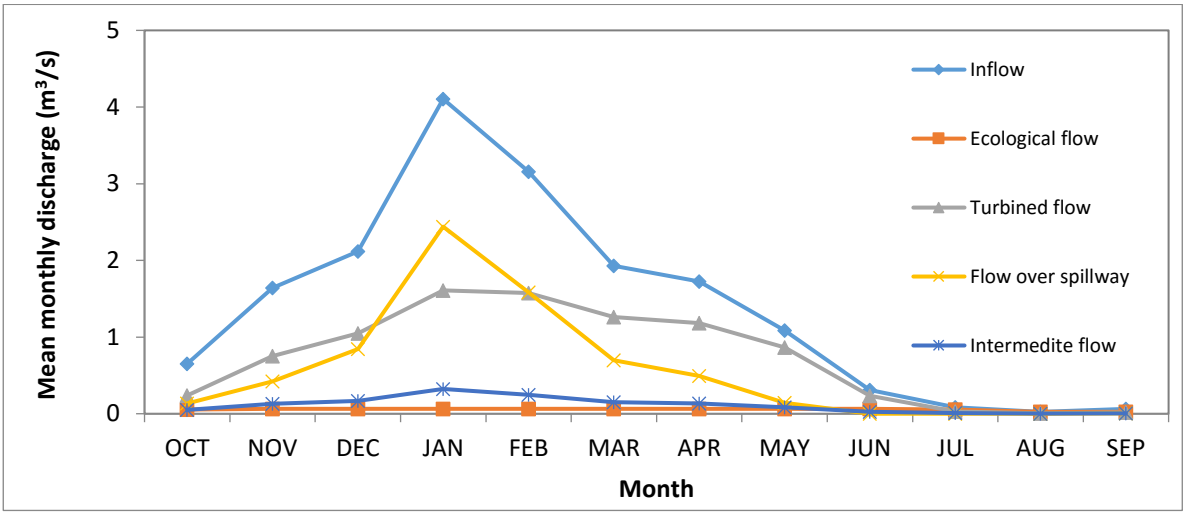


Figure 141 – Mean monthly flows at Bragado HPP scheme.

Along the hydrologic year, the turbined flow follows the inflow pattern, using as much water as possible in order to maximize revenues. Only when the inflow exceeds the ecological flow plus the design discharge of Bragado HPP then the water is released over the spillway, if the reservoir is at its full capacity. If not, the water is stored in the reservoir.

3.4.2.2.2. Fish populations

The fish assemblage community of the Avelames River is dominated by small sized native cyprinids, as it is typical of similar rivers in northern Portugal. Further downstream, close to the confluence with the Tâmega River, other species can be found, including the larger sized Iberian barbel (*Luciobarbus bocagei*). Further upstream some brown trout (*Salmo trutta*) can be found (see D2.2. Presentation of the tools).

To assess the fish assemblage composition in the vicinity of the Bragado HPP before the beginning of the study, in December 2017, a fish survey took place at the two sampling reaches (upstream and downstream Bragado HPP, Figure 142).



Figure 142 – Fish survey at Bragado ; a) upstream Bragado weir ; b) downstream Bragado HPP

A pool of three cyprinid species - Iberian chub (*Squalius pyrenaicus*), the calandino (*Squalius alburnoides*) and the Iberian nase (*Pseudochondrostoma almacai*) - were found at both sites.

Back to D2.2 Main index

Chub and nase were the predominant species, as expected given the patterns of fish assemblage variation in the Tâmega River basin (see Chapter 3.1). A few specimens of the European eel (*Anguilla anguilla*) were also found at the downstream river reach but were not measured or weighted. A summary of the survey data is shown in Table 13.

Table 13 – Fish survey at river reach upstream Bragado weir and downstream Bragado HPP

River reach	Fish species	N	Total weight (g)	Total length (cm)
Upstream Bragado weir	*Squalius alburnoides*	2	1.0±0.0	7.1±0.1
	Pseudochondrostoma duriense	1	1	4.1
	Squalius pyrenaicus	8	36.6±30	13.7±5.0
Downstream Bragado HPP	*Squalius alburnoides*	1	7.5	3.0
	Pseudochondrostoma duriense	94	4.2±4.3	7.9±2.0
	Squalius pyrenaicus	8	7.8±7.3	8.6±2.6

*Average values ± standard deviation

The low number of individuals caught upstream Bragado HPP was probably related to the low water level and to the negative influence of a quarry that was releasing polluted water into the river.

3.4.2.2.3. Habitat analysis

To characterize the habitat downstream and upstream Bragado HPP we have chosen a two-dimensional approach. The river bed topography was surveyed in September 2017 using a combination of a Nikon DTM330 total station and a Global Positioning System (GPS) (Ashtech, model Pro Mark2) (Figure 143). Trees, boulders, and large objects were defined by marking the object intersection with the river bed and by surveying the points necessary to approximately define its shape. The river bed substrate was also characterized.

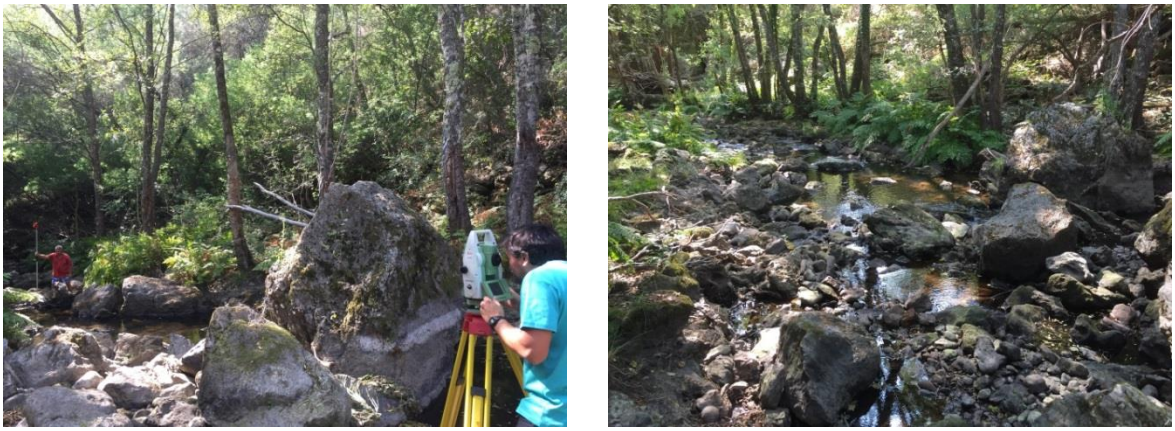


Figure 143 – Topography survey in the river reach downstream Bragado HPP

Back to D2.2 Main index

Altogether, 2506 points were surveyed at the river reach downstream the HPP and 2539 points at the upstream river reach (Figure 144 and Figure 145).

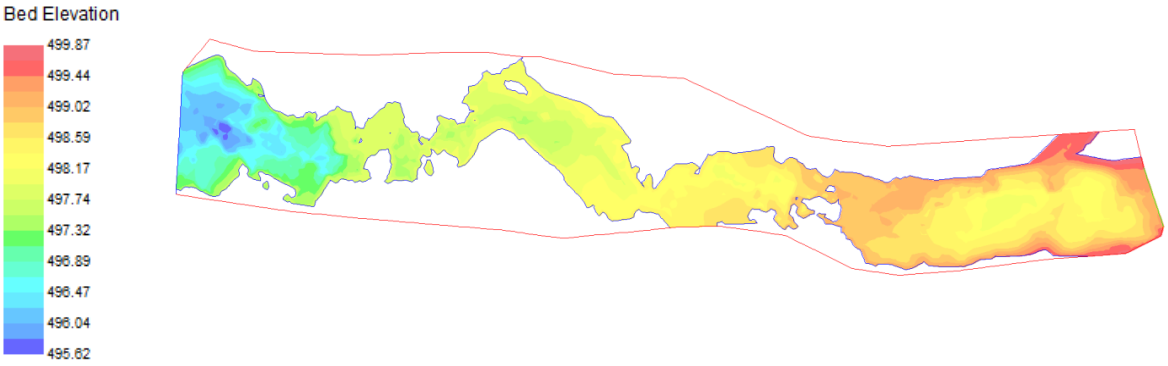
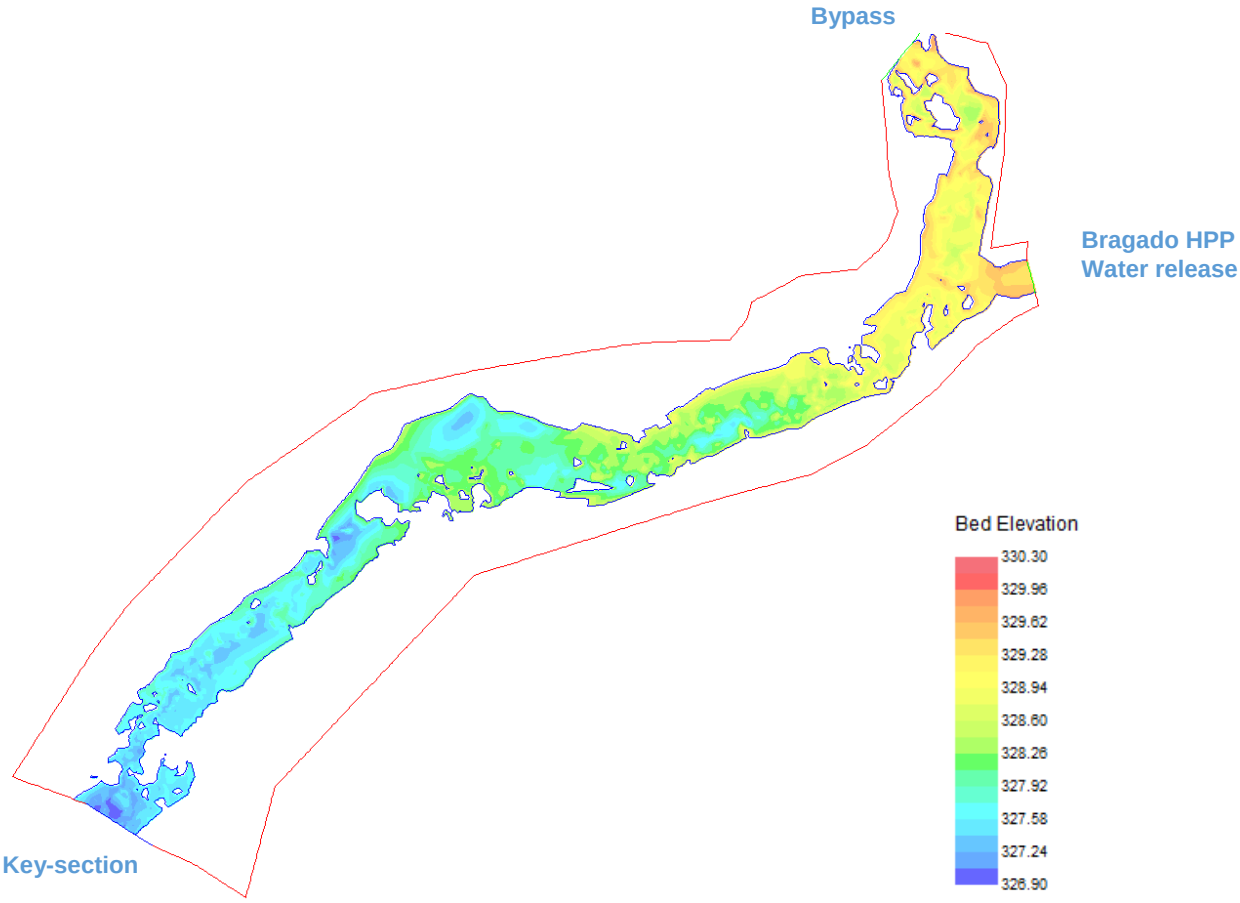


Figure 144 – River bed topography at the upstream river reach.



Back to D2.2 Main index

Figure 145 - River bed topography at the downstream river reach.

The upstream river reach did not meet the reference conditions from which it would be compared with the disturbed river reach, *i.e.* the downstream river reach. Therefore, we opted for not surveying and modelling the upstream reach.

3.4.3. Hydropeaking

3.4.3.1. Methodology

3.4.3.1.1. Characterization of hydropeaking

To characterize the Bragado HPP operation mode we applied the COSH tool, developed by Sauterleute & Charmasson (2014), to a 15 min interval flow series to identify and quantify rapid fluctuation in flow and water level with a subdaily resolution. The COSH tool allows to separate the peak events in rapid increases corresponding to upramping and rapid decreases of flow corresponding to the downramping. After detecting the peak events, the COSH tool identifies multiple peaking events, as a result of a successive starting and stopping of the turbines in an HPP. Additionally, the COSH tool also identifies peak events according to daylight conditions (daylight, darkness and twilight), because daylight strongly influences fish behaviour and movements.

To calculate the water level at the key-section, a rating curve was calculated. The limits adopted when computing the rating curve vary from 0.01 to 131.6 m^3/s (the highest recorded discharge), with an increment of 0.05 m^3/s. The values assumed for Ks and for the slope of the river bed were 15 $m^{1/3}/s$ (slow flow with deep zones and vegetation, Lencastre 1993) and 0.0332 m/m respectively. The rating curve is:

$$Q = 9.94 \times (h - 0.024)^{2.239} \qquad \text{Equation 5}$$

where *h* is the flow depth. To quantify hydropeaking impacts we have applied Carolli *et al.* (2015) methodology. This methodology consists of 2 indicators to characterize three different levels of physical alteration caused by hydropeaking. The two indicators are HP1, a dimensionless measure of the magnitude of hydropeaking and, HP2, which measures the temporal rate of flow changes in $m^3/s/h$.

The first parameter is defined as:

$$HP1_i = \frac{Q_{máx,i} - Q_{min,i}}{Q_{mean,i}} \; i \in [1, 365] \qquad \text{Equation 6}$$

$$HP1 = median|HP_i| \qquad \text{Equation 7}$$

where index *i* denotes the day of the year. HP1 is the annual median of daily discharges of $HP1_i$, calculated as the difference between the maximum and the minimum discharges ($Q_{max,i}$ and $Q_{min,i}$, respectively) over the *i*-th day, divided by the long term mean daily discharge ($Q_{mean,i}$)

The second parameter is defined as:

$$(HP2_k)_i = \left(\frac{\Delta Q_k}{\Delta t_k}\right) = \left(\frac{Q_k - Q_{k-1}}{t_k - t_{k-1}}\right)_i \; i \in [1, 365] \qquad \text{Equation 8}$$

$$HP2_i = P_{90}|(HP2_k)_i| \qquad \text{Equation 9}$$

Back to D2.2 Main index

$$HP2 = median|HP2_i| \quad \text{Equation 10}$$

where Q_k refers to each subdaily flow of the data series, HP2 is calculated as the annual median of daily values of $HP2_i$ in $m^3/s/h$ and $HP2_i$ is the 90th percentile (P90) of the discretized time derivative of the subdaily flow series.

To classify the level of impact of hydropeaking is necessary to calculate a threshold for each indicator: TR_{HP1} and TR_{HP2} which are defined by:

$$\mathrm{TR_{HP1}} = \mathrm{P_{75}}\left(\mathrm{HP1_i^{unp}}\right) + 1{,}5(\mathrm{P_{75}} - \mathrm{P_{25}})\left(\mathrm{HP1_i^{unp}}\right) \quad \text{Equation 11}$$

$$\mathrm{TR_{HP2}} = \mathrm{P_{75}}\left(\mathrm{HP2_i^{unp}}\right) + 1{,}5(\mathrm{P_{75}} - \mathrm{P_{25}})\left(\mathrm{HP2_i^{unp}}\right) \quad \text{Equation 12}$$

where $HP1_i^{unp}$ and $HP2_i^{unp}$ are the daily values of the 2 indicators for watercourses in natural regime and P75 and P25 are the 75th and 25th percentile of the distribution, respectively. Classification of the impact level of hydropeaking in watercourses in modified regime is:

- Class 1: non/low impact: $HP1 < TR_{HP1}$ and $HP2 < TR_{HP2}$
- Class 2a: medium impact: $HP1 > TR_{HP1}$ and $HP2 < TR_{HP2}$
- Class 2b: medium impact: $HP1 < TR_{HP1}$ and $HP2 > TR_{HP2}$
- Class 3: high impact: $HP1 > TR_{HP1}$ and $HP2 > TR_{HP2}$

3.4.3.1.2. Fish habitat use

To assess fish movements and habitat use downstream Bragado HPP due to hydropeaking, fishes were individually marked with PIT-Tags and tracked with an Oregon RFID portable reader and pole antenna (Cucherousset *et al.* 2005; Kelly *et al.* 2017) in the downstream river reach. With that aim, fish were captured during daylight in the selected river reach by electrofishing over the entire reach in 16 and 17 of May 2018, using a Pulsed DC electrofishing gear (Hans Grassl IG- 200), according to European norms - CEN EN 14011:2003, Water quality - Sampling of fish with electricity (European Committee for Standardization–CEN [CEN, 2003]) and national guidelines (INAG, 2008) Figure 142. After electrofishing, fish were stabilized in a fish corf in the Avelames River for at least 2h. Afterwards, fish were sorted by species, measured for total length (TL) and weighted for total weight (TW).

The abdominal region was disinfected with an iodine solution (betadine) in preparation for tag insertion. Fish measuring >60 mm and weighing more than 5 g were anaesthetized with eugenol before marking. Smaller fish were not marked to guarantee the tag weight is <2% of fish body (Winter 1983; Brown *et al.* 1999). Each fish was marked with a small HDX PIT-Tag (12 x 2.12 mm, weighing 0.1 g from Oregon RFID) previously placed in a pot with ethyl alcohol 96% for sterilization. The tag was injected in the intraperitoneal cavity with a sterilized needle linked to a grip injector (Oregon RFID). One hour following the insertion and after regaining equilibrium, fish were released at their capture location.

Detection campaigns were set after marking the fish to cover different seasons (i.e. late spring, late summer). In each campaign, the operator will walk the river upstream in a zigzag pattern, scanning the entire river reach with the portable reader and pole antenna (Kelly *et al.* 2017)

Back to D2.2 Main index

looking for tagged fish avoiding flow disturbance. Each time a fish is detected, the fish ID is recorded and water velocity and depth are measured, and the substrate is characterized. The portable Oregon high performance HDX RFID reader, ISO 11784 compatible, and pole antenna used (c. 50 cm in diameter) can have a detection range of approximately 45 cm for the PIT tags used.

3.4.3.1.3. Macroinvebrate assemblages

The macroinvertebrate community was characterized by collecting samples at the downstream river reach. Drift nets were installed upstream the water release from Bragado HPP (one) and downstream the river reach *c.* 100 m downstream the water release (two). The passive collection of macroinvertebrates present in the water column lasted 2h. Also, 2 “kick” samples were collected, one upstream and another downstream the water release, according to the protocol established by the Portuguese Environment Agency to determine the biological water quality. All samples were stored in 70% alcohol.

In the laboratory, all the samples were sorted, in order to separate the detritus and leaf litter from macroinvertebrates. Clean macroinvertebrate samples were stored in 70% alcohol and glycerol (9:1). After sorting, macroinvertebrate samples were identified with the help of a stereomicroscope.

3.4.3.2. Results

3.4.3.2.1. Characterization of Hydropeaking

To analyse the rapid fluctuations due to the HPP operation, the COSH-tool was applied to water level (h) series at the key-section (see Figure 139 and Figure 145). For that purpose, a time step of 15 min was adopted. Before computing the water levels, all null discharge at the section were replaced by 0.01 m^3/s, because COSH-tool would assume zero as a missing value. After that, a water level was assigned to each discharge, according to the rating curve previously presented (Equation). The discharge series is represented in Figure 146.

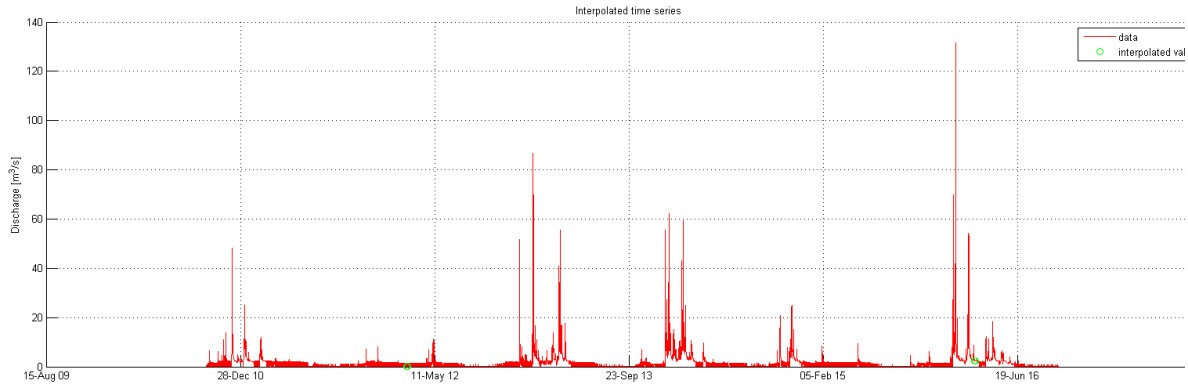


Figure 146 – Flow series from October 1st 2010 to September 30th 2016 at the key-section downstream Bragado HPP.

The highest discharge occurred during a flood in 2016. With an exception for the year 2012, all the others present flood events as a result of short intensive precipitation events in a very small watershed, as the one under analysis.

In order to smooth the input discharge data, a moving average (w) with a running length of 5 was applied. To identify the rapid increases and decreases different thresholds were set (

Back to D2.2 Main index

Table 14).

Table 14 – Threshold values for analysis of the water level time series for Avelames River.

W [-]	Cinc [-]	Cdec [-]	P [-]	T [min]	D [min]
5	0.13	0.13	0.2	120	45

The factors Cinc and Cdec, are usually in the range of 0.05-0.2 and are adjusted to assess the peak events (for more information see Sauterleute & Charmasson (2014)).

After applying the assigned thresholds we have run the COSH-tool for the 6 hydrologic years. The number of rapid increases and decreases per year is represented in Figure 147.

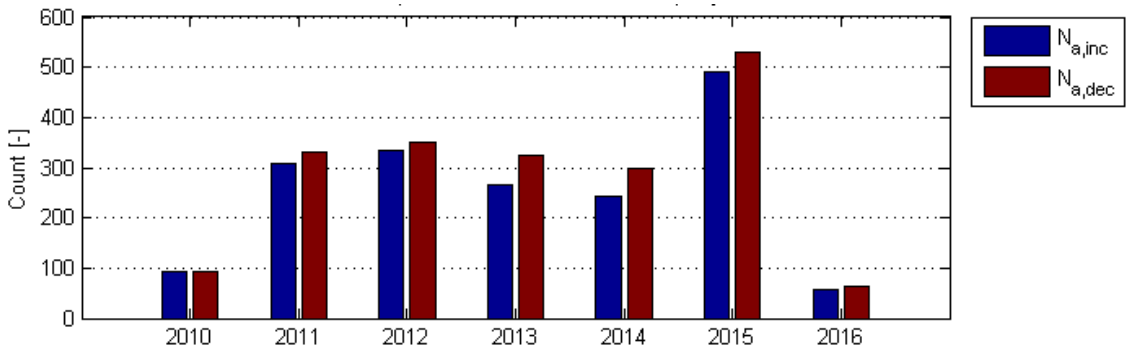


Figure 147 – Number of rapid increases (N_{inc}) and decreases (N_{dec}) per year for the Avelames River downstream Bragado HPP.

For the years 2010 and 2016, the data is not complete: in 2010 only data from September to December was available and in 2016 only data from January to September was available. The years with more peaking events were the ones with less water availability, like 2015. Based on data, we could conclude that Avelames River is very sensitive to rapid fluctuation of flow/water level during low flow periods. Hence the difference between turbine and river discharges is very high and COSH-tool detects the peaking events immediately.

Concerning the time between a rapid increase and the start of a rapid decrease (T_{high}) and the time between a rapid decrease and a rapid increase (T_{low}), the results show that T_{high} occurs mostly during the winter and T_{low} during the summer period (Figure 148).

Back to D2.2 Main index

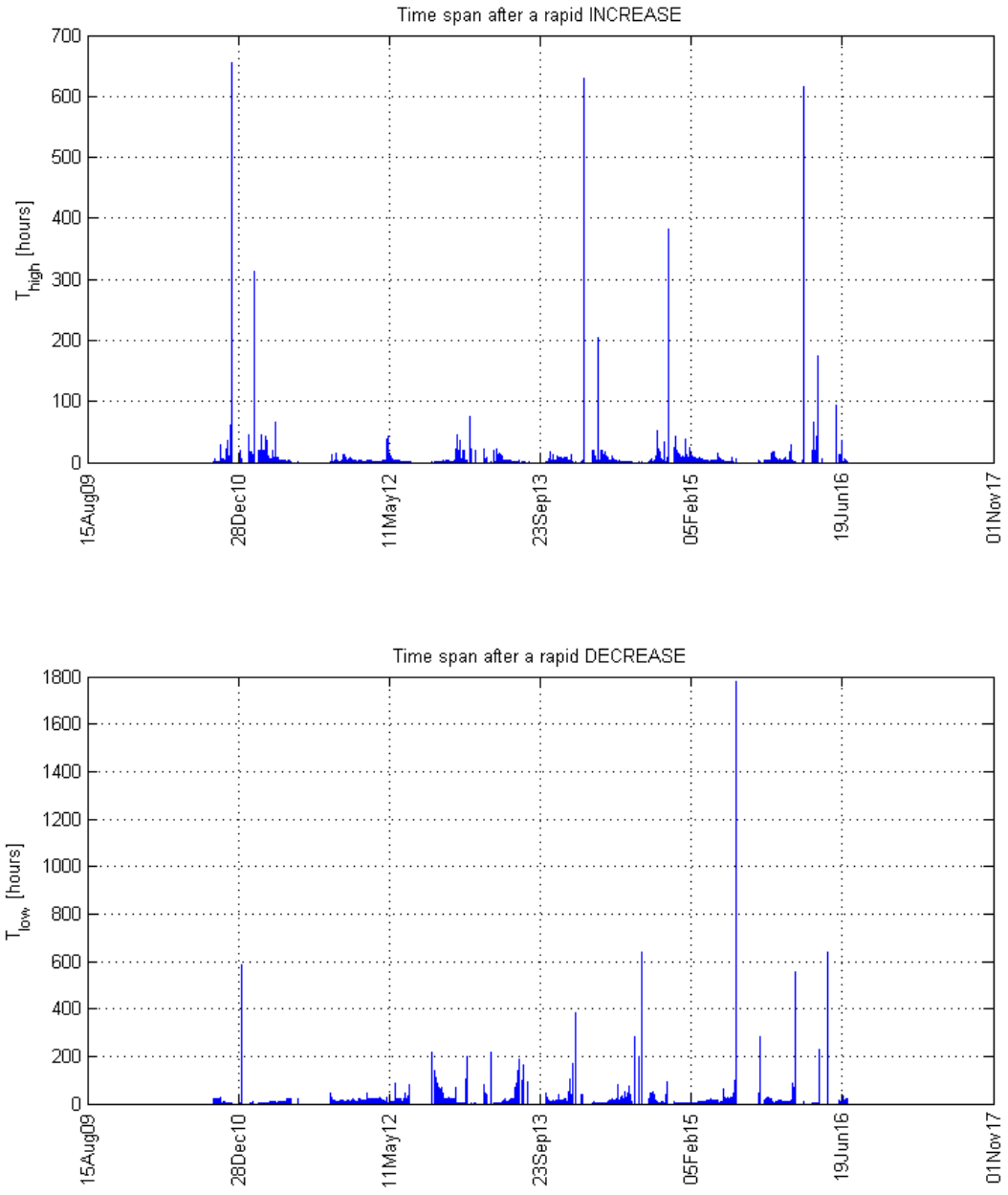


Figure 148 – T_{high} and T_{low} along the 6 years flow series.

When analysing the cumulative distribution of the time periods (Figure 149) we verify that 95% of the T_{high} last less than 24h and 50% of the T_{high} last 2h. Thus, in general, Bragado HPP turbines during 2h in continuous. The inflection point of the curve for T_{high} is observed at 17h, where the probability variation becomes asymptotic. For T_{low}, 90% of the events last 20h, while 50% last 5h.

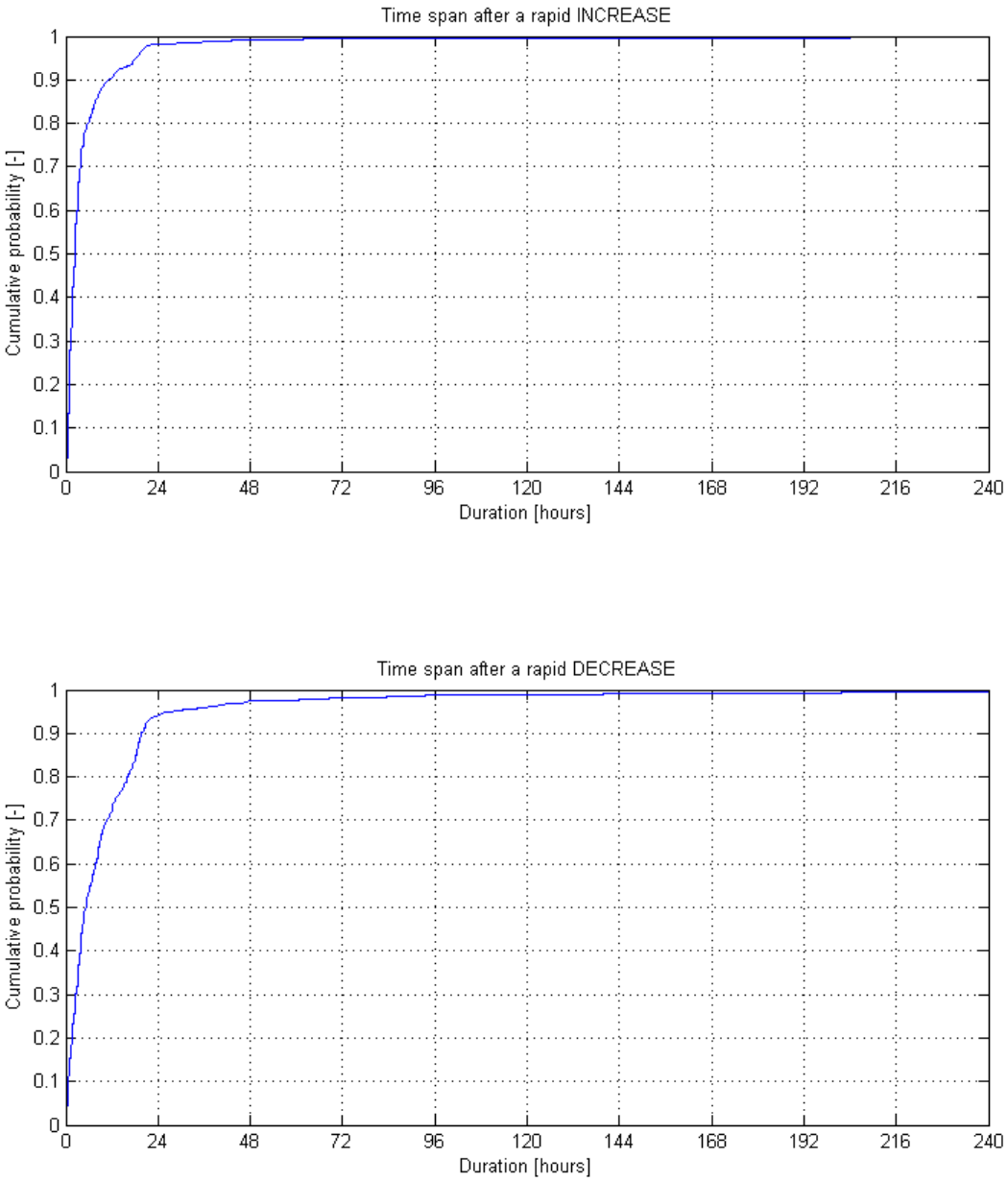


Figure 149 – Cumulative distribution of time span after a rapid increase and after a rapid decrease.

In general, Bragado HPP operates only once a day (Figure 151). Rapid increases and decreases tend to occur in the wet period from October to June. In the summer, the HPP does not operate due to the lack of water (Figure 151).

The operation scheme of Bragado HPP reflects the daily periods regarding the energy tariffs paid to the company. The rapid increase occurs in the morning followed by a rapid decrease around 14h (2 pm), the same pattern occurs at the end of the day c. 18h (6pm) (Figure 151).

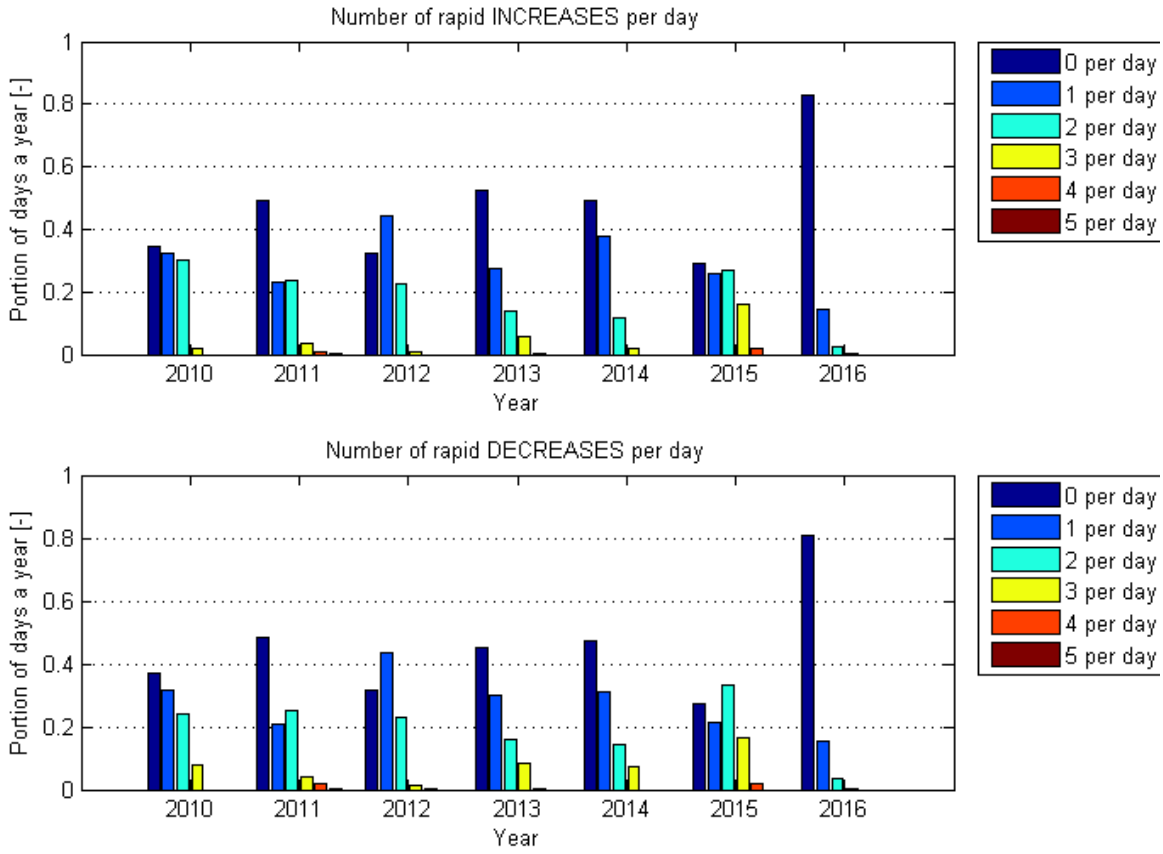


Figure 150 – Number of rapid increases and rapid decreases per day.

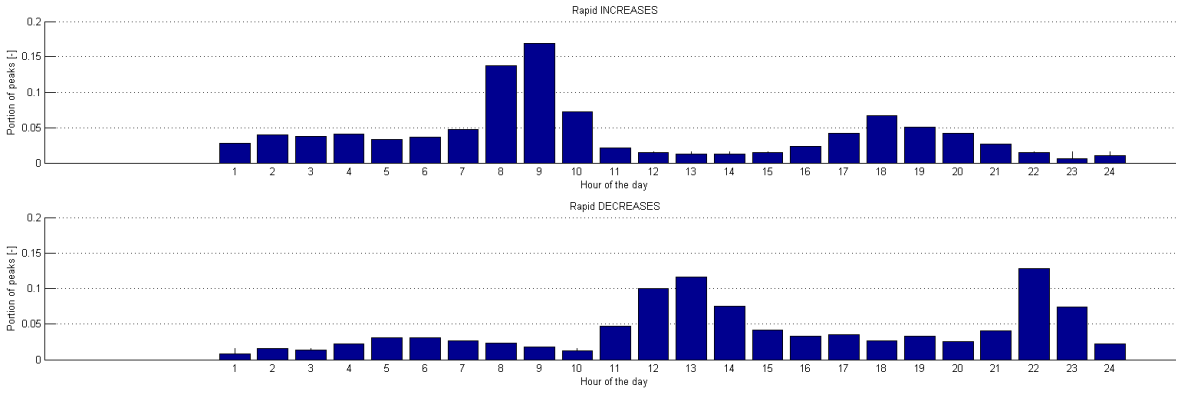


Figure 151 – Number of rapid increases and rapid decreases during the day.

According to Figure 152, most of the peaking events occur during daylight, 55% of rapid increases and 50% of rapid decreases. Along the year the peak events in darkness occur mainly in the autumn and winter season (Figure 153).

Back to D2.2 Main index

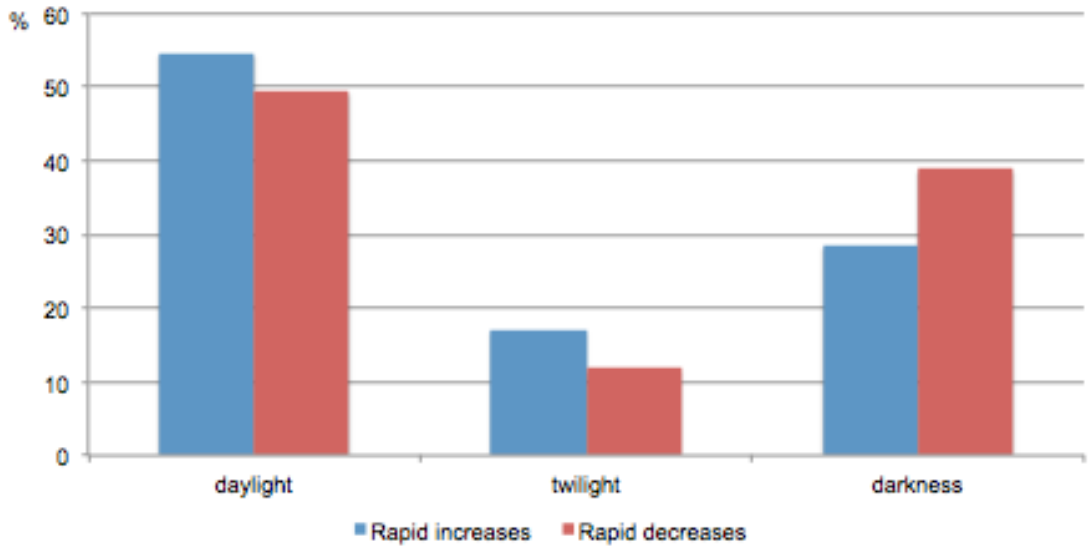


Figure 152 - Percentage of rapid increases and decreases according to daylight conditions (daylight, twilight and darkness).

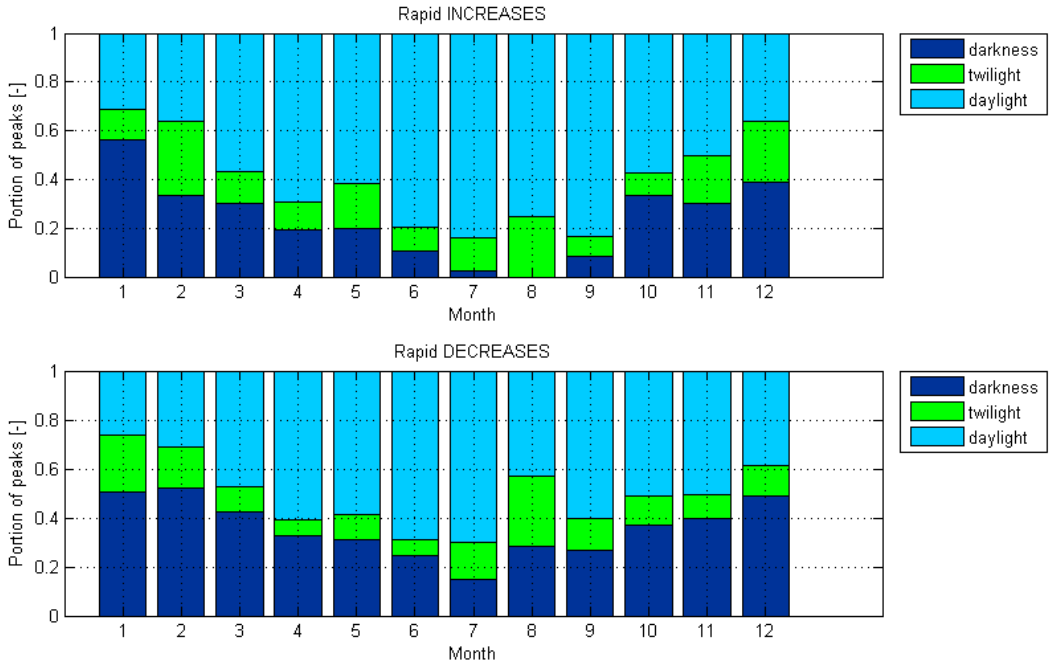


Figure 153 – Monthly distribution of rapid increases and rapid decreases according to light conditions, i.e. daylight, twilight and darkness.

The methodology proposed by Carolli *et al.* (2015) was applied to the subdaily flow series from 1st October 2010 to 30th September 2016 at the river reach downstream Bragado HPP. Two scenarios were considered: the actual scenario considering the flow regulation due to Bragado HPP operation and the pristine situation, prior to the existence of the HPP, i.e. the natural flow regime.

Back to D2.2 Main index

The natural flow series was used to calculate the limits TR_{HP1} and TR_{HP2} in order to characterize the level of impact of the HPP. The results of Carolli et al. (2015) parameters are shown in Table 15. The highest value concerning the modified flow regime for HP1 was 3.4 (2011/12) and for HP2 was 0.56 $m^3/s/h$ (2014/15). Considering the natural flow, both parameters HP1 and HP2 show values close to zero.

Therefore, Avelames River was classified as class 3, except for the 2015/16 year during which it was classified as class 2a. Concerning the natural flow regime, the classification of Carolli et al. (2015) returned class 1 for all the years analysed Table 15.

Table 15 – Values of Hydropeaking Impact (HP) and Threshold (TR) values for Avelames River downstream Bragado HPP considering the Carolli et al. (2015) methodology.

River reach	Hydrologic year	HP1 [-]	TR_{HP1} [-]	HP2 [$m^3/s/h$]	TR_{HP2} [$m^3/s/h$]	Class
Modified (with Bragado HPP)	2010/2011	1.65	0.45	0.30	0.07	3
	2011/2012	3.40	0.43	0.49	0.03	3
	2012/2013	1.03	0.63	0.27	0.09	3
	2013/2014	1.52	0.82	0.33	0.13	3
	2014/2015	1.62	0.49	0.56	0.06	3
	2015/2016	0.89	0.75	0.10	0.13	2a
Natural (without Bragado HPP)	2010/2011	0.09	0.45	0.01	0.07	1
	2011/2012	0.08	0.43	0.00	0.03	1
	2012/2013	0.11	0.63	0.01	0.09	1
	2013/2014	0.13	0.82	0.01	0.13	1
	2014/2015	0.08	0.49	0.00	0.06	1
	2015/2016	0.12	0.75	0.01	0.13	1

3.4.3.2.2. Fish location

Fish were tagged with the PIT-tag on the 16 and 17 of May 2018 (Figure 154).



Figure 154 – a) Electrofishing at the upstream river reach ; b) Fish measurements: weight and length.

In total, 104 individuals were individually marked with the PIT tags, 79 in the downstream river reach and 25 in the upstream river reach (Table 16).

Table 16 – Fish PITtagged in the upstream and downstream river reach.

Back to D2.2 Main index

River reach	Fish species	N	% of the total tagged fish	Total weight (g)	Total length (cm)
Upstream Bragado weir	*Squalius alburnoides*	7	28	6.1±2.8	8.3±1.4
	Squalius pyrenaicus	17	68	8.0±8.6	8.2±2.0
	Pseudochondrostoma duriense	1	4	6	8.6
Downstream Bragado HPP	*Squalius alburnoides*	8	10	3.9±1.8	7.2±0.7
	Squalius pyrenaicus	18	23	15.6±13.6	10.2±2.2
	Pseudochondrostoma duriense	53	67	7.0±5.3	8.5±1.7

After marking the fish caught with the PIT-tag we have returned to the river to check fish positions two more times, roughly corresponding to the seasons late spring and late summer. At the upstream river reach, that was planned to act as the reference site, we were unable to find any of the marked fish. Probably due to external factors, like the existence of a quarry upstream the river that was compromising the water quality.

The river reach downstream Bragado HPP was surveyed six times in each season. One person, carrying the portable antenna moved upstream in a zigzag pattern (Figure 155). The antenna was immediately above the water for low depths and immersed in the water for higher depths. The operator moved discretely to avoid fish displacement.



Figure 155 – Operator carrying the portable antenna looking for marked fish on the a) upstream river reach, and b) downstream river reach.

Each time a fish was recorded a sound was emitted by the receiver and another operator recorded: i) the fish code number associated to the PIT-tag; ii) the fish location, with a dual-frequency GNSS receiver (Trimble R2), iii) water depth, iv) velocity, v) bed substrate, and vi) the fish location regarding the water release from the HPP, either upstream or downstream. The first rough results are shown at

Back to D2.2 Main index

Table 17.

Table 17 – Number of fish records for each species in late spring and late summer.

Species	Late Spring						Late Summer					
	1	2	3	4	5	6	1	2	3	4	5	6
Squalius alburnoides	1	2	1	-	-	-	-	-	-	-	-	-
Squalius pyrenaicus	3	3	4	7	4	5	3	2	5	4	4	3
Pseudochondrostoma duriense	4	3	4	7	5	9	3	5	8	11	8	6
Total	8	8	9	14	9	14	6	7	13	15	12	9

On average, we have detected 10 individuals in each survey. The same fish was detected in different surveys occupying distinct habitats. Generally, fishes were recorded immediately upstream the water release from Bragado HPP and in the centre of the river channel - *c.* 50 m downstream the water release. In total, from the 79 PIT-tagged fish, 36 individuals were recorded; a few were recorded several times. From all the individuals detected, 2 were *S. alburnoides*, 13 were *S. pyrenaicus*, and 21 were *P. duriense* (Figure 156). The rank of the different species was the same for the marked and detected fish (Table 18 and Figure 156). Nevertheless, proportionally less S*. alburnoides* and *P. duriense* were detected, whereas the opposite was observed with *S. carolitertii*.

Table 18 - Proportion of each species in the specimens marked and detected in the downstream reach.

Species	% of the tagged specimens	% of the detected specimens
Squalius alburnoides	10	3
Squalius pyrenaicus	23	38
Pseudochondrostoma duriense	67	59

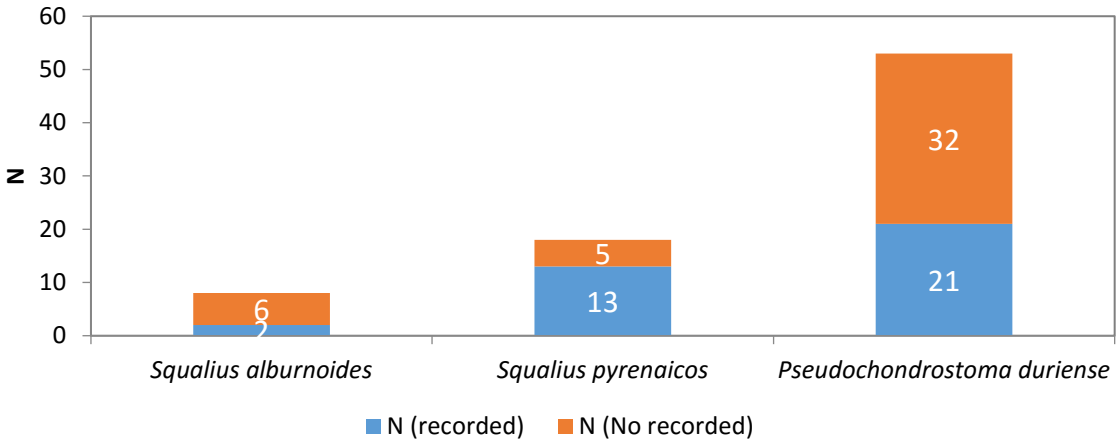


Figure 156 – Number of fish individuals detected and not detected by species during the seasons late Spring and late Summer.

During the late spring campaign, we have also identified potential spawning grounds grouped in 14 areas along the downstream river reach.

Back to D2.2 Main index

Another set of field campaigns is planned for the spring of 2019, including the marking of additional specimens and their tracking.

3.4.3.2.3. Macroinvertebrates

The samples were collected from the downstream river reach on the 19 of June of 2018. We have collected 3 drift samples (Figure 157): one upstream and two downstream of the HPP release. Also, 2 “kick” samples were collected, one upstream and the other was collected downstream of the HPP (Figure 157).



Figure 157 – Macroinvertebrates sampling.

The results for the samples of macroinvertebrates are presented in

Table 19, for the “kick” samples, and in

Table 20, for the drift samples.

Table 19 – Macroinvertebrate present in the “kick“ samples.

Taxa	Upstream	Downstream
Boyeria irene	3	1
Calopteryx virgo	0	1
Onychogomphus	5	24
Cordulegaster boltonii	0	1
Hydropsyche siltalai	1	1
Helicopsyche helicifex	0	2
Polycentropus corniger	9	0
Psychomyia ctenophora	5	0
Setodes	8	12
Ephemerella ignita	3	7
Baetis	48	15
Habroleptoides	13	7
Habrophlebia	11	0
Caenis	36	3
Ecdyonurus	16	0
Aphelocheirus aestivalis	3	4

Taxa	Upstream	Downstream
Gerris	32	0
Leuctra	16	9
Perla	1	0
Hydraena	1	0
Ochthebius	1	0
Limnebius	1	1
Oulimnius (adult)	7	7
Oulimnius (larvae)	2	5
Elmis (adult)	1	0
Elmis (larvae)	1	3
Esolus (adult)	1	0
Limnius (larvae)	1	1
Sialis fuliginosa	5	0
Atherix	3	2
Athrichops crassipes	0	1
Simulium	1	4
Ceratopogoninae	0	4
Chironomini	14	3
Tanytarsini	0	2
Orthocladiinae	29	12
Tanypodinae	17	5
Tabanidae	0	3
Tipula	0	1
Anthomyiidae	0	1
Dolichopodidae	0	1
Eriopterini	0	1
Hydracarina	8	1
Potamopyrgus	138	1376
Ancylus fluviatilis	1	8
Pisidium	1	1
Radix	0	1
Erpobdella	0	5
Dugesia	1	0
Lumbriculidae	1	2

Table 20 – Macroinvertebrates present in the drift samples.

Taxa	Upstream	Downstream left	Downstream right
Boyeria irene	2	1	0
Calopteryx virgo	0	1	0
Onychogomphus	0	0	1
Tinodes waeneri	1	0	0

Back to D2.2 Main index

Taxa	Upstream	Downstream left	Downstream right
Setodes	0	0	1
Ephemerella ignita	2	2	1
Baetis	6	6	2
Habrophlebia	0	3	0
Caenis	0	3	0
Aphelocheirus aestivalis	0	2	1
Gerris	4	0	1
Protonemura	0	2	1
Leuctra	0	2	1
Anacaena	1	0	0
Hydraena	1	0	0
Oulimnius adult	2	0	0
Elmis larvae	1	2	1
Esolus larvae	0	0	1
Bidessus	0	0	1
Simulium	12	2	78
Ceratopogoninae	0	0	1
Chironomini	3	0	1
Tanytarsini	2	1	3
Orthocladiinae	7	3	8
Tanypodinae	0	1	1
Hydracarina	1	3	7
Potamopyrgus	1	141	34
Ancylus fluviatilis	1	1	3
Erpobdella	0	0	2
Lumbriculidae	0	1	0

The abundance of the invasive mud snail (Potamopyrgus antipodarum) stands out in comparison with the other identified invertebrate taxa (

Table 19 and

Table 20). In a Mediterranean climate stream system, this invasive species interacted and competed with other grazing invertebrates, had a greater grazing impact in comparison with native snail species and reduced the survival of amphibian tadpoles (Bennett *et al.* 2015). Bennett et al. (2015) suggest that flow regulation could enhance their effects, by eliminating high flows that reduce their population sizes. However, this is likely not the case of Bragado, because the weir storage is small and does not affect the magnitude of the flood events.

3.4.4. References

Bennett, D.M., Dudley, T.L., Cooper, S.D. & Sweet, S.S. 2015. Ecology of the invasive New Zealand mud snail, Potamopyrgus antipodarum (Hydrobiidae), in a mediterranean-climate stream system. Hydrobiologia, 746, 375–399, https://doi.org/10.1007/s10750-014-2136-6.

Brown, R.S., Cooke, S.J., Anderson, W.G. & McKinley, R.S. 1999. Evidence to Challenge the “2% Rule” for Biotelemetry. North American Journal of Fisheries Management, 19, 867–871, https://doi.org/10.1577/1548-8675(1999)019<0867:ETCTRF>2.0.CO;2.

Cabral, M.J.J., Almeida, J., et al. 2005. Livro Vermelho Dos Vertebrados de Portugal. MJ, C., J, A., et al. (eds). Lisboa, Instituto da Conservação da Natureza.

Carolli, M., Vanzo, D., Siviglia, A., Zolezzi, G., Bruno, M.C. & Alfredsen, K. 2015. A simple procedure for the assessment of hydropeaking flow alterations applied to several European streams. Aquatic Sciences, 77, 639–653, https://doi.org/10.1007/s00027-015-0408-5.

CEN. 2003. Water quality: sampling of fish with electricity. European Standard EN 14011:2003.

Cortes, R.M., Calçada Duarte, J.P. & Monzon, A. 1990. Habitat and fish populations parameters in a headstream. SCIENTIA gerundensis, 53–60.

Cucherousset, J., Roussel, J.-M., Keeler, R., Cunjak, R.A. & Stump, R. 2005. The Use of Two New Portable 12-mm PIT Tag Detectors to Track Small Fish in Shallow Streams. North American Journal of Fisheries Management, 25, 270–274, https://doi.org/10.1577/M04-053.1.

Doadrio. 2001. Atlas y Libro Rojo de Los Peces Continentales de España. Doadrio, I. (ed.). Dirección General de Conservación de la Naturaléza Museo Nacional de Ciencias Naturales.

Ferreira, M.T., Pinheiro, A.N., et al. 2000. Avaliação Da Eficácia Das Passagens Para Peixes de Pequenos Aproveitamentos Hidroeléctricos e Suas Alterações Ecológicas Sobre a Ictiofauna Fluvial. Lisboa.

Filipe, A.F. 2004. Revisão Do Livro Vermelho Dos Vertebrados de Portugal: Peixes Dulciaquícolas e Migradores. Relatório Final.

Godinho, F.N., Ferreira, M.T. & Portugal e Castro, M.I. 1998. Fish assemblage composition in relation to environmental gradients in Portuguese reservoirs. Aquatic Living Resources, 11, 325–334, https://doi.org/10.1016/S0990-7440(98)80003-X.

Godinho, F.N., Pinheiro, P.J., Oliveira, J.M. & Azedo, R. 2014. Responses of intermittent stream fish assemblages to irrigation development. River Research and Applications, 30, 1248–1256, https://doi.org/10.1002/rra.2748.

INAG. 2001. Plano de Bacia Hidrográfica Do Rio Douro. Hidrorumo, Hidro4, Procesl e Prosistemas.

INAG. 2008. Manual para a avaliação biológica da qualidade da água em sistemas fluviais segundo a Directiva Quadro da Água: Protocolo de amostragem e análise para a fauna piscícola.

Kelly, B.B., Cary, J.B., Smith, A.D., Pregler, K.C., Kim, S. & Kanno, Y. 2017. Detection Efficiency of a Portable PIT Antenna for Two Small-Bodied Fishes in a Piedmont Stream. North American Journal of Fisheries Management, 37, 1362–1369, https://doi.org/10.1080/02755947.2017.1388886.

Lencastre, A. 1993. Hidráulica Geral. LNEC.

Madeira, J.M. 2002. Inventariação Da Ictiofauna Presente Na Bacia Hidrográfica Do Rio Douro.

Oliveira, J.M., Santos, J.M., Teixeira, A., Fereira, M.T., Pinheiro, P.J., Geraldes, A. & Bochechas, J. 2007. Avaliação Da Qualidade Ecológica de Rios Portugueses: Programa Nacional de Monitorização de Recursos Piscícolas de Águas Interiores. Lisboa.

Portela, M. 2014. Da Regionalização de Informação Hidromédrica Ao Dimensionamento de Albufeiras de Regularização e à Análise de Incertezas.

Reyjol, Y., Hugueny, B., et al. 2007. Patterns in species richness and endemism of European freshwater fish. Global Ecology and Biogeography, 16, 65–75, https://doi.org/10.1111/j.1466-8238.2006.00264.x.

Rodriguez-Ruiz, A. & Granado-Lorencio, C. 1992. Spawning period and migration of three species of cyprinids in a stream with Mediterranean regimen (SW Spain). Journal of Fish Biology, 545–556, https://doi.org/10.1111/j.1095-8649.1992.tb02682.x.

Santos, J.M., Godinho, F., Ferreira, M.T. & Cortes, R. 2004. The organisation of fish assemblages in the regulated Lima basin, Northern Portugal. Limnologica, 34, 224–235, https://doi.org/10.1016/S0075-9511(04)80047-1.

Sauterleute, J.F. & Charmasson, J. 2014. A computational tool for the characterisation of rapid fl uctuations in fl ow and stage in rivers caused by hydropeaking. Environmental Modelling & Software, 55, 266–278, https://doi.org/10.1016/j.envsoft.2014.02.004.

StatSoft. 2000. STATISTICA for Windows.

Winter, J.D. 1983. Underwater biotelemetry. In: Nielsen, L. A. & Johnsen, D. L. (eds) Fisheries Techniques. Bethesda, Maryland, American Fisheries Society, 371–395.

3.5 Freudenau

At Freudenau VERBUND will investigate the orientation of potamodromous fish and implications for the positioning of the fishway entrance using the method of numerical modelling of coupled hydro-thermo-chemical-mechanical cues. These results will be combined with the results and interpretations of fish swimming paths, obtained with 2D Telemetry. To identify possible locations and limitations for precise positioning of the acoustic tags and ensure a successfull mounting of hydrophones in the Danube a feasibility study is conduced prior to the 2D telemetry study.

3.5.1. Fish species

The Leitbild for the Danube at Vienna comprises 58 species including 8 key species.

Table 21: Fish ecological "Leitbild" (Leitbild according to BAW / IGF 2017); key species (l) in red, typical companion species (b) in orange, rare companion species (s) in yellow

Species	german name	type of species
Lota lota	Aalrutte	b
Squalius cephalus	Aitel	b
Thymallus thymallus	Äsche	s
Salmo trutta fario	Bachforelle	s
Barbatula barbatula	Bachschmerle	s
Barbus barbus	Barbe	l
Rhodeus amarus	Bitterling	b
Abramis brama	Brachse	l
Gymnocephalus baloni	Donaukaulbarsch	s
Phoxinus phoxinus	Elritze	s
Perca fluviatilis	Flussbarsch	b
Rutilus pigus	Frauennerfling	s
Carassius gibelio	Giebel	b
Acipenser nudiventris	Glattdick	s
Sabanejewia balcanica	Goldsteinbeißer	s
Gobio gobio	Gründling	s
Blicca bjoerkna	Güster	b
Leuciscus leuciscus	Hasel	l
Huso huso	Hausen	s
Esox lucius	Hecht	l
Hucho hucho	Huchen	l
Umbra krameri	Hundsfisch	s
Carassius carassius	Karausche	b
Gymnocephalus cernuus	Kaulbarsch	s
Romanogobio kesslerii	Kessler Gründling	s
Cottus gobio	Koppe	s
Alburnus alburnus	Laube	l
Leucaspius delineatus	Moderlieschen	s

Back to D2.2 Main index

Species	german name	type of species
Chondrostoma nasus	Nase	l
Leuciscus idus	Nerfling	l
Eudontomyzon mariae	Neunauge	s
Rutilus meidingeri	Perlfisch	s
Rutilus rutilus	Rotauge	b
Scardinius erythrophthalmus	Rotfeder	s
Vimba vimba	Rußnase	b
Aspius aspius	Schied	b
Misgurnus fossilis	Schlammpeitzger	s
Tinca tinca	Schleie	s
Alburnoides bipunctatus	Schneider	s
Gymnocephalus schraetser	Schrätzer	b
Alburnus mento	Seelaube	s
Barbus balcanicus	Semling	s
Pelecus cultratus	Sichling	s
Cobitis elongatoides	Steinbeißer	s
Romanogobio uranoscopus	Steingreßling	s
Acipenser ruthenus	Sterlet	s
Acipenser stellatus	Sternhausen	s
Zingel streber	Streber	b
Telestes souffia	Strömer	s
Acipenser gueldenstaedtii	Waxdick	s
Romanogobio vladykovi	Weißflossen Gründling	b
Silurus glanis	Wels	b
Cyprinus carpio	Wildkarpfen	s
Sander volgensis	Wolgazander	s
Sander lucioperca	Zander	b
Zingel zingel	Zingel	b
Ballerus sapa	Zobel	b
Ballerus ballerus	Zope	b

Number	key species (l)	8
	typical companion species (b)	18
	rare companion species (s)	32
	total	58
		58

Recent investigations (2010) of the fish fauna below the HPP (r-km 1880 - 1894) showed a good fish ecological status according to WFD compliant assessment. A total of 31 species of the Leitbild and seven species not included in the Leitbild were found. The fish biomass was about 184 kg /ha and was dominated by pike, bream, pike perch, catfish, and Giebel. The abundance was about 7.500 individuals per hectare and was dominated by bitterling, perch, roach, and rudd.

Back to D2.2 Main index

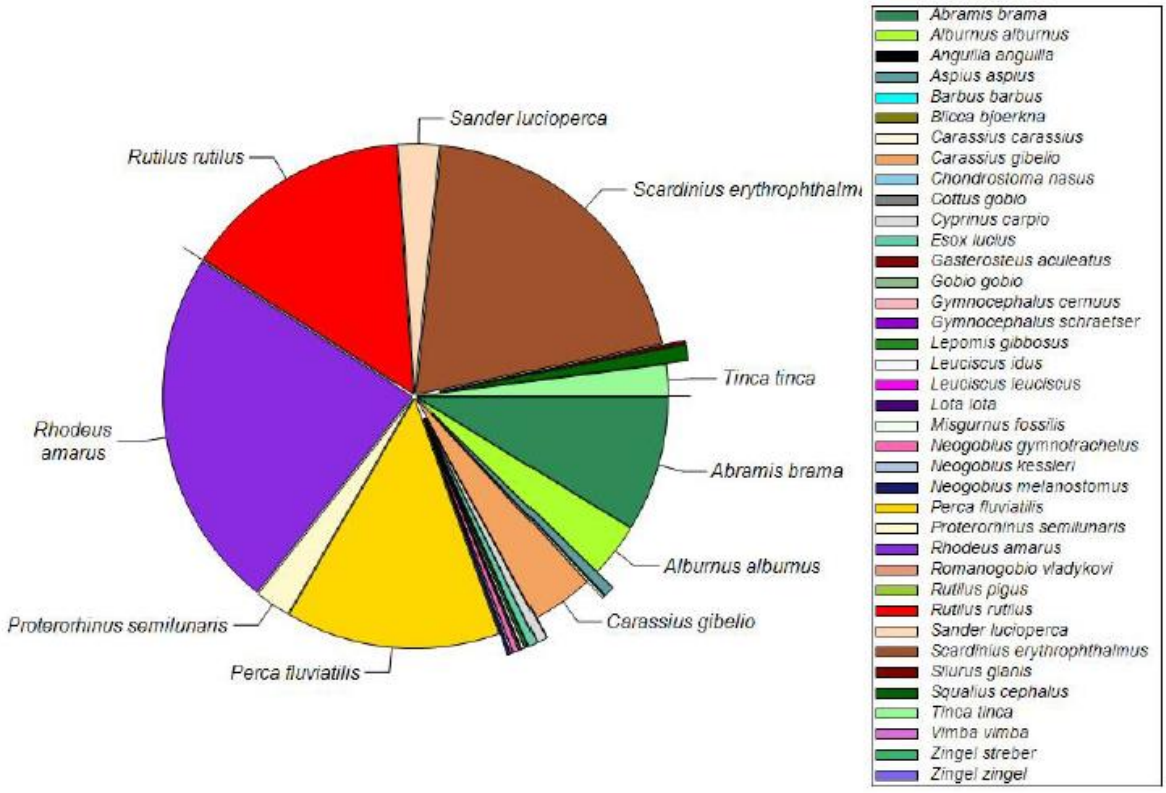


Figure 158: Relative abundance

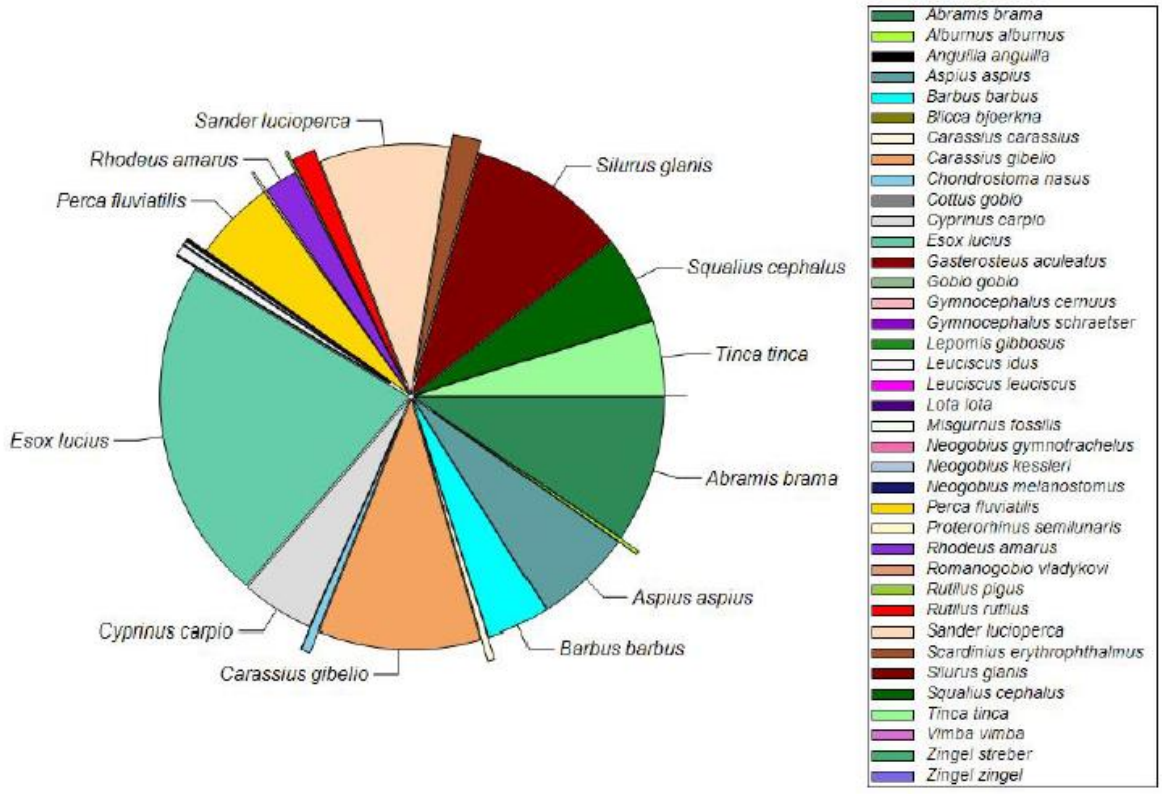


Figure 159: Relative biomass

Back to D2.2 Main index

3.5.2. Direct impacts on fish

The direct impact (turbine related impacts on survival and fitness) on fish populations depend on characteristics of the turbine with size and rotational speed being most important and on the species and size of fish under consideration, their behaviour with regard to migration, and their life history.

The turbine at Freudenau is one of the largest in Europe with a diameter of 7.5 m and a rotational speed of 65 rpm. Blade strike models predict turbine related injuries for small size classes (10-15 cm) in a range of <1-2 % and for spawning large sized fish (30-40 cm) in the range of 5 – 10 %.

At the Test Case Freudenau, no diadromous species are present. Most (> 90 %) of the down-migrating potamodromus fishes in rivers are larvae and juvenile with a total length < 15 cm (e.g. Pavlov 2002, Schmalz & Schmalz 2006, 2007, Schmalz 2010, Holzner 1999, Gubbels 2010, 20111012, 2013, Edler et al. 2011). These have a great chance of passing turbines without injuries due to blade strike. Of the various mechanisms believed to be responsible for injuries to fish during turbine passage, strike by turbine runner blades is one of the most predominant (Ploskey and Carlson 2004).

Only a small proportion of adults ever pass turbines and passage over several turbines is extremely unlikely. When considering published home range sizes and the size of the impoundments on the Austrian Danube the proportion of adult fish passing a turbine per year can be estimated at <5 %. Although some potamodromous fish species are able to migrate over large distances (see the literature survey on migration, D2.1), the average migration distances and home ranges of adult fish are relatively small. For the barbel a median home range size between two (2) and eleven (11) km is documented (Oviedo et al. 2007, Lucas & Frear 1997, Steinmann et al. 1937, Twine 2013), for the European grayling between one (1) and 16 km (Junge et al 2014, Heggenes et al. 2006, Ovidio et al. 2004), and for the nase between three (3) and nine (9) km (Ovidio & Philippart 2008, Huber & Kirchhofer 1998, Ovidio et al. 2012, Steinmann et al. 1937, Wagner 2010). The home range sizes are largely species specific but also differ between rivers. It seems that migration distances are smaller in natural and nature-like rivers providing high habitat heterogeneity and larger in channelized rivers. Although the investigated rivers differed in fragmentation, this parameter was only of minor importance for the median home range but had an effect on so called « strayers », i.e. the fish in the population which showed the largest home ranges and migration distances respectively.

Under these assumptions with regard to turbine encounter probability and turbine related injuries, effects on the population level caused by turbines are presumably <<1 % for larvae and juveniles and <<0.5 % for adults of the long distance migrating potamodromous guild.

The relationship between habitat heterogeneity and migration (and drift) distances is also a possibility to reduce the probability of turbine encounter for potamodromous fish, i.e. management measures to improve habitat conditions may lead to reduced home ranges (and drift distances) and thereby reduce the turbine encounter probability. Contrary to guidance structures this effect is not limited to size classes physically excluded by the bar spacing but also effects larval and juvenile fish.

At Freudenau several habitat measures have been implemented upstream and downstream of the power plant. Additionally, the nature-like bypass channel provides valuable habitat. All

these measures mitigate turbine related impacts on survival and fitness by reducing the probability of turbine encounter significantly.

3.5.3. Measures for habitat improvement

During the construction of the HPP Freudenau, the previously straight shoreline was reconstructed by creating backwaters, coves, gravel banks, and pools and thereby provide ecologically functional habitats for a wide range of species including fish and also different life stages.



Figure 160: Constructed shallow water areas (r-km 1936) out of gravel have a high ecological value especially for rheophilic fish species.

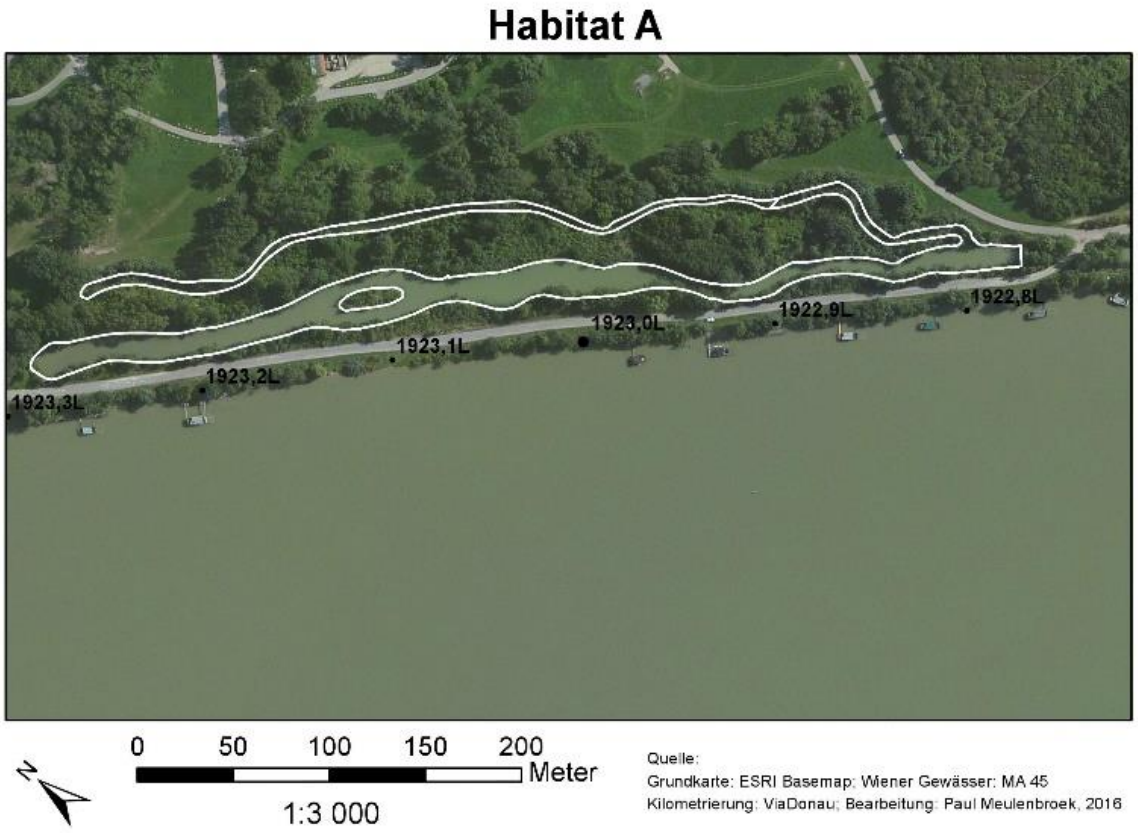


Figure 161: Side arm (r-km 1923).

Back to D2.2 Main index

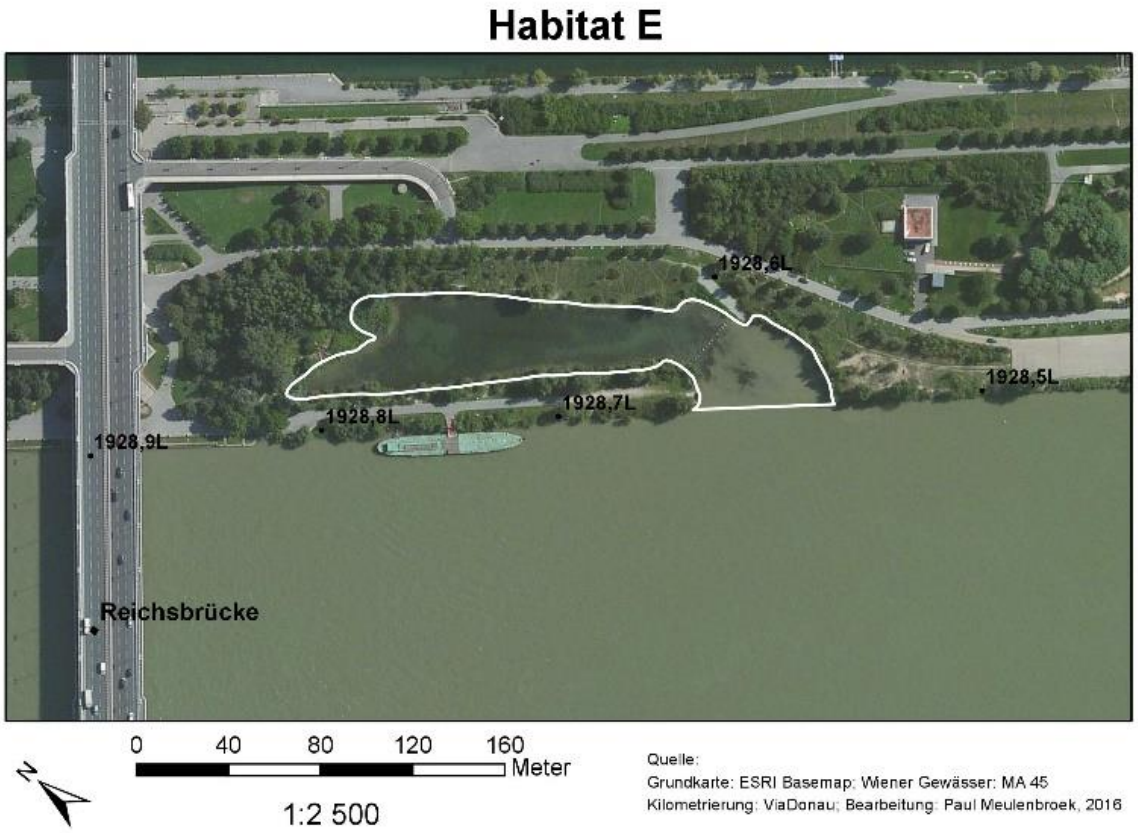


Figure 162: Artificial back-water (r-km 1928.5).

Monitoring results show their value for amphibians (Cabela et al. 2003), fish (Straif et al. 2003, Meulenbroek et al. 2018a), benthic invertebrates (Straif et al. 2003), odonates (Raab 2003a), reptiles (Cabela & Teufl 2003), and water fowl (Raab 2003b).

For instance, 44 species of waterbirds,six gulls, twelve amphibian species including the Danube Crested Newt (Triturus dobrogicus), 29 species of dragonflies including Leucorrhinia pectoralis one of Europeans most threatened dragonfly species and listed in Annex II of the Habitats Directive were observed. N. natrix uses the newly created structures at the Danube's bank for foraging, and L. agilis has established several small populations there.

The fish population structure and abundances showed an astonishing diversity (Straif et al. 2003). The central part of the impoundment and the transition area were characterised by an euryoecious and a stagnooecious fish species composition. The head of the impoundment was dominated by the two Danube fish species Chondrostoma nasus and Barbus barbus. Particularly a high abundance of juvenile fishes and larval stages were caught in the new structured habitats at the left Danube shoreline.

During a recent investigation of larval and juvenile fish (Meulenbroek et al. 2018a) about 15,000 fish larvae were trapped, and a subsample was determined to species level by DNA barcoding. In total, 26 different species were detected, including 10 species that are endangered or in danger of extinction. When species composition was considered, cyprinids become dominant at sites downstream of gravel bars, whereas in riprap sections, the majority

Back to D2.2 Main index

of the larvae consist of invasive Gobiidae. Side arm habitats provide spawning and nursery grounds for additional species. Furthermore, clear species-related seasonal patterns were observed with peak densities and multiple spawning periods of some species being recorded. The largest peak of Percidae occurred in the first half of May, followed by Cyprinidae at the end of May and Gobiidae in mid-June.

3.5.4. Use of bypass channel

(Excerpt from Meulenbroek et al 2013b)

The by-pass system consists of two major components, namely, a near-natural by-pass channel and a near-natural pool pass. The entrance is about 500 m downstream of the weir, with a delta system in the tailwater that has calm, shallow waters over some 200 m with two permanent wetted channels. The subsequent semi-natural by-pass channel has an average slope of 0.7% and is situated in a 7 m wide riverbed with and an average current speed of 0.6 $m.s^{-1}$. The first 160 m are straight, followed by a 300 m-long meandering section and a 140 m long branched section. One of the branches is blocked by a beaver dam and has calm to stagnant water. The remaining section of 170 m up to the weir is straight again. The total length of this free-flowing section is 1000 m. The channel bottom consists of gravel and sand; some rifle-pool sequences are developed and very dense riparian vegetation has been well established, consisting mainly of willows and alders. The uppermost part of the system is a pool pass of 19 pools (20–40 m in length and 3–16 m in width), a water-level difference of 11 cm from pool to pool, and a total length of 420 m. It is characterised by a pool depth of 1.5 m, different flow conditions, and a high abundance of reeds and macrophytes.

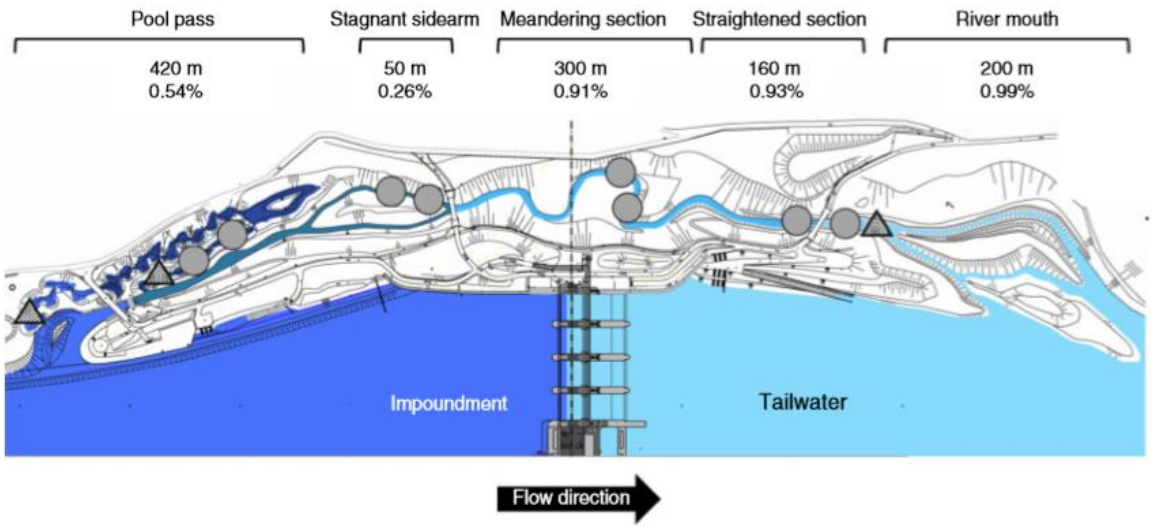


Figure 163: Fish by-pass system Freudenau. Triangles indicate fish larvae sampling points, circles indicate electrofishing points; length of the sections (m) and slope (%) are given beneath each section name (from Meulenbroek et al. 2018b, adapted after Eberstaller et al. 2001).

The chosen nature-like construction of the by-pass system functions like natural tributaries. More than 17 000 fish and 43 species, including several protected and endangered species, in all life stages, including eggs, larvae, juveniles and adults, were captured. Furthermore, the indicator species of the free-flowing Danube, nase (Chondrostoma nasus) and barbel (Barbus barbus), migrated into the fish by-pass and successfully spawned before returning. Therefore,

Back to D2.2 Main index

our results suggest that by-pass systems can function as an important habitat for the conservation of native fish fauna. The heterogenic habitat configuration provides conditions for all ecological guilds and, consequently, increases biodiversity.

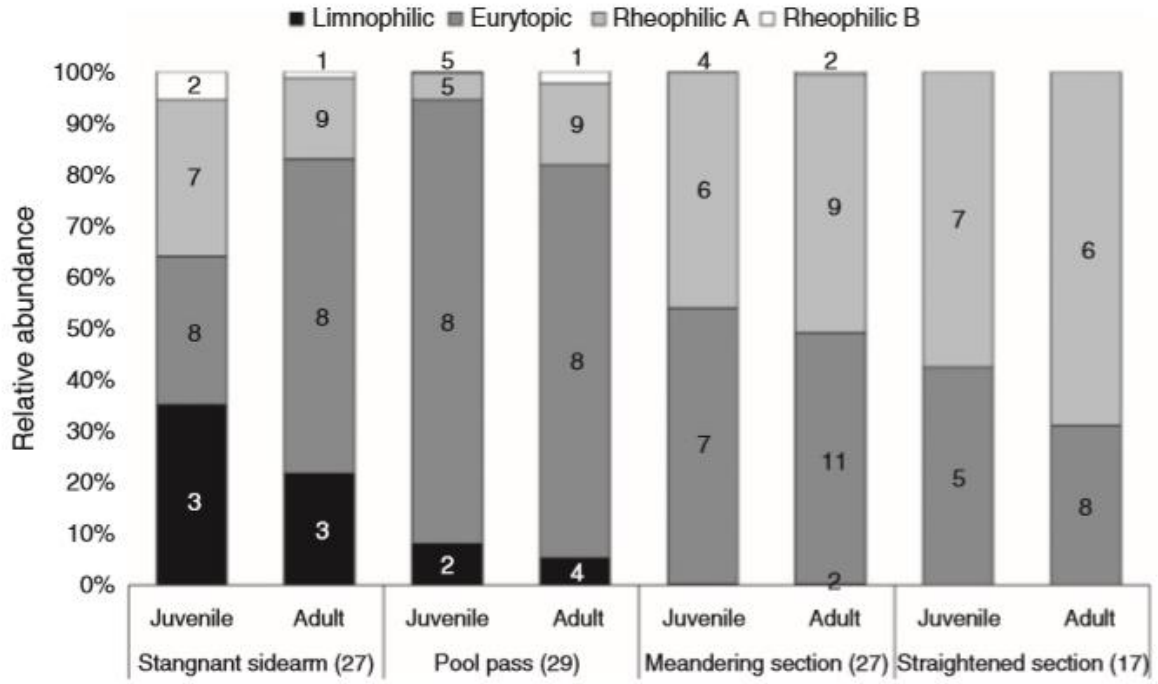


Figure 164: Relative abundances of flow guilds and number of species for the given sections. Bars indicate relative abundance of flow guilds for juvenile and adult of all caught fish; numbers within each category show the number of species per guild; numbers in parentheses indicate the total number of species per section (from Meulenbroek et al. 2018b).

Back to D2.2 Main index

3.5.5. Feasibility study for the investigation of fish migration paths with acoustic telemetry

The case study “Freudenau” aims to investigate the migration paths of key species in the Danube River at the Freudenau fish-pass. The ultimate goal is to set up a 2D telemetry survey to delineate migration routes and behaviour of monitored species. 2D telemetry is the best method to assess the behaviour of fish with a precise resolution of time and location (Silva et al., 2017).

The implementation of 2D arrays within a study area is a complex process. Hydrophones and acoustic tags react specifically to an environment and therefore need a precise and well developed setting. The functionality of a hydrophone-array depends on abiotic factors including topography, temperature, salinity, turbidity or discharge (Bergé et al., 2012). Additionally, turbulences and noise by ships, sediment transport or other sources influence the detection quality of tags in a negative way. Supersaturated water due to hydropower operation and high flow velocities additionally require precise knowledge of the functionality of the technology to be aware of the position-finding success. The development of a suitable hydrophone-array requires to run several trials with different hydrophone densities and positioning (Kraus et al., 2018).

Up to now, no experiences exist on establishing 2D telemetry arrays in the River Danube. Preliminary tests are therefore inevitable to identify local possibilities and limitations for the precise positioning of acoustic tags. The tests will be carried out at different locations in the proximity of the fish pass. The main focus is on the complex structural situation characterized by obstacles such as groynes or the high topographical heterogeneity next to the fish-pass. In addition to the functional testing of the technology and the identification of suitable arrays, solutions need to be developed to successfully mount hydrophones in the Danube. The local conditions downstream of the Freudenau power plant are characterized by high water velocities, high turbidity, obstacles, and intensive navigation. The installation of hydrophones, therefore, requires a comprehensive development phase and close cooperation and coordination with the competent authorities.

The feasibility study started in 2018 and will be finished in Q4 2018. The test series upstream of the power station Freudenau have been completed in December. Several hydrophone arrays were tested close to the influx building Langenzersdorf (see Figure 165). The applicability of the acoustic system in the Danube River could positively be tested. Satisfying positioning results could be obtained using up to six hydrophones and test tags (Figure 165).



Figure 165: Test array using six hydrophones close to the influx building Langentzersdorf. Yellow dots indicate the positive positioning of a test tag. The dots describe the path of the test tag. Hydrophones are indicated by blue squares.

Since December 2018 preparations were undertaken to start with the test series at the power station Freudenau. In a first step, a hydrophone array was conceived. Mounting devices were developed for hydrophones in the free water column as well as for hydrophones attached to the power plant (Figure 168). The test series started on January 30th 2019 with the installation of the devices. The first tests will be finished by the 6th of February 2019. Within that week test tags are dragged in the investigation area to generate positioning data. First results about the functionality will be perceived by mid-February.



Figure 166: Test array power station Freudenau. Eight hydrophones are tested in the proximity of the power station to test the positioning success with test tags.

A metal construction was developed which should be used for the longer deployment of hydrophones. The design allows that the hydrophones sit in perfect operating position and are protected from suspended load (Figure 167). Throughout February/March 2019 the deployment of the construction will be tested in the Danube. Negotiations with the responsible authorities will be carried out in February/March to retain necessary permissions for the deployment.



Figure 167: Mounting construction for open water hydrophones.



Figure 168: Mounting construction for the deployment at the power station

Back to D2.2 Main index

3.5.6. Hydraulic modelling with coupled diffusion models for temperature and chemicals

- A digital elevation model of the Danube and the fishway has been compiled as a basis for the hydraulic model.

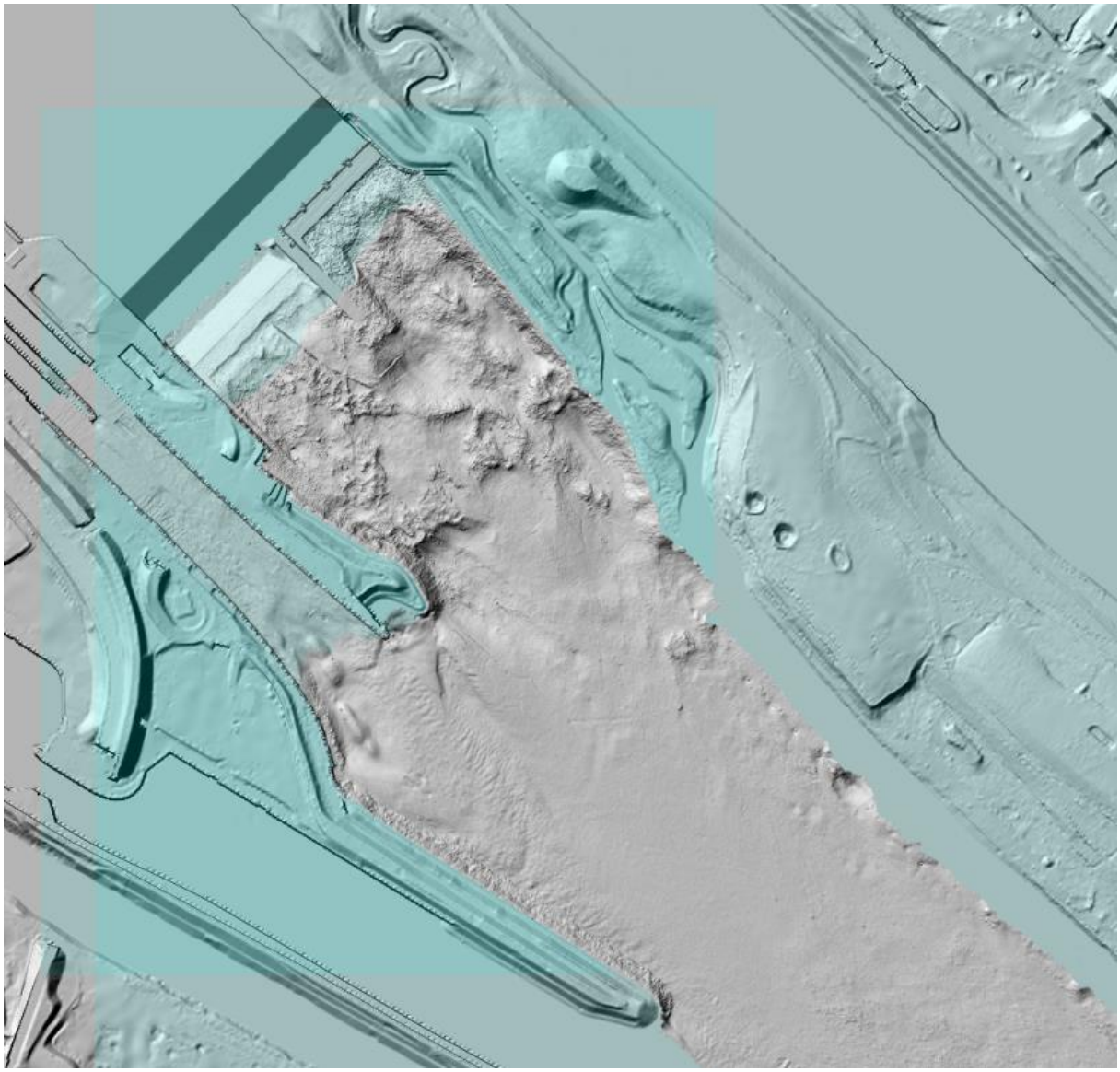


Figure 169: Digital elevation model of the Danube below the HPP Freudenau and the fishway

- Turbine data has been compiled as a basis for the hydraulic model
- Temperature and flow data have been compiled for model calibration
- Hydraulic and diffusion modelling is planned for 2019

3.5.7. Investigation and interpretation of fish swimming paths

- Planned for 2019/2020

3.5.8. References

Cabela, A., & Teufl, H. (2003). *Auswirkungen der Neugestaltung des Donauufers (Stauraum Freudenau) auf die Ausbreitung von Reptilien auf der Wiener Donauinsel*. *Denisia 10, 143-158*.

Cabela, A., Gressler, S., Teufl, H., & Ellinger, N. (2003). *Neu geschaffene Uferstrukturen im Stauraum Freudenau und Folienteiche auf der Wiener Donauinsel: Eine Studie über ihre Wirksamkeit als Trittsteinbiotope für Amphibien*. *Denisia 10, 101-142*.

Massinger*, G., & Michlmayr, F.* (2003) *Die Uferstrukturen der Donauinsel im Stauraum Freudenau. Denisia 10, 11-25..*

Meulenbroek, P., Drexler, S. S., Rauch, P., Geistler, M., & Waidbacher, H. (2015). Session B5: The Danube Fish Bypass System of Vienna/Freudenau and its Importance as a Lifecycle Habitat.

Meulenbroek, P., Drexler, S., Huemer, D., Gruber, S., Krumböck, S., Rauch, P., ... & Waidbacher, H. (2018a). Species-specific fish larvae drift in anthropogenically constructed riparian zones on the Vienna impoundment of the River Danube, Austria: Species occurrence, frequencies, and seasonal patterns based on DNA barcoding. *River Research and Applications*, *34*(7), 854-862.

Meulenbroek, P., Drexler, S., Nagel, C., Geistler, M., & Waidbacher, H. (2018b). The importance of a constructed near-nature-like Danube fish by-pass as a lifecycle fish habitat for spawning, nurseries, growing and feeding: a long-term view with remarks on management. *Marine and Freshwater Research*, *69*(12), 1857-1869.

Raab, R. (2003). Die Besiedlung neu geschaffener Uferstrukturen im Stauraum Freudenau (Wien, Niederösterreich) durch Libellen (Insecta, Odonata). *Denisia 10, 79-99*.

Raab, R. *Auswirkungen der Errichtung des Donaukraftwerkes Freudenau (Wien) auf die überwinternden Wasservogelbestände im Wiener Donauraum*. *Denisia 10, 159-179*.

Reckendorfer, W., Baranyi, C., Funk, A., & Schiemer, F. (2006). Floodplain restoration by reinforcing hydrological connectivity: expected effects on aquatic mollusc communities. *Journal of Applied ecology*, *43*(3), 474-484.

Schiemer, F., & Reckendorfer, W. (Eds.). (2000). *Das Donau-Restaurierungsprojekt: Gewässervernetzung Regelsbrunn* (Vol. 31). Verlag der Zoologisch-Botanischen Gesellschaft in Österreich.

Schiemer, F., & Reckendorfer, W. (Eds.). (2004). *Das Donau-Restaurierungsprojekt: Ökologische Auswirkungen* (Vol. 34). Verlag der Zoologisch-Botanischen Gesellschaft in Österrreich.1

Straif, M., Waidbacher, H., Spolwind, R., Schönbauer, B. and Bretschko, G. (2003) *Die Besiedlung neu geschaffener Uferstrukturen im Stauraum Wien-Freudenau (Donauinselhabitate) durch Fisch-und Benthosbiozönosen*. Denisia 10, 181-214.

Silva, A. T. et al., 2017. The future of fish passage science, engineering, and practice. Fish and Fisheries, 27 February, pp. 1-23.

Bergé, J. et al., 2012. Probability of detection and positioning error of a hydro acoustic telemetry system in a fast-flowing river: Intrinsic and environmental determinants. Fisheries Research, 5 February, pp. 1-13.

Kraus, R. T. et al., 2018. Evaluation of acoustic telemetry grids for determining aquatic animal movement and survival. Methods in Ecology and Evolution, 19 January, pp. 1489-1502.

Ploskey, G. R., & Carlson, T. J. (2004). Comparison of Blade-Strike modeling results with Empirical Data. U.S. Department of Energy under Contract DE-AC06-76RL01830

Ovidio, M., Parkinson, D., Sonny, D., & Philippart, J. C. (2004). Spawning movements of European grayling Thymallus thymallus in the River Aisne (Belgium). Folia Zoologica, 53(1)

Heggenes, J., Qvenild, T., Stamford, M. D., & Taylor, E. B. (2006). Genetic structure in relation to movements in wild European grayling (Thymallus thymallus) in three Norwegian rivers. Canadian Journal of Fisheries and Aquatic Sciences, 63(6), 1309-1319.

Junge, C., Museth, J., Hindar, K., Kraabøl, M., & Vøllestad, L. A. (2014). Assessing the consequences of habitat fragmentation for two migratory salmonid fishes. Aquatic Conservation: Marine and Freshwater Ecosystems, 24(3), 297-311.

Ovidio, M., & Philippart, J. C. (2008). Movement patterns and spawning activity of individual nase Chondrostoma nasus (L.) in flow-regulated and weir-fragmented rivers. Journal of Applied Ichthyology, 24(3), 256-262.

Huber, M., & Kirchhofer, A. (1998). Radio telemetry as a tool to study habitat use of nase (Chondrostoma nasus L.) in medium-sized rivers. Hydrobiologia, 371, 309-319.

Steinmann P., W. Koch and L. Scheuring 1937. Die Wanderungen unserer Susswasserfische dargestellt auf Grund von Markierungsversuchen. – Z. f. Fischerei, 35: 369-67.

Wagner (2010) Fischökologisches Monitoring im Rahmen des EU-LIFE-Projekts "Vernetzung Donau Ybbs“ mit Hilfe der Radiotelemetrie

Twine K.G. 2013 Conservation of barbel (Barbus barbus) in the River Great Ouse. Thesis,University of Hull

3.6 Gotein

3.6.1. Efficiency of downstream migration devices

3.6.1.1. Methodology

In 2016, a study was led by the French Agency for Biodiversity in order to assess the efficiency of Gotein's downstream migration device for Atlantic salmon smolts (Tomanova, et al., 2018).

3.6.1.1.1. Technology

The fishes are tracked with the PIT-Tag technology and detected with RFID antennas.

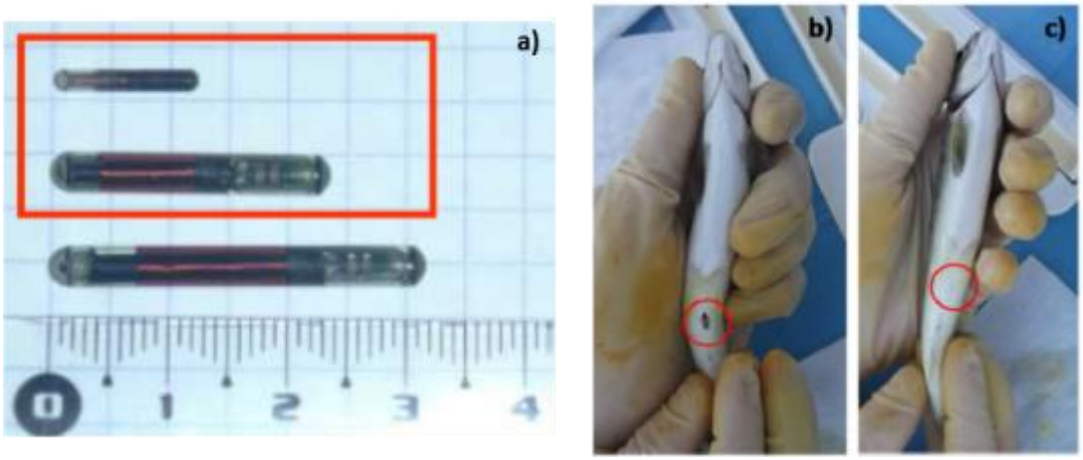


Figure 170: Tagging of fishes a) mark of 23 mm used b) and c) surgical insertion of the mark in the fish (source: (Tomanova, et al., 2018)).

The fishes were marked between the 29th and the 30th of March 2016 at the fish farm of Castels. The fishes were anaesthetized with eugenol for the surgery. The 11th of April they were moved to Trois-Ville and stabled in a pool with non-stop renewing of water.

6 batches of 50 to 52 fishes were released between 18h and 00h 100m upstream the power plant, in the headrace channel, see Table 22.

Table 22: Number of fishes and their size for each batch, date and time of release on Gotein's site (source : (Tomanova, et al., 2018)).

Batches	Number of fishes	Date of release	Time of release		Size (mm)			
					Average	Standard deviation	Min	Max
GOT_L1	50	12/04/2016	19:45	evening	188.0	8.0	171	202
GOT_L2	50	12/04/2016	22:40	night	188.0	11.4	158	212
GOT_L3	50	13/04/2016	00:40	night	186.5	10.9	155	211
GOT_L4	50	13/04/2016	18:37	evening	186.8	12.6	152	209
GOT_L5	50	13/04/2016	22:38	night	185.0	11.9	150	213
GOT_L6	52	14/04/2016	00:17	night	186.1	11.6	165	220

Back to D2.2 Main index

3.6.1.1.2. Set of detection antennas

Three antennas were installed in the downstream migration channel (metal) downstream the control weir and one in the resting pool of the fish pass, see Figure 172. The eel-pass was screened in order to avoid the smolts to enter it. If the fish is detected by an antenna in the downstream migration channel it means that it took this way of passage. The efficiency of the antennas in the channel was tested. 20 fishes were released one by one in the channel, then two groups of 5 fishes were released in the channel.

Table 23: Detection efficiency (%) of the antennas in the downstream migration channel (source: (Tomanova, et al., 2018)).

	test ind20	test gr5-1	test gr5-2
EXU1	100	80	80
EXU2	100	80	60
EXU3	100	40	100
EXU1+2+3	100	80	100

The efficiency decreases when several fishes go through the channel at the same time because of the collision between marks but the results after aggregation of detection of the three antennas shows that they are still satisfactory. We supposed that every fish going through the channel will be detected by the antennas.

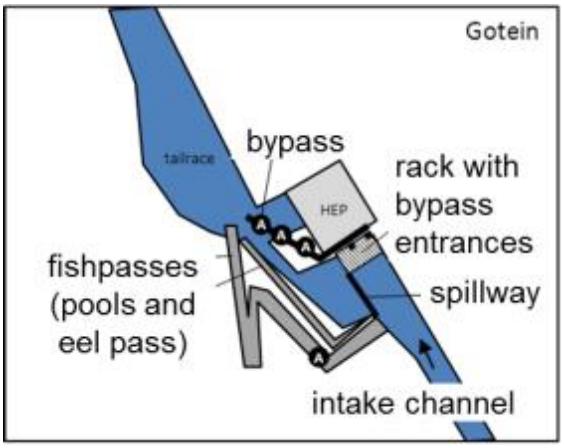


Figure 171: Schematic representation of the HPP and the antennas

Back to D2.2 Main index

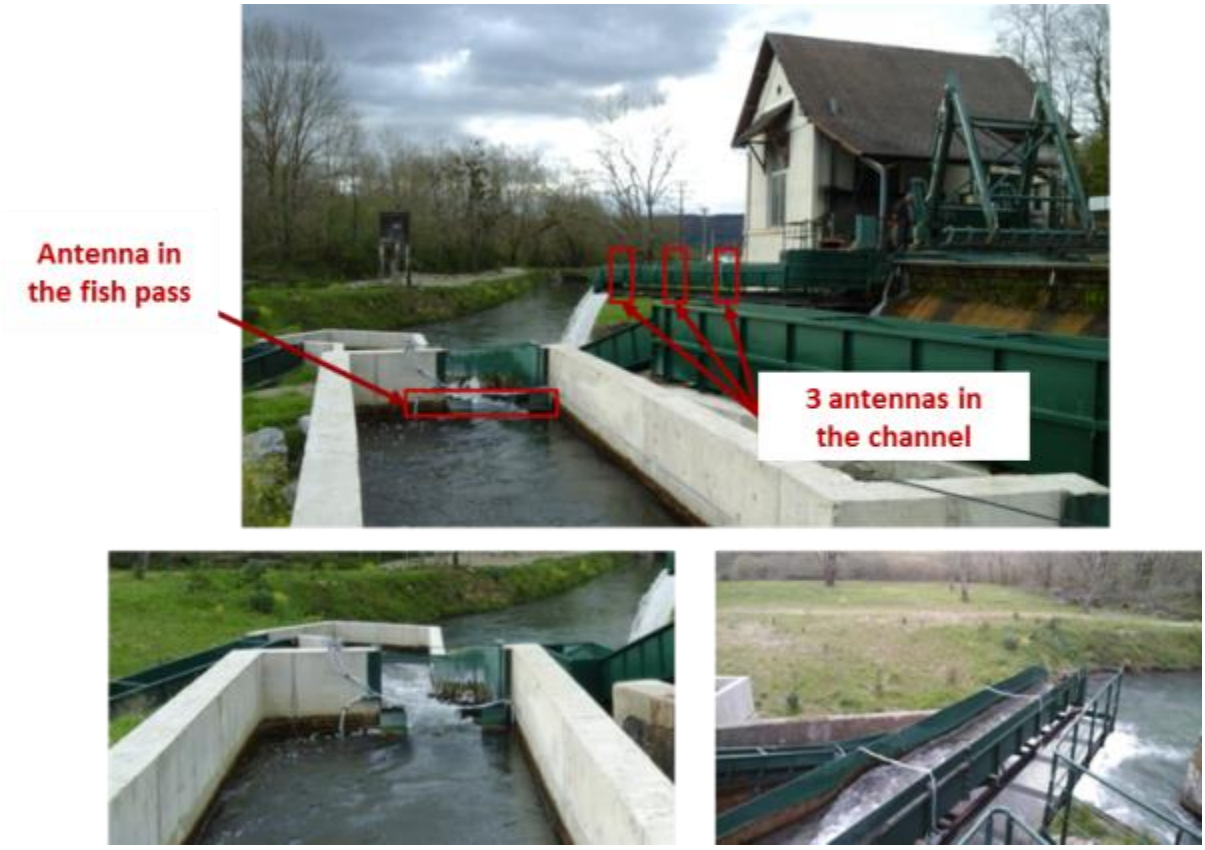


Figure 172: Pictures of the HPP and location of the antennas (source: (Tomanova, et al., 2018)).

It was not possible to directly detect the fishes going through the rack and therefore through the turbine. In a worst case scenario, we will consider that all non-detected fishes went through the turbine.

3.6.1.1.3. Hydrology of the Saison during the study

During the 5 days after the first release, the discharge varied between 29 and 46 m^3/s. Most of the fishes went downstream during this period. Goteins HPP worked stable, the discharge in the headrace channel is controlled at the dam. An ADCP measurement the 19th of Mai revealed a discharge of 6.7 m^3/s in the headrace channel and 0.35 m^3/s in the downstream migration channel.

3.6.1.2. Results

In average 80.9% of the fishes went through the downstream migration device and 2% used the fish pass, see Table 24. The efficiency is bigger for the fishes released in the evening: the difference is between 13 and 22%.

Back to D2.2 Main index

Table 24: number and distribution of detected or non-detected fishes in the different ways at Gotein (in blue: batches released in the evening) (source: (Tomanova, et al., 2018)).

Batch	Total of released fishes	Number of non detected fishes	Number of fishes detected in		Percentage of fishes detected in		Total percentage of fishes safely transfered downstream
			bypasses	fish pass	bypasses	fish pass	
GOT_L1	50	0	50		100	0	100
GOT_L2	50	11	38	1	76	2	78
GOT_L3	50	10	39	1	78	2	80
GOT_L4	50	5	44	1	88	2	90
GOT_L5	50	14	36		72	0	72
GOT_L6	52	12	37	3	71.2	5.8	76.9

A statistical test (Student test) was run in order to detect an eventual difference of size between fishes taking the downstream migration device or non-detected. The mean size of fishes taking the downstream migration device (188 mm) is bigger than the one non-detected (180.1 mm). The student test revealed that this difference is significant, see Figure 173. That means that the bar rack is more efficient for bigger fishes.

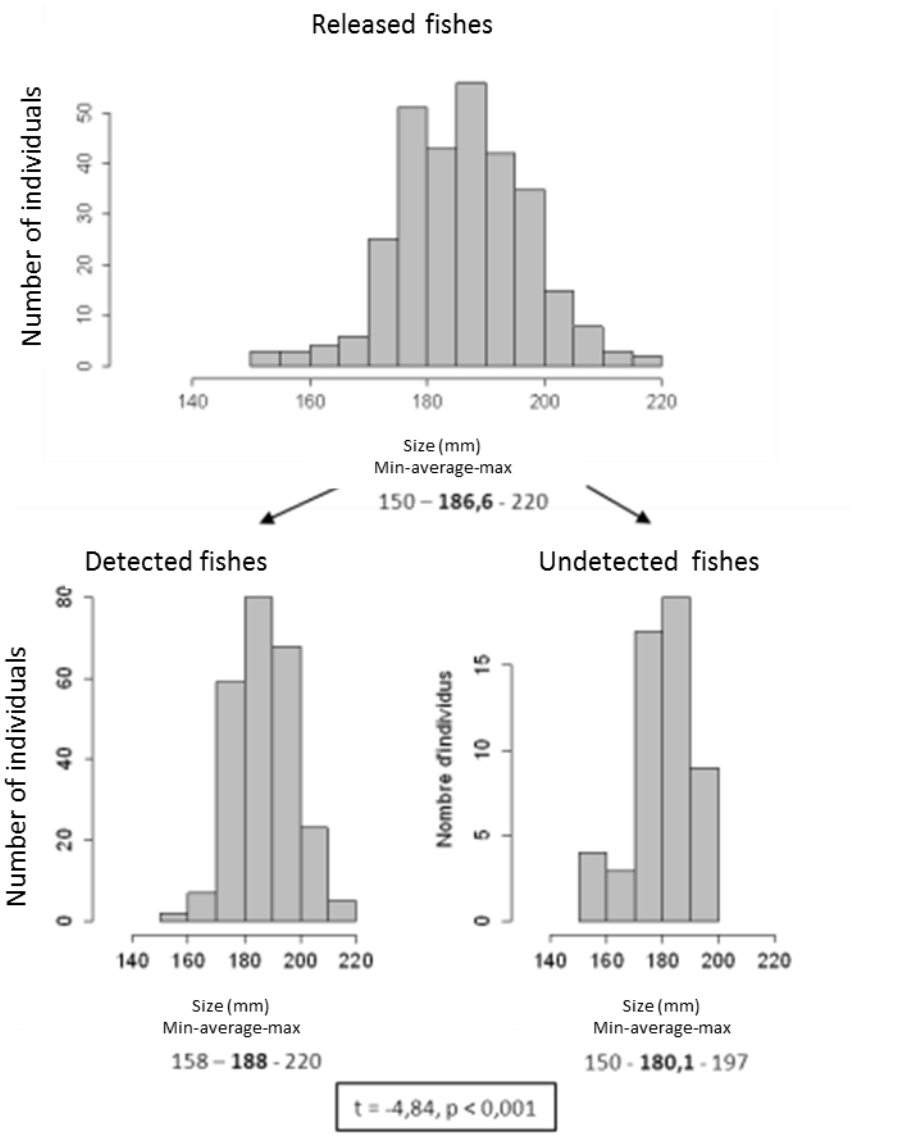


Figure 173: Distribution of released fishes' size, non-detected fishes' size and detected in the downstream migration channel fishes' size (source: (Tomanova, et al., 2018)).

The timing was also studied. For all batches, the first detections happened between 3 and 8 minutes after release. 50% of fishes take less than 20 minutes to circumvent the power plant through the downstream migration device, 75 % need less than 1h08, see Table 25. The timing passage is longer for the fishes released in the evening than at night.

Table 25: Timing of passage of smolts for the different batches, in grey the batches released in the evening (source: (Tomanova, et al., 2018)).

	Nb d'ind.	min	Q25	mediane	Q75	max
LOT1	50	0:06:35	0:14:48	0:51:29	1:57:16	187:33:21
LOT2	38	0:08:17	0:13:51	0:20:32	0:41:12	6:05:32
LOT3	39	0:03:25	0:07:02	0:11:53	0:19:57	1:31:24
LOT4	44	0:05:31	0:18:17	0:37:19	1:25:03	44:48:44
LOT5	36	0:03:47	0:10:56	0:19:45	0:53:25	52:22:36
LOT6	37	0:05:55	0:13:00	0:18:27	0:35:38	108:06:54
Total	244	**0:03:25**	0:12:05	**0:19:59**	**1:08:13**	187:33:21

3.6.1.3. Conclusion

The efficiency of the downstream migration device at Goteins HPP is **80.9 %.**

Taking into account the new efficiency of the infrastructure, the global survival rate can be updated, see Table 26.

Table 26: Summary of the distribution of fishes among the different ways, passage rate through turbines (this study) and their mortality rates (according (Voegtlé, 2010)), and global passage efficiency taking into account passage over the spillway, the downstream migration device and survival after passage through turbines (Tomanova, et al., 2018).

Dam		Power plant			**Total survival rate at Gotein**
Proportion (%) of fish passing over the spillway of the dam	Proportion (%) of fish led to headrace channel	Proportion (%) of fish passing through the turbine	Mortality through the turbine (%)	Proportion (%) of fish assumed dead due to passage through the turbine	
32.4	67.6	11.61	11	1.28	**98.72**

The global survival rate of Gotein is 98.72% which is not perfect but is considered satisfactory.

3.6.2. Characterization of the flow repartition between the 2 bypass entrances



Figure 174: Upstream view of the water intake and the two bypasses

Thanks to the law of spillways and the DEVER tool, developed by the AFB, the discharge over the control weir was calculated (see Table 27). Two water levels upstream the control weir were measured, one before the measurements in the bypass and one after.

Table 27: Calculation of the discharge over the weir

Parameter	1rst value, before the measure in the bypass	2nd value, after the measure in the bypass	Unit
Water level upstream the control weir (under the gate)	0.55	0.58	m
Floor level upstream the control weir	0.08	0.08	m
Width of downstream migration channel	0.9	0.9	m
Width of control weir	0.9	0.9	m
Water height upstream the control weir (under the gate)	0.47	0.5	m
Flow cross-section upstream the control weir (under the gate)	0.423	0.45	m²
Level of the control weir	0.23	0.23	m
Head on the weir	0.32	0.35	m
Discharge calculated by the DEVER tool	**0.326**	**0.376**	**m3/s**
Mean value	**0.351**		**m3/s**
Flow velocity upstream	0.771	0.836	m/s

The mean value allowed to downstream migration is 0.351 m^3/s.

Measurements in the bypass channel were also done downstream the first outlet thanks to a current meter. The discharge after the first outlet is 0.144 m^3/s. By subtraction, the discharge passing through the second outlet is 0.207 m^3/s.

Back to D2.2 Main index

Table 28: Distribution of discharge in the different outlets

		Value (m^3/s)	Proportion	Mean flow velocity in the outlet (considering H = 0.5 m and L = 0.8 m)
Discharge Outlet 1	Measure	**0.144**	**41.1%**	0.36
Discharge Outlet 2	Subtraction	**0.207**	**58.9%**	0.52
Total discharge	Spillway law	**0.351**	100.0%	

3.6.3. Hydraulic modelling of the fishfriendly water intake

The modelling will be done after the validation of the model developed in the WP3 this year for calculating the flow upstream the trashrack and the attractiveness of the bypasses.

3.6.4. References

Tétard, S., Tomanova, S., Courret, D., Sagnes, P., Alric, A., De Oliveira, E., . . . Frey, A. (2017). The efficiency of inclined and oriented racks to prevent Atlantic salmon smolts from entering turbines. International Conference on Engineering and Ecohydrology for Fish Passage. June 19th, 2017 - Corvallis.

Tomanova, S., Courret, D., Alric, A., De-Oliveira, E., Lagarrigue, T., & Tétard, S. (2018). Etude d'efficacité des exutoires associés à des grilles inclinées ou orientées pour la dévalaison des smolts de saumon atlantique - Etudes 2016 et synthèse des résultats 2015-2016. AFB - EDF - ECOGEA.

Voegtlé, B. (2010). Simulation des mortalités induites par les aménagements hydroélectriques lors de la migration de dévalaison des smolts de saumon atlantique. Rapport ECOGEA E080501.01.

3.7 Guma and Vadocondes

3.7.1 Population and habitat analysis

An assessment in terms of fish species and population structure of the river section affected by both HPPs will be done to provide reliable information of the fish population status. The study will focus mainly on cyprinid fishes, which are the dominant group in the study reach, and also in endemic species.

3.7.1.1 Methodology

The information will be collected from literature as well as on site by:

- The review of previous studies and data in historic, national and regional databases.
- Fish samples in the vicinity and in the two fishways. Fish samples have been done from May 2018 to date with electrofishing equipment (Hans-Grassl ELT60II backpack equipment) in the 60 m river length downstream of both fishways (Figure 175) with a sampling frequency of twice a month. In addition, fish sampling with nets has been carried out in the fishways, closing the upstream gate and taking out all the fish inside. All fish were put in holding tanks with oxygen supply until they were identified and measured (species, fork length, weight, sex and others). To manipulate fish, eugenol was used as an anaesthetic agent (variable dose depending on the species and water temperature). After fish recovery, they were released in their capture zones. Those species declared by the Spanish law as alien species were killed following the law and ethical guidelines about research with animals.



Figure 175: Electrofishing sample downstream of Guma fishway

3.7.1.2 Results

A brief summary of the main preliminary results on population analysis is presented in Table 29, Table 30 and

Back to D2.2 Main index

Table 31.

Table 29: Fish species of the study area (based on literature and previous studies review as well as during the fish samples).

Family	Scientific name	Status
Aguillidae	*Anguilla anguilla*[2]	Extinct native
Centrarchidae	*Lepomis gibbosus*	Invasive exotic
Centrarchidae	*Micropterus salmoides*	Invasive exotic
Cyprinidae	*Achondrostoma arcasii*[1]	Native*
Cyprinidae	*Alburnus alburnus*[1]	Invasive exotic
Cyprinidae	*Carassius auratus*[1]	Exotic
Cyprinidae	*Cyprinus carpio*	Invasive exotic
Cyprinidae	*Gobio lozanoi*[1]	Exotic
Cyprinidae	*Luciobarbus bocagei*[1,2]	Native
Cyprinidae	*Phoxinus bigerri*	Exotic
Cyprinidae	*Pseudochondrostoma duriense*[1,2]	Native*
Cyprinidae	*Squalius carolitertii*[1]	Native
Cyprinidae	*Tinca tinca*[1]	Exotic
Percidae	*Sander lucioperca*[1]	Invasive exotic
Poeciliidae	*Gambusia holbrooki*	Invasive exotic
Salmonidae	*Salmo trutta*[1,2]	Native

*Iberian endemism, cited at Annex II of Habitat Directive 92/43/EEC (IUCN Vulnerable).
[1]Presence confirmed by the field samples.
[2]Abundant in 1846 (Madoz, 1846).

Table 30: Preliminary results of the number of individuals captured during the samples from May to September 2018, by species and sampling point.

Species	GUMA		VADOCONDES		TOTAL
	Fishway	River	Fishway	River	
Achondrostoma arcasii	1	1	2	2	6
Alburnus alburnus	4762	1040	1753	863	8418
Carassius auratus	-	1	-	-	1
Gobio lozanoi	144	146	58	1158	1506
Luciobarbus bocagei	589	48	160	251	1079
Pseudochondrostoma duriense	4	-	2	4	10
Salmo trutta	5	-	1	11	17
Squalius carolitertii	-	-	-	8	8
Tinca tinca	1	1	-	-	2
TOTAL	5506	1237	1976	2297	11047

Back to D2.2 Main index

Table 31: Preliminary results of the length distribution of fish by species and sampling point: median (first and third quartiles) in mm

Fork length (mm)	GUMA		VADOCONDES	
	Fishway	River	Fishway	River
Achondrostoma arcasii	94	102	88 (84 – 92)	71 (52 – 90)
Alburnus alburnus	92 (88 – 98)	77 (58 – 85)	88 (57 – 116)	75 (66 – 120)
Carassius auratus	-	77	-	-
Gobio lozanoi	78 (36 – 110)	70 (42 – 80)	72 (50 – 90)	64 (39 – 108)
Luciobarbus bocagei	130 (113 – 173)	92 (42 – 116)	117 (98 – 140)	113 (75 – 155)
Pseudochondrostoma duriense	106 (94 – 111)	-	67 (66 – 68)	58 (55 – 61)
Salmo trutta	180 (175 – 206)	-	95	70 (65 – 75)
Squalius carolitertii	-	-	-	132 (120 – 142)
Tinca tinca	-	119	-	-

Despite crayfish were not defined as target species at the beginning of the samples, due to their continuous presence, they were taken into account but noting them only qualitatively. *Pacifastacus leniusculus* and *Procambarus clarkii* (both declared as alien species) were found in Guma fishway during all samples. *Procambarus clarkii* had a peak of abundance at the end of July and *Pacifastacus leniusculus* at the end of August.

Apart from these preliminary results, other analysis will be done with the data from this experiment. Frequency, length and condition factor distribution analysis will be carried out between sample points and along the time, as indices of peak migration movements, fishway use and general state of fish population.

3.7.1.3 Conclusion

Luciobarbus bocagei and *Gobio lozanoi* are the most abundant non-invasive species in the study reach, being the remainder species in decline. Throughout all sampling months, both species have been present. *L. bocagei* was more frequently found in Guma fishway whereas *G. lozanoi* was more frequently captured in the downstream vicinity of Vadocondes fishway. Length distribution for *L. bocagei* has shown a wide range (between 30 and 425 mm of fork length) although large individuals were not found (it has been possible to visually verify their existence in close sections). Previous studies focused on this species have shown a decrease in the migration movements of the larger individuals (Bravo-Córdoba et al 2017). The historical references include *Anguilla anguilla* as a species with a remarkable presence in this area (Madoz, 1846). However, nowadays it has completely disappeared in this river reach. The brown trout (*Salmo trout*) also had a greater distribution in the past (Madoz, 1846), with occasional appearances at present. *Pseudochondrostoma duriense* deserves a special mention since it was abundant a few years ago but has been suffering an important decline (own data and personal communications of river policy, fishermen and inhabitants) in these last years.

Current fish assemblage is mainly characterized by the presence of exotic and alien species, probably due to the dominance of lentic sections as a consequence of the presence of the HPP

dams. In this regard, *Alburnus alburnus* has shown great abundance. Its continuous presence suggests that the fishways and their river vicinity could be an acceptable habitat and/or movement path for this species. In the Spanish law, this species is declared as alien species (R.D. 630/2013), with a potential risk for native cyprinids due to the competition for the habitat and the food, egg predation, and hybridization risk (SIBIC, 2014).

Regarding crayfish, both species (*P. leniusculus* and *P. clarkii*) are declared as alien species by the Spanish law (R.D. 630/2013) with a high negative impact on native crayfish (*Austropotamobius pallipes*), amphibians and fish species. This threat is mainly due to their feeding habits (depredation risk on eggs and larvae), digging behaviour (changes in sediment balance) and disease transmission (the *afanomicosis* is a lethal disease for native crayfish) (GEIB, 2011). Its temporal abundance distribution is an indicative of the use of the fishway as a migration route by these crayfish species and may be related to pre-reproductive movements (spawning period for *P. leniusculus* in autumn; Salvador, 2015). This fact makes fishways as hotspots for another alien species, the American mink (*Neovison vison)* which depredates on the crayfish (numerous excrements have been found close to the fishways).

3.7.2 Analysis of the conceptual solutions and facilities for fish migration

In order to assess the current solutions and facilities for upstream fish migrations, an evaluation of the upstream fish passage is carried out based on fish monitoring data for different seasons and different hydraulic conditions.

3.7.2.1 Methodology

A processing of previously collected data on fish ascent in the two fishways (submerged notch with bottom orifice fishway at Guma HPP and vertical slot fishway at Vadocondes HPP) related to hydrodynamics features, was done. In addition, the characterization of the swimming performance of the main native cyprinids species in the river reach was carried out in order to define their swimming abilities and limitations. Both experiments were done by telemetry. The behaviour of fish was modelled through survival analysis methods. These statistical tools are really suitable to analyse this kind of data due to their particularities: events along the time, individuals without events, repeated events along the time, competing risk events and events dependent on time-varying covariates (for more details see full publications below).

3.7.2.2 Results and conclusions

Two scientific papers have been published in indexed journals (JCR): Ruiz-Legazpi, J., Sanz-Ronda, F. J., Bravo-Córdoba, F. J., Fuentes-Pérez, J. F., & Castro-Santos, T. (2018). Influence of environmental and biometric factors on the swimming capacity of the Iberian barbel (*Luciobarbus bocagei* Steindachner, 1864), an endemic potamodromous cyprinid of the Iberian Peninsula. *Limnetica*, *37*(2), 251-265. DOI: 10.23818/limn.37.21. [In Spanish].

Abstract: This paper analyses the volitional swimming capacity of the Iberian barbel (*Luciobarbus bocagei* Steindachner, 1864) in an open flume during its migration period, in relation to environmental and biometric factors. Water temperature, flow velocity and fish length were the most important factors which affected the swimming speed of barbels and their fatigue time. Within the range of values studied, the Iberian barbel was able to maintain sprint swim speeds (> 15 BL/s) for 3-10 s, and 17-117 s in prolonged swim mode (7-15 BL/s). The results can be used as a tool for the management of barbel populations, mainly in the design of fishways.

Bravo-Córdoba, F. J., Sanz-Ronda, F. J., Ruiz-Legazpi, J., Valbuena-Castro, J., & Makrakis, S. (2018). Vertical slot versus submerged notch with bottom orifice: Looking for the best technical fishway type for Mediterranean barbels. *Ecological Engineering, 122*, 120-125. DOI: 10.1016/j.ecoleng.2018.07.019.

Abstract: When engineers and ecologists face a fishway design, many issues need to be considered, the type of fishway being the first and foremost. It is an especially complex issue in areas with species whose migratory and swimming behaviour are as yet poorly known as Mediterranean barbels. The present study focuses on the fish passage of two of the most common types of technical fishways: Vertical Slot (VS), and Submerged Notch with Bottom Orifice (SNBO). Both types were studied and compared in terms of ascent ability (as the success rate and transit time) and motivation (as the proportion of attempts and attempt rate). Ascent ability in VS and SNBO were similar: more than 90% of fish did it successfully and the median transit time to ascend 2.25 m in height was lower than 23 minutes. Fish length had an effect on ascent time, being faster the biggest ones. Motivation was greater for VS, although not seeming to have a relevant influence in passage performance. These results provide new data of fishways performance and may help ecologists and engineers with their decision making, mainly in Mediterranean areas with similar habitats and species.

3.7.3 Assessment and improvement of fish mortality in the turbines

This task will focus on the technical issues of turbines and possible adaptive solutions of operation modes (more fishfriendly operation modes). Spanish Test Case will serve as a field test for other FIThydro partners (VOITH, TUT, TUM), being SAVASA and ITAGRA-GEA collaborators on fieldwork and data analysis. Voith is working on CFD/BioPA calculations and TUT will do the BDS (Barotrauma Detection System) tests. Furthermore, Voith will use the same models and focus on different operating modes to evaluate the possibility of adapting the operation for certain time period. Finally, the results from TUT and VOITH will be provided to TUM for fish turbine mortality assessment.

3.7.3.1 Methodology

Currently, we are collaborating and following the instructions of the leading partners in this subtask. Turbine data from the two HPPs (a total of four VOITH turbines in the range of 10 to 25 m^3/s) and the HPP facilities could be used for field trials (e.g. barotrauma and lateral line probe experiments and/or changes in operation modes). Leader partners think that Guma larger turbine is the most interesting for tests.

Experiments with the barotrauma detection sensors will be conducted during full load. The objective will be to collect 30 time series data sets of the pressure, linear acceleration, rotation rate and orientation during turbine passage. An injection system consisting of vertical tubes which can be flushed using water flow will be constructed. The system will allow the BDS to be injected at locations corresponding to the bottom blade tip, the bulb centre and the blade top. If the weather allows it, additional load scenarios may also be feasible. Based on previous field experiments, one day for testing the deployment, injection system and sensory recovery will be required. Each load scenario will also require one full day of fieldwork. The data will be provided to FITHydro project partners as comma delimited text files for assessment in the BioPA model by VOITH.

In May 2018 one pre-test was done in Vadocondes HPP together with TUT staff, in order to know the behaviour of barotrauma sensors (BDS) into these facilities and for training in the

recovery of these sensors in the river. Two different sensor types and some fake probes (Figure 7) were used. The sensors were thrown just upstream the turbines while several persons distributed in the outlet channel were waiting with capture devices at the riverbanks and on a boat to recover them.

3.7.3.2 Results

At present, we are waiting for adequate flow conditions in the Duero River and combining agendas of involved partners (scheduled for completion in December 2019).

Regarding the pre-test carried out in Vadocondes HPP, all devices (sensors and fake probes) were recovered in the outlet channel between 3 and 5 minutes after the release. An example of sensor output data capture can be seen in Figure 176.

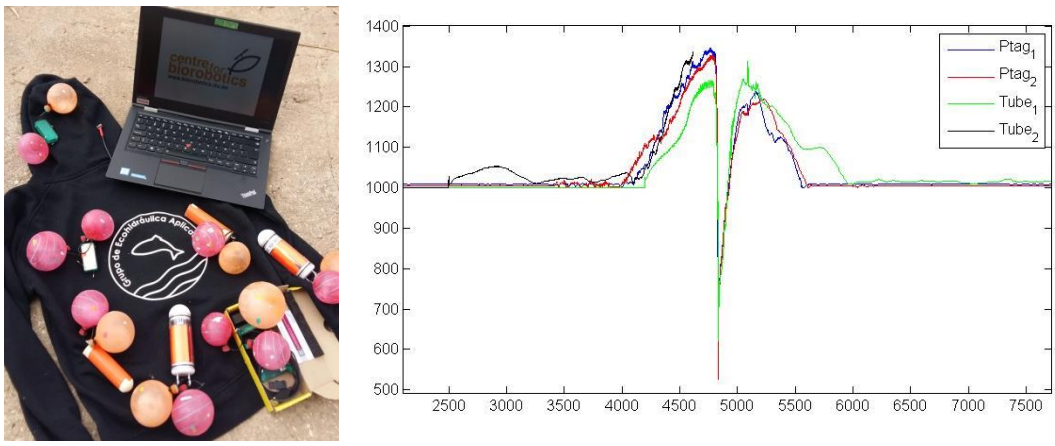


Figure 176: Left: Barotrauma sensors and fake probes with floating devices after the recovery used in the pre-test in Vadocondes HPP. Right: an example of output data of pressure (Y axis) along the time (X axis) registered by the sensors.

3.7.4 Spawning areas and hydro-morphology to attain self-sustainable populations

Spawning areas are affected by the HPP infrastructures (reservoir area) and the operational management (sediment dynamics). On this subtask, these effects would be briefly assessed.

3.7.4.1 Methodology

The study stretch was considered from Vadocondes HPP (downstream limit) up to a dam located in Guma village, upstream of Guma HPP (upstream limit) (Figure 178). The Guma village dam does not have a fishway, and it blocks the upstream fish migration.

First, visual recognitions of the study stretch were carried out, looking for the potential spawning areas during pre-spawning period (riffles with shallow water and gravel bed, during April and May 2018) for the main species of interest (native cyprinids – benthic spawners above gravel substrates).

After that, the potential spawning areas were mapped and visited several days looking for signs of spawning (fish groups, fights between fish, sign of nests, etc.).

Finally, larvae sampling was performed to confirm the spawning. These samples were done in August and September 2018 with a cone net with a mesh of 0.5 mm, doing *zig-zag* transects by foot in the river, from downstream to upstream in fast movements.

Back to D2.2 Main index



Figure 177: Potential area for spawning and cone net for trapping fish larvae.

3.7.4.2 Results

Table 31 shows the potential spawning areas within the study reach. The percentage of areas with enough conditions to serve as spawning sites was quite small, not exceeding 2% in all the study stretch (Table 32).



Figure 178: Potential spawning areas in the study reach. The downstream limit is Vadocondes HPP (section 1) and the upstream limit is the dam in Guma Village (section 2). Potential spawning areas are numerated from downstream to upstream (see table 10).

Table 32: Potential spawning areas between Vadocondes HPP and Guma village dam (see figure 9).

	Section 1	Section 2
Spawning subareas	1 = 1200 m^2 2 = 700 m^2 3 = 350 m^2	4 = 900 m^2 5 = 750 m^2 6 = 1900 m^2

Back to D2.2 Main index

Subtotal spawning areas	2250 m^2	3550 m^2
Subtotal river area	129000 m^2	283000 m^2
% spawning vs river area	1.74%	1.25%

Due to the unusual high flow conditions during the spawning period of 2018, a visual confirmation was not possible. Water level and turbidity were too high from April to July 2018, and made it impossible to see any evidence of spawning. In the previous spring (2017), it was possible to visually confirm the presence of some *L. bocagei* in the subarea number 2 with spawning behaviour.

Larvae sampling confirmed the presence of fish of the year (0^+) of different species but not in all the defined spawning areas (Table 33).

Table 33: Spawning areas (figure 9) and confirmation of fish larvae presence by species (X) for benthic spawners

Spawning areas	1	2	3	4	5	6
Achondrostoma arcasii						
Alburnus alburnus	x	x	x		x	x
Gobio lozanoi			x			x
Luciobarbus bocagei			x			x
Pseudochondrostoma duriense				x	x	x
Salmo trutta						
Squalius carolitertii						

3.7.4.3 Conclusion

The optimal potential spawning areas for native cyprinids was very small, clearly influenced by the flood storage area of Guma and Vadocondes HPP reservoirs. Also, the bed of the six potential spawning areas showed some problems of silting. Despite this, the presence of fish of the year of several species was confirmed both by larvae sampling and by periodical samples in the fishways (see

Table 31; minimum fork length of several species probably indicates fish of 0^+ age). In September 2018, with low flow conditions, it was possible to make an electrofishing sampling point just downstream of Guma village dam (that corresponds to the potential spawning area number 6. Figure 178). Although the fish were not fork length measured, the presence of fish of the year for *Luciobarbus bocagei, Pseudochondrostoma duriense, Gobio lozanoi* and *Alburnus alburnus* was confirmed, finding some big schools in the vicinity of the dam. Due to this impassable dam, the presence of these schools cannot be only attributed to a good recruitment of this point but also as a bottleneck point for fish dispersion.

Regarding the used methods for larvae sampling, for some species, this is probably not the most effective way to detect their presence. With adequate flow conditions and having

identified the potential areas, light larvae traps could be a good tool to confirm it, especially for post-hatching stages (see an example in Figure 179).

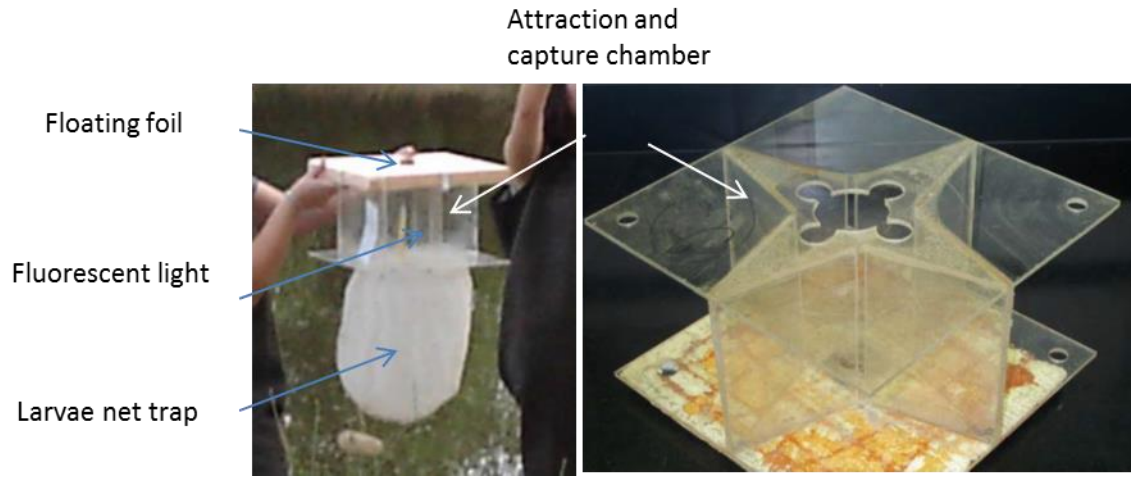


Figure 179: Fish larvae light trap. Right: bottom view of the trap without the net and the light. (modified from Pérez et al 2009)

3.7.5 Migration facilities and attraction flow

Fish passage will be analysed based on fish monitoring data and related to hydraulic variables (river and attraction devices). In particular, the attractiveness of fishway and the relationship with the river flow and operational management of HPP will be evaluated.

3.7.5.1 Methodology

Fish of direct sampling (subsection 3.7.1.) were marked with Visible Implant Elastomer (NMT®), that helps to recognize recaptures and previous location in subsequent samples (Figure 180). Fish from Guma were marked with yellow elastomer and fish from Vadocondes samples with red elastomer. In addition, fish from the fishways were marked in the dorsal fin and fish from the downstream section of the fishways were marked near the caudal fin. The first mark in a fish was done in its left side and, if a recapture happened, it was marked again but on the right side. All fish were anaesthetized before the marking procedure with eugenol.



Figure 180: Marking procedure with Visible Implant Elastomer. Left: yellow elastomer in the dorsal fin (fish from Guma fishway). Right: red elastomer near the anal fin (fish from downstream of Vadocondes fishway).

From May to October 2018, at least twice per month, native fish species (*Luciobarbus bocagei*, *Pseudochondrostoma duriense* and *Squalius carolitertii*) were PIT tagged. They were captured in different places downstream and upstream of the fishways and they were also released in different places downstream and upstream and in both river side banks. Passive integrated transponder (PIT) tags of 12 and 23 mm length and 0.1 and 0.6 g of weight (freevision®) were used not exceeding a maximum weight of the tag equal to 2% of the fish weight. All fish were anaesthetized (solution of eugenol), measured (mass and fork length) and PIT-tagged intraperitoneally by an incision posterior to the left pectoral fin (Figure 181).



Figure 181: Passive Integrated Transponder Tagging.

Back to D2.2 Main index

A pass-through antenna system was used to study fish movements in Guma fishway. Four antennas were placed in the notches and orifices. Each antenna was connected to a dedicated reader (ORFID® Half Duplex multiplexer reader), programmed to query the antennas at 14 Hz (3.5 Hz or 0.29 s per antenna) (Figure 182). Antennas system worked with solar power (40 W solar panel and charge controller) and two batteries (Pb-acid of 12 V and 60 Ah each one, connected in parallel) since mid of May until mid of September 2018. Then, due to the decrease of solar radiation/insolation, the equipment has been connected to the electrical network (Alternating Current) through an electronic battery charger and the batteries (Direct Current).

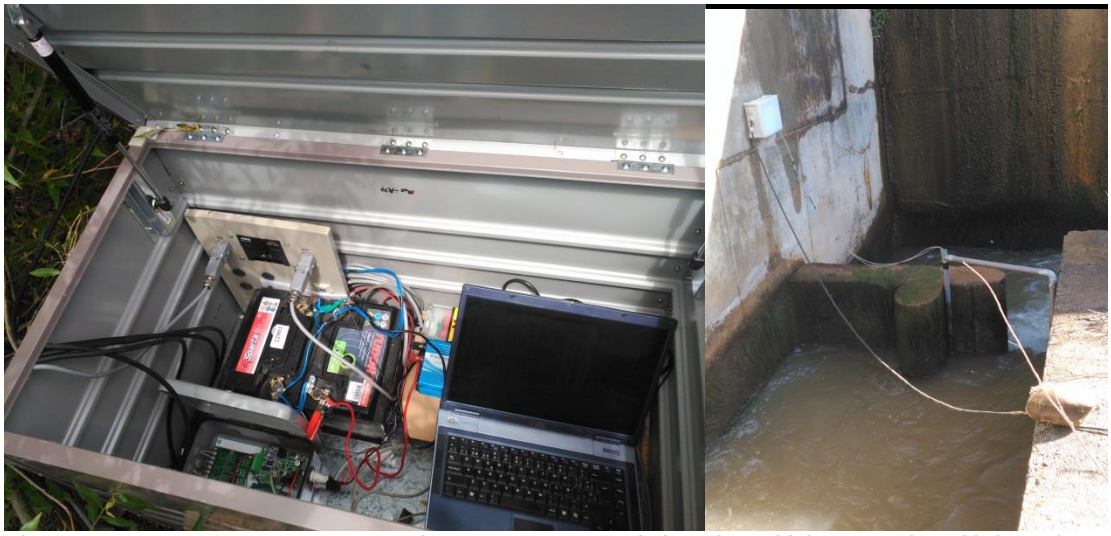


Figure 182: PIT tag antennas system (Oregon RFID® reader). Left: multiplexer reader with batteries and charge controller. Laptop is connected through an inverter. Right: hand-made RFID antenna with four loops of coil (2.5 mm2) enclosed in PVC pipe.

Variations of Duero River natural flow and changes in flow discharge through Guma turbines have been recorded for future fish attraction models, as well as water temperature (data provided by Hydrologic Automatic System of Duero River basin authority).

Eleven individuals of *Luciobarbus bocagei* were tagged with radio transmitters. They were caught at different dates and in different places (upstream and downstream Guma fishway) and released both upstream and downstream the fishway. Radio transmitter (model TXC007I of Scubla S.R.L®) has an internal coil antenna with a dimension of 19x10 mm (length x diameter) and weight of 2.9 g, with a theoretical life of about 4 months and 40 pulses per minute (frequency between 151.000 and 151.500 MHz). They were implanted in the intraperitoneal cavity through an incision of about 1.5 cm. The wound was closed with three absorbable stitches and liquid cutaneous suture. All the surgery process was done in a portable fish surgery box, where barbels could stay without movements, with the gills submerged in the water and with continuous water oxygenation with maintenance doses of anaesthetic (eugenol) (Figure 183). After the surgery, recovery of fish was confirmed carefully, by looking for the usual swimming activity and good equilibrium of the individuals. From July to October 2018, radiotracking was done once a week in the river reach between Vadocondes HPP and Guma village dam, with a three-fold element Yagi antenna and a VHF portable receiver (Telenax® R-1000 receiver).



Figure 183: Left: table with field surgery equipment for radio tagging. Right: Detail of Luciobarbus bocagei anaesthetized and sutured, with the gills submerged into the water with supply oxygen and the body of the fish secured (position and humidity) with the foam.

The schedule for 2019 includes:

- A fishcounter will be installed in Guma HPP fishway for evaluating the location and entrance of fish with this tool and comparing with the used ones.

- PIT antenna system will still be worked continuously.

- The influence of turbine operation and attraction flows in fishway location will be modelled using Survival Analysis methods.

3.7.5.2 Results

Results of marking and recapturing with elastomers:

Regarding visible elastomer implants, 1718 individuals of 8 species were marked, from which, 198 were recaptured (Table 34 and Table 35). Only *L. bocagei* and *G. lozanoi* were recaptured (they were also the most tagged species), mainly in the same sample place where they were marked for the first time, except for *L. bocagei* in Vadocondes, where a remarkable proportion was first tagged in the fishway and recaptured then in the river. Only one recapture of *L. bocagei* in Guma fishway was previously marked in Vadocondes fishway.

About the body marking location, although dorsal fin is generally recommended for other species, with small size cyprinids, we have observed that it is not the best place. In this case, the subcutaneous injection is quite difficult (very thin skin) and the visibility of the elastomer some time later was not good enough. However, based on our experience, near the caudal fin (the bottom of the fish) is a really good body part, being the marking procedure comfortable and it has good visibility in subsequent recaptures.

Table 34: Number of marked fish with Visible Implant Elastomer from May to September 2018, by species and sampling point.

Number of marked	GUMA		VADOCONDES		TOTAL
	Fishway	River	Fishway	River	
Achondrostoma arcasii	1	1	2	2	6
Carassius auratus		1			1

Back to D2.2 Main index

Number of marked	GUMA		VADOCONDES		TOTAL
	Fishway	River	Fishway	River	
Gobio lozanoi	120	146	58	378	702
Luciobarbus bocagei	567	42	160	216	985
Pseudochondrostoma duriense	4		2	4	10
Salmo trutta	3		1	1	5
Squalius carolitertii				8	8
Tinca tinca		1			1
TOTAL	695	191	223	609	1718

Table 35: Number of recaptured fish with Visible Implant Elastomer from May to September 2018, by species and sampling point. (In brackets: first number indicates the number of fish marked in the same sampling point in which it has been recaptured / second number indicates fish marked in different sampling points).

Number of recaptured	GUMA		VADOCONDES		TOTAL
	Fishway	River	Fishway	River	
Achondrostoma arcasii	-	-	-	-	0
Carassius auratus		-			0
Gobio lozanoi	-	1 (1/-)	-	5 (5/-)	6
Luciobarbus bocagei	126 (125/1)	1 (-/1)	53 (50/3)	12 (8/4)	192
Pseudochondrostoma duriense	-		-	-	0
Salmo trutta	-		-	-	0
Squalius carolitertii				-	0
Tinca tinca		-			0
TOTAL	126	2	53	17	198

Results of PIT tagging:

As preliminary results, a selection of data has been done focused only on *L. bocagei* (barbels) that were released downstream of Guma fishway, about 200 m from the entrance of the fishway, where both branches (fishway entrance channel and turbine outlet channel) join. Sample characteristics of marked fish with PIT tag can be seen in Table 36.

Table 36: Characteristics of fish sample (Luciobarbus bocagei) tagged with PIT tag for the analysis of upstream migration. There are three different sources of fish (all of them upstream the release place). [median (first quartile – third quartile)]

Source	Guma fishway	Guma village	San Esteban fishway*
N	164	43	60
Fork length (mm)	136 (113-175)	125 (112-145)	139 (119-193)
Weigth (g)	37 (21-78)	28 (20-42)	35 (22-95)
Condition Factor	1.42 (1.36-1.50)	1.40 (1.35-1.46)	1.35 (1.29-1.41)

* Fishway located 31 km upstream Guma village dam.

There were 149 of 267 barbels that located the fishway (56%), of which 79 had success in the ascent of the fishway (53%). Both fishway location and passage success were influenced by the source (origin) of the fish. About fishway location, Guma village origin had the lower location rate (19%), being similar in fish from San Esteban and Guma fishway origins (62% and 63% respectively). For the success in the ascent, the better rate was for San Esteban origin (81%), followed by Guma fishway (44%) and Guma village (38%) origins.

If dates of release are analysed, a decrease in the proportion of fish which locate the fishway along the migration season can be seen (Figure 184).

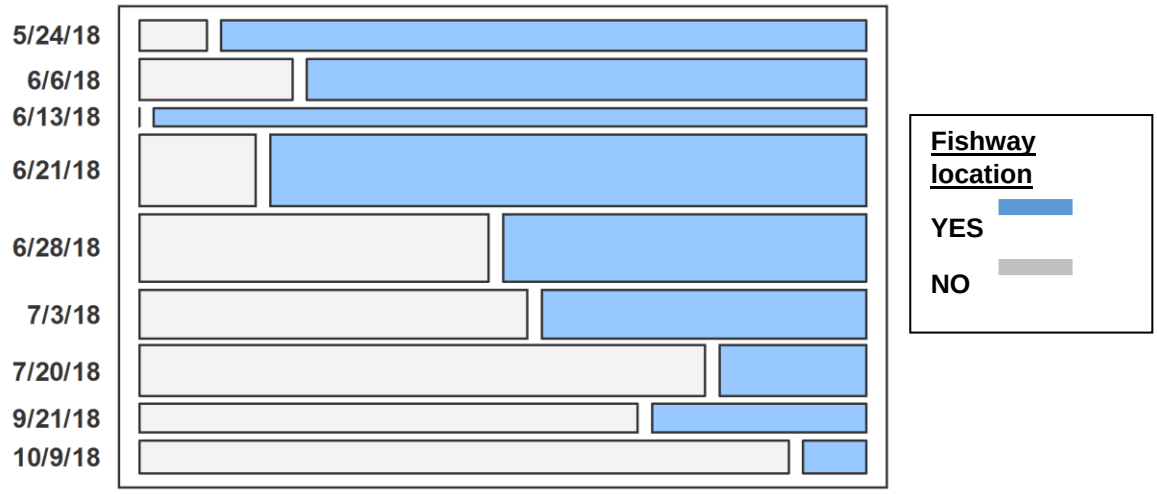


Figure 184: Proportion of barbels that located the fishway as a function of release date (month/day/year).

Regarding fish length, there were differences in the rate of fishway location. Median length of barbels which did not locate the fishway was 121 mm vs barbels that located the fishway = 154 mm; (Mann-Whitney test of median comparison; $p<0.001$). There were no differences in the ascent success due to the fish length.

Regarding Condition Factor ($K = 100*weight/length^3$), there were differences among condition factors of the different fish origin sources (San Esteban < Guma village < Guma fishway). For the Guma fishway origin, there were more fish with higher Condition Factor that located the fishway. Anyway, these results are preliminary, i.e. not conclusive, due to the need to assess the cross effect of other variables as for example the release date.

Fishway location and ascent success could be related to some environmental variables, for example, the total river discharge, discharge through the turbines or over the dam, and water temperature. These parameters have been represented in figure 12 to try to find some relationships. It can be seen a period of peak movement mainly during the second half of June and the first days of July, according to changes in the river discharge and water temperature.

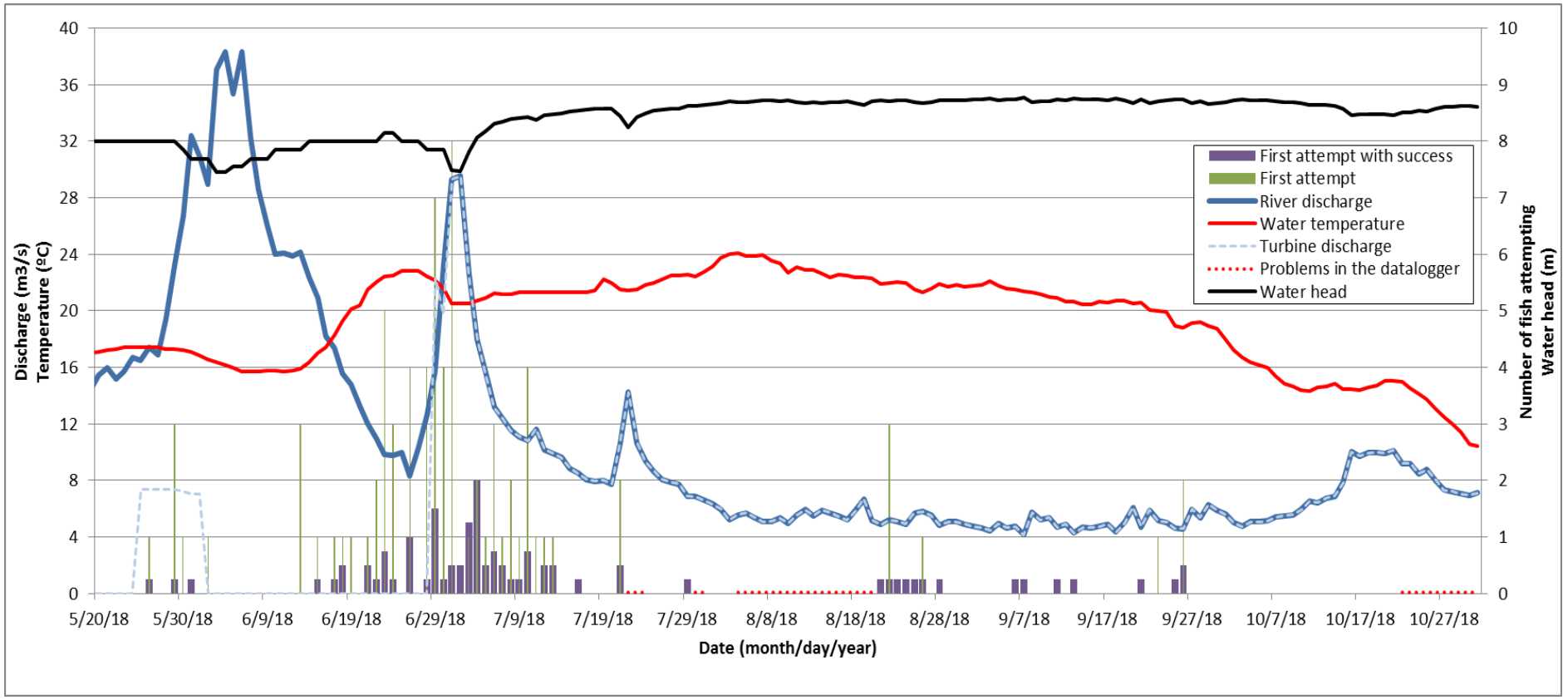


Figure 185: Fishway location and ascent success of Guma fishway, related to flow discharge and water temperature. Turbine discharge was affected by operational problems until 29th June. Water head refers to the difference between water level upstream and downstream.

.

Another important result is the ascent time or transit time. In this case, it is possible to know the time that takes to a fish to ascent between the entrance of the fishway (antenna 1) and the exit (antenna 4). It corresponds to an approximate total water head of 8 m (31 pools with water drops of 0.25 m between each one). In Table 37 the summary of the main ascent time results is shown. The global median time for ascending the fishway is about 3.5 hours, although quite variable according to the fish source. Of the data collected by the antennas, it is possible to see differences in ascent behaviour between fish source, with a higher motivation for the ascent of fish from upstream origins. However, fish that were caught in the fishway showed another kind of movements, probably more related to refuge and/or food search.

Table 37: Summary of the ascent time of Luciobarbus bocagei in Guma fishway, as a function of the source of the fish, in hours. Time is obtained between antenna 1 and antenna 4, corresponding to a total water head of 8 m (31 pools with mean water drops of 0.25 m.

Fish source	Guma fishway	Guma village	San Esteban fishway	Total
N	36	4	29	69
Median ascent time	9.3	2.3	1.9	3.4
First quartile	2.4	1.4	1.3	1.5
Third quartile	45.7	2.9	4.2	12.0

We expect to obtain more results from data about upstream migration and also downstream movement since we have tagged another 254 fish which were released upstream of Guma fishway. Of these fish, 132 were released in the right riverbank and 122 in the left riverbank, in different dates (summer and autumn) looking for results about fishway location in downstream movement. Until the 1st October 2018, at least 49 barbels released in the right riverbank and 13 of the left bank located the fishway, most of them moving downstream through the fishway and few of them seeming to move through the turbines (provisional data that need to be confirmed).

Results of radiotracking

Eleven barbels were radio tagged and also pit tagged to know exactly the moment of passing Guma fishway. In the beginning, ten fish were tagged but one of them died in August 2018 (number 1, Table 38) and we could recover the tag and reuse it in a new fish (number 11). Fish numbers one to five were captured some kilometres upstream of Guma fishway and released 250 m downstream of the fishway. Fish numbers 6 to 11 were captured in Vadocondes fishway and released approximately 600 m upstream of Guma fishway.

Table 38: Barbels (Luciobarbus bocagei) that were radiotagged (see figure 13 for details of their movements)

Barbel number	Length (mm)	Weight (g)	Sex	Condition Factor	Source	Release	Release date
1	250	213	Male	1.36	Upstream	Downstream	6/28/2018
2	205	115	Male	1.33	Upstream	Downstream	6/28/2018
3	213	121	Unknown	1.25	Upstream	Downstream	6/28/2018
4	210	128	Male	1.38	Upstream	Downstream	6/28/2018
5	200	105	Unknown	1.31	Upstream	Downstream	6/28/2018
6	224	149	Unknown	1.33	Downstream	Upstream	7/11/2018
7	185	76	Unknown	1.20	Downstream	Upstream	7/11/2018

8	255	210	Male	1.27	Downstream	Upstream	7/16/2018
9	200	110	Unknown	1.38	Downstream	Upstream	7/16/2018
10	255	200	Male	1.21	Downstream	Upstream	7/16/2018
11	233	164	Unknown	1.30	Downstream	Upstream	9/6/2018

The details of the movements performed by barbels are shown in Figure 185. As a summary, about the fish released downstream, three of them ascended Guma fishway (between 11 and 13 of July). Another descended more than 2 km, and then ascended till near the entrance of the fishway and finally, it was found dead near there. The other one descended more than 2 km and stayed there until batteries ran out. In relation to the six fish released upstream, four of them went upstream until they got the dam of Guma village (which has no fish passage), with three of these four fish staying there until the batteries ran out. The other one after arriving to Guma village descended till near Guma HPP dam. Another two fish (8 and 9) were impossible to locate after they were released.

It seems that only one fish descended Guma HPP during the life of the radiotag batteries, but we cannot know the way (the fishway or the turbines) because PIT antenna reader had some problems in the middle of its descent movement (fish 2).

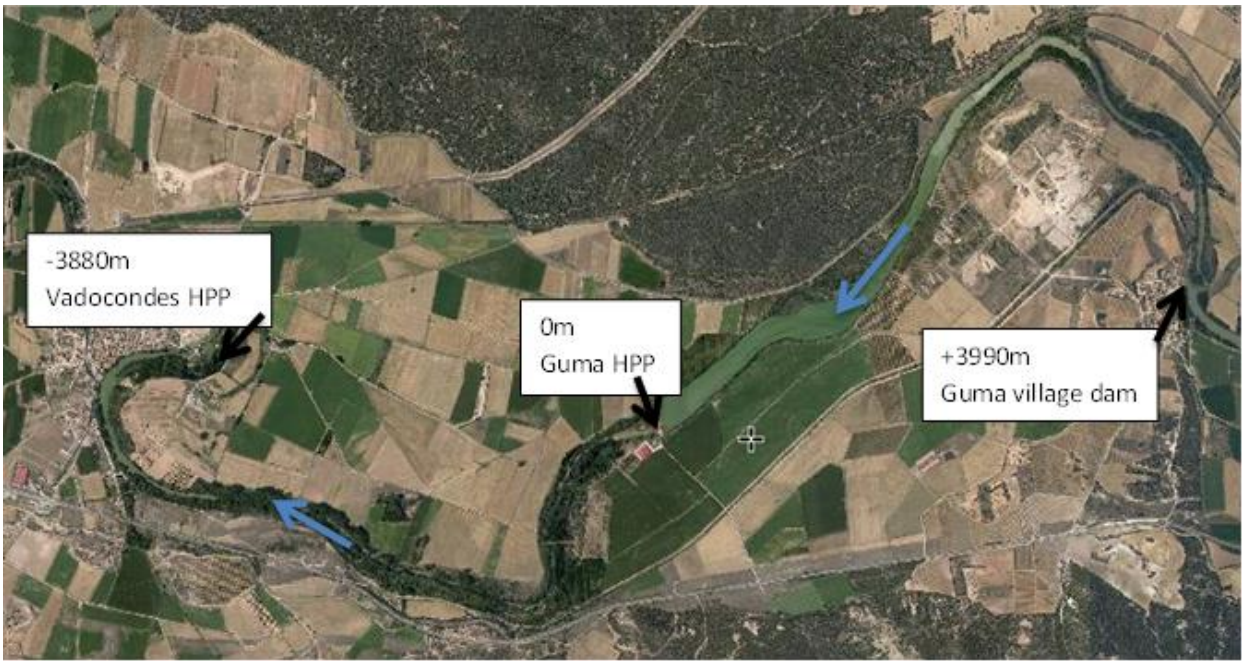


Figure 186: Scheme of movement for barbels with radiotag: map of the section under study where radiotracking was done once a week since July to October 2018.

Back to D2.2 Main index

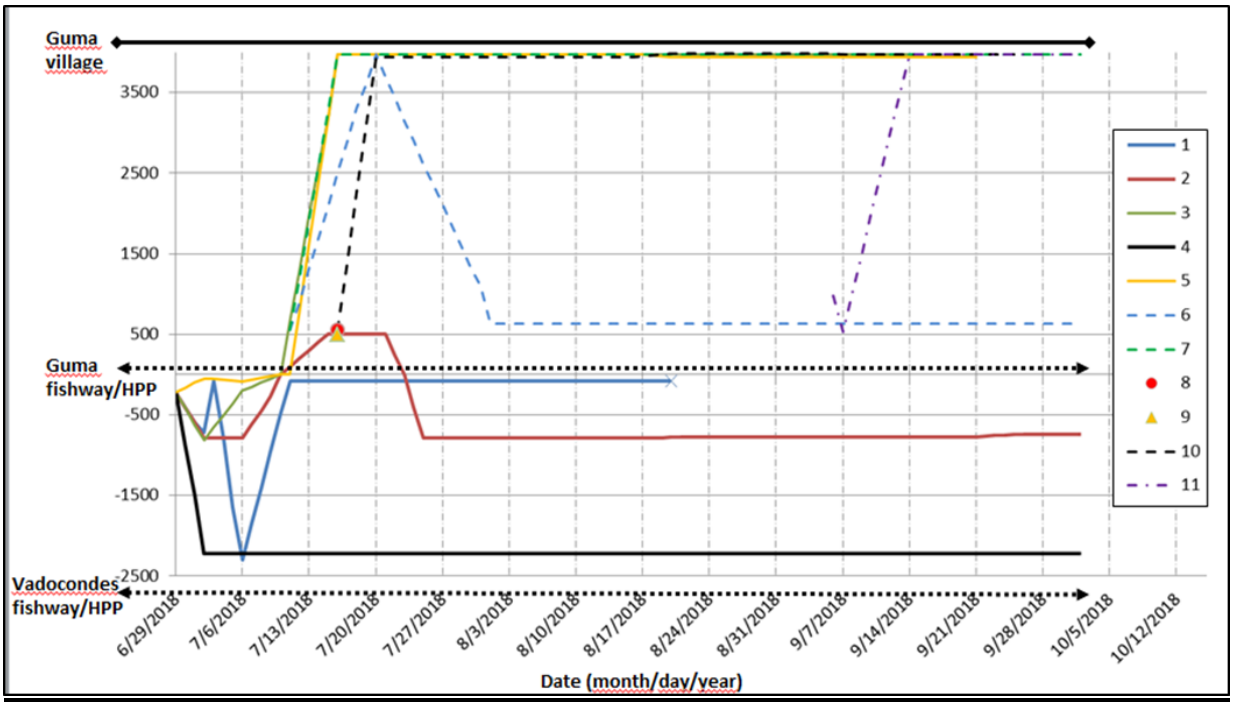


Figure 187: Scheme of movement for barbels with radiotag: graph of fish movements along the time (X axis) as a function of the distance from Guma HPP

3.7.6 Hydraulic modelling of the fishway and its attractiveness

The aim of this subtask is modelling the fishway and the downstream section of Guma HPP to analyse and improve its hydrodynamics by correlating it with fish behaviour. Mainly, we would like to improve the knowledge about the fishway hydrodynamics, its attractiveness, and the influence of the attraction flow on fish movements s.

Fishway hydrodynamics will be analysed under different flow regimes and operational constraints (like an orifice or notch clogging), using 3D numerical modelling.

To analyse the fishway attractiveness considering the competing turbined flow, different scenarios will be analysed using 2D and 3D modelling to try to find the scenarios that maximize fish upstream movement and hydropower production to try to establish more fishfriendly operation rules.

ITAGRA-GEA is responsible for data collection and IST is implementing the hydraulic model. Later, comparisons between these models and fish behaviour models will be done.

3.7.6.1 Methodology

With the 2D plans of the fishway facility of Guma HPP the 3D geometry of the fishway was created using Autocad. The geometry of the fishway was simplified, (22 pools were modelled instead of 31 pools) to allow for lower run times. This geometry was imported to the 3D model as stereolithography (STL) files. The computational domain was discretized using multi-block grids to optimize the mesh according to the simulated geometry. The flow field numerical modelling was performed using FLOW-3D®, a CFD commercial software that solves the governing equations of fluid motion in a Cartesian staggered grid using finite volumes method.

Back to D2.2 Main index

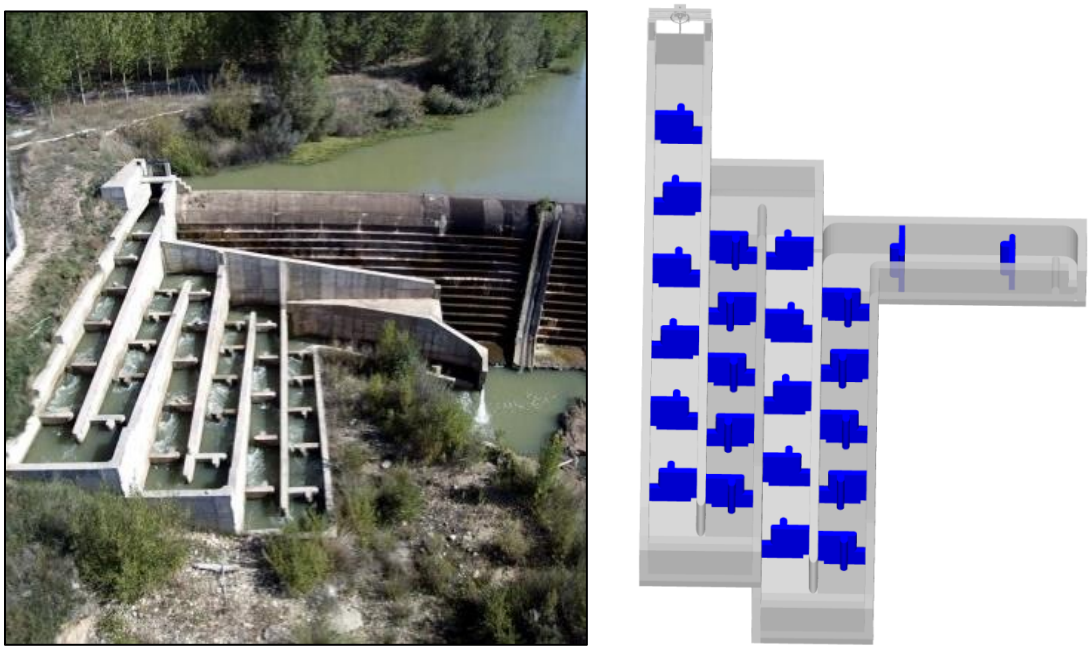


Figure 188: Left: Guma HPP fishway. Right: Guma HPP modelled fishway geometry.

The 2D and 3D numerical modelling of the downstream river reach is being performed with HEC-RAS and FLOW-3D® software. To build these numerical models several tasks were carried out:

- Hydraulic characterization of the downstream section (about 300 m) of Guma HPP with Doppler bathymetry ADCP, current meter and topographic equipment, under different flow conditions (Figure 189).



Figure 189: Hydraulic data acquisition on Guma HPP. Left: Doppler bathymetry in the turbine tailrace. Right: topographic survey of bathymetry sections.

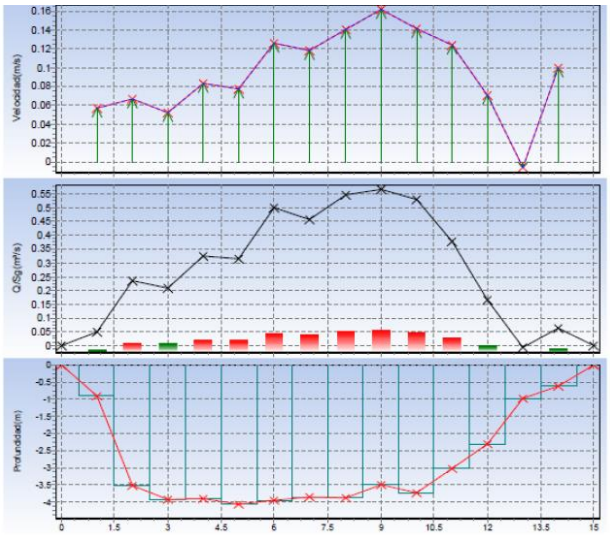


Figure 190: Example of bathymetry results of one section in Guma downstream reach. Up: current velocity; Middle: flow discharge; Down: water depth.

- Characterization of the river stretch under study through aerial photography (drone flight).



Figure 191: Photos from drone flight over Guma HPP

These data is being used to build (Figure 192), calibrate and validate the 2D and 3D numerical models.

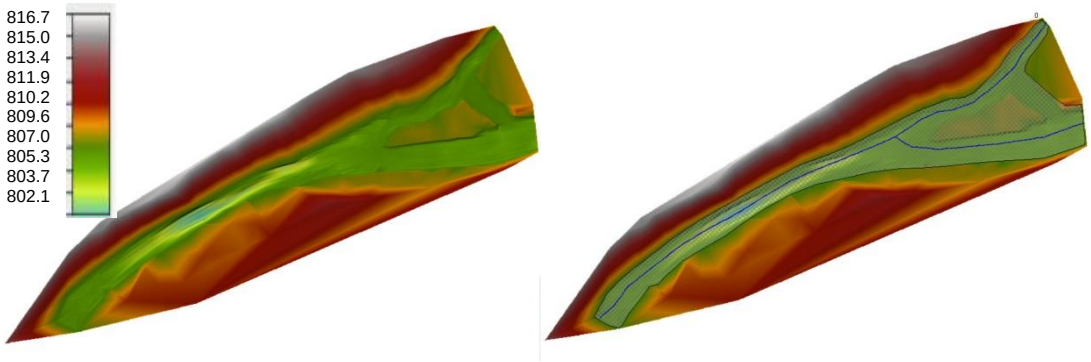
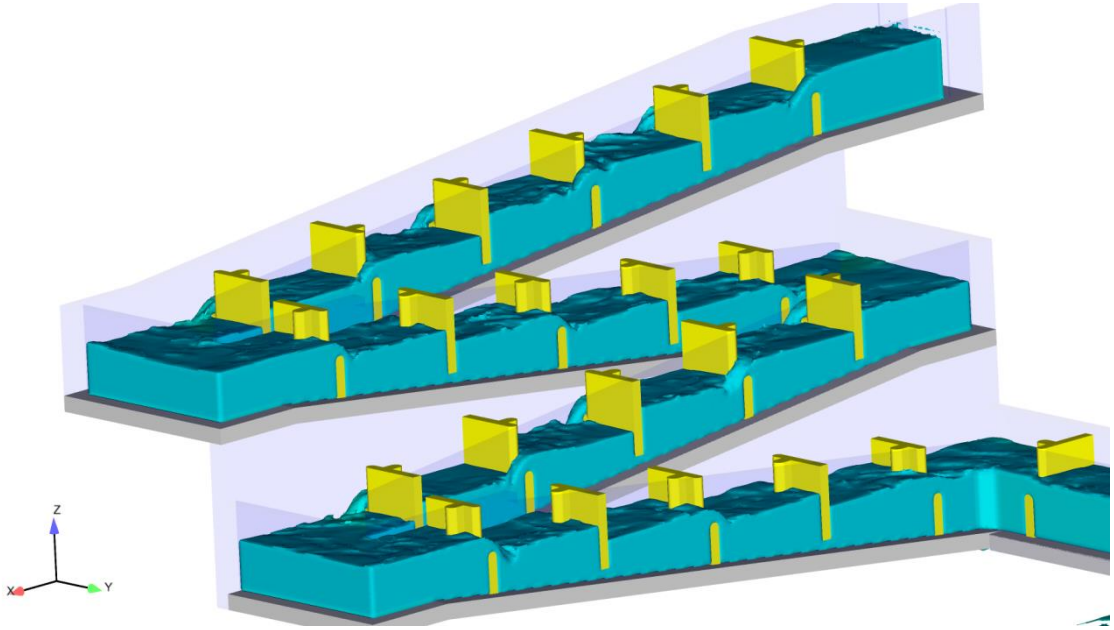
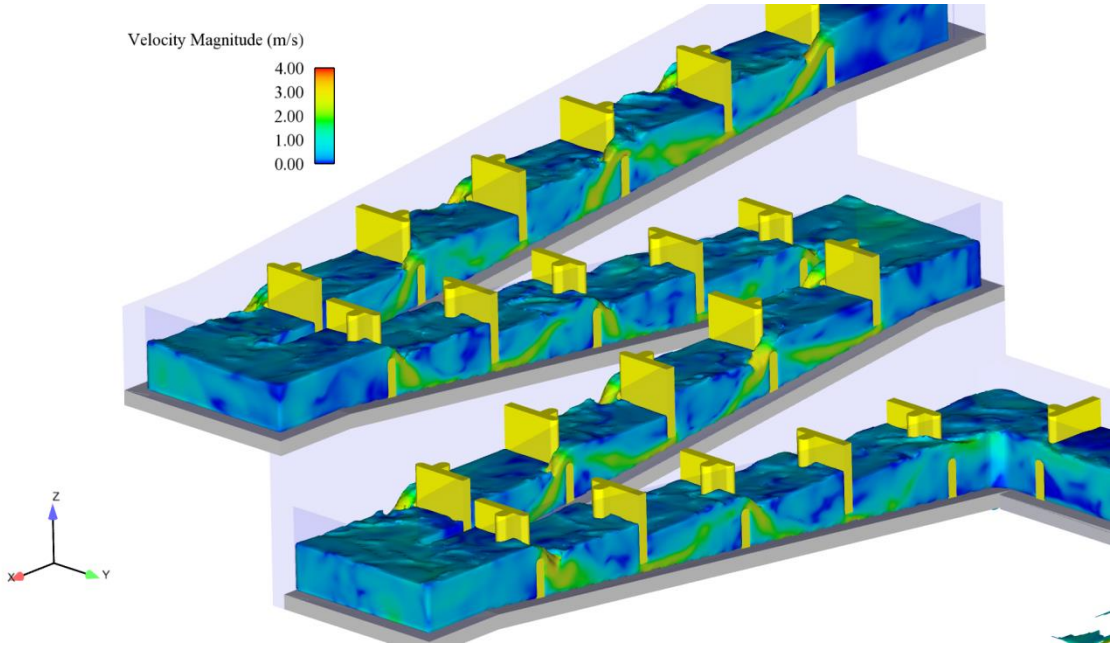


Figure 192: Downstream river stretch under study. Left: terrain elevation. Right: HEC-RAS 2D model area.

3.7.6.2 Results

The 2D and 3D modelling of the downstream river stretch and of the 3D modelling of the fishway is being carried out. The verification and validation procedure of the 3D fishway modelling is being performed to obtain valid accurate results. Some preliminary results are shown in Figure 193.





Back to D2.2 Main index

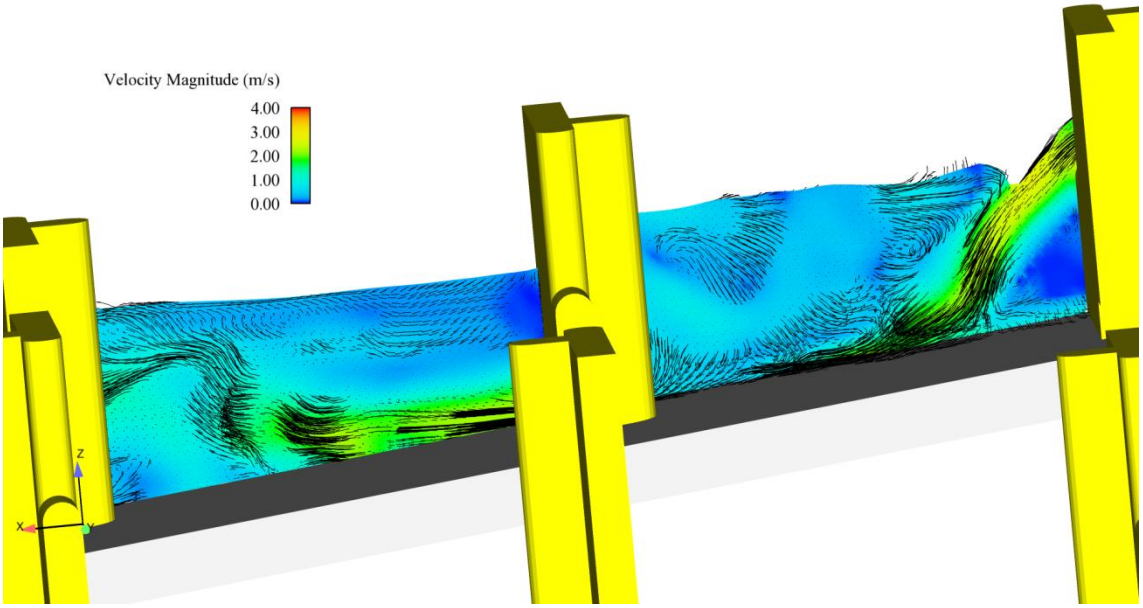


Figure 193: 3D fishway model preliminary results. Top: 3D flow and water surface configuration. Middle: 3D flow coloured by velocity magnitude. Bottom: Velocity magnitude and streamlines in two regular pools at y = 0.15 m (right located notch axis)

The model results will be analysed to characterize the flow hydrodynamics and turbulence patterns to try to correlate with the observed fish behaviour. The different pools (regular and turning pools) hydrodynamics will be fully characterized to understand differences and possible trapping zones. The hydrodynamics of non-uniform flow regimes caused by the river hydrological variability and/or operational constraints (like an orifice or notch clogging) will also be assessed.

The attractiveness of the fishway will be analysed by the characterization of the downstream river reach hydrodynamics, considering the competing turbined flow in order to investigate possible operational management options to enhance the attractiveness and thus upstream migration.

3.7.7 References

GEIB, 2011. Manual de las especies exóticas invasoras de los ríos y riberas de la cuenca hidrográfica del Duero. Grupo Especialista en Invasiones Biológicas. Confederación Hidrográfica del Duero, Valladolid, 215 pp.

SIBIC, 2014. *Carta Piscícola Española* (versión 01/2015). http://www.cartapiscicola.es/#/species/aalb (last Access on 14th of November, 2018).

Madoz, P. (1846). *Diccionario geográfico-estadístico-histórico de España y sus posesiones de ultramar*. Est. tip. de P. Madoz y L. Sagasti.

Pérez, R. 2009. Biología y ecología de las larvas de peces del río Guadamiar en zonas afectadas y no afectadas por el vertido tóxico de las minas de Aznalcollar. Tesis doctoral. Servicio de publicaciones de la Universidad de Córdoba.

R.D 630/2013. Real Decreto 630/2013 por el que se regula el Catálogo español de especies exóticas invasoras. Boletín Oficial del Estado núm. 185, España, 2 de agosto de 2013.

Salvador, V. 2015. Diagnóstico de la situación de las especies exóticas invasoras dentro del ámbito del proyecto LIFE11 NAT ES/699 MedWetRivers. Sociedad Pública de Infraestructuras y Medio Ambiente de Castilla y León S.A (SOMACYL).

Illies, J., Botoseanu, L., 1963. Problèmes et méthodes de la classification et de la-zonation écologique des eaux courantes, considérées surtout-du point de vue faunistique. Mitteilung Int. Vereinigung fuer Theor. unde Amgewandte Limnol. 12, 1–57.

Rosgen, D.L., Silvey, H.L., 1996. Applied river morphology. Wildland Hydrology, Pagosa Springs, Colorado, USA.

3.8 Günz

The Test Case HPP Oberegg includes 5 fish ladders – Deisenhausen, Höselhurst, Wattenweiler, Ellzee and Waldstetten. At the Test Case Günz the BEW will build compensation habitat structures in the fish bypass channels with the aim of improving the compensation habitat function, especially as spawning habitat and habitat for reophilie fish species.

3.8.1. Improvement of spawning habitats within the fish bypass

The BEW placed gravel into 3 of 5 fishladders to improve their functions as spawning habitats for the reophile target fish-species like nase and barbel. To see the possible immediate success of the measure the pools with fresh gravel and the pools with the existing substrate were sighted daily and compared from the day of placing gravel until about end of May. This period was chosen because of the spawning time of nase and barbel.

3.8.1.1. Data

Placing gravel into the fishways by BEW

On 9.4.2018 and 10.4.2018, BEW placed all in all about 42 tons of washed gravel with a grain size of 16/32 mm spread over the fishways Wattenweiler, Ellzee und Waldstetten. In each case, the gravel was placed over three pools of the fishways. The amount of gravel per pool was between 2 – 6 tons.



Figure 194: Placing gravel into Wattenweiler fishway.

Following aerial photos are showing the spots where the gravel was placed in.



Figure 195: Location of gravel input at Wattenweiler fishway.

.

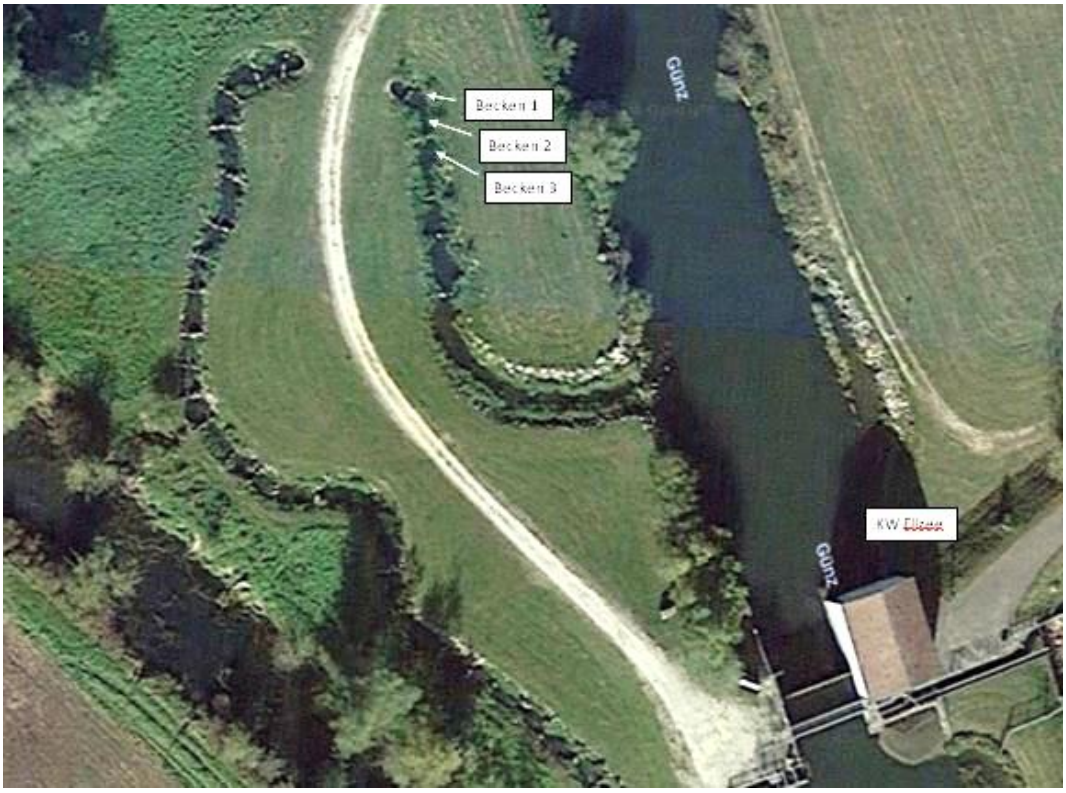


Figure 196 Location of gravel input at Ellzee fishway.

Back to D2.2 Main index



Figure 197 Location of gravel input at Waldstetten fishway.

3.8.1.2. Methodology

Immediate success control

As the spawning period of the species nase was expected to run within the time window when gravel was placed in the fishways were sighted daily if spawning business could be documented. Therefore samples of substrate from the ground of the pools with fresh gravel and also from a comparable number of pools without fresh gravel were extracted. These samples of substrate were sighted on fresh spawn.

3.8.1.3. Results

On the 13.4.2018 -only 4 days after placing gravel- there could be documented successful spawning of nases at the fishway Wattenweiler. In all 3 pools with fresh gravel, there could be found at about 50 % of the stones at least one or several glued nase-eggs.

Back to D2.2 Main index



Figure 198 spawn of nase on fresh gravel.

On the 13.4.2018 there could be also be documented spawning business of nase on the existing coarse substrate at the fishladder Ellzee. On some of the chunks of the old substrate, there could be detected glued eggs of nase. These only could be found within a shadowed area of the short technical part of the fishway under the bridge right below the upstream exit.



Figure 199 Spawn of nase at fishway Ellzee.

3.8.2. Population analysis

For the successful control of the planned and already done measurements there were performed inventorys of the present fish stock.

3.8.2.1. Data

The present fish fauna was invented on all 5 fishways by electric-fishing.

3.8.2.2. Methodology

The inventory of the fish-stock was done by electric fishing. Therefore it was used a batterie fed backpack electric-fishing device.

Data electric-fishing device:

- Type: Efgi 650
- Manufacturer : Bretschneider Spezialelektronik, Chemnitz
- Power: 650 W DC Power and 1300 W Pulse current



Figure 200 Electric fishing at Höselhurst fishway.

It was used solely DC – power to catch the fish gently. Before fishing, the flow of each fishladder was throttled to about 50 % to increase the catch- efficiency. At the point of throttling the flow the underwater entrance was closed with a net so that no fish could flee into the river. The fishing was done upstream pool after pool with a personnal strength of 3. All caught fish were kept within a basin and after measurement and documentation released back into the fishladder.

3.8.2.3. Results

Following data providing an overview of the results that were documented.

3.2.3.1. Fish-bypass Waldstetten

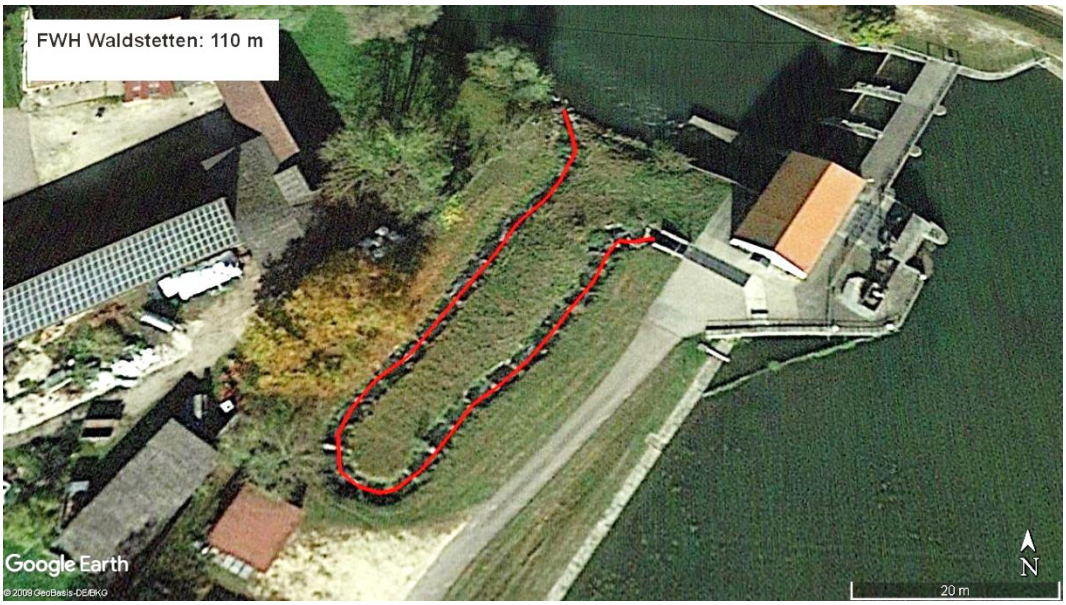


Figure 201 Aerial photo Walddstetten fishway.

Fishstock inventory: Fishladder Waldstetten 21.08.2018			
Species		Number	[%]
Eel	*Anguilla anguilla*	19	5,9
Chub	*Leuciscus cephalus*	44	13,8
Barbel	*Barbus barbus*	69	21,6
Perch	*Perca fluviatilis*	1	0,3
Prussian carp	*Carassius gibelio*	1	0,3
Gudgeon	*Gobio gobio*	3	0,9
Bleak	*Alburnus alburnus*	110	34,4
Nase	*Chondrostoma nasus*	14	4,4
Spirlin	*Alburnoides bipunctatus*	59	18,4
		320	100,0

Table 39 Fishstock inventory: Waldstetten fishway, 17.08.2018.

Back to D2.2 Main index

3.2.3.2. Fish-bypass Ellzee

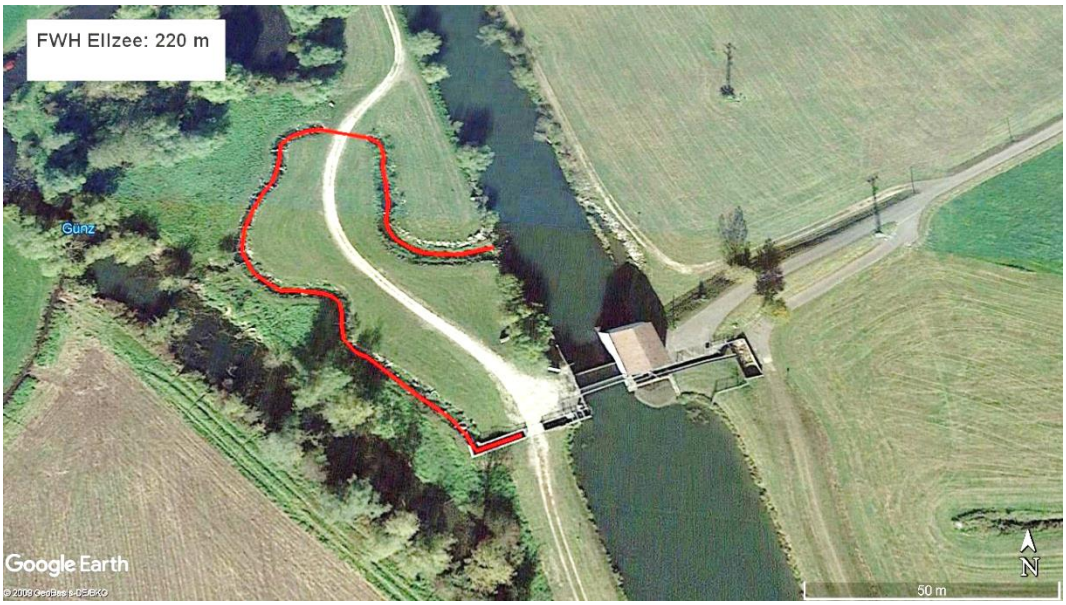


Figure 202 Aerial photo Ellzee fishway.

Fishstock inventory: Fishladder Ellzee 17.08.2018			
Species		Number	[%]
Eel	*Anguilla anguilla*	12	2,0
Chub	*Leuciscus cephalus*	84	14,0
Brown trout	*Salmo trutta*	11	1,8
Barbel	*Barbus barbus*	26	4,3
Perch	*Perca fluviatilis*	2	0,3
Prussian carp	*Carassius gibelio*	1	0,2
Silver bream	*Abramis bjoerkna*	45	7,5
Dace	*Leuciscus leuciscus*	1	0,2
Bleak	*Alburnus alburnus*	75	12,5
Nase	*Chondrostoma nasus*	117	19,5
Rainbow trout	*Oncorhynchus mykiss*	1	0,2
Roach	*Rutilus rutilus*	179	29,9
Tench	*Tinca tinca*	1	0,2
Spirlin	*Alburnoides bipunctatus*	44	7,3
		599	100,0

Table 40 Fishstock inventory: Ellzee fishway, 17.08.2018.

Back to D2.2 Main index

3.2.3.3. Fish-bypass Wattenweiler

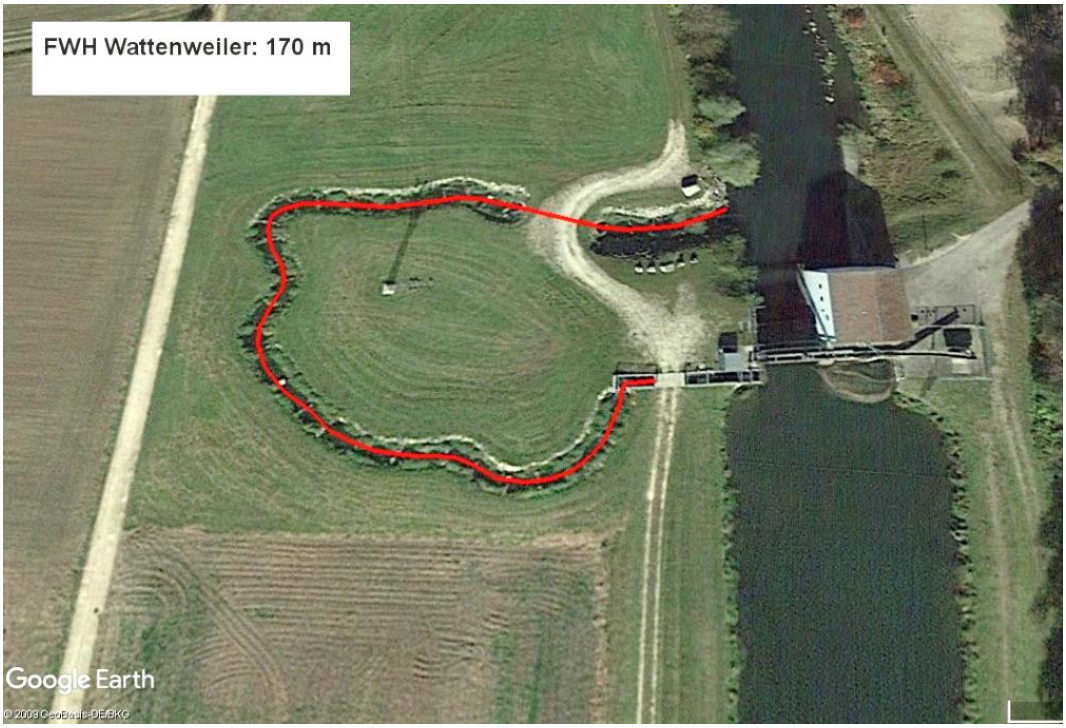


Figure 203 Aerial photo fishladder Wattenweiler

Fishstock inventory: Fishladder Wattenweiler 29.08.2018			
Species		Number	[%]
Eel	*Anguilla anguilla*	7	1,4
Chub	*Squalius cephalus*	82	16,9
Grayling	*Thymallus thymallus*	1	0,2
Brown trout	*Salmo trutta*	16	3,3
Barbel	*Barbus barbus*	203	41,9
Gudgeon	*Gobio gobio*	2	0,4
Dace	*Leuciscus leuciscus*	5	1,0
Nase	*Chondrostoma nasus*	31	6,4
Roach	*Rutilus rutilus*	31	6,4
Tench	*Tinca tinca*	1	0,2
Spirlin	*Alburnoides bipunctatus*	105	21,7
		484	100,0

Table 41 Fishstock inventory: Wattenweiler fishway, 29.08.2018.

Back to D2.2 Main index

3.2.3.4. Fish-bypass Höselhurst

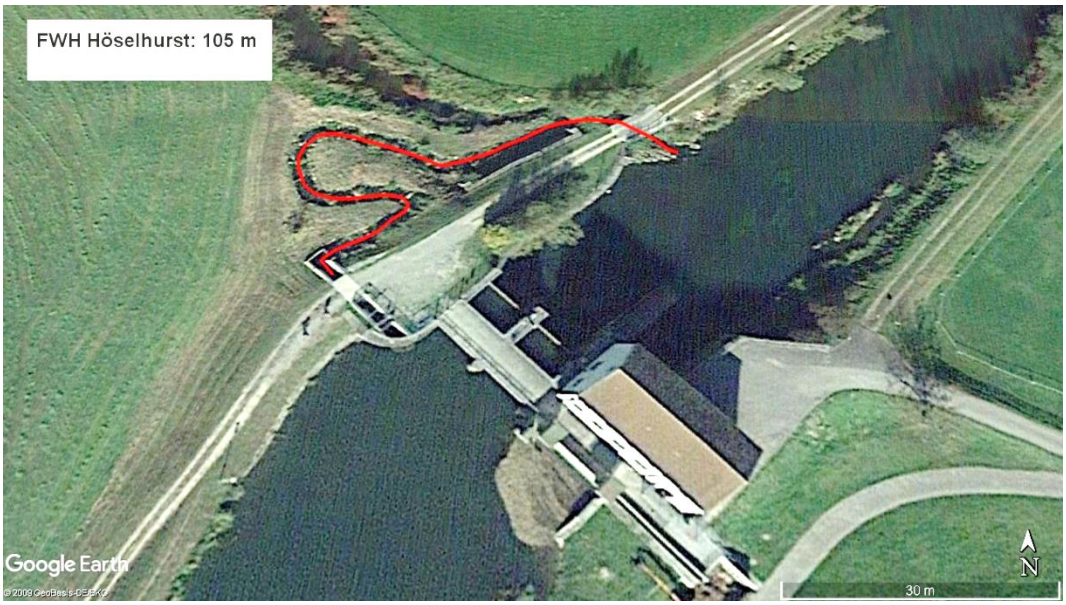


Figure 204 Aerial photo Höselhurst fishway.

Fishstock inventory: Fishladder Höselhurst 7.9.2018			
Species		Number	[%]
Eel	*Anguilla anguilla*	4	1,1
Chub	*Squalius cephalus*	69	18,2
Barbel	*Barbus barbus*	154	40,6
Perch	*Perca fluviatilis*	1	0,3
Gudgeon	*Gobio gobio*	30	7,9
Dace	*Leuciscus leuciscus*	1	0,3
Nase	*Chondrostoma nasus*	13	3,4
Roach	*Rutilus rutilus*	1	0,3
Spirlin	*Alburnoides bipunctatus*	104	27,4
Catfish	*Silurus glanis*	2	0,5
		379	100

Table 42 Fishstock inventory: Höselhurst fishway, 7.9.2018.

Back to D2.2 Main index

3.2.3.5. Fish-bypass Deisenhausen

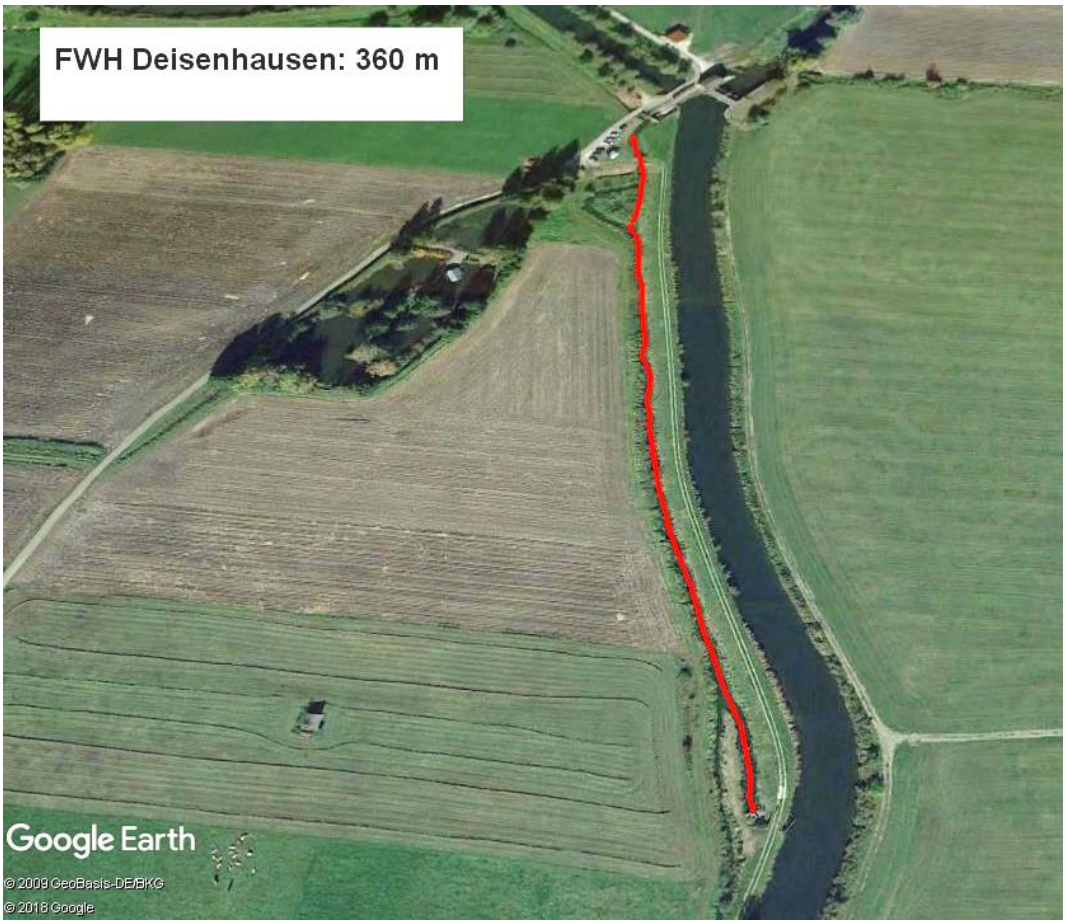


Figure 205: Aerial photo Deisenhausen, fishway.

Back to D2.2 Main index

Fishstock inventory: Fishladder Deisenhausen 23.8.2018			
Species		Number	[%]
Eel	*Anguilla anguilla*	11	0,8
Chub	*Squalius cephalus*	215	16,3
Grayling	*Thymallus thymallus*	2	0,2
Brown trout	*Salmo trutta*	1	0,1
Barbel	*Barbus barbus*	269	20,3
Perch	*Perca fluviatilis*	40	3,0
Topmouth gudgeon	*Pseudorasbora parva*	2	0,2
Minnow	*Phoxinus phoxinus*	48	3,6
Prussian carp	*Carassius gibelio*	2	0,2
Gudgeon	*Gobio gobio*	95	7,2
Silver bream	*Abramis bjoerkna*	2	0,2
Dace	*Leuciscus leuciscus*	70	5,3
Pike	*Esox lucius*	1	0,1
Bullhead	*Cottus gobio*	4	0,3
Bleak	*Alburnus alburnus*	67	5,1
Nase	*Chondrostoma nasus*	6	0,5
Roach	*Rutilus rutilus*	47	3,6
Rudd	*Scardinius erythrophthalmus*	1	0,1
Tench	*Tinca tinca*	7	0,5
Stone loach	*Barbatula barbatula*	217	16,4
Spirlin	*Alburnoides bipunctatus*	159	12,0
Carp	*Cyprinus carpio*	2	0,2
Stickleback	*Gasterosteus aculeatus*	55	4,2
		1323	100,0

Table 43 Fishstock inventory: Deisenhausen fishway, 23.8.2018.

Back to D2.2 Main index

3.9 Ham

3.9.1. Study of survival through Archimede screws

To investigate the impact of the hydropower station on fish that pass the screws (1), forced fish pass experiments are performed in which four species (in three repetitive groups of each 100 individuals (so, total of 300 individuals per species) are inserted at the top of one of the three screws, to pass it. The species investigated are European eel, Roach, Bream and Trout. The experiments are performed for all three possible turbine-operation modes, namely turbination at a discharge of 3, 4 and 5 m^3/s, respectively. Hence, in total 900 individuals of each species are forced into the screws to pass it, and evaluated on mortality, injury and potential delayed mortality. Second, (delayed) mortality and injury on individual fish that naturally passed the turbines is evaluated. Those fish are not forced into the turbines, but naturally passed it on their way down in the canal/by-pass channel. Those individuals can be of any species that is present in the canal. This measurement is performed on all fish that passed the turbines during one 24h cycle of hydropower generation with three screws on 5 m^3/s. The natural-pass experiments are repeated 10 times (ten 24h cycles, so a total of 240h of hydropower generation), and are spread over one year so that both periods of more and less fish migration activity are monitored.

As life fish experiments are part of another project, the methodology and the results are not included yet at this stage of the report. It should be included later after the “De Vlaamse Waterweg NV” project is finished.

The evaluation of the impact of the hydropower station by pressure related parameters is performed by the passage of barotrauma detection sensors (BDS) developed at the Tallinn University of Technology (TUT). For further details on the methodology see Figure 206 A.

3.9.1.1. Methodology

The objective of the fieldwork with the barotrauma sensors was to record 30 data sets per operational mode (3, 4 and 5 m^3/s). The sensors were deployed in the identical manner as the live fish in the forced fish-pass experiments (Figure 206 C), and are recaptured downstream with a hand-held fish net (Figure 206 D). Balloon tags were attached to each sensor and were set to inflate 1 minute after deployment in the Archimedes screw tail water. Metadata for each deployment were recorded including the time of deployment, passage duration, noticeable scratches, dents or if the sensor was crushed. The BDS collect the time series at 100 Hz including the total pressure, linear acceleration, rotation rate, magnetic field as well as the absolute orientation of the sensors during their passage through the screws.

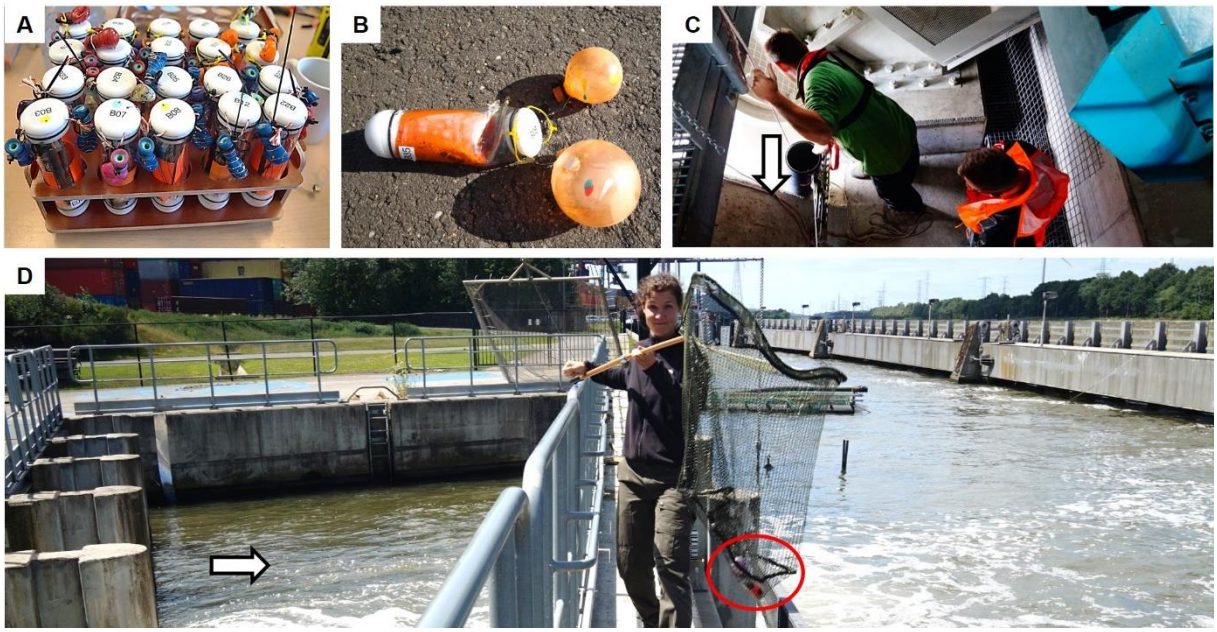


Figure 206: BDS deployment at Ham from 20-22.06.2018. A) Sensors outfitted with balloon tags ready for deployment. B) Sensor destroyed by crush event. C) Deployment of BDS into the Archimedes screw. D) Recovery downstream via balloon tags in a hand net.

3.9.1.2. Barotrauma sensors

The BDS time series data from this Test Case (I) to determine statistical properties of the passage conditions at the Archimedes screw under three different operational conditions operations, (II) to advance in understanding of the effect of screw operation on fish passage, (III) to evaluate fish passage through the screw (as an operational measure for downstream fish passage), and (IV) to create recommendations for fishfriendly passage at large Archimedes screws.

3.9.1.3. Results

The preliminary results of the sensor data are provided in the form of summary statistics in the following tables. Data post-processing and comparison with biological data and literature on Archimedes screws is currently ongoing. A peer-reviewed journal publication from the Ham BDS and live fish data set is under preparation and will be submitted in 2019.

The results of the BDS are a statistical analysis of the time series data for each of the sensor modes (e.g. pressure, acceleration, etc.). The following parameters are calculated for each individual measurement: min, max, mean, median, standard deviation, Q1, Q3 and the number of blade strikes. These statistical parameters are then aggregated according to flow scenario (full or half-load) and injection location (low, mid, high) into ensembles representing the distributions of each parameter. In this way, each hydropower plant can be compared using a set of reproducible, statistically-derived parameters. For example, if the number of blade strikes differs between flow scenarios but only significantly between two different injection heights, it is possible to “drill down” into the data by comparing the ensemble statistics to gain insight into the physical environment during passage and suggest corrective measures such as installing fish avoidance targeted at a particular location. The preliminary results from the BDS investigation at Ham are provided in the following tables and figures.

Table 44: Ensemble statistics of BDS deployment at Ham (n = 30), Q = 3 m³/s.

	PL (hPa)	PC (hPa)	PR (hPa)	Euler X (deg)	Euler Y (deg)	Euler Z (deg)	Acc X (m/s²)	Acc Y (m/s²)	Acc Z (m/s²)	Rot X (deg/s)	Rot Y (deg/s)	Rot Z (deg/s)
Min	983	989	985	0	-86	-181	-30	-33	-29	-959	-1717	-1009
Max	1229	1229	1227	362	87	182	31	30	30	1044	1723	979
Mean	1069	1068	1067	186	-1	79	0	-6	-2	15	-4	-3
Median	1047	1045	1045	191	-2	103	0	-8	-3	9	-1	-1
STD	58	58	58	104	26	78	4	5	5	137	185	138
Q1	1025	1024	1024	95	-16	60	-2	-9	-5	-38	-51	-53
Q3	1100	1098	1099	276	13	125	2	-4	0	67	48	50

Table 45: Ensemble statistics of BDS deployment at Ham (n = 28), Q = 4 m³/s.

	PL (hPa)	PC (hPa)	PR (hPa)	Euler X (deg)	Euler Y (deg)	Euler Z (deg)	Acc X (m/s²)	Acc Y (m/s²)	Acc Z (m/s²)	Rot X (deg/s)	Rot Y (deg/s)	Rot Z (deg/s)
Min	972	979	978	0	-86	-181	-32	-34	-34	-1099	-1786	-1017
Max	1227	1228	1226	360	86	182	33	27	32	1108	1748	984
Mean	1069	1069	1069	181	0	74	0	-6	-3	18	-1	-1
Median	1053	1053	1052	183	0	101	0	-8	-3	13	1	2
STD	56	56	56	104	30	89	5	5	5	169	220	162
Q1	1023	1024	1023	94	-19	55	-3	-9	-6	-52	-64	-68
Q3	1100	1100	1099	268	19	130	3	-4	0	88	67	69

Table 46: Ensemble statistics of BDS deployment at Ham (n = 33), Q = 5 m³/s.

	PL (hPa)	PC (hPa)	PR (hPa)	Euler X (deg)	Euler Y (deg)	Euler Z (deg)	Acc X (m/s²)	Acc Y (m/s²)	Acc Z (m/s²)	Rot X (deg/s)	Rot Y (deg/s)	Rot Z (deg/s)
Min	980	983	978	0	-87	-181	-31	-34	-34	-1012	-1750	-1010
Max	1191	1193	1192	361	85	182	32	28	31	1028	1681	1076
Mean	1052	1053	1052	185	-1	73	0	-7	-3	22	0	2

Back to D2.2 Main index

Median	1033	1034	1033	188	-2	92	0	-8	-3	18	3	3
STD	47	48	48	106	31	82	5	5	5	170	231	173
Q1	1016	1016	1015	97	-22	50	-3	-9	-6	-58	-70	-75
Q3	1081	1082	1081	274	19	126	3	-4	0	104	76	80

3.9.2. Fish tracking by acoustic telemetry

The impact of the hydropower plant on the local fish population and downstream migrating eel and salmon is investigated by acoustic telemetry on downstream migrating European eel and salmon smolts in the Albert canal. The tagged eels and salmons are released upstream of the sluice complex of Ham and their downstream migration route (passing the sluice complex through the ship locks, or passing it through the by-pass channel and the hydropower station) is evaluated by acoustic listening stations (ALSs or receivers) in the entire shipping canal, and the ship locks and by-pass channel of Ham). This evaluation should give a general estimation of the proportion of fish that take the route of the hydropower station, and is thus potentially harmed by the Archimedes screws. The results of this part of the study may also give further insight into potentially successful mitigation measures.

As fish tracking by acoustic telemetry is part of another project, the methodology and the results are not included yet at this stage of the report. It should be included later after the “De Vlaamse Waterweg NV” project is finished.

3.9.3. References

Elbatran, A. H., Yaakob, O. B., Ahmed, Y. M. & Shabara, H. M. (2015). Operation, performance and economic analysis of low head micro-hydropower turbines for rural and remote areas: A review. *Renewable and Sustainable Energy Reviews, 43*, 40-50. http://dx.doi.org/10.1016/j.rser.2014.11.045

Okot, D. K. (2013). Review of small hydropower technology. *Renewable and Sustainable Energy Reviews, 26*, 515-520.

3.10 Iller - Legau to Maria Steinbach

BEW, SJE, INBO and TUT cooperate to follow the fish swimming paths into the bypass channel with acoustic telemetry in order to reach the objectives and tasks mentioned in section 2 of the Iller presentation, please refer to D2.1. In general, INBO is responsible to collect 2D fish tracks in high resolution, and SJE is responsible to develop a hydraulic model on the flow situation around the fish pass outflow, downstream of the HPP of Altusried, which is situated between Legau and Maria Steinbach. Together SJE and INBO evaluate the relation between the fish tracks and the ecohydraulic modelling as mentioned in D2.1.

Below, the methodology and first results are given in separate sections, according to the content of the task (corresponding to the different sub-task managers: INBO for the fishtracks, SJE for the ecohydraulic model).

3.10.1. Population and habitat analysis (BEW)

3.10.1.1. Data

The fish fauna of the river Iller is mainly composed of reophelic species. The main target species are Danube salmon (*Hucho hucho*), grayling (*Thymallus thymallus*), brown trout (*Salmo trutta fario*), nase (*Chondrostoma nasus*), barbel (*Barbus barbus*), chub (*Squalius cephalus*). Futhermore there are pike (*Esox lucius*), perch (*Perca fluviatilis*), tench (*Tinca tinca*), burbot (*Lota lota*), bullhead (*Cottus gobio*), loach (*Barbatula barbatula*), bitterling (*Rhodeus amarus*), stickleback (*Gasterosteus aculeatus*), gudgeon (*Gobio gobio*), bleak (*Alburnus alburnus*), rainbow trout (*Oncorhynchus mykiss*), char (*Salvelinus sp*.) and spirlin (*Alburnoidus bipunctatus*) in the river Iller.

3.10.1.2. Methodology

The fish ecological data are collected with electrical fishing. Therefore, the area downstream of the HPP of Altusried is fished electrically on a length of 1500 m at both shorelines against the flow and in the middle of the river with the flow. The fishing is done from a boat. An electrical fishing unit with a power of 13 kW is used. All caught fishes are collected in a tub. The tub is evaluated every 500 m of fishing. All fishes in the tub are measured (total length) and determined on species level. The electrical fishing is done twice a year, once in spring and once in autumn.

3.10.1.3. Results

The fish community of the river Iller has been quite poor in the last view decades. The main reason of this is suggested in the anthropogenic changes of the river Iller. The main influences have been the construction of HPPs and straightening of the shoreline. This led to a decline of spawning and juvenile habitats. As a result, the fish populations have been decreasing. To change this state, the BEW started two restoration projects, the Illerstrategie 2020 and the EU-project ISOBEL. Within these projects, the main goals are to create fish-bypass channels and a nature-like bed load situation in the downstream parts of the HPPs. Thus, spawning and juvenile habitats have been constructed. During the last few years, the populations of the main species present in the river Iller, are increasing again. This was indicated by electrical fishing campaigns in 2016, 2017 and 2018, which indicated presence of all characteristic fish species of the river Iller (Table 47 and Table 48). Most of them, such as barbel, Danube salmon, grayling, chub and brown trout were caught in gratifying numbers, both the juvenile and adult stages. Only the population of nase is still in rather poor condition. There have been documented only a few individuals.

Back to D2.2 Main index

Table 47: Results of the electrical fishing session at 12.04.2017 in the downstream area of HPP Altusried.

Species	Species	Number of individuals
Stone loach	*Barbatula barbatula*	5178
Barbel	*Barbus barbus*	18
Bullhead	*Cottus gobio*	111
Pike	*Esox lucius*	1
Stickleback	*Gasterosteus aculeatus*	203
Gudgeon	*Gobio gobio*	94
Danube Salmon	*Hucho hucho*	2
Rainbow trout	*Oncorhynchus mykiss*	2
Perch	*Perca fluviatilis*	5
Brown trout	*Salmo trutta fario*	9
Rudd	*Scardinius erythrophthalmus*	1
Chub	*Squalius cephalus*	105
Grayling	*Thymallus thymallus*	24
Tench	*Tinca tinca*	1
Sum		**5754**

Table 48: Results of the electrical fishing session at 10.07.2018 in the downstream area of HPP Altusried.

Spring electrical fishing 2018 downstream area HPP Altusried			**Date: 10.07.2018**
Species	**Species**	**Individual with a total lenght under 20 cm**	**Individuals with a total lenght above 20 cm**
Grayling	*Thymallus thymallus*	1386	97
Brown trout	*Salmo trutta fario*	7	2
Stone loach	*Barbatula barbatula*	1388	0
Barbel	*Barbus barbus*	728	22
Bitterling	*Rhodeus amarus*	7	0
Chub	*Squalius cephalus*	70	0
Stickleback	*Gasterosteus aculeatus*	490	0
Perch	*Perca fluviatilis*	38	4
Gudgeon	*Gobio gobio*	191	0
Pike	*Esox lucius*	2	0
Danube salmon	*Hucho hucho*	6	0
Bleak	*Alburnus alburnus*	8	0
Bullhead	*Cottus gobio*	87	0
Nase	*Chondrostoma nasus*	12	0
Rainbow trout	*Oncorhynchus mykiss*	20	1
Char	*Salvelinus sp.*	0	1
Tench	*Tinca tinca*	6	0
Spirlin	*Alburnoidus bipunctatus*	2	0
Cyprinides, unknown	*Cyprinidae*	0	1
Sum		**4448**	**215**

Back to D2.2 Main index

3.10.1.4. Conclusion

All typical species of a river of the lower alpine region can be found in the downstream water area of the HPP Altusried. Especially the high number of young grayling (*Thymallus thymallus*) in spring 2018 is very gratifying, as well as the 6 young Danube Salmon (*Hucho hucho*).

3.10.2. Hydrodynamic modelling (SJE)

3.10.2.1. Setup of model

It is assumed that hydrodynamics are among the main factors for the behaviour of migrating fish. “Attraction flow” is one of the most commonly used terms when talking about fish finding the entrance of bypass installations at migration barriers. For that reason, a hydrodynamic model has been set up in the Altusried Test Case to deliver flow velocities and water depth as input parameters for the migration model to be developed. The model does not only cover the fish pass entrance area but also the river stretch downstream of the entrance and the area upstream of the entrance up to the area close to the weir. This wide coverage was chosen in order to analyse how fish approach the fish pass from downstream and how they behave when having passed by the fish ladder entrance.

In order to provide a sufficient resolution of the river bathymetry, cross sections have been measured with an approximate distance of 10 to 15 meters by flussbau IC. Deeper areas have been surveyed using a boat equipped with echosounder, reflector and total station, shallower areas close to the river banks have been surveyed wading. In addition to the terrestric survey, an aerial survey by flights with a camera equipped drone has been performed after having surveyed the position of ground control points (GCPs; Figure 207). This has been done for two reasons: 1) the orthophoto derived from the pictures support the setting up of the hydrodynamic model, 2) the evaluation of the pictures using the SfM (Structure from Motion) methodology provides a higher resolution of the river bathymetry than the cross sections alone (Figure 208). SJE has used a self-developed approach to derive bathymetrical information not only in the areas above the water surface but also for the underwater areas.



Figure 207: Drone used for the aerial survey (left), Ground control point (GCP, right)

The hydrodynamic calculations have been done using the software Hydro-As_2D that is based on the Saint-Venant or shallow water equations. The model has been calibrated using the water elevation measurements performed during the field survey.

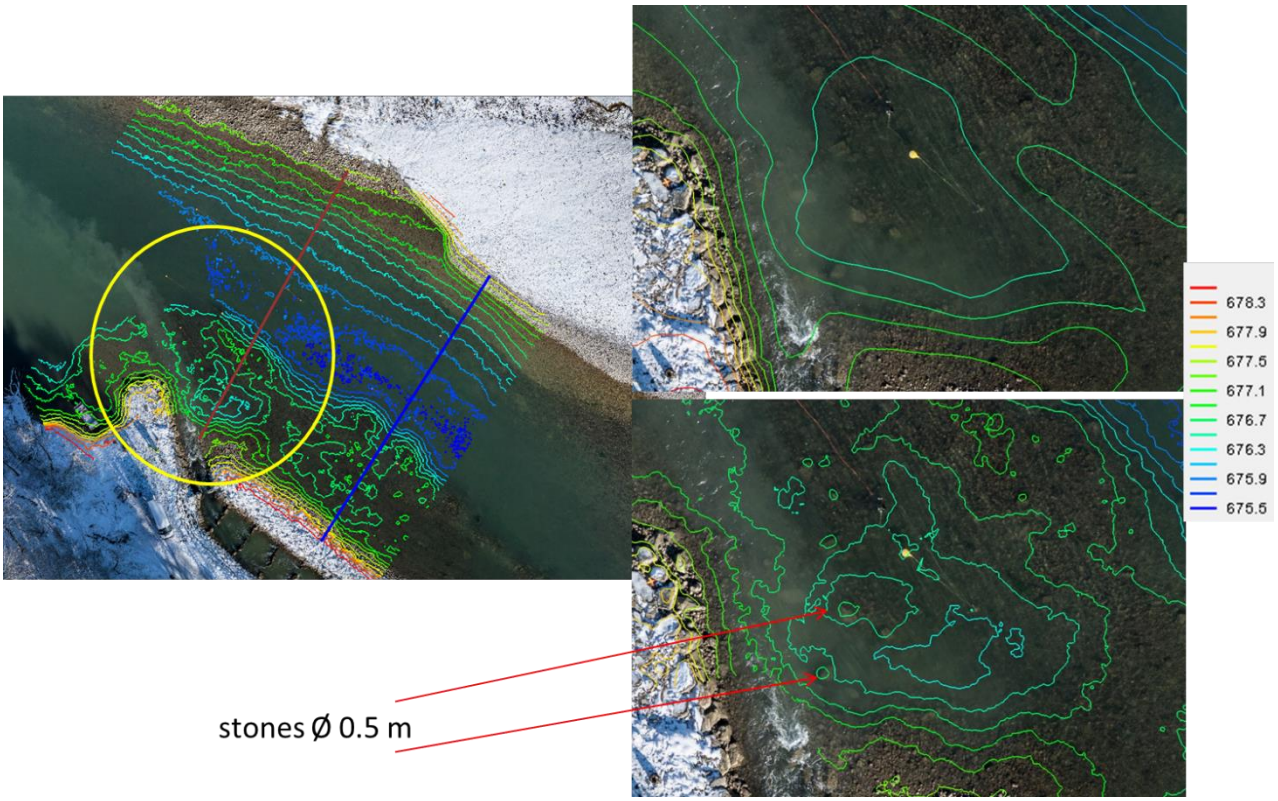
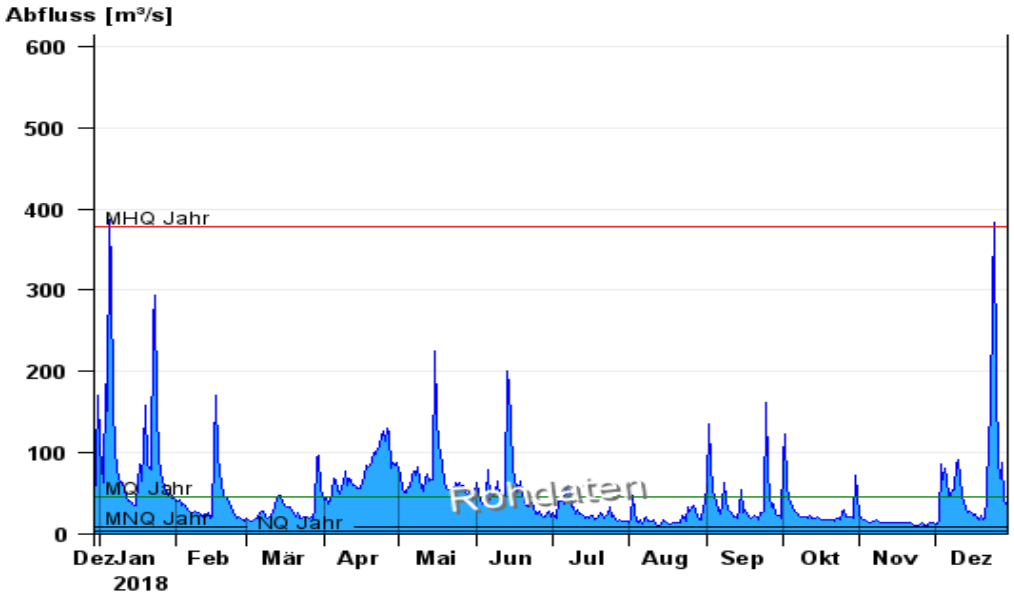


Figure 208: river bathymetry, derived by cross section interpolation (top), higher resolution derived by underwater SfM evaluation

3.10.2.2. Flow scenarios and results

The hydrological regime of the considered river stretch is pluvio-nival with low base flows in late summer, fall and winter and a high base flow in late spring and early summer during snow melt. However, the base flow is overlaid by regular mean and major flood events caused by rainfall events. In warm and rainy winter periods base flow can also be high, as can be seen in the following figure of the flow time series for the year 2018 (Figure 209).



Back to D2.2 Main index

Figure 209 : Flow registered at gage Kempten, approx. 8 km upstream of the Test Case site (from : https://www.hnd.bayern.de/pegel/iller_lech/kempten)

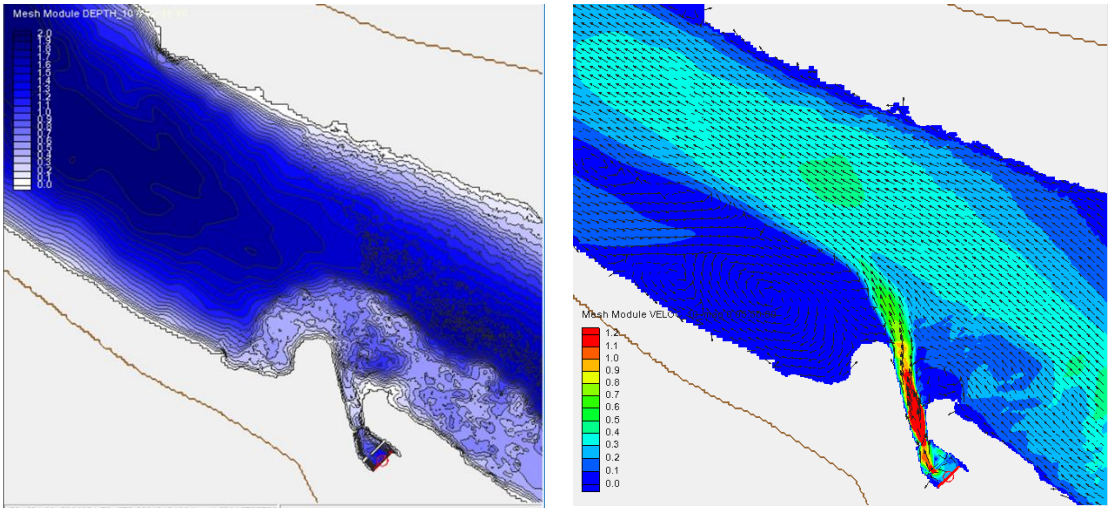
The flow scenarios to be modelled with the hydrodynamic model have been selected in order to cover a wide flow range with a certain probability to occur during the migration period of the considered fish species (grayling: March/April, barbel: May/June). However, since the HPP in the upper Iller are operated in a sort of storage mode during low flow situations, the probability of having a flow around 10 m³/s in the low flow season is increased. The following flows are considered:

Table 49: flows covered with model and hydrological characteristic

Flow	**Hydrological characteristic**
10 m³/s	Approx. MALF*, close to minimum flow (9 m³/s)
20 m³/s	Approx. 2·MALF
40 m³/s	Approx. MAF** winter
60 m³/s	Approx. MAF Summer
80 m³/s	Slightly increased summer flow

*MALF: Mean annual low flow
**MAF: Mean annual flow

Results from the hydrodynamic model are shown in Figure 210. It can be seen that for the low flow situation with 10 m³/s the flow velocities are increased in the area close to the fish ladder outlet. Usually, this zone of increased flow velocities is considered to have a guiding function for fish searching the fish ladder entrance. But even for the low flow situation, the increased flow velocities can only be detected in the direct vicinity of the fish ladder entrance (see figure top right). For higher flows, the extension of the higher flow velocity area is much less distinct (see figure bottom left).



Back to D2.2 Main index

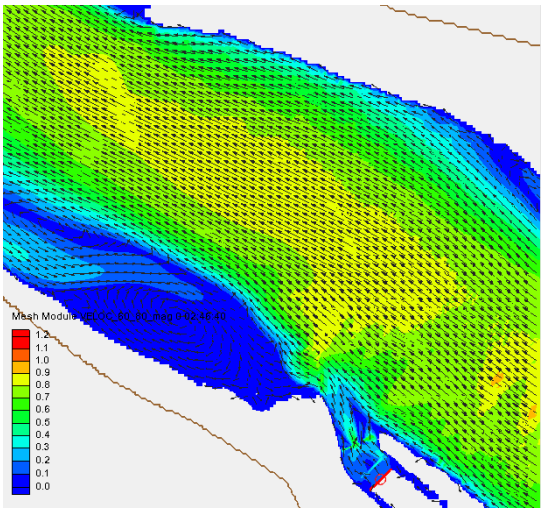


Figure 210 : Model results for 10 m³/s (top) and 60 m³/s (bottom), water depth (left), flow velocity (right)

3.10.3. Telemetry system (INBO)

Acoustic telemetry was chosen to analyse how upstream swimming fish approach the fish pass from downstream and how they behave when having passed by the fish ladder entrance. More precisely, the Vemco Positioning System (VPS) was applied to track the behaviour of the fish in 2 dimensions (2D telemetry). The area of interest is the same as for which the hydraulic model is developed, and includes the fish pass entrance area but also the river stretch downstream of the entrance and the area upstream of the entrance up to the area close to the weir.

3.10.3.1. Acoustic telemetry and the Vemco Positioning System (VPS)

Telemetry is used to monitor objects, such as animals, remotely. It involves placing electronic devices (“transmitters” or “tags”) on animals that autonomously transmit data to data logging or relay-receiving stations (“receivers” or “hydrophones”). Because radio waves do not propagate in salt water, most aquatic telemetry is rooted in two principal approaches: acoustic and satellite telemetry. Acoustically tagged animals are detected and logged by receivers moored at fixed locations that are retrieved periodically, or by mobile receivers (e.g., on a pursuit vessel), whereas satellite observations are sent to land-based receivers via orbiting satellites. Electronic tags may be secured externally, inserted into the stomach, or surgically implanted in animals and programmed to record and/or transmit various data types, ranging from simple presence and location to extensive time series records of the animal’s movements and environment (e.g., depth, temperature).

With rapid technological advancements over the past several decades more telemetry techniques, such as acoustic telemetry, became available to observe animal behaviour and movement in challenging environments (Hussey et al. 2015). Each technique has its opportunities and drawbacks and these greatly depend on the research question and characteristics of the environment where the studied animals behave and move. For instance, tracking aquatic animals under water requires techniques that allow propagation of info through water. As air is needed to transmit and receive satellite telemetric signals, satellite telemetry does not support tracking animals that exclusively behave and move below the water surface. Instead, radio telemetry, Passive Integrated Transponder (PIT) telemetry and acoustic telemetry are techniques that enable the monitoring of aquatic animal behaviour and movement under water. To study fish behaviour and movement in two dimensional space in

the area of interest in the river Iller, acoustic telemetry was selected and assumed to be the most (cost-) efficient technique.

Acoustic telemetry is a technique that makes use of the propagation of sound through water. It is much like speaking and listening under water. An acoustic tag emits a sound with regular or irregular time intervals. The sound is propagated through water as sound-waves and can be received by an underwater antenna or hydrophone. The hydrophone is part of what is called a receiver or acoustic listening station (ALS ; also simply named hydrophone). The sound that is emitted/transmitted by the acoustic tag is unique and encodes a unique series of numbers, called the ID code of the tag. When the tag is in the detection range of a hydrophone, the hydrophone hears and decodes the sound and logs the resulting ID code and precise timing of the detection.

In one dimensional acoustic telemetry, an autonomous hydrophone is placed under water to evaluate the potential presence of an acoustic tag within its detection range. The detection range is a spherical area around (but not below) the antenna of the hydrophone (Figure 211).

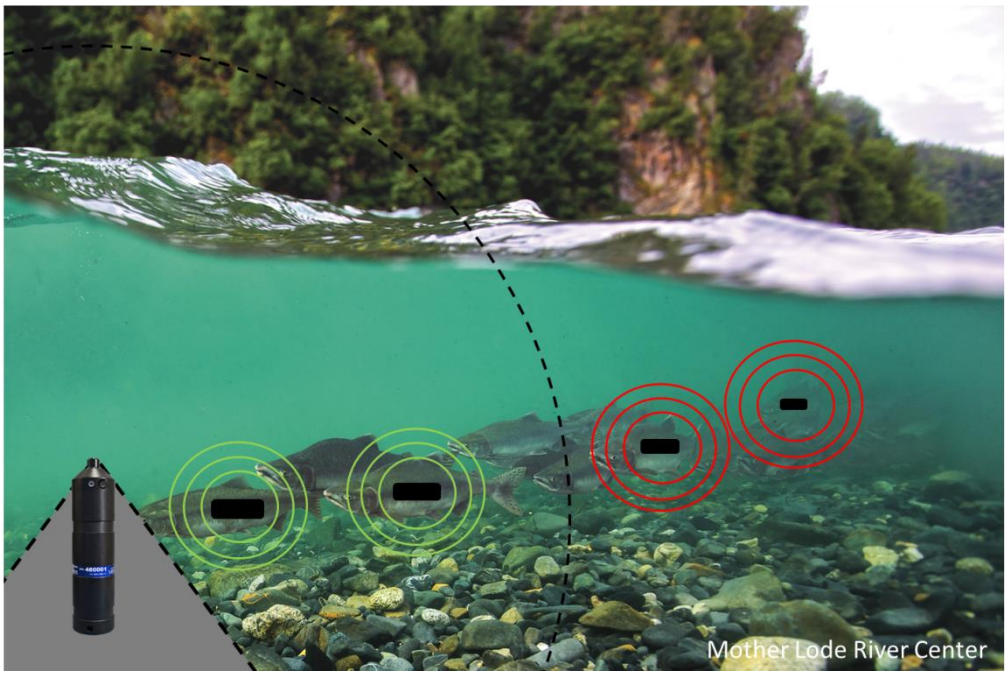


Figure 211: Schematic view of the detection range (outside the grey area within the dashed circle) of one autonomous hydrophone fixed at the bottom of a river. Tagged fish that are within the detection range (green encircled tags) are logged (ID code) as being present at each time stamp that their emitted signal is heard by the hydrophone. ID codes of tagged fish outside of the detection range of the hydrophone are not logged at those time stamps because they are not heard by the hydrophone and are thus assumed absent from the detection range of the hydrophone. One hydrophone can only define presence/absence and not the exact position of the tag within its detection range (1 dimensional acoustic telemetry).

The dimensions of the detection range are not static and depend on a variety of environmental cues, ranging from background noise over hydro morphology and bathymetry of the lake or river, type of substrate, and the stream velocities and signatures potentially causing turbulence and air bubbles. The exact relation between environment and dimensions of the detection range is different for each study area and difficult to disentangle. Therefore, in each newly installed acoustic telemetry network, range tests need to be performed to get a good idea of the detection coverage and detection probability before any conclusions can be drawn on the

presences of fish in a certain area (1 dimensional telemetry) or its exact position in the area (2 dimensional telemetry; Kessel et al. 2013).

In 2 and 3 dimensional acoustic telemetry, autonomous receivers are installed in a configuration so that every location in the area of interest is covered by the detection range of at least three receivers. Based on the theory of the propagation speed of sound through water and info on the exact timings of emission and detection of the acoustic signal of a tag, its position relative to the hydrophones that detected it, can be defined. More precisely, this method is called hyperbolic triangulation and is based on the time difference of arrival of the signals on the hydrophones detecting the signal. More info on hyperbolic triangulation can be found in the manual of the Vemco company (Smith 2013). The subsequent calculated positions of one tag give an idea of the track that the tagged fish has swum (Figure 212).

When Vemco hydrophones are used to set up a 2D/3D acoustic telemetry network, it is called VPS telemetry (Vemco Positioning System; https://vemco.com/products/vps/). Sometimes VPS telemetry is used as a synonym for 2D/3D acoustic telemetry, regardless of the company providing the acoustic devices. In this study, we used Vemco hydrophones and tags (see section 3.10.3.2).

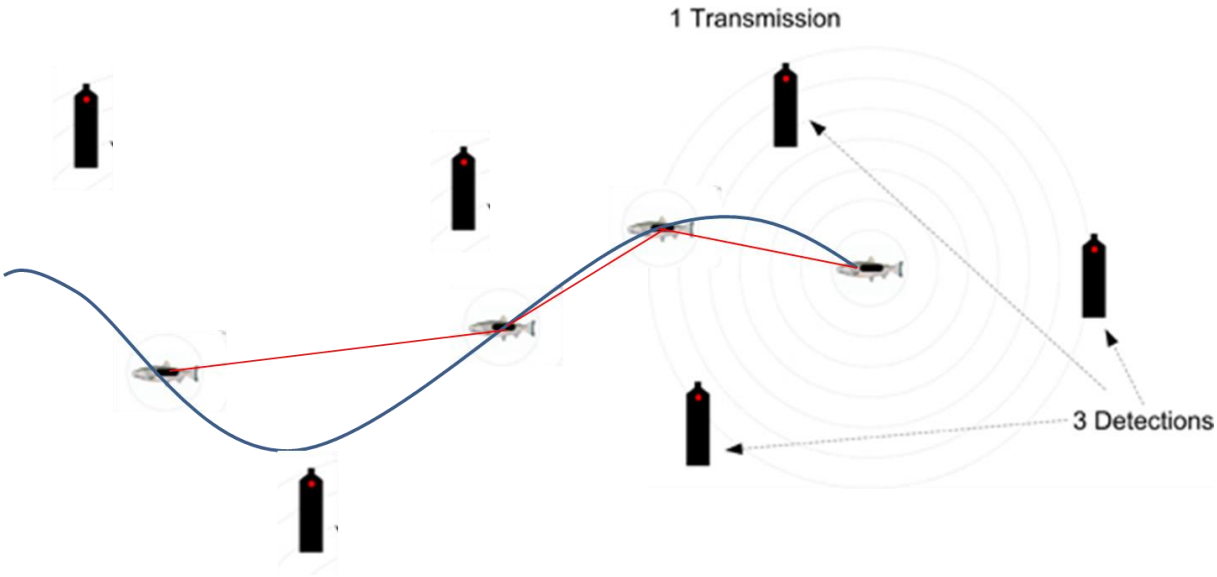


Figure 212: Schematic view of 2 dimensional acoustic telemetry. The relative position of a tagged fish towards the hydrophones (black bottles) is calculated based on the theory of the propagation speed of sound through water and info on the timing of emission of the tag signal and its detection on minimally three hydrophones. Subsequent positions give an idea (red line) of the track that the fish has swum (blue line).

Each calculated position has a certain error involved. This is due to a propagation of errors in each step of the detection and calculation process and the causes of these errors at each level are multiple and different. For instance, environmental cues that affect the arrival time of a detection can cause errors on the calculated position, but also errors on the defined positions of the hydrophones detecting the tag will cause an error on the calculated positions of the fish in its environment. Next, a certain error on each position also follows from the configuration of the hydrophone network and is inherent to the method of hyperbolic triangulation (see also Smith 2013). Specifically, tags that are within a triangle of hydrophones are far less sensitive to error than tags that are at the boundaries of the triangle or outside.

Error caused by static phenomenon's such as the configuration of the receiver network or an error on the positioning of the hydrophones is easier to define and deal with than errors that are caused by environmental cues, which are mostly spatially and temporally dynamic. For instance, the error following from the configuration of the network is calculated and reported by Vemco and defined in an HPE (Horizontal Positioning Error) value that comes along with each calculated position (see also Smith 2013). The relation between environmental cues and the error following from this is far more difficult to define and more difficult to assess. To date, no standard method is available to filter out all error present on calculated positions. Research on this topic is on-going (Baktoft et al. 2017, Meckley et al., 2014) and available methods will be tested in this study as well. Although detailed knowledge on the error on the calculated fish positions is necessary, it is not always needed to filter out all present error to solve a research question in a correct way, but it depends on the research question.

Regardless of any method to filter out error on calculated positions, it is necessary to get a clear view on the error present in each study before you can decide how this affects the correctness of your research result. To get a view on the present error, reference situations are created in the VPS network. For instance, test tracks can be created at the setup of the hydrophone network or during the study. A test track is a track of a test tag, which is not implanted in a fish but for instance, attached to a small floating vehicle and of which the exact position is permanently known (measured with a GPS). So, the observed (real) positions can be compared to the calculated positions. Another way to test for error during the continuation of the entire study is to install reference tags in the study area. These tags are fixed at a known (measured with a precise GPS), fixed position. The tags are detected throughout the entire study so that the fixed, known position can be compared with the calculated positions and errors can be defined on the calculated positions as the difference between the observed and calculated positions. The latter may also clarify potential temporal patterns in error.

Acoustic telemetry devices

Different types of telemetric systems and devices exist that can be used for acoustic telemetry. First of all, different companies exist that have their own specific products. In this study, we chose to work with Vemco (www.vemco.com). Generally, Vemco provides two different ways of ID code/signal emission from the tags. The signal can be either emitted as a pulse train of sounds, each encoding a small part of the ID code (called PPM way of transmitting the ID code), or it can be emitted as one sound that encodes the entire ID code at once (called HR way of transmitting the ID code). PPM and HR transmission each have their advantages and disadvantages and one or the other might be better suited depending on the study objectives and environment. Differences between PPM and HR that might affect the choice for one or the other are the duration of ID code emission, which is higher (up to 3 sec) in PPM than HR (less than 1 sec), their sensitivity to reflections of the signals, which is lower for PPM than HR, and their detection range. Only the first difference is not affected by the environment that is investigated.

Depending on the system that is selected for the study (PPM or HR) different hydrophone types are available. Hydrophones differ in the frequency that they can hear and decode. Vemco produces hydrophones that work either for emitted signals on 69 kHz or 180 kHz. No hydrophones exist that can hear and decode both frequencies. Hydrophones that hear and decode 69 kHz only work for PPM emitted signals, whereas the more recently developed 180 kHz hydrophones can hear and decode both PPM and HR emitted signals. Some types of hydrophones have a built-in tag, which is called the sync-tag and which enables the synchronisation of different hydrophones in the same (VPS) network and which can be used

as reference tags at the same time, and others don't have this ability built in. Next, some hydrophones contain sensors, measuring temperature, background noise and the vertical position of the hydrophone (the tilt), whereas others do not have these sensors built in.

3.10.3.2. Setup of the VPS network

To collect accurate and precise fish tracks in the study area of 500 m around the fish pass outflow, a VPS network of hydrophones had to be installed in the area. Previous to installation, the most efficient telemetric system (devices) had to be defined for this study and the study environment. Multiple tests were performed with different types of devices.

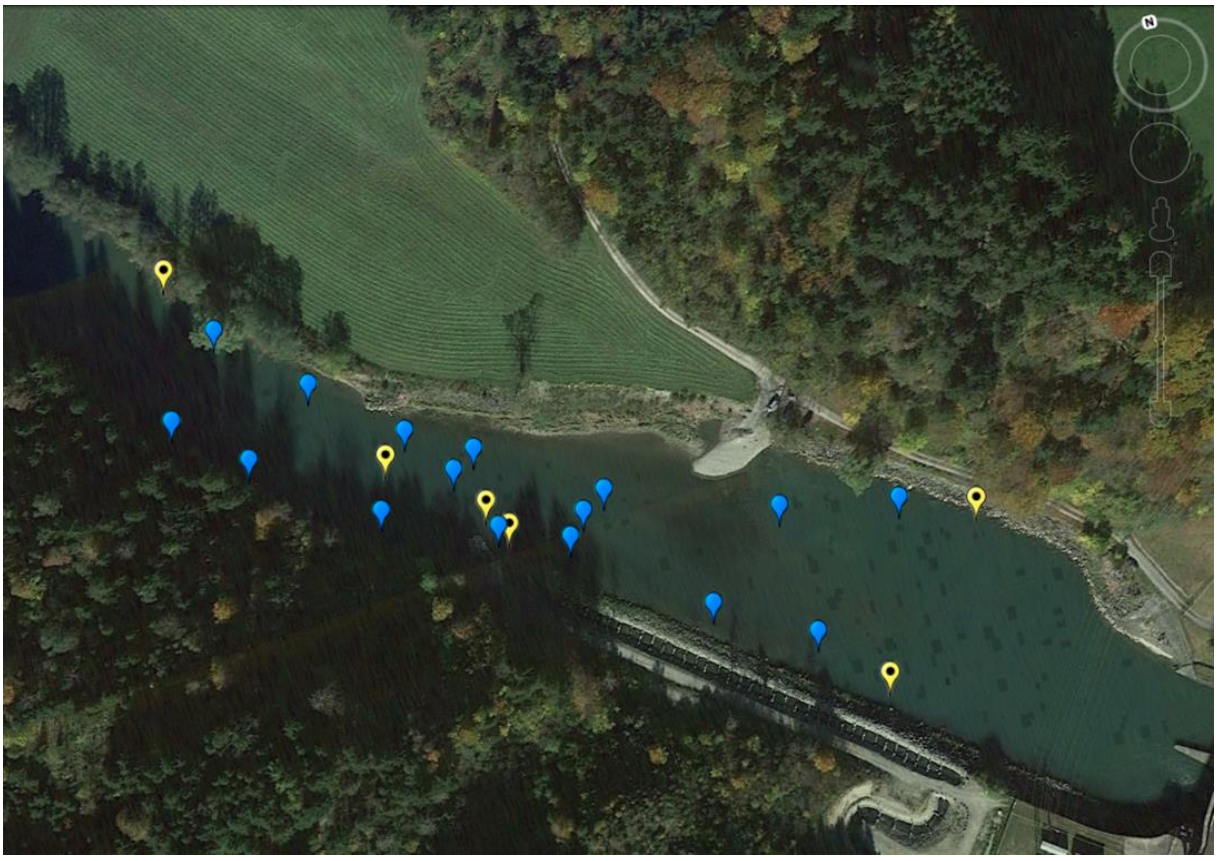
In May 2017 the 69 kHz PPM system of Vemco was tested with hydrophones having built-in sensors and a tag. In August 2017, range tests with the 180 kHz PPM and HR system were performed. The results of the tests indicated that the 180 kHz system performed better than 69 kHz in this study area, which is characterised by high flow velocities and a rough bathymetry causing turbulence (air bubbles and noise) and reflections of the tag signals, and background noise from the HPP turbines. Next, it was found that HR performed well and since it can have very short emission delays (the time between two emissions is called the delay of the tag) of only 1 sec, in contrast to PPM tags that already need up to 3 sec for one emission, it was selected above PPM. Very frequent emissions (delays of only 1,1 sec) are needed to get accurate tracks that are based on positions of the tagged fish every 1 to 3 m. Such 'high resolution' tracks are needed to make the link with flow velocity and bathymetry info in high detail resulting from the hydrodynamic model (section 3.10.2). Further, the tests indicated an optimal spacing of hydrophones of around 40 m (direct line of sight).

In February 2018 further profound tests were performed with the 180 kHz HR and PPM systems to clarify the number of hydrophones needed and their best positions so that the entire study area is covered with the detection ranges of minimally three receivers in the best possible way. Next, the mooring system needed to fix the hydrophones at their best position was tested. It is important that this mooring system holds the hydrophone near the bottom of the river, in a perfect vertical position (tilt of 0 to maximally 10°) for the entire study and thus also in harsh conditions with high discharges and flow velocities. At the same time, the mooring system should allow an easy recovery of the hydrophones at the end of the study to download the logged data. Figure 213 shows the mooring system used for the hydrophones and reference tags in this study.

The resulting VPS network existed of 16 180 kHz HR2 (High Residency) receivers with built-in sync-tags and temperature, noise and tilt sensors, and 6 reference tags (Figure 214). The hydrophones were moored on steel pyramid constructions that were fixed on the river bottom by means of steel chains running from one river bank to the other over the river bottom.



Figure 213: Pictures of the mooring of the reference tags (a) and the hydrophones with steel pyramid constructions (c) attached to a steel chain that is anchored at both sides of the river and runs over the river bottom (b). In total 16 pyramid constructions where attached to 7 chains spread over the study area. The hydrophone is held vertically by attachment to the top of the pyramid in picture c.



(a)



(b)



(c)

Figure 214: (a) Locations of the 16 hydrophones (blue marks) and 6 refefence tags (yellow marks) as positioned with a Trimble GPS at installation and recovery. (b) Location of all 19 hydrophones in the study, and 6 reference tags of the VPS network. (c) Zoom on the locations of the two hydrophones in the fish pass.

The fish tags were chosen to emit an HR signal with a variable delay between 1.1 and 1.3 sec and an additional PPM signal with a variable delay between 50 and 70 sec. Table 50 lists all specific receiver and tag characteristics used in this study.

Table 50: Overview of the type of devices (hydrophones and tags) used in this study and their specifications. The sensors in the hydrophones log temperature, tilt of the hydrophone and background noise.

Device (#)	**Delay of the (built-in) tag (sec)**	**Output power of the (built-in) tag**	**Sensor logging frequency**	**Estimated battery life**	**Weight (g)**
180 kHz HR2 hydrophones (19)	HR: 4-6 PPM: 25-35	Very High		6 months	-
V9-2x 180 kHz reference tags (6)	HR: 25-35 PPM: 270-330	High	-	min. 6 months	-
V9-2x 180 kHz fish tags (47)	HR: 1.1-1.3 PPM: 50-70	High	-	143 days	In air: 3.7 In water: 2

Apart from the 16 hydrophones installed in the area surrounding the fish pass outflow, three hydrophones (same type and characteristics) were placed around the study area to evaluate presence of tagged fish. One hydrophone was placed at app. 2 km downstream of the VPS network in the river Iller, covering the width of the river with its detection range to evaluate if

studied fish left the study area in downstream direction. Two other hydrophones were placed half way and upstream in the fish ladder, respectively (Figure 214). These hydrophones were used to evaluate if fish used the fish ladder to migrate upstream. Next, the upstream hydrophone helped to evaluate the efficiency of the counting pool (Figure 214). Not all fish that swim upstream to the counting pool are trapped in it and thus caught and marked by the BEW investigator.

3.10.3.3. Fish tagging and tracking

In the week of March 19th 2018, the VPS network was installed in its final position for the study. In the weeks following on the hydrophone installation, 47 wild fishes were caught, tagged and released in the VPS array at the most downstream hydrophone near the left bank (Table 51). The hydrophones were recovered again on the 22nd of August 2018 to download the logged data and were not re-installed in the water because the battery life of hydrophones and tags was ending. Furthermore, the aim was to monitor upstream fish migration and the spawning season (and so upstream spawning migration) is believed to last no longer than the beginning of July. None of the batteries of tags, neither hydrophones had run out before the end of the study. Some of the fish had left the VPS array before the end of the study (Table 51), but the reason is not known. They might have died and drifted downstream, might have been caught by anglers or might have swum downstream actively. Active escapement upstream was not possible as the dam is not passable unless the fish takes the fish pass. However, fish could not leave the fish pass upstream without being caught in the counting pool.

The aim was to tag and track as much individuals as possible of one species with a special focus on grayling and barbel as these species are known to be dominant in the river Iller and are known to swim upstream during the spawning period to find suitable spawning habitat. Grayling mainly spawn in March-April in this area, whereas barbel is known to spawn later in spring (late April, beginning of May). Therefore first grayling were caught until the spawning was believed to have started. To define the timing of spawning of grayling and barbel in the river Iller in spring 2018, the presence of eggs or sperm in the bellies of caught fish was evaluated during tagging surgery. 25 grayling were caught, tagged and released in the VPS array successfully (Table 51). Next, 22 barbel were successfully caught, tagged and released. Table 51 indicates the catch method and location of each of the tagged grayling and barbel as well as the dates of catch, tagging and release. Next, this table indicates the day at which the fish was detected by the VPS array the last time. Figure 215 shows the catch and release locations of the studied fish.

Table 51: Info on the 47 individual wild fish of two species (barbel and grayling) that were tagged and tracked in this study.

ID code	Species	Total length (mm)	Weight (g)	Catch method	Catch location	Release date	Last VPS detection
46838	Barbus barbus	570	2160	Counting pool Altusried	Fish pass	29/05/2018	22/08/2018
46839	Barbus barbus	594	2161,7	Counting pool Altusried	Fish pass	29/05/2018	22/08/2018
46840	Barbus barbus	456	932,6	Counting pool Altusried	Fish pass	29/05/2018	22/08/2018
46844	Barbus barbus	504	1285,8	Counting pool Altusried	Fish pass	24/05/2018	22/08/2018
46845	Barbus barbus	496	1106,8	Counting pool Altusried	Fish pass	24/05/2018	22/08/2018
46846	Barbus barbus	460	911,2	Counting pool Altusried	Fish pass	24/05/2018	5/06/2018
46847	Barbus barbus	619	2343,3	Counting pool Altusried	Fish pass	24/05/2018	22/08/2018
46848	Barbus barbus	545	1567,6	Counting pool Altusried	Fish pass	24/05/2018	22/08/2018
46849	Barbus barbus	480	1180,5	Counting pool Altusried	Fish pass	29/05/2018	22/08/2018
46850	Barbus barbus	526	1465,7	Counting pool Altusried	Fish pass	24/05/2018	22/08/2018
46851	Barbus barbus	330	327,2	Counting pool Altusried	Fish pass	24/05/2018	1/06/2018
46852	Barbus barbus	460	1053,2	E-fishing	Fish pass	24/05/2018	22/08/2018
46853	Barbus barbus	461	1010,6	Counting pool Altusried	Fish pass	24/05/2018	22/08/2018
46854	Barbus barbus	585	2105,1	Counting pool Altusried	Fish pass	24/05/2018	22/08/2018
46855	Barbus barbus	594	2212,7	Counting pool Altusried	Fish pass	24/05/2018	22/08/2018
46856	Barbus barbus	513	1544,1	Counting pool Altusried	Fish pass	24/05/2018	26/06/2018
46857	Barbus barbus	457	822,9	E-fishing	Fish pass	24/05/2018	22/08/2018
46858	Barbus barbus	516	1306,5	Counting pool Altusried	Fish pass	17/05/2018	22/08/2018
46859	Barbus barbus	387	648,4	Counting pool Altusried	Fish pass	17/05/2018	22/08/2018
46860	Barbus barbus	545	2074,4	Counting pool Altusried	Fish pass	17/05/2018	22/08/2018
46861	Barbus barbus	466	1009,6	Counting pool Altusried	Fish pass	17/05/2018	22/08/2018
46862	Barbus barbus	400	621,2	Counting pool Altusried	Fish pass	17/05/2018	18/05/2018
46863	Thymallus thymallus	403	673,3	E-fishing	Iller	11/04/2018	19/04/2018
46864	Thymallus thymallus	409	623,2	Counting pool Altusried	Fish pass	11/04/2018	18/04/2018
46865	Thymallus thymallus	350	315	NA	NA	11/04/2018	7/06/2018
46866	Thymallus thymallus	326	262,1	Counting pool Altusried	Fish pass	11/04/2018	24/04/2018
46867	Thymallus thymallus	439	755,4	Counting pool Altusried	Fish pass	11/04/2018	20/04/2018

46868	Thymallus thymallus	420	791,3	E-fishing	Iller	4/04/2018	15/04/2018
46869	Thymallus thymallus	508	1250,8	Counting pool Altusried	Fish pass	11/04/2018	11/04/2018
46870	Thymallus thymallus	426	756,8	Counting pool Altusried	Fish pass	11/04/2018	17/04/2018
46871	Thymallus thymallus	416	843,9	E-fishing	Iller	11/04/2018	19/04/2018
46872	Thymallus thymallus	411	640,1	Counting pool Altusried	Fish pass	11/04/2018	20/04/2018
46874	Thymallus thymallus	348	402,1	E-fishing	Iller	4/04/2018	23/05/2018
46901	Thymallus thymallus	383	657,7	E-fishing	Iller	4/04/2018	20/04/2018
46902	Thymallus thymallus	431	712,3	E-fishing	Iller	4/04/2018	4/04/2018
46903	Thymallus thymallus	371	444,6	Counting pool Altusried	Fish pass	4/04/2018	9/04/2018
46904	Thymallus thymallus	494	1048,5	E-fishing	Iller	4/04/2018	24/04/2018
46905	Thymallus thymallus	425	642,4	Counting pool Altusried	Fish pass	4/04/2018	15/04/2018
46906	Thymallus thymallus	498	1152,9	E-fishing	Iller	4/04/2018	15/06/2018
46907	Thymallus thymallus	331	317,3	Counting pool Altusried	Fish pass	4/04/2018	11/04/2018
46908	Thymallus thymallus	400	683	E-fishing	Iller	4/04/2018	15/04/2018
46909	Thymallus thymallus	389	634,2	E-fishing	Iller	4/04/2018	14/04/2018
46910	Thymallus thymallus	406	707,3	E-fishing	Iller	4/04/2018	18/04/2018
46911	Thymallus thymallus	309	233,4	E-fishing	Iller	4/04/2018	12/04/2018
46912	Thymallus thymallus	407	606,4	Counting pool Altusried	Fish pass	4/04/2018	13/04/2018
46913	Thymallus thymallus	318	312	E-fishing	Iller	28/03/2018	5/04/2018
46914	Thymallus thymallus	304	286	E-fishing	Iller	28/03/2018	10/04/2018

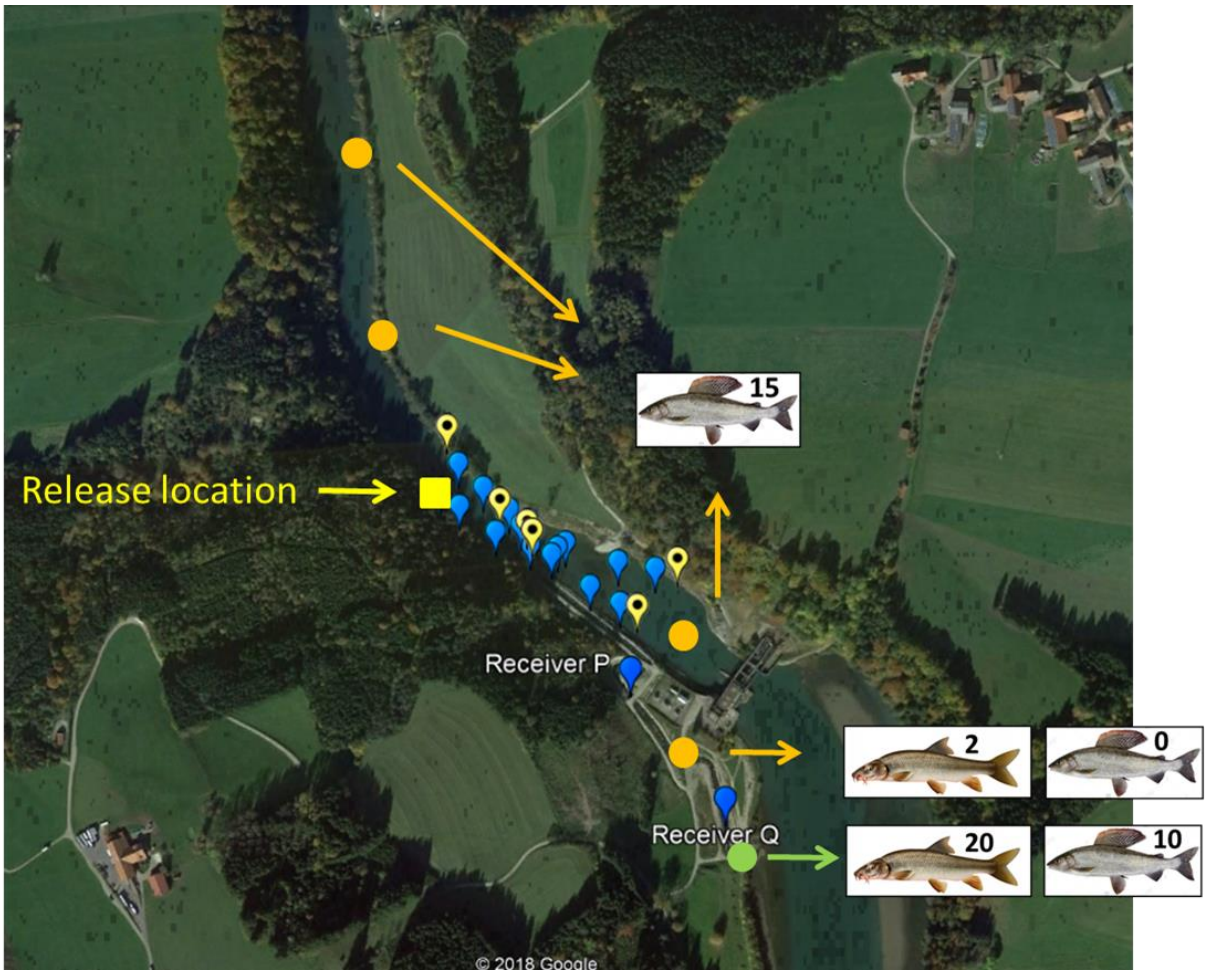


Figure 215: Indication of the number of grayling (top and right fish pictures) and barbel (left fish pictures) and their catch and release location in the study area. Yellow dots indicate locations where fish were caught electrically, whereas the green dot indicates the location of the counting pool, which was also used to catch studied fish. Further biometric info and info on the catch method is listed in Table 51.

Fish were caught electrically or in the counting pool. Once a fish was caught it was held in an aerated tank with water and brought to the hydropower plant, where the fish were operated on. Before surgery fish were put in an aerated tank with phenoxy-ethanol to sedate the fish (around 10 ml phenoxy-ethanol for 50 l of water). Once the fish was sedated (this took on average 6 +/- 1:46 min), it was laid on his back in a V-shaped tray placed in a water tank filled with a diluted solution of the anaesthetic so that the gills were constantly under water. The tag (Vemco V9-2X-180k, cylindrical shape 26x9 mm, weight 2·0 g in water, 180 kHz frequency, 143 days battery life, high power output and small HR delay of 1.1-1.3 sec) were implanted surgically by a 1·0–1·5 cm incision made behind the pelvic girdle, at the level of the upper edge of the pelvic fin, according to Nykänen et al. (2001). The weight of the tag in water was always < 0.85 % of the grayling weight and < 0.61 % of the barbel weight, remaining well below the recommended maximum of 2% (Winter, 1983). The surgery lasted for 7 min, on average. The tagged fish were transferred into another aerated tank with water to recover, and released into the river as soon as they could swim. Recovery generally took minimally 3 to maximally 12 min.

3.10.4. Fish tracks and evaluation – preliminary results (INBO)

Throughout the study, over 15 million fish positions of 47 fish were collected. Tagged fish stayed in the VPS network between 2 and 96 days (Table 52). Barbel resided on average far longer in the VPS network than grayling. Three of 25 tagged grayling were recovered at the hydropower plant of Fluhmhüle, downstream of Altusried. These fish were dead and infected

with a fungus. The fish itself was infected and not only the stitched incision of the tagging surgery. Also, not-tagged grayling were caught that were alive but infected with the parasite. The grayling positions and tracks collected do not indicate that grayling was highly affected by the tagging procedure. Nonetheless, it appeared that grayling was more sensitive to the handling and tagging than barbel, since no dead tagged barbel were found and most moved in the VPS network from the day of release until the end of the study.

3.10.4.1. Performance of the VPS network

As a broad, preliminary, measure, the median error of sync/ref positions was 0.32 m, and the 90% percentile error was 2.08 m. These numbers vary both spatially throughout the array, and temporally, as environmental conditions change. The primary source of error in the system was that of multipath signals, which are transmissions that reflect and are received later than they should if they were transmitted to the hydrophone in a straight line.

The mooring system withstood the highest discharges of 200 – 220 m³/s encountered during the studied period (Figure 216). Although some hydrophone movements were detected by Vemco during analyses of the detections of sync-tags, all calculated (based on the detections), hydrophone positions were within 1 m of the positions as measured with the Trimble GPS, after adjustments for hydrophone movement and time synchronisation of the hydrophone clocks. The trimble GPS measurements had a maximal error of 20 cm, but with hydrophone movement included finally each hydrophone position had a potential error of up to 1 m. Beside the hydrophone positions, the tilt was measured at the start and end of the study. The largest difference in tilt of a hydrophone observed between start and end of the study was 2°, which is minimal.

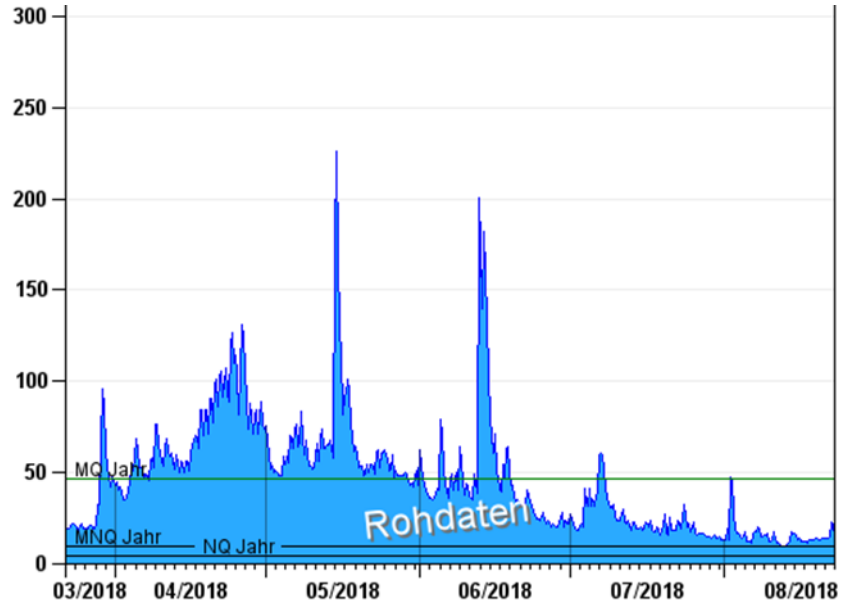


Figure 216: Discharge (in m³/s) of the river Iller in Kempten during the studied period (see also Figure 209).

3.10.4.2. Fish behaviour

So far, no fish tracks were evaluated although they are collected already. This is due to the fact that present errors on the fish positions still need to be evaluated and positions with low precision and accuracy need to be removed from the dataset before any further analysis can be performed.

Back to D2.2 Main index

The detections on the hydrophones in the fish pass give already info on which fish have found the fish pass entrance and have swum up the fish pass. These detections indicated that of all 25 tagged grayling, 12 found the entrance of the fish ladder at least once and swum up the fish ladder till halfway. Of these 12 grayling, 10 proceeded their way up until the counting pool (hydrophone upstream) of which two did this repeatedly (Table 52). Those two grayling were caught in the counting pool on 9th and 12th of April 2018, which is 5 and 8 days after their release in the VPS network, respectively. Of the 22 tagged barbel, eight found the entrance of the fish pass and swum upstream to the hydrophone halfway. Six of them proceeded their way up till the hydrophone upstream. Three of them moved upstream repeatedly and were finally caught in the counting pool respectively on the 2nd , 2nd and 12th of June 2018, which is 10, 10 and 19 days after their release in the VPS network. Hence, these data give a catch efficiency of the counting pool of 2 out of 10 (20%) for grayling and 3 out of 6 (50%) for barbel.

Table 52: Indication of the number of days that a tagged fish was detected in the VPS network and if the fish swum up the fish ladder or not, till where and only once or multiple times, and the date that a fish was caught in the counting pool if any catch occurred.

ID code	Species	Days detected (#)	Detection half way fish ladder	Detection upstream fish ladder	Repeated detections upstream fish ladder	Counting pool catch
46838	Barbus barbus	79	yes	yes	no	-
46839	Barbus barbus	83	yes	no	no	-
46840	Barbus barbus	71	no	n/a	no	-
46844	Barbus barbus	69	yes	yes	no	-
46845	Barbus barbus	72	no	n/a	no	-
46846	Barbus barbus	6	no	n/a	no	-
46847	Barbus barbus	70	yes	yes	yes	2/06/2018
46848	Barbus barbus	81	no	n/a	no	-
46849	Barbus barbus	81	no	n/a	no	-
46850	Barbus barbus	86	yes	yes	no	-
46851	Barbus barbus	9	no	n/a	no	-
46852	Barbus barbus	73	yes	yes	yes	2/06/2018
46853	Barbus barbus	84	no	n/a	no	-
46853	Barbus barbus	82	no	n/a	no	-
46854	Barbus barbus	90	no	n/a	no	-
46855	Barbus barbus	81	yes	yes	yes	12/06/2018
46856	Barbus barbus	32	no	n/a	no	-
46857	Barbus barbus	83	no	n/a	no	-
46858	Barbus barbus	96	yes	no	no	-
46859	Barbus barbus	90	no	n/a	no	-
46860	Barbus barbus	83	no	n/a	no	-
46861	Barbus barbus	89	no	n/a	no	-
46862	Barbus barbus	2	no	n/a	no	-
46863	Thymallus thymallus	6	no	no	no	-
46864	Thymallus thymallus	8	no	n/a	no	-

46865	Thymallus thymallus	14	no	n/a	no	-
46866	Thymallus thymallus	14	no	n/a	no	-
46867	Thymallus thymallus	7	no	n/a	no	-
46868	Thymallus thymallus	10	yes	yes	no	-
46869	Thymallus thymallus	1	no	n/a	no	-
46870	Thymallus thymallus	6	yes	yes	no	-
46871	Thymallus thymallus	8	yes	yes	no	-
46872	Thymallus thymallus	10	yes	yes	no	-
46874	Thymallus thymallus	7	no	n/a	no	-
46901	Thymallus thymallus	16	yes	no	no	-
46902	Thymallus thymallus	1	yes	yes	no	-
46903	Thymallus thymallus	6	no	n/a	no	-
46903	Thymallus thymallus	5	no	n/a	no	-
46904	Thymallus thymallus	21	no	no	no	-
46905	Thymallus thymallus	13	yes	yes	no	-
46905	Thymallus thymallus	12	yes	yes	no	-
46906	Thymallus thymallus	59	yes	no	no	-
46907	Thymallus thymallus	3	no	n/a	no	-
46908	Thymallus thymallus	12	yes	yes	no	-
46909	Thymallus thymallus	9	no	n/a	no	-
46910	Thymallus thymallus	14	yes	yes	yes	9/04/2018
46911	Thymallus thymallus	2	no	n/a	no	-
46912	Thymallus thymallus	9	yes	yes	yes	12/04/2018
46913	Thymallus thymallus	3	no	n/a	no	-
46914	Thymallus thymallus	9	no	n/a	no	-

3.10.4.3. Future work

The positions of sync- and reference tags should be analysed further to clarify how errors were induced spatially and temporally, and how these errors can be corrected for.

Next, three different methods will be applied on the data and their results compared, to filter out calculated fish positions of which the error is known to be too large to correctly aim for the study objective. The three methods that will be applied are (A) the YAPS method based on Time of Arrival (TOA) as developed by Baktoft et al. (2017), (B) a filtering based on HPE and RMSE values provided by Vemco, and (C) a filtering method developed by Vergeynst (not published) that is based on the receiver clusters that define fish positions with large errors.

Lastly the resulting accurate and precise fish tracks will be linked to the results of the hydrodynamic model and tracks will be evaluated in the light of the migration model that needs further fine-tuning (see objectives section).

3.10.5. Migration model (SJE)

3.10.5.1. Model development

The migration model under development is an extension of the habitat simulation system CASiMiR. Whereas the standard module for fish habitat simulations - CASiMiR-Fish - is focused on aquatic habitat suitability, the new module CASiMiR-Migration is designed to simulate the migration behaviour of fish. The current version of CASiMiR-Migration is based only on magnitude and direction of flow velocity and thresholds of water depth. It uses an agent-based approach, i.e. virtual fish in terms of programming objects are incorporated in the model that follow specific rules. In the model available up to now the virtual fish take the way against the flow direction as long as the flow velocity does not fall below or exceed velocity thresholds that can be defined species specific. As soon as these thresholds are reached the virtual fish stop migrating. Simultaneously there are thresholds for water depth.

It is assumed that other factors than basic hydraulic parameters as depth-averaged flow velocity and thresholds of water depth affect the fish behaviour in the environment of fish pass entrances. In the improved model more complex hydraulic features as well as morphologic conditions, spatial constellations and individual fish behaviour are planned to be integrated. For the development of the approach, it is necessary to find correlations between the evaluated fish tracks and the morphologic and hydraulic conditions around the fish ladder outlet but also further downstream and upstream.

3.10.5.2. Flow scenarios and results

The current version has been applied to the Altusried case study with a lower flow velocity threshold of 0.15 m/s and an upper one of 1.5 m/s (which is not reached in the model area). Results are shown in the following figure.

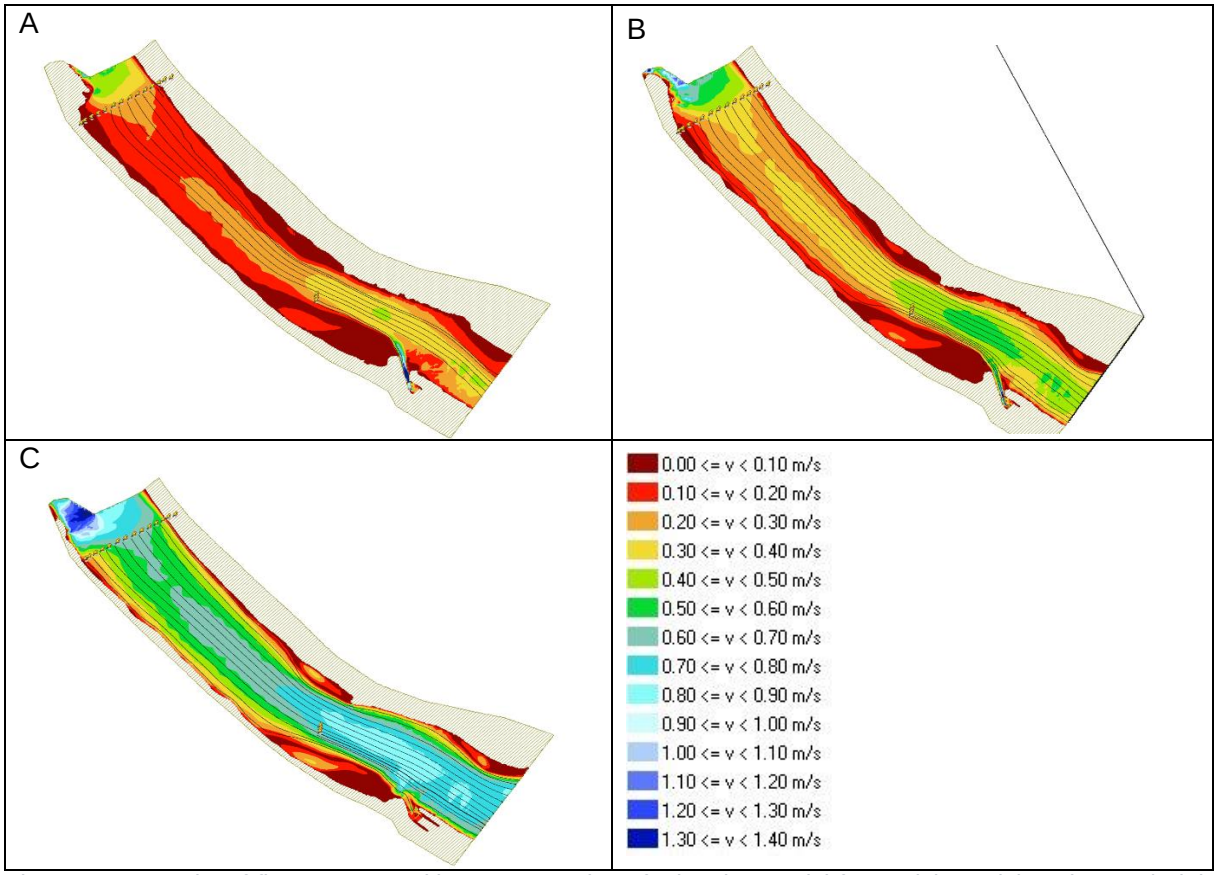


Figure 217: Results of first test runs with current version of migration model for 10 (A), 20 (B) and 60 m³/s (C), yellow pins indicate the start position of virtual fish, black lines the predicted track

When positioning the virtual fish equally over the river width in the lower part of the river stretch 10% of fish find the fish ladder entrance in case A with 10 m³/s, 7% in case B with 20 m³/s and 5 % in case C with 60 m³/s in the river. I.e. the higher the flow in river the less distinct is the attraction flow when considering only flow magnitude and direction.

By a first evaluation of the fish tracks, it is already clear that the percentage of fish finding the fish ladder entrance is much higher than these values. This indicates that the current model has to consider additional parameters as mentioned before.

3.10.6. References

Baktoft, H., Gjelland, K.O., Oakland, F., Thygesen, U.H. (2017). Positioning of aquatic animals based on time-of-arrival and random walk models using YAPS (Yet Another Positioning Solver). Scientific Reports 7, 142994. DOI:10.1038/s41598-017-14278-z.

Hussey, N.E., Kessel, S.T., Aarestrup, K., Cooke, S.J., Cowley, P.D., Fisk, A.T., Harcourt, R.G., Holland, K.N., Iverson, S.J., Kocik, J.F., Flemming, J.E.M., Whoriskey, F.G. (2015). Aquatic animal telemetry: A panoramic window into the underwater world. Science 348, 6240. DOI: 10.1126/science.1255642.

Jepsen, N., Thorstad, E. B., Baras, E., and Koed, A. (2002). Surgical implantation of telemetry transmitters in fish: how much have we learned? Hydrobiologia 483, 239–248. doi:10.1023/A:1021356302311

Jepsen, N., Mikkelsen, J. S., and Koed, A. (2008). Effects of tag and suture type on survival and growth of brown trout with surgically implanted telemetry tags in the wild. Journal of Fish Biology 72, 594–602. doi:10.1111/J.1095-8649.2007.01724.X

Kessel, S.T., Cooke, S.J., Heupel, M.R., Hussey, N.E., Simpfendorfer, C.A., Vagle, S., Fisk, A.T. (2014). A review of detection range testing in aquatic passive acoustic telemetry studies. Reviews in Fish Biology and Fisheries, 24 (1): 199-218. DOI 10.1007/s11160-013-9328-4.

Meckley, T.D., Holbrook, C.M., Wagner, C.M., Binder, T.R. (2014). An approach for filtering hyperbolically positioned underwater acoustic telemetry data with position precision estimates. Journal of Animal Biotelemetry 2: 7. https://animalbiotelemetry.biomedcentral.com/articles/10.1186/2050-3385-2-7.

Nykänen, M., Huusko, A., Mäki-Petäys, A. (2001). Seasonal changes in the habitat use and movements of adult European grayling in a large subarctic river. Journal of Fish Biology 58, 506-519. doi:10.1006/jfbi.2000.1467.

Smith, F. (2013). Understanding HPE in the VEMCO positioning system (VPS), published on the Vemco website: https://vemco.com/products/vps/. Link to the document: https://vemco.com/wp-content/uploads/2013/09/understanding-hpe-vps.pdf

Winter, J. D. (1983). Underwater biotelemetry. In Fisheries Techniques (Nielsen, L. A. & Johnson, D. L., eds), pp. 371–395. Bethesda, MD: American Fisheries Society.

3.11 Las Rives

3.11.1. Efficiency of downstream migration devices

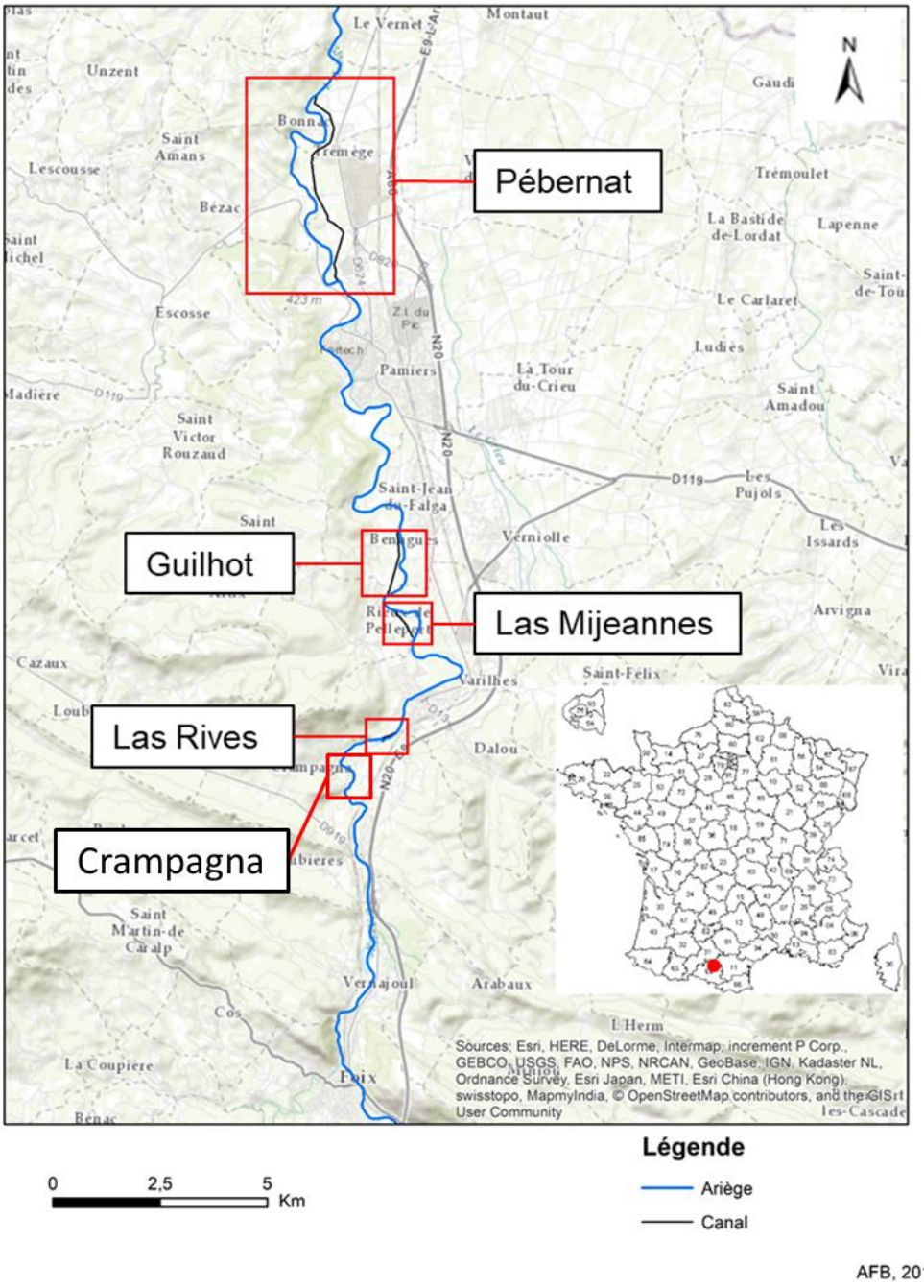
3.11.1.1. Introduction

In 2017, the French Agency for Biodiversity, EDF (Electricité de France) and the engineering office Ecogea launched the EFIGRI project (Etude de l'efficacité des prises d'eau ichtyocompatibles pour les smolts de saumon atlantique et les anguilles argentées – Study on the effectiveness of fishfriendly water intake for Atlantic salmon smolts and silver eels). The FIThydro project concerns only a part of this global project.

This study aims to assess the effectiveness of fishfriendly water intake for Atlantic salmon smolts and silver eels during two downstream migration periods, at hydropower plants with a maximum turbined flow between 30 and 50 m^3/s. Atlantic salmon smolts were monitored during spring 2017 and spring 2018. The silver eels were monitored during autumn-winter 2017-2018 and autumn-winter 2018-2019 (monitoring still on-going). These periods correspond to the natural downstream migration periods of these species.

The fishes are monitored along 5 hydropower plants: Crampagna – Las Rives – Las Mijeannes – Guilhot – Pébernat (only 4 for the smolts, without Crampagna).

Only the results at Las Rives will be presented.



AFB, 2017

3.11.1.2. **Methodology**

3.11.1.2.1. Technology

The fishes are monitored by Radio-telemetry in order to identify their downstream migration paths at hydroelectric schemes (over the weir, using the bypass or passing through the rack and the turbine). This technology has been chosen because it allows assessing precisely the efficiency of the downstream migration devices at each site and to monitor the progression of fish from upstream to downstream. This technology has already been used in previous studies and allows a reliable identification of fish and of their migration path.

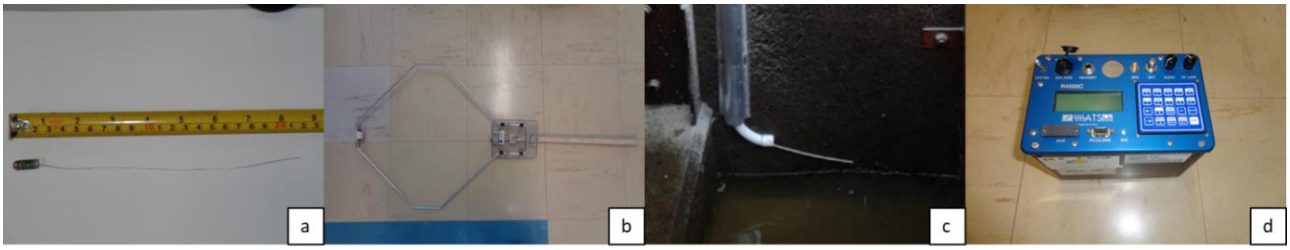


Figure 218: Radio telemetry material used: a) mark F1720 for Atlantic salmon smolts, b) aerial loop antenna, c) immersed strand antenna, d) receiving station RC4500 from ATS

3.11.1.2.2. Set of detection antennas

To identify the path of downstream migrating fish among the 3 possibilities (over the weir, using the bypass or passing through the rack and the turbine), 5 zones are equipped with antennas (Figure 219):

- ➔ Entry zone (E) upstream the trash rack, detecting the fishes coming in front the downstream migration device;
- ➔ Upstream zone of the downstream migration device (A) indicating the approach and the entry through the device;
- ➔ Zone in the downstream migration device settled in the downstream migration channel (P) confirming that the fish is using it;
- ➔ Zone in the headrace channel (C) indicating the passage through the trash rack towards the turbines;
- ➔ Zone in the bypassed reach of the Ariège (T) indicating passage through the weir (fishpass or spillway) or through the downstream migration device.

The efficiency of device for downstream migration is defined as the ratio between the number of smolts using the device (detected at P) and the number of smolts that enter the intake (detected at E).

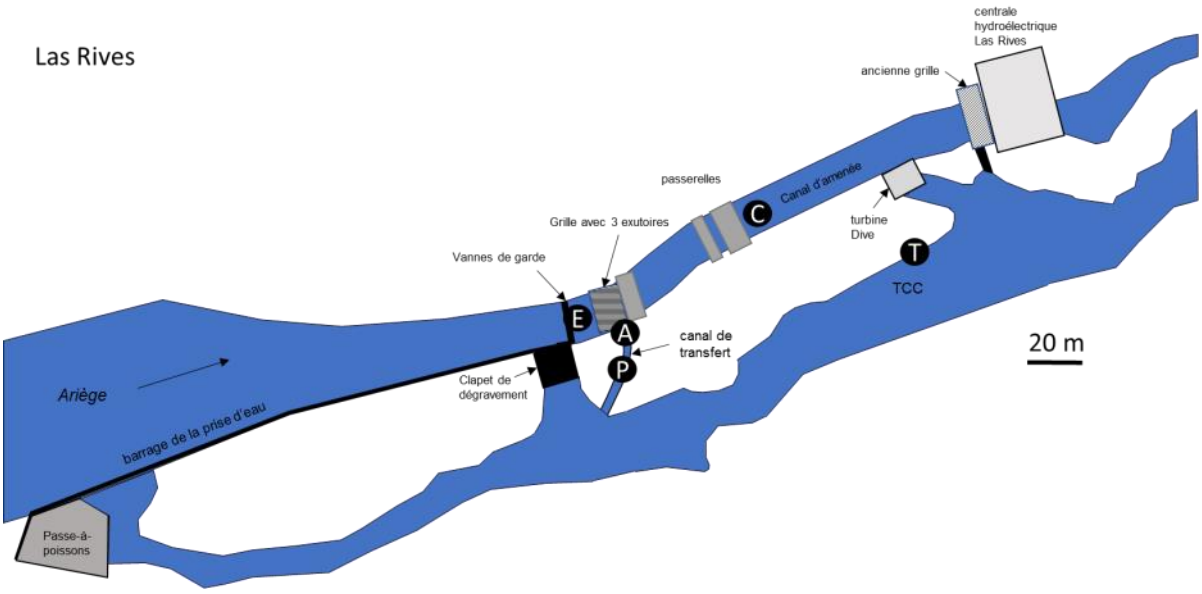


Figure 219: Set of detection antennas installed at Las Rives

3.11.1.2.3. Tagging and release

Atlantic salmon smolts are marked with type mark F1720 (Advanced Telemetry Systems, 45 ppm, guaranteed lifetime 1 day, observed lifetime 8-10 days, size of transmitter 20*7mm, 2g).

Eels are marked with type mark F1215C (Advanced Telemetry System, 45.80 ppm, guaranteed lifetime 25 days, observed lifetime 3 months, size of transmitter 55 or 65*10mm, 13g).

Smolts Spring 2017 and 2018

In spring 2017, 2 batches of 25 smolts were released upstream Las Rives.

In spring 2018, 4 batches of 25 smolts were released upstream Las Rives.

Silver eels winter 2017-2018 and 2018-2019

In January 2018, 2 batches of eels for a total of 96 were released upstream Las Rives.

In December 2018, 1 batch of 98 eels was released upstream Las Rives.

Table 53: Size of tagged fishes

Size (mm)	Smolts 2017	Eels 2018	Smolts 2018	Eels 2019
min	161	549	161	585
average	175	651	175	694
max	187	930	190	927

3.11.1.3. Results

Smolts Spring 2017

Table 54: Efficiency of the batches for released smolts at Las Rives in spring 2017

	Efficiency of the downstream migration devices (%)
Batch 1	94,4
Batch 2	70,8
Total	**81**

For the released smolts in spring 2017, the mean efficiency is 81 %.

Eels Winter 2017-2018

During winter 2017-2018, 20 passages of eels were recorded at the water intake of Las Rives. 100% of the eels went through the downstream migration outlet. The efficiency is 100%.

Smolts Spring 2018

Results to come

Eels Winter 2018-2019

On-going

3.11.1.4. Conclusion

To be continued

In Spring 2019, some tests will be carried out in order to assess the harmlessness of the downstream migration device at Las Rives. Indeed, fishes are falling from the downstream migration channel in the bypassed reach. The landing pool is 63 cm deep with the mean

interannual discharge. The early study of smolt data reveals that some fishes using the downstream migration duct accumulate some delay after Las Rives. This could be link to the fall and a possible injury downstream Las Rives. This will be studied at Las Rives in Spring 2019.

3.11.2. Hydraulic modelling

3.11.2.1. Characterization of currentology upstream the bar rack

3.11.2.1.1. Deployment of the ADCP probe

The currentology measures upstream the bar rack have been made with an Acoustic Doppler Current Profiler (ADCP) StreamPro Teledyne RDI (Figure 220). The probe is equipped with 4 sensors which issuance-reception beams are inclined of 20° to the axis of the probe. The width of a beam is 3°. The probe is vertically settled and slightly immersed (a few cm). The device measures the water depth, and the 3 components of flow velocity within 20 measurements cells uniformly distributed along the water column. The division of the cells is continuous during the measures and defined according to maximal depth provided by the operator. The frequency of measure acquisition is 1 Hz.



Figure 220: Pictures of the ADCP StreamPro assembled on its trimaran and the probe with a closer view of the 4 sensors

The flow conditions in Las Rives turned out to be too restless to deploy correctly the ADCP the common way, i.e. assembled on a trimaran and manoeuvred with a system of ropes. Furthermore, it is not certain that the “Bottom Tracking” system allows the device to measure its own movement to the bottom in the case where the ADCP stands above the inclined bar rack. Finally, the presence of metal pieces in the water intake could disturb the functioning of the compass and therefore the computing of its own path.

That is why a support and movement cart system was developed to deploy the ADCP in a more favourable way (Figure 221). The support is constituted of aluminium beams of square section (289*289 mm²) with different pieces of 2 or 3m long clipped with each other’s. These structures are usually used to set stages up for shows or stands. With a length 1 m higher than the water intake length, the weight was about 94 kg. Setting up such a support demands 6 persons. The movement cart has been made with NORCAN elements and handled with a rope system. This system allows a stationary and precise positioning of the ADCP probe, controlled by the operator and thus not using the “Bottom tracking” of the device.

In order to control the positioning of the probe, in particular, its altitude to the bending of the support, the exact positioning of the top of the probe was measured thanks to a tacheometer LEICA TS02-Ultra-7 (directly aimed in “laser beam” mode).



Figure 221 : Support and movement carts system allowing the deployment of the ADCP

The measures were made by positioning the probe at stationary points within time to get at least 30 valid measurements. Each transversal transect is described by several measurements points spaced with 1.0 m in general and 0.5 m for the transect at the top of the bar rack where a higher precision of measure was desired. Along the vertical banks of the water intake, the first and the last measurements points were placed between 1 m and 0.5 m from the bank to avoid that the measurements beams impact the wall.

At Las Rives, measures were made at 4 transversal transects located 2, 4, 6 and 10 m upstream the top of the bar rack (Figure 222). The immersion point of the bar rack is located about 0.65-0.7 m upstream the top of the bar rack. The entrance of the outlets stands about 1.85 m from the top. The transect at 10 m stands about the foot of the bar rack and the 2 m transect stand just upstream the entrance of the outlets (about 0.15 m).

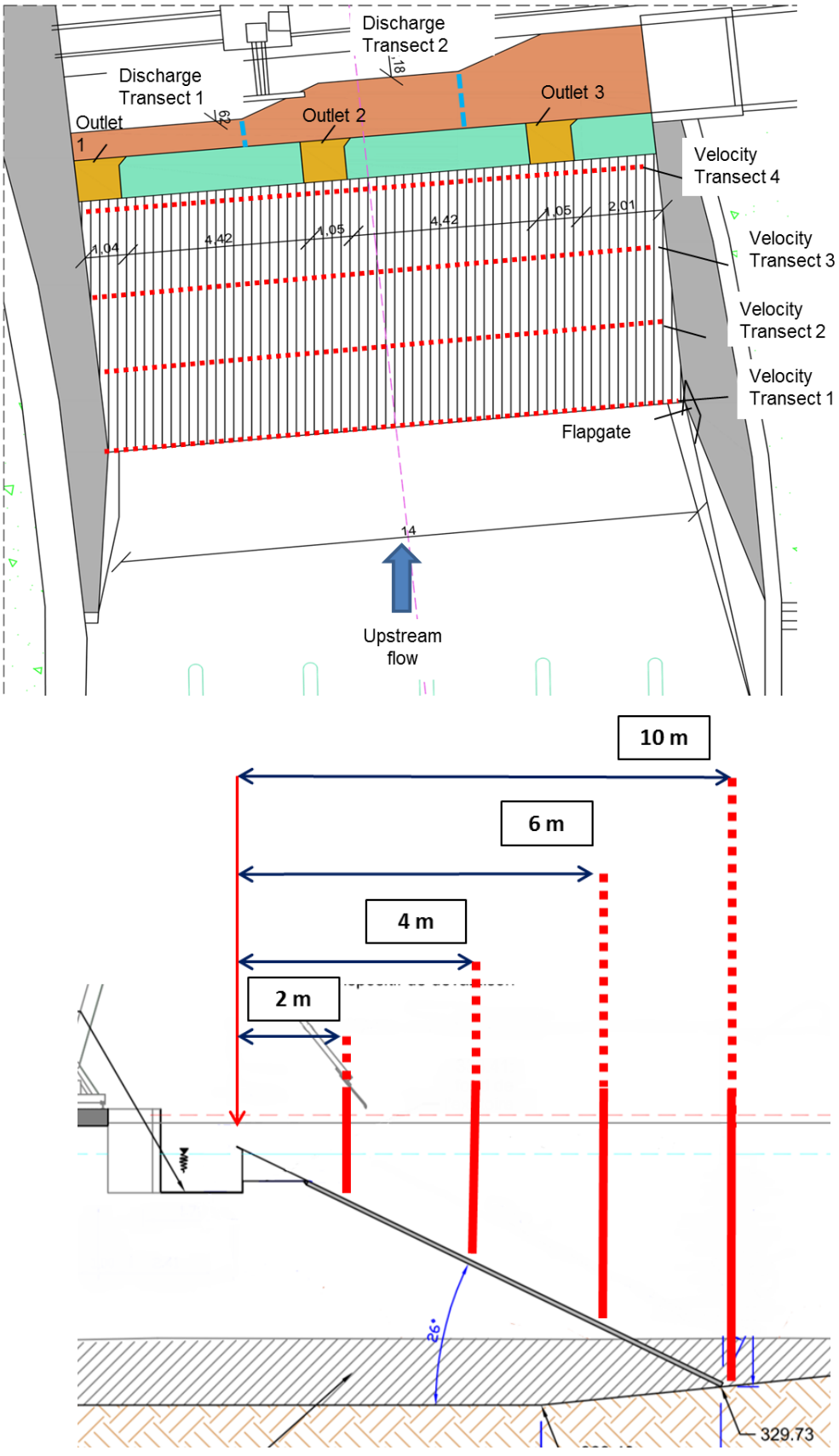


Figure 222: Positioning of the ADCP measurements transects at Las Rives.

3.11.2.1.2. Acquisition, processing and representation of the data

The date acquisition was performed with Teledyn Winriver II software. The data were then exported in ASCII format.

The results allow characterizing the different components of flow velocity (Figure 223):

- The component in the axis of the water intake $\mathbf{V_X}$
- The component transversal to the axis of the water intake $\mathbf{V_Y}$ (positive from the right bank to the left bank)
- The vertical component $\mathbf{V_Z}$ (positive bottom-up)
- The component normal to the bar rack $\mathbf{V_N}$
- The component tangential to the bar rack $\mathbf{V_T}$

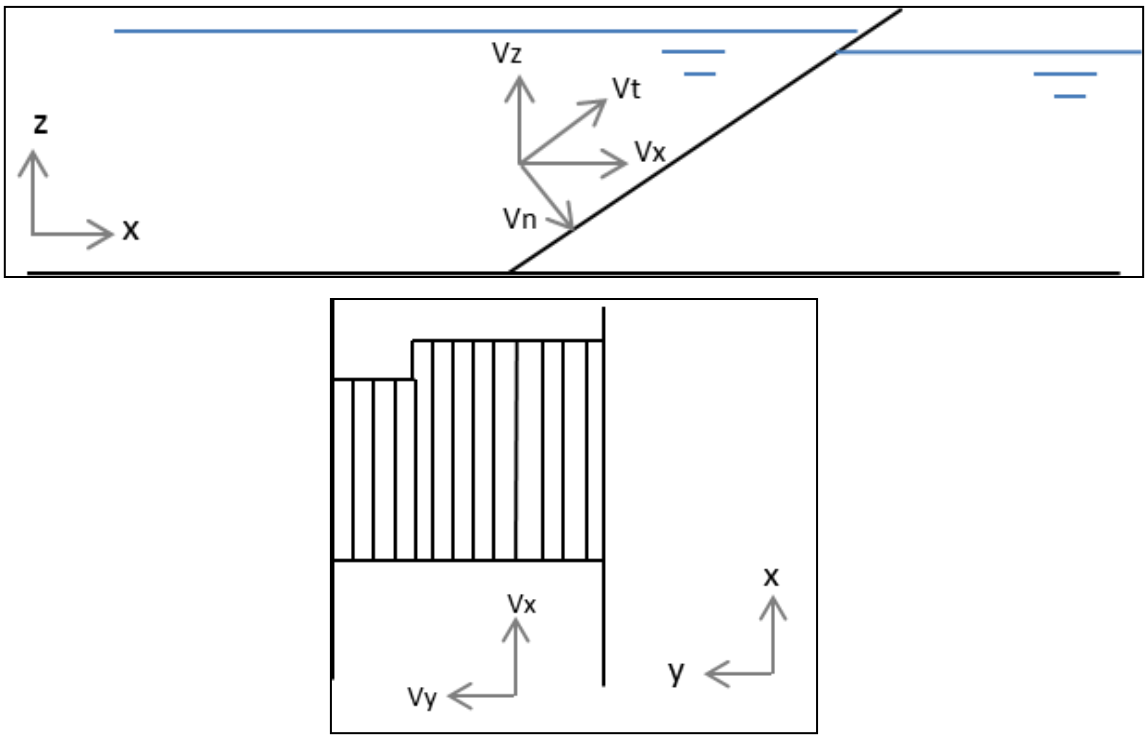


Figure 223: Diagram of the components of analysed velocity; longitudinal view (top) and plan view (down).

The results are presented either in dimensional form, or in dimensionless form by dividing the output velocity at the water intake by $\mathbf{V_0}$; determined from the mean turbined discharge during the measurements and the flow section at the foot of the bar rack (also called approach velocity).

3.11.2.2. Distribution of discharge between the 3 outlets

3.11.2.2.1. Methodology

The distribution between the 3 downstream migration outlets was characterized by carrying out:

- 2 gaugings with a flowmeter in the downstream migration duct
  - The first gauging in the portion between the first outlet at the left bank and the central outlet, just upstream the first enlargement

- And the second gauging in the portion between the central and the third outlet at the right bank, just upstream the second enlargement (section 1 and 2, see Figure 224)

- And an assessment of the total discharge transiting by the downstream migration duct thanks to a « weir law »

The discharges of the outlet in central and right bank position are obtained by subtraction of these different measurements.



Figure 224: Positioning of the gaugings in the downstream migration duct at Las Rives.

3.11.2.2.2. Gaugings with the flow meter in the downstream migration duct

The gaugings in the downstream migration duct were made with an electro-magnetic flow meter Marsh McBirney, FLO-MATE 2000. The measurements on each section were performed in the following way:

- Measure of the width of the section and cutting in verticals 10 cm from each bank then in equal parts from ± 20 cm, see Figure 226;
- For each vertical:
  - Measure of water depth;
  - Measure of the velocity in 6 points in the water column since the hypothesis of a logarithmical velocity profile cannot be made: bottom, 20%, 40%, 60% and 80% of water depth and finally at the surface. Each measure consists of a velocity average sampled over 30 seconds

Near lateral walls, the device had sometimes some measurements problems with certain values missing periodically. This had for consequence to avoid the computing of the average value by the device. To limit the waste of time due to this issue, 2 measurements of velocity over 15 seconds were made at each point.

The operator in the downstream migration duct was equipped with waders with felt soles to reduce risk of skidding on the metal bottom of the duct, a helmet, a life jacket and a harness to be secure via a rope by a second operator. Special care was brought to stand as downstream as possible from the measurement section in order not to skew the measure.

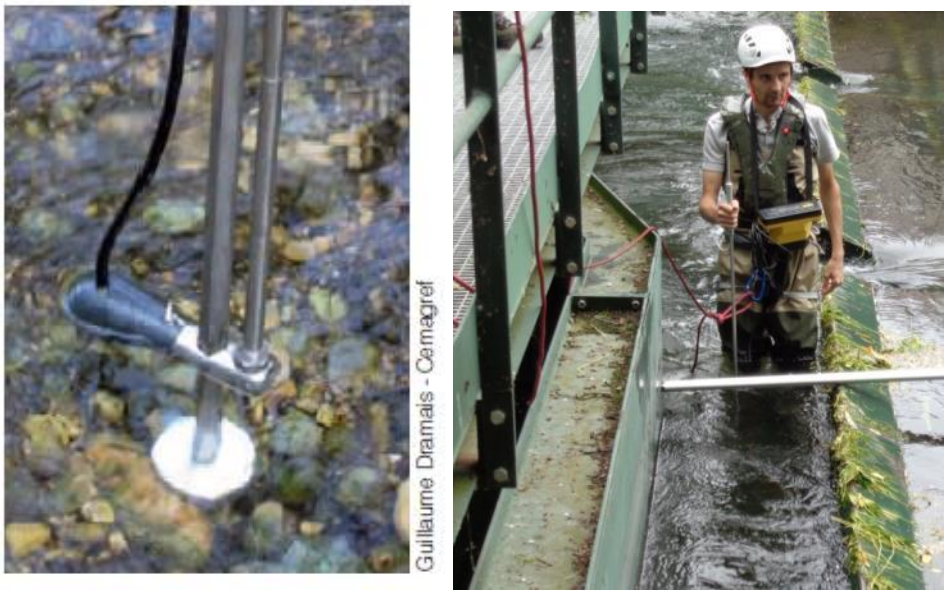


Figure 225: Example of an electro-magnetic flow meter

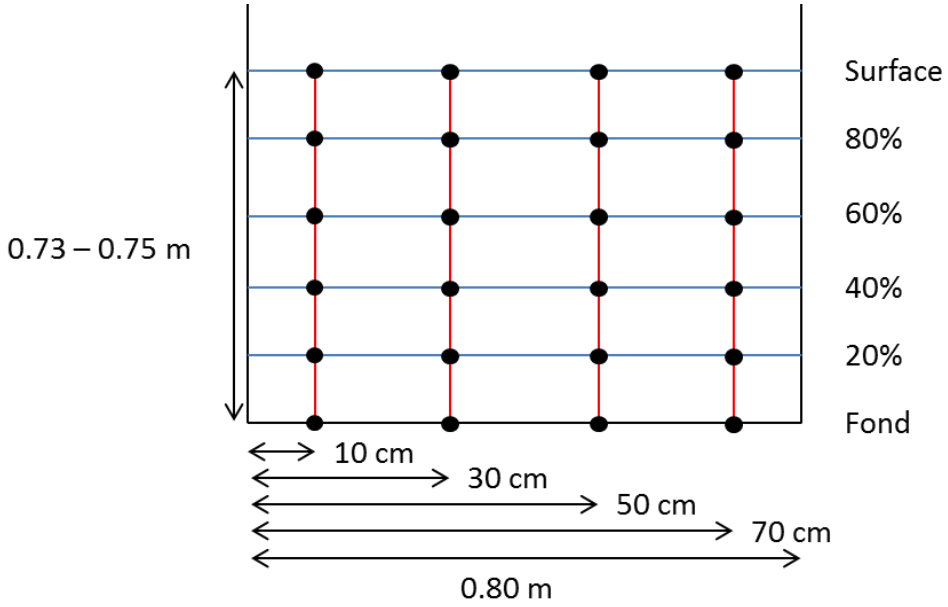


Figure 226: Cutting of a section during the measure by a flow meter, in red the verticals, the black dots correspond to the measurement points.

The discharge is calculated according to norm EN ISO 748:2007, by the method of mean section, by calculating the mean velocity between the banks and the closer verticals. The mean velocity on each vertical is calculated that way:

$$V_{moy} = 0.1(V_s + 2V_{0.8} + 2V_{0.6} + 2V_{0.4} + 2V_{0.2} + V_{pf})$$

Then a mean velocity is calculated for each flow section between the verticals and the closer bank; by making an average for the sections without including the banks, and by applying the following formula:

$$V_{moy\ section} = \frac{m}{m+1} * V_{moy\ closer\ vertical}$$

Here,$m = 10$ due to the smooth nature of the duct.

The discharge by flow section is then calculated:

$$Q_{section} = V_{moy\ section} * H_{eau\ moy} * L_{écoulement}$$

In order to have the total discharge, just sum up all sectional discharges.

3.11.2.3. Assessment of the total discharge transiting through the downstream migration duct thanks to a « weir law »

The total discharge transiting through the downstream migration duct could be evaluated by gauging in the duct downstream the third outlet. However, the gauging is quite complicated at this place. Indeed, the velocities are high and it is more complicated for the operator to stand in the duct.

That's why, it was preferred to assess the total discharge transiting through the migration duct at the control weir, from a transcript of the characteristics of the weir (width, level of overflow), of the duct when approaching the weir (width, bottom) and water level upstream.

The different levels have been measured thanks to a tacheometer LEICA TS02-Ultra-7 (aimed at a prism settled on a stick). The levels were readjusted in altitude referring to reference points.

To compute the total discharge, the tool Devers from Cassiopée® software was used, taking into account the correction linked to the high flow velocities in the duct when approaching the control weir (Bos correction (1989)). The calculation needs to determine the value of the flow coefficient, which depends on:

- The ration between the width of the weir and the width of the duct, which rules the intensity of lateral detachments. In this situation, the weir is as wide as the duct upstream, there is no lateral detachment. This leads to a high value of flow coefficient.
- The ratio between the head on the weir and the water level upstream (the difference being the height of the weir against the floor) which rules the intensity of vertical detachment.
- The type and the shape of the weir.

The resolution of the flow coefficient relied on elements from the « hydrometry » guide from the ONEMA (Le Coz et al. 2011).

3.11.2.4. Data of functioning during the measures

The data of functioning of the HPP during the measures were provided by the operator ONDULIA. These data included:

- At the HPP: water levels upstream and downstream, and power output produced, which allow calculating the turbined discharge according to an assessment of the global performance of the turbines.
- At the bar rack: the water level at the dam, upstream and downstream the bar rack.

These data were provided with a time slot of 10 minutes. This allows assessing the functioning conditions of the HPP during the measures. These spread over the day of 3rd July 2018. The discharge of the Ariège varied between 54.20 and 55.25 m^3/s at the hydrometric station of Foix located upstream.

The measures at Las Rives happened between 11:30 and 16:30. The turbined discharge at the HPP (G1 to G4) was quite steady and between 43.4 and 46.6 m^3/s. The HPP worked full power during the measurements (design discharge of 45 m^3/s). The total discharge of the Ariège was recalculated at the site of Las Rives and varied between 48.7 and 59.7 m^3/s. The

water level at the dam varied between -2.2 cm and 8.5 cm (to the crest of the dam), cf. Figure 227.

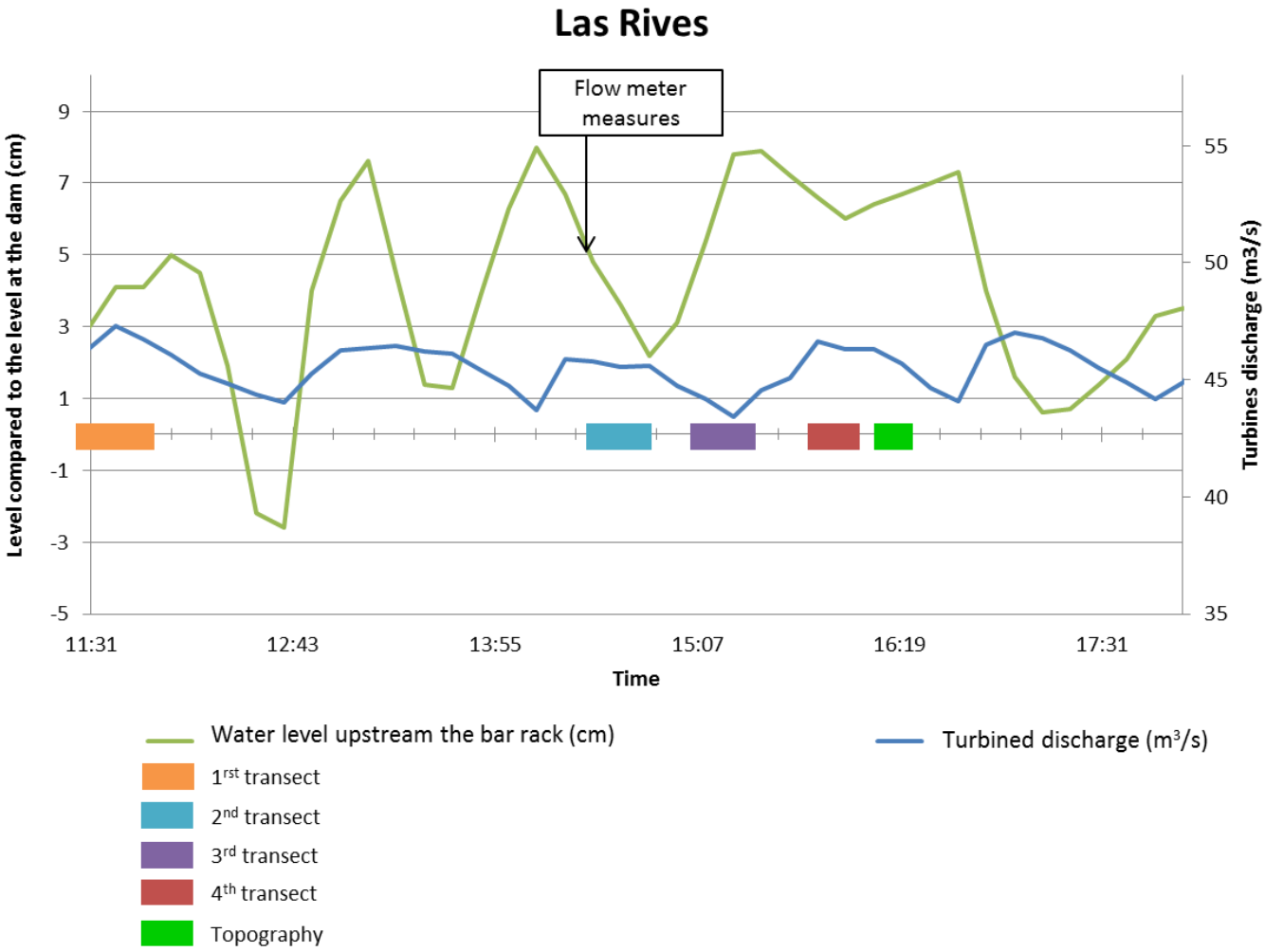


Figure 227: Variation of water level and total discharge of the Ariège during the measures at Las Rives.

Table 55: Mean discharge and velocity allowing the results to be dimensionless.

Transects	Mean discharge (m^3/s)	Velocity V_0 (m/s)
Transect 1 at 10m	49.02	0.87
Transect 2 at 6m	46.98	0.84
Transect 3 at 4m	47.52	0.85
Transect 4 at 2m	47.97	0.85

3.11.2.5. Discharge transiting through the downstream migration duct and distribution between the outlets

Table 56 presents the assessment of the total discharge transiting through the downstream migration duct, and the distribution of the discharge between the outlets (the detailed calculation are presented in Annex 1).

The total discharge allocated to downstream migration is assessed to 1.13 m^3/s, i.e. 84% of the theoretical value. The discharges of outlet 1 (left bank), 2 (central) and 3 (right bank) are 0.184 m^3/s, 0.488 m^3/s and 0.463 m^3/s respectively. The discharge supply of the first outlet

seems to be reduced with respect to the two others. It is a common phenomenon due to the head losses along the duct, but it seems here quite exacerbated for outlet 1.

The velocity at the entrance of outlet 1 (0.36 m/s) is therefore quite below the targeted theoretical value (0.90 m/s). The velocities at the entrance of outlets 2 and 3 are close to this value.

Table 56: Total discharge transiting through the downstream migration duct, and distribution of the discharges between the outlets at Las Rives.

		Value of discharge (m^3/s)	Proportion of total discharge	Velocity at the entrance of the outlet (m/s)
Discharge outlet 1	Gauging	**0.184**	**16.2%**	**0.36**
Discharge outlet 2	Difference	**0.488**	**43.0%**	**0.98**
Discharge outlets 1+2	Gauging	0.671	59.2%	-
Discharge outlet 3	Difference	**0.463**	**40.8%**	**0.93**
Total Discharge	Discharge formula	1.134	100.0%	-

3.11.2.6. Currentology upstream the bar rack

Figure 229 graphically illustrates the velocity components $\mathbf{V_X}$ and $\mathbf{V_Z}$ of the dimensionless velocity at the 4 transects. The bar rack is viewed from upstream.

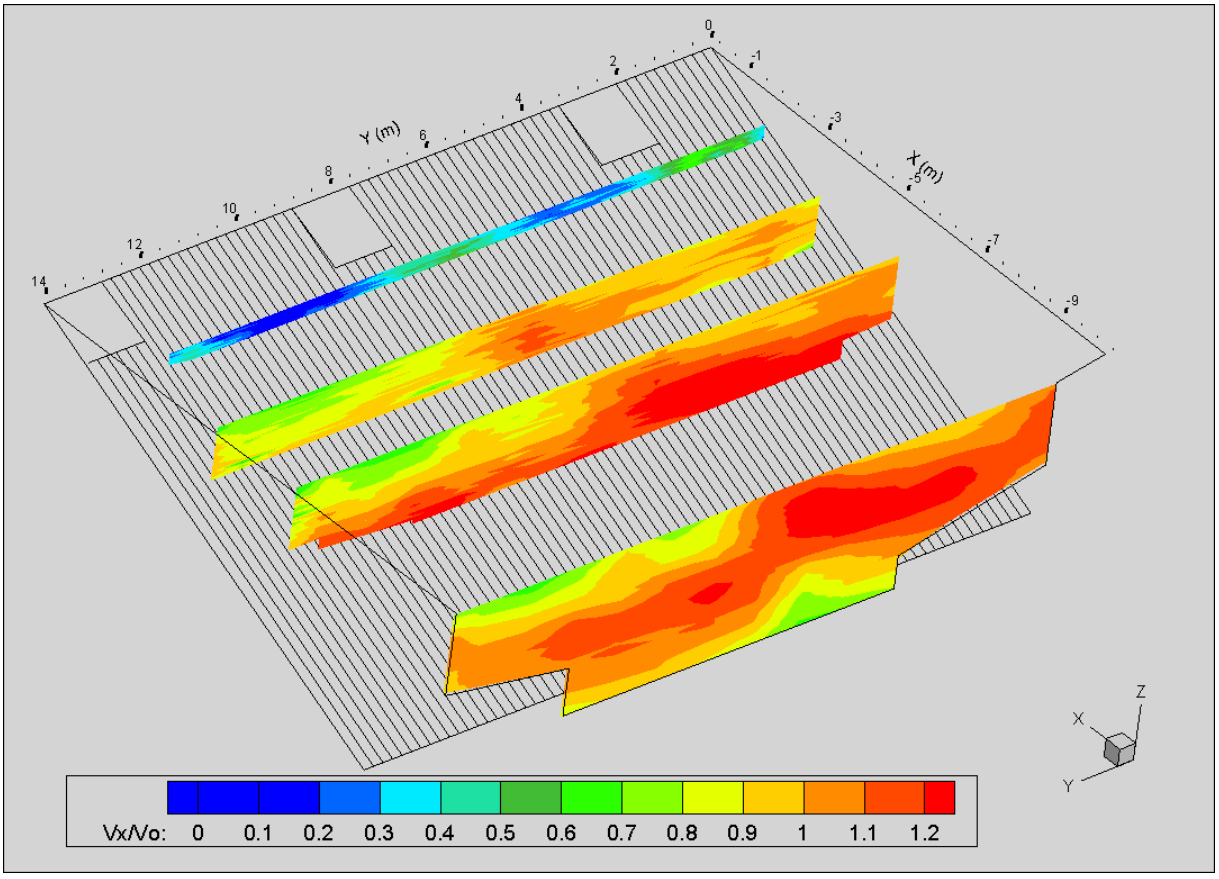
At the 3 transects located at 10 m, 6 m and 4 m upstream the top of the bar rack the components $\mathbf{V_X}$ vary between $0.6V_0$ and $1.1V_0$. Half of the water intake near the right bank presents velocities higher than the half at the left bank. This heterogeneity existing from the foot of the bar rack is probably linked to the general configuration of the water intake, and not to the bar rack itself. Between these 3 transects, no significant acceleration or deceleration of component $\mathbf{V_X}$ appears.

At the transect located 2 m upstream the top of the bar rack (about 0.15 m upstream the entrance of the outlets), the components $\mathbf{V_X}$ decrease significantly: between 0 and $0.3V_0$ beside the outlets and between $0.4V_0$ to $0.6V_0$ in front of the outlets. It is linked to the obturation of the top of the grid on the same depth of the outlets, see Figure 228.



Figure 228: Out of water bar rack at Las Rives, in the red rectangle, the grid is clogged in order to better guide fishes to the bypasses

The vertical components of $\mathbf{V_Z}$ seem low at the first 3 transects (value between -0.05V_0 and +0.15V_0) and slightly positive in average (oriented to the surface). At the transect, 2 m upstream the top of the bar rack, the components $\mathbf{V_Z}$ are noticeably negative (oriented to the floor), with values between -0.2V_0 and -0.3V_0 between the outlets and about -0.1V_0 near the outlets. This evolution is due to the fact that the flow has du “plunge” under the top of the grid which is clogged.



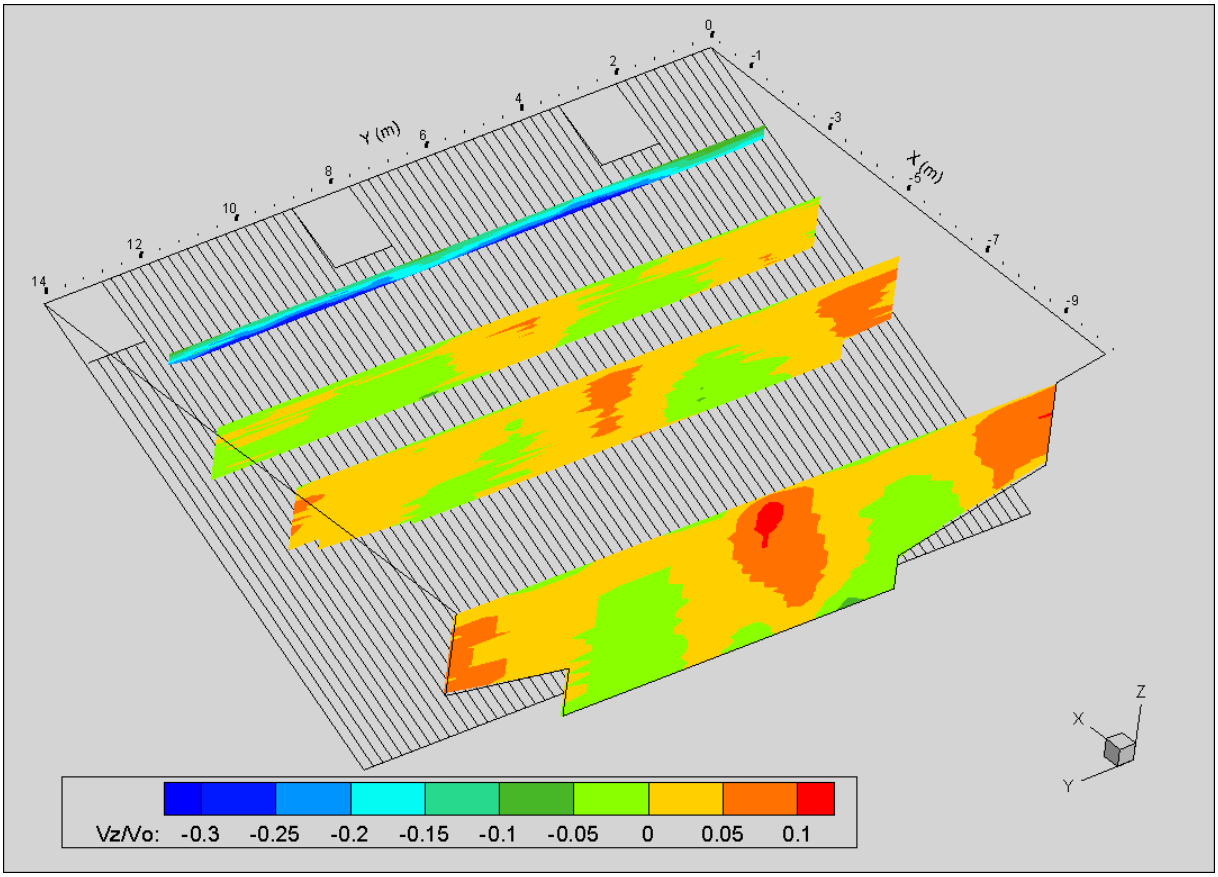


Figure 229: cartographies of the dimensionless velocities V_x/V_0 (up) and V_z/V_0 (down) measured at Las Rives.

Figure 231 graphically illustrates the dimensionless tangential and normal components $\mathbf{V_t}$ and $\mathbf{V_n}$ of the velocity at the 4 transects.

At the 3 transects located at 10 m, 6 m and 4 m upstream the top of the bar rack the tangential components $\mathbf{V_t}$ are mainly between $0.5V_0$ and $0.9\ V_0$. As for $\mathbf{V_x}$, the values are higher in the right hand part of the water intake.

At the transect at 2 m upstream the top of the grid (about 0.15 m upstream the entrance of the outlets), the components $\mathbf{V_t}$ decrease significantly linked to the clogging of the top of the grid: value nearly zero between the outlets and between 0.3 to $0.5V_0$ in front of the outlets.

The normal components $\mathbf{V_n}$ of the velocity vary between 0.2 to $0.5V_0$ on the 4 transects, including the 4th transect where the flow is plunging under the clogged top of the grid.

Figure 232 presents the ratio between the tangential and normal velocities $\mathbf{V_t/V_n}$.

At the 3 transects located at 10 m, 6 m and 4 m upstream the top of the bar rack, this ratio varies between, 1.5 and 3, with mean values of 2. This is compliant with the theoretical value.

At the transect 2 m upstream the top of the grid (about 0.15 m upstream the entrance of the outlets), the ration is close to 0 between the outlets and close to 1.0-1.5 in front of the outlets. This is consistent with the evolution of the tangential components seen above.

Figure 233 illustrates the transversal component $\mathbf{V_y}$ at the transect located 2 m upstream the top of the grid.

The dimensionless velocity is globally negative. The general currentology points towards the right outlet. The main reason for this non-uniformity is due to the outlet that leads to the end of

the duct where the flow is more intense and where the velocity is higher. The local variations of $\mathbf{V_y}$ near the entrances of the outlets can hardly be measured even if weak variations exist. The location of the transect could be an explanation for this.

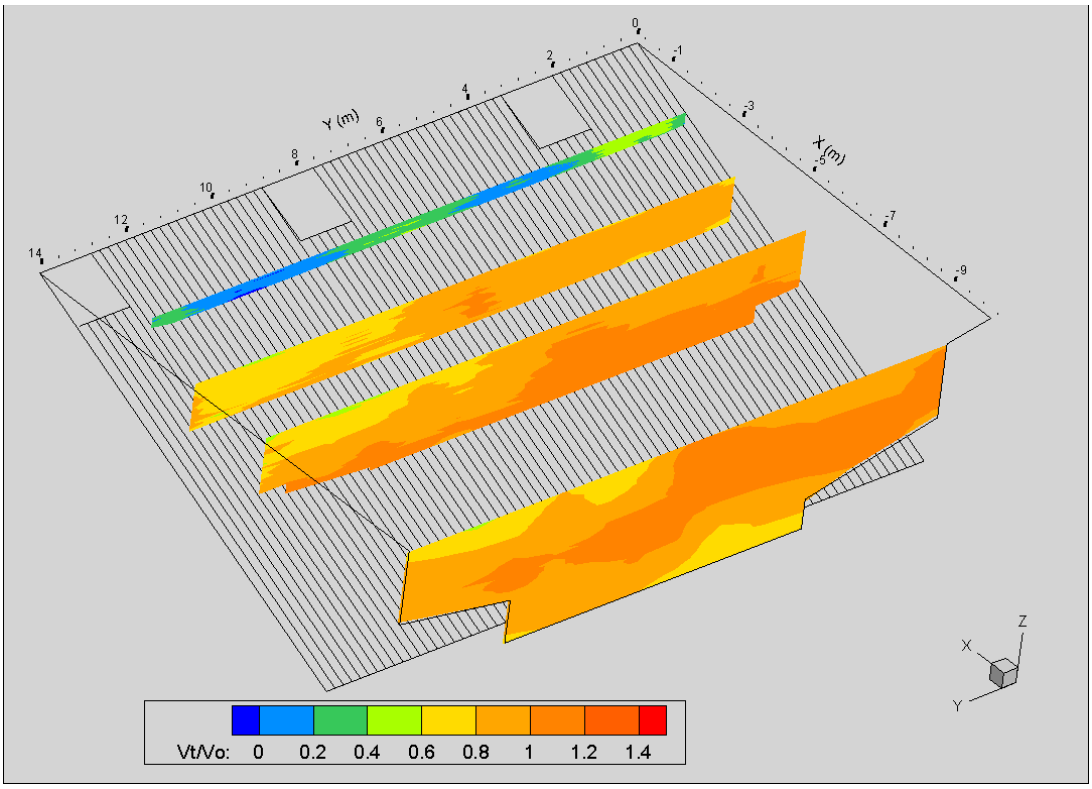


Figure 230: Cartographies of Vt/V0 measured at Las Rives

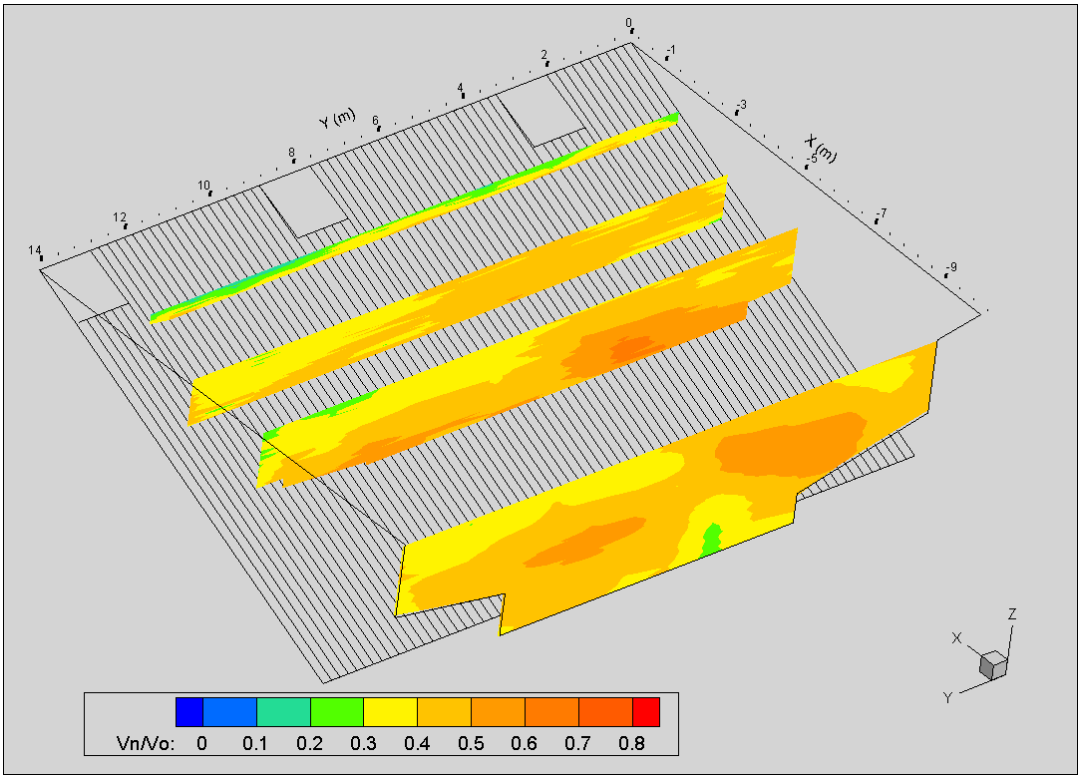


Figure 231: Cartographies of V_n/V_0 measured at Las Rives.

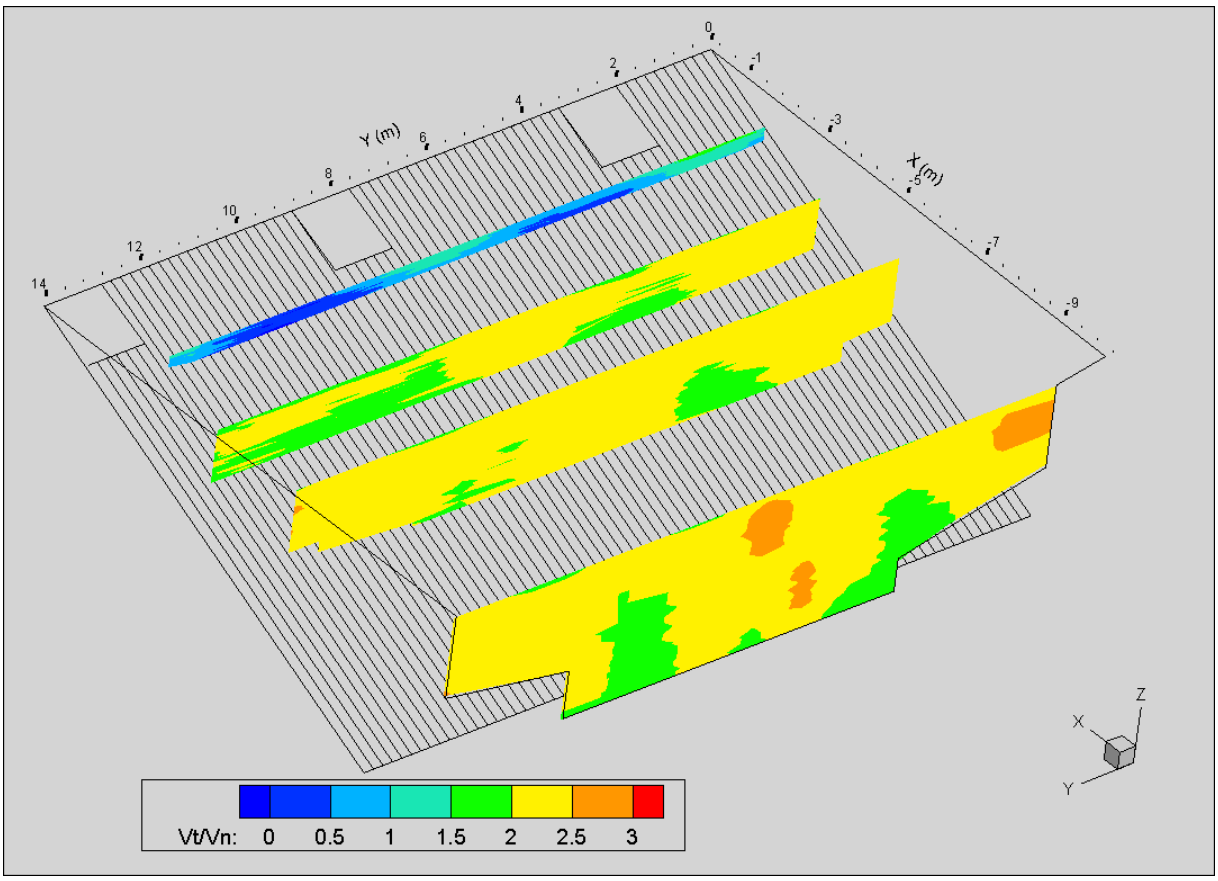


Figure 232: Cartography of ratio V_t/V_n measured at Las Rives.

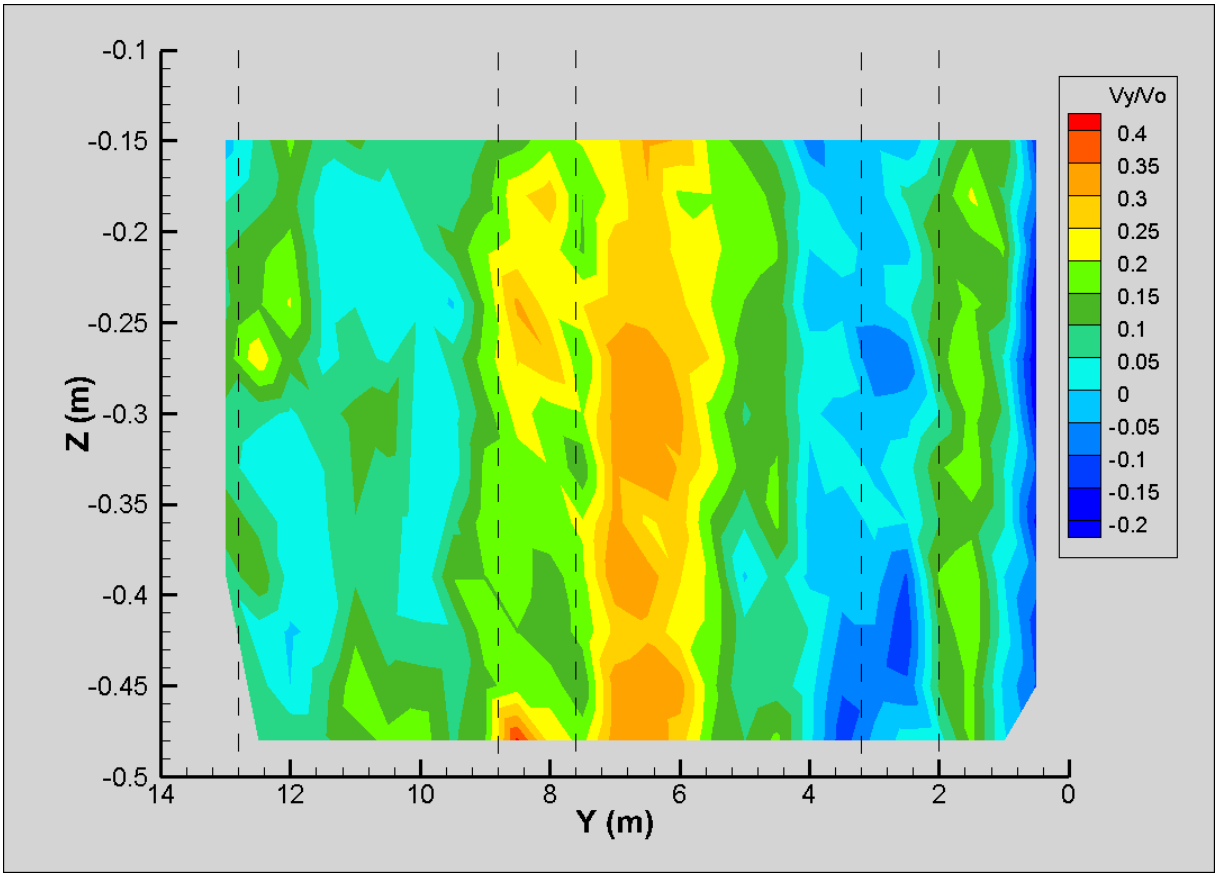


Figure 233: Cartography of V_y/V_0 of transect located 2 m upstream the top of the bar rack (about 0.15 m upstream the entrance of the outlets). Positive direction is oriented from the right bank to the left bank. The location of the outlets is indicated by the vertical dotted lines.

The modelling will be done after the validation of the model developed in WP3 this year which serves to calculate the flow upstream the trashrack and the attractiveness of the bypasses.

3.11.3. Assessment of global survival rate at Las Rives

Upcoming

3.11.4. References

Hydrec. 2014. Centrale hydrauélectrique de Las Rives - Rivière Ariège - Commune de Varilhes et Saint Jean de Verges - Dimensionnement du plan de grille ichtyocompatible et des dispositifs de dévalaison des poissons. 2014.

Le Coz, J., et al. 2011. Contrôle des débits réglementaires - Application de l'article L 214-18 du Code de l'Environnement. 2011.

3.11.5. Annex 1: Gauging of the discharge in the downstream migration duct and assessment of the total discharge

Table 58 and Table 59 present the results of the gaugings in the downstream migration duct at Las Rives. For the first gauging, corresponding to the discharge in the first outlet, the discharge is **0.184 m³/s**. For the second gauging, corresponding to the discharge of the two first outlets, the discharge is equal to **0.671 m³/s**.

The topography measurement were postponed to the gauging with the flow meter. The water levels varied during this period of time (Table 57). This will be taken into account during the exploitation of the results.

Table 57: Variation of water levels during the measures

	Gauging 1	Gauging 2	Upstream gates
Water level during the gauging (m)	0.73	0.77	-
Water level during topography measurements (m)	0.76	0.75	0.69

Table 58: Exploitation of measured velocities at Las Rives at the first point of gauging

Verticale	Mesure de vitesse à différentes hauteurs (m/s)						Vitesse moyenne (m/s)	Vitesse moyenne (m/s)
	Fond	0.2	0.4	0.6	0.8	Surface		
Berge RD								
1	0.19	0.14	0.33	0.33	0.28	0.32	0.267	0.301
	0.18	0.31	0.40	0.38	0.31	0.36	0.334	
2	0.18	0.31	0.31	0.33	0.32	0.37	0.309	0.294
	0.16	0.27	0.28	0.27	0.32	0.34	0.278	
3	0.36	0.29	0.26	0.33	0.33	0.34	0.312	0.314
	0.25	0.25	0.35	0.30	0.39	0.32	0.315	
4	0.37	0.40	0.37	0.38	0.39	0.40	0.385	0.375
	0.32	0.36	0.40	0.36	0.37	0.34	0.364	
Berge RG								

Verticale	Hauteur d'eau (m)	Distance depuis la rive gauche (m)	Section	Vitesse moyenne (m/s)	Largeur d'écoulement (m)	Hauteur d'eau moyenne (m)	Débit par section (m³/s)
Berge RD	0.75	0.80	RD - 1	0.27	0.10	0.75	0.020
1	0.75	0.70	1 - 2	0.30	0.20	0.74	0.044
2	0.73	0.50	2 - 3	0.30	0.20	0.73	0.044
3	0.73	0.30	3 - 4	0.34	0.20	0.73	0.050
4	0.73	0.10	4 - RG	0.34	0.10	0.73	0.025
Berge RG	0.73	0.00					

Table 59: Exploitation of measured velocities at Las Rives at the second point of gauging

Verticale	Mesure de vitesse à différentes hauteurs (m/s)						Vitesse moyenne (m/s)	Vitesse moyenne (m/s)
	Fond	0.2	0.4	0.6	0.8	Surface		
Berge RD								
1	0.17	0.20	0.14	0.20	0.14	0.10	0.163	0.1655
	0.23	0.16	0.19	0.20	0.16	0.03	0.168	
2	0.24	0.38	0.16	0.20	0.10	0.17	0.209	0.211
	0.24	0.41	0.23	0.17	0.13	0.01	0.213	
3	0.38	0.44	0.32	0.32	0.33	0.36	0.356	0.353
	0.34	0.46	0.31	0.31	0.34	0.32	0.35	
4	0.62	0.75	0.71	0.73	0.74	0.68	0.716	0.7035
	0.58	0.70	0.75	0.65	0.68	0.77	0.691	
5	0.72	0.87	0.95	0.96	0.90	0.74	0.882	0.876
	0.66	0.93	0.91	0.95	0.85	0.76	0.87	
6	0.83	0.90	0.89	0.96	0.91	0.85	0.9	0.8735
		0.92	0.99	0.98	0.94	0.81	0.847	
Berge RG								

Verticale	Hauteur d'eau (m)	Distance depuis la rive gauche (m)	Section	Vitesse moyenne (m/s)	Largeur d'écoulement (m)	Hauteur d'eau moyenne (m)	Débit par section (m^3/s)
Berge RD	0.76	1.58	RD - 1	0.15	0.10	0.760	0.011
1	0.76	1.48	1 - 2	0.19	0.23	0.760	0.033
2	0.76	1.25	2 - 3	0.28	0.25	0.760	0.054
3	0.76	1.00	3 - 4	0.53	0.30	0.770	0.122
4	0.78	0.70	4 - 5	0.79	0.30	0.780	0.185
5	0.78	0.40	5 - 6	0.87	0.30	0.780	0.205
6	0.78	0.10	6 - RG	0.79	0.10	0.780	0.062
Berge RG	0.78	0.00					

Table 60 presents the measured data pour le calculation of the total discharge on the downstream migration duct by the discharge formula. It is necessary to determine the discharge coefficient of the weir from its characteristics. According to the hydrometric guide of the ONEMA (Le Coz, et al., 2011), 2 approaches are possible:

- Considering that the weir is thick (Figure 234) as planned in the initial sizing (Hydrec, 2014). In a thorough manner, the head **h** on the weir should be lower or equal to the thickness **e** of the weir. At Las Rives, the measured head is 0.38 m; the condition is respected only if the thickness of the weir is equal or greater than 0.24 m (which has not been checked). Table 61 allows determining the coefficient **A1** according to the ratios **h/e** and **h/p** (p is the height of the weir from the floor of the duct). The discharge coefficient is then deduced:

$$C = 0.385A_1 = 0.385 \times 1.195 = 0.46$$

- Considering that the weir is thin (Figure 235). The weir doesn't have a reduction of the width compared to the duct (ratio **b/B** =1), so the coefficient **Cr** is equal to 0.05. The ratio h/p is equal to 1.16. The discharge coefficient is deduced:

$$C = 0.40 + C_r * \frac{h}{p} = 0.40 + 0.05 * 1.16 = 0.458$$

The two values of discharge coefficient are very close. The value of 0.46 is chosen.

Table 60: Measured data for the calculation of the total discharge thanks to the discharge formula

Water level upstream the bar rack	333.970	m
Water level upstream the weir	333.877	m
head losses between the upstream level and the weir	0.093	m
Level of the floor upstream the weir	333.184	m
Width of the duct	2.410	m
Width of the weir	2.410	m
Water level upstream the weir	0.693	m
Flow section upstream the weir	1.670	m²
Measured level of the weir	333.522	m
Level of the weir in the project	333.450	m
Head on the weir	0.355	m

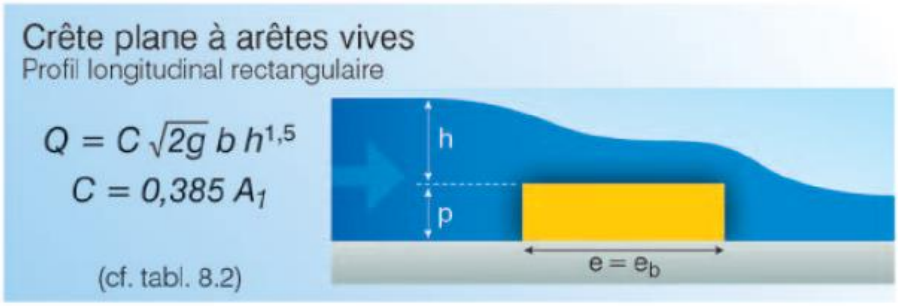


Figure 234: Expression of the discharge coefficient for a thick weir with a plane crest and sharp edges (source: (Le Coz, et al., 2011)).

Table 61: Determination table of A1 coefficient (source (Le Coz, et al., 2011))

	h/e																	
h/p	0,1	0,2	0,3	0,4	0,5	0,6	0,7	0,8	0,9	1,0	1,1	1,2	1,3	1,4	1,5	1,6	1,7	1,8
0,1	0,850	0,850	0,850	0,861	0,870	0,885	0,893	0,925	0,948	0,971	0,993	1,016	1,039	1,062	1,085	1,106	1,130	1,148
0,2	0,855	0,855	0,855	0,864	0,874	0,888	0,907	0,930	0,954	0,977	1,001	1,026	1,050	1,074	1,096	1,120	1,142	1,159
0,3	0,864	0,864	0,864	0,868	0,879	0,894	0,913	0,936	0,961	0,986	1,011	1,037	1,061	1,085	1,110	1,132	1,152	1,169
0,4	0,873	0,873	0,873	0,874	0,885	0,901	0,920	0,945	0,969	0,995	1,021	1,047	1,072	1,097	1,122	1,144	1,163	1,180
0,5	0,882	0,882	0,882	0,883	0,894	0,909	0,929	0,954	0,978	1,005	1,032	1,057	1,083	1,109	1,133	1,154	1,173	1,188
0,6	0,892	0,892	0,892	0,894	0,904	0,920	0,941	0,964	0,990	1,016	1,043	1,067	1,094	1,120	1,143	1,164	1,182	1,196
0,7	0,901	0,901	0,901	0,906	0,916	0,932	0,952	0,975	1,000	1,026	1,052	1,077	1,104	1,129	1,152	1,171	1,188	1,203
0,8	0,911	0,911	0,912	0,916	0,926	0,942	0,962	0,985	1,010	1,036	1,062	1,086	1,112	1,136	1,158	1,176	1,194	1,209
0,9	0,921	0,921	0,922	0,926	0,936	0,952	0,972	0,996	1,021	1,046	1,072	1,096	1,120	1,143	1,163	1,181	1,199	1,214
1,0	0,929	0,929	0,931	0,936	0,946	0,962	0,982	1,006	1,031	1,056	1,081	1,106	1,128	1,150	1,169	1,187	1,204	1,220
1,1	0,935	0,937	0,940	0,946	0,956	0,972	0,993	1,017	1,042	1,066	1,092	1,115	1,138	1,159	1,177	1,195	1,212	1,228
1,2	0,941	0,944	0,949	0,956	0,966	0,982	1,004	1,028	1,053	1,077	1,103	1,126	1,148	1,168	1,186	1,204	1,222	1,237
1,3	0,946	0,951	0,957	0,966	0,977	0,993	1,016	1,040	1,063	1,089	1,114	1,136	1,158	1,178	1,196	1,214	1,232	1,250
1,4	0,953	0,959	0,967	0,975	0,986	1,005	1,028	1,050	1,075	1,101	1,124	1,147	1,168	1,187	1,206	1,224	1,244	1,266
1,5	0,961	0,968	0,975	0,984	0,997	1,018	1,040	1,061	1,088	1,111	1,134	1,156	1,176	1,196	1,215	1,235	1,258	1,277
1,6	0,972	0,978	0,985	0,994	1,010	1,030	1,050	1,073	1,096	1,119	1,142	1,164	1,184	1,204	1,224	1,245	1,268	1,289

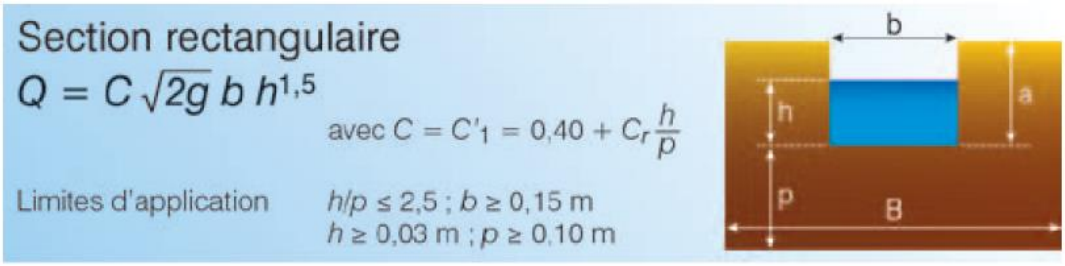


Figure 235: Expression of discharge coefficient for a weir with thin wall and rectangular section (Le Coz, et al., 2011)

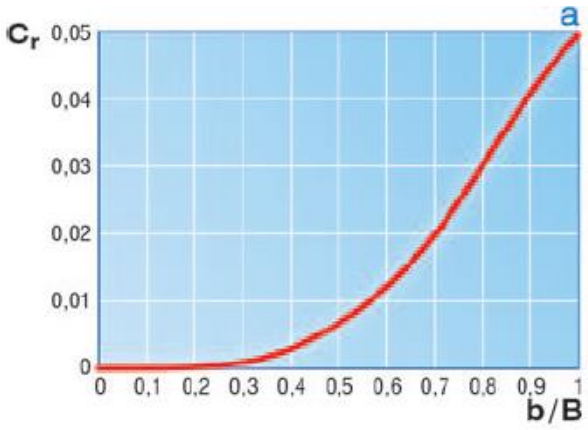


Figure 236: Abacus for the determination of Cr for a weir with thin wall and rectangular section (Le Coz, et al., 2011)

Figure 237 presents the results of the discharge calculation made with the Devers tool from Cassiopée software. A discharge of 1.13 m^3/s is obtained; it is a few lower than the theoretical value of 1.35 m^3/s (84%).

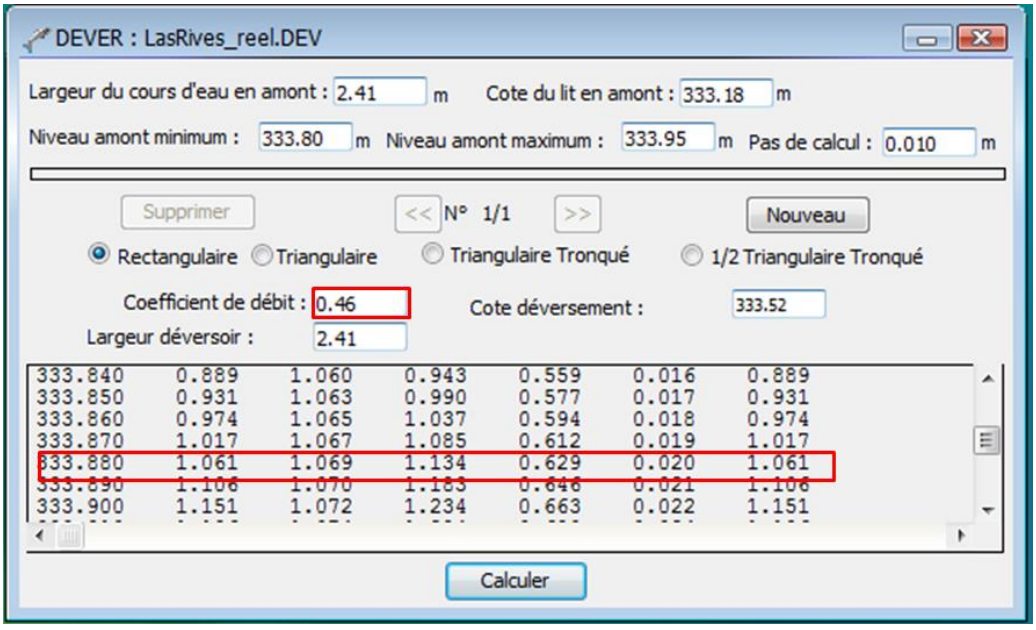


Figure 237: calculated discharge by Devers tool (C=0.46).

3.12 Schiffmuhle

3.12.1 Monitoring of bedload transport through a vortex tube

In this study, we aim to quantify (i) the total bedload mass and (ii) the grain size distribution of the bedload transported through the vortex tube, and (iii) to provide the operator of HPP Schiffmühle with recommendations on the vortex tube operation. A field calibration was performed to relate the obtained signals to bedload transport characteristics. In this report, only the data of the geophone and accelerometer are processed and the analysis is based solely on the signal amplitude. Further data analysis is ongoing

3.12.1.1 Data

The negative impact of hydropower plants on the bedload continuity in the Limmat River is of strong interest for the assessment of habitat quality (see section 3.12.3). HPP Schiffmühle is equipped with a vortex tube, a diversion structure for bedload. The vortex tube consists of a steel tube embedded in the side weir, connecting the headwater channel to the residual flow reach (Figure 238). The section of the tube extending into the headwater channel has a slot opening along its soffit and an open end. A gate valve is positioned in the side weir, which is automatically opened when a critical discharge is exceeded. When it is open, a spiral flow develops and bedload transported across the bed of the headwater channel may be entrained into the vortex tube and flushed to the residual flow reach by the combination of the approach flow and the pressure gradient between the headwater channel and the residual flow reach (Mtalo 1988, Atkinson 1994a, Atkinson 1994b, Awasthi 2001). To quantify the diversion efficiency of the vortex tube, three passive acoustic sensors, a geophone, an accelerometer, and a microphone, have been attached to the steel vortex tube (Gray *et al.* 2010). All measurements only concern the sediment transported as bedload, because suspended sediment transport is not an issue.

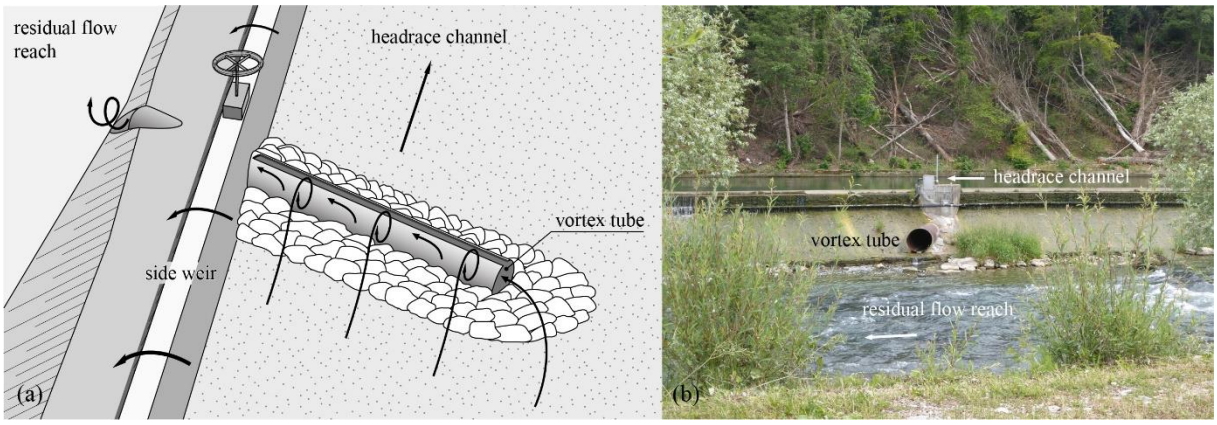


Figure 238: (a) Conceptual sketch of the vortex tube functionality and (b) the vortex tube at HPP Schiffmühle.

The gate valve operation is controlled by the discharge signal of the Swiss Federal Office for the Environment (FOEN) hydrometric station Baden, Limmatpromenade (Station ID 2243), approximately 4800 m upstream of the vortex tube. No major tributaries join the Limmat River in between. The gate valve is opened when the discharge exceeds Q_{open} = 150 m^3/s during the rising limb of a hydrograph and closes when the discharge falls below Q_{close} = 130 m^3/s during the receding limb. Since the beginning of October 2018, the vortex tube is also opened weekly for approximately 22 min, opening and closing time of approx. 5 min included. The goal of the operator is to more regularly divert bedload transported during discharges < Q_{open} into the residual flow reach. To test the functionality of the monitoring system, a test file of 2-4 s length is recorded every day at a set time.

The automatically recorded events up to December 23, 2018 can be sorted into the three main categories (i) flood events (4 events), (ii) weekly flushing (12 events), and (iii) tests (191 events). Figure 239 shows the data set collected until December 23, 2018, including unforeseen operational problems of the HPP or the data recording system. The geophone was installed first in April 2018, later followed by the installation of the accelerometer and the microphone in June 2018. Only the geophone data is thus available for the spring flood events.

Table 62 shows the characteristics of the four spring flood events. Due to difficulties with data storage during the 16-May-18 event, data is only available for 32.3% of its total duration. During the period marked 'frontal weir out of order', the discharge allocation to the headwater channel and the residual flow reach was not representative of normal operating conditions. Therefore, the pressure difference between the headwater channel and the residual flow reach may have been influencing the hydraulic conditions and bedload transport in the vortex tube. For this reason, the flood 13-Jun-18 is excluded from the data analysis. Similarly, the first weekly flushing event is excluded due to ongoing gravel extraction works that may have influenced the functioning of the vortex tube.

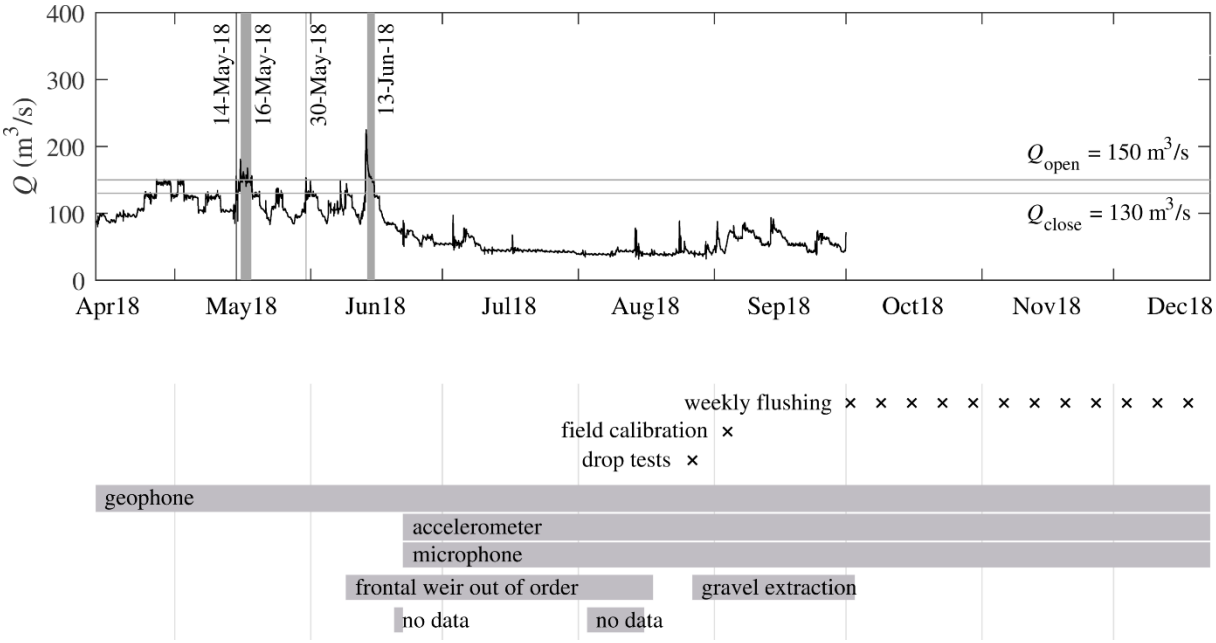


Figure 239: Overview of the data set collected between April 13, 2018 and December 23, 2018. The discharge data (FOEN hydrometric station ID 2243) for October, November, and December 2018 is not yet available. The vortex tube is automatically opened for $Q > Q_{open}$ and closed for $Q < Q_{close}$. Flood events are labeled with their start date. The bottom panel informs about the installation dates of the sensors and restrictions on the data availability due to operational problems of either the HPP or the data recording system. The test events are not displayed individually.

Table 62 : Recorded flood events between April 13, 2018 and December 23, 2018.

Notation	Start time (UTC)	End time (UTC)	Duration	recorded	Q_{max}
			dd / hh:mm:ss	(%)	(m^3/s)
14-May-18	2018/05/14 22:14:00	2018/05/15 01:24:05	-- / 03:10:05	100	155.7
16-May-18	2018/05/16 01:03:40	2018/05/18 09:47:33	02 / 08:43:53	32.3	180.9
30-May-18	2018/05/30 20:35:12	2018/05/30 23:12:16	-- / 02:37:04	100	153.2

13-Jun-18 *	2018/06/13 10:56:24	2018/06/15 12:56:29	02 / 02:00:05	100	224.8

* frontal weir out of order

.

3.12.1.2 Methodology

3.12.1.2.1 Passive acoustic sensors

Three passive acoustic sensors were installed on the vortex tube at HPP Schiffmühle to measure the oscillations of the steel tube caused by grain impacts. A geophone (GS-20DX manufactured by Geospace Technologies, Houston TX, USA), a single axis accelerometer (ICP352C03 manufactured by PCB Piezoelectronics, Depew NY, USA), and a microphone (ICP130A24 manufactured by PCB Piezoelectronics, Depew NY, USA) were mounted in a 0.22 m long, 0.12 m high, and 0.081 m deep, water-tight aluminum housing that was welded to the side of the vortex tube (Figure 240). All signals are recorded by an analog-digital converter with a sampling frequency of f_s = 51.2 kHz. These raw signals are then transmitted and further processed.



Figure 240: The bedload monitoring setup with (a) the housing and the geophone and (b) the housing mounted to the vortex tube and all sensors installed.

Figure 241 shows an exemplary geophone and accelerometer signal with the threshold A_{min} (V) above the background noise level, the maximum amplitude A_{maxmax} (V) and the impulse count *SumIMP* for the period shown. To facilitate data analysis, all recorded raw signals are aggregated in the summary values *IMP*, the sum of the impulse count per second, and A_{max}, the maximum positive amplitude value within a second (Rickenmann *et al.* 2014). The parameters *SumIMP* and A_{maxmax} represent the same summary values, but they are calculated over the duration of an entire event (e.g. a flood).

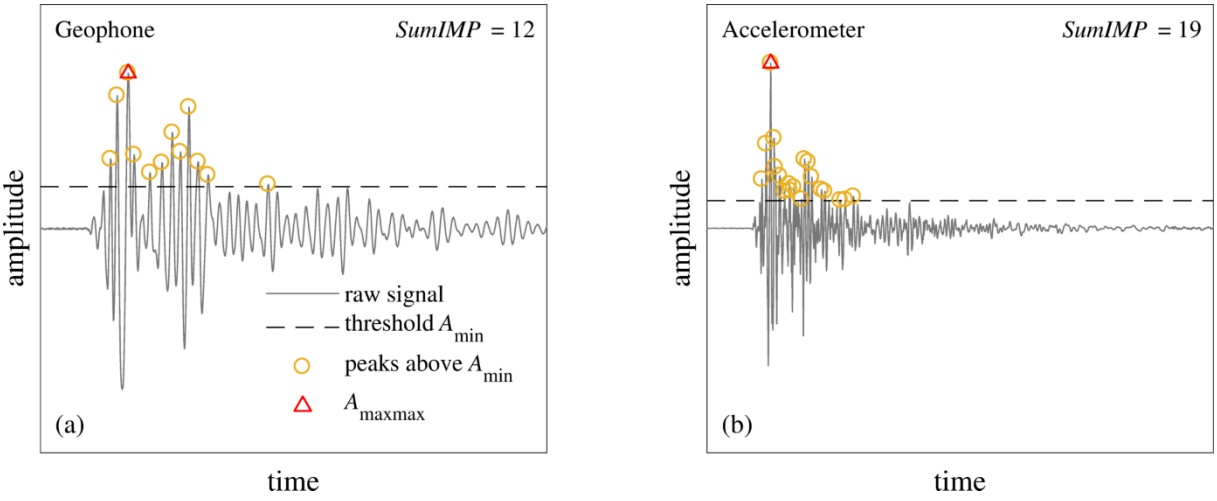


Figure 241: Exemplary (a) geophone and (b) accelerometer signal of the same grain impact. SumIMP denotes the total number of peaks above the threshold amplitude A_{min} for the event shown. A_{maxmax} is the maximum amplitude registered during this event. Only positive amplitude values are considered.

3.12.1.2.2 Pressure sensor

In addition to the bedload monitoring sensors, a pressure sensor (26W manufactured by Keller AG, Winterthur, Switzerland) was installed next to the vortex tube outlet to record water levels in the residual flow reach relative to the vortex tube bottom (Figure 242). The sampling frequency is 1 min^{-1}, independent of the vortex tube operation. The information on the water level at the vortex tube outlet is of interest because the vibration signals may be influenced by submergence of the vortex tube outlet. Additionally, the diversion efficiency of the vortex tube is attenuated by a rising water level at the outlet (VAW 2001, VAW 2017). The pressure sensor data will not, however, be analyzed in this report.

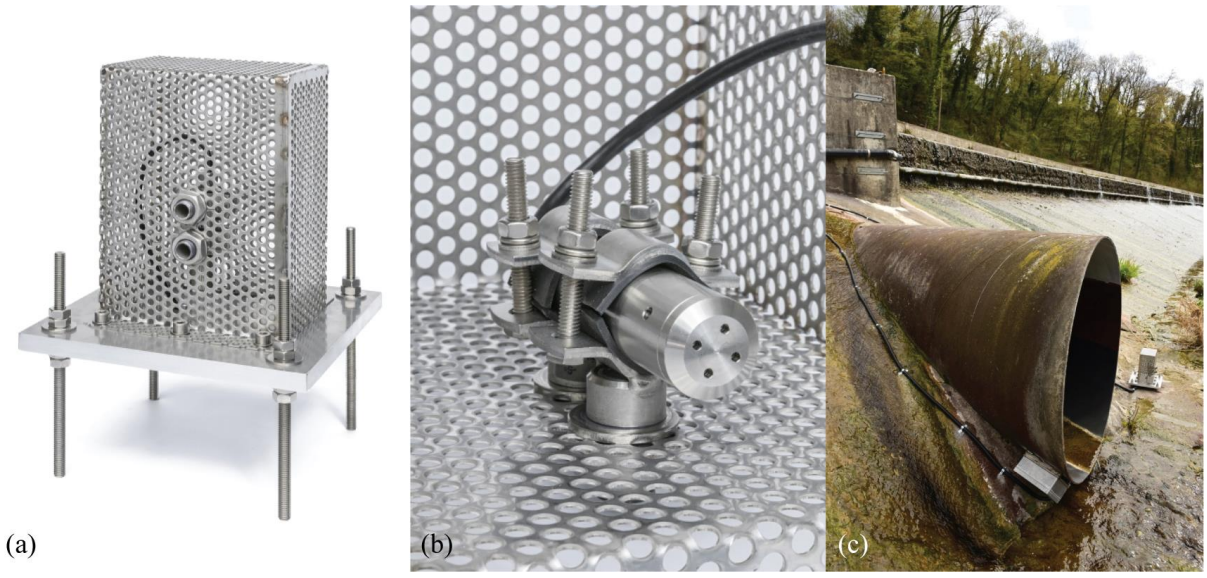


Figure 242: The setup for water level measurements with (a) the housing, (b) the sensor, and (c) the installation next to the vortex tube outlet.

3.12.1.2.3 Field calibration

On September 4, 2018, the vortex tube was calibrated in the field with four sediment mixtures of known grain size distributions that were flushed through the vortex tube. The grain size distribution analysis of these mixtures was conducted by square-hole sieving and with the grain-detection software BASEGRAIN (Detert and Weitbrecht 2013). The images for

BASEGRAIN were taken with a SONY ILCE-6000 and no distortion correction was applied. To obtain the real *b*-axis of the grains, a correction factor of b_{sieve} / *b* = 0.80 (Graham *et al.* 2010) and $b_{BASEGRAIN}$ / *b* = 0.85 (Stähly *et al.* 2017) was applied.

The samples *fine*, *medium*, and *coarse* were obtained from an external gravel extraction site, whereas the sample *channel* is gravel directly excavated from the headwater channel. Table 63 and Figure 243 show the grain size distributions (GSD) and characteristic grain sizes of all sediment mixtures used in the field calibration.

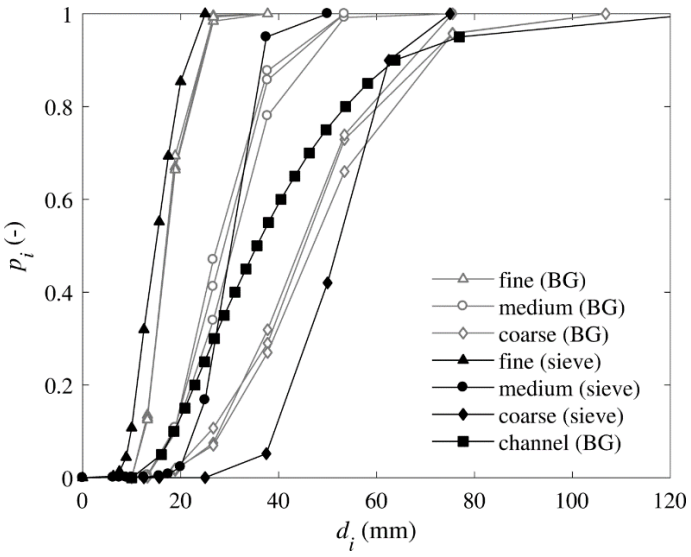


Figure 243: Grain size distribution of the four gravel mixtures used in the field calibration. The legend indicates whether the grain size sample was processed by square-hole sieving (sieve) or by BASEGRAIN analysis (BG).

Table 63: Characteristic grain sizes and the geometric standard deviation $\sigma_g = (d_{84}/d_{16})^{1/2}$ of the sediment mixtures used in the field calibration and in the turbine inlet (BG = BASEGRAIN, sieve = square-hole sieve).

sediment mixture	d_{16} (mm)	d_{50} (mm)	d_{84} (mm)	σ_g (-)
fine (sieve)	10.6	14.9	19.8	1.36
medium (sieve)	24.7	30.3	35.7	1.20
coarse (sieve)	41.2	52.1	60.9	1.22
channel (BG)	21.3	35.6	57.3	1.64
turbine inlet (BG)*	16.9	27.2	46.1	1.65

* not used in field calibration

During the field calibration, the vortex tube was opened and closed six times (Table 64). The first opening CW served as calibration of the clear water signal and the flushing of any movable sediment in the vicinity of the vortex tube. During the subsequent calibration runs, the sediment mixtures were dumped in the upstream vicinity of the vortex tube by an excavator set up on a float (Figure 244). The material was dumped with the vortex tube closed and it was opened only afterwards. The river discharge *Q* was 72.5 m^3/s.

The field calibration is based on the assumption that all of the dumped material was transported through the vortex tube. It is questionable if this assumption holds, as part of the sample may have been entrained by the flow to pass the vortex tube and be transported further along the headwater channel or it may have been deposited and not entrained by the increased flow velocity following the opening of the vortex tube. The relative importance of these processes can be assessed by considering the hydrological conditions. The bed shear stresses during the calibration runs (Q = 72.5 m^3/s) are too small to entrain grains larger than 4-8 mm, as was deduced from ADCP measurements in March 2018 with Q = 62-71 m^3/s (Section 3.3.3.1). Compared to the GSD of the sample mixtures shown in Figure 243, it is therefore unlikely that a large fraction of the sample was by-passing the vortex tube. Moreover, laboratory tests have shown that the opening of the vortex tube strongly influences the local flow field and establishes a suction effect that is especially strong when the water level difference between the headwater channel and the residual flow reach is large (VAW 2017). As a result of the low discharge and therefore large water level difference on the day of the calibration, the relative flow field change caused by the vortex tube was strong and likely entrained most of the dumped gravel. Nevertheless, there is no way of knowing exactly what fraction of the total bedload volume was passing through the vortex tube and has thus induced impact signals. This uncertainty would have been reduced if the number of calibration runs and the variation in sample volume had been increased or if it had been possible to conduct systematic flume experiments, as it is generally recommended for indirect bedload monitoring systems (Gray *et al.* 2010, Wyss *et al.* 2016b, Wyss *et al.* 2016c). Also, a bedload sampling system downstream of the vortex tube outlet would have been necessary to improve the calibration (compare Rickenmann *et al.* 2012). The simple and relatively inexpensive calibration approach applied here was adjusted to the study purpose.

Table 64: Field calibration runs of September 4, 2018. The duration includes the opening and closing time of the vortex tube. The material was dumped in between the calibration runs, when the vortex tube was closed.

Notation	Sediment mixture	Volume (m^3)	Start time (UTC)	End time (UTC)	Duration (s)
CW	-	-	2018/09/04 08:06:53	2018/09/04 08:18:57	725
CF1	fine	0.5	2018/09/04 08:22:52	2018/09/04 08:34:56	725
CF2	fine	0.5	2018/09/04 08:36:53	2018/09/04 08:48:57	725
CM	medium	1	2018/09/04 08:50:53	2018/09/04 09:08:57	1085
CC	coarse	1	2018/09/04 09:10:53	2018/09/04 09:24:57	845
CCH	channel	approx. 2	2018/09/04 09:28:53	2018/09/04 09:43:57	905

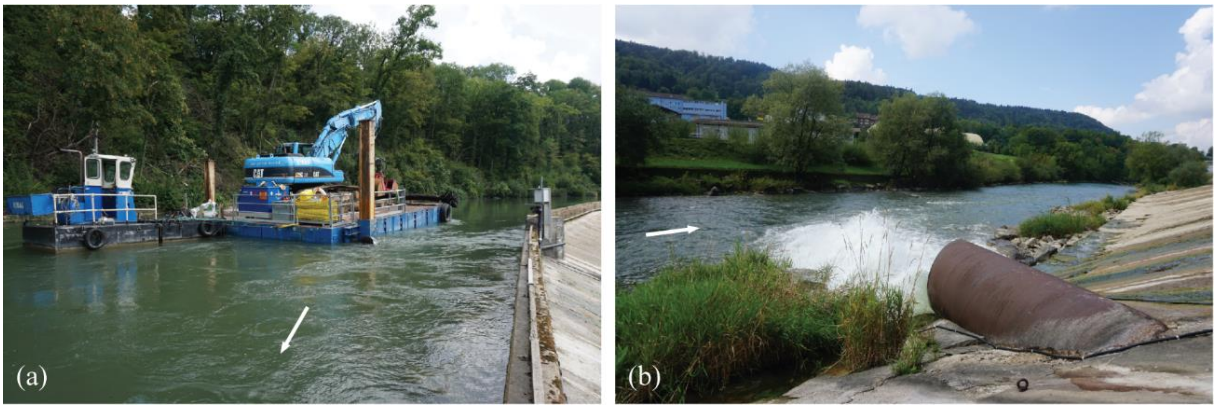


Figure 244: Field calibration on September 4, 2018 with (a) an excavator set up on a float and (b) the outlet of the vortex tube during a calibration run.

3.12.1.2.4 Data analysis

From the field calibration data, the background noise level was determined to be 0.015 V for the geophone and 0.01 V for the accelerometer. To investigate the influence of the grain size diameter on the vibration signal, the dataset of the field calibration was used to relate the maximum recorded amplitude per event A_{maxmax} (V) to the maximum grain size diameter D_{max} (mm). D_{max} was determined from the square-hole sieve analysis and largest detected particle in the BASEGRAIN analysis (Figure 243). Following Wyss *et al.* (2016a), a power law function of D_{max} is fitted to A_{maxmax} (Figure 245)

$$A_{max\,max} = 2.85 \cdot 10^{-4} \cdot D_{max}^{\ 1.80} \quad (1a)$$

$$A_{max\,max} = 1.62 \cdot 10^{-3} \cdot D_{max}^{\ 1.44} \quad (1b)$$

where Eq. (1a) represents the geophone data with an RMSE = 0.11 V and Eq. (1b) the accelerometer data with an RMSE = 0.20 V. This corresponds to the 95% quantile at ± 0.22 V for the geophone data and ± 0.40 V for the accelerometer data, respectively. The smallest detectable grain is 9.0 mm for the geophone (A_{min} = 0.015 V) and 3.5 mm for the accelerometer (A_{min} = 0.01 V). This relation will be used during future data analysis to extract the GSD of the impulse signals.

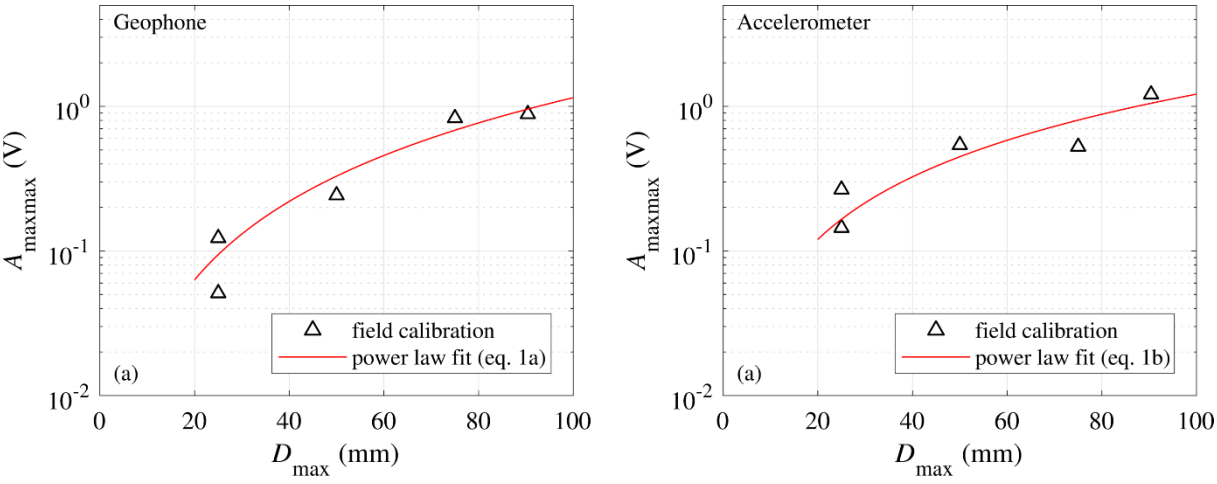


Figure 245: The maximum amplitude A_{maxmax} as a power law function of the maximum transported grain size D_{max} for each field calibration runs.

To extract information about the transported bedload volume from the monitoring system, it is linked to the sum of impulses *SumIMP* above a certain amplitude threshold A_{min}. A linear regression has been shown to be a good model for several impact plate geophone systems (Rickenmann *et al.* 2014)

$$SumIMP = a + b \cdot V_b \quad (2)$$

where *SumIMP* (-) is the total of impulses above a certain threshold A_{min} (V) and V_b (m^3) is the total transported bedload volume during an event. For A_{min}, the background noise level was used. In addition, the sum of the impulse counts and the bedload volumes of CF1, CF2, CM and CC calibration runs (Table 60) were also used as a fifth data point. This is possible when adapting the assumption that the relation between total impulse count and bedload volume is linear (Rickenmann *et al.* 2014). The calibration run CCH was used to validate the model as its bedload volume (Table 60).

Figure 246 shows the best linear regression fit for both datasets with its calibration and validation data points. The parameters of Eq. (2) are a = −484 and b = 10210 m^{-3} for the geophone and a = −781 and b = 7508 m^{-3} for the accelerometer. The model based on the accelerometer data (Figure 246b) seems to be slightly more accurate.

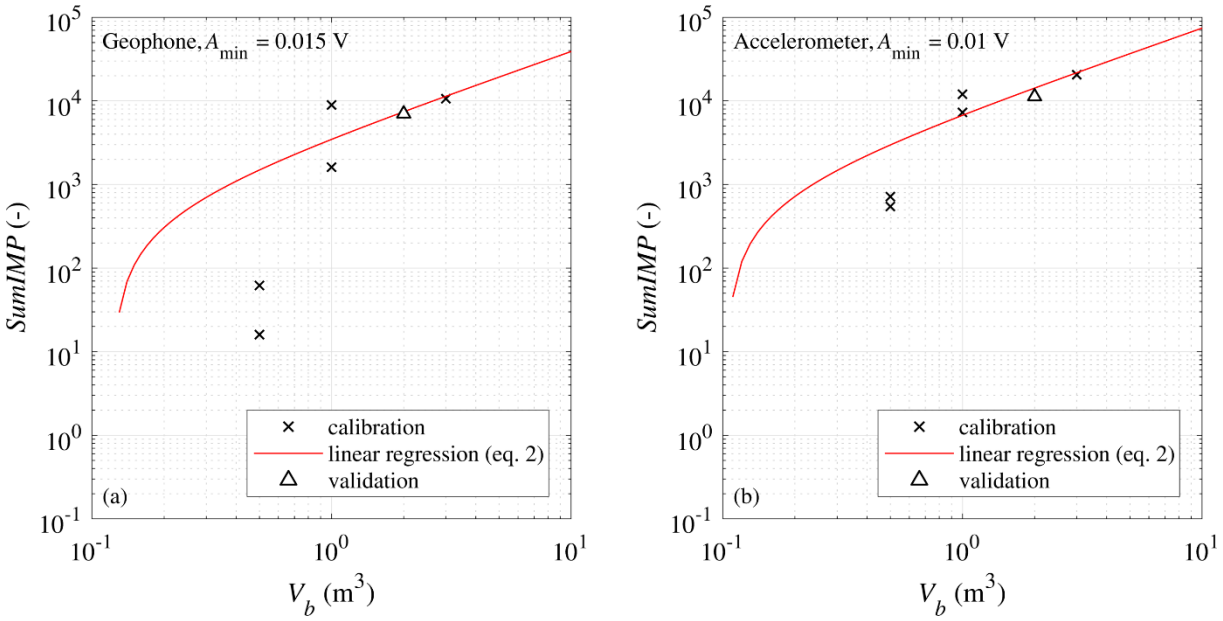


Figure 246: Linear relation between the total transported bedload volume V_b and the sum of impulses SumIMP during the field calibration runs for (a) geophone data and (b) accelerometer data.

3.12.1.3 Results

The transported bedload volumes during eleven weekly flushing events and three spring floods were determined by applying the linear relation to the sum of impulses (Eq. 2). Figure 246 was extended with the results (Figure 247). According to the fit of the geophone data based on A_{min} = 0.015 V, the transported bedload volumes were (i) 0.16 m^3 on May 14, 2018, (ii) 0.27 m^3 on May 16, 2018, and (iii) 0.48 m^3 on May 30, 2018. The accelerometer was not yet installed during these flood events. The transported bedload volume during the weekly flushing events ranged from 0.13 to 0.91 m^3 for the geophone and from 0.10 to 0.33 m^3 for the accelerometer data. The calculated values for bedload transport during the floods and flushing events are thus mostly lower than the volumes dumped during the calibration runs. Some weekly flushing events did not record any impulses on the accelerometer.

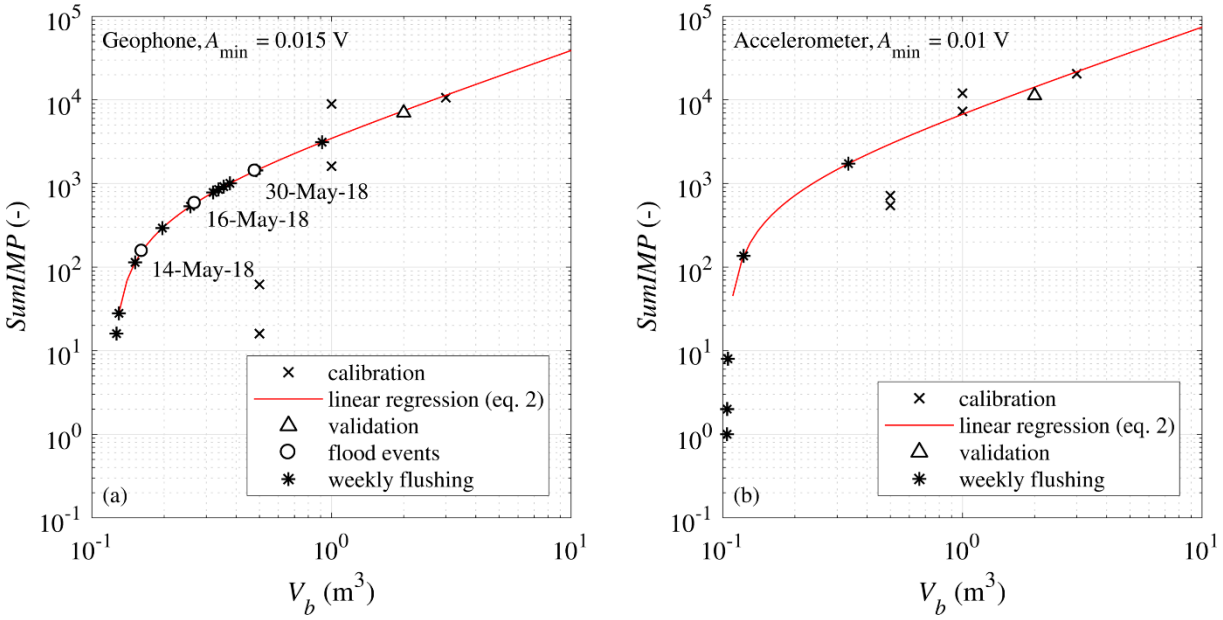


Figure 247: The linear regression between the total transported bedload volume V_b and the sum of impulses SumIMP fitted to the calibration runs and the resulting bedload volumes for the flood events and weekly flushings for (a) geophone data and (b) accelerometer data. Note that the flood events were only recorded by the geophone, as the accelerometer was not yet installed.

The duration of the recorded flood events was either short or they were incompletely recorded (Table 62). It is reasonable that the resulting bedload volumes are relatively small (Figure 247), given that during the calibration runs, material was directly dumped upstream of the vortex tube, while the currently occurring bedload transport in the Limmat River is relatively low. However, with only three flood events recorded so far, it is nearly impossible to assess validity of these results. A record of a prolonged period of vortex tube flushing, i.e. several days, would allow putting the results into perspective. The bedload volumes diverted during the weekly flushing events are in the same range as the flood events, but the data set collected so far is not yet sufficient to make any operational recommendations.

Further insights are expected from the 3D hydro-numerical model that will be set up by AF-Consult (section 0). Bed shear stresses along the headwater channel obtained through the simulation of flood events will enable the estimation of the grain sizes that are transported as bedload. These scenarios will help to assess the quality of the bedload volume determination as well as serve as a validation for future GSD analyses. Furthermore, the ongoing data collection during flood events will eventually allow the connection of the measured bedload transport to the discharge and the comparison to the long-term hydrology and estimates for bedload transport (Flussbau AG, 2017).

3.12.1.4 Conclusions and Outlook

A bedload monitoring system with a geophone, an accelerometer, and a microphone has been installed on a vortex tube, a bedload diversion system at HPP Schiffmühle. It was calibrated in the field by repeatedly dumping sediment samples of known grain size distribution and volume upstream of the vortex tube and subsequently flushing them to the residual flow reach. The results allowed to relate the transported bedload volumes to the impact signals of the geophone and accelerometer. During the flood events and weekly flushing events recorded so far, bedload volumes of < 1 m^3 were determined. These results seem reasonable, but a reliable assessment of their validity is only possible once a larger number of events will be recorded. The amplitude has been shown to also contain information on the transported grain size fractions, however, the quantitative analysis thereof is pending. Additional information on the

grain size distribution will be extracted from the frequency spectrum of the impact signals. It can be concluded that the usage of the steel vortex tube as a conveyance body and impact plate for passive acoustic bedload monitoring is possible. The first results are promising, but the data analysis will be refined and extended. Furthermore, a larger number of flushing events has to be recorded.

In this report, data collected until December 23, 2018 was processed. The measurement system will continue to record flood events and the analysis of transported total bedload and its grain size distribution will be updated in further dissemination documents. The following steps will be taken during the remaining duration of the FIThydro research project:

- The appropriateness of the correction factors b_{sieve} / b = 0.80 (Graham *et al.* 2010) and $b_{BASEGRAIN}$ / b = 0.85 (Stähly *et al.* 2017) will be tested by manual measurement of the *b*-axis of all volume sample grains and of all grains being detected on images analyzed with BASEGRAIN.
- A relation between particle size and weight will be established for the bedload at HPP Schiffmühle and the calibration samples from the gravel plant (Bunte and Abt, 2001).
- Parameters influencing the signals, e.g. the grain size, the drop location, or the drop height, will be thoroughly examined by the analysis of several in-situ drop tests that were already performed.
- The probability of signal overlapping will be assessed with the approach of Wyss *et al.* (2016a).
- The analysis of the grain size distribution of the transported bedload will first be completed with the signal amplitude approach (Wyss *et al.* 2016a) and later extended to include the frequency spectra (Wyss *et al.* 2016b, Wyss *et al.* 2016c)
- The microphone data will be analyzed.
- All recorded flood and weekly flushing events will be analyzed.

3.12.2 Downstream impact of sediment management at HPPs (NTNU, ETHZ)

The dynamic changes in bedload transport rates and total transported masses are quantified and their effects on river ecology and morphology are qualitatively and numerically evaluated.

3.12.2.1 Data

Data will be collected from the field campaign and literature. The information on the sediment structure is collected using different techniques as sieving, pebble count and picture based information based on the evaluation software BASEGRAIN, developed at VAW, ETH Zurich (Detert & Weitbrecht, 2013) Further information about the shelter availability are collected following the Finstad method and the redox potential is measured for potential habitats to get information about the interstitial in this area.

3.12.2.2 Methodology

- Bathymetry measurements around HPP (section 2.12.3)
- Habitat mapping, sediment sampling, shelter measurements and substrate characterization

3.12.2.3 Results

Habitat mapping, sediment sampling, shelter measurements and substrate characterization

For habitat mapping and sediment sampling in the residual flow reach three different well established techniques are used, such as collecting and sieving of the sediment material, picture based sediment distribution evaluation (Buscombe et al 2010) with the program BASEGRAIN and the pebble count method (Bunte at al. 2004). The results will be compared throughout the whole project period and will be used to evaluate the substrate based shelter evaluation. The results described in this report are based on the first field trip in March 2018.

The spots in which the samples are taken represent a broad variety of potential habitats for the relevant fish species in the area (Figure 162). The techniques used for each spot might differ based on the applicability at each location (Table 61). For instance, depending on the water depth and turbidity, it is not possible to use BASEGRAIN in submerged areas as the quality of the pictures is not sufficient. The results are used to compare the different measurement techniques but also to gain information about the structural changes over time in the residual flow reach using further samples which were and will be taken. These results will be linked with the data gathered in the numerical simulations conducted by the FIThydro partner AF Consult to be able to evaluate the development of the sediment structure as a result of flow changes.



Figure 248: Locations of the sediment sampling in March 2018

Table 65: List of the different methods applied at the testing spots

Data Point	Basegrain	Sieving	Pebble Count
#1	x	x	x
#2		x	x
#3		x	
#4			x
#5	x	x	x
#6		x	x
#7			
#8		x	x
#9			
#10			
#11	x	x	x
#12	x	x	x
#13		x	x
#14	x	x	x
#15	x		x
#16			x

All the three different techniques show advantages and disadvantages as a results of the circumstances of the sampling such as submerged spots vs. non-submerged spots etc. This can be seen in Figure 163 where smaller fractions are underrepresented in comparison with the other two methods. A reason might be that collecting / sieving is an invasive method and the very fine fractions might get lost during sampling. A more detailed evaluation will be available after the evaluation of the other field campaigns.

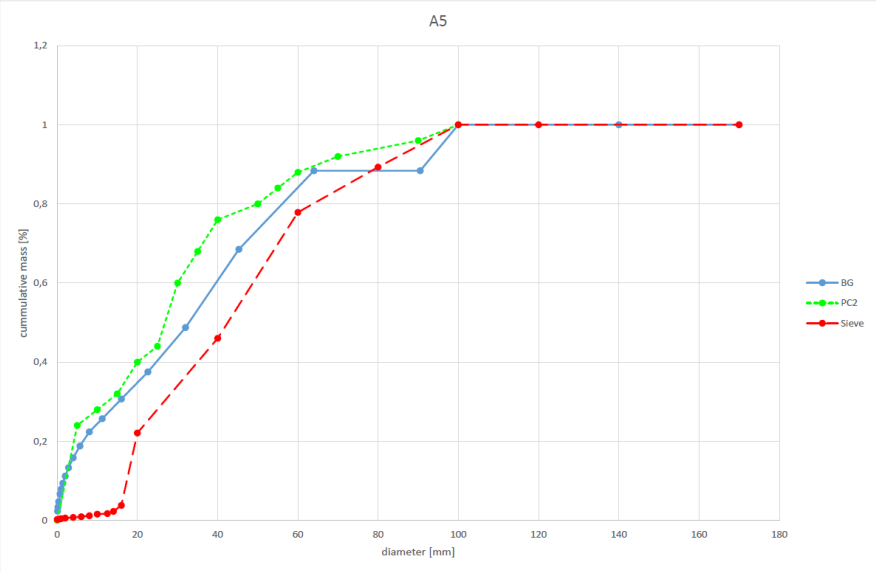


Figure 249: Results of sieving (red dashed), pebble count (green dotted) and BASEGRAIN (blue line) at spot number 5.

The shelter availability is investigated with the method of Finstad (Finstad et al., 2007, Figure 250). The original method shall be adapted to the endemic species in the river Limmat within FIThydro. The availability and the size of the opening in the interstitial are measured with a plastic tube with respect to diameter and depth of the openings. The results are structured in

different categories based on the depth S1: 2-5 cm, S2: 5-10 cm, and S3: >10 cm according to Forseth et al. (2014).

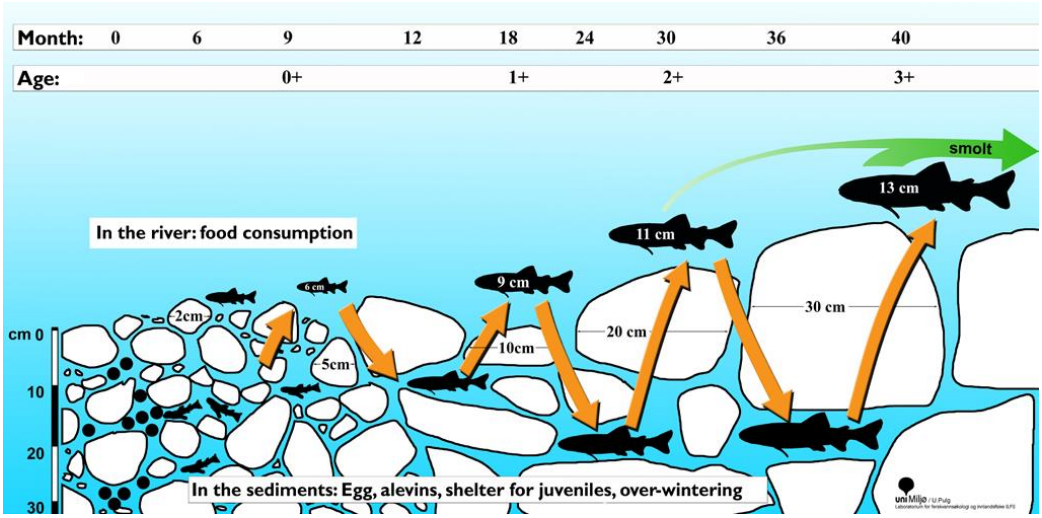


Figure 250: Shelter needs and availabilities depending on the different body sizes of salmons for different ages (Forseth et al., 2014).

Then a weighted shelter availability (Forseth et al., 2014) is calculated:

S1 + S2 x 2 + S3 x 3

and assigned to a class: "low shelter" (< 5), "moderate shelter" (5-10) or "high shelter" (> 10).

The results will be also linked to the grain size distribution. In the river Limmat the sediment percentiles D5 and D10 are much smaller than the ones the method was developed for in Norwegian rivers, therefore also other percentiles and distribution parameters will be evaluated and fitted with the results of the field campaigns.

3.12.2.4 Conclusion & Outlook

First results are promising. Data analysis is on-going and a new field measurement will be conducted in 2019.

3.12.3 Efficiency of downstream and upstream migration devices (ETHZ, FCO, LKW, AF-CONSULT)

At **HPP Schiffmühle** an angled fish guidance structures with horizontal bars, i.e. a Horizontal Bar Rack (HBR) has been implemented regarding downstream fish migration. The current situation is documented through field monitoring and 3D numerical modelling in the area near the HBR and the frontal weir. The monitoring comprises the characterization of the flow field and bathymetry using an Acoustic Doppler Current Profiler (ADCP) and a survey of the fish movements. The latter is made with the PIT-tagging technique.

The detailed hydraulic data on the HBR will be obtained from the laboratory investigation in WP3, Task 3.5, and will serve as a basis for the implementation of the HBR into the numerical model. The flow field around the HBR, its bypass system, head losses and upstream and downstream flow fields at HPP Schiffmühle will be simulated using the 3D numerical model. The results from the simulation will be compared to the measured values to assess the performance of the numerical model and to deduce potential paths for improvement. Furthermore, fish movements and fish guidance efficiency of the implemented HBR and fish ladders will be quantified by PIT-tagging technique (FCO). An antenna mounted in the bypass and fish ladders will confirm the fish passage. Similar fish monitoring campaigns are carried out in two other HPPs upstream and downstream of HPP Schiffmühle on the river Limmat and

the obtained data will be shared by the operator Limmatkraftwerke. Finally, a comprehensive data set is compiled to study the fish movements on a larger scale. Hydraulics and fish data are evaluated to assess the fish guidance efficiency (FGE) of the HBR and fish ladders. If required, further investigation will be conducted to improve the HBR geometry for better FGE.

3.12.3.1 Data

Data are collected from the field campaigns, the HPP operator and literature.

3.12.3.2 Methodology

- Velocity and bathymetry measurements using ADCP and Drone
- Numerical modelling of HBR and weir flow
- Fish monitoring using PIT-tagging technique

Hydraulics and bathymetry measurements (ADCP)

Acoustic Doppler Current Profiler (ADCP)

High resolution 3D velocity, as well as bathymetry measurements, were conducted using an Acoustic Doppler Current Profiler (ADCP) mounted on a remote control boat in March and October 2018. The models of the ADCP and the boat are River Pro 1200 kHz including piston style four-beam transducer with a 5th, independent 600 kHz vertical beam and Q-Boat supplied by Teledyne Marine, USA, respectively (Figure 251).

The first campaign took place during an average river discharge of Q = 70 m^3/s from 13-15 March 2018, while the second campaign was done on 31st October and 1st November 2018 with an average river discharge of Q = 45 m^3/s. The main goals of both campaigns were to map river bathymetry and measure flow velocities in the upstream and downstream river reaches of the HPP. The data are used to construct, calibrate and validate the 3D numerical model, study the hydraulics of the HBR at the HPP and quantify sediment erosion and deposition in the river. The post-processing was done according to the workflow sketched in Figure 252 using the software WinRiver II[4] and VMT[5]. In addition to the ADCP measurements, we measured flow velocities inside the downstream bypass inlet using a propeller type handheld probe.



Figure 251: ADCP and Q-boat.

[4] Data collection and post processing software provided by U.S. Geological Survey
[5] Matlab based software for processing and visualizing ADCP data provided by U.S. Geological Survey

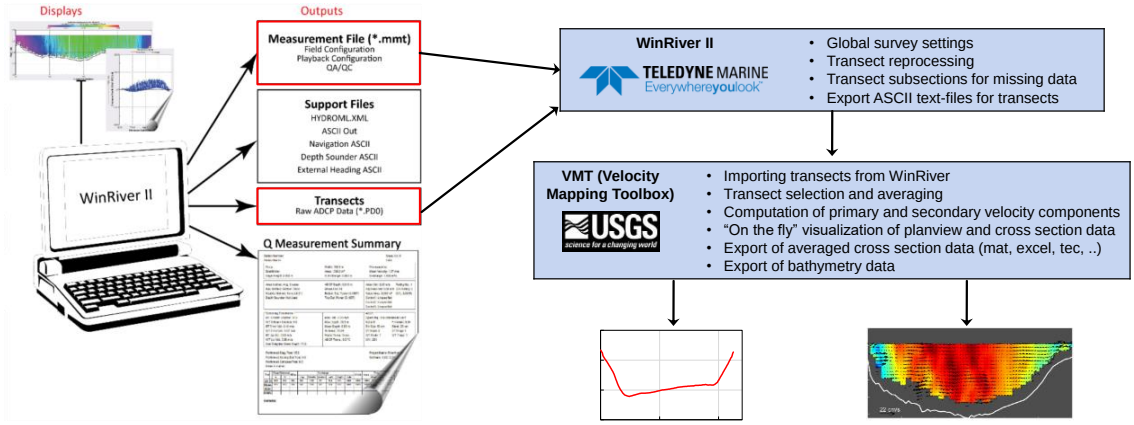
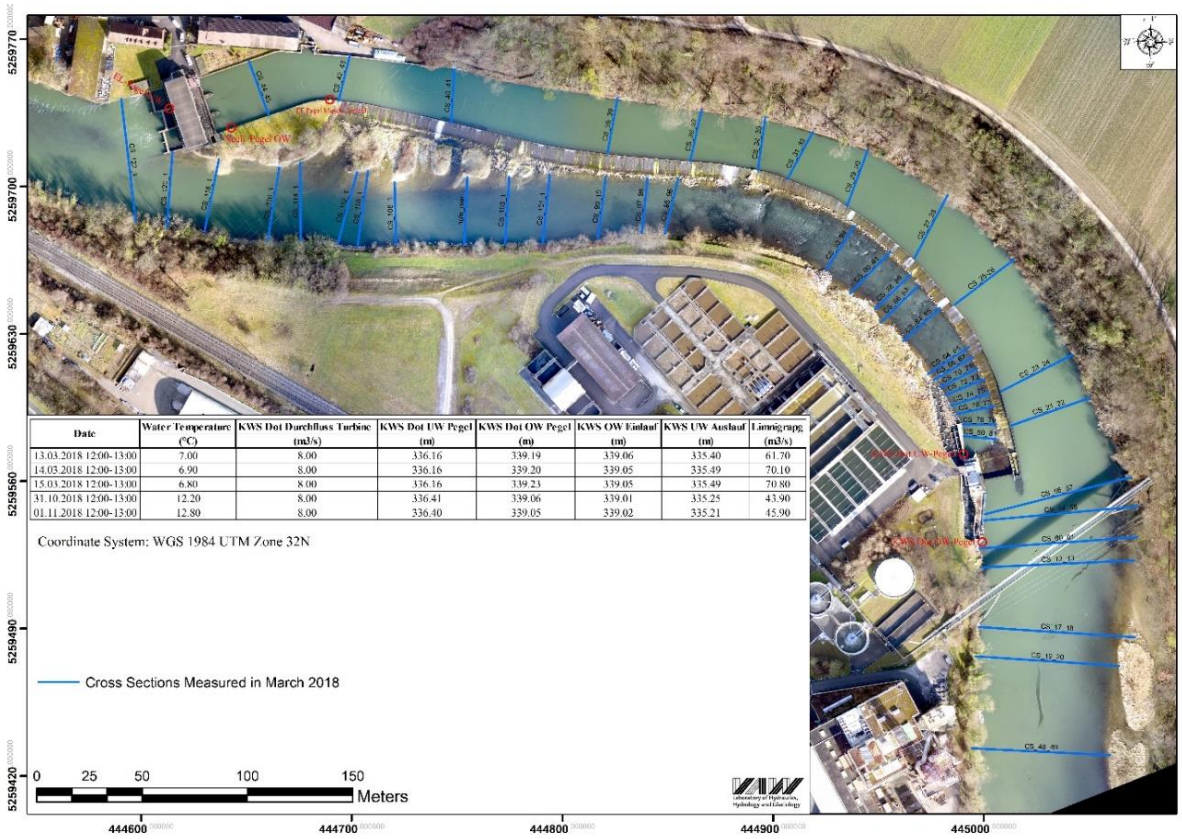


Figure 252: ADCP data analysis workflow.

ADCP measurement cross-sections at the first (46 cross-sections) and second field campaigns (69 cross-sections) are shown in Figure 253 and Figure 254. Due to a low accuracy of altitude measurement with the DGPS system of the ADCP, we used a TS02 Leica total station and a target on the boat to determine the water surface elevation at each transect during the second field campaign (Figure 255).



Date	Water Temperature (°C)	KWS Dot Durchfluss Turbine (m3/s)	KWS Dot UW Pegel (m)	KWS Dot OW Pegel (m)	KWS OW Einlauf (m)	KWS UW Auslauf (m)	Limnigraph (m3/s)
13.03.2018 12:00-13:00	7.00	8.00	336.16	339.19	339.06	335.40	61.70
14.03.2018 12:00-13:00	6.90	8.00	336.16	339.20	339.05	335.49	70.10
15.03.2018 12:00-13:00	6.80	8.00	336.16	339.23	339.05	335.49	70.80
31.10.2018 12:00-13:00	12.20	8.00	336.41	339.06	339.01	335.25	43.90
01.11.2018 12:00-13:00	12.80	8.00	336.40	339.05	339.02	335.21	45.90

Figure 253: Velocity and bathymetry measurement locations at HPP Schiffmühle in March 2018.



Figure 254: Velocity and bathymetry measurement locations at HPP Schiffmühle in October 2018.



Figure 255: Water surface elevation measurements using a total station and a target on the boat.

Hydraulics (Airborne Image Velocimetry (AIV))

Measurement of dry topography

Regionalwerke Baden AG (Zabah, 2018) performed measurements to get detailed data of the non-wetted topography. To this end, eleven ground control points (GCP) had been measured by geotechnical surveying on 2018/03/08 and a measurement flight had been performed on 2018/03/08 between 10:00-11:00 at a height of 140–145 m over ground. Based on 104 images, a high resolution 3D point cloud had been computed by photogrammetry software *PIX4D*, which combines structure from motion (SfM) technique with MultiView Stereo (MVS) methods. A Digital Surface Model (DSM), as well as an RGB ortho-image each with raster sizes of 0.0244 m, had been computed out of it (Figure 256). Georeference is given by the new Swiss survey LV95.

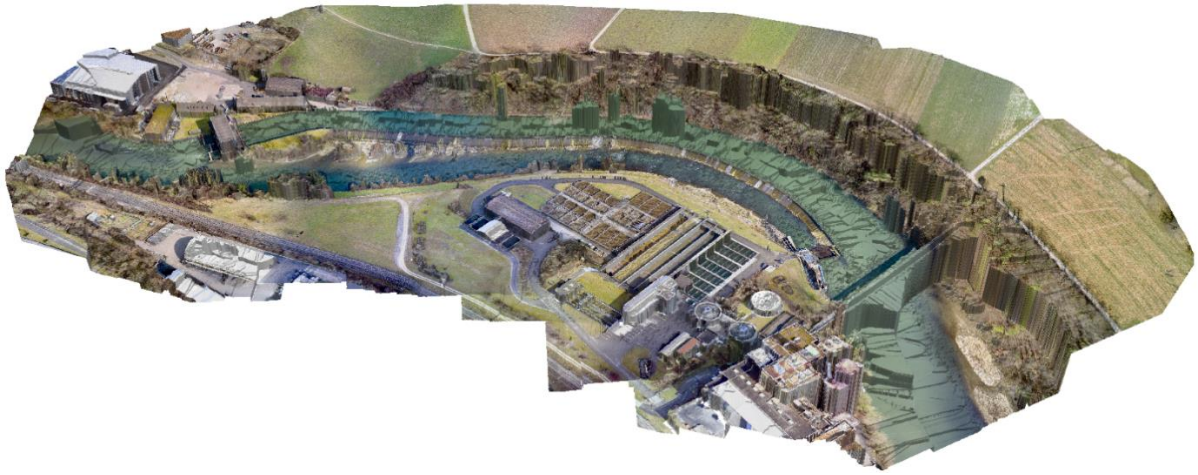


Figure 256: 3D snapshot view to the dry topography area observed by Regionalwerke Baden AG.

Measurement of surface velocity fields by Airborne Image Velocimetry

Airborne Image Velocimetry (AIV) measurements of surface velocities fields were performed on 2018/03/13 between 11:00-11:45 by VAW/ ETH Zürich. The flow discharge at this time was almost constant at 71–72 m^3/s, as deduced from the FOEN gauging station Baden-Limmat[6]. The goal of these measurements was to get an overview of the time-averaged far field approach flow.

The AIV technique applied was similar to the one presented by Detert at al. (2017). A crude description of the set-up, performance and image analysis is given in the following, with more information at details deviating from Detert at al. (2017). The AIV measurement setup consisted of an UAV *DJI Phantom 4 Pro+* with a weight of 1.4 kg including a three-axis Gimbal-stabilized action-camera. The latter has a 1” CMOS-sensor and the lens providing a field of view of 84° and a 35 mm focal length equivalent (Figure 257). The total cost of the quadcopter and accessories was below 2 kCHF (March 2018).

Surveying flights were performed at 30–70 m over ground, recording in h.256 video mode at 23.976 fps with a resolution of 4096×2160 px^2. To have a significant grayscale contrast on the video frames the flow was seeded with tracer from the upstream bridge, from a boat and from diverse riparian points during the measurements. Eco foam chips (*FILL-PAC Bio* from *MEDEWO*, Switzerland) were selected with diameters of 30-40 mm (Figure 257).

[6] Station #2243, located 4.6–5.1 km upstream, with assumption of an average flow velocity of 1–2 m/s.

The total length of the video data set comprises > 20 min, which is too large to be analyzed in total. Therefore, a reduced data set consisting of 579 image pairs each with an internal time shift of $\Delta t_{0:1}$ = 5/23.976 s and a median time shift of $\Delta t_{0:1–4:5}$ = 40/23.976 s between the image pairs had been chosen manually for the subsequent image analysis.

Image orthorectification was performed using the photogrammetry software *PhotoScan*, based on the 2×579 = 1158 image frames, combined with the eleven GCPs from Regionalwerke Baden AG (Zabah, 2018) and, to provide more supporting points for the computation, 17 additional characteristic markers as virtual GCPs (e.g. gully holes, larger stones) identified on their dry topography data set.

During the workflow process of *PhotoScan* a frame camera type setting was used to initialize implementation of a camera model that adequately fits the actual lens distortions. The whole process of photograph alignment at original resolution, including computation of camera parameters and positions took about 10 h computational time on a standard PC. The camera positions of the resulting sparse cloud had a reprojection error of ±0.2 px (in image coordinates). *PhotoScan* corrected the 3D coordinates of the GCPs by an average value of ±1.26 m according to the positions measured in the field and gave a reprojection error of ±1.2 px (in image coordinates) for all GCPs. The dense point cloud was reconstructed with medium quality, i.e. the images had been resized by a factor of four, and aggressive depth filtering within 17 h computational time on a typical office PC. The resulting point cloud had a density of 8.1 million points, which is >25 times higher than the density of the sparse cloud. A mesh with 420,000 vertices was build based on 4.5 million manually selected points of the point cloud, i.e. the dense point cloud with misleading points at the water surface and non-riparian points deleted. Finally, 1158 RGB orthoimages with raster sizes of 0.016 m have been exported for the subsequent image velocimetry analysis.

Flow velocities were determined by PIV via the previously described geo-referenced images. The images were converted to 8-bit grayscale, with each individual Gaussfilter-computed background image substracted, and the image intensity was adjusted and pixel values < 40 were capped – as described by the following MATLAB-code lines

```
I = rgb2gray(I);
J = imerode (imbinarize(I,0),strel('square',40));
I = imadjust((I-imgaussfilt(I,10)).*uint8(J));
I(I<40)=0;
```

Then, the MATLAB-based open source software *PIVlab* by Thielicke and Stamhuis (2014) was used to determine the surface flow velocities. PIV analysis was performed to the 579 image pairs in mode [(0,1), (4,5), (8,9), . . .] on a final window size of 64×64 px^2 with 50% overlap. Postprocessing comprised masking out non-water surface areas and applying a universal outlier detection method (Westerweel & Scarano, 2005) to the instantaneous velocity fields to eliminate misleading velocity vectors. The median value of the time series at each grid point was chosen to describe a characteristic time averaged surface velocity. Due to inhomogeneous flow-seeding conditions and non-perfect image orthorectification results (shivering between image pairs) the chosen approach is prone to overestimate near-zero flow velocities. Therefore, velocities <0.2 m/s finally have been deleted.



Figure 257: DJI Phantom 4 Pro and Ecofoam as seeding particles.

Fish monitoring

Fish have been monitored at HBR-BS and both technical and nature-like fish passes using the PIT-tagging technique since 2017 (Figure 258 and Figure 259).

Two antennas in the nature-like fish pass and another two antennas in the vertical-slot fish pass detect the entrance behaviour of fishes. One additional antenna at the exit of the fish pass registers the fish leaving the pass. One antenna has been installed in the downstream bypass to detect downstream migrating fish (Figure 259). All six antennas are connected to readers recording detections at a rate of about 14 scans per second. Data from the readers are remotely downloaded and the function of the readers is controlled from the office.



Figure 258: PIT-Tag antennas (left picture in the nature-like fish pass, right picture in the vertical-slot pass.

Fish tagging started in September 2017. In the first year (2017), we tagged 549 fishes belonging to 10 different species. In 2018, 1’782 fishes belonging to 17 species were tagged. A total of 2’331 individuals tagged in 2017 and 2018 were released downstream of the fish ladder. Most of the fish were caught in the counting facilities, except 73 individuals that were electrofished on 26-9-2018 upstream of the hydropower plant and translocated to downstream areas. Smaller fishes (< 160 mm) were tagged with 12 mm PIT tags, larger fishes (> 159 mm) with 32 mm tags. With a small incision the tags were placed in the body cavity. For the handling fishes were anaesthetized with clove oil (30 mg/l) (Figure 259). Before releasing fish back to the water they could fully recover from anaesthesia.




Figure 259: left: bleak with 12 mm PIT-tag, right: barbel, one of the most abundant species in the Limmat River.

Hydraulics (Numerical modelling)

Flow conditions upstream and downstream of the HPP are simulated with the software FLOW-3D (Flow Science, 2014). The goal is to simulate flow conditions at the in- and outlets of the fish migration structures at variable Limmat discharges and, accordingly, with variable operating conditions of the hydropower plants. The following modelling concepts are applied.

Trash rack

The horizontal trash rack is simulated in FLOW-3D by applying a baffle. This allows to account for the hydraulic effects of the rack without having to simulate each individual bar by direct numerical simulation with a resolution fine enough to properly resolve its hydraulic effects – an almost impossible endeavour given the trash rack size and bar spacing. It has been shown by specific research (Krzyzagorski, 2016), that the representation of a trash rack by a baffle leads to correct hydraulic effects.

Since the trash rack is not aligned with the orthogonal model cells, FLOW-3D fits the rack in a stepped shape on the grid. This artificially increases the rack surface. By reducing the porosity of the rack, the increase can be compensated as follows:

$$\phi_{model} = \sin(\alpha) \cdot \phi_{rack}$$

where:

ϕ_{model} Porosity to be entered into model
ϕ_{rack} Porosity of the rack
α Angle between grid and rack (0 = aligned)

With this correction, the open surface of the rack and therewith the flow velocities within the rack are properly represented.

The horizontal direction of the approach flow is not influenced by the rack since the bars are horizontally arranged. The impact on the vertical flow direction is not considered here because of the small vertical velocity component.

The loss coefficient assuming a 5 % obstruction and perpendicular flow is calculated based on the formula developed by Meusburger (2002, pages 170/171).

$$\zeta_{obstruction} = \left(\frac{P}{1-P}\right)^{\frac{3}{2}}$$

where *P* is the obstructed flow area. With 5 % obstruction the coefficient is 0.012. Oblique flow direction is directly accounted for by the FLOW-3D simulation.

Turbine

The flow through the turbine has not been simulated. The model ends before the impeller with an outflow rate boundary condition equalling to the turbine flow. The water is returned to the model by an equivalent inflow boundary condition at the end of the suction tube.

Fish downstream migration device

The fish downstream migration device is designed for a flow of 170 l/s when the weir flap is fully raised. The inlet of the device consists of two rectangular openings at different depth in the side wall of the HPP structure approximately 4 m upstream of the weir. The openings lead to a chamber from where a pipe leads to the residual flow river section. In the model, this flow is specified by an outflow boundary condition at the top and an inflow boundary condition at the bottom of the pipe.

Fish passes for upstream migration devices

To limit the computational power of the simulations the flow through the technical fish pass and the near-natural bypass is not explicitly simulated over the entire length of these structures. Only the flow through the lowest pools of each of the structures is simulated, such that the attracting flows in the residual water section are well represented by the model. The discharges are known and set in the model with outflow and inflow boundary conditions.

Model geometry

For generation of the model geometry, two types of data are combined:

1. As-built drawings of the structures of the residual HPP and of the near-natural bypass.
2. Bathymetry data measured in the present project and additional cross sections further upstream and downstream recorded by FOEN in 2013.

From the as-built drawings, a 3D geometry of the residual HPP has been established (Figure 260). The bathymetric cross sections used for establishing the geometry of the Limmat river, the headwater channel and the residual flow section are displayed in Figure 261.

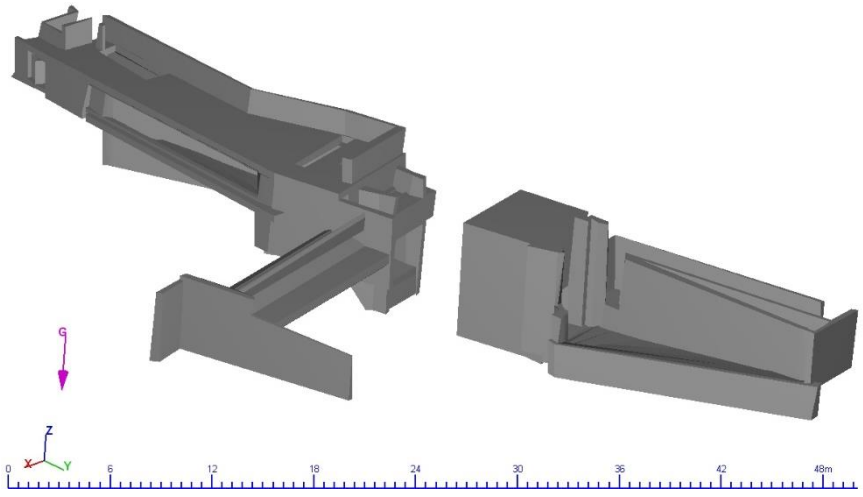


Figure 260: 3D geometry of the residual HPP with upstream (left) and downstream (right) parts.

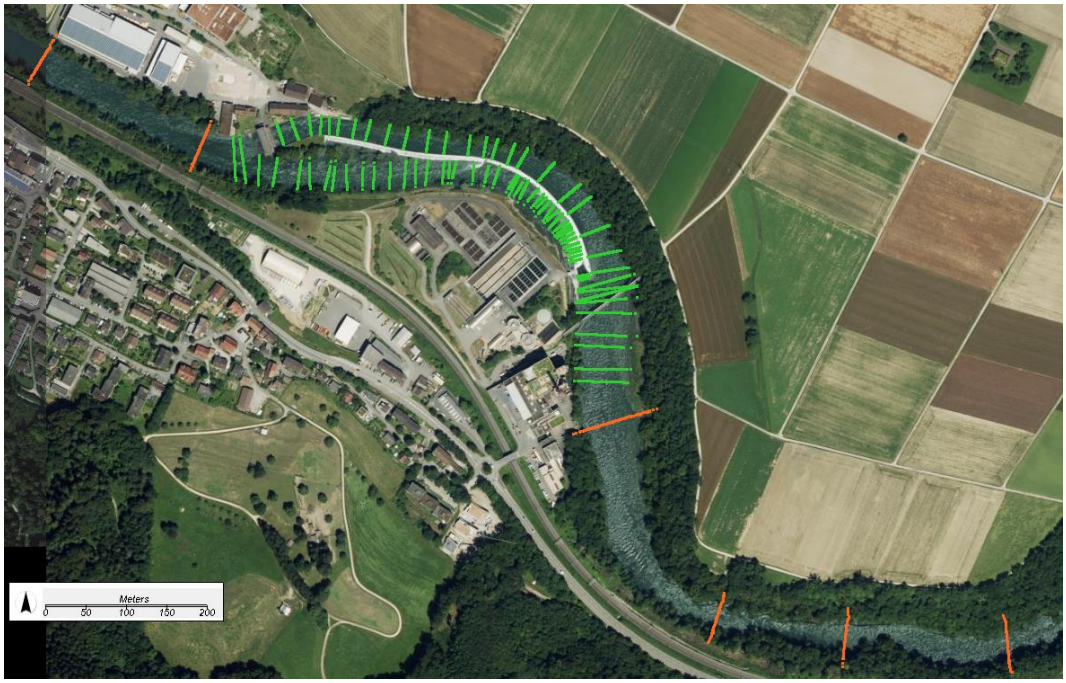


Figure 261: Available bathymetric cross sections, green (this project) and orange (FOEN, 2013).

Boundary conditions

Inner model boundary conditions for individual elements such as the turbine, the fish downstream migration device and the fish upstream migration devices have been described in above sections. The outer model boundary conditions are defined as:

- Inflow boundary condition at the upstream
- Water level to discharge relation at the downstream

Flow condition scenarios

The goal is to simulate flow conditions at the in- and outlets of the fish migration structures at variable Limmat discharges and, accordingly, with variable operating conditions of the hydropower plants.

The Limmat discharge conditions and operating conditions for which the model is to be applied are selected in a two-step approach:

1. Only the periods in which fish migration occurs are considered. These are mid-May to mid-June in springtime and September till the beginning of October in fall. In these periods the three residual flow allocations of 8, 10 or 14 m^3/s can occur. As seen in 10, four sub-periods with different prescribed residual flows must be considered.
2. For these four sub-periods, the Limmat hydrograph is analysed and Limmat flows of 5 %, 20 %, 50 % and 95 % are evaluated (Table 66, Figure 262). In total, a set of 16 flow conditions are thus considered to be studied as scenarios.

It can be noted that weir overflow, starting at 123 m^3/s, takes places for 6 out of the 16 scenarios.

Table 66: Limmat flow conditions and prescribed residual flows during fish migration periods in spring and fall

Period	Q_{Limmat} 5%	50%	80%	95%	$Q_{residual}$ min.
2nd half of May	295	125	98	68	10
1st half of June	289	136	95	62	14
September	227	91	61	45	10
1st half of October	173	82	57	43	8

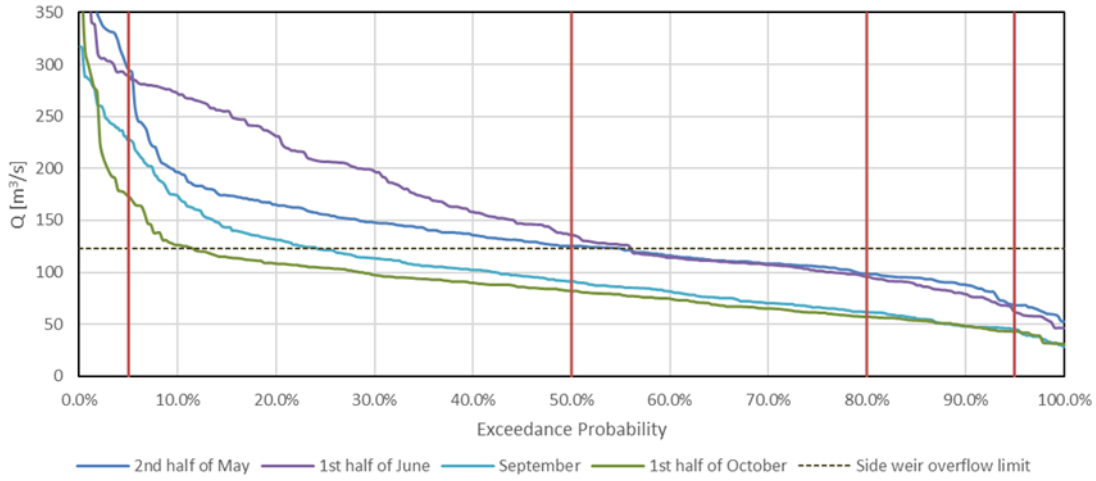


Figure 262: Flow duration curves established based on 1997-2018 Limmat flow data for the four sub-periods of fish migration.

Model calibration and validation

River bed roughness values of the model are calibrated in a trial and error approach such as to fit the simulated water levels to the observed ones. Roughness values will be assigned to model sub-areas as shown in Table 67.

Table 67: Calibration of roughness values

Model sub-area	Manning's roughness n [s/m$^{1/3}$]
Upstream & downstream river	TBD
Headwater channel	TBD
Residual flow section	TBD
Concrete structures (overflow weir, headwater channel walls, HPP inlet, vertical-slot fish pass)	TBD
Near-natural fish pass	TBD

Model validation will be against the measured flow velocities and has not yet been conducted.

3.12.3.3 Results

Hydraulics and Bathymetry data (ADCP)

During the field measurements, the discharge in the river Limmat slightly fluctuated around *Q* = 70 m^3/s and 49 m^3/s in March and October 2018, respectively. The discharge of the residual flow HPP was around 8 m^3/s and total discharge in the residual flow reach was approx. 10 m^3/s including the discharges from the HPP, fish ladder, downstream bypass flow and the side weir along the headwater canal in both field measurements.

Figure 263 shows the upstream and downstream river reach bathymetry in March and October 2018. It is clearly seen that the bathymetry in the headwater canal changed and deepened from March to October 2018. This is mainly because of the removal of settled gravels from the headrace channel in September 2018. The removed gravels amounted to approx. 5300 m^3 calculated using the bathymetry maps and were dumped into the residual flow reach (Figures 169, 178). Such replenishment of gravels is considered as a measure to improve the downstream fish habitat and to mitigate river bed armouring, bank erosion, channel incision. Major bathymetry and flow depth changes occurred between the vortex tube and the residual flow HPP causing high flow velocities around the fish ladder inlets (Figure 263). We expect that after several flood events, the dumped gravels will be transported further downstream of the main HPP and the bathymetry of the residual flow reach will become similar to that in March 2018 with improved habitat quality. Therefore, for 3D numerical model, the bathymetries of the residual flow reach in March 2018 and that of the headrace channel in October 2018 are used.

Figure 263a and b show the depth-averaged flow velocity distribution in the upstream and downstream flow reaches of the HPP Schiffmühle in March and October 2018, respectively. Note that the river discharges were different but the discharges in the residual flow reach were similar in March and October in 2018. The flow velocity increases from the downstream of the residual flow HPP up to the entrance of the fish ladder and reaches its maximum of 250 cm/s in October 2018 due to bathymetry changes caused by gravel replenishment in September 2018. Downstream of that location, it gradually decreases along the river reach until the downstream of the main powerhouse. In this region, a similar trend is observed in velocity distribution measured in March 2018 (Figure 264a). Although velocity magnitudes are different in March and October 2018, the overall velocity distribution in the headrace channel has changed because of gravel removal in September 2018 compared to that in March 2018.

One of the foci of the present study is to investigate the hydraulics and efficiency of HBR-BS in HPP Schiffmühle. To this end, we conducted densely-spaced ADCP measurements as well as velocity measurement inside the bypass at the HPP. Figure 265 shows the depth-averaged velocity distribution and streamlines around the HPP measured in October 2018. The flow velocities are high just upstream of the HPP close to the left bank of the river. Velocities slightly decrease towards the turbine intake. A discharge of 8 m^3/s goes into the turbine intake and a little flow goes towards the weir and the bypass inlet. The rest of the flow, i.e. about 41 m^3/s, goes into the headrace channel corresponding to about 80% of the river discharge. As indicated with red arrows in Figure 265, most of the fish in the river follow the main stream towards the headrace channel, while a small portion swims towards the HPP. When fish arrive at the HPP, it is likely that they do not find the bypass entrance because of the re-circulation zone and low velocities between the weir and the bypass inlet compared to high flow velocity at the turbine intake (Figure 265 and Figure 266). The design discharge of the bypass is 0.170 m^3/s and the corresponding average velocities in front of the bypass, at two rectangular bypass openings and in the pipe are approx. 0.35 m/s, 2 m/s and 3.46 m/s, respectively (Figure 267). However, the ADCP field data show that the velocity in front of the bypass is around 0.10 m/s instead of 0.35 m/s (Figure 266). To confirm this result, we measured velocities inside the bypass and show the measurement points and velocity data in Figure 266. The average flow velocity at the two rectangular bypass openings is 0.66 m/s and the total bypass discharge amounts to 0.055 m^3/s. For this bypass discharge, the average flow velocity in front of the bypass is 0.11 m/s (Figure 268a), which is in agreement with the ADCP measurement. The measured bypass discharge is less than 1/3 of the design discharge, which is likely due to clogging of the bypass pipe. Although the bypass pipe entrance is regularly cleaned according to the operator, the clogging seems to be unavoidable. Overall, due to mainly the re-circulation zone, low flow velocities in front of the bypass as well as almost zero tangential velocity

between the turbine and bypass intakes, the fish guidance efficiency of the bypass system is expected to be low. We will discuss this result together with the fish monitoring result in the next subsection.

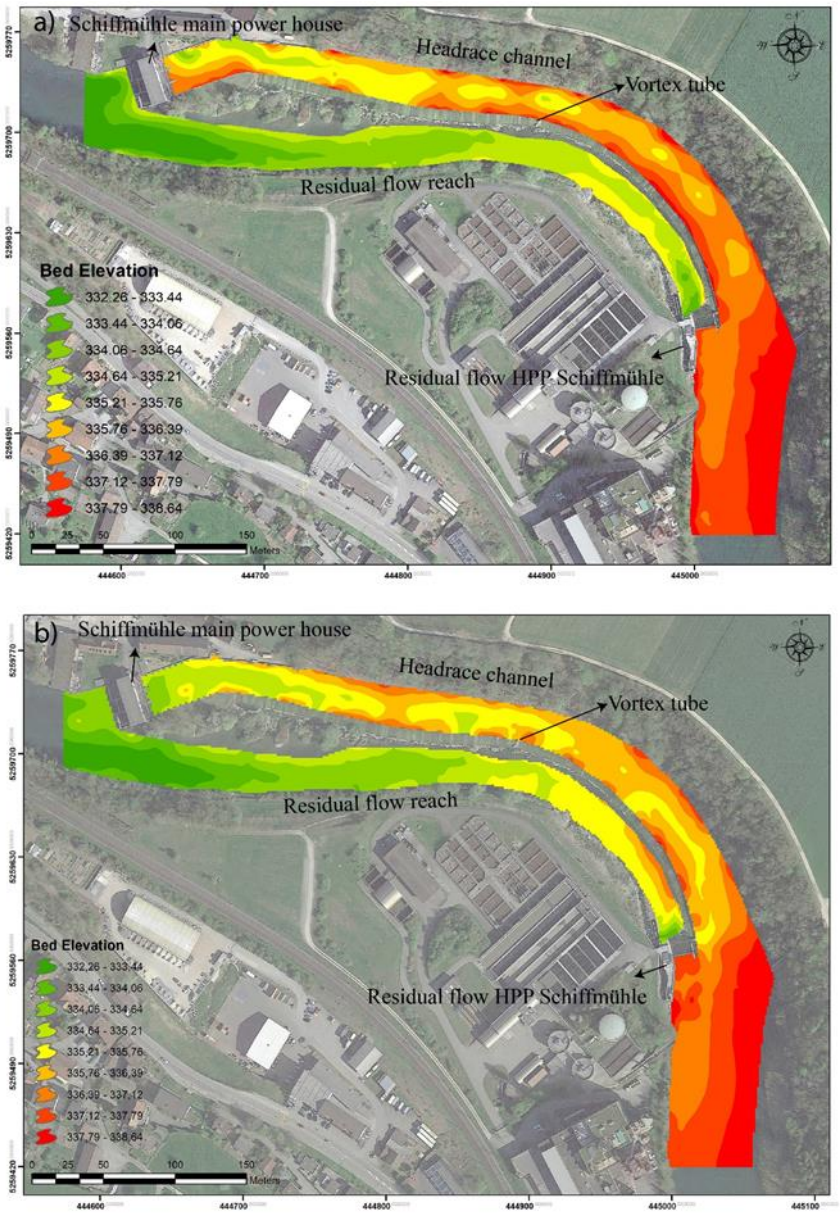


Figure 263: Bathymetry of upstream and downstream flow reaches of the residual flow HPP Schiffmühle in March (a) and October (b) 2018.



Figure 264: Photos of residual flow reach in March (a) and October (b) 2018.

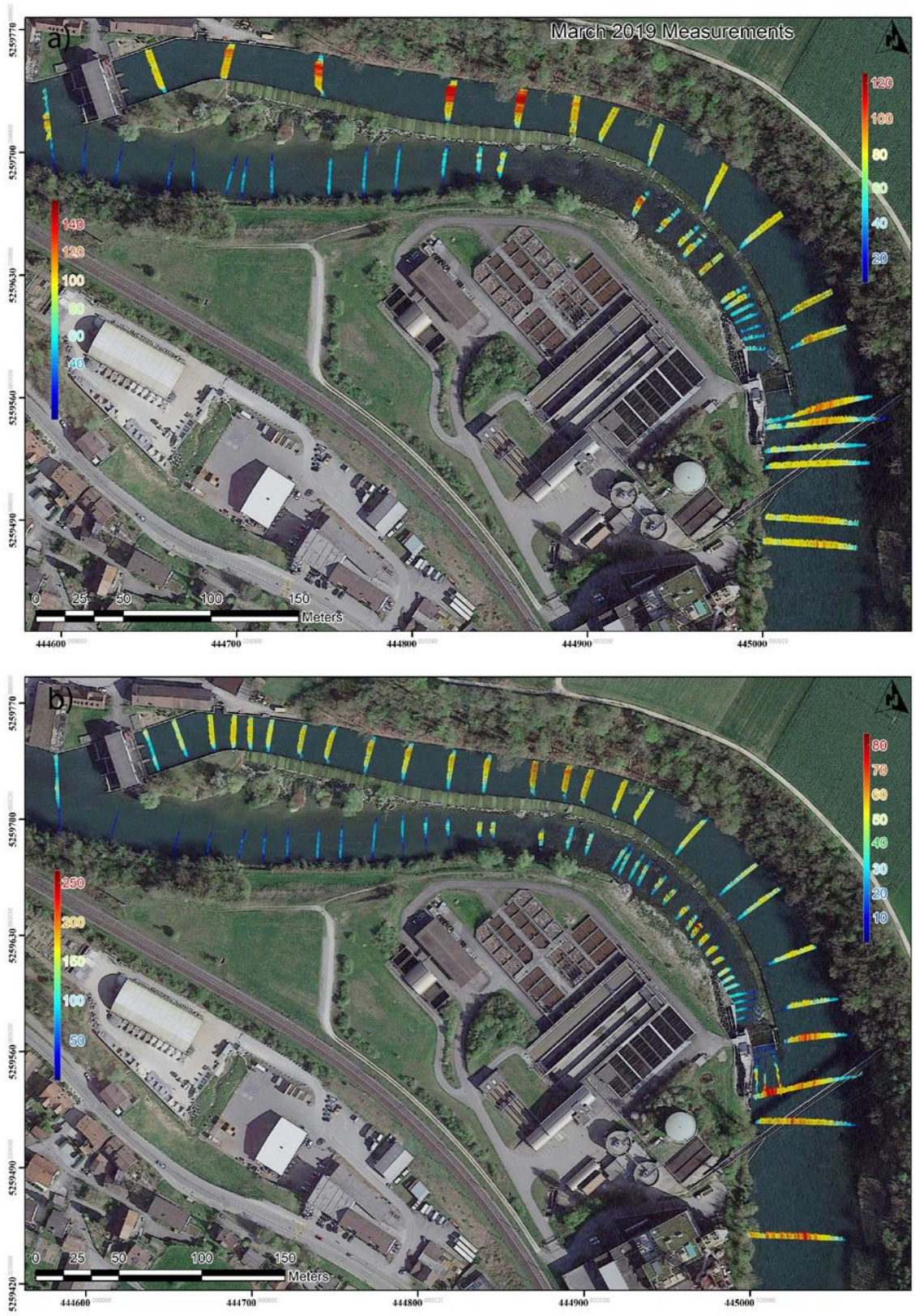
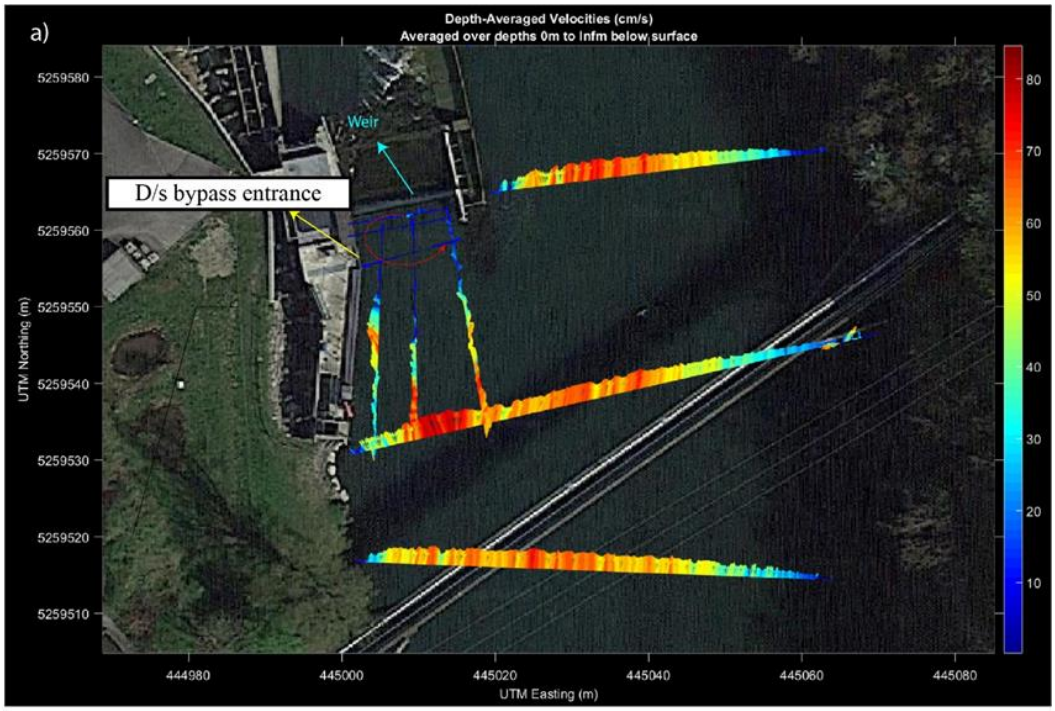


Figure 265: Depth-averaged velocity profiles from ADCP measurements at HPP Schiffmühle in (a) March and (b) October 2018. Note that the left and right colorbars are for the residual flow reach and headrace channel, respectively.



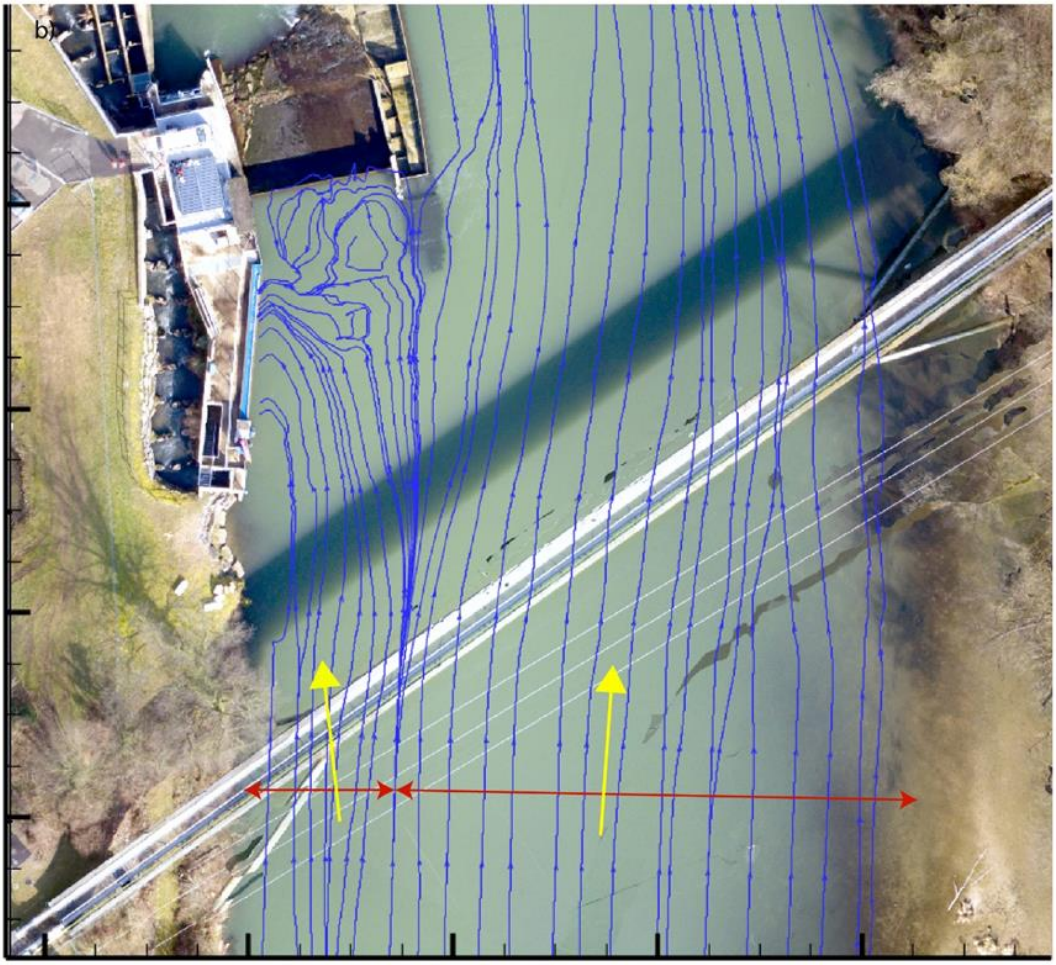


Figure 266: Depth-averaged velocity profiles (a) and streamlines (b) from ADCP measurements at HPP Schiffmühle in October 2018.

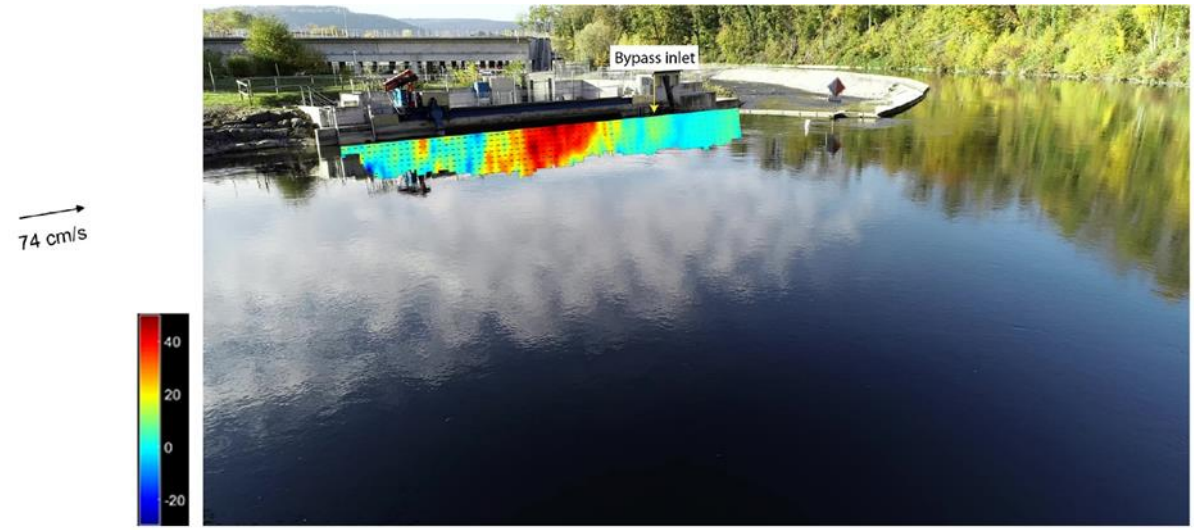
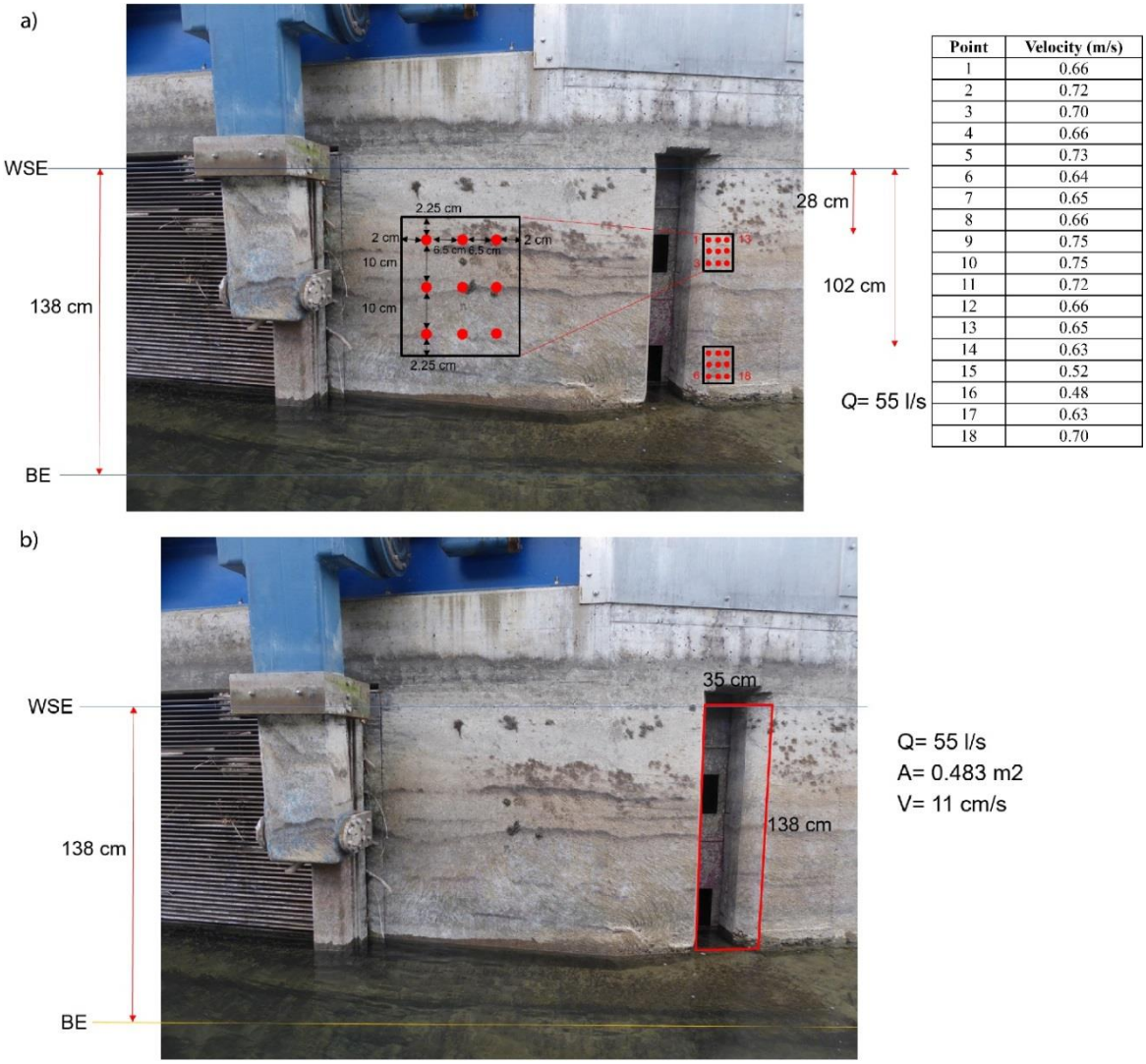


Figure 267: Velocity distribution along the HBR-BS in October 2018.



Point	Velocity (m/s)
1	0.66
2	0.72
3	0.70
4	0.66
5	0.73
6	0.64
7	0.65
8	0.66
9	0.75
10	0.75
11	0.72
12	0.66
13	0.65
14	0.63
15	0.52
16	0.48
17	0.63
18	0.70

Figure 268: Velocity measurement points inside the bypass and velocity data (a) and average velocity in front of the bypass (b).

Hydraulics (AIV)

Figure 269 shows the resulting time-averaged surface velocity field. Note that according to Le Coz et al. (2010), depth-averaged velocities can be estimated by multiplying the surface velocity by factors of between 0.79 and 0.89, with a central value close to 0.85. Figure 270 presents the corresponding streamlines. It becomes obvious how the main flow is deflected to the outer bend of the headrace channel. The main flow must be accompanied by a strong streamwise-clockwise rotating secondary current that dives down a few meters before it reaches the right bank. There, a smaller streamwise-anticlockwise rotating secondary current is indicated by much slower flow velocities. The turbine approach flow upstream of the HBR-BS at the residual flow HPP has surface flow velocities of around 0.6–0.7 m/s, with the streamlines being deflected towards the turbine only a few meters upstream of the horizontal bar rack, which is in a good agreement with ADCP data (Figure 265a and Figure 266a). The reach of the residual flow can be subdivided into two parts: (i) The area around the fish pass is affected by the turbine outlet of the residual flow power plant with surface velocities slightly above 1.0 m/s and (ii) the transverse ground sill downstream of the nature-like fish pass entrance that retains the water and slows down the surface velocity to 0.6–0.7 m/s. Downstream of the ground sill the flow is quite inhomogeneous and locally reaches surface velocities of up to 2.0 m/s in maximum.

Unfortunately, some areas show misleading flow velocities that obviously do not represent reliable flow physics. They are exemplarily highlighted in Figure 269. There are multiple reasons for this noise, such as a lack of seeding, white water, sun reflections, and higher riparian vegetation apparently moving with the moving camera position. Currently, VAW develops adequate techniques to avoid such noise directly during the video recording and to filter out falsified velocity vectors afterwards. As wrong velocity vectors in AIV are, in tendency, smaller than the real velocity, falsified time-averaged velocities are typical too low. Thus, local velocities have to be compared with neighbouring velocities every time, and, in case of doubts, faster velocities are supposed to be closer to real–world situations.

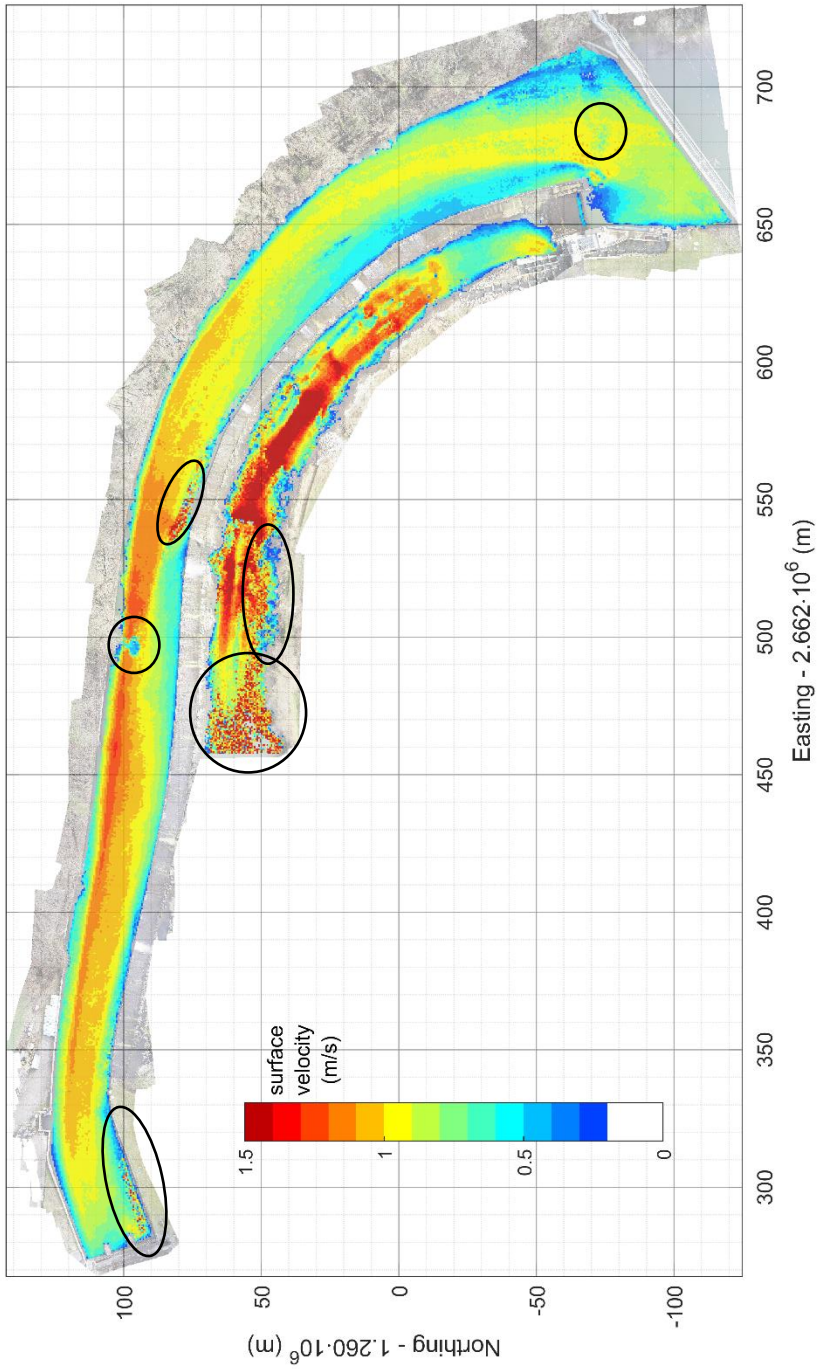


Figure 269: Geo-referenced surface velocity field measured using AIV on 2018/03/13 between 11:00-11:45 at a flow discharge of 71–72 m^3/s, with exemplary areas of misleading (noisy) velocity data highlighted by black ellipses.

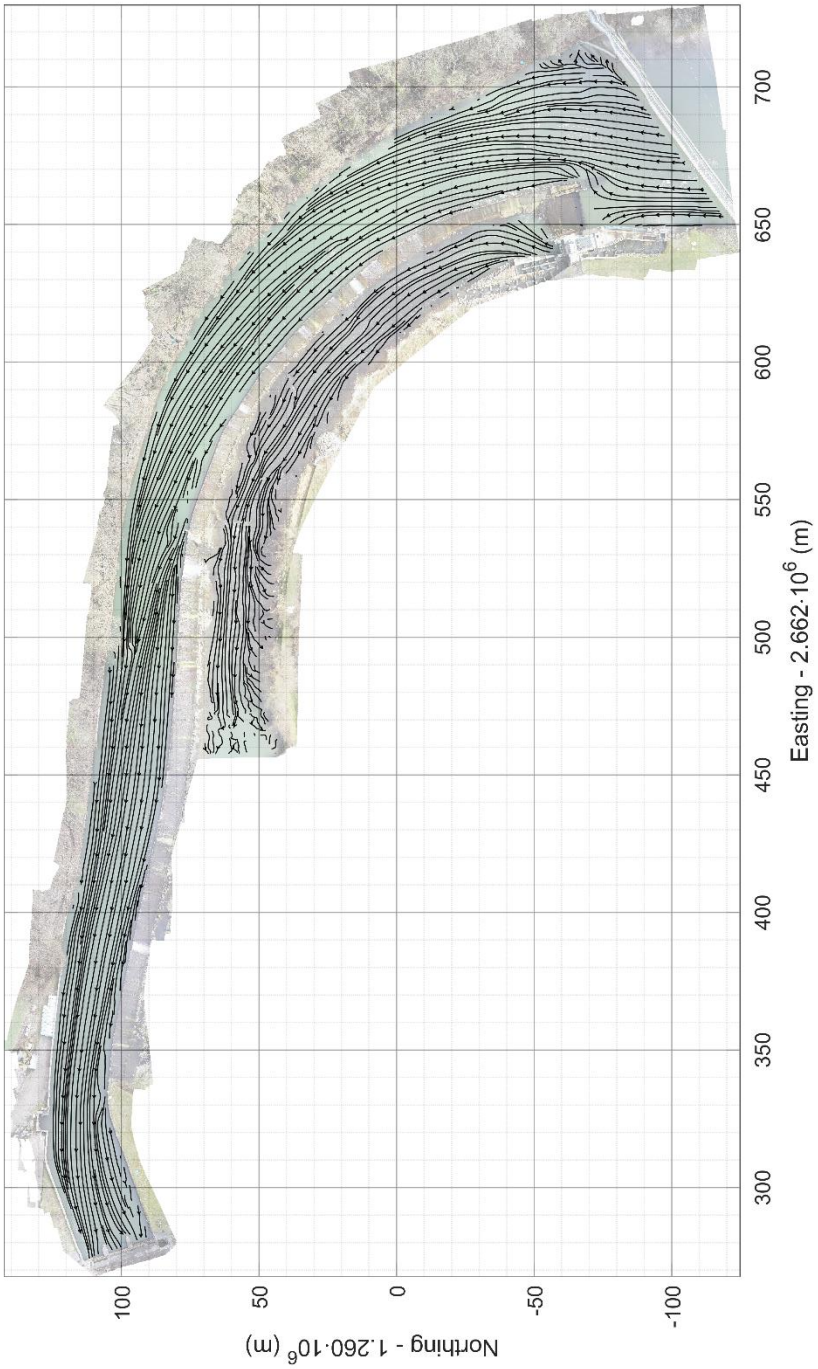


Figure 270: Geo-referenced surface velocity streamlines computed from AIV results.

Fish monitoring

Figure 271 presents an overview of all tagged fishes. The range of the total length was from 82 to 900 mm (median 130 mm).

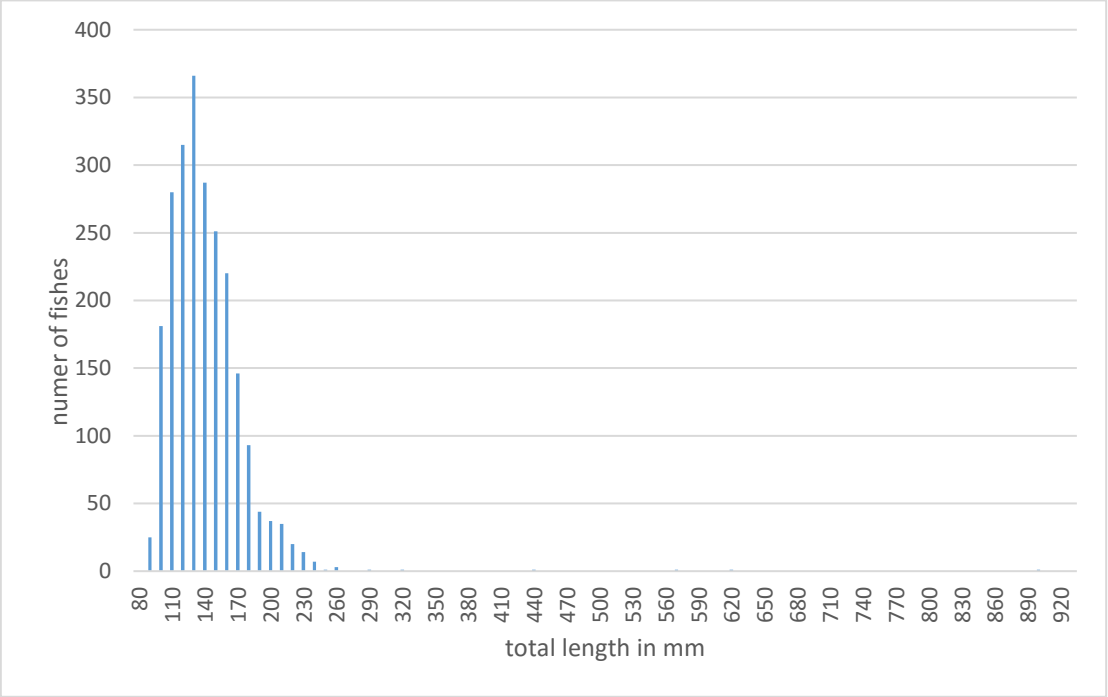


Figure 271: Total length of tagged fishes (N=2'331) belonging to 17 fish species. Only 5 individuals were larger than 300 mm.

Between 28 September 2017 and January 6, 2019, 251'570 detections were registered at the installed antennas. In Table 64 an overview of the detected fishes in the fish pass is presented. 1'601 of the tagged fishes (68.7 %) were detected. This can be considered as a very high rate. 1'280 tagged fish (54.9 %) successfully ascended the fish pass. Barbel prefer the entrance of the vertical-slot pass, while chub, roach and dace prefer to enter in the nature-like pass.

Additional analysis showed that for all fish species together the attraction efficiency (42.5 %) of the nature-like fishway was higher than in the vertical slot pass (31.6 %). However, the entrance efficiency in the vertical slot pass was with 98.8 % distinctly higher than in the nature-lake pass (86.5 %). On the other hand, the passage efficiency for the vertical slot and the nature-like pass was very similar (≈ 80 %). Passage efficiency was calculated by dividing the number of fish that exited the fish pass by the number that was detected at the second antenna at the entrance.

Concerning the downstream migration, only one of the tagged fish was registered in the bypass. As shown in section 2.12.3.2.4, the re-circulation zone, low velocities between the weir and the bypass inlet compared to high flow velocity at the turbine intake as well as low velocities inside the bypass make it difficult for fish to find the bypass. This problem needs considerable attention. However, additional results from the year 2019 have to be included. In 2019 special downstream migration experiments will be carried out.

Table 68: Fish monitoring results

Species	N tagged	N detected	% detected	N ascended in vertical slot pass	N ascended in nature-like pass	Passage efficiency whole fish pass %
eel	1	1	100	1	0	100
chub	371	221	59.6	43	135	85.2
Brown trout	2	1	50	0	0	0
barbel	985	644	65.4	334	186	85.4
perch	131	86	65.6	16	40	69
gudgeon	5	1	20	0	0	0
bullhead	3	0	0	0	0	0
dace	81	73	90.1	6	46	85.9
carp	1	0	0	0	0	0
bleak	102	74	72.6	25	29	79.2
nase	5	3	60	0	2	100
roach	257	210	81.7	14	153	90.3
rudd	2	1	50	0	0	0
tench	2	0	0	0	0	0
spirlin	379	283	74.7	147	84	84.1
pumpkinseed	3	3	100	2	1	100
total	**2331**	**1601**	**68.7**	**588**	**676**	**84.6**

Hydraulics (Numerical modelling)

Results from 3D hydraulic modelling are foreseen in 2019 and will serve as an important input to the habitat modelling.

3.12.3.4 Conclusions & Outlook

We documented the current situation and investigated the hydraulics, bathymetry and fish guidance efficiency of HBR-BS at HPP Schiffmühle by means of field monitoring and 3-D numerical modelling in the area near the powerhouse, and weir. The monitoring comprises:

- characterization of the flow field and river bathymetry using ADCP
- 3D numerical simulation
- survey of the fish movements using PIT-tagging technique

High resolution 3D velocity, as well as bathymetry measurements, were conducted using an Acoustic Doppler Current Profiler (ADCP) mounted on a high-speed remote control boat in March and October 2018. The ADCP data are used to construct the 3D numerical model of the HPP and calibrate and validate the model. Fish have been monitored at HBR-BS and both

technical and nature-like fish passes using the PIT-tagging technique since 2017. The key results of these works include:

1) River bathymetries were mapped in March and October 2018 and used in 3D numerical model
2) Gravel replenishment from the headrace channel into the residual flow reach as sediment connectivity measure was done and its effects are quantified
3) Both ADCP and AIV velocity measurements indicate that most fish in the river are expected to follow the main stream towards the headrace channel while a small portion swims towards the HPP.
4) The attraction flow to the bypass for downstream migration seems inefficient and a re-circulation zone possibly affects fish searching the bypass entrance.
5) No fish was detected in the bypass confirming the poor velocity field around the bypass
6) Clogging of the bypass pipe is a problem affecting the bypass discharge and velocity
7) the downstream bypass system needs optimization

Both the technical and natural upstream fishways function efficiently

Based on the present results, we plan to conduct ADCP measurements in 2019 again. Moreover, fish monitoring will be continued in 2019. Numerical model results for various discharge scenarios will be available in 2019. Furthermore, optimization of bypass geometry and hydraulics, and options of possible new bypass locations such as at the left side of the weir will be numerically studied to improve the bypass attraction flow and hence fish guidance efficiency of HBR-BS.

3.12.4 Habitat modelling (SJE, TUT)

The attraction flow from the fish pass outlets will be investigated with the habitat simulation system CASiMiR. A Lateral Line Probe (LLP) will be used to study fish habitats and potential migration pathways using machine learning algorithms which are based on a spectral analysis of the recorded narrowband pressure fields. The results from LLP and CASiMiR will be compared.

To characterize the relationship between the local hydrodynamic conditions in the fishway outlet flow (“attraction flow”) and the spatial distribution of local flow variables, an artificial lateral line probe (LLP) as well as an acoustic Doppler velocimeter (ADV) are used and are shown in Figure 272. The use of the ADV provides velocity data comparable to available studies on attraction flows, and the use of a LLP provides body-oriented differential pressure fluctuations in order to explore the additional data gained using the lateral line probe (higher sampling rate and distributed sensing). Compared to point velocity measurements delivered by ADV, LLP captures the physical metrics (body-oriented pressure gradients) which may be closer to the “fish’s perspective”.

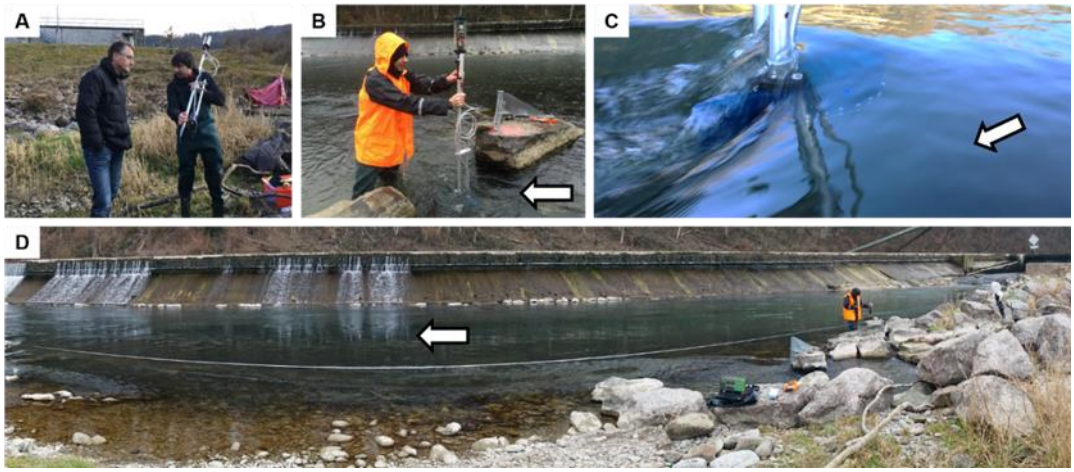


Figure 272: A) Lateral line probe can be used easily, and requires a short field training. B) The LLP measurements can be made directly in the attraction flow jet. C) Close-up view of the LLP near the top of the water column, illustrating the water flow around the probe body. D) A measuring tape extended in the field along the jet core facilitates reproducible measurement locations for future studies using ADV or LLP.

3.12.4.1 Data

Data are collected as pressure time series from the ADV (velocity *U*,*V*,*W*) and LLP (differential pressure sensor readings, water temperature, water depth). All data files are stored on a secured server and shared with FITHydro project partners as required in the consortium agreement.

3.12.4.2 Methodology

CASiMiR and LLP

The results of the bathymetric and hydrodynamic model are the basis for the analysis of fish migration; yet they are currently not available (as of January 2019). The telemetric investigations in the Test Case Schiffmühle do not deliver tracks of fish approaching the fish pass, but the fish entering and leaving the fish pass are counted. Thus, it is not possible to use the telemetric data for the development of CASiMiR migration which aims on the assessment of attraction flow. The Test Case Schiffmühle will instead be used for testing the migration model, which is developed based on data from the Test Case Altusried, Iller, where fish tracks are available. The intention is to find relations between the flow rates that provide good conditions in terms of attraction flow and the number of fish entering the fish ladder from downstream.

The lateral line probe measurements were performed by TUT and SJE on March 13 and 14, 2018 along the center of the jet core at the bottom, mid-depth and top of the water column (Figure 273). This was done for two reasons: 1) Some fish species are known to be bottom-oriented, but there is no available information on the hydraulic conditions in-situ near the bottom for attraction flow studies. 2) 2D models cannot capture the vertical distribution of the velocity and it is therefore important to determine the physical differences between the bottom, mid (velocity in 2D models is depth-averaged and corresponds roughly to this region), and top of the water column.

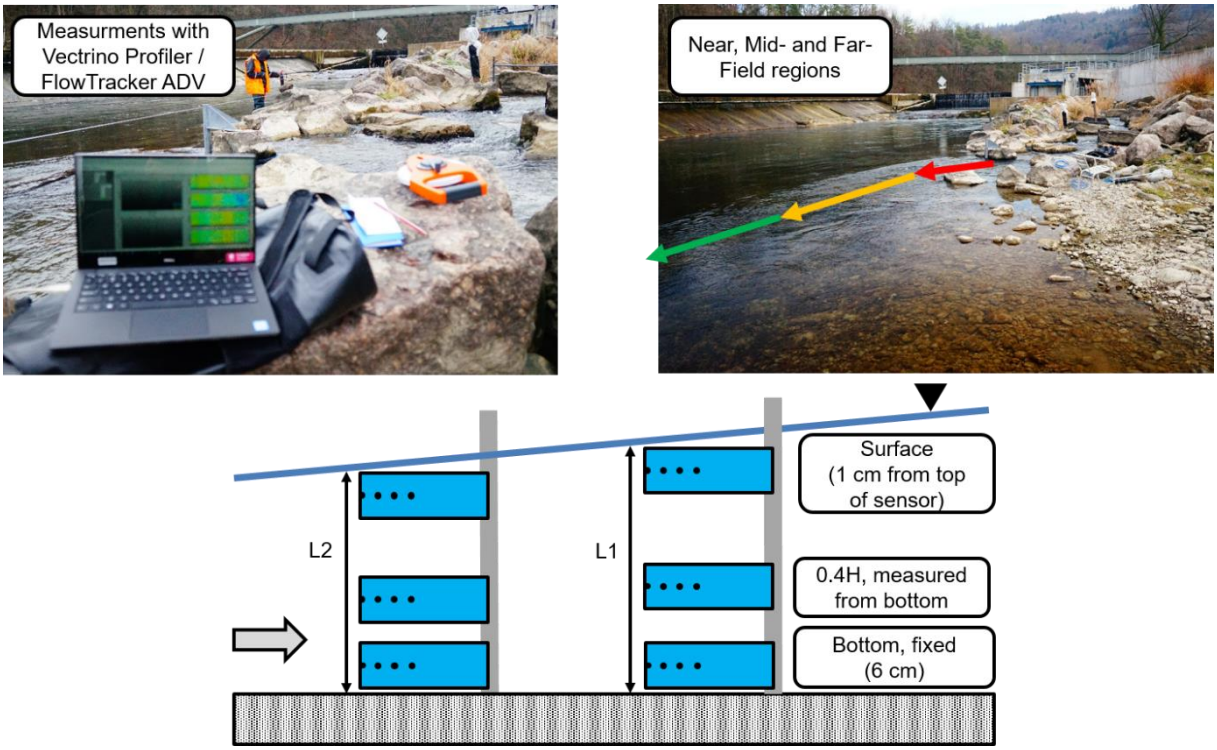


Figure 273: Top images show LLP and ADV measurement locations at the Schiffmühle case study site which correspond to the near, mid- and far-field regions of the jet core. Lower image depicts the vertical measurement locations for the LLP and ADV in order to capture the hydrodynamic conditions of the jet core at the bottom, middle and top of the water column.

3.12.4.3 Results

Data processing from the LLP is currently ongoing. Based on our work using the LLP as part of the live fish behaviour studies in Portugal, as series of best-performing LLP pressure metrics has been compiled and will be compared to the ADV data and are listed in Table 69.

Table 69 : Pressure-based variables from LLP measurements.

Variables	Equation
Mean pressure[1]	$\bar{p}_i = \frac{\sum_{j=1}^{n} p_{i,j}}{N}$
Mean fluctuations[1]	$\bar{p}'_i = \frac{\sum_{j=1}^{n} \lvert p_{i,j} - \bar{p}_i \rvert}{N}$
Mean front pressure ($\bar{p}_{12}$)	$\bar{p}_{12} = \frac{\sum_{j=1}^{n} p_{1,j} + p_{2,j}}{N}$
Mean pressure ($\bar{p}_{1-6}$)	$\bar{p}_{1-6} = \frac{\sum_{j=1}^{n} \frac{\sum_{k=1}^{6} p_{k,j}}{6}}{N}$

Mean front fluctuations ($\bar{p}'_{12}$)	$\bar{p}'_{12} = \frac{\bar{p}'_1 + \bar{p}'_2}{2}$
Mean fluctuations ($\bar{p}'_{1-6}$)	$\bar{p}'_{1-6} = \frac{\sum_{i=1}^{n} \bar{p}'_i}{N}$
Mean front pressure asymmetry ($\Delta\bar{p}_{12}$)	$\Delta\bar{p}_{12} = \frac{\sum_{j=1}^{n} \left(p_{1,j} - p_{2,j}\right)^2}{N}$
Mean pressure asymmetry ($\Delta\bar{p}_{1-6}$)	$\Delta\bar{p}_{1-6} = \frac{\sum_{k}^{m} \frac{\sum_{j=1}^{n} \left(p_{2k-1,j} - p_{2k,j}\right)^2}{N}}{M}$
Mean front fluctuations asymmetry ($\Delta\bar{p}'_{12}$)	$\Delta\bar{p}'_{12} = \frac{\sum_{j=1}^{n} \left(p'_{1,j} - p'_{2,j}\right)^2}{N}$
Mean fluctuations asymmetry ($\Delta\bar{p}'_{1-6}$)	$\Delta\bar{p}_{1-6} = \frac{\sum_{k}^{m} \frac{\sum_{j=1}^{n} \left(p'_{2k-1,j} - p'_{2k,j}\right)^2}{N}}{M}$

[1]Only for the variable definition above. Sensors are not considered individually.

3.12.4.4 Conclusion

Results for the forthcoming LLP evaluation will be published in the form of a peer-reviewed paper in 2019.

Results of the attraction flow assessment can only be delivered after the hydrodynamic model is available and after the migration model based on the correlation between fish tracks and hydrodynamic measurements and modelling from the Test Case Altusried will be available.

3.12.5 References

Atkinson, E. (1994a). Vortex-tube Sediment Extractors. I: Trapping Efficiency. Journal of Hydraulic Engineering, 120(10), 1110-1125.

Atkinson, E. (1994b). Vortex-tube Sediment Extractors. II: Design. Journal of Hydraulic Engineering, 120(10), 1126-1138.

Awasthi, A.K. (2001). Desanding for Small Hydro - An Innovative Approach. Proceedings of the 2nd International Conference 'Silting Problems in Hydropower Plants', Bangkok, Thailand.

Bunte, K., Abt, S.R. (2001). Sampling surface and subsurface particle-size distributions in wadable gravel- and cobble-bed streams for analyses in sediment transport, hydraulics, and streambed monitoring. Gen. Tech. Rep. RMRS-GTR-74. Fort Collins, CO: US Department of Agriculture, Forest Service, Rocky Mountain Research Station. 428 p.

Detert, M., and Weitbrecht, V. (2013). User guide to gravelometric image analysis by BASEGRAIN. Advances in science and research (S. Fukuoka, H. Nakagawa, T. Sumi, and H. Zhang eds.), Taylor & Francis, London, 1789-1795.

Detert, M., Johnson, E.D., Weitbrecht, V. 2017. Proof-of-concept for low-cost and non-contact synoptic airborne river flow measurements. International Journal of Remote Sensing 38(8–10), 2780–2807. doi:10.1080/01431161.2017.1294782

Finstad, A.G., Einum, S., Forseth, T., Ugedal, O., 2007. Shelter availability affects behaviour, size-dependent and mean growth of juvenile Atlantic salmon. Freshwater Biology 52, 1710–1718. https://doi.org/10.1111/j.1365-2427.2007.01799.x

Flow Science, Inc (2014): FLOW-3D Version 11.0.3 – User manual

Flussbau AG (2017). Geschiebehaushalt Limmat, Geschiebedurchgängigkeit Streichwehre (Bedload balance Limmat, bedload conveyance of side weirs). Technical Report [unpublished, in German].

Forseth, T., Harby, A., Ugedal, O., Pulg, U., Fjeldstad, H.-P., Robertsen, G., Barlaup, B.T., Alfredsen, K., Sundt, H., Salveit, S.J., Skoglund, H., Kvingedal, E., Sundt-Hansen, L.E.B., Finstad, A., Einum, S., Arnekleiv, J.V., 2014. Handbook for environmental design in regulated salmon rivers (NINA temahefte No. 53). Norsk institutt for naturforskning.

Graham, D.J., Rollet, A.-J., Piégay, H., and Rice, S.P. (2010). Maximizing the accuracy of image-based surface sediment sampling techniques. Water Resources Research, 41(7), 1-12.

Gray, J.R., Laronne, J.B., Marr, J.D.G. (2010). Bedload-surrogate Monitoring Technologies, US Geological Survey Scientific Investigations Report 2010-5091. US Geological Survey: Reston VA.

Kzyzagorski, S., Gabl, R., Seibl, J. et al. (2016) Implementierung eines schräg angeströmten Rechens in die 3D-numerische Berechnung mit FLOW-3D. Österr. Wasser- und Abfallw. 68: 146. doi:10.1007/s00506-016-0299-2

Le Coz, J., Hauet, A., Pierrefeu, G., Dramais, G., Camenen, B. 2010. Performance of Image-Based Velocimetry (LSPIV) Applied to Flash-Flood Discharge Measurements in Mediterranean Rivers. Journal of Hydrology 349(1–2), 42–52. doi:10.1016/j.jhydrol.2010.05.049.

Meusburger, H. (2002): Energieverluste an Einlaufrechen von Flusskraftwerken. VAW Mitteilungen Nr. 179 (H.-E. Minor, ed.), ETH Zürich. http://people.ee.ethz.ch/~vawweb/vaw_mitteilungen/179/179_g.pdf

Mtalo, F. (1988). Geschiebeabzug aus Kanälen mit Hilfe von Wirbelröhren (Bedload diversion from channels with vortex tubes). Report No. 58, Hydraulic Research Institute Obernach, Technical University of Munich, Germany [in German].

Rickenmann, D., Turowski, J.M., Fritschi, B., Klaiber, A., Ludwig, A. (2012). Bedload transport measurements at the Erlenbach stream with geophones and automated basket samplers. Earth Surface Processes and Landforms, 37, 1000-1011.

Rickenmann, D., Turowski, J.M., Fritschi, B., Wyss, C., Laronne, J., Barzilai, R., Reid, I., Kreisler, A., Aigner, J., Seitz, H., Habersack, H. (2014). Bedload transport measurements with impact plate geophones: comparison of sensor calibration in different gravel-bed streams. Earth Surface Processes and Landforms, 39, 928-942.

Stähly, S., Friedrich, H., Detert, M. (2017). Size Ratio of Fluvial Grains' Intermediate Axes Assessed by Image Processing and Square-Hole Sieving. Journal of Hydraulic Engineering, 143(6): pages??.

Thielicke, W., Stamhuis, E. J. 2014. PIVlab – Towards User-Friendly, Affordable and Accurate Digital Particle Image Velocimetry in MATLAB. Journal of Open Research Software 2:e30. doi:10.5334/jors.bl

VAW (2001). Kraftwerk Schiffmühle (Hydropower plant Schiffmühle). VAW-Report 4158, ETH Zurich, Laboratory of Hydraulics, Hydrology and Glaciology (VAW), Switzerland [unpublished, in German].

VAW (2017). Wirbelröhre Kraftwerk Turgi (Vortex tube hydropower plant Turgi). VAW-Report 4343, Laboratory of Hydraulics, Hydrology and Glaciology (VAW), ETH Zurich, Switzerland [unpublished, in German].

Westerweel, J., Scarano, F. 2005. Universal outlier detection for PIV data. Experiments in Fluids 39(6), 1096–1100. doi:10.1007/s00348-005-0016-6

Wyss, C.R., Rickenmann, D., Fritschi, B., Turowski, J.M., Weitbrecht, V., Boes, R.M. (2016a). Measuring Bed Load Transport Rates by Grain-Size Fraction Using the Swiss Plate Geophone Signal at the Erlenbach. Journal of Hydraulic Engineering, 142(5): 04016003.

Wyss, C.R., Rickenmann, D., Fritschi, B., Turowski, J.M, Weitbrecht, V., Boes, R.M. (2016b). Laboratory flume experiments with the Swiss plate geophone bed load monitoring system: 1. Impulse counts and particle size identification. Water Resources Research, 52, 7744-7759.

Wyss, C.R., Rickenmann, D., Fritschi, B., Turowski, J.M, Weitbrecht, V., Boes, R.M. (2016c). Laboratory flume experiments with the Swiss plate geophone bed load monitoring system: 2. Application to field sites with direct bed load samples. Water Resources Research, 52, 7760-7778.

Zabah E. 2018. KWS_26-03-2018.zip, KWS_26-03-2018ply.zip. Regionalwerke Baden AG (pers. communication)

3.13 Trois-Villes

3.13.1. Efficiency of downstream migration devices

3.13.1.1. Methodology

In 2016, a study was led by the French Agency for Biodiversity (AFB) in order to assess the efficiency of Trois-Villes' downstream migration device for Atlantic salmon smolts (Tomanova, et al., 2018).

3.13.1.1.1. Technology

The fishes are tracked with the PIT-Tag technology and detected with RFID antennas.

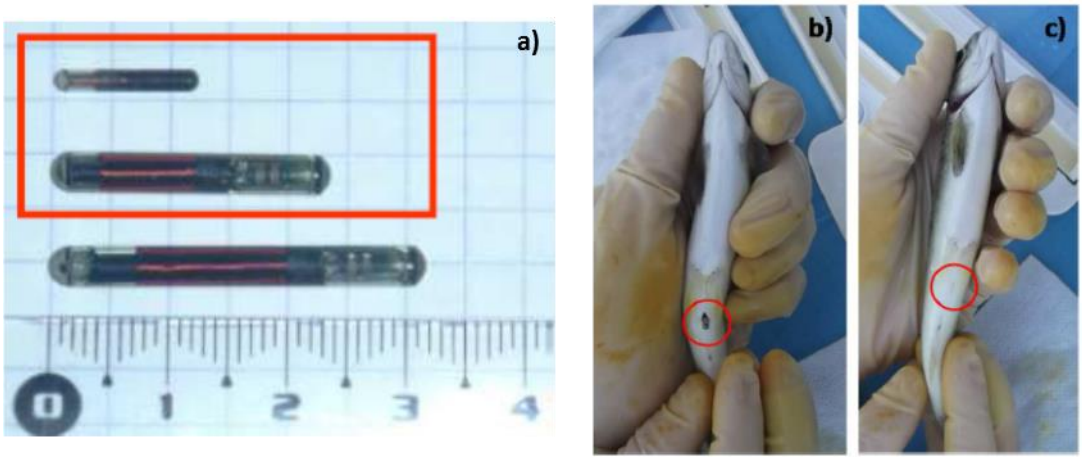


Figure 274: Tagging of fishes a) mark of 23 mm used b) and c) surgical insertion of the mark in the fish (source: (Tomanova, et al., 2018)).

The fishes were marked between the 29th and the 30th of March 2016 at the fish farm of Castels. The fishes were anaesthetized with eugenol for the surgery. The 11th of April they were moved to Trois-Ville and stabled in a pool with non-stop water renewing.

6 batches of 50 fishes were released between 18h30 and 00h30 100m upstream the power plant, in the headrace channel, see Table 22.

Table 70: Number of fishes and their size for each batch, date and time of release on Trois-Villes' site (source : (Tomanova, et al., 2018)).

Batches	Number of fishes	Date of release	Time of release		Size (mm)			
					Average	Standard deviation	Min	Max
TV_L1	50	12/04/2016	18:28	evening	187.7	10	166	205
TV_L2	50	12/04/2016	22:20	night	186.9	9.3	162	210
TV_L3	50	13/04/2016	00:12	night	185.8	8.3	165	205
TV_L4	50	13/04/2016	18:07	evening	186.3	9.4	161	211
TV_L5	50	13/04/2016	22:07	night	187.2	10.6	165	221
TV_L6	50	13/04/2016	23:34	night	185.7	10.6	159	204

3.13.1.1.2. Set of detection antennas

Two antennas were installed in the downstream migration channel (metal) downstream the control weir and one upstream, another antenna in the resting pool of the fish pass, one last was installed in the dump channel, see Figure 172. The dump channel is fed in water

automatically when the discharge in the headrace channel is bigger than the max turbined discharge (a valve opens). The eel-pass was screened in order to avoid the smolts to enter it. If the fish is detected by an antenna in the downstream migration channel it means that it took this way of passage. The efficiency of the antennas in the channel was tested. 20 fishes were released one by one in the channel, then two groups of 5 fishes were released in the channel.

Table 71: Detection efficiency (%) of the antennas in the downstream migration channel (source: (Tomanova, et al., 2018)).

	test ind20	test gr5-1	test gr5-2
EXU1	95	60	20
EXU2	90	20	0
EXU3	100	40	60
EXU1+2+3	100	80	60
EXU2+3	100	40	60

The efficiency decreases when several fishes go through the channel at the same time because of the collision between marks but the feedback on the other sites prove that in most case passage of smolts in the channel are more spaced. We supposed that every fish going through the channel will be detected by the antennas.

The detection by EXU1 doesn't allow confirming passage through the downstream migration channel because the antenna is before the control weir and the fishes can turn back.

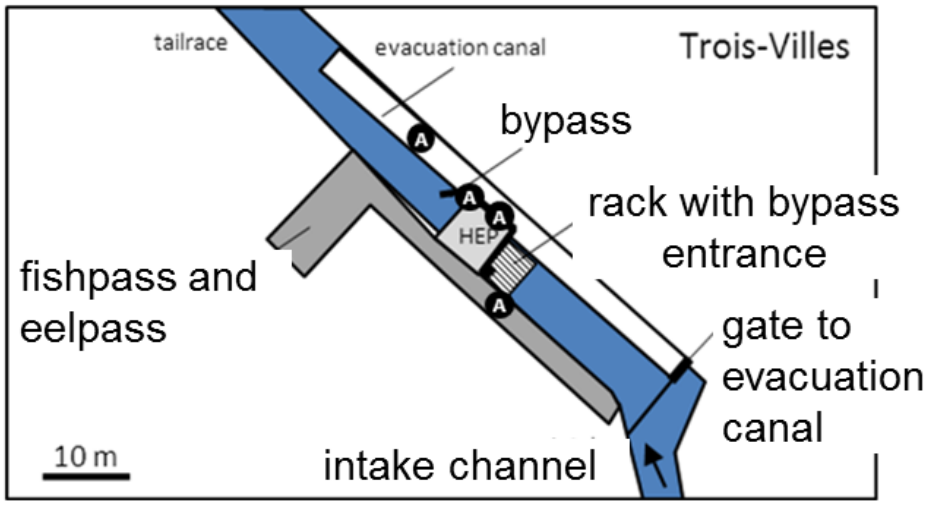


Figure 275: Schematic representation of the HPP and the antennas



Figure 276: Pictures of the HPP and location of the antennas (source: (Tomanova, et al., 2018)).

It is not possible to detect the fishes going through and the rack and therefor through the turbine. We will consider that non-detected fishes went through the turbine.

3.13.1.1.3. Hydrology of the Saison during the study

During the 5 days after the first release, the discharge varied between 29 and 46 m^3/s. Most of the fishes went downstream during this period. Trois-Villes HPP worked stable, the discharge in the headrace channel is controlled at the dam. An ADCP measurement the 19th of Mai revealed a discharge of 3.9 m^3/s in the headrace channel and 0.22 m^3/s in the downstream migration channel.

3.13.1.2. Results

30.7% of fishes went through the dump channel when the valve opens.

In average 61% of the fishes went through the downstream migration device and 0.7% used the fish pass, see Table 24.

When we exclude the fishes taking the dump channel, 87.5 % of fishes went through the downstream migration device and 1% through the fish pass.

Table 72: number and distribution of detected fishes or not in the different ways at Trois-Villes (in blue: batches released in the evening) a) with b) without fishes detected in the dump channel (source: (Tomanova, et al., 2018)).

a)

Batch	Total of released fishes	Number of non-detected fishes	Number of fishes detected in			Percentage of fishes detected in			Total percentage of fishes gone
			bypasses	fish pass	dump channel	bypasses	fish pass	dump channel	
TV_L1	50	4	37	1	8	74	2	16	92
TV_L2	50	6	24		20	48	0	40	88
TV_L3	50	3	25	1	21	50	2	42	94
TV_L4	50	2	38		10	76	0	20	96
TV_L5	50	1	33		16	66	0	32	98
TV_L6	50	7	26		17	52	0	34	86
Mean efficiency						61	0.7	30.7	92.3
Standard deviation						12.6	1	10.6	4.6

b)

Batch	Total of released fishes	Number of non-detected fishes	Number of fishes detected in			Percentage of fishes detected in			Total percentage of fishes gone
			bypasses	fish pass	dump channel	bypasses	fish pass	dump channel	
TV_L1	42	4	37	1		88.1	2.4		90.5
TV_L2	30	6	24			80.0	0		80.0
TV_L3	29	3	25	1		86.2	3.4		89.7
TV_L4	40	2	38			95	0		95
TV_L5	34	1	33			97.1	0		97.1
TV_L6	33	7	26			78.8	0		78.8
Mean efficiency						87.5	1		88.5
Standard deviation						7.5	1.5		7.6

A statistical test (Student test) was run in order to detect an eventual difference of size between fishes taking the downstream migration device or non-detected. The mean size of fishes taking the downstream migration device (186.5 mm) is bigger than the one non-detected (183.4 mm). The student test revealed that this difference is not significant, see Figure 277.

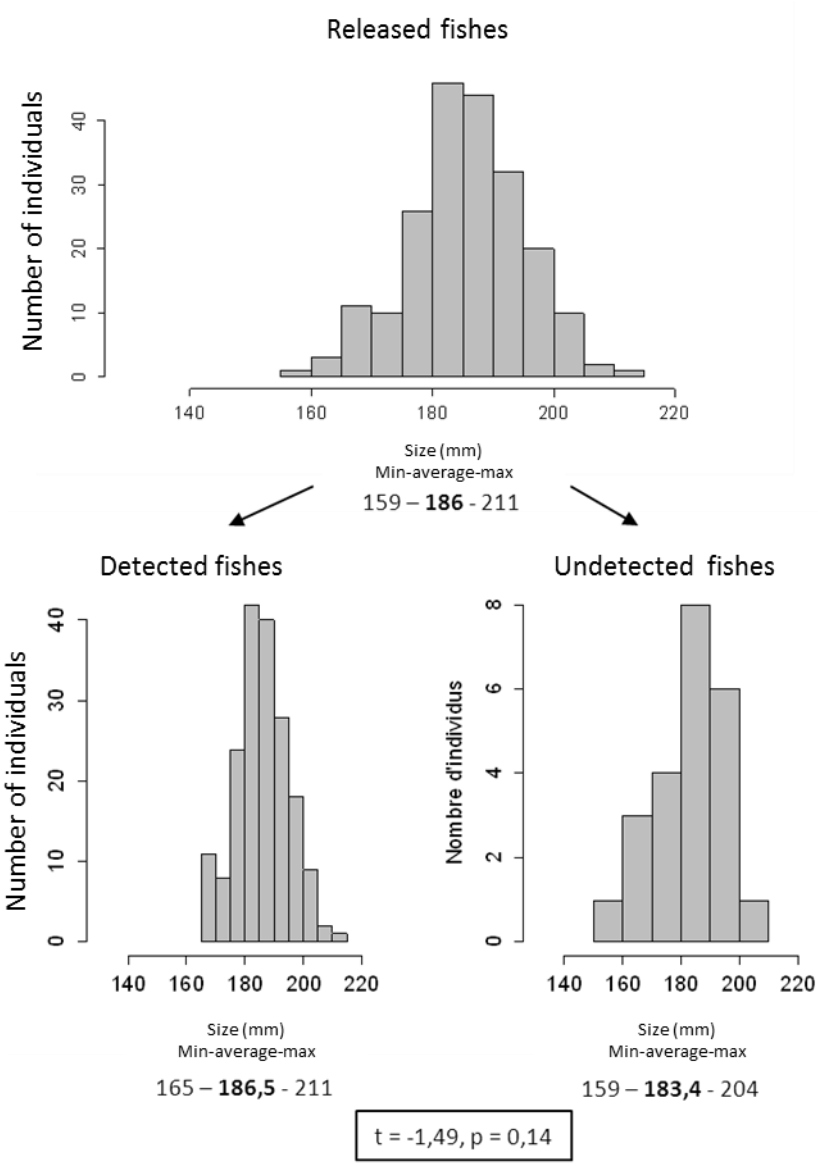


Figure 277: Distribution of released fishes' size, non-detected fishes' size and detected in the downstream migration channel fishes' size (source: (Tomanova, et al., 2018)).

The timing was also studied. For all batches, the first detections happened between 4 and 12 minutes after release. 50% of fishes take less than 1 hour to circumvent the power plant through the downstream migration device, 75 % need less than 3h15, see Table 25. The timing passage is longer for the fishes released in the evening than at night.

Table 73: Timing of passage of smolts for the different batches, in grey the batches released in the evening (source: (Tomanova, et al., 2018)).

Exutoire et canal de transfert

	Nb d'ind.	min	Q25	mediane	Q75	max
LOT1	37	1:08:10	3:21:13	4:24:06	7:00:07	9:45:10
LOT2	24	0:12:11	0:21:43	0:54:07	1:42:09	4:06:33
LOT3	25	0:07:12	0:11:23	0:28:17	1:21:26	5:00:13
LOT4	39	0:06:41	0:46:15	1:11:41	3:49:30	40:58:52
LOT5	33	0:04:25	0:17:55	0:24:41	0:49:04	3:08:22
LOT6	27	0:08:55	0:18:03	0:37:32	1:06:16	16:35:00
Total	185	**0:04:25**	0:24:41	**1:02:01**	**3:15:39**	40:58:52

Canal de décharge

	Nb d'ind.	min	Q25	mediane	Q75	max
LOT1	8	2:45:05	3:11:58	3:33:18	4:21:07	6:49:54
LOT2	20	0:09:30	0:11:05	0:15:27	0:18:04	7:15:55
LOT3	21	0:03:27	0:05:49	0:10:20	0:18:12	1:23:00
LOT4	10	0:12:41	3:40:36	6:13:02	7:08:14	27:42:28
LOT5	16	0:07:39	0:22:30	0:33:22	1:32:47	23:12:45
LOT6	17	0:04:50	0:11:09	0:13:04	0:21:51	46:34:01
Total	92	**0:03:27**	0:11:06	**0:19:12**	**2:36:16**	46:34:01

3.13.1.3. Conclusion

The configuration of Trois-Villes is quite specific because of the presence of the dump channel. Its entrance is located in a calm area upstream the trash rack where the fishes stagnate. The dump valve opened regularly during the study, in short duration and suddenly. This area seems to be more used during the night.

Some detections revealed that some fishes were detected by the first antenna in the downstream migration channel but then were detected in the dump channel. This shows a reluctance of fishes to go through the downstream migration device. However, these reluctances don't question reaching a good efficiency.

Table 74: Summary of the distribution of fishes among the different ways, passage rate through turbines (this study) and their mortality rates (according (Voegtlé, 2010)), and global passage efficiency taking into account passage over the spillway, the downstream migration device and survival after passage through turbines (Tomanova, et al., 2018).

Dam		Power plant			**Total survival rate at Trois-Villes**
Proportion (%) of fish passing over the spillway of the dam	Proportion (%) of fish led to headrace channel	Proportion (%) of fish passing through the turbine	Mortality through the turbine (%)	Proportion (%) of fish assumed dead due to passage through the turbine	
8.4	91.6	7.02	11	0.77	**99.23**

3.13.2. Hydraulic modelling

In spring 2016, the AFB team made some measurements in order to assess the discharge assign to downstream migration.

3.13.2.1. ADCP measurements

These measures aim to assess the efficiency of the flow upstream the bar rack installed at Trois-Villes hydropower plant.

The mapping of each component of the velocity results from the processing of these measures.

They allow validating, after computation of the tangential and normal velocities, the fishfriendly criteria of the rack.

3.13.2.1.1. The technology used

The currentology measurements upstream the bar rack have been made with an Acoustic Doppler Current Profiler (ADCP) StreamPro Teledyne RDI (Figure 220). The probe is equipped with 4 sensors which issuance-reception beams are inclined of 20° to the axis of the probe. The width of a beam is 3°. The probe is vertically settled and slightly immersed (a few cm). The device measures the water depth, and the 3 components of flow velocity within 20 measurements cells uniformly distributed along the water column. The division of the cells is continuous during the measures and defined according to maximal depth provided by the operator. The frequency of measure acquisition is 1 Hz.



Figure 278: Pictures of the ADCP StreamPro assembled on its trimaran and the probe with a closer view of the 4 sensors

The data analysis is made by a software Teledyne Winriver II. Trois-Villes was the French first Test Case where the ADCP was tested. The protocol was not optimized. The choice was made to acquire the data continuously when the ADCP was moving along the section. The measure has uncertainties due to this acquisition mode: the ADCP is installed on a catamaran and is handled with a pole.

In Trois-Villes, four measurement sections have been made, see Figure 279.

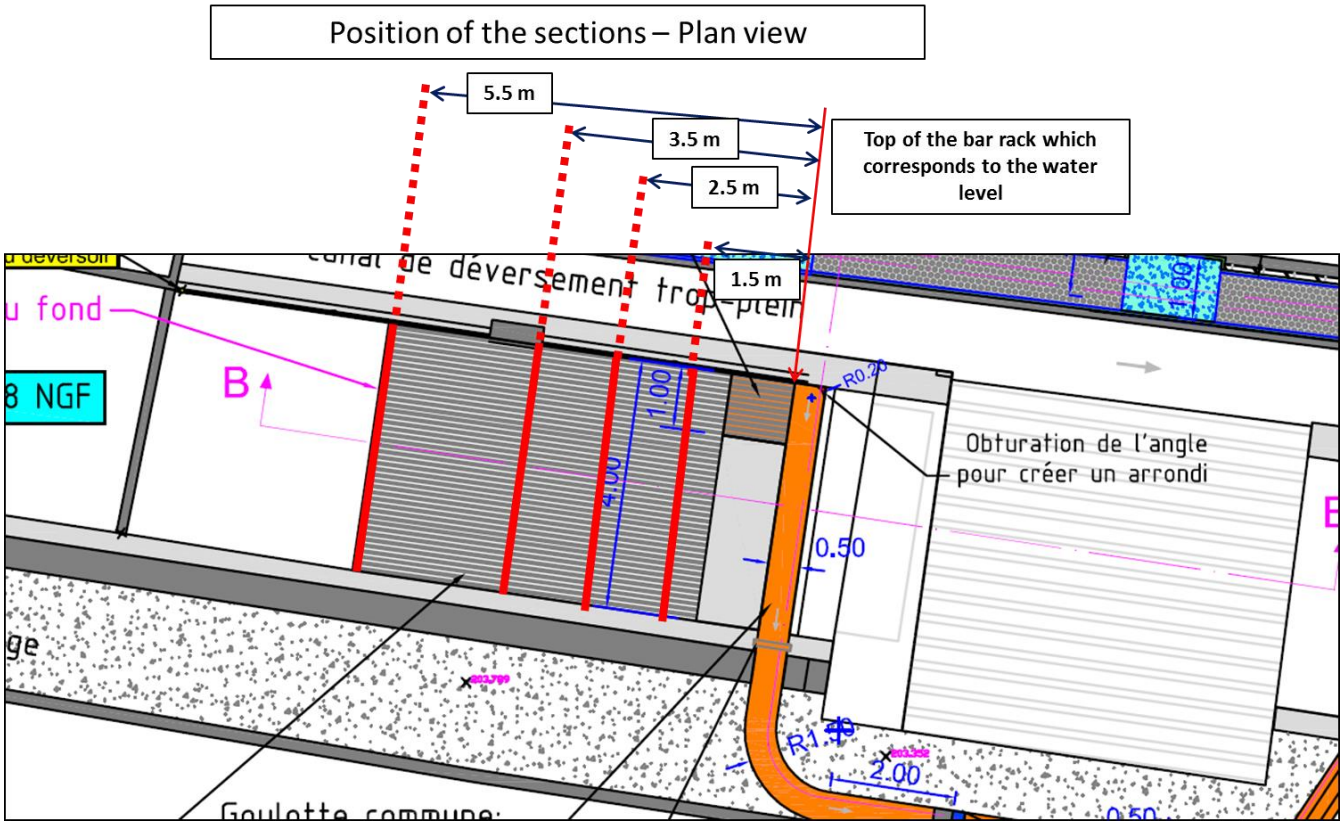


Figure 279: Positioning of the four sections upstream the bar rack in Trois-Villes

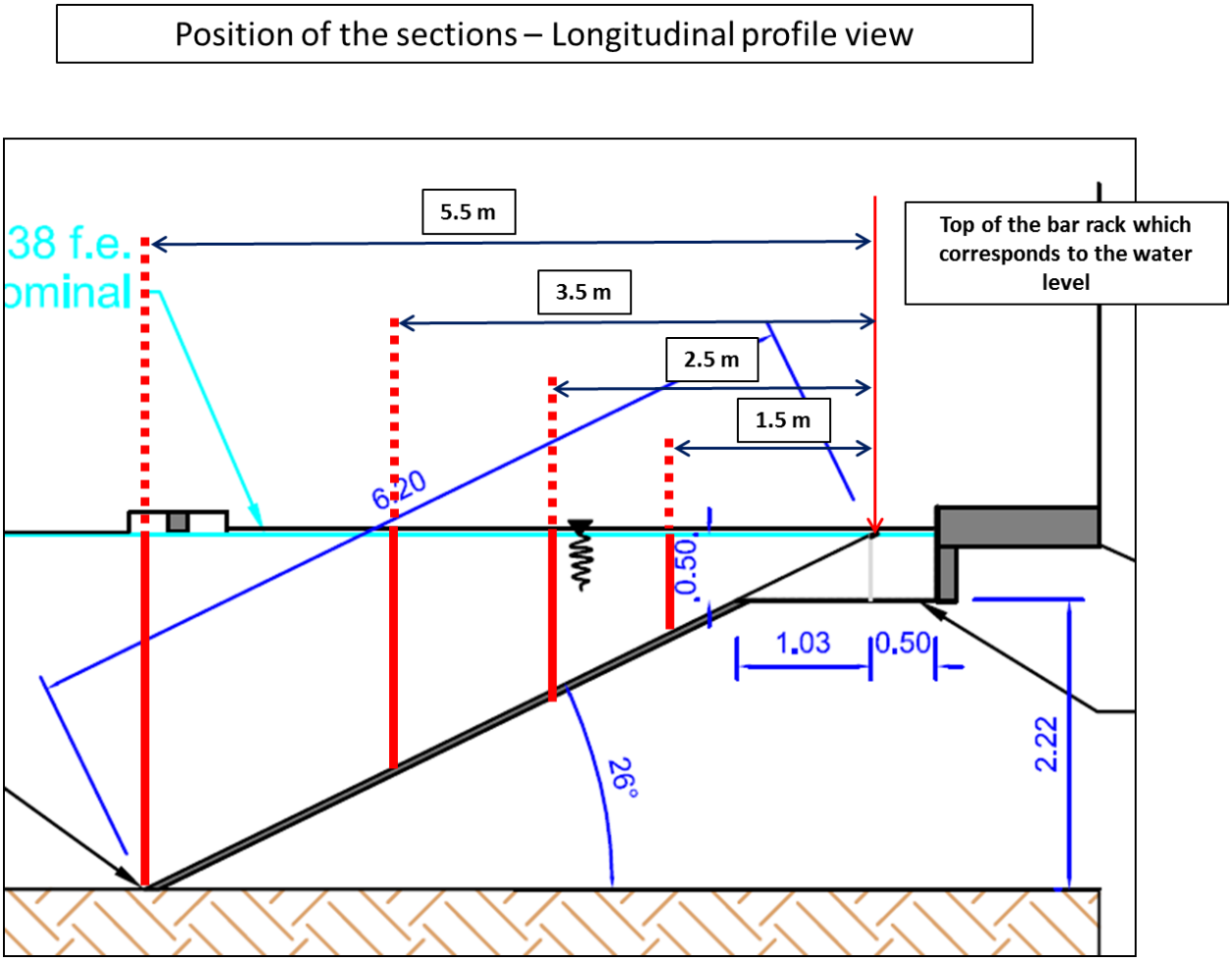


Figure 280: Positioning of the different sections

The North, East and Earth Up velocities are extracted, as well as the coordinates. These data are projected under Vx, Vy and Vz velocities. Then the outliers and empty values are delated. Finally, an average is made every 0.1 m.

The maps are made with the Tecplot software from these mean values by interpolation of the point according to the direction of Y and Z axes, see Figure 281 and Figure 282.

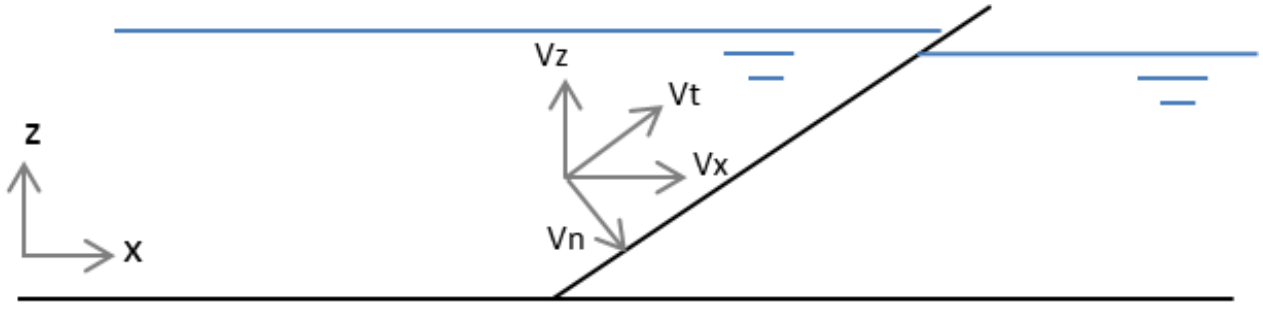


Figure 281: longitudinal section of a water intake and representation of the different components of the velocity.

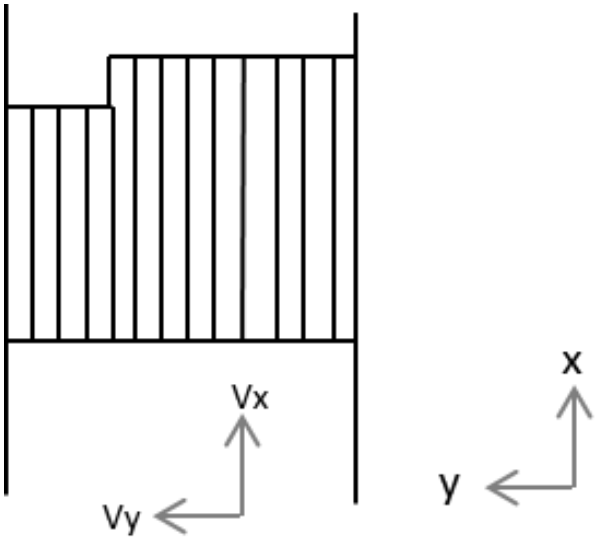


Figure 282: Plan view of a water intake and representation of the different components of the velocity.

3.13.2.1.2. Conditions during the measurements

During the measurements the mean discharge in the Saison was 18 m^3/s.

3.13.2.1.3. Results

The results will be discussed later.

3.13.2.2. Discharge measurements

We made ADCP measurements in the headrace channel 20 meters upstream the bar rack.

The data processing gives a global discharge in the headrace channel of 4.24 m^3/s.

Thanks to spillway lay and the DEVER tool, developed by the AFB, the discharge over the control weir was calculated:

Table 75 : Calculation of the discharge over the weir

Water level upstream the control weir (under the gate)	0.670	m
Bedlevel upstream the control weir	0.150	m
Width of downstream migration channel	0.490	m
Width of control weir	0.490	m
Water depth upstream the control weir (under the gate)	0.520	m
Flow cross-section upstream the control weir (under	0.255	m^2
Level of the control weir	0.300	m
Head on the weir	0.370	m
Discharge calculated by the DEVER tool	**0.224**	**m^3/s**
Flow velocity upstream	0.879	m/s

The calculated discharge is of 0.224 m^3/s, it is close to the targeted value of 200 L/s.

3.13.2.3. Conclusion

To be completed

The modelling will be done after the validation of the model developed in WP3 this year for calculating the flow upstream the trashrack and the attractiveness of the bypasses.

3.13.3. References

Tétard, S., Tomanova, S., Courret, D., Sagnes, P., Alric, A., De Oliveira, E., Frey, A. (2017). The efficiency of inclined and oriented racks to prevent Atlantic salmon smolts from entering turbines. International Conference on Engineering and Ecohydrology for Fish Passage. June 19th, 2017 - Corvallis.

Tomanova, S., Courret, D., Alric, A., De-Oliveira, E., Lagarrigue, T., & Tétard, S. (2018). Etude d'efficacité des exutoires associés à des grilles inclinées ou orientées pour la dévalaison des smolts de saumon atlantique - Etudes 2016 et synthèse des résultats 2015-2016. AFB - EDF - ECOGEA.

3.14. Conclusion

All the activities conducted at the 14 Test Cases are not yet completed, but results are already available that allowed to determine application ranges, knowledge gaps and needs. The missing results at each Test Case will be presented at the end of the project - November 2020 - in an updated document. This document will present the configuration of all sites, the objectives of the activities and their results.

The application ranges, the knowledge gaps and needs will be discussed in the next sections.

4. Upstream migration

Authors	Manon Dewitte (CNRS), Laurent David (CNRS)
Contributors	Armin Peter (FishConsulting), Christian Milzow (AF Consult), Marcell Szabo-Meszaros (NTNU), Cornelia Felber (UNIPER), Javier Sanz-Ronda (ITAGRA-SAVASA), Francisco Javier Bravo (ITAGRA-SAVASA), Sylvain Richard (AFB), Antonio Pinheiro (IST), Ine Pauwels (INBO), Ismail Albayrak (ETHZ), Nicole Smialek (TUM)
Reviewers	Armin Peter (FishConsulting)

List of tables

Table 76: Application ranges of the different techniques of fish tracking - Quality of the study. 383
Table 77: Approximative budget needed for the 4 different techniques of fish tracking. 384
Table 78: Environmental conditions entering into consideration for choosing a fish tracking technique 384
Table 79: Advantages and drawbacks of hydraulic modelling: 1D, 2D or 3D. 386
Table 80: Principal factors entering into consideration to choose the type of crossing devices in France. 388
Table 81: Application ranges of Baffle type fishways in France. 388
Table 82: Application range of pool type fishways in France. 389
Table 83: Application range of Rustic fishways in France. 390
Table 84:Principal conception criteria of devices depending on the targeted species and their abilities of swim/jump in France. 391
Table 85: Principal factors entering into consideration to choose the type of crossing devices in Spain. 393
Table 86: Application ranges of rocky ramps in Spain. 394
Table 87: Principal conception criteria of devices depending on the targeted species and their abilities of swim/jump in Spain, ... 395
Table 88: Principal factors entering into consideration to choose the type of crossing devices in Flanders - Belgium. 396
Table 89: Application ranges of pool-type fishways in Flanders – Belgium. 397
Table 90: Principal conception criteria of devices depending on the targeted species and their abilities of swim/jump in Flanders – Belgium. 398

Upstream migration concerns all kind of migratory fishes, potadromous and diadromous species. Fish need different environment for the main phases of their life cycle i.e. reproduction, production of juveniles, growth and sexual maturation. Diadromous species, like salmon and eels, share their life time between freshwater and sea while potadromous species spend their entire life time in freshwater.

Hydropower plants (HPP) may block upstream migration. Many mitigation measures exist allowing fishes to migrate upstream. Please refer to deliverable D2.1. Upstream migration is studied in seven Test Case HPPs within FIThydro: Altheim (see 3.1), Iller (see 3.10), Anundsjoe (see 3.2), Günz (see 3.8), Guma and Vadocondes (see 3.7) and Schiffmühle (see 3.12). Herein all types of tools used in these Test Cases are compared and the application ranges of the mitigation measures for upstream fish migration are discussed for each involved country.

4.1. Specific tools for upstream migration

For the topic of upstream migration 3 categories of tools have been used at the Test Case HPPs: fish monitoring, field measurements and finally hydraulic numerical modelling. Each tool or method is already presented in chapter 2. Tools and methods – general description.

4.1.1. Fish Monitoring

One or more of the following four different fish monitoring techniques were employed at the Test Cases:

- Radio telemetry
- Acoustic Telemetry
- RFID with PIT-tag
- Visible Implant Elastomer.

Each technique is already described, see 2. Tools and methods – general description.

In order to choose one or more of the techniques, it is important to consider the objectives of the study:

- **Radio telemetry**: detection of linear movements (migration corridor), analysis of delay at HPP, mortality, temperature use (need of temperature sensor), turbine mortality, survival.
- **Acoustic telemetry:** fish behaviour and movement patterns during upstream migration, turbine mortality.
- **RFID with PIT-Tag:** passage questions, attraction and entrance efficiency, fish ladder efficiency, efficiency of downstream migration bypass, use of habitat, survival.
- **Visible implant Elastomer:** stocking experiments, group marking, survival; Temporary habitat use studies. In the case of fishways, tagging fish downstream, upstream and inside the fishway, and recapturing some of them, can provide information about their movements. Usually, this technique is used as a **complement to other tracking techniques**.

It is possible to combine several techniques. It is important to take into account the impact of tagging and the tag on the fish when selecting the technique (size of the transmitter compared to the size of the fish, the weight of the transmitter compared to the weight of the fish should not exceed 2%, etc.).

All tagging procedures need anaesthesia. The authorities of most countries require permission for fish tagging and classify fish monitoring studies as animal experiments, which also applies

for visible implant elastomer. The external apparition of the fish should not be changed (only small dots with elastomer). Preventing unnecessary handling and avoiding stress are of prime importance for such studies. Surgery should only be carried out by experienced researchers and entirely should be conducted with trained personnel.

The following table allows comparing the different techniques.

Table 76: Application ranges of the different techniques of fish tracking - Quality of the study.

Quality of study	Radiotelemetry	Acoustic telemetry	RFID PIT	Visible Implant Elastomer
Study over 1 year	+	+	+++	-
Mobile prospecting	++	++	+ (not everywhere)	+ (not everywhere)
Stationary station	++	+ (not everywhere)	+ (not everywhere)	+ (not everywhere)
Distance of detection	++	++	+	- (video/catch)
Precise movement of individual	+	++	+	-
Parasites/ false detection	+	--	++	+
Dysfonction due to environmental noises	-	--	--	++
Number of individuals to mark	+	+	++ (a lot of codes)	+ (lot of individuals but few unique codes)
Usable for small fishes	+ (10-15cm)	+ (10-15cm)	++ (5cm)	++(4cm)
Speed of identification/ detection	+	+	+++	+
External mark	++	+	(+)	+
Internal mark	+ (if antenna)	++	+++	-
Intrusive mark for the individual	--	--	++	+++
Lifetime	limited	limited	unlimited	Limited (usually less than 1 year)

Table 77: Approximative budget needed for the 4 different techniques of fish tracking.

Approximative budget	radiotelemetry	Acoustic telemetry	RFID PIT	Visible Implant Elastomer
costs	-	-	++	+(very low cost per tag, but it is necessary to do fish samples to recapture fish)
tag	200-300€	300-400€	2 €	From 0.05 € (depending on the length of the tag and the number of tags per fish)
coffret/receiver	2500-6000€	1500-3000 and more	2000-3000€	Costs of fish samples

Table 78: Environmental conditions entering into consideration for choosing a fish tracking technique

Environment and conditions	radiotelemetry	Acoustic telemetry	RFID PIT	Visible Implant Elastomer
Freshwater	++	++	+	++
Saltwater	-	++	(+)	++
Depth	< 10m Depending on conductivity	> 1m	< 1m	-- (only applicable for video recognition)
Flow speed	- depending on pulse rate	- (transmission of signal)	++	-- (only applicable for video recognition)
Turbulence and air bubbles	-	-- (transmission of signal)	++	-- (only applicable for video recognition)
Turbidity	++	- (transmission of signal)	++	-- (only applicable for video recognition)
Ice/ frost	++	- (transmission of signal + damage)	+ (damage)	Not Applicable
Thermal stratification	++	- (transmission of signal)	++	Not Applicable
Conductivity	- (if freq >30Mhz)	+	-	Not Applicable

These tables are built after the experiences of partners taking part in the project and from (Tomanova, et al., 2017).

4.1.2. Field measurements

4.1.2.1. Velocity and Bathymetry measurements with ADCP and ADV

Within FIThydro activities dealing with upstream migration, two different techniques are used to measure velocities: ADCP and ADV. Please refer to 3. Tools and methods – general description for the description of the techniques.

Despite the same goal of measuring velocities, ADCP and ADV are not used in the same cases. Indeed, ADCP allows measuring in areas with high discharges and velocities whereas ADV can hardly be deployed in this context. The ADCP measures the velocity on a profile/ cross section whereas the ADV measures the velocity point by point. Therefore, ADCP is more appropriate for large cross sections where the velocity profile is needed. One major drawback of ADCP is the limitation to conduct measurements in shallow water. It needs at least 30 cm water depth to measure the velocity while ADV is adapted to shallow water. Due to the assembly of the ADCP on a boat for the measurements, it is not possible to do measurements in narrow channels/pools (like in a fish pass), ADV is way more adapted to that kind of measurement (see the section 5.1 for comparison of ADCP deployment types).

To resume, the ADCP technique is recommended for bathymetry and velocity profiling upstream or downstream of a fishpass to study the currentology around the fishpass, the attraction flow etc. while the ADV is adapted to velocity measurement within the fish passes, which are narrow and shallow.

4.1.2.2. Measurement of the discharge in a pool-fish pass

The discharge within the fish pass is a major factor influencing the functionality of the fish pass. The following two techniques are widely used to measure in-situ discharge.

Hydraulic Formula

In pool fish ways, knowing the geometry of the slot or the notch and the water levels in the upstream and downstream pools allows applying weir laws. Considering that the water level in the pools is fluctuating within each pool, the discharge and its mean values can be computed in several pools within a fish pass.

Dilution gauging (or tracer dilution method for flow measurement)

This method requires the release of a known tracer concentration in a section of the river or fishway and the subsequent determination of the tracer concentration in a downstream section. It is based on the dilution relationships between the injection of the tracer and the discharge to be determined.

4.1.3. Hydraulic modelling tools

For assessing the velocity fields related to upstream migration devices, 2D or 3D numerical modelling techniques are applied. In some cases, even 1D modelling is applied for preliminary assessments. At the entrance of the device, i.e. at its downstream end, 2D modelling is often used to get the flow topology in the river such as to validate the local velocities and the attraction flow. If the entrance is more complex with vertical variations of the structure as could be for instance with a submerged inlet, 3D modelling is better adapted to accurately capture the 3D effects. Inside of the different devices, for nature-like fishways or vertical slot fishways without additions, 2D modelling is sufficient. If the device contains macro-roughness elements, sills or complex 3D designs, a 3D modelling becomes necessary to capture the main topology of the flow. The use of turbulence models is also necessary to close the system of equations.

One can note that in 3D modelling the choice of the turbulence model is still an open debate. The main options are to apply Reynolds-averaged Navier-Stokes (RANS) turbulence closure schemes, which can also be unsteady (URANS) for transient problems or large eddy simulation (LES), which is more computationally intensive. Another issue to be handled by the software is the evaluation of the free water surface, which is a complex issue because of the moving boundary between air and water. Different 3D softwares apply different methods for the free surface issue.

When selecting a numerical software, it is of prime importance to have a support from the developers and user-community in terms of normal application of the software (user manual, user forum, specific support by developers) and in terms of continuous update of the software to ensure compatibility with new other software (e.g. for pre- and postprocessing) and data formats.

Table 79: Advantages and drawbacks of hydraulic modelling: 1D, 2D or 3D.

	1D **(e.g. HEC-RAS, BASEMENT)**	**2D** **(e.g BASEMENT, hydro_AS-2D, River 2D; HEC RAS, TELEMAC-2D)**	**3D** **(e.g. FLOW-3D, OpenFOAM, TELEMAC-3D, STAR CCM+)**
Advantages	• Fast first assessment of approximate flow velocities and depths	• Same dimensionality as habitat models such as e.g. CASiMiR • Computation times usually not a limiting factor	• Representation of flows at different depths, important with complex geometries; 3D Velocities
Drawbacks	• Variations within a cross sections, important when studying attraction flows, cannot be simulated	• Depth-averaged velocity values only	• More complicated model set-up • Long computation times, which limit calibration and scenario analyses • Available freeware is complex in application; commercial products are expensive
Output parameters	• E.g. cross-sectional mean velocities, water depths, discharge	• Spatially distributed (vertically averaged) parameters such as e.g. velocities, water depth, turbulent kinetic energy, shear force (along river bed), large scale recirculations	• 3D distribution of all parameters • Additional parameters such as: eddy/vortex characteristics (if necessary), internal normal and shear forces (more detailed turbulence descriptors) • Time resolved data • Free surface evaluation

4.2. Application Ranges

4.2.1. In France

In France, a reference framework tool is created by the ONEMA – National Office for water and aquatic environment (today AFB – French Agency for Biodiversity): RefMADI – Hydroelec (Référentiel Milieux Aquatiques – Document d'Incidences appliqué à l'HYDROELECtricité / Referential Aquatic environment – Impact document applied to hydropower). Indeed in France, any project for creating, renewal or modification of a hydropower plant need a study on the impacts of those works or an "impact document".

This tool, therefore, helps the operators to build the project and to draw up the service of the state.

The following tables are from this tool and present the principal factors entering into consideration to choose the type of crossing devices in France, the application ranges of the different type of fishways and the principal conceptions criteria of devices according to the target species.

These tables are not a regulatory guideline. It is a tool to help designers and operators to find the best solutions for each situation. Once the type of fishways is chosen, the most important steps consisting of sizing and designing the fishpass are following. These tables don't handle this part of the project.

In order to choose the type of fishway, seven factors are compared for baffle fishways, pool fishways, pre-barrage and rustic fishways. To have more information on each type of fishways, please refer to Deliverable D2.1 released in October 2018.

Table 80: Principal factors entering into consideration to choose the type of crossing devices in France.

	Baffle-type fishway	Pool fishway	Pre-barrage	rustic fishway
Height of fall range (m)	limited height < 2.5	middle to high fall (to 8-10 m)	Low height of fall (<1.5-2m)	Low height of fall (<2m)
Supplied discharge range (m3/s)	0.2 to 1 m3/s	0.1 to 1.5-2 m3/s	0.15 to several m3/s	0.2 to more than 10 m3/s
Slope range (%)	10 to 20 %	8 to 15%	the water course slope	2-3 to 8-10 %
Targeted species	Large salmonids and sea lamprey	Every species depending on the design (height of fall, type of jet at the walls)	Salmonids	Every species depending on the design (slope, location and size of hydraulic singularities)
Adaptability to water level variations	moderate tolerance to upstream water level variations	high tolerance to upstream water level variations	high tolerance to upstream water level variations	Low tolerance to upstream water level variation
Land hold constraint	Low	Low	Moderate	High
Maintenance constraint	Moderate	High sensitivities to clogging by logjam and engraving	limited	limited

Table 81: Application ranges of Baffle type fishways in France.

Baffle-type fishway	plane baffle	Super-active type bottom baffle fishway
Slope range (%)	12 to 20 %	10 to 16 %
Supplied discharge range (m3/s)	0.2 to 0.6 m3/s	0.2 to 1 m3/s
Width of the device (m)	0.5 to 1m	0.5 to 1.2 m
Adaptability to water level variations	Limited tolerance to upstream water level variations (30 to 60 cm)	
maximal length of the flights	6 to 8 m for brown trout 10 to 12 m for atlantic salmon and sea trout	8 to 15 m for brown trout 30 to 50 m for atlantic salmon and sea trout
Maintenance constraint	high sensitivity to clogging	low sensitivity to clogging

Table 82: Application range of pool type fishways in France.

Pool fishways	Vertical slots	Deep notches	Surface non-submerged notches
Height of fall range (m)	middle to high fall (to 8-10 m)	middle to high fall (to 8-10 m)	middle to high fall (to 8-10 m)
Slope range (%)	5 to 12 %	10 to 15 %	15 to 20 %
Supplied discharge range (m3/s)	0.5 to 1.5-2 m3/s	0.3 to 0.7 m3/s	0.1 to 0.6 m3/s
Type of flow at the walls	surface jets	surface jets	plunging jets
Targeted species	every species	salmonids, living waters cyprinids	salmonids
Adaptability to water level variations	high adaptability to upstream and downstream water level variations	high adaptability to upstream and downstream water level variations	limited adaptability to upstream and downstream water level variations
Maintenance constraint	high sensitivity to clogging by logjam and engraving		
Land hold constraint	low (possibility to fold the pools)		

Table 83: Application range of Rustic fishways in France.

Rustic fishways	Joint rockfill ramps	Ramps with evenly placed blocks	Ramps with periodic rows of blocks
Height of fall range (m)	max 1-1.5 m	max 2-2.5 m	max 2-2.5 m
Slope range (%)	5 to 10 %	4 to 8 %	6 to 9%
Supplied discharge range (m3/s)	0.2 to 1.3 m3/s/m	0.1 to 0.6 m3/s/m	0.06 to 0.55 m3/s/m
Maximal length (m)	10-20 m	/	/
Adaptability to water level variations	low tolerance to upstream water level variation	low tolerance to upstream water level variation (20 to 40 cm depending on the block height)/ reduced sensitivity to flooding by downstream	low tolerance to upstream water level variation (20 to 40 cm depending on the block height)/ reduced sensitivity to flooding by downstream
Targeted species	Salmonids, shads, sea lampreys, big rheophilic cyprinids (+ eventually eels at edges)	Every species depending on the design (slope, size and concentration of blocks)	Every species depending on the design (slope, spacing of the rows, size of blocks)
Maintenance constraint	Low	moderate	Sensitive to clogging by logjam and engraving
Land hold constraint	Low	High	High

Table 84:Principal conception criteria of devices depending on the targeted species and their abilities of swim/jump in France.

Type of species	Salmon, sea trout	Shad	Sea lampreys, European river lampreys	river trout, graylings	Big rheophilic cyprinids, northern pikes (LT>30cm)	Other rheophilic cyprinids (LT<25-30 cm)	Little benthic species (bullhead, brook lampreys, apron)	Eels (>20-25 cm)
Pool type fishways (included ramps with periodic rows of blocks and pre-barrage)								
Type of jet at the walls	plunging jet/ surface jet	surface jet	surface jet	plunging jet/ surface jet	surface jet	surface jet	surface jet	surface jet
minimum hydraulic head on the notch (plunging jet)	0.3			0.25-0.3				
minimal width of passage sections (m)	0.3	0.4	0.2	0.15	0.3	0.2	0.15	0.15
recommended fall between pools (m)	0.3	0.25	0.25	0.25-0.30	0.25	0.2	0.15	0.2
minimal depth of pools (m)	1	1	0.5-0.75				0.5	0.5
recommended dissipated energy (W/m3)	200-250	150	150-200		150		100-150	150
Ramps with evenly placed blocks								
minimal water height on the ramp (m)	0.4		0.15	0.3		0.2-0.3	0.2	0.05
maximal velocities between the blocks (m/s)	2.5	2	2	2	2	1.5	1.5	1.5
Recommended slope (maximal, in %)	7	6	7	7	6	4-5	4	

Type of species	Salmons, sea trout	Shad	Sea lampreys, European river lampreys	river trout, graylings	Big rheophilic cyprinids, northern pikes (LT>30cm)	Other rheophilic cyprinids (LT<25-30 cm)	Little benthic species (bullhead, brook lampreys, apron)	Eels (>20-25 cm)
Baffle Fishways (PB: plane baffle, BB: bottom baffle) Targeted species: Salmon and trout only								
minimum draght on the baffles (m)	PB: 0.3 BB: 0.2		PB: 0.2/0.25 BB: 0.1					
maximal slope of the flights (%)	PB: 20 BB: 16		PB: 15-18 BB: 16					
maximal lenght of the flights (m)	PB: 30-50 BB: 10-12		PB: 8-15 BB: 6-8					
minimum width (m)	PB: 0.8 BB: 0.6		PB: 0.5 BB: 0.5					

4.2.2. In Spain

In the case of Spain, two agencies (Water-Federal and Environmental-Regional) have the responsibilities for fish passage at HPPs. However, there are no official guidelines. Therefore, solutions are selected depending on the budget (public or private) and the experience of the people involved in the project. There are many differences between river basins, regions and people.

In general, the same criteria as in France are used in Spain based on two resources: Larinier, et al. (2002) and the German guideline DVWK/FAO.

Table 85: Principal factors entering into consideration to choose the type of crossing devices in Spain.

	Baffle-type fishway	Pool fishway	Pre-barrage	Rocky ramps	Bypass or artificial river
Height of fall range (m)	Same as in France	Same as in France	Same as in France	Low height of fall (<2m)	Low height of fall (<2m)
Supplied discharge range (m3/s)				0.2 to more than 10 m3/s	0.2 to more than 10 m3/s
Slope range (%)				5-8%	2-4%
Targeted species				Every species depending on the design (slope, location and size of hydraulic singularities)	Every species
Adaptability to water level variations				Low tolerance to upstream water level variation	Low tolerance to upstream water level variation
Land hold constraint				High	High
Maintenance constraint				limited	limited

Table 86: Application ranges of rocky ramps in Spain.

Rocky ramps	Joint rockfill ramps	Ramps with evenly placed blocks	Ramps with periodic rows of blocks	Bypass or artificial river
Height of fall range (m)	Same as in France	Same as in France	Same as in France	max 2-2.5 m
Slope range (%)				2 to 4 %
Supplied discharge range (m3/s)				0.1 to 2 m3/s/m
Maximal length (m)				10 to 200 m
Adaptability to water level variations				low tolerance to upstream water level variation (20 to 40 cm depending on the block height)/ reduced sensitivity to flooding by downstream
Targeted species				Every species depending on the design
Maintenance constraint				Sensitive to clogging by logjam and engraving
Land hold constraint				High

For pool fishways and baffle fishways, the application ranges in Spain are the same as in France except than Spain doesn't recommend surface non-submerged notches.

Table 87: Principal conception criteria of devices depending on the targeted species and their abilities of swim/jump in Spain,

Type of species	Salmon, sea trouts	Shad	Sea lampreys, European river lampreys	river trout	rheophilic cyprinids	Little benthic species	Eels (>20-25 cm)
Pool type fishways (included ramps with periodic rows of blocks and pre-barrage)							
Type of jet at the walls	plunging jet/ surface jet	surface jet	surface jet	plunging jet/ surface jet (Convenient way: without plunging flow)	**surface jet**	surface jet	surface jet
minimum hydraulic head on the notch (plunging jet)	0.3			**0.3**			
minimal width of passage sections (m)	0.3	0.4	0.2	0.15	**0.2**	0.15	0.15
recommended fall between pools (m)	0.3	0.25	0.25	0.25-0.30	**0.25**	0.15	0.2
minimal depth of pools (m)	1	1	**0.6**			0.5	0.5
recommended dissipated energy (W/m3)	200-250	150	150-200		**125-150**	100-150	150
Ramps with evenly placed blocks							
minimal water height on the ramp (m)	0.4		**0.3**	**0.3**		0.2	0.05
maximal velocities between the blocks (m/s)	2.5	2	2	2	**2**	1.5	1.5
Recommended slope (maximal, in %)	7	6	7	7	**7**	4	

4.2.3. In Belgium

In the case of Belgium, the application ranges are different in Flanders and in Wallonia. Below are the application ranges for Flanders.

In Belgium, only pool fishways and nature-like fishways are widely used. There is a difference in design criteria between the smaller non-navigable and larger navigable waterways in Flanders. The target species are non-salmonid species and the policy/goal is to mitigate the barriers also for those species with the weakest swimming capacities.

Table 88: Principal factors entering into consideration to choose the type of crossing devices in Flanders - Belgium.

	Pool fishway	**Nature-like fishway**
Height of fall range (m)	(very) low head (<1 - 5 m)	(very) low head (<1 - 3 m)
Supplied discharge range fish pass (m3/s) small waterways	0.1 to 2 m3/s	0.1 to 2 m3/s
Supplied discharge range fish pass (m3/s) navigable waterways	0.8 tot 3 m3/s	1 to 3 m3/s
Supplied discharge range auxiliary flow (m3/s) navigable waterways	1 to 4 m3/s	1 to 4 m3/s
Slope range (%)	< 5%	< 0,5%
Targeted species	all species (ranging from species with poor swimming capacities like three-spined stickleback to species with better swimming capacities like the rheophilic chub)	all species (ranging from species with poor swimming capacities like three-spined stickleback to species with better swimming capacities like rheophilic cyprinids
Adaptability to water level variations	high tolerance to upstream water level variations	average tolerance to upstream water level variations
Land hold constraint	Low	High
Maintenance constraint	vertical slot: high sensitivities to clogging by logjam and engraving	Low

Table 89: Application ranges of pool-type fishways in Flanders – Belgium.

Pool fishways	Vertical slots	V-shaped-weir
Height of fall range (m)	(very) low fall (<1m - 5 m)	(very) low fall (<1m - 3 m)
maximum drop per pool	0.08 to 0.12 m	0.08 to 0.12 m
optimal drop per pool	0.09 m	0.10 m
Slope range (%)	< 5 %	< 5 %
Supplied discharge range fish pass (m3/s)	0.8 to 1.2 m3/s	1.5 to 3 m3/s
Supplied discharge range auxiliary flow (m3/s)	1 to 4 m3/s	1 to 4 m3/s
Type of flow at the walls	surface jets	surface jets
Targeted species	all species	all species
Adaptability to water level variations	high adaptability to upstream and downstream water level variations	limited adaptability to upstream and downstream water level variations
Maintenance constraint	high sensitivity to clogging by logjam and engraving	low maintenance
Land hold constraint	low ('turning pools' can create a more compact design	average (higher than vertical slot fishways but lower than nature-like fishways)

Table 90: Principal conception criteria of devices depending on the targeted species and their abilities of swim/jump in Flanders – Belgium.

Type of species	Sea lampreys, european river lampreys	rivers trouts	Big rheophile cyprinids, northern pikes (LT>30cm)	Other rheophile cyprinids (LT<25-30 cm)	Little benthic species (bullhead, brook lampreys)	Eels (>20-25 cm)
Pool type fishways (included ramps with periodic rows of blocks and pre-barrage)						
Type of jet at the walls	surface jet					
minimal width of passage sections (m)	0.3	0.3	0.3	0.3	0.3	0.3
recommended fall between pools (m)	0,08 - 0,12	0,08 - 0,12	0,08 - 0,12	0,08 - 0,12	0,08 - 0,12	0,08 - 0,12
minimal depth of pools (m)	0,5 - 1				0,5 - 1	0,5 - 1
recommended dissipated energy (W/m3)	<100		<100		<100	<100
Nature-like fishways						
Type of jet at the walls	DNA	DNA	DNA	DNA	DNA	DNA
minimum hydraulic head on the notch (plunging jet)	DNA	DNA	DNA	DNA	DNA	DNA
minimal width of passage sections (m)	>1m (variable fishway width)	>1m (variable fishway width)	>1m (variable fishway width)	>1m (variable fishway width)	>1m (variable fishway width)	>1m (variable fishway width)
recommended fall between pools (m)	DNA	DNA	DNA	DNA	DNA	DNA
minimal depth of pools (m)	DNA	DNA	DNA	DNA	DNA	DNA
recommended dissipated energy (W/m3)	<100	<100	<100	<100	<100	<100

4.2.4. In Portugal

In the case of Portugal, there are no official guidelines, or thresholds for the design of upstream migration devices. The guidelines of Larinier et al., FAO (Food and Agriculture Organization of the United Nations) and DVWK (worksheets from “Deutsche Vereiningung für Wasserwirtschaft Abwasser und Abfall”) are normally used, but the solutions depend on the people involved in the project.

4.2.5. In Germany

In Germany operators and designers use the general guideline for the construction of fish-passes, fish-ways and fish-lifts to restore up-stream fish migration in Germany. The methodology presented here is translated from German to English from the following publication:

DWA 2014. Merkblatt DWA-M-509: Fischaufstiegsanlagen und fischpassierbare Bauwerke – Gestaltung, Bemessung, Qualitätssicherung." *Deutsche Vereinigung für Wasserwirtschaft, Abwasser und Abfall e. V.(DWA), Hennef* (2014).

Methodology to determine geometric and hydraulic threshold values

Geometric and hydraulic threshold values are dependent on both adult specimens of the largest species and the weak swimmers, as well as on the defined fish ecological region (Dußling et al. 2005) of the respective location. Accordingly, in order to establish the site-specific limit values, it is necessary to determine the fish ecological region and the autochthonous fish fauna. The autochthonous fish fauna can comprise both, resident species as well as species already extinct but expected to recolonise the system in the future. This is generally done by experienced and qualified experts in fish biology. Geometric and hydraulic limit values are in principle determined by five steps:

1. **Step: Determination of the fish ecological region of the watercourse and determination of the maximum values for the power density during the energy dissipation.**

   The procedure for the determination of the fish ecological region of the watercourse is described in DWA (2014, p. 38-41). The information given in table 3 (DWA 2014, p. 39) is used as an aid. If the fish ecological region of the specific river stretch is known, table 21 provides the thresholds for the specific power density during the energy dissipation in the fish migration facility or fish pass.

2. **Step: Defining the construction type**

   The design type is determined primarily on the basis of the topographical features at the respective location. The decisive criterion here is that the fish migration system or the migration corridor in a fish pass/ fish migration facility has the optimal location and can be optimally found by the fishes willing to mover ore migrate and all geometric and hydraulic limits can be maintained according to best fish passability (DWA 2014, p. 116-123 and DWA 2014, 126-128). Beyond that, also the available provision of water, the construction expenditure and the cost for the choice of the construction method need to be taken into account. Thus, exclusion of certain construction types may be technically justified.

3. **Step: Determination of the required length of the facility and height difference to be overcome on site as well as the maximum permissible flow speed.**

If the intended construction method has been determined and the height difference and the overall length to be overcome is known (table 17, 18 and 19 DWA 2014 p. 127, 128) contain the suitable thresholds for the maximum permissible flow speeds. Table 17 contains the limit values for pool type fish ways, table 18 for nature like construction schemes and table 19 for constructions with placed blocks.

4. Step: Determination of the relevant species guild or the target species.

In order to determine all other limiting values from a species perspective, the relevant target species and the fish species guild must be determined in accordance with the values given in the DWA (2014). There, the autecology of all relevant fish species comprising maximum and minimum values for species morphology as well as their ability to cope with environmental factors such as current speed or water depth are given. To address not only a certain target species, the individual requirements for the technical details of the fishpass according to the fish regions guilds under planning are described in detail (DWA 2014, p. 38-41).

5. Step: Determination of geometric limits.

The geometric limits for the construction of the fish migration device can be found in table 16 (see pdf, book p. 123). There, the species-specific minimum requirements, which most likely ensure a successful upstream migration, are presented. This means that values for the water depth in the migration corridor and the gaps, as well as the slot width and the pool length of a fish pass structure, are specified for all larger species of the native fish fauna. The relevant value for the construction detail of the location is always the minimum required value of all species-specific values. Due to the different proportions of fish species of different size, the required water depth, for example, may be based on a certain species that can be different from those considered for the determination of the required pool length or slot width.

4.2.6. In Switzerland

In Switzerland, the operators use the German guideline “DWA”, with very little modifications, see above.

4.2. Knowledge gaps

Six Test Cases are dealing with upstream migration. Three kinds of activities have taken place:

- Hydraulic Modelling
- Fish monitoring
- Fish habitat studies within the fish pass

At HPP Altusried, fish monitoring and hydraulic modelling are carried out. The goals are to have a better understanding of the fish behaviour approaching the fish pass and within the fish pass, to study the attraction of the fish pass and link it to the behaviour of fishes for finding the entrance of the fish pass. At this stage of the study at HPP Altusried, some comments can be made:

- Even if the hydraulic conditions are not favourable, fishes have been detected within the fish pass. The behaviour is very different between the species.
- The behaviour of fishes will be linked to hydraulics and morphology, but a big effort for data processing and evaluation will be needed.

Altusried will try to correlate the behaviour of different fish species and the hydraulic conditions before entering and within the fish pass.

At HPP Anunsdjoe, a hydraulic modelling of the fish pass is planned. It will allow to assess the passability and the attraction of the fish pass.

At HPP Günz habitat within the fish pass is studied. The activity will seek an improvement of spawning habitats within the nature-like fish pass by adding gravels. Performance evaluation of fish pass will be assessed using electro-fishing technique within the fish pass. Some lessons learnt from the study are:

- Nase were spawning on fresh gravel within the fishway just a few days after gravel was deposited in. The fresh gravel is moving downstream slowly in the fishway pool after pool. The fish-stock inventory with electric fishing showed a high amount of the target species like nase and barbel with ages about 2-3 years. Generally, it also showed a relatively high quantity of fish-biomass living there and all in all 25 species were documented. Especially relict populations of grayling, minnow, bullhead and brown trout which are very rare at HPP Günz.

The activities at Günz are showing that nature-like fishpass seems to constitute a good habitat area for many species. Thus, it gives a good indication of the potential of the fish pass as a compensation habitat. It is important to note that these observations were made at short term.

At HPPs Guma and Vadocondes fish monitoring and hydraulic modelling were conducted. The studies aim to assess the behaviour of the fishes downstream and within the fish pass and its efficiency, and to improve knowledge about fishway hydrodynamic and attractiveness (performance of attraction flow and influence on fish movement). At this stage some lessons have been learnt:

- Despite a long pool-type fish way (over 8 m height), several fishes (mainly Iberian barbels) ascented the fishway without problem or without important delays;
- The first results of fish tracking showed the relevance of the use of fishway by exotic and mainly alien species like bleak;
- The fish monitoring also showed some difficulties for radiotracking of radiotags with internal antenna (detection range).

The fishes that were monitored come from different locations (upstream, downstream areas), the study data coming from the fish tracking will give information on fish behaviour, use of the fish pass over time. The hydraulic modelling is still in progress, the results will be very important and will be linked to fish monitoring in order to correlate the fish behaviour and the currentology downstream and within the fish pass.

At HPP Schiffmühle, fishes are monitored to assess the entrance preferences and efficiency of the fish ladder for different species: two entrances for the fish pass, species-specific preference of the entrance. The attraction and entrance efficiency, time used for the passage, the efficiency of the fish pass (combination of vertical slot fishway and nature-like fish way). The present results lead to the following key findings:

- The detection rate of the tagged fish is high (69 %), the protocol of tagging and the site setting will allow to give some recommendation at the end of the project;

- Both entrances are used. Barbel and spirlin prefer the vertical slot. Roach, dace and chub prefer the nature-like bypass. Other species do not have preferences and use both entrances equally (e.g. bleak);
- The attraction efficiency for all species was higher for the nature-like fishway, however, the entrance efficiency was higher for the vertical slot pass;
- The passage efficiency of the fish ladder is high (> 80 % for most species). However, the downstream bypass seems not to work;
- PIT-Tagging is a suitable approach to determine the efficiency of a fish ladder. A total of 2331 fishes were tagged in 2017 and 2018. Additional tagging will be realized for upstream migration.

Additional downstream experiments will be carried out in 2019. PIT-Tagging is a suitable approach to determine the efficiency of a fish ladder.

In Altheim, the mapping of the fish pass is planned in order to assess the habitat quality within the nature-like fish pass. However, the methodology and results are not yet available.

The studies at Altheim and Günz will be complementary.

4.3. References

Dußling, U.; Bischoff, A., Haberbosch, R.; Hoffmann, A.; Klinger, H.; Wolter, C.; Wysujack, K.; Berg, R. (2205). Der Fischregionsindex (FRI) – ein Instrument zur Fließgewässerbewertung gemäß EG-Wasserrahmenrichtlinie, Wasserwirtschaft, 7/8, 19–24.

DWA 2014. "Merkblatt DWA-M 509: Fischaufstiegsanlagen und fischpassierbare Bauwerke – Gestaltung, Bemessung, Qualitätssicherung." *Deutsche Vereinigung für Wasserwirtschaft, Abwasser und Abfall e. V.(DWA), Hennef* (2014).

Larinier, M., Travade, F., Porcher, J.P., 2002. Fishways : biological basis, design criteria, and monitoring. *Bulletin Français de la pêche et de la pisciculture*, p. 208

RefMADI, Pincipaux critères de conception des dispositifs en fonction des espèces ciblées et de leur capacité de nage/saut, juillet 2016

Tomanova, S.; Guillemin, A.; Destouches, J-P.; Allou, S., 2017. Journée d'échange technique AFB - Utilisation de la RFID, 13-15 Novembre 2017

5. Downstream migration

Authors	Ismail Albayrak (ETHZ), Robert Boes (ETHZ)
Contributors	Dominique Courret (AFB), Manon Dewitte (CNRS), Laurent David (CNRS), Armin Peter (Fish Consulting), Christian Milzow (AF Consult), David Vetsch (ETHZ), Stephan Kammerer (ETHZ), Raf Bayens (INBO), Johan Coeck (INBO), Ine Pauwels (INBO)
Reviewers	Laurent David (CNRS), Nils Rüther (NTNU)

List of Figures

Figure 283:Photos from Las Rives showing the movable support platform for ADCP measurements. 405

Hydropower plants (HPP) and dams in rivers may block or delay up- and downstream migration of all kind of migratory fish species i.e. anadromous, catadromous and potadromous and cause injury or mortality of fish passing turbines or spillways. Consequently, species populations can decline. For an efficient restoration of water bodies, the European Water Framework Directive was enacted in 2000 and the revised Swiss Water Protection Act and Water Protection Ordinance was introduced in 2011. As to downstream fish protection technologies, this poses particular challenges to HPP operators, engineers and local authorities due to the current lack of design standards. Detailed information on several types of downstream fish migration technologies are presented in Deliverable 2.1. In the scope of FIThydro, hydraulics and fish guidance efficiencies of two types of fish protection and guidance structures categorized as mechanical barriers are studied at HPPs Gotein, Las Rives and Trois-Villes in France and HPP Schiffmühle in Switzerland. Furthermore, fish passage through an Archimedes screw (see chapter 6 on turbine passage) and ship-locks at HPP Ham in the Albert canal are studied by fish monitoring. Fish monitoring, velocity measurements and numerical modelling are done to investigate possible downstream fish migration measures such as the implementation of a fish guidance structure and weir passage at HPP Bannwil in Switzerland. In this section of D.2.2, all tools and devices used within the reseach activities on downstream fish migration in these Test Cases are compared and application ranges of fish guidance structures and ship-lock passage are discussed.

5.1. Specific tools and devices for downstream migration

The tools and devices used in the case study HPPs are categorized into ‘fish monitoring’, ‘field hydraulic measurements’ and ‘Hydraulic numerical modelling’. General information on all the tools as well as methods are reported in section 3 and a comparison between the tools and devices based on the experiences gained from the case studies is presented below.

5.1.1. Fish monitoring

The fish monitoring techniques used for downstream fish migration studies are listed in the following for each case study HPP:

- Radio Telemetry (HPPs Bannwil and Las Rives)
- Acoustic Telemetry (HPP Ham)
- RFID with PIT-tag (HPPs Gotein, Trois-Villes and Schiffmühle)
- ARIS/DIDSON (HPP Bannwil)

Comparison of such fish monitoring techniques with regard to the advantages, limitations and costs is presented in section 4.4.1. Therefore, a short comparison of ARIS/DIDSON technique with others is presented in the following.

Acoustic cameras with high resolution such as DIDSON/ARIS are dual-frequency identification sonars. They send out multibeam fans. The camera can image individual fish and record the behaviour. DIDSON/ARIS cameras operate at frequencies between 0.7-3.0 MHz. The maximum detection ranges depend on the frequency and the type of camera. Most acoustic cameras have ranges of about 30 m and 60 m for long range systems. However, in most applications, fishes begin to disappear at distances of about 25 m. Imaging sonar data in combination with a powerful detection and classification software has strong capabilities to detect downstream migrating fishes at large hydropower plants. The cameras are useful at longer ranges than most available optical equipment. In addition, they also work at night or under turbid water conditions. At HPP Bannwil, an ARIS Explorer sonar was used with the frequencies 1.8 and 3.0 MHz. The detection range for fishes was 0.7–14 m. With this

installation, it was possible to detect the presence, the swimming depth, and behaviour of fishes in front of the trash rack.

Acoustic telemetry can be used in a way to assess fish behaviour in detail. At the case study at the HPP of Ham (Belgium), a Vemco VPS system has been used to determine the specific downstream route choice of salmon smolts and silver eels in front of a ship-lock complex that is equipped with an Archimedes screw turbine. The set-up of the system is described in the case study presentation file (section 2.10). The advantages of using acoustic telemetry are: (i) the number of fish that were used is under full control, (ii) fish could be recognised individually, as well as their passing attempts, (iii) specific fish behaviour could be assessed in the vicinity of lock filling structures, (iv) passage mortality could be assessed for each type of route and (v) fish could be followed after passage through deep estuarine water up to the sea.

5.1.2. Field hydraulic measurements

The instruments for velocity and/or bathymetry measurements used for downstream fish migration studies are listed in the following for each case study HPP:

- ADCP (HPPs Schiffmuhle, Bannwil, Trois-Villes and Las Rives)
- Airborne Image Velocimetry (HPP Schiffmuhle)
- Hand-held propeller (HPP Schiffmühle)
- Electromagnetic current meter (HPPs Las Rives and Gotein)

Three different ADCP deployments were used within the FIThydro studies at different HPPs. An ADCP system based on a remote-controlled boat platform is used at Swiss HPPs Bannwil and Schiffmühle for velocity and bathymetry measurements. A tethered boat ADCP application from banks was made in French HPP Trois-Villes (4.0 m wide intake) while an ADCP on a movable support platform was used at another French HPP Las Rives (14.0 m wide intake, Figure 282). The following table (Table 91) compares these three deployments. ADCP application for upstream fish migration studies is documented in section 4.1.2.



Figure 283:Photos from Las Rives showing the movable support platform for ADCP measurements.

A handheld propeller was used to measure flow velocities inside the bypass of the horizontal bar rack fish guidance structure at the HPP Schiffmühle where ADCP measurement was not possible (see section 2.12). Similarly, an electromagnetic current meter was used at the HPPs Las Rives and Gotein to measure flow velocities inside the bypass of the vertically inclined bar rack fish guidance system.

Table 91: Advantages and disadvantages of three ADCP deployment techniques.

	ADCP on remote-controlled boat platform (HPPs Schiffmühle and Bannwil)	ADCP on a tethered boat from banks (HPP Trois-Villes)	ADCP on a movable support platform (HPP Las Rives)
Man power required for medium to large rivers (Q > 100m³/s)	Low (+++)	Low (+++)	(-) Not possible to construct a long bridge (≤ 20-25 m).
Man power required for small rivers (Q < 100m³/s)	Low (+++)	Low (+++)	High for bridge installation (+), low for measurement itself
Cost of devices	Relatively high due to the cost of the remote-controlled boat (+)	Low (+++)	Medium depending on the cost of the support system (++)
Overall long-term cost of the measurements	Low (+++) the cost of the boat is justified in long-term use due to less man power requirement	Low (+++)	Low (+++) The structure is composed of several elements that are 2 or 3 m long each. At each site, the number of element you combine has to be adapted.
Total duration of a measurement for the same amount of data	Shorter because of easy deployment (+++)	Medium because of manually moving the ADCP position (++)	Medium because of manually moving the ADCP position (++)
Limitations	Approx. 0.50 m from each bank of the rivers and closer to cannot be measured due to width of the boat. (+)	Approx. 0.50 m from each bank of the rivers cannot be measured due to width of the boat. (+)	Approx. 0.10 m from each bank of the rivers cannot be measured due to width of ADCP. (+++)
	Note that: This minimum distance from a bank or vertical wall at the intakes for measurement is also related to the angle of beams from vertical (20°) and water depths. Therefore, impact of beam on the sidewalls or banks before it reaches the bottom or the inclined rack has to be avoided.		
Coverage area for the velocity and bathymetry measurements in the river	No limit (+++)	Limited to close area of the bank or a bridge (+)	Limited to length of the support platform (++)
Stationary measurements at low turbulent flows	(+++)	(+++)	(+++)
Stationary measurements at high turbulent flows	Possible but difficult due to high motion of the boat (+)	Possible but difficult due to high motion of the boat (+)	Easier because of fixed and robust ADCP position (+++)
Velocity measurements in front of bypass	Possible if flow is not shallow (+++)	Possible if flow is not shallow (+++)	Possible if flow is not shallow (+++)
Velocity measurements inside bypass	Not possible (-)	Not possible (-)	Possible if flow is not shallow and bypass is not narrow (+)
Qualitative ranking per category:			

- advantageous (+++)
- moderate (++)
- unfavourable (+)
- not possible (-)

5.1.3. Hydraulic numerical modelling

The numerical software for hydraulic modelling used for downstream fish migration studies are listed in the following for each case study HPP:

- FLOW-3D (HPPs Schiffmuhle and Bannwil)
- OpenFOAM (HPPs Las Rives, Trois Villes)

Comparison between the software is presented in section 4.1.3. FLOW-3D is a commercial software and is easy to use thanks to its graphical user interface (GUI), has detailed documentation and provides access to the high performance computing services (see section 3.9). Therefore, it is used to simulate various flow conditions at two Swiss HPPs. The goals of the studies at Swiss HPPs could be achieved using FLOW-3D.

In the case of modelling complex geometries such as fish guidance structures, unstructured or body-fitted computational grids could be an advantage. OpenFOAM is a promising alternative to FLOW-3D since it can accurately represent such geometries and is an open-source software (see section 3.15). Therefore, OpenFOAM is applied to model vertically inclined bar racks used at French HPPs for fish guidance.

5.2. Design criteria and application ranges

Within the FIThydro project, the following downstream fish migration measures are studied:

- Vertically inclined bar rack with top bypass (HPPs Gotein, Trois-villes and Las Rives))
- Horizontal Bar Rack - Bypass System (HBR-BS) (HPP Schiffmühle)
- Spillway passage (HPP Bannwil)
- Ship-Lock Sluice complex fish passage (HPP Ham)

The application ranges of these measures are presented for each country based on official guidelines if available. In section 5.3, these ranges and knowledge gaps are discussed.

5.2.1. In France

Vertically inclined bar racks are installed perpendicularly to the flow direction and at an angle *ß* to the horizontal in order to guide fish towards one or several surface bypasses located at the top of the rack. The following criteria are recommended by the French Agency for Biodiversity (AFB) for inclined rack and angled bar rack (Courret and Larinier 2008; Courret et al. 2015):

- Maximum clear bar spacing: 20 mm for silver eels (> 55-60 cm long), 25 mm for smolts of Atlantic salmon and sea trout
- Maximum value of normal velocity to rack: $V_N \leq 0.5$ m/s
- For inclined bar rack: maximum angle of the rack from the horizontal: $ß \leq 26°$; for angled bar rack: maximum angle to the wall $\alpha \leq 45°$
- For inclined bar rack: bypass entrance width around 1.0 m and maximum distance between 2 entrances is 4-5 m ➔ cumulative width of entrances is at least ≈ 20-25% of

the intake width; for angled bar rack: as deep as possible and minimum depth 0.5 m at the downstream end of the rack
- Minimum bypass flow depth: 0.5 m
- For inclined bar rack: bypass entrance velocity equals 1.1 times the mean approach velocity; for angled bar rack: entrance velocity equals 1.7 times the mean approach velocity for α=45° and equals 1.0 times the mean approach velocity for angled bar racks with streamwise bars
- The combination of criteria on the bypass number (linked to the maximum distance between 2 bypasses), the bypass dimensions (width and depth) and the entrance velocity allows determining the discharge needed for the device according to the characteristics of the water intake. The implementation of French criteria for vertically inclined bar rack leads to bypass discharges varying from 5-6% of design discharge for small intakes, down to 2-3% for intakes > 50 m^3/s. For angled bar rack, the approach in France is case by case.

Up to now, inclined bar racks are installed at intake with design discharge up to 100 m^3/s.

References:

Courret, D., Larinier M. (2008). Guide pour la conception de prises d'eau "ichtyo-compatibles" pour les petites centrales hydroélectriques [Guide for the design of fish-friendly intakes for small hydropower plants]. France: Agence de l'Environnement et de la Maîtrise de l'Energie (ADEME). Report No: RAPPORT GHAAPPE RA.08.04. http://www.onema.fr/IMG/pdf/2008_027.pdf (in French).

Courret, D., Larinier, M., David, L., Chatellier, L. (2015). Development of criteria for the design and dimensioning of fish-friendly intakes for small hydropower plant. Fish Passage 2015, Groningen, June 22-24.

5.2.2. In Switzerland

The Swiss Federal Office for Environment (FOEN) published a guideline on the restoration of upstream and downstream fish migration at small to medium HPPs (Hefti, 2012). The guideline gives a practical procedure on how to meet the requirements of the revised Swiss Water Protection Act (WPA) and Water Protection Ordinance (WPO) introduced in 2011, and presents examples of best practices. The following criteria are recommended by FOEN for the design of angled bar racks, vertically inclined bar racks and HBR-BS:

- Maximum clear bar spacing: 20 mm
- Maximum value of normal velocity to rack: $V_N \leq 0.5$ m/s
- Maximum angle of the rack with respect to the flow direction (HBR-BS, angled bar racks): $\alpha \leq 45^o$
- Maximum angle of the rack with respect to the horizontal (vertically inclined bar rack): $ß \leq 26^o$
- Minimum bypass discharge: 2 to 10% of the max. turbined discharge
- Minimum dimensioning of a bypass: 0.5 m width and 0.5 m height
- Minimum water level in the bypass: 0.40 m
- Discharge into the downstream flow above the downstream water level in freefall of maximum 2.5 m
- Downstream water depth at least a quarter of the freefall height, but at least 0.9 m

Vertically inclined bar racks (French case studies) and HBR-BS (Swiss case study) are studied in FIThydro.

These guidelines are under revision and some criteria will be adapted according to available best practice experiences. This is applicable for maximum clear bar spacing and downstream water depth.

For large HPPs, only limited guidelines are available. However, studies to develop or test downstream fish migration solutions have started at large pilot HPPs on River Aare. Furthermore, an innovative fish guidance structure with vertical-curved bars for small-to-large HPPs is developed and tested in the Laboratory of Hydraulics, Hydrology and Glaciology (VAW) of ETH Zurich (see deliverable D3.4, published in 2020).

For detailed information on downstream fish passage technologies, please refer to Deliverable D2.1 released in October 2018.

References:

Hefti, D. (2012). Wiederherstellung der Fischauf- und -abwanderung bei Wasserkraftwerken (Restoration of fish up- and -downstream fish migration at hydropower plants). Checkliste Best practice. Bundesamt für Umwelt (FOEN), Bern. Umwelt-Wissen Nr. 1210: 79 S. http://www.bafu.admin.ch/uw-1210-d.

5.2.3. In Belgium

Belgium or Flemish law does not provide stringent regulations for fish migration at the ship-lock complexes. Nevertheless, Stevens & Coeck (2010) designed a prioritization map to solve fish migration obstacles, which was imposed by the Benelux Decision about free fish migration. The Albert Canal is considered as a waterway that needs special attention, but that is not prioritized highly to solve fish migration obstacles for being an artificial canal. The eel management plan for Belgium (Steven et al., 2009) states that downstream fish migration obstacles, like ship-lock complexes should pay special attention to fish passage when these structures are adapted in any way. The local water manager (DVW) adopted this recommendation by installing less harming Archimedes screw turbines at the ship-lock complexes.

References:

Stevens, M., Coeck, J., Van Vessem, J., Philippart, J.C., Thirion, A. (2009). Eel management plan for Belgium. COUNCIL REGULATION (EC) No 1100/2007 of 18 September 2007 establishing measures for the recovery of the stock of European eel. 172 pp.

Stevens M. & Coeck J. (2010). Wetenschappelijke onderbouwing van een strategische prioriteitenkaart vismigratie voor Vlaanderen (Benelux Beschikking M(2009)01). Rapporten van het Instituut voor Natuur- en Bosonderzoek 2010. (INBO.R.2010.33). Instituut voor Natuur- en Bosonderzoek, Brussel.

5.3. Results and knowledge gaps

Downstream fish migration measures are studied in six case study HPPs. The following three types of activities are conducted:

- Fish monitoring
- Field velocity measurements
- Numerical modelling

5.3.1. France

At the Test Cases in France, assessment of biological efficiency of the downstream migration devices was conducted for Atlantic salmon smolts (HPPs Gotein, Trois Villes and Las Rives) and silvers eels (HPP Las Rives). At the three Test Cases, the French design criteria were respected. The present studies conducted at the Test Cases, therefore, allow assessing the actual French design criteria recommendations.

Efficiencies for smolts are stable among sites and ranged from 80% to 90%, with short delay for passage. Concerning silvers eels (> 55-60 cm), the efficiency at Las Rives is 100% (no eel pass through the rack) with also short delay of passage (Tomanova et al. 2018). These findings give credence to the recommended design criteria for low-sloping racks, which is the main solution implemented in France for small to medium HPPs.

Field velocities were measured at Trois Villes and Las Rives HPP with ADCP and analyses of data are under progress but validate the upstream velocity and the discharge in the bypasses. Numerical modelling of these 2 intakes using OpenFOAM is also planned during 2019. The goal is to properly characterize the flow fields that allow reaching the good biological efficiencies mentioned. Then, this can be used as a reference for other projects using the calibrated modelling tool to forecast the flow field.

From French point of view, knowledge gaps mainly concern large HPPs (design discharge > 100 m^3/s) where the building of low bar spacing racks is technically difficult and costly.

Reference:

Tomanova, S., Courret, D., Alric, A., De Oliveira, E., Lagarrigue, T., Tetard, S. (2018). Protecting efficiently sea-migrating salmon smolts from entering hydropower plant turbines with inclined or oriented low bar spacing racks. *Ecological Engineering*. Volume 122, 15 October 2018, Pages 143-152.

5.3.2. Switzerland

At HPP Schiffmühle, all three activities have been conducted. The goals of the activities are to document current situation, assess the fish guidance efficiency (FGE) of the state-of-the art fish guidance structure (FGS) i.e. horizontal bar rack – bypass system (HBR-BS) and if needed, further improve the HBR-BS geometry for better FGE (See section 2.12). The design of the HBR follows the recommendations from FOEN but the bypass dimensions are not compatible with the recommendations (section 1.2.2). The results of the activities have led to the following conclusions:

- Both ADCP and AIV velocity measurements indicate that most of the fish in the river are expected to follow the main stream towards the headrace channel while a small portion swims towards the HPP.
- The attraction flow to the bypass for downstream migration seems inefficient and a re-circulation zone possibly affects fish searching the bypass entrance.
- No fish was detected in the bypass confirming the poor velocity field around the bypass
- Clogging in the bypass pipe is a problem affecting the bypass discharge and velocity
- Current bypass system needs optimization

- Alternative bypass system needs to be relocated either closer to the HBR or at the left bank of the weir

A numerical model of the HPP Schiffmühle is constructed, calibrated and validated in early 2019. The numerical model will allow optimizing the bypass geometry and hydraulics and options of possible new bypass locations such as at the left side of the weir to improve bypass attraction flow and hence fish guidance efficiency of HBR-BS. Numerical model results will be available in mid-2019. The lesson-learnt from the studies at HPP Schiffmühle indicate that design, location and operation of a bypass system are of prime importance for a successful implementation and high fish guidance efficiency of HBR-BS.

Similarly, all above listed three activities have been also conducted at HPP Bannwil. The goals of the activities are to document the current situation, investigate the efficiency of spillway fish passage as an operational measure and investigate numerically structural measures i.e. innovative fish guidance structures and spillway passage under various operational scenarios (see Deliverable D3.4 in 2020). The results of the activities have led to the following conclusions:

- No fish injury is expected during fish spillway passage since fish terminal velocity is higher than the spillway velocity.
- Due to back-roll and possible atmospheric gas supersaturation (>100%) in the stilling basin of spillway, fish can be exposed to predation and strike to baffle blocks and gas-bubble disease, respectively. Therefore, stilling basin geometry needs to be optimized if spillway passage is considered as a measure at this HPP.
- Hydraulic conditions at potential positions of FGS are unfavourable.
- ARIS acoustic fish monitoring results were non-conclusive due to low number of fish detection.

Fish monitoring using radio telemetry technique at HPP Bannwil will be conducted starting from early 2019 for a year. The collected fish monitoring, hydraulic and 3D numerical model data will be used to develop measures to improve down fish migration. The lessons learnt from the studies at HPP Bannwil indicate that:

- Fish monitoring using a hydro-acoustic technique (ARIS/DIDSON) should be conducted during various fish migration seasons and under various flow conditions to obtain concrete data on fish behaviour.
- The 3D numerical model is a powerful tool to develop and/or test potential downstream fish migration measures such as spillway passage and fish guidance structures.
- Velocity and bathymetry data are of prime importance for calibration and validation of the 3D numerical model.
- For large HPP with high discharges such as HPP Bannwil, ADCP with a remote-controlled boat is convenient, easier and faster to measure bathymetry and velocities at low cost of manpower (two people are enough) compared to tethered ADCP technique.

5.3.3. Belgium

The goals of the monitoring study at the ship-lock complex of Ham (Belgium) using acoustic telemetry are to assess searching behaviour and to determine the specific passage route of both tagged salmon smolts end silver eels. Fish can pass the complex via the turbine intake when it is in operation or by using the locks. The latter can be passed by using the lock filling

intakes or by swimming into the locks together with ships (open gates). Almost all tagged fish passed the complex by using the lock; 88% of the silver eels (n=58) and 100% of the salmon smolts (n=42). So only 12% of the eels passed the complex by using the HPP route whereas no single smolt used this route. For both species, a distribution of approximately 50/50 was met regarding the choice between the lock filling intakes versus open lock gates (Vergeynst et al., 2016, 2018).

Mortality after lock passage was severe for both species (20% for salmon smolt and 36% for silver eel), indicating unknown negative impact due to ship-lock passage. No clear difference in mortality rate between the 2 lock entrance routes was demonstrated, so lock emptying could play a negative role as well. Further research is needed to fill this existing knowledge gap.

The use of an acoustic array at 69 kHz, together with a random ppm signal delay of 15-30 sec could distinguish the different passage routes. However, gathered fish tracks to indicate fish behaviour were not accurate for further data analysis. Fast swimming fish generated too little closely located consecutive positions to shape a precise and accurate fish track. Erroneous data appeared more frequently at the outer range of the acoustic array and were filtered out if the error was too large. Acoustic arrays working at a higher frequency with the use of very short signal delays have proved to overcome these drawbacks, even in challenging environments and hence recommended for future studies.

5.4. Conclusions

The section 5 reports on (i) a wide range of tools and devices used in the research activities on downstream fish migration at the test cases for velocity and bathymetry measurements, hydraulic numerical modelling and fish monitoring, (ii) design criteria and application range of measures for safe downstream fish migration and (iii) overall results and knowledge gaps determined from the research activities.

Advantages and disadvantages of three different deployment methods of Acoustic Doppler Current Profiler for velocity measurements are presented in a table based on the experiences gained from the test cases. Furthermore, Airborne Image Velocimetry, hand-held propeller and Electromagnetic Current Meter used for velocity measurements are described. In a similar way, a brief information on advantages and disadvantages of fish monitoring techniques and numerical modelling software is presented Depending on the application and goal of the studies, users should select one of those techniques using the table 91 and information given in section 5.1.

Vertically inclined bar rack with top bypass and Horizontal Bar Rack – Bypass System (HBR-BS) used at the test cases are mechanical barriers used for fish protection and guidance at HPPs. Swiss and French guidelines for design of such Fish Guidance Structures (FGS) are similar and presented in section 5.2. Swiss guideline is currently under revision and some criteria will be adapted according to available best practice experiences. Overall, the vertically inclined bar rack and HBR-BS are designed for small to medium size HPPs due to their velocity limitations. For large HPPs, only limited guidelines are available. Fish passage at ship-lock complexes is an alternative measure for safe fish migration. However, Belgium or Flemish law does not provide stringent regulations for such measure.

The French design criteria for vertically inclined bar racks are respected at three French cases and the findings of the research activities at these test cases showed that such FGSs efficiency

guided smolts and silver eels with a short delay of passage. The knowledge gaps exist for large HPPs with discharge > 100 m^3/s in France. Regarding the research activities in Swiss test cases, the findings indicate that the attraction flow to the bypass of HBR-BS at the HPP Schiffmühle is inefficient with low fish guidance efficiency and hence the bypass system needs optimization, which will be done using 3D numerical modelling in the scope of FIThydro. No fish injuries during the spillway or weir passage at HPP Bannwil is expected but stilling basin geometry needs optimization to avoid predation, fish strike to the baffle blocks and gas-bubble disease. The findings of the activities from HPP Bannwill show that there are still knowledge gaps on the design of a FGS for such block-type and large HPP with complex hydraulics and topography in front of the turbines. Fish monitoring study at the ship-locks of the HPP Ham (Belgium) showed that high percentage of fish used the ship-lock as a passage route instead of turbine intake. However, severe fish mortality during the ship-lock passage was observed and hence further research is need to identify the causes of fish mortality and improve fish passage at such locks.

Overall, the present studies provide basic knowledge on the design and operation of FGSs, spillway and ship-lock fish passages and, tools and devices for development and efficiency evaluation of such downstream fish migration measures despite some knowledge gaps. Furthermore, the present findings will contribute to fish-friendly and sustainable use of HPPs and underpin the follow-up studies (laboratory and complementary field studies) on such measures for safe downstream fish migration.

5.5. References

Vergeynst, J., Baeyens, R., Coeck, J., Pauwels, I.S., Nopens, I., Mouton, A., De Mulder, T. (2018). Fish behaviour in the vicinity of a navigation lock complex: the challenges. International Symposium on Hydraulic Structures 8:.

Vergeynst, J., Baeyens, R., Pauwels, I., De Mulder, T., Nopens, I., Mouton, A. (2016). Behaviour of downstream migrating European eel at sluices and turbines. http://lib.ugent.be/catalog/pug01:8075115.

6. Passage through turbine

Authors	Franz Geiger (TUM), Mathilde Cuchet (TUM)
Contributors	Jeffrey Tuhtan (TUT), Ulli Stolz (VOITH)
Reviewers	Joachim Pander (TUM), Nicole Smialek (TUM)

List of figures

Figure 284: Exemplary cumulative influence of multi facility passages on the overall survival rates in function of the number of passed facilities and the survival rate of each facility. 415
Figure 285: Application range of hydraulic machines with regard to site specifications, based on (Giesecke et al. 2014) – modified. 422
Figure 286: Typical survival rate relations of common (and comparable) turbine types. 423
Figure 287: Schematic overview of damage rate assessment SMTDs. 428
Figure 288: Schematic workflow with regard to turbine passage issues. 434
Figure 289: 35 kW turbine runner at the Obernach laboratory from upstream (top left) and downstream (top right) and longitudinal section of the test section (bottom, [m]). 436
Figure 290: Injection points at turbine intake (left), dummy damage distribution (mid) and dummy damage incidence in dependency of load case and insertion point (right). 438
Figure 291: Estimated strike probabilities for turbine passage in the investigated test and lab case scenarios in dependency of full load (FL) and half load (HL) as well as object length, for object passage with flow velocity and orientation aligned with flow (left) or perpendicular to blade relative velocity (right). 439
Figure 292: Estimated strike probabilities for turbine passage in the investigated test and lab case scenarios in dependency of passage radius as well as object length, for object passage with flow velocity and orientation aligned with flow and full load (left) and half load (right). . 439
Figure 293: BDS sensor, sensor injection, injection point in front of turbine intake, sensor retrieval from tailwater, tailwater barrier. 440
Figure 294: Exemplary BDS data, pressure and acceleration values in dependency of time. 441
Figure 295: Preliminary analysis of nadir pressure distribution for incidence assessment. . 441
Figure 296: Exemplary stress level distribution at runner entrance, as deduced from numerical simulation. 442
Figure 297: Stress level hill charts for the investigated stressors (vertical axis: head, horizontal axis: discharge) 442
Figure 298: Combined fish passage hill chart for 10 cm acclimation depth. 443

List of tables

Table 92: Basic damage potential assessment of turbine types. 422
Table 93: Summary of basic parameters for investigated Kaplan turbines 435

6.1. Background to fish mortality in hydraulic machines

The key items of hydropower usage are hydraulic machines which transform the potential or related kinetic energy of water into mechanical energy, usable for a further purpose, mostly electricity production. In almost all cases, the transformation is implemented by a rotating “runner” and the respective machine referred to as a turbine. Without respective means (c.f. SMTDs for downstream migration), fish within the water body can pass with the water through the turbines. This is especially important with regard to fish downstream migration and drift. Such movement patterns are part of the life cycle of many species for various reasons, as described in respective deliverables (Lucas, et al., 2001).

Fish passage through turbines is in general related to potential injury and mortality, also referred to as fish damage. The actual incidence and severity of injury and mortality of fish due to turbine passage depend on the fish (size, species, condition) and the turbine (type, design specifications, operating point) (Cramer et al. 1964, Davies 1988, Cada 1990, Monten 1985, Larinier et al. 1989, Turnpenny 1998, Holzner 2000). It can only be assessed as a statistical average and is characterized by the damage or mortality rate. Alternatively, the corresponding survival rates can be addressed. The mortality rates of fish during turbine passage can in principle vary from almost 0 to 100 % for particular setups, while most hydropower plants show differentiated values (Montén 1985, Dumont et al. 2005). Whereas injury or death of single fish are commonly considered acceptable face to the necessities and benefits of hydropower, the mortality rates have to be considered in relation to population protection requirements (Dudgeon et al. 2006).

Fish mortality during turbine passage can be of major importance for population stability. This gets especially eminent with regard to diadromous fish species, mainly salmon and eel, as these species are frequently obligated to pass numerous hydropower facilities for their reproduction cycle with respective cumulative damage (Dumont 2005). Figure 284 illustrates the exemplary influence of multiple facility passages on overall survival rates. But also potamodromous fish species can in principle be seriously affected by mortality rates due to turbine passage and the impact on their populations has to be assessed individually. Site specific thresholds for mortality have to account for the given population, habitat and migration conditions and need to be coordinated with facilities in the surrounding river system.

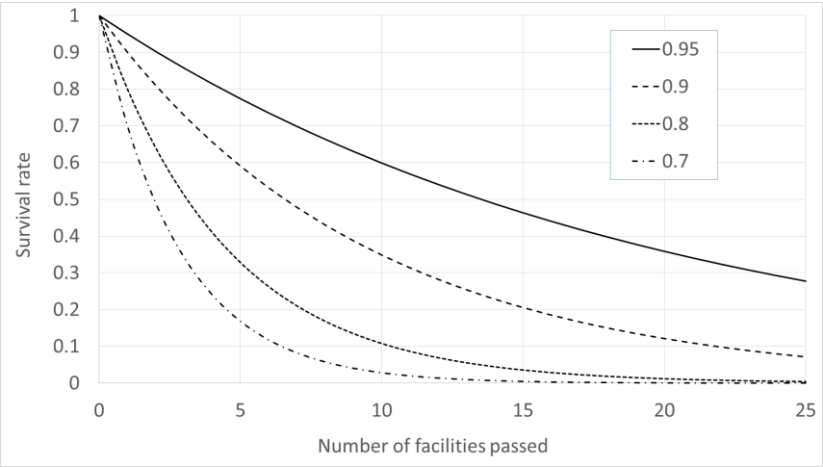


Figure 284: Exemplary cumulative influence of multi facility passages on the overall survival rates in function of the number of passed facilities and the survival rate of each facility.

A major issue is the evaluation of fish mortality rates during turbine passage for given conditions, especially as turbines are in general customized to local service conditions with resulting individual variability. Moreover, the knowledge of damage processes can be utilized to develop design or operation management in order to reduce mortality rates. In this context, the drivers of fish damage during turbine passage and the particularities of different turbine types with regard to fish passage need to be considered.

6.2. Injury and mortality of fish due to turbine passage

Sources of fish injury and fish mortality during turbine passage have already been summarized in D2.1 – Survey on turbines, but are briefly recalled in the context of the present deliverable to facilitate the subsequent considerations. A number of damage mechanisms have been identified. Beside immediate mortality, delayed mortality due to internal injury has to be considered, especially with regard to hydrodynamic damage mechanisms. Additional damage in relation to turbine passage can arise e.g. from trash rack passage, but is not related directly to turbine issues.

6.2.1. Strike and gaps

The most obvious damage mechanism is related to collisions with fixed (e.g. guide vanes) or moveable (e.g. runner) parts of the turbine. Injury can reach from scale loss to spinal fracture, amputation or decapitation (Davies 1988, Schneider et al. 2012, Müller et al. 2017). The actual injury scheme and severity depend on the impact velocity and the shape and size of the obstacle (in relation to the fish), and in more detail also on impact location, orientation, fish species and individual size of the fish (Amaral et al. 2011). Face to the relative velocities at that instance, runner blade leading edge is of primary relevance for this damage mechanisms in most turbines.

A second source for mechanical damage is given by gaps, e.g. between runner and housing or between moveable runner blades and hub. The size of the fish and the gap, its shape and the local hydraulic conditions have high influence on resulting damage and depend largely on turbine type and design (Cada 2001).

6.2.2. Pressure and cavitation

Hydraulic machines are in general related to pressure changes in the working fluid. The pressure regime experienced by fish during turbine passage can cause injury or mortality, e.g. swim bladder rupture (Foye et al. 1965, Abernethy et al. 2001, Jacobson et al. 2012). Beside fish species (especially concerning swim bladder aspects of physostome and Physoclisti), the acclimation pressure of the fish, the minimum pressure during turbine passage and the pressure gradient are main influences (Becker et al. 2003). The actual pressure regime depends highly on underlying turbine type, design and operating mode.

If the pressure drops below given limits (c.f. vapor pressure or critical pressure), cavitation occurs due to a phase change of fluid to vapor. Related phenomena, especially face to vapor bubble collapse, can also cause injury and mortality to fish (Weitkamp et al. 2003, Deng et al. 2005, Boys et al. 2018). The occurrence of cavitation is, however, an extraordinary situation, which is not meant to happen during common turbine operation, at least in relevant scale, as it is also related to efficiency reduction and potential machine damage.

6.2.3. Shear and turbulence

Similar to pressure, the hydrodynamic processes in hydraulic machines entail shear stress and turbulence. These aspects are also known to be potentially harmful to fish. The damage

mechanisms are less distinct than for strike and pressure and relatively few references are available but given investigations show damage ranging from scale loss to decapitation (Neitzel et al. 2004).

6.2.4. Indirect mortality

Turbine passage related stress entails unfavourable conditions for fish survival in the tailwater area, e.g. disorientation (Coutant et al., 2000). This can entail increased mortality with regard to natural hazards, like predation. Exemplary data for a Kaplan turbine with 7 % loss to be expected, reports up to 30 % mortality for juvenile Coho salmon when indirect mortality due to predation was considered (Larinier 2001). Relatively few information is available on this topic and the related mortality rates depend evidently on the specific site. Subsequent considerations only focus on turbine specific mortality aspects.

6.3. Discussion on tools and methods

The most relevant SMTDs with regard to the management of turbine related fish mortality concern the hydraulic machines themselves and tools/methods to assess the mortality rates of fish caused by the passage of these machines.

6.3.1. Hydraulic machines

This chapter provides an overview and relevant background information about common hydraulic machine types for hydropower production as well as available information on a number of traditional and innovative solutions which try to address these issues. Face to numerous uprising ideas and products in this field, completeness cannot be provided and the presentation is restricted to most relevant aspects in the given context. With regard to references on mortality rates it has to be acknowledged, that such findings depend largely on underlying test conditions (e.g. fish length) and cannot be compared directly. Summarized information on application ranges of particular machine types (including head and discharge references) and their principle damage potential to fish is provided at the end of the chapter.

6.3.1.1. Classic impulse turbine types

In impulse turbines, the potential energy of the water is transformed into kinetic energy, which subsequently drives a runner. These setups are mostly dedicated to high to mid head applications and achieve efficiencies towards 90 %. Regulation of the turbine is in general done by regulation of the water discharge by a nozzle in front of the runner. The relative unfavourable fish passage conditions have to be seen face to the relevance for fish migration issues and fish protection capabilities.

6.3.1.1.1. Pelton turbine

Pelton design turbines are impulse-type turbines using the principal of a traditional overshot waterwheel designated for high head applications. They are related to correspondingly high pressure values and gradients in the approach flow and high impact velocities on the runner. Consequently, fish are not likely to survive Pelton turbine passage in general. However, the ecological shortcoming has to be considered face to typical application of this turbine type. The high head facilities are rarely related to run-of-the-river schemes but supplied form respectively large and mostly artificial reservoirs in mountain areas. Thus, fish migration issues are mostly less relevant and feasibility of fish protection measures at intakes is relatively easy.

6.3.1.1.2. Turgo turbine

Turgo turbines are for medium head applications, which show application ranges in between Pelton and Francis turbines. While a number of economic advantages are claimed in

comparison to Pelton and Francis designs, few implementations and information are given. The impulse type characteristics suggest unfavorable fish passage conditions in comparison to Francis reaction type design.

6.3.1.1.3. Crossflow turbine

Crossflow turbines are hydraulic machines with non-radial and non-axial flow conditions, where water crosses twice through the runner blades. Producers reference the application range with 2 – 200 m head, 0.03 – 16 m³/s discharge and 10 – 7000 kW power. Most implemented facilities show modest power size. The design can provide advantages with regard to self cleaning characteristics and for part load efficiency but reduced peak efficiency. Concerning fish mortality, the impulse-type characteristics, unfavourable leading edge geometry, high numbers of blades and relatively high rotational speed suggest unfavourable conditions. Experimental mortality investigations show values from 10 to 70 % mortality rate, depending on turbine design, fish species and fish length (Gloss et al. 1983).

6.3.1.2. Classic reaction turbine types

In reaction turbines, flow velocity and related pressure forces around the submerged runner are used for energy conversion. Respective turbine types are designated for mid to low head applications. Regulation of the turbine to given river discharge condition is achieved by control devices in front of the runner as well as moveable blades or variable speed, depending on the respective turbine type. The regulation devices allow an efficient performance for a wide operating range in head and flow. Efficiency at optimum condition is commonly well above 90%. The energy conversion also requires an adequate draft tube downstream of the turbine runner for these turbine types. In general, fish damage during turbine passage can vary largely, depending on the given fish and turbine specifications.

6.3.1.2.1. Francis turbine

Francis turbines feature fixed runner geometry and are the most common turbine type for mid head conditions. Radial inflow is deviated to axial outflow. Discharge adaption is provided by a guide vane control device. Spiral casing installations, as well as free approach flow chamber setups, can be found. The fixed runner geometry entails relatively unfavourable part load efficiency. Pressure regimes, blade shape and numbers (mostly 7 to 19 blades) and rotational speeds, as well as a number of given experimental investigations, suggest higher mortality in comparison to Kaplan turbines. However, the references mortality rates of 1.1 – 50 % (FIThydro D1.2) do not show distinct differences and actual comparison has to account for the given boundary condition. This can be based on mortality modelling approaches, which are available for this turbine type (Collins et al. 1982, Eicher 1987, Dedual 2007).

6.3.1.2.2. Diagonal turbine

Diagonal turbines (aka Deriaz turbines) combine aspects of Francis and Kaplan turbines. While general flow is comparable to Francis setups and the turbine type thus adapted to mid head application, double regulation by guide vanes and runner blades provides improves part load efficiency. Blade numbers (8 – 12 blades for 25 – 100 m head, 0.1 – 10 m³/s discharge) are relatively small in comparison to Francis design and suggest improved fish passage conditions. Additional aspects have to be considered for actual assessment, especially rotational speed. Actual fish passage investigations or mortality considerations are not provided and adequate assessment would require respective work. Only few installations are given so far, and no relevant information on fish mortality can be provided.

6.3.1.2.3. Kaplan turbine

Kaplan turbines are employed for low to mid head applications and the most common turbine type for low head facilities of respectable discharge/power output. The design refers to double regulated axial machines. Guide vane and runner blade adjustment provide favorable conditions for part load operation (e.g. efficiency > 80 % for discharges from 20 - 120 % design discharge). Blade numbers range typically from 3 to 8 and increase with head. While traditional design mostly featured vertical axis with a spiral case at the inflow, bulb setups with horizontal or inclined axis are also common, especially for very low head applications. Moreover, s-type and straflo-setups can be found but are less common. While hydraulic conditions at the runner and related considerations are comparable for different Kaplan turbine types, it should be distinguished between vertical Kaplan machines and bulb machines, as the inflow situation is different and influences the path of the fish from inflow to where it passes the turbine (hub or shroud).

Face to the large deployment of Kaplan turbines, especially at run-of-the-river hydropower facilities with obvious fish migration issues, a respective number of experimental fish passage investigations have been conducted throughout the decades (Long et al. 1967, Bell et al. 1985, Taylor et al. 1985, Stier et al. 1986, Dainys et al. 2017). Mortality rates of 0.9 – 47 % (FIThydro D1.2) have been reported. Several models for mortality prognosis have been deduced and are discussed in further detail in subsequent chapters.

6.3.1.2.4. Propeller turbine

A variety of axial turbines can be found, which mostly represent simplified approaches of the Kaplan design. Often single regulation (guide vanes or runner blades) is employed for economic reasons to face particular boundary conditions. In some cases, variable runner speed is included to compensate the related part load shortcomings. This aspect, as well as gap issues, can be of interest for the improvement of fish mortality during turbine passage, e.g. related to part load operation. So far, only few reliable information is available concerning the large and heterogeneous variety of such turbine designs. In principle, adapted mortality modelling approaches can be employed, similar to those which will be discussed for the more relevant case of Kaplan turbines.

6.3.1.3. Traditional hydropower approaches

A number of hydraulic machines are based on rather traditional approaches for hydropower usage. They are typically restricted to low or very low head applications and limited power per unit. Relatively large dimensions, small rotational speeds and flow velocities are associated with relatively favourable fish passage conditions. Gap aspects are the main issues for fish mortality and have to be considered in relation to required machine efficiency.

6.3.1.3.1. Water wheel

Traditional waterpower usage was based on water wheels and such installations are still in service for very low head applications with limited discharge at numerous mill sites. A variety of different types have emerged. Most water wheels feature horizontal axis. Overshot, breastshot and undershot wheels can be found. The most frequent design in middle Europe is Zuppinger wheels (0.5 – 2.5 m head and 0.3 – 3 m^3/s discharge) and overshot wheels (50 – 500 l/s discharge and > 2 m head). Efficiencies in a range of 70 - 80 % with favourable part load comportment and fish mortality rates of 0 - 23 % can be found (Adam et al. 2015, Tombek et al.), but actual values depend largely on wheel specifications (e.g. gaps).

6.3.1.3.2. Hydraulic pressure machine

The hydraulic pressure machine was developed in the scope of the HYLOW project, intending advanced energy conversion for very low head applications. The basic design compares to water wheel setups, whereas the headwater side of the wheel is impounded up to the wheel axis. So far only one prototype facility was installed within the scope of the R&D project. Fish downstream passage investigations resulted in an overall mortality of 19 % for the given fish distribution (Uzunova et al. 2014). Similar approaches have been implemented at several sites but no information on ecological evaluation is available (e.g. application range 20 – 2000 kW power and 1 – 5 m head). Similar to water wheels and screw turbines the actual efficiency and fish mortality rates will depend largely on given specifications.

6.3.1.3.3. Screw turbine

Hydropower implementations by Archimedes screw setups have emerged throughout the last decades. This approach is limited to low head and low discharge sites with regard to mechanical engineering challenges. Common power output shows a range of several 10 kW, up to several 100 kW and potential up to 1 MW (e.g. 20 – 80 rpm, 0.5 – 10 m head, 0.2 – 5 m^3/s discharge, screw diameter up to 4 m). In general, these techniques suggest favourable conditions for fish downstream passage, as the rotation speed of the screw is relatively slow. However, several investigations revealed mortality rates up to 23 % (0.02 – 23 % c.f. D1.2) (Edler et al. 2011, Schmalz 2011, Ebel 2013). The related damage can be ascribed to the leading edge of the screw and to the gap between screw and hub. Modifications of the leading edge and a rotating housing can reduce or eliminate these issues. Accordingly, such implementations are highly recommended with regard to fish downstream passage. However, a rotating housing, in turn, increases mechanical engineering challenges.

6.3.1.3.4. Free flow hydropower

A number of innovations try to provide hydropower implementation without generation of head water and tail water but by exploiting flow conditions in given rivers (Giesecke, et al., 2014). Frequently, these approaches claim advances in ecological features also with regard to fish mortality. The stream wheel setup is a traditional implementation of the basic principle. However, the power output is derived from the kinetic energy of the flowing water. For common river conditions, this corresponds to a magnitude of only a few 10 cm head. Moreover, only a relatively small partition of this power can be utilized. Consequently, this approach and its various implementations show few potential to get remarkable relevance for energy production and are thus not further considered.

6.3.1.4. Innovative “fishfriendly” turbine types

During the last decades, a number of turbine producers have tried to improve fish downstream passage conditions through turbines by special turbine modifications or design. The main features of four examples for these innovations are summarized in this context.

6.3.1.4.1. MGR

The MGR (Minimum Gap Runner) technology refers to enhanced Kaplan turbines, developed by Voith Hydro. Similar design improvements have been adopted by other turbine manufacturers. The main feature of these turbines is the reduction of gaps at tip and hub by full spherical hub and discharge ring geometry. Related mechanical damage, as well as hydrodynamic load due to unfavorable flow conditions, are thus reduced, which however only affects fish passing in the respective area. Such design is related to increased design and manufacturing costs but also has the potential to increase the efficiency for rehabilitation projects. Moreover, the MGR turbine design can address improved overall hydrodynamic

conditions (e.g. pressure regime) and geometric details (e.g. leading edge shape) to improve fish downstream passage.

Experimental investigations are given for exemplary implementation on U.S. west coast facilities, where survival was e.g. increased from 94 to 97 % but remained rather similar at such magnitudes for other cases (USACE 2013). While such improvements are recommended in order to improve fish passage conditions, the efficiency of these measures seems so far limited and in general not capable to reduce damage rate ranges on a large scale. Significant changes of mortality rates require significant modifications of the hydraulic machines and finally a specialized design in regard to strike and pressure distribution.

6.3.1.4.2. VLH

The VLH (Very Low Head) technology is based on special turbine development, characterized as runner blade regulated propeller turbine with variable speed. Main features are large runner diameter (3.1 – 5 m), low rotational speed and limited pressure load. Moreover, gaps and leading edge profile have been addressed (Lagarrigue et al. 2010). In turn, a large number of runner blades and small flow velocities are reluctant for strike probability reduction. The hydraulic design does not require a draft tube and modular units for different head and discharge ranges are available (1.5 – 4.5 m head, 10 – 27 m³/s discharge). Implementation is related to small civil engineering constructional efforts, but turbine related costs in general increase with reduced energy density of the machine and efficiency decreases.

First fish passage investigations indicated survival rates close to 100 % (Lagarrigue et al. 2008), but showed issues of the employed methodology with regard to the fish injection system. Recent investigations suggest positive findings for certain facilities but also remarkable fish damage for other facility specifications. According to observed damage schemes, depending on the facility specifications, runner impact velocities might be just above or underneath biological limits for relevant damage. Provided a clarification of the ongoing ecological evaluation, this approach might be of high interest for fish downstream passage compatible hydropower usage in the given application range.

6.3.1.4.3. Pentair

Based on works about fish passage in pumps, a design for fishfriendly bulb turbine is proposed by Pentair (Van Esch, et al., 2015). Relatively few information of this type of machines is available so far, but first fish experimental campaigns have been conducted for the assessment of fish mortality during turbine passage (Pentair, 2013). A test series with eel showed 0 % mortality, while methodical issues might have influenced this finding. Another investigation concerning several fish species and conducted under better boundary conditions but with differing turbine characteristics showed mortality rates between 0 and 6 %.

While further clarification of mortality rates is required for actual assessment of these turbine designs, the present data indicate relatively low mortality rates face to given runner speed and blade thickness. Beside the small runner blade number (2 – 3) the findings suggest, that spiral shape (respectable circumferential development) of runner blades can be favourable to achieve relatively large blade surface with respectively suitable pressure conditions and moreover a spiral geometry of the leading edge could reduce damage incidence and/or severity in case of blade impact. The rotational direction of runner and leading edge spiral have to be accounted for.

6.3.1.4.4. Alden

The Alden turbine was developed by Alden Labs and features a specialized design to minimize fish damage (Foust, et al., 2011). It is based on a Francis turbine with a vertical axis, non-regulated runner, with radial approach flow and axial outflow. Regulation is provided by wicket gates upstream the runner. The particular shape of the runner was developed in order to reduce fish damage face to pressure, shear and strike. The turbine type application range is for instance assessed as 6 – 40 m head and 15 – 80 m³/s discharge. Fish survival close to 100 % is targeted for large scale facilities. For 28 m head, 43 m³/s discharge, 4 m runner diameter and 120 rpm a survival rate of 98 % is expected for fish of 200 mm length. While the concept might be the most developed and promising approach for fishfriendly turbine in the given head range, no prototype implementation and investigations are provided yet and respectable costs, especially for refitting at existing plants have to be accounted for. Similar to VLH type, the turbine was designed with regard to acceptable pressure regime for fish passage, entailing reduced energy density and thus increased machine volume.

6.3.1.4.5. Summary

Figure 285 shows typical application ranges of the various hydraulic machines. Table 92 provides a basic assessment of the relevance of different damage sources for the machine types and an overall assessment for the aspect of fish injury and mortality due to turbine passage. In some cases, such assessment remains unresolved so far or a broad variability has to be stated. The intended low mortality rates on innovative turbine technologies require further evaluation for broad application.

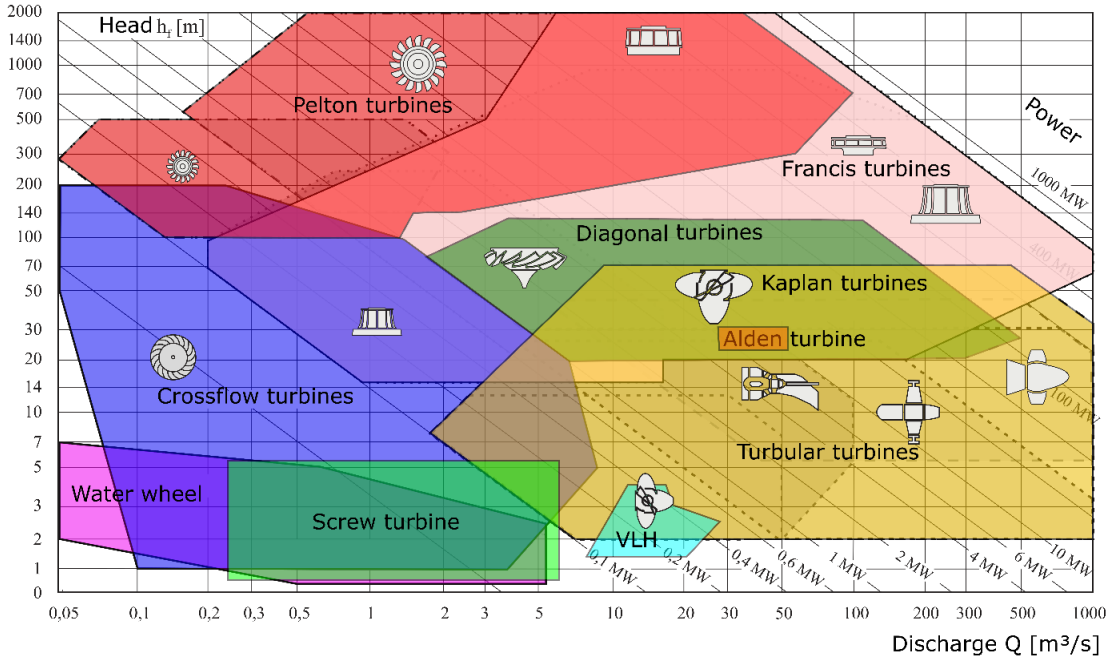


Figure 285: Application range of hydraulic machines with regard to site specifications, based on (Giesecke et al. 2014) – modified.

Table 92: Basic damage potential assessment of turbine types.

	Strike probabilities	Impact fatality	Gaps issues	Pressure load	Shear and turbulence	Overall mortality
Pelton	High	High	-	High	-	Lethal
Turgo	High	High	-	High	-	Lethal
Crossflow	High	Variable	-	Variable	-	High
Francis	High-medium	High-medium	Low	High-medium	Variable	Variable
Diagonal	High-medium	High-medium	High-medium	High-medium	Unresolved	Unresolved
Kaplan	Variable	Variable	High-medium	Low-medium	Low-medium	Variable
Propeller	Variable	Variable	Variable	Low-medium	Low-medium	Variable
Water wheel	Variable	Low	Variable	Low	Variable	Low
Hydraulic pressure	Low	Low	Variable	Low	Low	Low
Screw turbine	Low	Variable	Variable	Low	Low	Low
MGR (Kaplan)	Low-medium	Low-medium	Low	Low-medium	Low	Potentially low
VLH (Propeller)	Medium	Low-medium	Low-medium	Low	Low	Potentially low
Pentair (Bulb)	Medium	Low-medium	Unresolved	Unresolved	Unresolved	Potentially low
Alden (Francis)	Low	Low	Low	Low	Low	Potentially low

A number of turbine types show overlapping application ranges. With regard to basic machine principles, a ranking of typical mortality rates can be stated for the most common turbine types. Different relations can be given for particular machine specifications and the typical ranking has to be considered face to typical application ranges, especially with regard to facility head and the related potential for fish damage. Upcoming deliverables (D 3.1) will address these aspects is more detail.

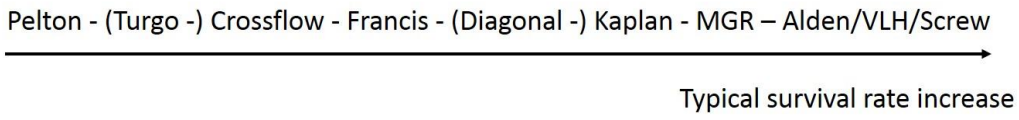


Figure 286: Typical survival rate relations of common (and comparable) turbine types.

6.3.2. Machine modification, management and further mitigation measures

Apart from general particularities for fish passage of different turbine types, SMTDs for mitigation of mortality rates are given, which are especially of interest with regard to existing hydropower plant.

6.3.2.1. Machine modifications

One potential mitigation measure for fish mortality due to turbine passage at given hydropower setups is a modification of the hydraulic machine. Examples range from the modification of leading edges of screw turbines up the replacement of conventional Kaplan runners by MGR turbines. Such measures correspond finally to the choice of hydraulic machines and their design details, already discussed in the previous chapter.

6.3.2.2. Machine management

Mortality rates of fish during turbine passage depend in detail not only on basic geometric and hydraulic design of the turbines but also on the given operating point. The actual head and turbine discharge, as well as the setting of control device, runner blades or rotational speed, can have remarkable influence of blade strike probabilities, impact velocities, pressure regimes, shear and turbulence load. Consequently, these relations can be used to reduce fish mortality rates by targeted turbine management (ATV-DVWK 2005). This approach is of special interest with regard to fish species with distinct downstream migration periods, like eel and salmon smolt.

During respective migration periods, two basic options, as well as combinations of them, can be considered to improve fish passage conditions: Total or partial turbine shutdown and fish passage via weirs or spillways, which might be adapted for fishfriendly downstream passage. Modified turbine operating points which entail reduced fish mortality. As such measures reduce energy production, the accurate prognosis of relevant migration periods is of special interest. Different approaches have been developed, based on compartment observation of stocked fish or the detection of fish activity in the headwater of hydropower facilities (Brujis et al. 2003, Egg et al. 2017).

The machine management method, especially in combination with alternative downstream passage corridors is related to FIThydro work on downstream passage. In the context of turbine passage, the aspect of operating point resolved fish mortality rate assessment is of main relevance, which is discussed in the subsequent chapter. In general, turbine management should be considered for hydro facilities with several turbine units in order to provide favourable ecologic conditions for turbine passage. For example, discharge distribution between several Kaplan units should take into account that fish mortality typically increases with decreasing turbine discharge (Geiger et al. 2016a). Detailed consideration has to be based on turbine specific fish mortality rate assessment and should also account for site specific aspects of hydrology, fish migration and machine efficiency.

6.3.2.3. Further mitigation measures

The issue of turbine related fish mortality is governed by the given turbine type, design and operating point (see above) on the one hand side, and the given fish species and sizes (c.f. D1.2) and the other hand side. While it is frequently neglected in fish mortality rate assessment (see below), the actual mortality rates are also influenced by the fish condition and comportment during turbine passage (Solomon 1988). Theoretical considerations of runner blade strike show relations with passage velocity (c.f. swimming movement), body orientation and passage location (c.f. hub, mid, tip), which is in accordance with preliminary experimental findings (Geiger et al. 2018). Such relations of fish mortality and fish condition/comportment could be used to reduce mortality by influencing fish behaviour. A respective approach has been developed at the TUM and will we treated in WP3.

6.3.3. Fish mortality assessment

Actual mortality rates of fish due to turbine passage depend on the given turbine design and specifications as well as the operating conditions and the affected fish (Larinier 2008). A number of methods and tools for the determination of actual mortality rates are available, from direct damage monitoring to different approaches for damage rate modelling (Geiger 2018, Müller et al. 2017). They vary in their respective application requirements and informational content.

6.3.3.1. Direct fish monitoring

The injury and mortality of fish during turbine passage can be investigated directly, by investigation of fish damage due to turbine passage. Respective activities require in general the consideration of animal welfare regulations (e.g. bioassay permits), fishery rights and site particular regulations (Adam et al. 2013).

The investigation of fish damage due to turbine passage can in principle be based on the observation of passage events of the natural fish stock (Calles et al. 2012, Dumont et al. 2012). Sufficiently high case numbers are required for reliable statements face to various influences and related statistical spread. This is in most cases difficult to achieve face to the boundary conditions at river sites and practical aspects of such observations (c.f. net operation). Eel show particular high downstream migration intensities during limited periods, which can be addressed to obtain respective case numbers. The unknown initial condition of fish remains a methodical issue (c.f. potential damage face to upstream HPPs).

Alternatively, fish can be inserted in order to achieve respective case numbers (Linde 2018, Müller et al. 2017). Insertion points can be chosen with regard to different aspects (e.g. in front of the screen, in front of the turbine, in front of the recovery device). The insertion method should provide natural/undisturbed turbine approach and passage, to avoid methodical issues. Fish species, sizes and condition similar to the natural stock in the river system are desirable for representative statements. Face to availability, frequently fish from hatchery has to be employed and the transferability of results has to be accounted for.

The actual registration of fish injury or mortality requires the catching of the fish in the tailwater. This can be done by specialized net installations, which span the entire turbine outflow area. Catch rate and net related injury and mortality have to be considered, e.g. by reference tests (Pander et al. 2018). The operation of such net installations at river sites is in most cases complicated by floating debris load and resulting clocking, which results in temporal restrictions for the deployment. In general, difficulties increase with the size/discharge of the turbine and so far investigations up to 80 m^3/s have been conducted (Schneider et al. 2012).

Alternatively, to the netting of the entire outflow area, so called balloon tags can be attached to the fish, which inflate after a given time and allow to catch the fish in the tailwater (Schneider, et al., 2017). Additional radio tags can be employed to locate the fish by respective receivers if required, e.g. in large rivers (English et al. 2005). The consideration of telemetry data without fish recovery is less adapted as mortality is difficult to identify and to assign. The influence of the tagging procedure and the tag itself on the fish behaviour and passage and the resulting injury and mortality remain methodical issues to be accounted for.

The number of inserted fish depends on the employed recovery method for example with regard to specific recapture rates and the influence on deduced statements. Typical magnitudes range from one to several hundred fish for each investigated parameter combination (fish species, size, operation point, injection point). To account for potential long

term mortality e.g. due to internal injury, the fish should be observed under adequate conditions for a certain time, mostly 48 to 96 h (Brown et al. 2012). Autopsy, radiology, histology and further techniques can be employed to provide further information.

Respectable efforts are required for direct fish damage investigations at common river site hydropower plants, especially for facilities of larger size. Therefore, a number of indirect approaches have been developed to assess fish damage rates by modelling. Some of these approaches need to be combined in order to provide actual injury and mortality statements and some require reference data from direct fish monitoring or laboratory experiments.

6.3.3.2. Fish laboratory experiments

Hydraulic aspects of turbines can be investigated in scaled models under laboratory conditions. The complex biological influences of fish injury and mortality during turbine passage do, in the first instance, not allow for a respective approach. But laboratory investigations can, at first, provide valuable information about these biological aspects.

A number of targeted laboratory investigations has already been conducted to gain information about resulting injury and mortality of fish face to given exposure to blade strike, pressure fluctuation or shear stress (Turnpenny 1998, Neitzel et al. 2000, Abernethy et al. 2001). So far, most respective studies have been conducted in North America (Foust et al. 2011). The available information can provide orientation on fish vulnerability face to given exposure, but clarification for relevant European species is recommended.

The relations about physical stress and resulting fish damage can in principle be used for the transfer of results from scaled investigations to prototype conditions. Moreover, they can provide the missing link for indirect methods of mortality assessment, which deduce physical stress levels of fish during by sensor passage or modelling different approaches.

6.3.3.3. Sensor passage investigations

Autonomous measurement devices can be inserted into the water upstream the turbine and pass through the turbine with the flow. They are recovered in the tailwater, in case facilitated by balloon tag and radio telemetry. The data recorded during turbine passage can be analyzed to evaluate the physical stress which fish are exposed to. Beside other parameters, pressure linear acceleration and rotation grade are typically recorded with respective temporal resolution (Deng et al. 2007). This enables an assessment of fish exposure to strike and pressure fluctuation related stress. Targeted investigations of passage conditions at specific turbine positions (e.g. hub, blade tip) can be achieved by specialized injection systems. Sensor passage and fish passage have to be differentiated due to fish comportment. The FIThydro project includes the development and deployment of a corresponding device, the BDS (Barotrauma Detection System). Further information is provided in the respective instances.

6.3.3.4. Numerical modelling

The hydraulic conditions inside a turbine can be simulated by numerical models. Based on the specific turbine geometry and the operating point of interest, CFD simulations (Computational Fluid Dynamics) provide detailed pressure and flow fields. Assuming fish passage along streamlines, the fish stress with regard to pressure, shear and turbulence can be quantified. Biological reference data for fish response to given stress levels would in principle enable mortality prognosis. So far, only relative statements with regard to fish stress for different turbine designs or operating points are considered. The influence of strike is included by analytical modelling (see below). The FIThydro project includes the development and

application of numerical based fish stress assessment and further information is provided in the respective instance.

6.3.3.5. Statistical modelling

Data from experimental investigations of fish mortality at hydropower plants can be used for statistical modelling in order to obtain mortality prognosis for further facilities. Several models can be found in literature, mainly for eel and salmon passage through Kaplan and Francis turbines (Larinier et al. 1989, Ebel 2008, Gomes et al. 2008). Fish length and basic turbine parameters are required as input variables. While such models might provide a suitable orientation of mortality magnitude in certain cases, the application should be restricted to parameter ranges corresponding to the underlying data sets. Moreover, these models mostly do not account for actual operating points. Ecological turbine management or design is not supported. Face to these restrictions, merely statistical models are not considered in further detail.

6.3.3.6. Analytical modelling

The most obvious source of fish injury and mortality during turbine passage is runner blade strike. A number of approaches have been developed to predict fish mortality rates during turbine passage for a given turbine from analytical considerations (Montén 1985, Raben 1957). Based on assumptions/simplifications, the probability of runner blade strike can be calculated. Models for Kaplan and Francis turbines can be found, which take into account basic turbine dimensions, the actual operating point and the fish length. Moreover, fish species specific calibration parameters are included in these models, which describe the probability of relevant injury/mortality in case of runner blade strike. Other sources of damage (e.g. pressure) are included in the calibration but not represented correctly for general application. More recent developments of analytical based models also address pressure and shear, based on reference data from CFD and biological experiments (Turnpenny 2000).

6.3.3.7. Conclusions

The overall possibilities for mortality rate assessment are illustrated in Figure 287. Two main directions are available for injury and mortality rate assessment, the direct monitoring of fish passage and the modelling of damage rates. An adequate modelling need to cover the various damage sources and thus requires the combination of different STMDs. While strike related impact is addressed by analytical models, hydrodynamic influences require sensor passage or numerical calculations. Any modelling requires reference data from laboratory experiments or monitoring, to account for underlying biological aspects, i.e the biological response in form of injury or mortality face to given physical stress levels.

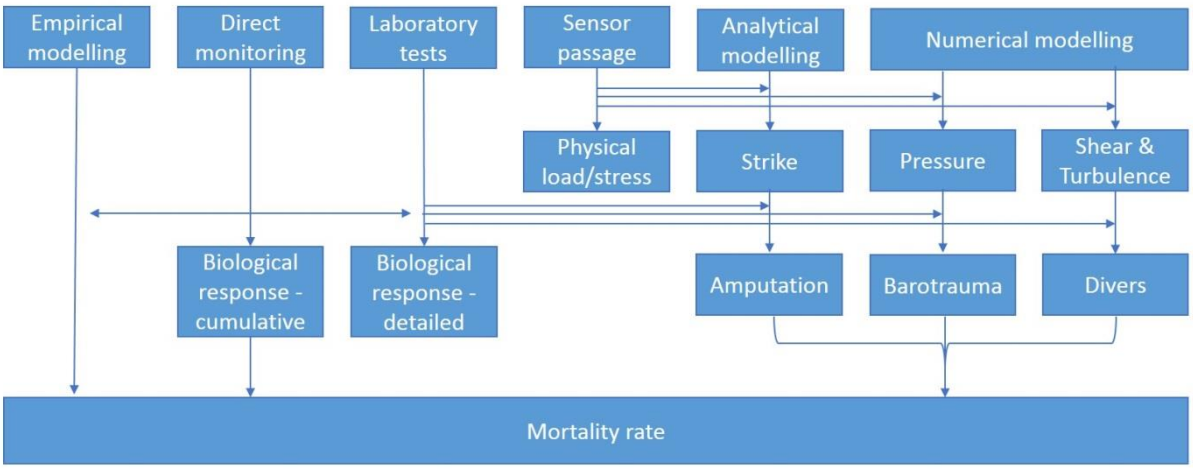


Figure 287: Schematic overview of damage rate assessment SMTDs.

6.3.4. Application range

Subsequent tables provide summarized overview, typical applications and individual application aspects of mortality assessment techniques. Application ranges for turbine types are referenced in the respective discussion summary in the previous chapter.

Overview on SMTDs for mortality assessment		
	Main restrictions	**Main application**
Direct fish monitoring - Net based	- Very high practical efforts - Limited turbine discharge - Given boundary conditions - Methodical difficulties	- Limited discharge - Traditional and innovative hydraulic machine types, especially types with no available reference data - Site specific monitoring
Direct fish monitoring - Tag based	- High practical efforts - Given boundary conditions - Methodical difficulties	- Large scale facilities - Site specific monitoring
Sensor passage investigation	- Practical efforts - Only physical load along sensor trajectory	- Potential fish replacement for fish monitoring - Detailed analysis for R&D and sensitive sites
Statistical modelling	- No consideration of service conditions - Transferability and accuracy problems	- If any other method is not applicable
Analytical modelling	- Accuracy issues - Hydrodynamic load requires combination - Biological & behavioral reference required	- Kaplan and Francis turbines
Numerical modelling	- Computational efforts - Strike requires combination - Biological & behavioral reference required	- Reaction turbines - Detailed analysis for R&D and sensitive sites
Advisable mortality rate assessment in function of the given turbine type		

Turbine type	**Damage rate assessment suggestion**
Pelton Turgo Crossflow	Direct fish monitoring if required. Based on such experimental references modelling might be developed.
Francis Kaplan	Modelling approaches available, improvements required. Direct fish monitoring in single cases and for modelling enhancement.
Diagonal Propeller	Direct fish monitoring desirable for unreferenced setups. Modelling development by adaption of Kaplan and Francis ansatz possible.
Water wheel Hydraulic pressure Screw turbine	Direct fish monitoring advisable as gap issues are dominant and influenced by fish comportment. Limited size and boundary conditions facilitate monitoring. Modelling could only be developed on a statistical basis with limited reliability.
MGR	Variable (Monitoring, sensor passage, modelling), case dependent
VLH Pentair Alden	Direct fish monitoring is appropriate face to high requirements and innovative character, where limited size of VLH and Pentair also facilitate this approach. Possible modelling development subsequently with monitoring reference data.

Fish passage monitoring	
turbine types and sizes	Any relevant but limited size face to feasibility restrictions
range of hydraulic conditions	Any relevant but limited size face to feasibility restrictions
deducted parameters	Injury and mortality, directly but cumulative
accuracy of results	Statistical inaccuracy, depending on recapture rates and case numbers Influences of boundary conditions (e.g. available discharge) and methodical issues (e.g. wild fish – farm fish, influences of handling, netting, sensors on fish behaviour and mortality)
requirements for application	Legal requirements (bioassay, fisheries, security) Material and qualified personnel Fish in case of insertion Tag and receiver technology in case of tagging Potential production loss during procedure Adequate hydrological conditions (sufficient discharge but limited floating debris load)
restrictions	Feasibility of netting face to season, test duration, discharge (e.g. < 80 m^3/s per turbine) Feasibility of tag recovery face to tailwater conditions

Sensor passage investigations (BDS)	
turbine types and sizes	Archimedes, Francis, Kaplan, Vortex -

	Distance between blades must allow for min 4 cm dia. Sensor passage
range of hydraulic conditions	Any speed, discharge and load Head up to 250 m
deducted parameters	Strike: Peaks in linear accelerometer Pressure: Total pressure in kPa Shear: Total pressure gradient across 1.25 and 2.5 mm pressure sensors Turbulence: Pressure fluctuations from moving time average Sampling rate: 100 Hz
accuracy of results	Pressure: 0.5 cm water column or better Shear: 0.25 cm H20 / cm or better Turbulence: 0.5 cm H20 or better Dependency on deployment location and number of sensors to achieve statistically reliable results
requirements for application	The sensors cost approximately 500 EUR / unit. When the deployment and recovery teams are experienced, sensors can be deployed at a rate of 1-5 min. 30 measurements for each load case / discharge scenario are recommended, typically taking 2-4 days of field work. Experience has shown that the loss / destruction rate can be estimated as 10% for Kaplan, bulb turbines and Archimedes screws.
restrictions	Sensors must be able to enter the hydropower plant. This may require modifications to the trash rack if it does not allow the minimal 4 cm diameter spacing. An injection system in the form of a tube may be required if different heights (e.g. blade top, hub, blade bottom) are to be investigated. Passive drift does not account for fish behavior influences.

Statistical modelling	
turbine types and sizes	Kaplan, Francis Development for futher machine types possible if data available
range of hydraulic conditions	Mostly based on full load considerations Development for futher conditions possible if data available
deducted parameters	Overall mortality rate in function of fish species and length
accuracy of results	Frequently found inaccurate
requirements for application	Basic turbine parameters (diameter, discharge, head, number of blades, runner speed) Fish species and length
restrictions	Application should be restricted to conditions comparable to underlying statistical modelling (often not well referenced) Transferability remains unresolved Only references for salmon and eel

Analytical modelling	
turbine types and sizes	Kaplan, Francis

	Adaption to Propeller and innovative schemes is possible
range of hydraulic conditions	Ordinary operating conditions (full load, part load)
deducted parameters	Runner blade strike probabilities Mortality rate via empirical factors or functions
accuracy of results	Limited accuracy, e.g. 10 -15 % survival rate accuracy
requirements for application	Basic turbine parameters (diameter, discharge, head, number of blades, runner speed) Preferentially guide vane and runner blade angles for relevant operating points and passage radius Fish species and length with impact response reference
restrictions	Only few reference data for mortality factors/functions, mainly for salmon and eel Accounts only for mortality due to strike, hydrodynamic aspects require combination with CFD based approach or mortality factors with statistical and thus imprecise consideration of additional stress factors

Numerical modelling (CFD + BioPA)	
BioPA was developed by PNNL in the US. It derives the risk of a mechanical injury of a fish, based on prototype CFD calculations, following a streamline through the turbine and deriving the maximum impact of different stressors like pressure, shear and turbulence. Additionally strike events are considered, the impact velocity is derived from CFD results. The mechanical stressors are then evaluated with the biological response of a fish. Within FIT-Hydro Voith investigates the Test Cases Bannwil and Guma using CFD calculation, derives Streamlines using a post-processing tool and applies the response data used in BioPA. Results showed to be comparable with the original BioPA approach.	
turbine types and sizes	Kaplan, Francis and other reaction turbines
range of hydraulic conditions	normal operation at power plant, no transient operation modes
deducted parameters	pressure change (minimum pressure), velocity for strike, shear, turbulence
accuracy of results	depends on 2 things, quality of CFD and quality of biological response data CFD quality dependents on the operating conditions and the degree of numeric modelling, Part load and off-cam conditions are less accurate in CFD prediction, as the modelling of turbulences and vortexes is difficult in stationary CFD Accuracy of biological response data depends on stressor - Pressure: can be predicted well with experiment using pressure chambers - shear stress, turbulence: effects difficult to assess results can be compared relatively to a base solution, so far no absolute mortality rate can be predicted
requirements for application	Geometry data of hydraulic part of power plant required, information on operating points needed

	BioPA is licensed by PNNL, CFD simulation requires licenses Effort to prepare a calculation is approximately 2 weeks - 1 preparing setup, 1 perfoming CFD and do analysis (main operating points) Costs depend on licensing deals and personnel costs
restrictions	Biological data difficult to assess. So far only data for salmonids available assumption that fish follows streamline, no fish movement considered stressors are considered as single events, combination of events are not assessed acclimation depth is important for pressure related injuries, value not necessarily equals the depth the fish swims in

6.4. Knowledge gaps

6.4.1. Required SMTDs for fish mortality in turbines

The foremost requirement with regard to turbine passage of fish is the quantification of fish mortality rates. While a number of reference data and modelling approaches can be found (c.f. D1.2), SMTDs for mortality rate assessment are still insufficient. Direct fish passage monitoring is related to remarkable efforts and hindered by methodical issues. A broad application of first damage rate assessment requires preferentially a relatively simple modelling method.

Most relevance for broad European river ecology has to be ascribed to classic reaction turbine types, mainly Kaplan and Francis turbines (Pracheil et al. 2016). Especially Kaplan turbines are installed in numerous run-of-the river plants and can show large spread of mortality rates in function of machine size and operation. Respective work should consequently focus on this machine type.

To achieve sufficient accuracy and applicability, a simple mortality assessment has to account for turbine specifications and thus correspond to analytical modelling approaches. Face to the eminence of Kaplan turbines, respective model approaches have already been developed. These models focus on strike issues and show heterogenic formulations. Improved strike modelling requires clarification of model differences and suitability.

Moreover, mortality modelling has to account for hydrodynamic aspects. Possibilities to cover the impact of pressure, shear and turbulence related stress on fish have ti be investigated. Such work requires detailed reference data for pressure regimes for different relevant turbine sizes and operating conditions.

Detailed hydrodynamic investigations of turbine passage conditions can be conducted by sensor passage investigations and numerical modelling. Comparable work was conducted for large scale facilities in North America, but adaption of respective techniques to European conditions is required. Experimental and numerical investigations of suitable and representative hydropower sites can provide comprehensive data to deduce modelling of hydrodynamic load.

To assess actual mortality rates caused by physical load, biological reference data is needed. Available data has to be reviewed. Transferability of data from North America has to be considered for European fish species and passage conditions. Experimental work is desirable

and especially required for the clarification of potential fish condition and comportment influence.

Related to work on the fish protection system IDA in WP3, investigations with live fish will be conducted in the Obernach laboratory. These experiments will also serve to gain biological reference data for fish mortality and especially to evaluate the influence of fish condition and comportment on injury and mortality resulting from turbine passage.

An improved understanding and modelling of mortality rates, can subsequently be used to optimize design and operation of turbines in order to mitigate fish mortality rates. Figure 288 illustrates the workflow related to turbine passage issues. The knowledge gaps will be addressed by different tasks, carried out at several Test Cases and laboratory setups.

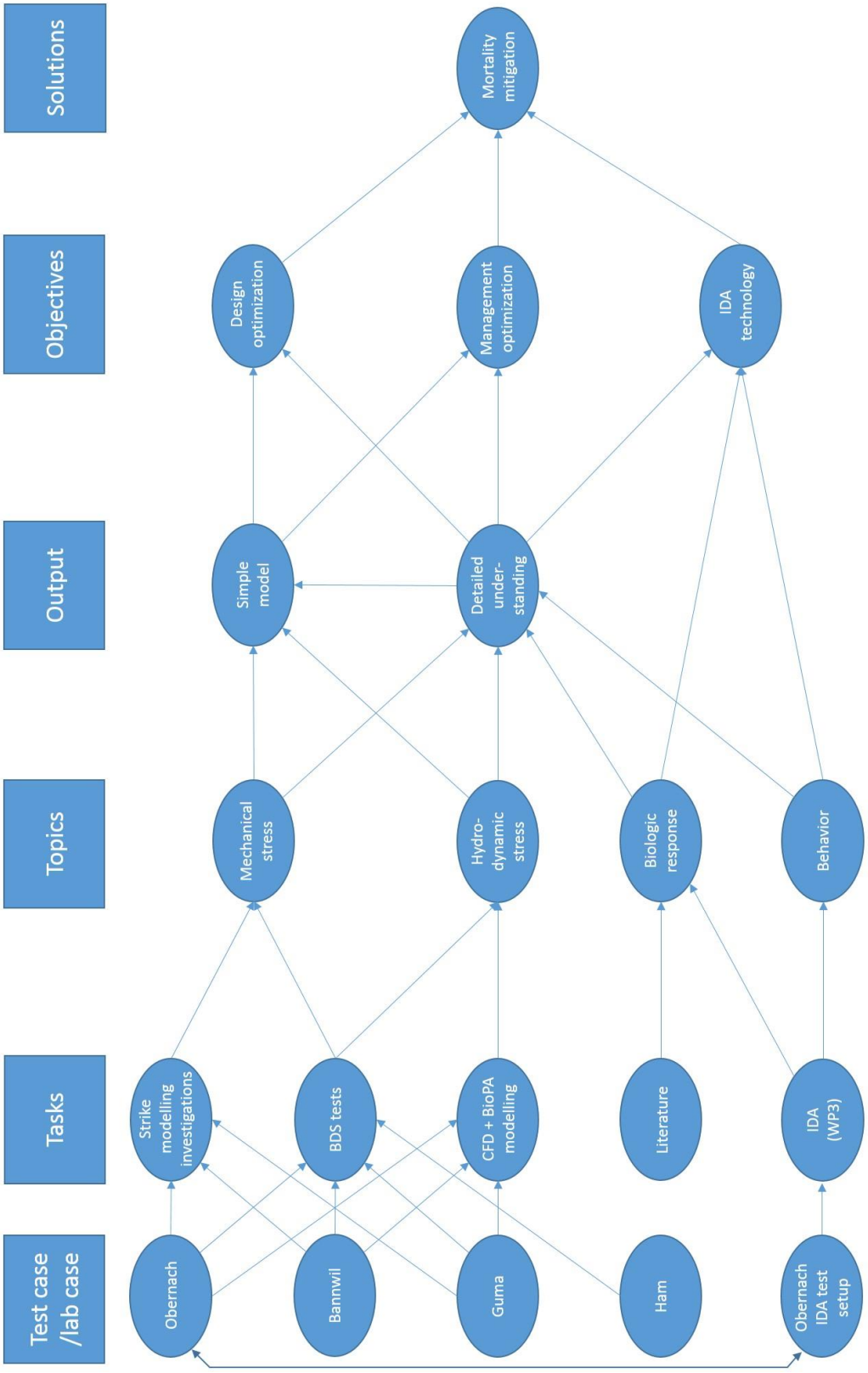


Figure 288: Schematic workflow with regard to turbine passage issues.

Back to D2.2 Main index

6.4.2. Work on SMTDs for fish mortality in turbines

Based on the previous analysis of fish mortality and turbine issues, the work focuses on the modelling of fish mortality rates in Kaplan turbines and includes:

- Analytical modelling of runner blade strike probabilities and the resulting fish damage
- Sensor passage investigations of physical conditions during turbine passage by BDS sensor deployment
- Numerical modelling of hydrodynamic stress during turbine passage (pressure, shear, turbulence) by CFD and BioPA based software

The work aims towards an improved fish mortality rate quantification. An improved understanding of fish damage can subsequently also be utilized for damage rate reduction by management or design measures. The considerations cover mechanical damage due to strike as well as mortality related to hydrodynamic stress. With regard to mortality prognosis, the considerations need to account for probabilities and levels of exposure as well as the probabilities for relevant injury/response face to the given stress levels. The latter is not addressed by direct means but has to be deduced from literature references and will be promoted in D3.1. The relations between turbine design/operation and the resulting stress are examined in several aspects.

The respective activities focus on two exemplary Test Cases, Bannwil and Guma, which feature Kaplan turbines of relevant specifications for numerous European hydropower sites. Moreover, experiments with a Kaplan turbine at the Obernach laboratory are included. Table 93 summarizes the basic parameters of the considered turbines. The parameter ranges show coverage of relevant spread, required for the research purpose, especially with regard to European hydropower conditions. For each site, analytical modelling, BDS deployment and numerical modelling are conducted.

Table 93: Summary of basic parameters for investigated Kaplan turbines

	Bannwil Test Case	Guma Test Case	Obernach laboratory
Power (per unit)	9.5 MW	1.8 MW	35 kW
Design discharge [m³/s]	142	25	1.5
Design head [m]	7.2	8	2.5
Runner diameter [m]	4.4	2.1	0.75
Runner speed [rpm]	107	220	333
Number of blades	4	4	4
Design	Bulb	S-type	Bulb

Detailed information about Test Cases and related activities are provided in the respective chapters. Relevant information on the laboratory setup and work is given in the subsequent chapters. Additional BDS test is conducted at Ham Test Case with regard to sensor deployment. By instance of the present deliverable, the Test Case investigations, as well as numerical investigations, have not been completed, due to various influences, especially hydrological restrictions. The present document provides the intermediate findings while final results will be provided at a given time.

6.4.2.1. Laboratory investigations

The research and development activities are facilitated by experimental work in an existing test setup in the hydraulic laboratory of the TUM in Obernach, which features a 35 kW Kaplan

turbine, in bulb design with almost horizontal axis (10°). Machine specifications are provided in Table 93. Figure 289 shows the turbine runner and its installation. Double regulation by guide vanes and runner blades is controlled manually, providing constant boundary conditions during tests. The turbine is embedded in the laboratory channel system. Water supply is provided from the Isar river and discharge can be controlled by an upscaled Rehbock gauge flume. The tailwater surface elevation can be controlled by a gate at the end of the downstream channel reach. The laboratory environment enables thus targeted and controlled test conditions.

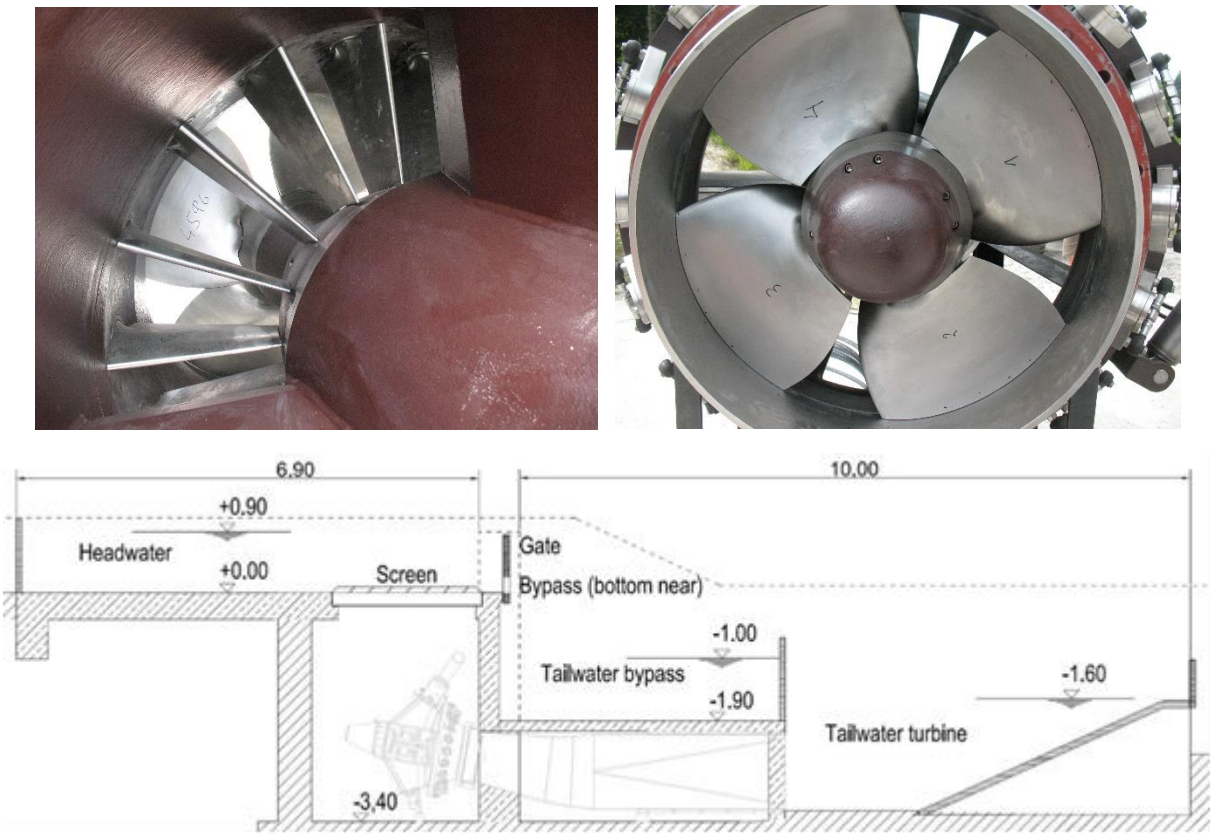


Figure 289: 35 kW turbine runner at the Obernach laboratory from upstream (top left) and downstream (top right) and longitudinal section of the test section (bottom, [m]).

The turbine is part of a test setup for the TUM Hydro Shaft concept (Sepp 2014). As small scale prototype of this innovative hydropower scheme, the facility was employed to clarify fish downstream passage conditions. In the scope of these works, a number of fish also passed through the turbine and respective data concerning fish injury and mortality due to turbine passage is already available (Geiger et al. 2016b). Tests were conducted for turbine discharges of 1.5 m³/s, 1.3 m³/s and 1.0 m³/s.

A variety of relevant European potamodromous species was included in the test series. Most data is available for brown trout (*Salmo trutta fario*) and grayling (*Thymallus thymallus*), but also barbel (*Barbus barbus*), bullhead (*Cottus gobio*) and minnow (*Phoxinus phoxinus*) were involved. Fish length ranged from 4.5 – 22 cm. As tests mainly addressed fish protection and bypass passage issues, the auxiliary injury and mortality observations featured relatively small case numbers. Only 233 of 1974 inserted fish passed through the turbine. Nevertheless, the observed injury and mortality rates showed statistical significant relations in coherence with literature, i.e. an increase of damage rates with increasing fish length and with decreasing

turbine discharge. Detailed information on the injury and cause of death of each individual were recorded and provide reference data for the occurrence of the different damage sources.

In addition to the live fish passage tests, a number of experiments have been conducted with dummies and inanimate fish (Geiger 2018). The respective data provides further insight to assess runner blade strike probabilities and especially the influence of fish body and fish behaviour on the occurrence of relevant damage in case of runner blade strike. Further live fish turbine passage tests are scheduled in conjunction with WP3 and will provide further data for mortality references and modelling details, especially with regard to the influence of fish comportment.

To address the aspect of passage location on strike probabilities, an injection system was installed in the laboratory site, which enabled dummy injection close to hub and tip position just upstream of the turbine intake. Details of injection system service were designed in order to assure that dummies were completely injected and in order to minimize hydraulic influence of the injection system. Sausage dummies (11 cm length) were marked with different color tags on each side. For constant turbine service conditions, dummies were subsequently injected into the turbine, iteratively for hub and tip position. This procedure assures identical test conditions for tip and hub investigations.

Tests were conducted for three different turbine discharges. For design discharge and 2/3 design discharge, 120 dummies were deployed for each injection point. For 1/3 design discharge, 100 dummies were deployed for each injection point. All test were conducted under design head conditions. An inclined plane of perforated metal sheets in the downstream channel enabled dummy recovery after each test. All 680 deployed dummies were recovered. Geometric and hydraulic conditions in the tailwater area assure, that dummy damage can exclusively be assigned to turbine runner blade strike. Runner blade strikes resulted in cutting of the dummy body. Damage incidence ,as well as the relative position on the dummy body and the orientation, was documented. Different colour codes on both ends of the dummies and a targeted insertion direction accounted for the damage location with regard to passage direction.

The observed damage showed arbitrary distribution along the dummy body. The direction of cuttings was mostly perpendicular to the body axis or with less than 45° aberration to this. Only single dummies indicated impacts with flat angles of blade and body axis. The damage incidence was in general remarkable smaller than theoretical values for objects with flow alignment. These results refer to an arbitrary orientation of the dummies during runner passage. Moreover, the incidence of damage depends on the body orientation. The results confirm dependency of damage incidence not just on operating point, but on the actual passage radius.

A comparison of the damage incidence with results of previous dummy tests without injection system demonstrates methodical issues of turbine passage investigations. Results for full load scenario correspond to those for passage near hub, while values for 2/3 part load show proximity to tip near passage findings. Dummy insertion during previous studies was done from identical positions in the approach flow area above the turbine intake for both discharge scenarios. The differing approach flow of both operating points can entail systematic influence on the actual passage position and with respective impact on damage incidence. These findings illustrate the eminence of adequate dummy and sensor injection.

Figure 290 provides exemplary images of the employed injection points, the dummy damage and the damage incidence. The decrease of damage incidence with decreasing discharge

seems contradictory to strike probability increase model predictions with decreasing discharge but is in turn plausible when taking into account the local relative velocity, which does not result in relevant damage in case of strike.

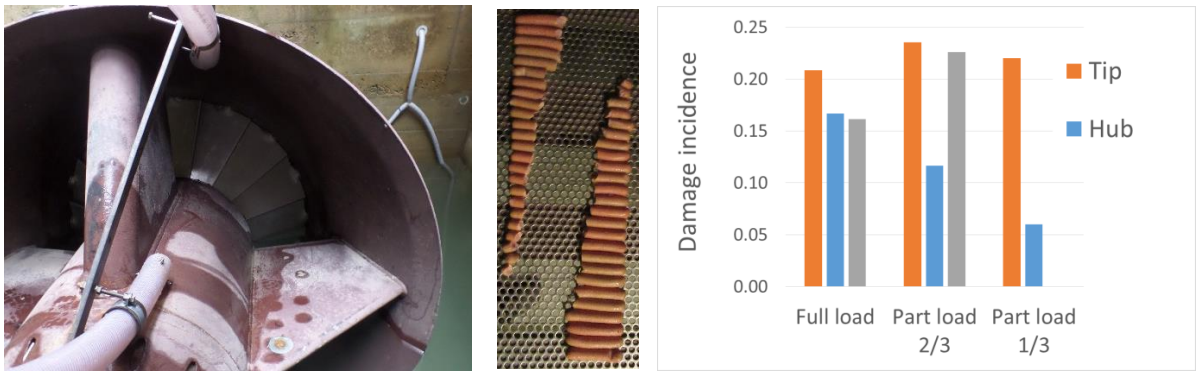


Figure 290: Injection points at turbine intake (left), dummy damage distribution (mid) and dummy damage incidence in dependency of load case and insertion point (right).

6.4.2.2. Analytical modelling (Strike)

Collisions with runner blade leading edge are one major source for fish injury and mortality during turbine passage. The understanding of this issue requires the quantification of blade strike probabilities on the one side and the assessment of fish mortality in case of a strike event on the other side.

A variety of models have been developed to predict fish mortality based on blade strike considerations. Concerning the calculation of strike probabilities, two main approaches can be identified, the one of von Raben (von Raben 1957) and the one of Montén (Montén 1985). Various authors developed mortality models which feature strike probability modelling corresponding to that of von Raben but combine it with different stress response modelling. A number of authors moreover proposed further modifications to von Raben's approach, e.g. with regard to fish width, fish body circumferential extension or runner blade thickness (Franke et al. 1997, Hecker et al. 2005, van Esch et al. 2014).

In general, the modelling takes into account the hydraulic situation at the runner entrance and deduces the probability of blade strike for an idealized one dimensional object with the length of the fish body. A number of details, however, influence the results, as for example the orientation of the fish. This aspect represents the actual difference in the modelling of von Raben and Montén. Von Raben's approach corresponds to fish alignment with the local flow velocity, which is consistent with common rheotaxis of fish. Montén originally suggested arbitrary fish orientation and his modelling corresponds to fish orientation perpendicular to the relative velocity of fish and blade, which is relevant in this context.

The actual fish orientation during turbine passage remains mostly unresolved. General rheotaxis behaviour and experimental findings with regard to strike occurrence and orientation of injury clearly indicate non-arbitrary orientation (Hogan et al. 2014), but no sufficient data is available for detailed assessment face to complex behavioural influences. Due to turbine design, both modelling approaches frequently provide similar results for full load and aberrations only manifest in part load conditions. Figure 291 shows exemplary strike probabilities for investigated the Test Cases and lab scenarios in function of fish orientation and load case.

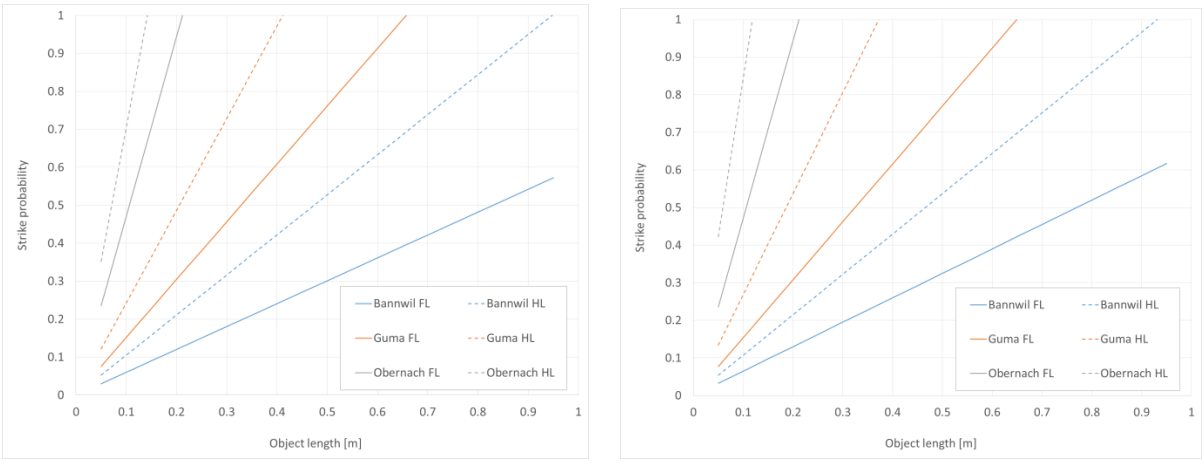


Figure 291: Estimated strike probabilities for turbine passage in the investigated test and lab case scenarios in dependency of full load (FL) and half load (HL) as well as object length, for object passage with flow velocity and orientation aligned with flow (left) or perpendicular to blade relative velocity (right).

The previous results have been calculated for mid runner radius, as mortality modelling generally refers to that specific location. The actual passage radius, in turn, can have a remarkable influence on the resulting strike probability. Figure 292 provides the respective modelling results for passage at hub or tip radius. The real passage location distribution of fish in turbines remains unreferenced. Especially with regard to large scale facilities and fish species with particular surface near or bottom near swimming preference, the fish trajectories are likely to be oriented rather towards hub or tip area.

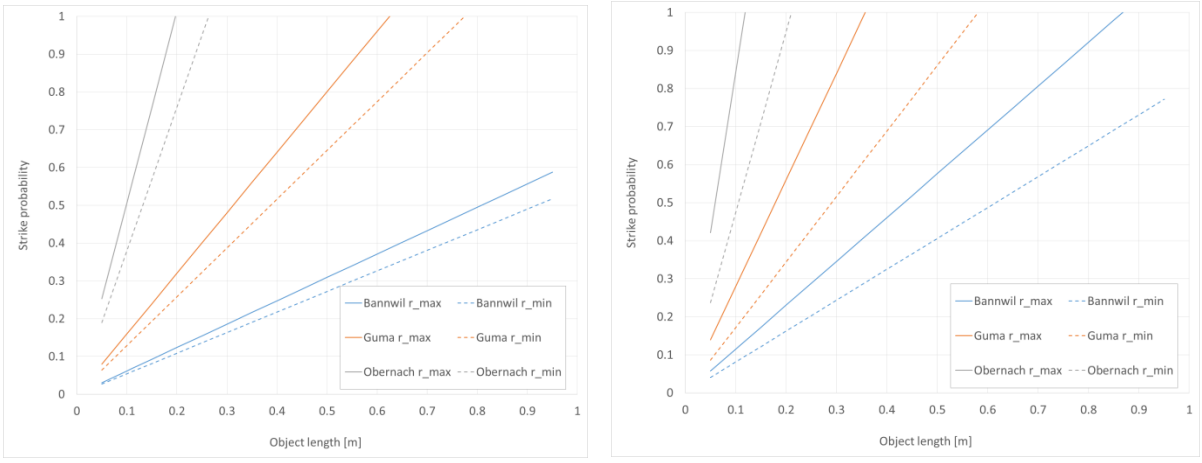


Figure 292: Estimated strike probabilities for turbine passage in the investigated test and lab case scenarios in dependency of passage radius as well as object length, for object passage with flow velocity and orientation aligned with flow and full load (left) and half load (right).

The modelling of strike is further developed in view of sensor passage findings and CFD results. Strike/acceleration measurements from BDS test will be used as a reference for strike occurrence and strength. Reference data from numerical simulations will be employed as a reference for the detailed geometric and hydraulic conditions, which govern strike dynamics. The enhanced strike modelling will account for passage orientation, location and also potential swimming speed of fish. It will be combined with experimental and literature based modelling of strike response, to achieve mortality prognosis. The work will also be related to task 3.5.2,

with special emphasis on the influence of fish behaviour on mortality and possibilities of mortality reduction.

6.4.2.3. Sensor passage investigations (BDS)

BDS sensors are deployed at Test Cases and in laboratory in order to achieve reference data on the physical conditions during turbine passage. The acquired data is to be compared with analytical as well as numerical modelling, to obtain comprehensive understanding and modelling of fish stress during turbine passage. A detailed presentation of BDS technology is provided in the Test Case presentations. At the time of this deliverable, investigations at Obernach laboratory and Ham Test Case have been accomplished. Data analysis is ongoing.

The first BDS sensor devices were deployed in the laboratory facility. Three different sensor types were used (A, B, F). Sensors were injected in front of the turbine intake by a specialized injection system and recovered from the tailwater by hand nets. A screening barrier in the tailwater excluded sensor loss. 183 sensors deployments were conducted. All sensors were recovered. Tests were conducted for three different hydraulic conditions/operating points, which corresponded to those from live fish experiments and dummy tests (1.5 m³/s, 1.3 m³/s, 1 m³/s, each 2.5 m head). Figure 293 illustrated test conditions and procedure.

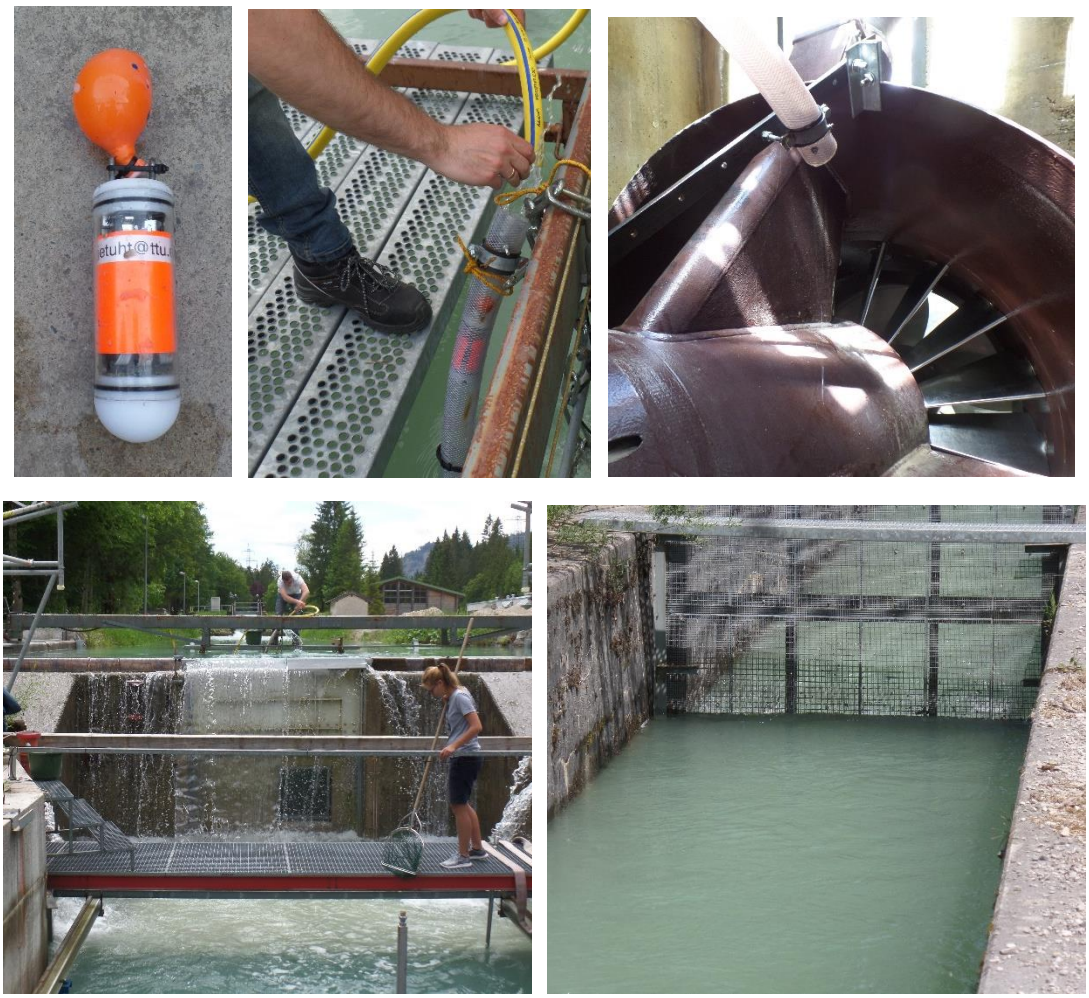


Figure 293: BDS sensor, sensor injection, injection point in front of turbine intake, sensor retrieval from tailwater, tailwater barrier.

The BDS sensor data provides various information, which is still being processed. Figure 294 shows exemplary pressure and acceleration data for a single sensor turbine passage with typical pressure increase towards the runner and distinguished pressure drop / nadir face to runner passage.

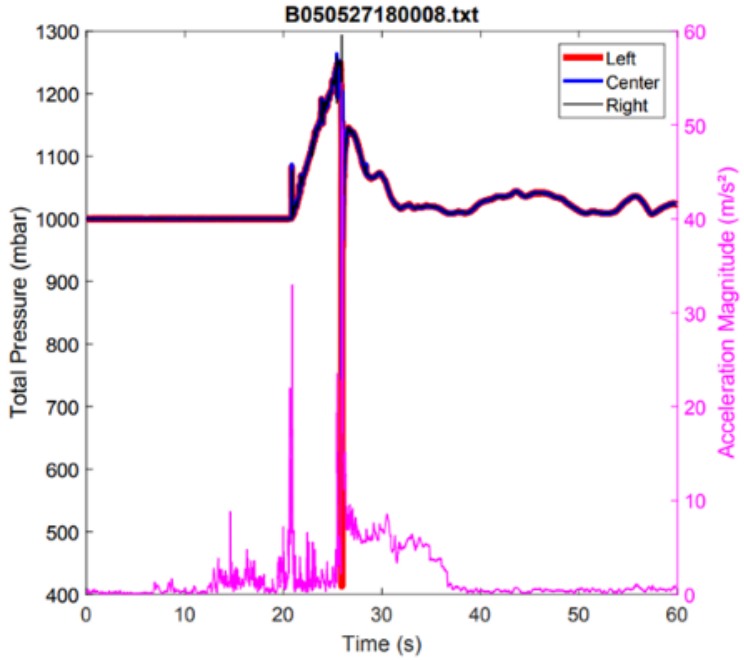


Figure 294: Exemplary BDS data, pressure and acceleration values in dependency of time.

The magnitude of the nadir pressure is relevant for mortality rates and depends on the actual passage location/instance of time in relation to runner passage. A preliminary statistical analysis of the BDS tests at Obernach is illustrated in Figure 295, which presents the nadir pressures of all B-type sensor passages for full and 2/3 part load. It provides the probability to encounter respectable low nadir pressures during runner passage. The clarification of these pressure distributions, as well as the residual stress factors at the Test Cases is a main objective of the related work.

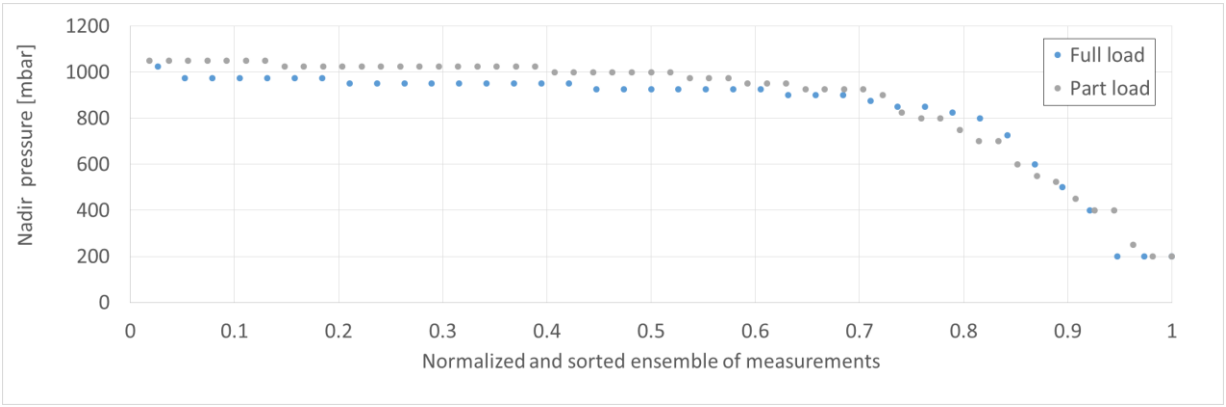


Figure 295: Preliminary analysis of nadir pressure distribution for incidence assessment.

6.4.2.4. Numerical modelling (CFD+BioPA)

Numerical modelling in principle provides the most comprehensive information about hydrodynamic conditions during turbine passage and thus, the most detailed assessment of related stress for fish. For instance, the CFD modelling and the subsequent analysis of fish stress with regard to strike, pressure, turbulence and shear have been conducted for Bannwil Test Case. Respective work for Guma Test Case and Obernach laboratory facility are in progress.

Figure 296 provides an exemplary visualization of fish stressor at the runner leading edge for Bannwil Test Case study. Detailed information about the modelling and the deduced results is given in the respective Test Case presentation. As summarized in Figure 297, the modelling and data processing can deduce fish stress levels for each stressor in function of the operating point.

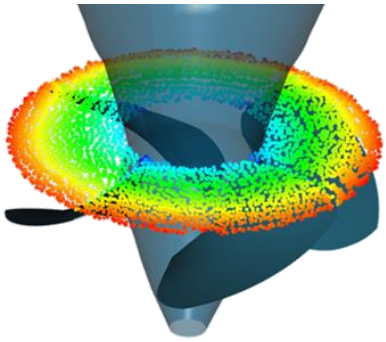


Figure 296: Exemplary stress level distribution at runner entrance, as deduced from numerical simulation.

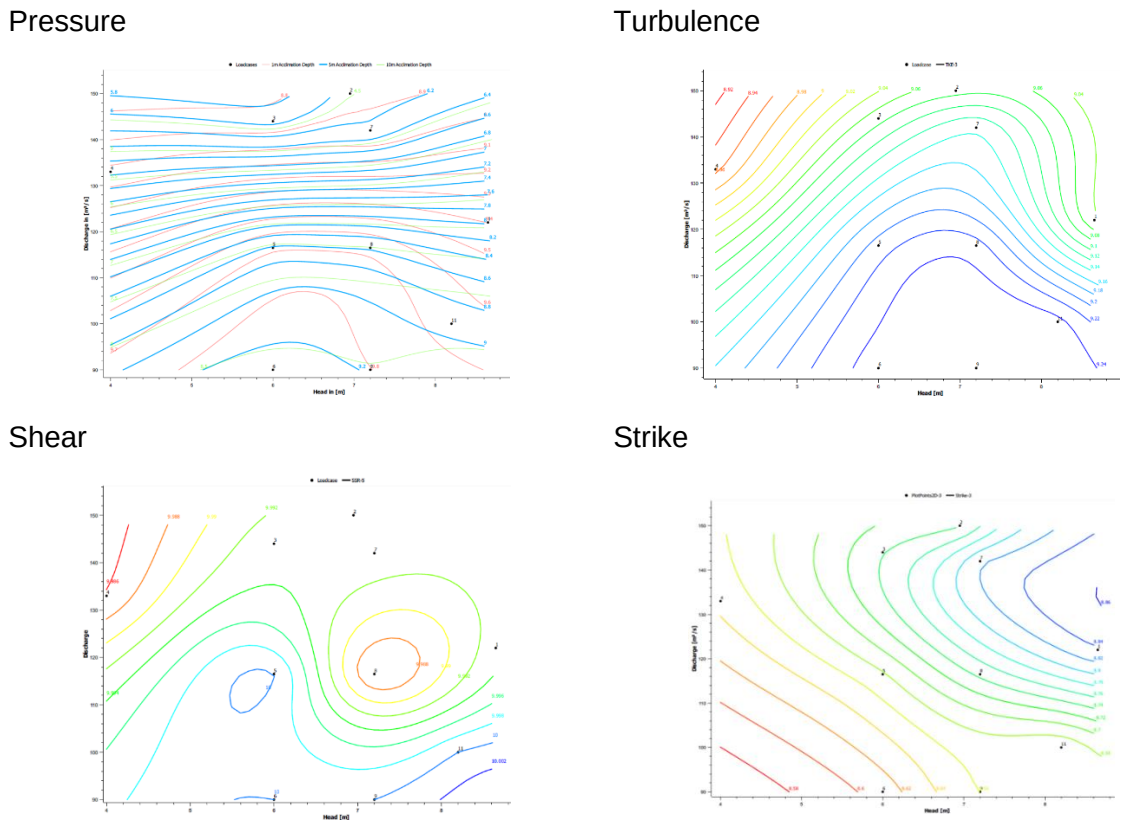


Figure 297: Stress level hill charts for the investigated stressors (vertical axis: head, horizontal axis: discharge)

The numerical based modelling enables a profound understanding of fish stress during turbine passage. It can thus be utilized for targeted design towards ecologically improved turbines but can also be employed for the development of favourable operating schemes. Work is still required as single stress levels need to be combined to meaningful overall values and fish response to stress levels needs to be addressed for actual mortality assessment. Figure 298 shows an example of overall stress levels in function of operating points as deduced by present approaches. The comprehensive information with regard to various operating point subsequently enables mortality rate assessment for the entire range of service conditions throughout a year.

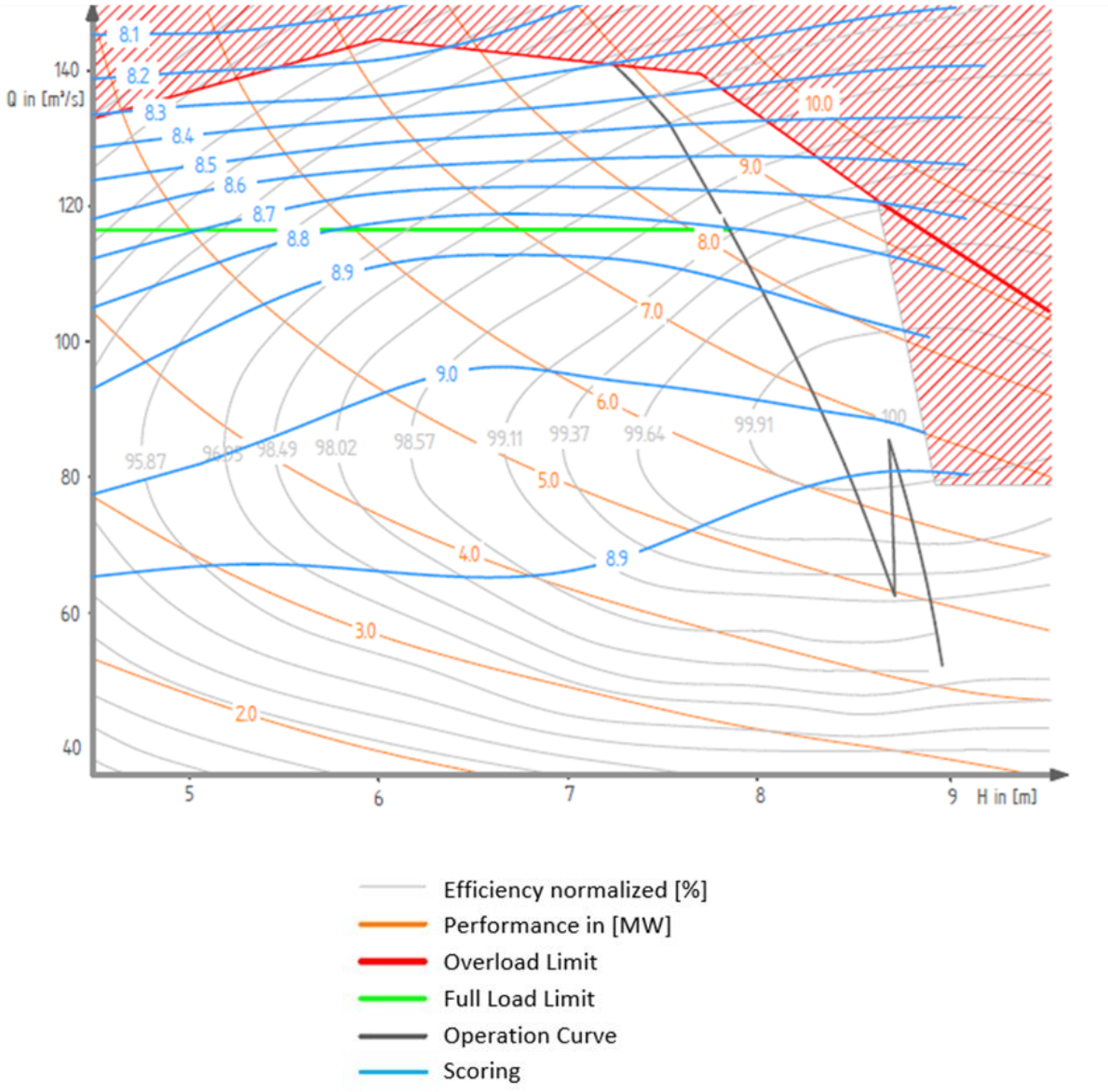


Figure 298: Combined fish passage hill chart for 10 cm acclimation depth.

6.4.3. Conclusion

Work on fish mortality face to turbine passage is ongoing, targeting improved and adapted ways of mortality rate assessment as well as methods of mortality rate reduction. General damage sources of fish face to turbine passage, turbine types and their particularities with

regard to fish downstream migration and SMTDs for mortality rate reduction have been identified and relevant relations were deduced. The further work is focused on the most relevant turbine type for fish downstream migration issue in Europe and those SMTDs most promising for the research goals.

Supported by experimental data from sensor passage investigations with BDS technology, modelling of runner blade strike as well as numerical modelling of turbine hydrodynamic and the resulting stress of fish is advanced. The work is elaborated for two Test Cases with representative range and supported by laboratory investigations, but the developed STMDs will provide applicability for a large range of European HPP conditions and promise general knowledge on mortality rate assessment and mitigation.

By instance of the present deliverable, the work is still ongoing and a comparison and analysis of Test Case results will be provided at a given time. All single procedures have been conducted successfully by now for individual cases: BDS deployment, runner blade strike modelling and numerical modelling with fish stress analysis. These steps will be completed for all sites within 2019. Moreover, actual fish mortality investigations will be conducted at the laboratory site in conjunction with works in WP3.

The developed mortality rate assessment will be presented in D3.1, also including the respective information on mitigation measures. A remaining bottle neck of actual mortality rate modelling will be the lack of reference data concerning fish response to given stress levels with regard to relevant fish species. This might only be resolved by targeted experimental investigations.

6.5. References

Abernethy, C. S., B. G. Amidan, and G. F. Cada. „Laboratory Studies of the Effects of Pressure and Dissolved Gas Supersaturation on Turbine- Passed Fish.“ Tech. rep., Pacific Northwest National Laboratory, 2001.

Adam, B., O. Gler, and H. E. RIK Hufgard. „Zur Wirkung von Wasserrädern auf Fische.“ Artenschutzreport, 2015.

Adam, Beate, Maren Schürmann, and Ulrich Schwevers. Zum Umgang mit aquatischen Organismen: Versuchstierkundliche Grundlagen. Springer-Verlag, 2013.

Amaral, S., G. Hecker, S. St. Jean, and B. McMahon. „2010 Tests Examining Survival of Fish Struck By Turbine Blades.“ Tech. rep., EPRI, Palo, Alto, 2011.

ATV-DVWK, Deutsche Vereinigung für Wasserwirtschaft, Abwasser und Abfall e. V. „Fischschutz und Fischabstiegsanlagen - Bemessung, Gestaltung, Funktionskontrolle.“ Tech. rep., 2005.

Becker, James M., Cary S. Abernethy, and Dennis D. Dauble. „Identifying the effects on fish of changes in water pressure during turbine passage.“ Hydro review (HCL PUBLICATIONS) 22 (2003): 32-42.

Bell, Charles E., and Boyd Kynard. „Mortality of adult American shad passing through a 17-megawatt Kaplan turbine at a low-head hydroelectric dam.“ North American Journal of Fisheries Management (Wiley Online Library) 5 (1985): 33-38.

Boys, Craig A., Brett D. Pflugrath, Melanie Mueller, Joachim Pander, Zhiqun D. Deng, and Juergen Geist. „Physical and hydraulic forces experienced by fish passing through

three different low-head hydropower turbines.“ Marine and Freshwater Research (CSIRO) 69 (2018): 1934-1944.

Brown, Richard S and Pflugrath, Brett D and Colotelo, Alison H and Brauner, Colin J and Carlson, Thomas J and Deng, Z Daniel and Seaburg, Adam G. „Pathways of barotrauma in juvenile salmonids exposed to simulated hydroturbine passage: Boyleś law vs. Henryś law.“ Fisheries Research (Elsevier) 121 (2012): 43-50.

Bruijs, MCM and Polman, HJG and Van Aerssen, GHFM and Hadderingh, RH and Winter, HV and Deerenberg, C and Jansen, HM and Schwevers, U and Adam, B and Dumont, U and others. „Management of silver eel: Human impact on downstream migrating eel in the river Meuse.“ EU-Report Contract Q5RS-2000-31141, 2003.

Cada, G. F. „The Development of Advanced Hydroelectric Turbines to Improve Fish Passage Survival.“ Fisheries 26 (2001).

Cada, G. F. „A Review of Studies Relating to the Effects of Propeller-Type Turbine Passage on Fish Early Life Stages.“ North American Journal of Fisheries Management (Taylor & Francis) 10 (1990): 418-426.

Calles, Olle, Simon Karlsson, Mats Hebrand, and Claudio Comoglio. „Evaluating technical improvements for downstream migrating diadromous fish at a hydroelectric plant.“ Ecological Engineering 48 (2012): 30-37.

Collins, N. H., and C. P. Ruggles. „Fish Mortality in Francis Turbines.“ Research and Development Report - Canadian Electrical Association, 01 1982: var paging.

Coutant, Charles C., and Richard R. Whitney. „Fish Behavior in Relation to Passage through Hydropower Turbines: A Review.“ Transactions of the American Fisheries Society (Taylor & Francis) 129 (2000): 351-380.

Cramer, Frederick K., and Raymond C. Oligher. „Passing Fish Through Hydraulic Turbines.“ Transactions of the American Fisheries Society 93 (1964): 243-259.

Dainys, J., S. Stakėnas, H. Gorfine, and L. Ložys. „Mortality of silver eels migrating through different types of hydropower turbines in Lithuania.“ River Res Applic 34 (2017): 52-59.

Davies, J. K. „A review of information relating to fish passage through turbines: implications to tidal power schemes.“ Journal of Fish Biology (Blackwell Publishing Ltd) 33 (1988): 111-126.

Dedual, M. „Survival of Juvenile Rainbow Trout Passing through a Francis Turbine.“ North American Journal of Fisheries Management 27 (2007): 181-186.

Deng, Z., T. J. Carlson, J. P. Duncan, and M. C. Richmond. „Six-Degree-of-Freedom Sensor Fish Design and Instrumentation.“ Sensors, 2007: 3399-3415.

Deng, Zhiqun, Gregory R. Guensch, Craig A. McKinstry, Robert P. Mueller, Dennis D. Dauble, and Marshall C. Richmond. „Evaluation of fish-injury mechanisms during exposure to turbulent shear flow.“ Canadian Journal of Fisheries and Aquatic Sciences (NRC Research Press) 62 (2005): 1513-1522.

Dudgeon, David and Arthington, Angela H. and Gessner, Mark O. and Kawabata, Zen-Ichiro and Knowler, Duncan J. and Lévêque, Christian and Naiman, Robert J. and Prieur-Richard, Anne-Hélène and Soto, Doris and Stiassny, Melanie L. J. and Sullivan, Caroline A. „Freshwater biodiversity: importance, threats, status and conservation challenges.“ Biological Reviews (Blackwell Publishing Ltd) 81 (2006): 163-182.

Dumont, U., P. Anderer, and Dr. U. Schwevers. „Methoden zur Untersuchung von Fischwanderungen und der Schädigung von Fischen an Wasserkraftstandorten.“ Tech. rep., Umweltbundesamt, Umweltbundesamt Wörlitzer Platz 1 06844 Dessau-Roßlau, 2012.

Dumont, U., and U. Schwevers. Handbuch Querbauwerke. Ministerium für Umwelt und Naturschutz, Landwirtschaft und Verbraucherschutz des Landes Nordrhein-Westfalen, 2005.

Ebel, G. Fischschutz and Fischabstieg an Wasserkraftanlagen - Handbuch Rechen- und Bypasssysteme. Bd. Band 4. Halle (Saale): Büro für Gewässerökologie und Fischeribiologie Dr. Ebel, 2013.

Ebel, G. „Turbinen bedingte Schädigung des Aales (Anguilla anguilla) – Schädigungsraten an europäischen Wasserkraftanlagenstandor-ten und Möglichkeiten der Prognose.“ Mitteilungen aus dem Büro für Gewässerökologie und Fischereibiologie Dr. Ebe 3 (2008).

Edler, C., O. Diestelhorst, and M. Kock. „Untersuchungen zur Abwanderung und Schädigung von Fischen an der Wasserkraftschnecke Rhede-Krechting (Bocholter Aa, Kreis Borken) im Sommer und Herbst 2010.“ Tech. rep., Abschlussbericht im Auftrag des Landesfischereiverbandes Westfalen und Lippe e.V., Münster und Planungsgemeinschaft terra aqua, Bochum, Bochum., 2011.

Egg, Leonhard, Melanie Mueller, Joachim Pander, Josef Knott, and Juergen Geist. „Improving European Silver Eel (Anguilla anguilla) downstream migration by undershot sluice gate management at a small-scale hydropower plant.“ Ecological Engineering 106 (2017): 349-357.

Eicher, G. J. „Turbine-related fish mortality: Review and evaluation of studies: Final report. [Contains glossary].“ Tech. rep., 1987.

English, Karl K., William R. Koski, Cezary Sliwinski, Anita Blakley, Alan Cass, and James C. Woodey. „Migration Timing and River Survival of Late-Run Fraser River Sockeye Salmon Estimated Using Radiotelemetry Techniques.“ Transactions of the American Fisheries Society (Taylor & Francis) 134 (2005): 1342-1365.

Foust, J., G. Hecker, S. Li, and G. Allen. „Fish-Friendly Hydropower Turbine Development & Deployment: Alden Turbine Preliminary Engineering and Model Testing.“ Tech. rep., Electric Power Research Institute, 2011.

Foye, Robert E., and Matthew Scott. „Effects of pressure on survival of six species of fish.“ Transactions of the American Fisheries Society (Taylor & Francis) 94 (1965): 88-91.

Franke, Gary F., D. R. Webb, and R. K. Fisher Jr. „Development of environmentally advanced hydropower turbine system design concepts.“ Tech. rep., Lockheed Idaho Technologies Co., 1997.

Geiger, Franz. „Fish Mortality Rate During Turbine Passage – Generalized Runner Blade Strike Probability Modelling.“ 12th International Symposium on Ecohydraulics. Tokyo, Japan, 2018.

Geiger, Franz, Mathilde Cuchet, and Peter Rutschmann. „Fish downstream migration at hydro power plants-screen passage and mortality investigations.“ 11th International Symposium on Ecohydraulics (ISE 2016). 2016a. 286.

Geiger, F., and P. Schäfer S.and Rutschmann. „Monitoring of downstream passage of small fish at the TUM-Hydro Shaft Power Plant Prototyp.“ Versuchsbericht des Lehrstuhls und der Versuchsanstalt für Wasserbau und Wasserwirtschaft, TU München, 2016b.

Giesecke, Jürgen, Stephan Heimerl, and Emil Mosonyi. Wasserkraftanlagen: Planung, Bau und Betrieb. Springer-Verlag, 2014.

Gloss S., P., and R. Wahl J. „Mortality of Juvenile Salmonids Passing through Ossberger Crossflow Turbines at Small-Scale Hydroelectric Sites.“ Transactions of The American Fisheries Society - TRANS AMER FISH SOC 112 (03 1983): 194-200.

Gomes, P., and M. Larinier. „Dommages subis par les anguilles lors de leur passage au travers des turbines Kaplan – Etablissement de formules prédictives.“ Anguilles-ouvrages Programme national de recherche développement, 2008.

Hecker, G. E., and G. S. Allen. „An Approach to Predicting Fish Survival for Advanced Technology Turbines.“ Hydro Review 24 (2005): 36-43.

Hogan, Timothy W., Glenn F. Cada, and Stephen V. Amaral. „The status of environmentally enhanced hydropower turbines.“ Fisheries (Wiley Online Library) 39 (2014): 164-172.

Holzner, M. „Untersuchungen über die Schädigung von Fischen bei der Passage des Mainkraftwerks Dettelbach.“ Ph.D. dissertation, Technische Universität München - Institut für Tierwissenschaften, 2000.

Jacobson, P. and Amaral, S. and Castro-Santos, T. and Giza, D. and Haro, A. and Hecker, G. and McMahon, B. and Perkins, N. and Pioppi, N. „Environmental Effects of Hydrokinetic Turbines on Fish: Desktop and Laboratory Flume Studies.“ Tech. rep., Electric Power Research Institute, 2012.

Lagarrigue, T., B. Voegtle, and J. M. Lascaux. „Tests for evaluating the injuries suffered by downstream migrating salmonid juveniles and silver eels in their transiting through the VLH turbogenerator unit installed on the Tarn River in Millau.“ Tech. rep., Ecogea, 2008.

Lagarrigue, T., and A. Frey. „Test for evaluating the injuries suffered by downstream-migrating eels in their transiting through the new spherical discharge ring VLH turbogenerator unit installed on the Moselle River in Frouard.“ Report E. CO. GEA for MJ2 Technologies. ECOGEA, Muret, France, 2010.

Larinier, M., and J. Dartiguelongue. „La circulation des poissons migrateurs: le transit à travers les turbines des installations hydroélectriques.“ Bulletin Fran{\c{c}}ais de la P{\^e}che et de la Pisciculture (EDP Sciences), 1989: 1-87.

Larinier, Michel. „Environmental issues, dams and fish migration.“ Dams, Fish and Fisheries: Opportunities, Challenges and Conflict Resolution, 01 2001.

Larinier, Michel. „Fish passage experience at small-scale hydro-electric power plants in France.“ Hydrobiologia (Springer) 609 (2008): 97-108.

Linde, P. „Fischökologisches Monitoring an innovativen Wasserkraftanlagen.“ 7. Workshop des Forums "Fischschutz und Fischabstieg". Dresden, 2018.

Long, C. W., and W. M. Marquette. „Research on Fingerling Mortality in Kaplan Turbines.“ Tech. rep., 1967.

Lucas, Martyn C., Etienne Baras, Timothy J. Thom, Annie Duncan, and Ondrej Slavĺik. Migration of freshwater fishes. Blackwell Science, 2001.

Montén, Erik. Fish and turbines : fish injuries during passage through power station turbines. Stockholm: Vattenfall, 1985.

Mueller, M., J. Pander, and J. Geist. „Evaluation of external fish injury caused by hydropower plants based on a novel field-based protocol.“ Fisheries Management and Ecology 24 (2017): 240-255.

Neitzel, Duane A and Richmond, Marshall C and Dauble, Dennis D and Mueller, Robert P and Moursund, Russell A and Abernethy, Cary S and Guensch, Greg R. „Laboratory studies on the effects of shear on fish.“ Tech. rep., Pacific Northwest National Lab.(PNNL), Richland, WA (United States), 2000.

Pander, J., M. Mueller, J. Knott, and J. Geist. „Catch-related fish injury and catch efficiency of stow-net-based fish recovery installations for fish-monitoring at hydropower plants.“ Fish Manag Ecol. 25 (2018): 31-43.

Pentair. „Fish-friendly pump safe for eel and scalefish.“ Tech. rep., Pentair, 2013.

Pracheil, Brenda M., Christopher R. DeRolph, Michael P. Schramm, and Mark S. Bevelhimer. „A fish-eye view of riverine hydropower systems: the current understanding of the biological response to turbine passage.“ Reviews in Fish Biology and Fisheries (Springer) 26 (2016): 153-167.

Raben, K. Von. „Zur Beurteilung der Schädlichkeit der Turbine für Fische.“ Wasserwirtschaft 48 (1958): 60-63.

Raben, K. Von. „Zur Frage der Beschädigung von Fischen durch Turbinen.“ Wasserwirtschaft 47 (1957): 97-100.

Schmalz, Wolfgang. „Fischabstieg durch eine Wasserkraftschnecke an einem Ausleitungskraftwerk.“ Wasserwirtschaft 7 (2011): 82-87.

Schneider, Jörg, Dirk Hübner, and Egbert Korte. „Funktionskontrolle der Fischaufstiegs- und Fischabstiegshilfen sowie Erfassung der Mortalität bei Turbinendurchgang an der Wasserkraftanlage Kostheim am Main.“ Tech. rep., BFS Bürogemeinschaft für Fisch- & Gewässerökologische Studien, Frankfurt, am, 2012.

Josef Schneider and Clemens Ratschan and Paul Heisey and Chris Avalos and Jeffrey Tuhtan and Christian Haas and Walter Reckendorfer and Martin Schletterer and Andreas Zitek. „Flussabwärts gerichtete Fischwanderung an mittelgroßen Fließgewässern in Österreich.“ Wasserwirtschaft (Springer Vieweg), 2017: 39-44.

Sepp, A. and Rutschmann, P. „Ecological Hydroelectric Concept "Shaft Power Plant".“ International Seminar on Hydro Power Plants. Vienna, 2014.

Solomon, D. J. Fish passage through tidal energy barrages. Energy Technology Support Unit (ETSU), 1988.

Stier, David J., and Boyd Kynard. „Use of Radio Telemetry to Determine the Mortality of Atlantic Salmon Smolts Passed through a 17-MW Kaplan Turbine at a Low-Head Hydroelectric Dam.“ Transactions of the American Fisheries Society (Taylor & Francis) 115 (1986): 771-775.

Taylor, Ralph E., and Boyd Kynard. „Mortality of Juvenile American Shad and Blueback Herring Passed through a Low-Head Kaplan Hydroelectric Turbine.“ Transactions of the American Fisheries Society (Taylor & Francis) 114 (1985): 430-435.

Tombek, Bernd, Mandred Holzner, Ulrich Pulg, and Johannes Schnell. „Untersuchungen zur Effektivitätalternativer Triebwerkstechniken undSchutzkonzepte für abwanderndeFische beim Betrieb von Kleinwasser-kraftanlagen.“ Tech. rep., kein Datum.

Turnpenny, A. W. H. and Clough, S. and Hanson, K. P. and Ramsay, R. and McEwan, D. „Risk assessment for fish passage through small, low-head turbines.“ Tech. rep., United, Kingdom, 2000.

Turnpenny, A. W. H. „Mechanisms of fish damage in low head turbines: An experimental appraisal.“ Fish migration and fish bypasses, 1998: 300.

USACE. „Turbine Optimization for Passage of Juvenile Salmon, Phase II Main Report,.“ Tech. rep., U.S. Army Corps of Engineers, 2013.

Uzunova, Eliza P., and Dimitar Kisliakov. „Fischdurchgängigkeit der Wasserdruckmaschine.“ KW - Korrespondenz Wasserwirtschaft, 2014: 93-100.

Van Esch, B. P. M., and I. L. Y. Spierts. „Validation of a model to predict fish passage mortality in pumping stations.“ Canadian journal of fisheries and aquatic sciences (NRC Research Press) 71 (2014): 1910-1923.

Van Esch, B. P. M., and J. Van Berkel. „Model based study of fish damage for the Pentair Fairbanks Nijhuis Modified Bulb Turbine and the Water2Energy Cross Flow turbine.“ Tech. rep., Pro-Tide, 2015.

Weitkamp, Don E., Robert D. Sullivan, Tim Swant, and Joe DosSantos. „Gas Bubble Disease in Resident Fish of the Lower Clark Fork River.“ Transactions of the American Fisheries Society 132 (2003): 865-876.

7. Hydropeaking

Authors	Antonio Pinheiro (IST)
Contributors	Isabel Boavida (IST), Julie Charmasson (SINTEF), Matthias Schneider (SJE)
Reviewers	Peter Rutschmann (TUM)

List of figures

Figure 299 - Lunz Mesocosm Infrastructure: total view upstream direction; https://www.aquacosm.eu/mesocosm/lunz-mesocosm-infrastructure-lmi/) 452
Figure 300: Aerial view of the compensation and regulation basin Innertkirchen. Up right: Inn2 power house. Centre: PUW outlet and regulation structure. Low left: BB restitution and regulation structure into the Hasliaare River. Along the right image border, the Gadmerwasser River and the initial restitution structure upstream of the railway bridge are visible (in Muller et al. 2016 455

List of tables

Table 94 – Appropriateness of hydropeaking mitigation measures relatively to hydropeaking impacts..... 455

7.1. Introduction

The main goal of the hydropeaking related work in FITHYDRO is the assessment of hydropeaking impacts and, in that way, also the effectiveness of hydropeaking mitigation measures. Basically, there is a distinction between hydrological and ecological assessment. However, it is known that purely hydrological assessment by factors such as hydropeaking amplitudes, flow ramping rates or peaking frequencies can differ a lot from ecological assessment. It has been shown that, in this context, river morphology is one of the most important factors, and in stretches with comparable hydrological impact factors the ecological status has been found better in the ones with higher morphological heterogeneity (ezb, limnex, sje 2012, ARGE Trübung Alpenrhein 2001). In conclusion, for the ecological assessment, the hydrological and morphological factors must be considered.

Within FIThydro, only two Test Cases have hydropeaking operation: Bragado, in Portugal, and GKI, in Austria. At the date of this deliverable, this last Test Case was not yet officially integrated in FIThydro by the EU. Moreover, it presents the specificity of being under construction. Nevertheless, the GKI reach is presently affected by the hydropeaking operation of the immediately upstream Swiss hydropower plant (HPP) of Martina. The construction of GKI is actually a hydropeaking impact mitigation measure, which comes with the advantage that the effectiveness of this mitigation can be assessed as one of several potential scenarios.

The two Test Cases are very different from each other. While Bragado has a high head and low discharge power plant, which with no significant regulation upstream, GKI has a high head and medium discharge power plant, where most of the flows are regulated in Martina HPP and on the two other Swiss HPP, further upstream in river Inn.

In Bragado, the downstream reach of Avelames river affected by hydropeaking is very short (2 km), since this stream is tributary of a much larger river (Tâmega), where the hydropeaking effects of Bragado do not produce a significant impact. Regarding GKI, the conveyance circuit, the available storage for regulation and the operation rules imposed by the environmental permit will allow smoothing the hydropeaking effects caused by Martina operation along the bypass reach, which has a significant length (24.8 km).

7.2. Knowledge gaps and needs

7.2.1. Hydropeaking impacts

The literature review carried out within the scope of Deliverable D2.1 showed that, although several studies on hydropeaking effects and mitigation measures were published in recent years (e.g., Young et al. 2011; Greimel et al. 2018), so far, only few studies published quantitative hydropeaking thresholds for operational mitigation measures (Bejarano et al. 2017a), most of them established for salmonid fish through stranding trials in the field (Saltveit et al. 2001) and in experimental channels (Halleraker et al. 2003).

As recent important quantitative investigations with direct relation to ecological impacts for fish (mortality probability), the stranding experiments of BOKU in Vienna in large scale experimental channels can be cited. These investigations were focused mainly on stranding and drift risk for juvenile fish under controlled hydropeaking events and with local morphological variations. The outcomes of these experiments were thresholds for water level down- and upramping rates that indicate a low risk for juvenile (Schmutz et al. 2013).

The tolerance of different fish species, at different life-stages to hydropeaking effects, such stranding risks, are still poorly known, being difficult in most of the situation to establish

thresholds. There is a lack of adequate relationships between flow-thresholds (e.g., ramping rates, peak ratios) and fish abundance, longitudinal displacement, and stranding. There has been an effort to establish quantitative thresholds (Schmutz et al. 2015), yet they remain useful for regional use due to their site and species specificities.

Furthermore, literature indicates that the impact of hydropeaking is strongly dependent on river reaches morphology (Bradford 1997; Scruton et al. 2008; Boavida et al. 2015), especially site-specific characteristics, such as lateral bar angle, grain size distribution, shelters or potholes, which must be considered when prescribing mitigation measures. Stranding experiments that have been carried out in quasi-natural facilities - Figure 1 (Schülting et al. 2018) must be encouraged, as well as experiments in the rivers (Capra et al. 2017), in order to widen the knowledge about key fish species of that region.



Figure 299 - Lunz Mesocosm Infrastructure: total view upstream direction; https://www.aquacosm.eu/mesocosm/lunz-mesocosm-infrastructure-lmi/)

Current studies report about different results concerning the slowdown of these rates along the course of the river. Whereas some studies find a positive correlation between retentions of peak flow and morphological parameters (Hauer et al. 2013), other studies have found quite diverse water level changes in heterogeneous morphologies independent of the distance from the source of the peaking (Kopecki & Schneider. 2016).

Another impact on fish ecology is the risk exposure of reproduction areas by hydropeaking. Areas providing suitable spawning conditions during the increased flows can fall dry during periods of low flows. Areas suitable during low flows can suffer from sediment movement during peak flows, which increases the probability of redds to be destroyed. Current guidelines for hydropeaking take this into consideration (Tonolla et al. 2017) and, as an important aspect of fish population stability, it must be part of an integrated assessment.

Temporal aspects such as peaking frequency or peaking period (daily and seasonally), as well as the time of the day when peaking occurs, play another important role in the assessment of hydropeaking impacts (Bakken et al. 2016). In the case of salmonids, the risk of stranding is higher if peaking occurs during daylight in winter. Indeed, salmonids have limited movements during day because they hide from predators and because of cold water temperature in winter (Saltveit et al. 2001). The temporal distribution of peaking events over the year is another important factor as the consequences on fish are different given that water level reductions occur regularly every day during a time period or if they occur irregularly over the year (Bakken et al 2016). If the discharge decreases daily, fish will tend to avoid the regulated area.

Lately, new insights on the effects of water quality (e.g., temperature) due to peak flows on fish populations have been described (Toffolon et al. 2010; Zolezzi et al. 2011; Pulg et al. 2016). However, it is unclear to what degree peak flows affect water quality and how that influences fish behaviour (e.g. predation and migration) (Young et al. 2011).

Furthermore, the cumulative effects on fish populations should be expected. For example, repeated small pulses may decrease feeding time, then growth, then species survival, and ultimately community composition (Young et al. 2011). Information on that has been rarely assessed.

7.2.2. Mitigation measures

The mitigation measures can be divided in two categories: operational and structural ones. The selection of the mitigation measures to apply to each Test Case would be improved by a clearer understanding of the mechanisms and relationships that trigger the effects.

Regarding the operational measures, again, the literature review showed that more knowledge is required to perform cost-benefit analysis to evaluate the involved tradeoffs, wherever hydropeaking problems occur (Niu and Insley 2013). The costs imposed on hydropower operators, in terms of revenue losses can be estimated with the aid of existing production models. But the environmental improvements resulting from those measures, namely the positive impacts that they may have on fish populations, are still very difficult to be balanced with those lost profits.

Other studies recommend management approaches to improve spawning and rearing success, such as restricting peak flows during spawning and raising minimum flows during incubation to prevent dewatering (Casas-Mulet et al. 2016) . Also, in this area, further research is required, to cover a complete set of key European fish species requirements.

A recent review on hydropeaking (Moreira et al. 2019) also pointed out that Austria is the only EU Member State that has already established hydropeaking thresholds. On a Federal level, the Autonomous Province of Bolzano, Italy, did it as well. Other countries or regions, like Spain and the German Province of Baden- Württemberg, have recommendations, in river basin management plans, for the mitigation of hydropeaking, while many countries still work on a case by case basis.

Therefore, it is evident that there is a lack of legislation/guidelines regarding hydropeaking mitigation. Most probably, this lack is closely related to the lack of information on the impacts of hydropeaking in the fish species at the different life-stages, and the inherent difficulty in establishing legislation/guidelines.

7.3. Tools for hydropeaking assessment and related knowledge gaps

The CEDREN research center led by SINTEF, one of the FIThydros's partners, developed a method to assess the impacts of hydropeaking on fish population (Harby et al., 2016). This method has been originally developed for salmon and is now under development in FIThydro for the Iberian barbel and the grayling. The assessment method will be available as an Excel-based tool called the Hydropeaking Tool. The Hydropeaking Tool will be applied in both Test Cases (Bragado and GKI) to assess the impacts of hydropeaking in the flow regime, in the present situation and, for GKI, after the implementation of the operation rules defined in the environmental permit.

The work carried out so far in the two case-studies has shown that some revisions of hydropeaking criteria and thresholds are required to adapt the hydropeaking tool to different species. For instances, in Bragado, during the summer period the rivers in this region experience severe droughts, adding to this, evaporation in the reservoir increases, leading to a shut in energy production in an attempt to store water in the reservoir. Some authors refer to the flow ratio as one metric to define the hydropeaking impact (Carolli et al. 2011; Meile et al. 2008). But when calculating the flow ratio for hydropower schemes like this one the value obtained is very high, sometimes 10 times higher than the values obtained for Central Europe. This must be recognized when defining thresholds. Furthermore, the analysis has emphasized the lack of knowledge regarding the vulnerability to hydropeaking of other fish species than salmon'. Therefore, these will be topics that will be addressed in the subsequent deliverables from WP3 and WP4, but that will require a strong research investment, out of the scope of FIThydro, to achieve results that may allow the Hydropeaking Tool or other similar tools be applied in the different European regions.

7.4. Appropriateness, constraints and limitation of the mitigation measures

Deliverables D2.1 and 4.1 extensively present and discuss the use of structural mitigations measures. Regarding structural mitigation measures for the hydropeaking impacts, none was implemented in Bragado and none is foreseen for GKI. However, in the GKI example, morphological mitigation has been performed in one river reach which the impacts will be assessed for. In this latter Test Case, as mentioned before, a set of operational constraints are established in the environmental permit, regarding the reduction of the hydropeaking impacts.

Without the intention of being exhaustive, and depending on the site-specific conditions, a set of structural mitigation measures related with habitat management may be appropriate to mitigate the hydropeaking impacts:

- Morphology adaptations;
- Shelter/ current deflectors;
- River-in-the-river;
- Off-channel habitats;
- Regulating basins (Figure 300).



Figure 300: Aerial view of the compensation and regulation basin Innertkirchen. Up right: Inn2 power house. Centre: PUW outlet and regulation structure. Low left: BB restitution and regulation structure into the Hasliaare River. Along the right image border, the Gadmerwasser River and the initial restitution structure upstream of the railway bridge are visible (in Muller et al. 2016

These mitigation measures are site-specific, and therefore they must address the site conditions and the hydropeaking impacts that may exist at that site. Nevertheless, some *a priori* indications may be given relatively to the appropriateness the mitigation measures regarding the different impacts – Table 94.

Table 94 – Appropriateness of hydropeaking mitigation measures relatively to hydropeaking impacts

	Morphology adaptations	Shelter / Current deflectors	River-in-the-river	Off-channel habitats
Stranding	X			
Downstream displacement of fish		X	X	X
Movements and home range	X		X	
Diel variations		X		X
Reduced spawning	X			X
Nest site dewatering	X			
Reduced rearing survival	X		X	X
Altered migration	X	X	X	

In the GKI Test Case the operational mitigation measures will be implemented by the construction of the power plant, in the way that the construction of the HPP is changing the hydrology downstream of the weir to a regime with attenuated hydropeaking. Since the flow data for the current and future situation are available, this enables the comparison of the situation before and after. On the other hand, three morphologically different stretches are under investigation. One with uniform morphology comparable to about 90% of the affected river section and two with morphological enhancements. This will enable a comparison “before-after” as well.

7.5. Range of application, accuracy and limitation of existing on-site monitoring tools and methods

The range of application of the developed hydropeaking assessment method is not restricted in terms of the methodology itself. But the affected fish species may have quite different demands and sensitivities. If these demands are not defined for the species affected in a given case, the application of the hydropeaking assessment methodology is restricted. However, with the application of the method, the knowledge about the related fish requirements is assumed to increase. In a first approach, it might also be appropriate to use expert judgement for the parameters of the method and apply adapted values to rivers dominated by other species than the ones already studied in more detail.

The accuracy of the assessment methodology is high in terms of the physical parameters, i.e. flow rates and their change in time is high, if there is calibration data available, such as gauging stations and water level measurements. But, as in any method linking physical parameters and ecological reactions, there is a high uncertainty in the ecological impacts.

None of the FIThydro's Test Cases related with hydropeaking has on-site monitoring tools regarding the impacts on fish population.

To date, a fish monitoring campaign with fish tagging was set up at Bragado. During 2018, 79 individuals were individually marked with PITtags. After that, fish were monitored during two field campaigns, roughly corresponding to late spring and late summer. Generally, fishes were recorded immediately upstream the water release from Bragado and in the centre of the river channel - *c.* 50 m downstream the water release. In total, from the 79 PIT-tagged fish, 36 individuals were recorded; a few were recorded several times. From all the individuals detected, 2 were *S. alburnoides*, 13 were *S. pyrenaicus*, and 21 were *P. duriense*. The rank of the different species was the same for the marked and detected fish. Nevertheless, proportionally less S*. alburnoides* and *P. duriense* were detected, whereas the opposite was observed with *S. carolitertii*. This work is still under development.

It seems clear that no application ranges can be defined for the mitigation measures considered for hydropeaking impacts. Moreover, the accuracy of those measures can only be addressed with numerical simulations of the hydrodynamic conditions integrated with the knowledge about fish preferences in the different life-stages (Costa et al. 2018). But the success of those measures can only be evaluated with extensive monitoring campaigns after their implementation and by comparing the results with pre-implementation data.

Similarly, it is not possible to discuss the limitations of those measures, since they are essentially site-specific. Nevertheless, in WP3 we will apply the COSH tool software to test-cases where hydropeaking is an issue to characterize and assess hydropeaking impact.. Moreover, what will be crucial to do, once the site-specific limitations are identified, is to assess the cost-effectiveness of the measures, which will be addressed in WP4.

7.6. References

Bakken, T.H.; Forseth, T.; Harby, A.; Alfredsen, K.; Arnekleiv, J.V.; Berg, O.K.; Casas-Mulet, R.; Charmasson, J.; Greimel, F., Halley, Duncan John; Hedger, R.D.; Larsen, B. M.l; Leo, F.; Melcher, A.; Puffer, M.; Pulg, U.; Reitan, O.; Ruther, N.; Saltveit, S. J.; Sauterleute, J. Friedrich; Schneider, M.; Skoglund, Helge; Sundt, H.; Timalsina, N. P.; Ugedal, O.; van Dijk, J. J.; Vollset, K.; Zakowsky, T.Zinke, P (2016). Miljøvirkninger av effektkjøring: Kunnskapsstatus og råd til forvaltning og industri. Trondheim, Norway: Norsk institutt for

naturforskning (NINA) 2016 (ISBN 978-82-426-2834-3) 205 s. NINA temahefte(62). sENERGISINT NINA NTNU UiO UNI

Bejarano MD, Sordo-Ward Á, Alonso C, Nilsson C (2017a) Charactering effects of hydropower plants on sub-day flow regimes. J Hydrol 550:186–200. doi: 10.1016/j.jhydrol.2017.04.023

Bejarano MD, Sordo-Ward Á, Alonso C, Nilsson C (2017b) Characterizing effects of hydropower plants on sub-daily flow regimes. J Hydrol 550:186–200. doi: 10.1016/j.jhydrol.2017.04.023

Boavida I, Santos JM, Ferreira MT, Pinheiro AN (2015) Barbel habitat alterations due to hydropeaking. J Hydro-Environment Res 9:237–247. doi: 10.1016/j.jher.2014.07.009

Bradford MJ (1997) An experimental study of stranding of juvenile salmonids on gravel bars and in sidechannels during rapid flow decreases. Regul Rivers Res Manag 13:395–401. doi: 10.1002/(SICI)1099-1646(199709/10)13:5<395::AID-RRR464>3.0.CO;2-L

Capra H, Plichard L, Berge J, et al (2017) Fish habitat selection in a large hydropeaking river: Strong individual and temporal variations revealed by telemetry. Sci Total Environ 578:109–120. doi: 10.1016/j.scitotenv.2016.10.155

Casas-Mulet R, Alfredsen K, Brabrand Å, Saltveit SJ (2016) Hydropower operations in groundwater-influenced rivers: implications for Atlantic salmon, Salmo salar , early life stage development and survival. Fish Manag Ecol 23:144–151. doi: 10.1111/fme.12165

Costa MJ, Boavida I, Almeida V and Pinheiro AN (2018) Do artificial velocity refuges mitigate the physiological and behavioural consequences of hydropeaking on a freshwater Iberian cyprinid? Ecohydrology. doi: 10.1002/eco.1983

Greimel F, Schülting L, Graf W, et al (2018) Hydropeaking Impacts and Mitigation. In: Schmutz S, Sendzimir J (eds) Riverine Ecosyst. Manag., Aquatic Ec. Springer, pp 91–110

Halleraker JH, Saltveit SJ, Harby A, et al (2003) Factors influencing stranding of wild juvenile brown trout (Salmo trutta) during rapid and frequent flow decreases in an artificial stream. River Res Appl 19:589–603. doi: 10.1002/rra.752

Moreira M, Hayes DS, Boavida I and Pinheiro, AN (2019) Ecologically-based criteria for hydropeaking mitigation: A review. Sci Total Environ 657:1508–1522. doi: 10.1016/J.SCITOTENV.2018.12.107

Müller, M., Keller, Y., Billeter, P.A., Kaderli, R., Gehri, M., & Kost, M. (2016). Hydropeaking mitigation measures-planning , realization and operation of the first Swiss hydropeaking compensation basin in Innertkirchen BE. In proceedings Hydro 2016, 10-12 October, Montreux, Switzerland

Niu S, Insley M (2013) On the economics of ramping rate restrictions at hydro power plants: Balancing profitability and environmental costs. Energy Econ 39–52. doi: 10.1016/j.eneco.2013.04.002

Pulg U, Vollset KW, Velle G, Stranzl S (2016) First observations of saturopeaking: Characteristics and implications. Sci Total Environ 573:1615–1621. doi: 10.1016/j.scitotenv.2016.09.143

Saltveit SJ, Halleraker JH, Arnekleiv JV, Harby A (2001) Field experiments on stranding in juvenile Atlantic salmon (Salmo salar) and brown trout (Salmo truta) during rapid flow

decreases caused by hydropeaking. Regul Rivers Res Manag 609–622. doi: DOI: 10.1002/rrr.652

Schmutz S, Bakken TH, Friedrich T, et al (2015) Response of Fish Communities to Hydrological and Morphological Alterations in Hydropeaking Rivers of Austria. River Res Appl 31:919–930. doi: 10.1002/rra.2795

Schülting L, Feld CK, Zeiringer B, et al (2018) Macroinvertebrate drift response to hydropeaking: An experimental approach to assess the effect of varying ramping velocities. Ecohydrology e2032. doi: 10.1002/eco.2032

Scruton DA, Pennell CJ, Ollerhead LMN, et al (2008) A synopsis of 'hydropeaking' studies on the response of juvenile Atlantic salmon to experimental flow alteration. Hydrobiologia 609:263–275. doi: 10.1007/s10750-008-9409-x

Toffolon M, Siviglia A, Zolezzi G (2010) Thermal wave dynamics in rivers affected by hydropeaking. Water Resour Res 46:W08536. doi: 10.1029/2009WR008234

Young PS, Cech JJ, Thompson LC (2011) Hydropower-related pulsed-flow impacts on stream fishes: a brief review, conceptual model, knowledge gaps, and research needs. Rev Fish Biol Fish 21:713–731. doi: 10.1007/s11160-011-9211-0

Zolezzi G, Siviglia A, Toffolon M, Maiolini B (2011) Thermopeaking in Alpine streams: event characterization and time scales. Ecohydrology 4:564–576.

Schmutz S., Fohler N., Friedrich T., Fuhrmann M., Graf W., Greimel F., Höller N., Jungwirth M., Leitner P., Moog O., Melcher A., Müllner K., Ochsenhofer G., Salcher G., Steidl C., Unfer G., Zeiringer B. 2013: Schwallproblematik an Österreichs Fließgewässern – Ökologische Folgen und Sanierungsmöglichkeiten. BMFLUW, Wien.

Harby A.; Forseth T.; Ugedal O.; Bakken T.H.; Sauterleute J.. 2016. A method to assess impacts from hydropeaking. IAHR, International Symposium on Ecohydraulics, 2016, Melbourne, Australia

ARGE Trübung Alpenrhein 2001: Trübung und Schwall im Alpenrhein. Synthesebericht, Fachberichte und Literaturstudie im Auftrag der Internationalen Regierungskommission Alpenrhein, Projektgruppe Gewässer- und Fischökologie, Vaduz, Projektordner.

ezb, limnex, sje. 2012. Alpenrhein D6: Quantitative Ana¬lyse von Schwall-Sunk Ganglinien für unterschiedliche Anforderungsprofile Arbeitspaket 5: Habitatmodellierung zur quantitativen Bewertung der Grösse des Schwallein-flusses am Alpenrhein. IRKA: 185 S.

Hauer, Christoph & Schober, Bernhard & Habersack, Helmut. (2013). Impact Analysis of River Morphology and Roughness Variability on Hydropeaking Based on Numerical Modelling. Hydrological Processes. 27. 2209-2224

Kopecki, I., Schneider, M. (2016): Operational and structural measures to reduce hydropeaking impact on fish larvae. La Houille Blanche, 2016/6.

Tonolla D.; Chaix O.; Meile T.; Zurwerra A.; Büsser P.; Oppliger S.; Essyad K. 2017. Schwall-Sunk – Massnahmen. Ein Modul der Vollzugshilfe Renaturierung der Gewässer. Bundesamt für Umwelt, Bern. Umwelt-Vollzug Nr. 1701: 133 S.

8. Hydromorphology

Authors	Kordula Schwarzwälder (NTNU)
Contributors	Ismail Albayrak (ETHZ); Matthias Schneider (SJE), Manon Dewitte (CNRS)
Reviewer	Peter Rutschmann (TUM)

Hydromorphology deals with hydraulics, morphology and their interactions. Within FIThydro the different hydromorphological applications are highly linked to the testing and development of different sediment management measures and strategies.

Sediment management strategies and measures can be described and calculated with complex numerical tools. These allow the simulation and prediction of effects of different activities undertaken. The current tools are very detailed and need far too much computational time and input accuracy for a fast approach on a large scale. At the moment there is no tool available with a less sophisticated approach that would allow such evaluations to be faster and on larger scales and hence poses a knowledge gap to be investigated further. The sediment strategies and measures described in the following are related to the FIThydro Test Cases and are using the existing complex tools mentioned above.

The second large field of interest related to hydromorphology is the linking of morphological patterns in a river to habitat quality and hence to how sediment management can influence habitat quality and availability. Section 8.1.4 of this deliverable describes computational habitat models, which usually use flow and sediment properties to define habitat quality for fish. Yet, such tools are also quite sophisticated, not available to everyone and mainly used on a smaller scale. Some of these different methods and tools are used and further developed within the project at different Test Cases in Switzerland, Sweden and Germany. However, at this stage of the FIThydro project, a linkage between sediment management and fish habitat suitability still represents a knowledge gap.

8.1. Specific tools for hydromorphology

For the topic of hydromorphology, one method and two tools are applied at the Test Cases to evaluate the different approaches. The method is used to investigate the possibilities of sediment management for habitat improvement; the tools are the vortex tube used at the Test Case Schiffmühle and the habitat modelling tool Casimir used at the Test Case Altusried. The vortex tube is in turn also a part of the sediment management method. The tools have already been presented in the FIThydro Deliverable 2.1.

8.1.1. Sediment Management for habitat improvement

This method will allow a link between different management measures for sediment such as the vortex tube (see 8.1.2) and the effects of such measures on the habitat quality in a certain area on a relatively small scale such as the residual flow reach in Schiffmühle where this method is developed and tested.

Different devices and tools are used to collect and produce the necessary input parameter for this method. These devices and tools will be described in the following subsections. The results of sediment sampling and shelter measurements are compared to gather information about potential links between the sediment distribution and the shelter availability. Using these results

the overall method is developed based on the results of four different field campaigns gathering the named data on site which then are linked to a numerical simulation evaluating different hydraulic and morphologic scenarios using the collected data as input.

8.1.1.1. Sediment sampling

The sediment sampling is conducted applying three different methods:

- Sieving
- Picture-based evaluation using the software Basegrain
- Pebble count method

All three methods were applied at the same spots if possible, however, in some submerged areas especially the method using Basegrain but sometimes even collecting the samples for sieving was not possible.

All three methods are surface sampling methods. Sieving and pebble count will be described in the following while the method using Basegrain can be found in the FIThydro deliverable 2.1 and Detert & Weitbrecht 2013. Both sieving and pebble count aredescribed further and in more detail also in the relevant literature such as Bunte et al 2001.

Sieving is a type of area sampling. This means that in a certain area which needs to be defined beforehand all particles of the surface without including any subsurface particles are collected. In submerged areas this can lead to a loss and following an underestimation of very fine material. The collected sediment is then dried and sieved in the lab. This is done using sieves with a defined mesh size (size classes [mm]: 256, 128 – 256, 64 – 128, 32 – 64, 16 – 32, 8 – 16, 4 – 8, 2 – 4, 1 – 2, < 1). The method allows to count all particles, including the fine material (as mentioned if not washed out before), however it needs field time as well as lab time.

Pebble counts is a line counting method, when on a certain line with a defined length (which can be different in size depending on the specific method chosen) all sediment particles are counted with their size. The size is defined by the intermediate axis (width). Hence it is also a surface measure. Other than the sieving this method is mostly neglecting or at least underestimating the fine particles as they can hardly be seen and picked up.

While the sieving is an invasive type of sampling, the pebble count can be either invasive (picking the sones) or non-invasive (only counting under a certain line) and basegrain is non-invasive. For these picture based method the quality of the results is for submerged areas more depending on the turbidity.

The sampling was conducted at 16 different spots which were chosen according to their assumed suitability as a habitat and in addition to allow a various picture of the residual flow reach tested. The results are compared among the different sampling methods and among the different spots.

8.1.1.2. Shelter measurements

The shelter measurements are conducted following the method of Finstad et al 2007 at the same spots as the sediment sampling. The method is described as part of FIThydro deliverable 2.1, the Wiki and in more detail in Forseth et al 2014. The original method was developed for salmonids in Norwegian rivers. Within FIThydro it will be developed further and adapted to fish species more typical for Mid-European rivers.

The outcome of the sampling provides information on the number of certain categories of shelter available for fish within a specified area. Depending on the weighted number of the different categories this is either good, moderate or poor.

8.1.1.3. Numerical modelling

The numerical modelling is conducted in two steps. Step one is the hydraulic modelling of the whole system of the Schiffmühle Test Case, step two the hydromorphological modelling of the residual flow reach.

I. The hydraulic conditions for different scenarios are modelled by the FIThydro partner AF Consult using the commercial software Flow3D. As calibration and validation data the bathymetry and velocity data collected with the ADCP are used (see 3.12).
II. These data are used as input and comparison for the hydromorphological modelling by NTNU using the software SSIIM, which is developed at NTNU. Using the hydraulic scenarios modelled with Flow3D possible sediment management scenarios are added and the results compared with the taken samples.

The results will be linked to the results of the different samplings (8.1.1.1 and 8.1.1.2) to get retrieve information how sediment management can affect the habitat quality and availability.

8.1.2. Vortex Tube / Bedload monitoring

The monitoring of bedload transport is a challenging task due to its strong temporal and spatial stochasticity (Gray and Simões 2008, Gray et al. 2010). Traditionally, direct sampling technologies, either portable or installed in-stream, have been applied. Examples include pit traps, pressure-difference samplers, and basket samplers (Ryan et al. 2005). Major limitations of these technologies include (i) their often difficult and hazardous deployment during floods, (ii) the spatially and temporally discrete record, and (iii) the difficulty to calibrate their sampling efficiency (Gray et al. 2010). Thus, no universally applicable and reliable technology for direct bedload sampling is available (Ryan et al. 2005).

In addition to direct bedload sampling, several indirect monitoring methods have emerged in the past 10-20 years (Ryan et al. 2005, Gray et al. 2010, Rickenmann 2017). These bedload-surrogate monitoring technologies use different sensor types to record signals that are produced by the bedload transport. These sensors can be classified into active and passive sensors. Technologies using active sensors include acoustic Doppler current profilers (ADCP), sonar, radar, and tracers. With the exception of tracers, active sensors are more suitable for monitoring bedload transport in sand-bed rivers (Gray et al. 2010). Technologies using passive sensors include geophones, microphones, accelerometers, hydrophones, piezoelectric sensors, and magnetic detectors (Rickenmann 2017). These methods are more suitable for bedload monitoring in gravel-bed rivers and can be designed in a stand-alone mode, e.g. a hydrophone (Geay et al. 2017), or in a combination with some impact structure, e.g. a pipe or a plate (Gray et al. 2010, Mizuyama et al. 2010, Rickenmann et al. 2012, Tsutsumi et al. 2017). Due to the variability in sedimentological and hydraulic characteristics of the monitored streams as well as in sensors and monitoring setups, the field calibration of each monitoring system is indispensable (Rickenmann et al. 2014). Indirect bedload monitoring is therefore still reliant on traditional bedload sampling methods for calibration, but enables continuous monitoring during flood events and extends the observation period to much longer time spans (Gray et al. 2010).

Within the FIThydro case study HPP Schiffmühle, the goal is to monitor bedload diverted from the headwater channel to the residual flow reach through a vortex tube (cf. **0**). As the vortex

tube is operated only during flood events, the utilization of a direct bedload sampling method would require flexible scheduling of labour-intensive field measurements and short, unexpected flood events would most likely not be recorded. Additionally, the vortex tube is not safely accessible during flood events. Therefore, an indirect method with passive acoustic sensors is developed based on the principle of Swiss Plate Geophone System (SPGS) (see 2.6).

In the case of HPP Schiffmühle, the vortex tube not only served as a diversion structure but also as an impact plate. The field calibration of the monitoring system can be achieved by collecting the transported bedload within a known time period, e.g. with a bedload collection basket (Rickenmann et al. 2012), or by flushing a known quantity of gravels. At HPP Schiffmühle, the first option was impracticable due to its complexity and cost. Instead, four gravel samples of known volume and grain size distribution were flushed through the vortex tube.

8.1.3. Bathymetry measurements with ADCP

Bathymetry measurements can be conducted using single or multi-beam sonars and various models of ADCP, airborne LIDAR, Ariel photography and Optical Satellite technique. Within the FIThydro project, ADCPs have been commonly used because they allow not only to map the river bed but also to measure 3D flow velocities at a high resolution. The velocity data are of prime importance for sediment transport studies, as allow determining the bed shear stresses and hence threshold particle sizes for initiation of sediment motion. For this reason, an ADCP system based on a remote-controlled boat platform is used at the Swiss HPP Schiffmühle. General information on ADCP and comparison of three different deployment platforms are given in section **2.21** and 5.1. The present deployment platform for the ADCP is a remote-controlled boat and highly recommended because of less man-power needed, faster and more measurements in shorter time, no flow disturbance and interference with beams and smoother movement of the boat.

Bathymetry and velocity measurements were conducted in the headwater channel and residual flow reach of HPP Schiffmühle in March and October 2018. Due to the shallow flow and large boulders in parts of the residual flow reach, one person had to be in the water to steer the ADCP boat in order to avoid damage to the boat. This could be the case for tethered ADCP application as well. If the goal is only to measure river bathymetry in a shallow river with low discharge, the use of a total station is recommended instead of ADCP. Based on our experiences at HPP Schiffmühle, a RTK GPS instead of a DGPS is highly recommended for accurate bathymetry measurements using an ADCP.

Another advantage of ADCP for hydro-morphology studies is its ability to allow indirect measurement of suspended sediment transport as well as bed load transport based on the backscatter acoustic signal and bottom tracking data, respectively. Note that such ADCP applications are still under development.

8.1.4. Habitat modelling with Casimir

The fish habitat simulation module CASiMiR-Fish is based on hydromorphological information. In the current version, it uses on one hand results from hydrodynamic modelling in terms of water depth and depth-averaged flow velocity and on the other hand information on substratum on the river bottom and cover types (morphological features that server as a shelter for fish) to derive habitat suitability indices. This habitat suitability can be calculated for different flow scenarios (from low flow to high flow) but also for different morphological scenarios (status quo, morphological enhancements, flood protection measures etc.)

In FITHYDRO an extension of the fish habitat model is developed that focusses onthe upstream migration behaviour of fish. The new module CASiMiR-Migration is developed to assess the attraction flow of fish passes. It is based on hydromorphology as well but uses additional information such as flow directions, flow velocity gradients and on morphology such as river bottom gradients, vicinity of morphological features, preferences for spatial units (bank zone, river centre). In contrast to the existing fish habitat model, it is taking the networking of different habitat types into account.

8.1.5. Double averaging method

The Double Averaging Method (DAM) is not a hydromorphological method itself, however, it is linked to rough bed flows and hence will be considered very briefly in this section.

The method was developed for hydrodynamics and fluvial hydraulics (Nikora et al 2007a, Nikora et al 2007b) and so far used mainly in laboratory applications (Navaratnam et al 2018) mainly with a focus on porous media.

With this method, the fluid momentum equations are doubleaveraged in time and in space. The method was then theoretically applied to rough-bed flows, such as present in the residual flow reach in the FIThydro Test Case Anundsjø in Sweden. Following Nikora et al 2007a and b the main advantage of the DAM is “a consistent link between spatially averaged roughness parameters, bed shear stress, and double-averaged flow variables”. This also includes taking into account drag forces (viscous, form) and form-induced stresses.

Within FIThydro the method will be applied in the field using ADV measurements in the residual flow reach as an input parameter to this method. Following it will be compared with results from laboratory testings to allow us to determine the accuracy of the method and the application ranges for field applications.

8.2. Knowledge Gaps and application ranges

8.2.1. Sediment Management

2.2.1.1. Vortex Tube

Bedload transport restoration measures include (i) structural measures, e.g. sediment bypass tunnels, (ii) operational measures, e.g. reservoir drawdown during natural or artificial flood events, and (iii) sediment replenishment (Bunte 2004, Boes 2015, Boes et al. 2017, Sumi 2017). Within the FIThydro project, the vortex tube built in the year 2003 at HPP Schiffmühle is studied as an example of a bedload continuity restoration measure (section 2.12). The vortex tube is a diversion structure, conceptionally similar to sediment bypass tunnels, but adapted to low-head hydropower plants. At HPP Schiffmühle, the headwater channel and the residual flow reach are parallel to each other and the vortex tube is embedded in the side weir between the two channels. The distance to cover by the vortex tube is short and therefore the construction costs remain reasonably low. The vortex tube is thus generally suitable for bedload diversion at low-head hydropower plants with short distances between the headwater channel and the residual flow reach.

When planning a vortex tube, careful consideration has to be given to the HPP operation and layout in order to ensure its functionality (VAW 2001, VAW 2017). The vortex tube needs to be located where significant bedload transport occurs during flood events. If, for example, the HPP is out of operation during flood events, the bedload transport in the headwater channel may be inhibited due to reduced bottom shear stresses and a diversion structure along this channel is therefore obsolete.

Furthermore, the local hydraulic conditions may influence the diversion efficiency of the vortex tube. The vortex flow within the tube is maintained by a combination of approach flow and the pressure gradient between the headwater channel and the residual flow reach. It was found that a difference in water table elevation of at least 0.5 to 1 m between the two channels is required to maintain the vortex flow in the tube. For lower differences, which generally occur during high flood discharges, the vortex tube may block and lose its functionality. It was shown that this block will dissolve, once the water table elevation in the residual flow reach has declined sufficiently, but the diversion effect of the vortex tube is essentially non-existent during the period of blockage. Careful consideration is therefore required to ensure that the discharge range of vortex tube functionality overlaps with the range of significant bedload transport (VAW 2017).

2.2.1.2. Sediment Sampling and Structure

The sediment structure and distribution at the test site in Schiffmühle is mainly gravel with a slight tendency of colmation. Within the first field campaigns, the distribution of the fine material differed highly from one sampling to the next, probably as a result of the sediment management activities taking place. The results achieved with such a sediment distribution can not necessarily be transferred for instance to rivers with e.g. sandy soil material. Hence linking the sediment and the shelter availability and following the habitat quality needs to be done carefully.

2.2.1.3. Numerical Simulation and habitat evaluation

Using the vortex tube and its contributions to sediment management as well as the results achieved with sediment sampling and habitat evaluation the effect of sediment management measures on the habitat quality is modelled by linking these results with numerical simulations. The application range of the method linking the sediment management with habitat availability,

in general, is not limited to the Test Case Schiffmühle. However it will be done as a first step specifically for the habitat requirements of fish species present in Limmat river, hence additional adaptions might be necessary for other species and their requirements of certain sediment and habitat conditions. In addition, the hydraulic conditions defined as relevant for the Test Case might not be directly applicable also for other HPPs and rivers.

8.2.2. Swimming paths and Casimir

In Switzerland, as in other European countries, there are only general guidelines for the positioning of fish ladder entrances. These are rather related to basic criteria as e.g. the distance to the migration barrier, the position in relation to the main river flow or the vicinity of turbine outlets. The use of hydromorphological information and habitat aspects for the assessment of attraction flow is not common.

In the Test Case Schiffmühle, information on fish upstream migration is not available in terms of fish tracks but the telemetry data from this site provide information on the passage of certain cross sections at the lower and upper entrance and within the fish ladder. This is the reason why it is not feasible to use the data for the development of CASiMiR migration since the fish movement when approaching the fish pass is not covered by the telemetry. However, the model can be applied using the information from the 2D hydrodynamic model and information on the river morphology. The results from the assessment of the attraction flow for different flow situations can then be compared to the number of fishes detected when entering the fish ladder.

As in all European countries, the positioning of fish passes is based on basic rules considering distances to barriers or sources of main flow like turbine outlets or open gates, rather than hydromorphological and habitat information. In the Test Case Altusried an acoustic telemetry system has been installed to detect the fish movement approaching the fish pass from downstream. This information is used to find a correlation between hydraulics, morphology and fish behaviour. First results indicate that different fish species show different behaviour and that movement seem to be closely correlated to specific hydraulic and morphologic patterns. The objective within FITHYDRO is to use these the correlations for the assessment of attraction flow in different flow situations but also for modified morphology. It is assumed that outcomes of the investigations can be transferred to other sites and additional rules for the beneficial placement of fish pass installations can be derived.

8.2.3. Double Averaging Method

As the Double Averaging Method is a theoretically based approach, which is not limited to the specific Test Case but tested and developed further at this specific FIThydro test site, the application range is not directly related to the Test Case in Sweden. The Test Case provides the rough bed bottom surface in the residual flow reach necessary to develop the method for field applications and makes it comparable to the laboratory studies carried out so far. However, the method will be applicable to different independent cases within its application range which is investigated as part of the experiments.

8.3. Lessons learned / recommendations

HPP Schiffmühle

Within the FIThydro project, the bedload monitoring system was installed to improve the understanding of the bedload diversion efficiency of the vortex tube at HPP Schiffmühle. The vortex tube was built in the year 2003 and the operator of HPP Schiffmühle stated that the need to excavate gravel from the headwater channel has reduced since then, which is an indicator for the functionality of the vortex tube. However, quantitative conclusions are challenging, because the entrainment of bedload into the headwater channel is difficult to estimate.

The data collected by the bedload monitoring system up to date shows that bedload is in fact transported through the vortex tube (section 2.12). These results also confirm that the concept of the SPGS is adaptable to a non-standard impact plate, such as the vortex tube. However, due to the dry year 2018, the number of recorded flood events was not yet sufficient to deduce diverted bedload volumes with reasonable certainty. The bedload monitoring campaign will thus be continued and a larger dataset is expected to improve the estimation of diverted bedload volumes. In addition, repeated bathymetry measurements with ADCP were conducted at HPP Schiffmühle within the FIThydro project (section 8.1.2). The detailed analysis of the topographic changes over a certain time period and the link to the bedload monitoring data recorded during the same period will further improve the overall assessment of the bedload continuity and efficiency of the vortex tube at HPP Schiffmühle.

Also, the sediment sampling and shelter measurements will be continued to allow a clearer view of the changes of the system being linked to the sediment management strategies. Combined with the numerical simulations of the hydromorphological processes which are currently running this will improve our knowledge about the potential and limitations of sediment management strategies for the development of habitat availability.

HPP Anundsjö

With respect to hydromorphology the Double Averaging Method will be developed further to be able on a later stage to be linked to fish swimming paths and further indication potential habitats. Presumably, this cannot fully be done as part of FIThydro, as there not all data will be available during the project.

8.4. References

Boes, R.M. (ed.) (2015). Proceedings of the 1st International Workshop on Sediment Bypass Tunnels. VAW-Mitteilungen 232 (R. M. Boes ed.), Laboratory of Hydraulics, Hydrology and Glaciology (VAW), ETH Zurich, Switzerland.

Boes, R.M., Albayrak, I., Friedl, F., Rachelly, C., Schmocker, L., Vetsch, D., Weitbrecht, V. (2017). Geschiebedurchgängigkeit an Wasserkraftanlagen (Sediment conveyance at hydropower plants). Aqua Viva, 2, 23-27 [in German].

Bunte, K., Abt, S.R., 2001. Sampling surface and subsurface particle-size distributions in wadable gravel-and cobble-bed streams for analyses in sediment transport, hydraulics, and streambed monitoring (No. RMRS-GTR-74). U.S. Department of Agriculture, Forest Service, Rocky Mountain Research Station, Ft. Collins, CO. https://doi.org/10.2737/RMRS-GTR-74

Bunte, K., Abt, S.R., Potyondy, J.P., Ryan, S.E., 2004. Measurement of Coarse Gravel and Cobble Transport Using Portable Bedload Traps. Journal of Hydraulic Engineering 130, 879–893. https://doi.org/10.1061/(ASCE)0733-9429(2004)130:9(879)

Bunte, K. (2004). Gravel Mitigation and Augmentation below Hydroelectric Dams: A Geomorphological Perspective. Report. USDA Forest Service, Fort Collins, Colorado.

Detert, M., Weitbrecht, V., 2013. User guide to gravelometric image analysis by BASEGRAIN 9.

Finstad, A.G., Einum, S., Forseth, T., Ugedal, O., 2007. Shelter availability affects behaviour, size-dependent and mean growth of juvenile Atlantic salmon. Freshwater Biology 52, 1710–1718. https://doi.org/10.1111/j.1365-2427.2007.01799.x

Finstad, A.G., Einum, S., Ugedal, O., Forseth, T., 2009. Spatial distribution of limited resources and local density regulation in juvenile Atlantic salmon. Journal of Animal Ecology 78, 226–235. https://doi.org/10.1111/j.1365-2656.2008.01476.x

Finstad, A.G., Ugedal, O., Forseth, T., N?sje, T.F., 2004. Energy-related juvenile winter mortality in a northern population of Atlantic salmon (Salmo salar). Canadian Journal of Fisheries and Aquatic Sciences 61, 2358–2368. https://doi.org/10.1139/f04-213

Foldvik, A., Einum, S., Finstad, A.G., Ugedal, O., 2017. Linking watershed and microhabitat characteristics: effects on production of Atlantic salmonids (Salmo salar and Salmo trutta). Ecology of Freshwater Fish 26, 260–270. https://doi.org/10.1111/eff.12272

Foldvik, A., Finstad, A.G., Einum, S., 2010. Relating juvenile spatial distribution to breeding patterns in anadromous salmonid populations. Journal of Animal Ecology 79, 501–509. https://doi.org/10.1111/j.1365-2656.2009.01652.x

Forseth, T., Harby, A., Ugedal, O., Pulg, U., Fjeldstad, H.-P., Robertsen, G., Barlaup, B.T., Alfredsen, K., Sundt, H., Salveit, S.J., Skoglund, H., Kvingedal, E., Sundt-Hansen, L.E.B.,

Finstad, A., Einum, S., Arnekleiv, J.V., 2014. Handbook for environmental design in regulated salmon rivers (NINA temahefte No. 53). Norsk institutt for naturforskning, Trondheim, Norway.

Geay, T., Belleudy, P., Gervaise, C., Habersack, H., Aigner, J., Kreisler, A., Seitz, H., Laronne, J.B. (2017). Passive acoustic monitoring of bed load discharge in a large gravel bed river. Journal of Geophysical Research: Earth Surface, 122, 528-545.

Gray, J.R., and Simões, F.J.M. (2008). Estimating sediment discharge, appendix D of Sedimentation engineering – Processes, measurements, modeling, and practice (M. Garcia ed.): American Society of Civil Engineering Manuals and Reports on Engineering Practice No. 110, 1067-1088.

Gray, J.R., Laronne, J.B., Marr, J.D.G. (2010). Bedload-surrogate Monitoring Technologies, US Geological Survey Scientific Investigations Report 2010-5091. US Geological Survey: Reston VA.

Haun, S., Kjærås, H., Løvfall, S., Olsen, N.R.B., 2013. Three-dimensional measurements and numerical modelling of suspended sediments in a hydropower reservoir. Journal of Hydrology 479, 180–188. https://doi.org/10.1016/j.jhydrol.2012.11.060

Hedger, R.D., Naesje, T.F., Fiske, P., Ugedal, O., Finstad, A.G., Thorstad, E.B., 2013. Ice-dependent winter survival of juvenile Atlantic salmon. Ecology and Evolution 3, 523–535. https://doi.org/10.1002/ece3.481

Mizuyama, T., Laronne, J.B., Nonaka, M., Sawada, T., Satofuka, Y., Matsuoka, M., Yamashita, S., Sako, Y., Tamaki, S., Watari, M., Yamaguchi, S., Tsuruta, K. (2010). Calibration of a Passive Acoustic Bedload Monitoring System in Japanese Teichert, M.A.K., Kvingedal, E., Forseth, T., Ugedal, O., Finstad, A.G., 2010. Effects of discharge and local density on the growth of juvenile Atlantic salmon Salmo salar. Journal of Fish Biology 76, 1751–1769. https://doi.org/10.1111/j.1095-8649.2010.02614.x

Mountain Rivers. In Bedload-surrogate Monitoring Technologies (J.R. Gray, J.B. Laronne, J.D.G. Marr eds.), US Geological Survey Scientific Investigations Report 2010-5091. US Geological Survey: Reston, VA, 296-318.

Navaratnam, C.U., Aberle, J., Qin, J., Henry, P.-Y., 2018. An experimental investigation on the flow resistance over a porous gravel-bed surface and its non-porous counterpart. E3S Web of Conferences 40, 05073. https://doi.org/10.1051/e3sconf/20184005073

Nikora, V., McEwan, I., McLean, S., Coleman, S., Pokrajac, D., Walters, R., 2007a. Double-Averaging Concept for Rough-Bed Open-Channel and Overland Flows: Theoretical Background. Journal of Hydraulic Engineering 133, 873–883. https://doi.org/10.1061/(ASCE)0733-9429(2007)133:8(873)

Nikora, V., McLean, S., Coleman, S., Pokrajac, D., McEwan, I., Campbell, L., Aberle, J., Clunie, D., Koll, K., 2007b. Double-Averaging Concept for Rough-Bed Open-Channel and Overland

Flows: Applications. Journal of Hydraulic Engineering 133, 884–895. https://doi.org/10.1061/(ASCE)0733-9429(2007)133:8(884)

Olsen, N.R.B., 1994. SSIIM - a three-dimensional numerical model for simulation of water and sediment flow. Transactions on Ecology and the Environment 8.

Rickenmann, D., Turowski, J.M., Fritschi, B., Klaiber, A., Ludwig, A. (2012). Bedload transport measurements at the Erlenbach stream with geophones and automated basket samplers. Earth Surface Processes and Landforms, 37, 1000-1011.

Rickenmann, D., Turowski, J.M., Fritschi, B., Wyss, C., Laronne, J., Barzilai, R., Reid, I., Kreisler, A., Aigner, J., Seitz, H., Habersack, H. (2014). Bedload transport measurements with impact plate geophones: comparison of sensor calibration in different gravel-bed streams. Earth Surface Processes and Landforms, 39, 928-942.

Rickenmann, D. (2017). Bed-Load Transport Measurements with Geophones and Other Passive Acoustic Methods. Journal of Hydraulic Engineering, 143(6): 03117004.

Rüther, N., Olsen, N.R., 2005. Three-Dimensional Modeling of Sediment Transport in a Narrow 90° Channel Bend. Journal of Hydraulic Engineering 131, 917–920. https://doi.org/10.1061/(ASCE)0733-9429(2005)131:10(917)

Rüther, N., Olsen, N.R.B., 2007. Modelling free-forming meander evolution in a laboratory channel using three-dimensional computational fluid dynamics. Geomorphology 89, 308–319. https://doi.org/10.1016/j.geomorph.2006.12.009

Ryan, S.E., Bunte, K., Potyondy, J.P. (2005). Breakout session II, bedload-transport measurement – Data needs, uncertainty, and new technologies, Proceedings of the Federal Interagency Sediment Monitoring Instrument and Analysis Research Workshop (J.R. Gray ed.), September 9-11, 2003, Flagstaff, Arizona, U.S. Geological Survey Circular 1276, 16-28.

Stähly Severin, Friedrich Heide, Detert Martin, 2017. Size Ratio of Fluvial Grains' Intermediate Axes Assessed by Image Processing and Square-Hole Sieving. Journal of Hydraulic Engineering 143, 06017005. https://doi.org/10.1061/(ASCE)HY.1943-7900.0001286

Sumi, T. (ed.) (2017). Proceedings of the 2nd International Workshop on Sediment Bypass tunnels, Kyoto University, Kyoto, Japan.

Szabo-Meszaros, arcel, Rüther, N., Alfredsen, K., 2016. Correlation between the shelter of juvenile salmonids and bed substrate, in: Wieprecht, S., Haun, S., Weber, K., Noack, M., Terheiden, K. (Eds.), River Sedimentation: Proceedings of the 13th International Symposium on River Sedimentation (Stuttgart, Germany, 19-22 September, 2016).

Teichert, M.A.K., Kvingedal, E., Forseth, T., Ugedal, O., Finstad, A.G., 2010. Effects of discharge and local density on the growth of juvenile Atlantic salmon Salmo salar. Journal of Fish Biology 76, 1751–1769. https://doi.org/10.1111/j.1095-8649.2010.02614.x

Tsutsumi, D., Fujita, M., Nonaka, M. (2018). Transport measurement with a horizontal and a vertical pipe microphone in a mountain stream: taking account of particle saltation. Earth Surface Processes and Landforms, 43, 1118-1132.

VAW (2001). Kraftwerk Schiffmühle (Hydropower plant Schiffmühle). VAW-Report 4158, ETH Zurich, Laboratory of Hydraulics, Hydrology and Glaciology (VAW), Switzerland [unpublished, in German].

VAW (2017). Wirbelröhre Kraftwerk Turgi (Vortex tube hydropower plant Turgi). VAW-Report 4343, Laboratory of Hydraulics, Hydrology and Glaciology (VAW), ETH Zurich, Switzerland [unpublished, in German].

Wyss, C.R., Rickenmann, D., Fritschi, B., Turowski, J.M, Weitbrecht, V., Boes, R.M. (2016). Laboratory flume experiments with the Swiss plate geophone bed load monitoring system: 1. Impulse counts and particle size identification. Water Resources Research, 52, 7744-7759.

9. Conclusion

In this deliverable, the SMTDs used within the project at 14 Test Cases of the project were described. These tools will be included in the wiki which will be avalaible online by the end of the project in November 2020.

Moreover, the activities conducted at the Test Cases so far have been presented. Although the complete results are not yet available, it has been possible to analyse, compare and discuss the results to deduce application ranges, knowledge gaps and needs according the 5 topics: upstream migration, downstream migration, passage through turbine, hydropeaking and hydromorphology.

This deliverable is complementary to D2.1 which presented a survey of existing mitigation measures. These mitigation measures will be also included and updated in a wiki system developed in WP4. Therefore this deliverable D2.2 is highly linked to WP3 and WP4. Please refer to corresponding deliverables in the respective work packages.

10 Acknowledgement

The main authors would like to thank all the partners who contributed to this deliverable, who sometimes delivered their contributions within very short times.

11. Appendix

11.1. A-1 Programs of the workshops the 25th January 2019 in Lisbon, Portugal

Meeting information

Meeting : The 5th SC and 5th CSMB meetings and workshops	Location Lisbon, Portugal
Initiated by : CNRS-Institut P'	Date: 25th January 2019
Distribution SC and CSMB	Time : Please check detailed program below
Hôte: IST-ID	Venue : IST-ID

Agenda

1. Habitat modelling

Time	Tool/Topic	Speaker
13:30 – 13:40	Cosh Tool	Julie Charmasson (SINTEF)
13:40 – 13:50	Hydropeaking indicator	Dominique Courret (AFB)
13:50 – 14:00	Hydropeaking tool	Julie Charmasson (SINTEF)
14:00 – 14:15	General discussion on hydropeaking	All
14:15 – 14:30	River-2D	Isabel Boavida (IST)
14:30 – 14:45	Casimir	Matthias Schneider (SJE)
14:45 – 15:00	General discussion on differences and advantages and disadvantages of using the different tools/softwares available	All

2. Hydraulic modelling

Time	Tool/Topic	Speaker
15:30 – 15:45	1D/2D (HEC-RAS)	Ana Quaresma (IST)
15:45 – 16:00	3D (OpenFOAM+FLOW-3D)	David Vetsch (ETHZ)
16:00 – 16:15	Basement	David Vetsch (ETHZ)
16:15 – 16:30	Sediment transport modelling	Nils Rüther (NTNU)
16:30 – 17:00	General discussion on differences and advantages and disadvantages of using the different tools/softwares available	All
17:00 – 17:15	Final Remarks	Laurent David (CNRS)

Contact: Manon Dewitte (manon.dewitte@imft.fr); Ana Quaresma (analopesquaresma@tecnico.ulisboa.pt)